



Environmental Engineering and Management Journal

Founding Editor: Matei Macoveanu

Editor-in-Chief: Maria Gavrilescu

Guest Editor: Dan Cascaval

Innovative Materials and Processes (2)



"Gheorghe Asachi" Technical University of Iasi



Environmental Engineering and Management Journal

An International Journal

Founding Editor: Matei Macoveanu

Editor-in-Chief: Maria Gavrilescu

Guest Editor: Dan Cascaval

Innovative Materials and Processes (2)



“Gheorghe Asachi” Technical University of Iasi

EcoAdvertising Offer

The **Environmental Engineering and Management Journal** encourages initiatives and actions concerning the improvement of education, research, marketing and management, in order to achieve sustainable development. This journal brings valuable opportunities for those offering products, technologies, services, educational programs or other related activities, creating thus a closer relation with the request of the market in the fields of environmental engineering, management and education.

This journal address researchers, designers, academic staff, specialists with responsibilities in the field of environmental protection and management from government organizations (central and local administrations, environmental protection agencies) or from the private or public companies. Also, graduates of specialization courses or of the Environmental Engineering and Management profile, as well as other specialists may find in this journal a direct linkage between the offer and request of the market concerned with the protection of the environment and the administration of natural resources in the national and international context.

The journal was conceived as a means to develop scientific and technical relationships between people who offer and request solutions for environmental protection and conservation of natural resources, creating thus the premises to enhance the transfer of technology and know-how, the confirmation and implementation of ecological products and services.

Taking these aspects into consideration, we gladly welcome any persons or companies which correspond to the above-mentioned purposes and objectives to use our journal to identify potential collaborators, thus contributing to the support of this self-financed journal, which has a special section for eco-advertising.

Costs of advertising material publication

- I. Color ad – whole page, inside 160 €
Color ad – ½ page, inside 90 €
Color ad – ¼ page, inside 50 €
Color ad – other format, inside 0.50 €/cm²
- II. Black and white ad – whole page, inside 120 €
Black and white ad – ½ page, inside 75 €
Black and white ad – ¼ page, inside 45 €
Black and white ad – other format, inside 0.40 €/cm²
- III. Covers III, IV 220 €
- IV. Advertising article 80 €/page

At a constant publication of the advertising material, the following discounts will be offered:

- ✓ 3 publications 10%
- ✓ 6 publications 15%
- ✓ 12 publications 20%

For subscriptions and orders please contact us at:

**OAIMDD (Academic Organization for Environmental Engineering and Sustainable Development),
71 Mangeron Blvd., PO 10, Box 2111, 700050 Iasi, Romania, CIF: 10150285**

Phone/Fax: 0040-232-271759

E-mail: bmrobu.at.gmail.com mgav_eemj.at.yahoo.com

In LEI:

ALPHA BANK ROMANIA (ABR)

SWIFT Code: BUCUROBU

IBAN: RO87BUCU1032235333663RON

Beneficiary: OAIMDD-EEMJ

Adress: PO 10, Box 2111, 700050 Iasi, Romania

In EURO:

ALPHA BANK ROMANIA (ABR)

SWIFT Code: BUCUROBU

IBAN: RO79BUCU1031215940036EUR

Beneficiary: OAIMDD-EEMJ

Adress: PO 10, Box 2111, 700050 Iasi, Romania

Department of Environmental Engineering and Management

OAIMDD-EcoZone Publishing House

73 Prof.Dr.docent Dimitrie Mangeron Street, 700050-Iasi, Romania

Phone/Fax: 0040-232-271759

EDITORIAL BOARD

Founding Editor:

Matei Macoveanu *Gheorghe Asachi* Technical University of Iasi, Romania

Editor-in-Chief:

Maria Gavrilescu, *Gheorghe Asachi* Technical University of Iasi, Romania

Editorial Assistants:

Raluca-Maria Hlihor, *Gheorghe Asachi* Technical University of Iasi, Romania
Laura Bulgariu, *Gheorghe Asachi* Technical University of Iasi, Romania

SCIENTIFIC ADVISORY BOARD

Maria Madalena dos Santos Alves
University of Minho, Braga
Portugal

Abdeltif Amrane
University of Rennes, ENSCR
France

Ecaterina Andronesco
University *Polytechnica* of Bucharest
Romania

Robert Armon
Technion-Israel Institute of Technology, Haifa
Israel

Adisa Azapagic
The University of Manchester
United Kingdom

Hamidi Abdul Aziz
Universiti Sains Malaysia, Penang
Malaysia

Pranas Baltrenas
Vilnius *Gediminas* Technical University
Lithuania

Hans Bressers
University of Twente, Enschede
The Netherlands

Han Brezet
Delft University of Technology
The Netherlands

Dan Cascaval
Gheorghe Asachi Technical University of Iasi
Romania

Aleg Cherp
Central European University, Budapest
Hungary

Yusuf Chisti
Massey University, Palmerston North
New Zealand

Philippe Corvini
University of Applied Sciences Northwestern Switzerland,
Muttens, Switzerland

Igor Cretescu
Gheorghe Asachi Technical University of Iasi
Romania

Silvia Curteanu
Gheorghe Asachi Technical University of Iasi
Romania

Andrew J. Daugulis
Queen's University Kingston
Canada

Valeriu David
Gheorghe Asachi Technical University of Iasi
Romania

Katerina Demnerova
University of Prague
Czech Republic

Gheorghe Duca
State University of Moldavia, Kishinev
Republic of Moldavia

Emil Dumitriu
Gheorghe Asachi Technical University of Iasi
Romania

Jurek Duszczek
Delft University of Technology
The Netherlands

Anca Duta Capra
Transilvania University of Brasov
Romania

Fabio Fava
Alma Mater Studiorum University of Bologna
Italy

Eugenio Campos Ferreira
University of Minho, Braga,
Portugal

Cristian Fosalau
Gheorghe Asachi Technical University of Iasi
Romania

Anton Friedl
Vienna University of Technology
Austria

Anne Giroir Fendler
University *Claude Bernard* Lyon 1
France

Ion Giurma
Gheorghe Asachi Technical University of Iasi
Romania

Yuh-Shan Ho
Peking University
People's Republic of China

Arjen Y. Hoekstra
University of Twente, Enschede
The Netherlands

Nicolae Hurdud
Gheorghe Asachi Technical University of Iasi
Romania

Ralf Isenmann
Munich University of Applied Sciences
Germany

Marcel Istrate
Gheorghe Asachi Technical University of Iasi
Romania

Ravi Jain
University of Pacific, Baun Hall Stockton
United States of America

Michael Sogaard Jørgensen
Aalborg University
Denmark

Nicolas Kalogerakis
Technical University of Crete, Chania
Greece

Gheorghe Lazaroiu
University *Polytechnica* of Bucharest
Romania

Thomas Lindhqvist
International Institute for Industrial Environmental
Economics, Lund University, Sweden

Andreas Paul Loibner
University of Natural Resources and Life Sciences,
Vienna, Austria

Tudor Lupascu
Academy of Sciences, Institute of Chemistry, Kishinev,
Republic of Moldavia

Antonio Marzocchella
University of Naples *Federico II*,
Naples, Italy

José Mondéjar Jiménez
University Castilla-La Mancha, Cuenca
Spain

Shin' ichi Nakatsuji
University of Hyogo
Japan

Valentin Nedeff
Vasile Alecsandri University of Bacau
Romania

Alexandru Ozunu
Babes-Bolyai University of Cluj-Napoca
Romania

Yannis A. Phillis
Technical University of Crete, Chania
Greece

Marcel Ionel Popa
Gheorghe Asachi Technical University of Iasi
Romania

Marcel Popa
Gheorghe Asachi Technical University of Iasi
Romania

Valentin I. Popa
Gheorghe Asachi Technical University of Iasi
Romania

Tudor Prisecaru
University *Polytechnica* of Bucharest
Romania

Gabriel-Lucian Radu
Polytechnica University of Bucharest
Romania

Ákos Rédey
Pannon University, Veszprém
Hungary

Joop Schoonman
Delft University of Technology
The Netherlands

Dan Scutaru
Gheorghe Asachi Technical University of Iasi
Romania

Bogdan C. Simionescu
Gheorghe Asachi Technical University of Iasi
Romania

Florian Statescu
Gheorghe Asachi Technical University of Iasi
Romania

Carmen Teodosiu
Gheorghe Asachi Technical University of Iasi
Romania

Saulius Vasarevicius
Vilnius *Gediminas* Technical University
Lithuania

Angheluta Vadineanu
The University of Bucharest
Romania

Colin Webb
The University of Manchester
United Kingdom

Peter Wilderer
Technical University Munich
Germany

Petra Winzer
Bergische University Wuppertal
Germany

Environmental Engineering and Management Journal

Environmental Engineering and Management Journal is included and indexed in

CABI

Chemical Abstracts Service/SciFinder (ACS) (since 2002)

EBSCO Database (since 2002)

EVISA

ICAAP (International Consortium for Advancement of Academic Publications)

Index Copernicus Journal Master List (ICV/2012=16.20)

Journal Citation Reports® (IF=1.258), (*Environmental Sciences*, Ranked **146 of 206**), (5-Year Impact Factor: 0.970

Article Influence® Score: 0.085)

MedSci

ProQuest (since 2002)

The National University Research Council (RO)

Science Citation Index Expanded™ (Thomson ISI)

SJR (SCImago Journal&Country Rank) (*Environmental Sciences*, Ranked **480 of 825**,

H=14, SJR index/2014 = 0.311, SNIP index/2014 = 0.64)

SCOPUS (since 2008)

Thomson ISI Master Journal List

Web of Science® (Thomson ISI) (**H=20**)

Home page: <http://omicron.ch.tuiasi.ro/EEMJ/>

Full text: <http://www.ecozone.ro>

Founding Editor: Matei Macoveanu, Iasi (RO)

Editor-in-Chief: Maria Gavrilescu, Iasi (RO)

Environmental Engineering and Management Journal is edited by

Gheorghe Asachi Technical University of Iasi and **EcoZone** Publishing House of the **Academic Organization for Environmental Engineering and Sustainable Development (O.A.I.M.D.D.)**

Editorial and Production Office:

Department of Environmental Engineering and Management - Faculty of Chemical Engineering and Environmental Protection

73 Prof.Dr.docent Dimitrie Mangeron Street, 700050 Iasi, Romania

Phone: +40-232-278680, ext. 2259, 2137

Fax: +40-232-271759

e-mail: eejournal.at.yahoo.com, ee_journal.at.yahoo.com, eejeditor.at.yahoo.com, eejm_editor.at.yahoo.com,

eejournal.at.gmail.com, eejm.editor.at.gmail.com, eejm.office.at.gmail.com

Editorial production and secretariat:

Raluca-Maria Hlihor, Editorial Assistant 1

Laura Bulgariu, Editorial Assistant 2

Cristina Ghinea

Isabela Simion

Elena - Diana Comanita

Petronela Cozma

Mihaela Roşca

Camelia Smaranda

Administrative and financial support:

O.A.I.M.D.D., President Brindusa Mihaela Robu

Published 12 issues per year, under the aegis of the

"Gheorghe Asachi" Technical University of Iasi, Romania

by **EcoZone** Publishing House of the **Academic Organization for Environmental Engineering and Sustainable Development (OAIMDD)**, <http://www.ecozone.ro>

Annual subscription rate 2015 (12 issues)

Print:

EURO 500 per volume

EURO 50 per issue

Electronic:

400 per volume

40 per issue

Order directly to the Editorial Office

73 Prof.Dr.docent Dimitrie Mangeron Street, 700050 Iasi, Romania

Phone/Fax: Fax: +40-232-271759

e-mail: bmrobu.at.gmail.com

eejm.office.at.gmail.com

Electronic, full text:

Order or purchase on-line at: www.ecozone.ro

Bank account (EURO):

ALPHA BANK ROMANIA (ABR)

SWIFT Code: BUCUROBU

IBAN: RO79BUCU1031215940036EUR

Beneficiary: OAIMDD-EEMJ

Adress: PO 10, Box 2111, 700050 Iasi, Romania

Bank account (LEI):

ALPHA BANK ROMANIA (ABR), IBAN: RO87BUCU1032235333663RON, Beneficiary: OAIMDD-EEMJ

All rights reserved, including those of translation into foreign languages. No part of each issue may be reproduced in any form (photoprint, microfilm, or any other means) nor transmitted or translated without written permission from the publishers. Only single copies of contributions, or parts thereof, may be made for personal use.

This journal was carefully produced in all its parts. Even so, authors, editors and publisher do not guarantee the information contained there to be free of errors. Registered names, trademarks etc. used in this journal, even when not marked as such, are not be considered unprotected by law.



"Gheorghe Asachi" Technical University of Iasi, Romania



CONTENTS

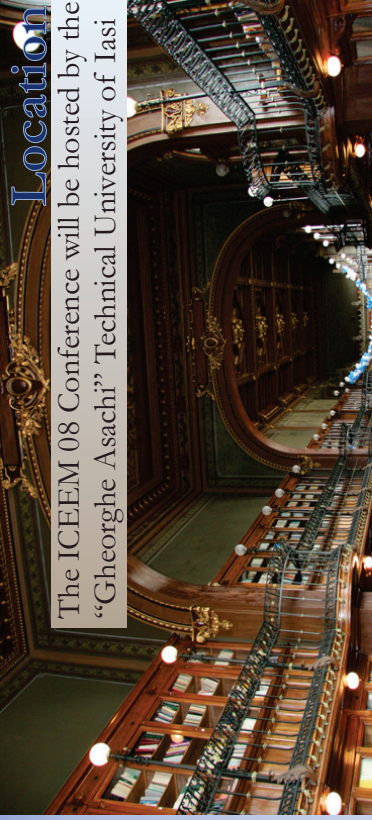
ICEEM08 Call

Papers

| | |
|---|-----|
| Adsorption equilibrium and effective diffusivity in cylindrical alumina particles impregnated with calcium chloride <i>Eugenia Teodora Iacob Tudose, Etelka David, Marius Sebastian Secula, Ioan Mamaliga.....</i> | 503 |
| Design and performance evaluation of a plant for glycerol conversion to acrolein <i>Ionut Banu, Georgiana Guta, Costin Sorin Bildea, Grigore Bozga.....</i> | 509 |
| Influence of nanoporous materials on the chemical composition of Merlot and Cabernet Sauvignon wines <i>Camelia Elena Luchian, Valeriu V. Cotea, Lucia Cintia Colibaba, Catalin Zamfir, Maria Codreanu, Marius Niculaua, Antoanela Patraş.....</i> | 519 |
| Cellulose cellets as new type of adsorbent for the removal of dyes from aqueous media <i>Daniela Suteu, Gabriela Biliuta, Lacramioara Rusu, Sergiu Coseri, Gabriela Nacu.....</i> | 525 |
| Separation of succinic acid from fermentation broths. Modelling and optimization <i>Elena-Niculina Dragoi, Silvia Curteanu, Dan Cascaval, Anca Irina Galaction.....</i> | 533 |
| Equilibrium performances of <i>Crystal-Right™</i> CR100 zeolite used in water softening process <i>Liliana Lazar, Bogdan Bandrabur, Ramona-Elena Tataru-Fărmuş, Mioara Drobota, Silviu-Gabriel Stroe, Gheorghe Gutt.....</i> | 541 |
| Adsorption of endocrine disruptors on exfoliated graphene nanoplatelets <i>Elena Radu, Alina Catrinel Ion, Florinela Sirbu, Ion Ion.....</i> | 551 |

| | |
|---|-----|
| Evolution of trophic parameters from Amara Lake <i>Ofelia Axinte, Iulia Simona Bădescu, Cristina Stroe, Valeria Neacsu, Laura Bulgariu, Dumitru Bulgariu</i> | 559 |
| A new strategy for pentachlorophenol monitoring in water samples using ultra-high performance liquid chromatography-mass spectrometry tandem <i>Yassine Kadmi, Lidia Favier, Maria Harja, Andrei Ionut Simion, Lacramioara Rusu, Dominique Wolbert</i> | 567 |
| Comparative studies on kinetics of anaerobic and aerobic biodegradation of lipids from olive oil mill wastewaters with mixture of <i>Bacillus spp.</i> cells <i>Ramona-Mihaela Matran, Alexandra-Cristina Blaga, Dan Cașcaval, Alexandra Tucaliuc, Anca-Irina Galaction</i> | 575 |
| Magnetic contamination of environment – laboratory simulation of mixed iron oxides impact on microorganism cells <i>Lacramioara Oprica, Claudia Nadejde, Maria Andries, Emil Puscasu, Dorina Creanga, Maria Balasoiu</i> | 581 |
| “Green synthesis” and characterization of gold nanoparticles obtained by a direct reduction method and their fractal dimension <i>Razvan State, Florica Papa, Gianina Dobrescu, Cornel Munteanu, Irina Atkinson, Ioan Balint, Adrian Volceanov</i> | 587 |
| Enhancing the Fenton process by UV light applied in textile wastewater treatment <i>Vasilica-Ancuta Simion, Igor Cretescu, Doina Lutic, Constantin Luca, Ioannis Poullos</i> | 595 |
| Mathematical modelling of mechanical behaviour of cellulose-based fibres exposed to gamma rays and hydrothermal treatment <i>Angelica Olaru, Teodor Măluțan, Maria Geba, Cristina M. Ursescu, Corina Măluțan</i> | 601 |
| PNiPAM-functionalized mesoporous carbon for the adsorption of vitamin B2 <i>Maria Ignat, Maria Emiliană Fortuna, Liviu Sacarescu Mirela-Fernanda Zaltariov, Valeria Harabagiu</i> | 607 |
| Supercritical fluids and ultrasound assisted extractions applied to spruce bark conversion <i>Adina Iulia Talmaciu, Irina Volf, Valentin I. Popa</i> | 615 |
| Selective recovery of phenolic derivatives through the technique of liquid membranes <i>Ioana Diaconu, Cristina Monica Mirea, Elena Ruse, Gheorghe Nechifor</i> | 625 |
| Simple eco-friendly β -galactosidase immobilization on functionalized magnetic particles for lactose hydrolysis <i>Kalim Belhacene, Elena Florentina Grosu, Alexandra Cristina Blaga, Pascal Dhulster, Mariana Pinteala, Renato Froidevaux</i> | 631 |

| | |
|--|-----|
| Removal of carbamazepine by electrocoagulation: investigation of some key operational parameters <i>Tania Yehya, Lidia Favier, Yassine Kadmi, Fabrice Audonnet, Nidal Fayad, Maria Gavrilescu, Christophe Vial</i> | 639 |
| Impact of urbanization on urban heat island effect based on TM imagery in Wuhan, China <i>Qijiao Xie, Zhixiang Zhou</i> | 647 |
| Research on the production of forage for the agro-touristic farms in Romania by cultivating perennial leguminous plants <i>Aurel Călina, Jenica Călina</i> | 657 |
| Effect of hydrogen addition on exhaust emissions and performance of a spark ignition engine <i>Yasin Karagöz, Emre Orak, Levent Yükek, Tarkan Sandalcı</i> | 665 |
| Gridded population distribution map for the Hebei Province of China <i>Yu Zhang, Chun Dong, Jiping Liu, Shouzhi Xu, Tinghua Ai, Fengguang Kang</i> | 673 |
| Optimization of ISEs for simultaneous NH_4^+ , NO_3^- and NO_2^- monitoring in synthetic wastewater using <i>Solver</i> <i>Natalija Velić, Olivera Galović, Milan Sak-Bosnar, Tonči Rezić, Božidar Šantek, Ana Stanić</i> | 681 |
| Challenges and oportunities in green plastics: An assessment using the ELECTRE decision-aid method <i>Elena-Diana Comaniță, Cristina Ghinea, Raluca Maria Hlihor, Isabela Maria Simion, Camelia Smaranda, Lidia Favier, Mihaela Roșca, Irina Gostin, Maria Gavrilescu</i> | 689 |
| Facile synthesis of bismuth oxide nanoparticles by a hydrolysis solvothermal route and their visible light photocatalytic activity <i>Xiaowen Luan, Jian Jiang, Qingya Yang, Minmin Chen, Maolin Zhang, Longfeng Li</i> | 703 |
| Degradation and adsorption behavior of dibutyl phthalate in methanogenic phase refuse <i>Chengran Fang, Yuyang Long, Dongsheng Shen</i> | 709 |



Location

The ICEEM 08 Conference will be hosted by the "Gheorghe Asachi" Technical University of Iasi

Abstract Submission

The **extended abstract submission** should be done **no later than March 30, 2015**, via www.iceem.eu. After the review process, the accepted abstracts (2 pages) will be published electronically in a Book of Abstracts.

The 2nd Conference Call and decisions on **abstract acceptance** will be available after **May 1st 2015**.

Selected papers by the International Scientific Committee will be published in special issues of the journals:

• Process Safety and Environmental Protection

(ISI impact factor: 1.829) will publish papers with the topics:

- *Environmental pollution and monitoring*
- *Water and wastewater treatment and management*
- *Air pollution, prevention and treatment*
- *Waste management for resources and energy recovery*

• Environmental Engineering and Management Journal

(ISI impact factor 1.258) will publish papers with the topics:

- *Sustainable production and consumption*
- *Environmental management and sustainability assessments*
- *Environmental education*

• New Biotechnology (ISI impact factor 2.106) will publish papers in:

- *Environmental biotechnology*

The Conference language is English.

Fees

The fees for the ICEEM 08 Conference will include the conference materials (Program, Abstracts book), coffee breaks, lunches and conference dinner.

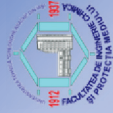
- Full fee: **300 EUR**,
- M.Sc. and PhD students fee: **150 EUR**. More details on www.iceem.eu

Contacts

For details please visit the conference site: www.iceem.eu, or contact the Conference Organizing Committee: iceem08@gmail.com



The "Gheorghe Asachi" Technical University of Iasi
Faculty of Chemical Engineering and Environmental Protection
Department of Environmental Engineering and Management



8th INTERNATIONAL CONFERENCE ON ENVIRONMENTAL ENGINEERING AND MANAGEMENT

1st Call for Papers



9 - 12 September 2015
IASI, ROMANIA
www.iceem.eu

Partners:

- European Federation of Biotechnology, Environmental Biotechnology section
- InterMEDIU - Information, Consultancy and DL Department, TUTIASI, Romania
- Academic Organization for Environmental Engineering and Sustainable Development (OAIMDD), Iasi, Romania



EUROPEAN FEDERATION OF
BIOTECHNOLOGY

Foreword

After two editions abroad, in Hungary and Austria, the 8th edition of ICEEM will be organized in Iasi, Romania between 9 and 12 September 2015 by the “Gheorghe Asachi” Technical University of Iasi.

This ICEEM edition aims to bring together international researchers, academics, professionals and students activating in the fields of environmental engineering and management and to support knowledge exchange and dissemination of specific research and educational programmes.

Like before, ICEEM 08 strongly encourages contributions that focus on innovation, multidisciplinary and cross-sectorial approaches related to environmental issues and sustainability.

Furthermore, the ICEEM conference welcomes contributions of young and senior scientists, and at the same time it encourages practitioners and specialists in various environmental fields to add a more practical-oriented approach to the conference sessions.

We hope that the plenary sessions, oral and poster presentations, workshops and side-events of ICEEM 08 will enhance multidisciplinary, international cooperation and effective communication of scientists, engineers and managers.

Conference chairperson

Prof.dr., dr.h.c. Carmen Teodosiu
“Gheorghe Asachi” Technical University of Iasi

Topics

- I. Environmental pollution and monitoring
- II. Water & wastewater treatment and management
- III. Air pollution, prevention and treatment
- IV. Environmental biotechnology
- V. Environmental management and sustainability assessments
- VI. Sustainable production & consumption
- VII. Waste management for resources and energy recovery
- VIII. Environmental education, Workshops and Exhibitions

Events

Key note lectures
 Plenary Sessions
 Seminars
 Workshops
 Posters Sessions
 Social Events

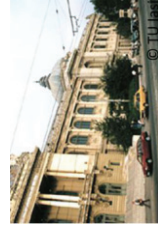
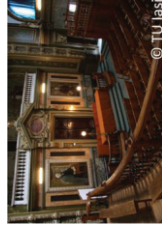
International Scientific Committee

| | |
|---|---|
| Prof.dr., dr.h.c. Maria Madalena dos Santos Alves <i>University of Minho, Portugal</i> | Prof.dr. Maria Gavrilescu <i>Technical University of Iasi, Romania</i> |
| Prof.dr. Tiberiu Apostol <i>Politehnica University, Bucharest, Romania</i> | Prof.dr. Ion Giurma <i>Technical University of Iasi, Romania</i> |
| Prof.dr. Adisa Azapagic <i>The University of Manchester, UK</i> | Assoc. Prof.dr. Almuđena Hospido <i>University of Santiago de Compostela, Spain</i> |
| Prof.dr. Hans Bressers <i>University of Twente, The Netherlands</i> | Prof.dr. Ovidiu Gabriel Iancu <i>A.I.Cuza University Iasi, Romania</i> |
| Prof.dr. Han Brezet <i>Delft University of Technology, The Netherlands</i> | Prof.dr., dr.h.c. Michael Jørgensen <i>Aalborg University, Denmark</i> |
| Prof.dr. Dan Cascaval <i>Technical University of Iasi, Romania</i> | Prof.dr. Nikolas Kalogerakis <i>Technical University of Crete, Greece</i> |
| Prof.dr. Francisc Castells Piqué <i>University of Rovira i Virgili Tarragona, Spain</i> | Prof.dr. Emmanuel G. Koukios <i>National Technical University of Athens, Greece</i> |
| Prof.dr., dr.h.c. Yusuf Chisti <i>Massey University, New Zealand</i> | Prof.dr. Gabriel Lazar <i>Vasile Alecsandri University of Bacau, Romania</i> |
| Prof. dr. Philippe Corvini <i>University of Applied Sciences and Arts Northwestern, Switzerland</i> | Prof.dr., dr.h.c. Thomas Lindqvist <i>IIIIEE, Lund University, Sweden</i> |
| Prof.dr. Cristina Costache <i>Politehnica University, Bucharest, Romania</i> | Assoc.prof.dr. Florica Manea <i>Politehnica University Timisoara, Romania</i> |
| Prof.dr. Igor Cretescu <i>Technical University of Iasi, Romania</i> | Prof.dr. Antonio Marzocchella <i>University Federico II, Naples, Italy</i> |
| Prof.dr. Camelia Draghici <i>Transilvania University of Brasov, Romania</i> | Prof.dr. Mircea Nicoara <i>A.I.Cuza University Iasi, Romania</i> |
| Prof.dr. Fabio Fava <i>Alma Mater Studiorum-University of Bologna, Bologna, Italy</i> | Prof.dr. Alexandru Ozunu <i>Babeş Bolyai University, Cluj, Romania</i> |
| Prof.dr. Sorin Filipescu <i>Babeş Bolyai University, Cluj Napoca, Romania</i> | Prof.dr. Carmen Postolache <i>University of Bucharest, Romania</i> |
| Prof.dr., dr.h.c. Anton Friedl <i>Vienna University of Technology, Austria</i> | Prof.dr., dr.h.c. Akos Rédey <i>Pannonia University, Veszprem, Hungary</i> |
| | Prof.dr. Wilhelm Schabel <i>Karlsruhe Institute of Technology, Germany</i> |
| | Acad.prof.dr. Bogdan Simionescu <i>Technical University of Iasi, Romania</i> |

Organizing Committee

Dr. Brindusa Robu
 Dr. Adela Buburuzan
 Dr. Catalin Balan
 Dr. Daniela Fighir
 Dr. Petronela Cozma
 Dr.d. Irina Morosanu

Dr. George Barjoveanu
 Dr. Daniela Gavrilescu
 Dr. Camelia Smaranda
 Dr. Gabriela Sorceanu
 Dr. Raluca Hlihor
 Dr.d. Diana Comanita





"Gheorghe Asachi" Technical University of Iasi, Romania



ADSORPTION EQUILIBRIUM AND EFFECTIVE DIFFUSIVITY IN CYLINDRICAL ALUMINA PARTICLES IMPREGNATED WITH CALCIUM CHLORIDE

Eugenia Teodora Iacob Tudose, Etelka David, Marius Sebastian Secula, Ioan Mamaliga*

*"Gheorghe Asachi" Technical University of Iasi, Department of Chemical Engineering,
73 Prof. Dr. Docent Dimitrie Mangeron Str., 700050 Iasi, Romania*

Abstract

Adsorption equilibrium and effective diffusion coefficients of water vapor, in cylindrical particles of activated alumina (A) and activated alumina impregnated with calcium chloride (MCA), are experimentally determined. The experiments were conducted at 303 K and 323 K using cylindrical particles with 2.5 mm in both length and diameter. Diffusion coefficients were determined from the kinetics of water sorption. The measurements were conducted in a constant pressure unit based on a magnetic suspension balance (Rubotherm) under isothermal conditions. The sorption capacity depends on temperature and it was found to be higher by 25 % for the MCA material compared with the A material. The water diffusion coefficient depends itself on the adsorption equilibrium taking into account the local slope of the water sorption isotherm. The effective diffusivity of water is almost 2 times lower in impregnated than in non-impregnated alumina. The obtained diffusion data could be used to model the dynamic adsorption.

Key words: adsorption equilibrium, composite alumina - calcium chloride, effective diffusion coefficient

Received: November, 2014; Revised final: March, 2015; Accepted: March, 2015

1. Introduction

Adsorption processes are encountered at a wide scale in industry for gas separation and purification, for humidity control, for environmental protection etc. To calculate and design the adsorption apparatus, equilibrium and diffusion data are needed. In literature, several experimental methods to determine the equilibrium and diffusion coefficients in porous materials are presented (Figueiredo and Matos Freitas, 2013; Igwe et al., 2013; Luis et al., 2014; Mamaliga et al., 2009; Mamaliga et al., 2010; Simonova et al., 2009; Terzyk and Gauden, 2002; Witek-Krowiak, 2013). Studies of adsorption kinetics of water vapors in porous materials offer information to design and operate air conditioning and gas purification plants (Aristov et al., 2006; Simonova et al., 2009; Solomon et al., 2013). Porous alumina

particles are obtained by dehydration of alumina hydrates (commonly $\text{Al}_2\text{O}_3 \cdot 3\text{H}_2\text{O}$), in controlled temperature conditions, up to approximately 6 percent moisture content. The surface has stronger polarity than silica gel and has both acid and basic characteristics, reflecting the amphoteric nature of aluminum. At room temperature, the affinity of activated alumina for water is comparable to the affinity of silica gel, but the adsorption capacity is lower. At elevated temperatures, activated alumina has a higher adsorption capacity than silica gel. Thus, activate alumina is used as drying agent for water vapor and is also employed for removal of polar gases from hydrocarbon streams.

Analytical solutions to Fick's second law of diffusion for the kinetics of adsorption in planar sheet, spherical and cylindrical adsorbents, are well known, but the numerical applications are limited

* Author to whom all correspondence should be addressed: e-mail: imamalig@ch.tuiasi.ro; Phone: 0040 749 036662; Fax: 0040 232 271311

because the solutions are given as infinite series. In various studies (Terzyk and Gauden, 2002; Terzyk et al., 2003) a method to determine diffusion coefficient within cylindrical and spherical carbon granules was developed. They expressed diffusion coefficient as a function of normalized adsorption for spherical adsorbents. For cylindrical adsorbents, the diffusion coefficient was defined in normalized adsorption using both the cylinder length and radius. In this paper, we give a practical approach to adsorption kinetics for cylindrical adsorbents.

Time dependent adsorption for a finite cylinder with radius R and length L is given as (Carslaw and Jaeger, 2005; Crank, 1979) (Eq. 1):

$$\frac{q_t}{q_{max}} = 1 - \left(\frac{4}{\pi^2} \sum_{n=1}^{\infty} \frac{1}{\alpha_n^2} \exp\left(-\frac{\alpha_n^2 Dt}{R^2}\right) \right) \times \left(\frac{8}{\pi^2} \sum_{m=1}^{\infty} \frac{1}{2m-1} \exp\left(-\frac{\pi^2 (2m-1)^2 Dt}{L^2}\right) \right) \quad (1)$$

where q_t and q_{max} are the quantities retained at time t and, respectively, at saturation, D is the effective diffusion coefficient and α_n are roots of the zero-order Bessel function: $J_0(\alpha_n)=0$.

Eq. (1) is computationally exact, but cannot be conveniently used in practical numerical valuation.

The expression for adsorption within a finite cylinder could be obtained using the expressions for adsorption within an infinite cylinder and an infinite planar sheet. An expression for adsorption within an infinite planar sheet of L thickness is given as (Carslaw and Jaeger, 2005; Crank, 1979) (Eq. 2):

$$\frac{q_t}{q_{max}} = 1 - \frac{8}{\pi^2} \sum_{m=1}^{\infty} \frac{1}{2m-1} \exp\left(-\frac{\pi^2 (2m-1)^2 Dt}{L^2}\right) \quad (2)$$

A solution for small Dt/L^2 can be obtained in the form of (Carslaw and Jaeger, 2005; Crank, 1979) (Eq. 3):

$$\frac{q_t}{q_{max}} = 4 \left(\frac{Dt}{\pi L^2} \right)^{0.5} + 8 \left(\frac{Dt}{L^2} \right)^{0.5} \sum_{m=1}^{\infty} (-1)^m \operatorname{ierfc}\left(\frac{mL}{2D^{0.5}t^{0.5}} \right) \quad (3)$$

where $\operatorname{ierfc}(y)$ is the integral of the error function $\operatorname{erfc}(y)$, and, $\operatorname{ierfc}(y) = \exp(-y^2)/\pi^{0.5} - y \operatorname{erfc}(y)$.

For $Dt/L^2 < 0.08$, the second part of Eq. (3) is negligible, so the equation becomes (Eq. 4):

$$\frac{q_t}{q_{max}} = 4 \left(\frac{Dt}{\pi L^2} \right)^{0.5} \quad (4)$$

For adsorption in an infinite planar sheet, Rong and Vadgama (Rong and Vadgama, 2006) derived the Eq. (5):

$$f_{i,s} = \frac{a_t}{a_{t,max}} = 1 - \frac{8}{\pi^2} \exp\left(-\frac{\pi^2 Dt}{L^2}\right) \quad (5)$$

valid for $t > 0.05326 L^2 / D$, $a_t / a_{t,max} > 0.52$, and (Eq. 6):

$$f_{i,s} = \frac{a_t}{a_{t,max}} = \frac{4}{L} \left(\frac{Dt}{\pi} \right)^{0.5} \quad (6)$$

for $t < 0.05326 L^2 / D$, $a_t / a_{t,max} < 0.52$.

The diffusion coefficient is calculated from the half time of saturation as (Eq. 7):

$$D = 0.04908 \frac{L^2}{t_{0.5}} \quad (7)$$

A similar equation at the adsorption in an infinite cylindrical granule is given as (Eq. 8):

$$\frac{a_t}{a_{t,max}} = 1 - 4 \sum_{n=1}^{\infty} \frac{1}{\alpha_n^2} \exp\left(-\frac{\alpha_n^2 Dt}{R^2}\right) \quad (8)$$

where: R is the granule radius and α_n are roots of the zero order Bessel function: $J_0(\alpha_n)=0$.

At the adsorption in an infinite cylinder, for small dimensionless time (Dt/R^2), Eq. (8) becomes Eq. (9):

$$\frac{a_t}{a_{t,max}} = \frac{4}{R} \left(\frac{Dt}{\pi} \right)^{0.5} - \frac{Dt}{R^2} - \frac{(Dt)^{1.5}}{3\pi^{0.5} R^3} \quad (9)$$

For the adsorption in an infinite cylinder, a bipartite expression can be obtained (Eq. 10):

$$f_{i,c} = \frac{a_t}{a_{t,max}} = 1 - 4 \sum_{n=1}^{\infty} \frac{1}{\alpha_n^2} \exp\left(-\frac{\alpha_n^2 Dt}{R^2}\right) \quad (10)$$

valid for $t > 0.03598 L^2 / D$, $a_t / a_{t,max} > 0.3908$, and (Eq. 11):

$$f_{i,c} = \frac{a_t}{a_{t,max}} = \frac{4}{R} \left(\frac{Dt}{\pi} \right)^{0.5} - \frac{Dt}{R^2} - \frac{(Dt)^{1.5}}{3\pi^{0.5} R^3} \quad (11)$$

for $t < 0.03598 L^2 / D$, $a_t / a_{t,max} < 0.3908$

The diffusion coefficient is calculated from the half time of saturation as (Eq. 12):

$$D = 0.06306 \frac{R^2}{t_{0.5}} \quad (12)$$

The equation for adsorption within a finite cylinder is (Rong and Vadgama, 2006) (Eq. 13):

$$f_{f,c} = f_{i,s} + f_{i,c} - f_{i,s}f_{i,c} \quad (13)$$

For our particular cylindrical granule, with radius $R=1.25 \text{ mm}$ and length $L=2.5 \text{ mm}$, Eq. (13) is a function of the product $D \times t$ and, the apparent diffusion coefficient, D , can be estimated from the half adsorption time as (Eq. 14):

$$D_{ap} = \frac{4.6 \cdot 10^{-8}}{t_{0.5}}, m^2 / s \quad (14)$$

Further, the effective diffusion coefficient can be calculated using the equation (Aristov et al., 2006) (Eq. 15):

$$D_e = D_{ap} \frac{\varepsilon + (1 - \varepsilon)K}{\varepsilon}, m^2 / s \quad (15)$$

where: ε is the material porosity and K is the local slope of the adsorption isotherm.

In this paper, we present an experimental study on water vapor equilibrium and diffusion in alumina (A) and composite material (MCA) cylindrical particles.

2. Experimental part

2.1. Materials

Two different materials were used in our experiments, namely: activated alumina (A) and activated alumina impregnated with a calcium chloride solution (MCA) (Table 1). The materials consist of cylindrical granules of 2.5 mm diameter and length. The porous matrix was dried in an oven for 4 hours, at 160°C , and left afterwards to cool down in a dessicator, at room temperature.

The composite material was obtained by impregnating alumina with a calcium chloride solution of 15% mass, at 25°C , in a stirring vessel, at a rotation of 300 rpm. After 2 hours of impregnation, each sample of porous material was separated from the salt solution by vacuum filtration, at room temperature. The retained granules were again dried for 4 hours in an oven, at 160°C , and left to cool down in a dessicator, at room temperature. The resulting CaCl_2 impregnated alumina (MCA) had a salt content of 7.92%. The nitrogen adsorption-desorption isotherms obtained for A and MCA materials correspond, according to the IUPAC classification, to the Type IV isotherm with hysteresis.

Table 1. Characteristics of the materials used in the experimental study on water vapor equilibrium and diffusion

| Materials | Total specific surface (m^2/g) | Total porosity (%) | Pore diameter (nm) |
|-----------|--|--------------------|--------------------|
| A | 96.275 | 64.133 | 5.390 |
| MCA | 43.339 | 37.153 | 5.517 |

One can observe that in the pressure range when the adsorption monolayer is formed, the two curves presented in Fig. 1 have an identical behavior, of Type II isotherm. An enhanced adsorption is registered at higher vapor pressures, fact corresponding to the capillary condensation in mesopores.

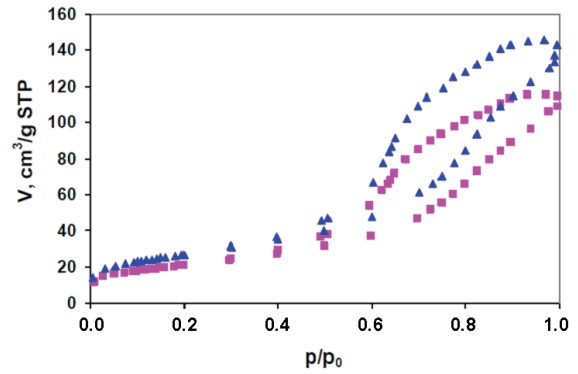


Fig. 1. Sorption isotherms for N_2 in cylindrical granules of A and MCA materials

2.2. Experimental set up

In order to obtain the experimental equilibrium data and diffusion coefficients a magnetic suspension balance system (Rubotherm, Germany, accuracy $\pm 0.1 \text{ mg}$) was used. This allows the measurement of the material mass variation in time. The scheme of the experimental set-up was presented in previous works (Mamaliga, 2004; Mamaliga et al., 2004; Mamaliga et al., 2010). The investigated material was situated on a support suspended by the hook of magnetic coupling. Mass was measured using a balance (Sartorius: $210 \text{ g} \pm 0.1 \text{ mg}$). Adsorption experiments were carried out at constant temperature and different pressure values in an adsorption cell. Pressure in the adsorption cell was controlled by means of the evaporating water and was measured with a pressure sensor.

The amount of solvent absorbed is very small, thus the buoyancy forces at different pressures are important and were taken into account (Mamaliga et al., 2010).

2.3. Experimental protocol

To determine the diffusion coefficient, experiments were led as follows:

1. The porous material was placed into the adsorption cell and dried under vacuum (pressure lower than 0.5 mbar) until a constant mass is obtained. The temperature in sorption cell is maintained at a certain value by means a thermostat.

2. Temperature in the water evaporator is adjusted and maintained to a prescribed value.

3. Water vapors will be kept in contact with the porous material until adsorption equilibrium is

reached. The mass variation of adsorbent material is recorded in time.

4. In order to start a new experiment, parameters such as the evaporator temperature or water vapor pressure would be adjusted. Each experiment gives a point on the equilibrium isotherm.

3. Results and discussion

An example of adsorption kinetics at 303 K, for the same sample of MCA, at two different water vapor pressure values, successively applied is given in Fig. 2. For the investigated materials, kinetic curves were obtained at different values of water vapor pressure. From these plots was determined the half time of diffusion ($t_{0.5}$), used to calculate the apparent diffusion coefficient. Using Eq. (14), apparent diffusion coefficient for cylindrical granules of A and MCA was calculated. Values obtained at a temperature of 323 K and at various pressures of water vapors are shown in Fig. 3.

Equilibrium isotherms, expressed in two different ways, for the investigated materials at an adsorption temperature of 323 K, are presented in Fig. 4. The slopes of adsorption isotherms, K , are determined from Fig. 4b. The amount of water uptake and the slope K of MCA is significantly higher (20-25 %) than for activated alumina (A). The local slope K is presented in Table 2.

With these values and taking into account material porosities (Table 1), the effective diffusion coefficients were calculated based on Eq. (15). The MCA values at a temperature of 323 K, in comparison with those obtained for diffusion in activated alumina (A), are shown in Fig. 5. At low vapor pressure, the effective diffusion coefficients are almost constant and for alumina decrease slightly from values of vapor pressure in the range 60-120 mbar.

Analyzing data shown in Fig. 5, it can be seen that the water vapor effective diffusion coefficient values in activated alumina (A) are higher than in composite materials. The presence of calcium chloride modifies the porous structure of alumina and the pore distribution. The effective diffusion coefficients in the composite material are almost 60 % lower than those obtained in non-impregnated alumina. The difference between the values of effective diffusion coefficients could be attributed to the unequal contributions of the three transport mechanisms (bulk, Knudsen and surface diffusion) occurring in the materials.

For the MCA material, an average effective diffusion coefficient has been determined to have a value of $8.5 \cdot 10^{-7} \text{ m}^2/\text{s}$. For activated alumina, the effective diffusion coefficient values were lower at higher vapor pressures. This could be due to the sorption mechanism changes and occurrence of phenomena such as capillary vapor condensation. Thus, the obtained values are closer to the liquid diffusion coefficients. The temperature influence on

the sorption isotherms for the MCA material is presented in Fig. 6 (a, b).

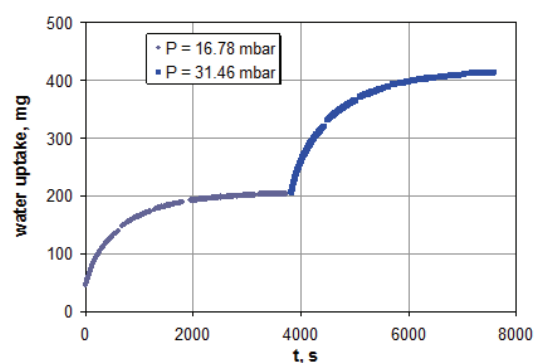


Fig. 2. Water uptake at 303 K in cylindrical MCA granules (diameter and length of 2.5 mm) at two values of water vapor pressure, 16.78 and 31.46 mbar

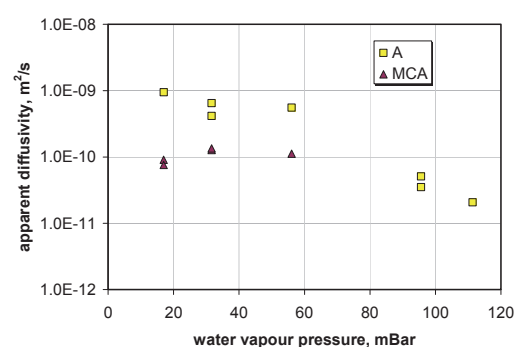


Fig. 3. Apparent diffusion coefficient of water vapors in A and MCA at 323 K

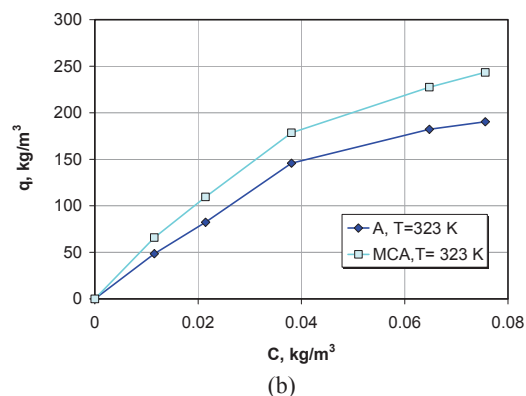
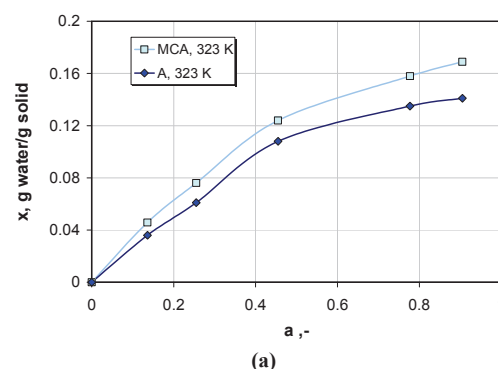


Fig. 4. Sorption isotherm for A and MCA materials at 323 K

The diffusion data obtained at water vapor adsorption on MCA granules at a temperature of 303 K are presented in Table 3. It includes, also, the local slopes determined from Fig. 6b. In Fig. 7 the temperature influence on the effective diffusion coefficients for the MCA material is presented.

Table 2. Sorption Equilibrium (slope K) at 323 K

| Water vapor pressure, mbar | A Local slope, K | MCA Local slope, K | Water activity, - |
|----------------------------|------------------|--------------------|-------------------|
| 16.97 | 4216.7 | 5722.2 | 0.138 |
| 31.57 | 3403.6 | 4400.1 | 0.257 |
| 56.07 | 3813.1 | 4145.2 | 0.456 |
| 95.37 | 1365.6 | 1834.3 | 0.777 |
| 111.32 | 747.7 | 1462.2 | 0.905 |

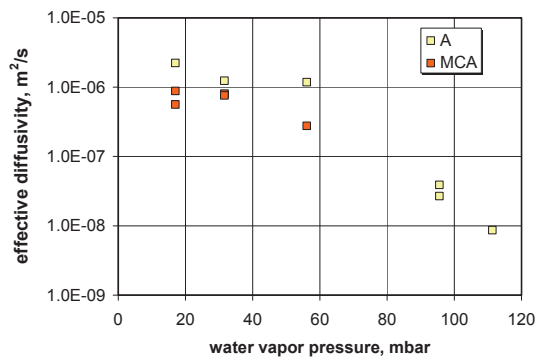


Fig. 5. Effective diffusion coefficients of water vapors in A and MCA at 323 K

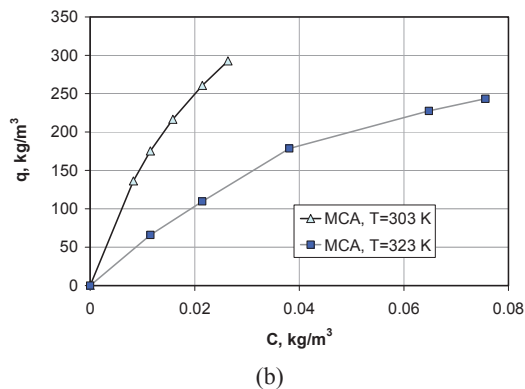
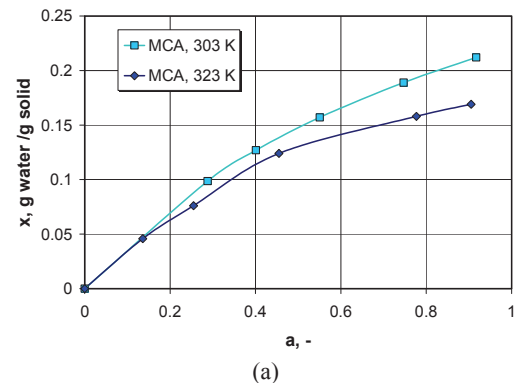


Fig. 6. Sorption isotherms for the MCA material at 303 K and 323 K

Table 3. Diffusion data for MCA at a sorption temperature of 303 K

| Water vapor pressure, mbar | Apparent diffusivity, m²/s | Local slope, K | Effective diffusivity, m²/s |
|----------------------------|----------------------------|----------------|-----------------------------|
| 16.97 | 8.177E-11 | 16450 | 2.2421E-06 |
| 23.29 | 7.272E-11 | 12028 | 1.99397E-06 |
| 31.6 | 8.345E-11 | 9637 | 2.28786E-06 |
| 31.6 | 4.694E-11 | 9637 | 1.28692E-06 |

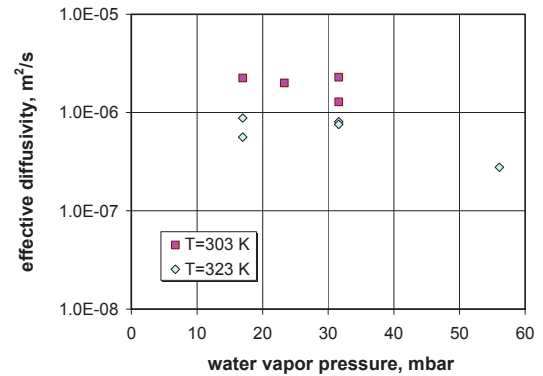


Fig. 7. Effective diffusion coefficients of water vapors in MCA at two temperatures

Analyzing data shown in Fig. 7, it can be seen that the water vapor effective diffusion coefficient values in the MCA material at 303 K are higher than values at 323 K. This could be explained based on an increase in vapor viscosity with temperature.

4. Conclusions

Effective diffusion coefficients of water vapors in cylindrical granules of activated alumina (A) and activated alumina impregnated with calcium chloride (MCA) were determined.

Experiments were performed at 303 K and 323 K granules having the same diameter and length (2.5 mm). The experiments were conducted at constant vapor pressure by means of a technique based on a magnetic suspension balance (Rubotherm, Germany). The apparent diffusion coefficient was determined from half time of diffusion. The effective diffusion coefficients depend on the apparent diffusion coefficients, the local slopes of the sorption isotherms and the material porosities.

For the impregnated alumina, the effective diffusion coefficients are almost 60 % lower than for non – impregnated activated alumina. The temperature has a certain influence on the vapor diffusion coefficients.

References

- Aristov Y.I., Glaznev I.S., Freni A., Restuccia G., (2006), Kinetics of water sorption on SWS-1L (calcium chloride confined to mesoporous silica gel): Influence of grain size and temperature, *Chemical Engineering Science*, **61**, 1453-1458.
- Carslaw H.S., Jaeger J.C., (2005), *Conduction of Heat in Solids*, Oxford Univ. Press, Oxford.

- Crank J., (1979), *The Mathematics of Diffusion*, Clarendon, Oxford.
- Figueiredo S.A., Matos Freitas O., (2013), Adsorption kinetics of removal of yellow lanasol dyestuff using gallinaceous feathers, *Environmental Engineering and Management Journal*, **12**, 2061-2070.
- Igwe C.J., Arukwe U., Anioke N.S., (2013), Isotherm and kinetic studies of residual oil adsorption from palm oil mill effluent (pome) using boiler fly ash, *Environmental Engineering and Management Journal*, **12**, 417-427.
- Luís P., Cheng C.Y., Boaventura R.A.R., (2014), Adsorption of a basic dye onto esmegel clay, *Environmental Engineering and Management Journal*, **13**, 395-405.
- Mamaliga I., (2004), Diffusion coefficients in ternary systems solvent-solvent-polymer (in Romanian), *Journal of Plastics (Revista de Materiale Plastice)*, **41**, 180-184.
- Mamaliga I., Schabel W., Kind M., (2004), Measurements of sorption isotherms and diffusion coefficients by means of a magnetic suspension balance, *Chemical Engineering and Processing*, **43**, 753-763.
- Mamaliga I., Baciú C., Petrescu S., (2009), Adsorption equilibrium study of some wet air-composite material systems, *Environmental Engineering and Management Journal*, **2**, 253-257.
- Mamaliga I., Schabel W., Petrescu S., (2010), Characterization of water vapour diffusion into spherical silica gel particles, *Journal of Chemistry (Revista de Chimie)*, **61**, 1231-1234.
- Negrea A., Lupa L., Ciopec M., Negrea P., (2014), Silica impregnated with cyphos IL-101 for Cs⁺ adsorption, *Environmental Engineering and Management Journal*, **13**, 2005-2013.
- Rong Z., Vadgama P., (2006), Simple expressions for diffusion coefficient determination of adsorption within spherical and cylindrical absorbents using direct simulation method, *Journal of Colloid and Interface Science*, **303**, 75-79.
- Simonova I.A., Freni A., Restuccia G., Aristov Y.I., (2009), Water sorption on composite "silica modified by calcium nitrate", *Microporous and Mesoporous Materials*, **122**, 223-228.
- Solomon I., Ribeiro A.M., Santos J.C., Loureiro J.M., Rodrigues A., Sandu I., Mamaliga I., (2013), Adsorption equilibrium of water vapor onto activated carbon, activated alumina, carbon and alumina impregnated with hygroscopic salt, *Turkish Journal of Chemistry*, **37**, 358-365.
- Terzyk A.P., Gauden P.A., (2002), The simple procedure of the calculation of diffusion coefficient for adsorption on spherical and cylindrical adsorbent particles-experimental verification, *Journal of Colloid and Interface Science*, **249**, 256-261.
- Terzyk A.P., Rychlicki G., Biniak S., Lukaszewicz J.P., (2003), New correlations between the composition of the surface layer of carbon and its physicochemical properties exposed while paracetamol is adsorbed at different temperatures and pH, *Journal of Colloid and Interface Science*, **257**, 13-30.
- Witek-Krowiak A., (2013), Kinetics and equilibrium of copper and chromium ions removal from aqueous solutions using sawdust, *Environmental Engineering and Management Journal*, **12**, 2125-2135.



“Gheorghe Asachi” Technical University of Iasi, Romania



DESIGN AND PERFORMANCE EVALUATION OF A PLANT FOR GLYCEROL CONVERSION TO ACROLEIN

Ionut Banu*, Georgiana Guta, Costin Sorin Bildea, Grigore Bozga

*University Politehnica of Bucharest, Department of Chemical and Biochemical Engineering,
313 Spl. Independentei, 060042 Bucharest, Romania*

Abstract

The development of biodiesel industry in the recent past brought into discussion the valorization of glycerol as the byproduct of this technology. Dehydration of glycerol leads to acrolein, mainly used as a raw material in the production of acrylic acid and its esters. Several research efforts dealing with the synthesis of acrolein from glycerol are reported in the literature. However, they are limited to catalyst testing on laboratory scale, no attention being paid to the process feasibility at an industrial scale. The goal of this paper is to fill this gap by presenting an integrated design study of the glycerol dehydration process. A simplified kinetic model was developed based on published data, this one being able to predict with sufficient accuracy the rate of the main reaction and the formation of relevant by-products (carbonyl compounds, hydrocarbons, carbon monoxide and coke). A reaction system was designed, similar to the reactor-regenerator unit usually used in hydrocarbon catalytic cracking (FCC). Moreover, the operating conditions were determined in such a way to maximize the selectivity and ensure the autothermal operation. The reactor effluent is sent to a separation section consisting mainly in distillation units. Due to formation of a low-boiling azeotrope, extractive distillation is employed for separating the acrolein-water mixture, using a part of the fresh glycerol feed as solvent. For a set of typical operating conditions, the separation section was designed in Aspen Plus environment. An economic evaluation study was performed using Aspen Economic Evaluation module, following which an acrolein price of 1.13 EUR/kg was determined. By comparing this value with the market one of 3.3 EUR/kg, the feasibility of the proposed process from the economical point of view will be emphasized.

Key words: economic evaluation, glycerol valorization, kinetic model, plant design, reactor-regenerator system

Received: November, 2014; Revised final: March, 2015; Accepted: March, 2015

1. Introduction

The continuous increase in energy demand corroborated with the accentuate depletion of the fossil fuels resources, made the scientific world to give more attention to conversion of renewable and bio-degradable resources to bio-fuels and value-added chemicals.

The biodiesel industry knew a considerable development in the last decade, 1.6% of transport fuel used worldwide being represented by liquid biofuels (Nogueira, 2011). Considered as the most important biofuel, the biodiesel is produced from natural triglycerides (vegetable oils or animal fats)

and methanol through a catalytic transesterification process using either methanol or ethanol as a reagent (Corma et al., 2008; Olivieri et al., 2013). The byproduct of biodiesel industry is glycerol, produced with a ratio of 1 kg of glycerol to 10 kg of biodiesel (McNeil et al., 2012). The glycerol resulting from biodiesel industry, usually known as “raw glycerol” is an aqueous solution containing 80-85 wt.% glycerol. This raw glycerol can be subjected further to advanced separation processes to produce pure glycerol, but the purification processes can be rather difficult to implement, expensive and inefficient from the energetic point of view. Among the purification processes worth to be mentioned vacuum distillation

* Author to whom all correspondence should be addressed: e-mail: i_banu@chim.upb.ro; Phone: (+)4 021 402 3938

at pressures of 10^{-5} bar and 120°C , refining on ion exchange resins, membrane separation etc. (Bozga et al., 2011). As reported by Talebian-Kiakalaieh et al. (2014), over 1.54 million ton of glycerol is anticipated to be produced in 2015. Due to the high amount of glycerol released on the market, new utilizations of this chemical compound as “raw glycerol” have to be explored. The valorization of glycerol will produce also a decrease in biodiesel price from 0.63 to 0.35 USD/L as reported by Talebian-Kiakalaieh et al. (2014). Nowadays, glycerol has over two thousand different applications as pure compound in food and cosmetic industry, pharmaceuticals and personal care products industry, solvent or as a major ingredient in toothpastes as reported by Tan et al. (2013).

Several processes has been proposed for glycerol valorization, among them being worth to mention its conversion into acetals, steam reforming to obtain synthesis gas, conversion to acrolein and propane diols (Zaharia et al., 2013). Acrolein, an important chemical compound, is used as an intermediary in acrylic acid and its derivatives synthesis, methionine synthesis, as a monomer for acrylic resins or as a reagent in herbicides industry (Bozga et al., 2011). Glycerol can be converted to acrolein by dehydration in gas or liquid phase, using homogeneous or heterogeneous catalysts (Gu et al., 2012). The commercial technology for acrolein synthesis is based on gas-phase selective propylene oxidation in the presence of BiMoO_x catalyst, in a multi-step process involving utilization of chlorine (a corrosive reagent). The negative environmental impact as well as the economic drawback due to the continuous increase in propylene price, makes the acrolein synthesis from glycerol a commercially and environmentally attractive route (Bozga et al., 2011; Talebian-Kiakalaieh et al., 2014).

Several types of catalysts have been proposed in the literature for the conversion of glycerol to acrolein. Heteropolyacids catalyst supported on silica has been used by Chai et al. (2009). Total glycerol conversion along with selectivity in acrolein of about 87% was reported in the study of Chai et al, but with an increase catalyst deactivation due to coke deposition. Yadav et al. (2013) reported the activity of a dodecatungstophosphoric acid catalyst supported on mesoporous silica. Glycerol conversions of 94% with an acrolein selectivity of 80% were obtained, but severe catalyst deactivation due to coke deposition have been reported. The most promising type of catalysts for glycerol dehydration to acrolein is zeolites, materials possessing large surface area and sufficient acid sites. Gu et al. (2012) tested H-Beta, HY and HZSM-5 zeolites and among them, the latter shown a good catalytic activity in acrolein synthesis, due to the porous structure that ensure a significant specific surface area

In order to develop a kinetic model for the acrolein synthesis process from glycerol, detailed information about the distribution of by-products in typical operating conditions is required. From our

knowledge, there are only few studies in the literature reporting information about the by-products produced in glycerol dehydration to acrolein process. Sabater-Prieto (2007) used a WO_3/ZrO_2 catalyst, to perform the process in a fixed-bed reactor. Acetaldehyde, phenol, acrolein, propanal, acetone, hydroxyacetone have been identified in the reaction mixture, for reaction temperatures in the range $230 - 280^{\circ}\text{C}$ and atmospheric pressure, using aqueous glycerol solution of 20 wt %. Even if the catalyst deactivation plays an important role in the mentioned process, no relevant information can be extracted from the study of Sabater-Prieto (2007).

A comprehensive study regarding glycerol dehydration on a HZSM-5 catalyst was reported by Corma et al. (2008). A circulating bed reactor that allows catalyst regeneration in a continuous way was used and glycerol conversions over 86 % with selectivities in acrolein up to 62 %. A reaction scheme accounting for dehydration, cracking, and hydrogen transfer reactions catalyzed by the acid sites of the zeolite was reported. Acrolein was the major product, short olefins, aromatics, acetaldehyde, hydroxyacetone, acids, and acetone were identified and accounted through a complex reaction network. In order to develop a kinetic model, extensive information about reaction products distribution is required.

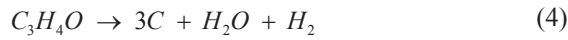
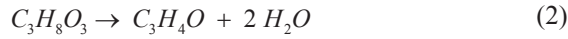
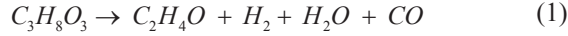
From our knowledge, no kinetic model that takes into account the distribution of by-products is reported in the literature. In order to efficiently design a chemical reactor, a representative kinetic model is required, and consequently, a first goal of our study is to develop a kinetic model for the glycerol dehydration to acrolein process. In spite of several research efforts, the acrolein synthesis process by glycerol dehydration is still limited to laboratory scale. The main goal of the present paper is to report and evaluate the conceptual design of a glycerol dehydration plant.

2. Development of a kinetic model

The experimental data, used in the present study to develop a kinetic model for the glycerol dehydration process to acrolein, has been published by Corma et al. (2008). The authors are reporting that the experimental work was performed on two types of reactors, a fixed-bed one and a circulating-bed reactor using a ZSM-5 type catalyst. The operating conditions are presented in Table 1. Several compounds have been identified as reaction byproducts in the mentioned study, among the most important being carbon monoxide, carbon dioxide, alkanes, olefins (ethylene, propylene, butene), acetaldehyde, acetone, 2-propenol, acetol, acids, BTX fractions and coke.

Due to the limited amount of experimental data, in the developed kinetic model the considered reaction products were restricted to acrolein (the main product), carbon monoxide, hydrocarbons (lumped as ethylene), carbonyl compounds (lumped

as acetaldehyde), and coke. The selectivities of glycerol transformation to products and by-products, as well as the glycerol conversion are given in Table 1. Based on the selected reaction products, the global reactions describing the stoichiometry of the glycerol dehydration process are represented by Eqs. (1-4):



The rates of these global reactions were written in terms of partial pressures following the classical power law approach. Each of the four kinetic constants was expressed in terms of two parameters by the Arrhenius relationship (Eq. 5).

$$k_i = A_i \exp\left(-\frac{E_i}{RT}\right) \quad (5)$$

The reactor model used in the estimation was written in the following hypotheses:

- one-dimensional plug flow model
- isothermal regime
- constant physical properties

The mass balance equation written in terms of degree of advancement of reactions is (Eq. 6).

$$\frac{d\xi_{mi}}{dx} = \frac{1}{WHSV} \cdot v_{Ri}^{(m)}; x=0, \xi_{mi}=0, i=1,4 \quad (6)$$

A nonlinear parameter estimation procedure based on the classical least-square method has been developed, and the model error function has the form given by Eq.(7), where y_i represents the experimental (exp subscript) and calculated (c subscript) values of glycerol conversion and the selectivities of its transformation into the byproducts taken into account (Puaux et al., 2007).

$$J = \sum_{i=1}^N e_i^T W e_i; e_i = y_{\text{exp},i} - y_{c,i} \quad (7)$$

The parameter calculation was performed using the MATLAB® “lsqcurvefit” procedure coupled with the “ode15s” integration function. The calculated parameter numerical values are presented in Table 2.

The agreement between the calculated data and the experimental results are emphasized through the parity diagrams of the glycerol conversion (Fig. 1a) and selectivities of the products and byproducts (Fig. 1b). The results given in the parity diagram shows a good agreement between calculated and experimental conversion values as well as for the selectivities used in the estimation calculations. This finding is also supported by a very good correlation coefficient ($R^2=0.973$). The estimated parameter values are presented in Table 2.

Table 1. Experimental data used in kinetic model development (Corma et al., 2008)

| Exp | Temperature, [K] | COR, [kg cat / kg feed) | WHSV, [h ⁻¹] | t_0 [s] | σ_{CO} | σ_{Hc} | $\sigma_{Acrolein}$ | σ_{Coke} | $\sigma_{Carbonyl}$ | X_G |
|-----|------------------|-------------------------|--------------------------|-----------|---------------|---------------|---------------------|-----------------|---------------------|-------|
| 1 | 773 | 11 | 431 | 0.7 | 0.104 | 0.094 | 0.39 | 0.062 | 0.35 | 1 |
| 2 | 773 | 48 | 55 | 1.4 | 0.16 | 0.179 | 0.232 | 0.177 | 0.252 | 1 |
| 3 | 923 | 45 | 121 | 0.7 | 0.268 | 0.296 | 0.11 | 0.057 | 0.269 | 1 |
| 4 | 563 | 12.6 | 282 | 1 | 0.034 | 0.019 | 0.588 | 0.206 | 0.153 | 0.98 |
| 5 | 623 | 5.6 | 1243 | 0.5 | 0.019 | 0.016 | 0.589 | 0.078 | 0.298 | 0.89 |
| 6 | 623 | 10.7 | 360 | 1 | 0.034 | 0.024 | 0.588 | 0.122 | 0.232 | 1 |
| 7 | 623 | 11.5 | 335 | 0.9 | 0.034 | 0.025 | 0.621 | 0.15 | 0.17 | 1 |
| 8 | 623 | 5.4 | 1315 | 0.5 | 0.021 | 0.019 | 0.591 | 0.101 | 0.268 | 0.86 |
| 9 | 623 | 9.9 | 388 | 0.9 | 0.029 | 0.028 | 0.586 | 0.162 | 0.195 | 0.97 |

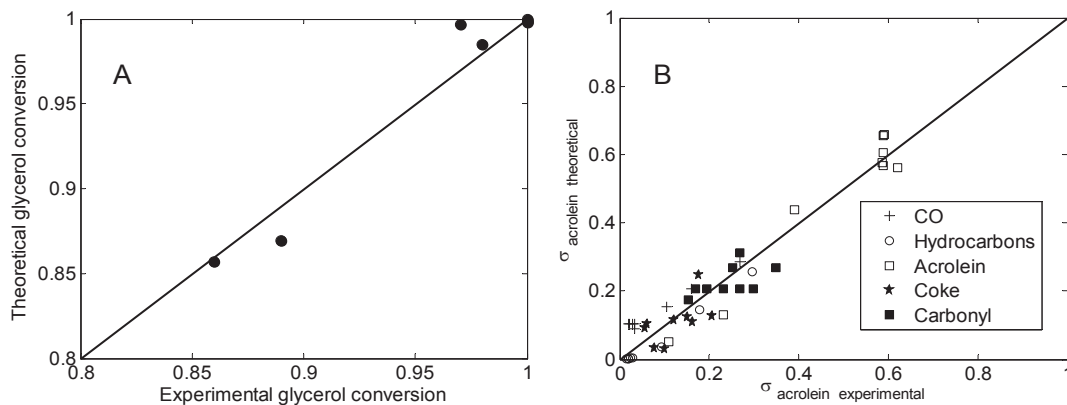


Fig. 1. Parity diagrams for conversion (A) and selectivities in byproducts (B)

Table 2. Estimated kinetic parameters

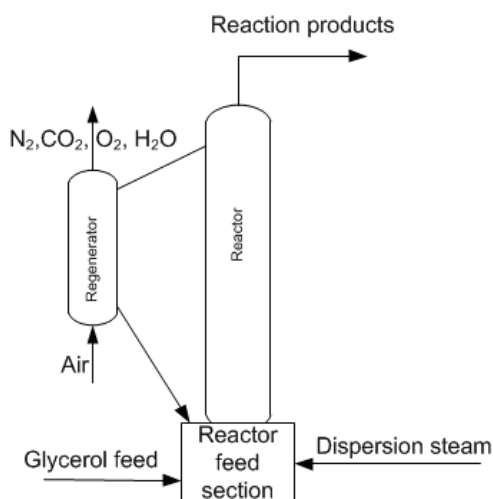
| Chemical reaction | 1 | 2 | 3 | 4 |
|--|-------------------|-------------------|-------------------|-------------------|
| A_i , kmol kgcat ⁻¹ s ⁻¹ | $3.75 \cdot 10^4$ | $1.05 \cdot 10^4$ | $6.31 \cdot 10^4$ | $1.92 \cdot 10^2$ |
| E_i , kJ kmol ⁻¹ | $3.79 \cdot 10^4$ | $2.7 \cdot 10^4$ | $6.62 \cdot 10^4$ | $1.05 \cdot 10^4$ |

3. Design of the acrolein synthesis plant

The conceptual design of the glycerol dehydration plant was performed following the hierarchical procedures detailed in references (Dimian and Bildea, 2008; Dimian et al., 2014). In order to provide relevant details, the study will be divided in two parts, one regarding the analysis of the process in a reactor-regenerator system and the second dedicated to the design of the separation section to produce products with high purity. In this work, it was designed a glycerol dehydration plant with a production capacity of 100 000 t/y.

3.1. Analysis and design of the reactor-regenerator system

Due to the significant catalyst deactivation, Corma et al. (2008) proposed that the glycerol dehydration process to be carried out in a circulating bed reactor with continuous catalyst regeneration, a system similar with the one used in the fluid catalytic cracking of hydrocarbons. The schematic diagram of the reactor is given in Fig. 2. The aqueous solution of glycerol (80 wt %) is fed at the reactor inlet along with the regenerated catalyst and a dispersion steam flowrate that will enhance the catalyst transport over the reactor length and the vaporization of glycerol feed. The circulating bed reactor model was written in the following hypotheses: one-dimensional plug-flow of the gas phase and adiabatic regime, constant physical properties, gaseous phase and catalyst has the same temperature.

**Fig. 2.** Diagram of the reactor-regenerator system

The vaporization of the reaction mixture at the reactor inlet was considered instantaneous. The reactor model consisting in mass balance equations, thermal balance and pressure drop equations is expressed by differential Eqs. (8-10).

$$\frac{d\xi_{m,i}}{dx} = \frac{1}{WHSV} v_{R,i}^{(m)}; x=0, \xi_{m,i}=0, i=1,4 \quad (8)$$

$$\frac{dT}{dx} = \frac{(1-\varepsilon)\rho_{cat}A_tL\sum_i(-v_{R,i}\Delta H_{R,i})}{D_{m,sol}c_{s,g} + F_{cat}c_{s,cat}}; x=0, T=T_r \quad (9)$$

$$\frac{dp}{dx} = -\rho_{cat}g(1-\varepsilon)L; x=0, p=p_0 \quad (10)$$

The weight-hourly space velocity (WHSV) and the catalyst residence time have been expressed by Eqs. (11) and (12).

$$WHSV = \frac{D_{m,sol}}{t_{0,cat}D_{m,cat}} \quad (11)$$

$$t_{0,cat} = \frac{xL A_t (1-\varepsilon) \rho_{cat}}{D_{m,sol} COR} \quad (12)$$

The reaction rates were considered to be affected by the catalyst deactivation due to coke deposition by a function φ , depending on the temperature and catalyst residence time, with the decay coefficient expressed by an Arrhenius relation as for the FCC process (Ahari et al., 2008) (Eq. 13).

$$\varphi = \exp(-at_{0,cat}); a = a_0 \exp\left(\frac{-E_{cat}}{R_g T}\right) \quad (13)$$

In order to evaluate the possibility to operate the reactor in an autothermal regime, the thermal balance equations for reactor and regenerator were written. The necessary heat required for rising up the catalyst temperature comes from the coke combustion, according to the Eq. (14).

$$D_{m,cat}c_{s,cat}(T_{reg}-T_{i,reg}) + D_{m,air}c_{s,air}(T_{reg}-T_a) = D_{m,cat}c_{coke}X_{coke}(-\Delta H_{R,coke}) \quad (14)$$

The coke composition was taken as 92 % carbon and 8 % hydrogen (Corma et al., 2008). The amount of air necessary for the coke combustion was calculated from a stoichiometric relation, considering the combustion products to be only in CO₂ and H₂O, and taking into account a 20% (mol) excess of oxygen. The evaluation of thermal balance for the reactor took into account that the heat transported from the regenerator with the catalyst (at the regeneration temperature) is used for feed heating up, vaporization and raising further temperature to the required value for the reaction to be performed in adiabatic regime. The global heat balance equation for the regenerator is given by Eq. (14).

$$D_{m,cat}c_{s,cat}(T_{reg}-T_{e,r})=D_{m,G}c_{s,GL}(T_{vap}-T_{go})+D_{m,W}c_{s,WL}(T_{vap}-T_{go})+D_{m,G}\lambda_G+D_{m,W}\lambda_W \\ +D_{m,steam}c_{s,W}(T_r-T_s)+D_{m,G}c_{s,GV}(T_r-T_{vap})+D_{m,W}c_{s,WV}(T_r-T_{vap})+Q_{react} \quad (14)$$

The reaction enthalpies calculated by using Kirchhoff law (Reid et al., 1987) were used to evaluate the reaction thermal effect by Eq. (15).

$$Q_{react}=\frac{D_{MC}}{3}\cdot\Delta H_{R,4}+D_{M,jc}\cdot\Delta H_{R,3}+(D_{M,A}+D_{M,jc})\cdot\Delta H_{R,2}+D_{M,carbonyl}\cdot\Delta H_{R,1} \quad (15)$$

In order to determine the reactor geometrical characteristics, a specific mass flowrate similar with the one in the FCC process was considered. The reactor diameter was evaluated by expressing the reactor cross-section by Eq. (17).

$$A_t=\frac{D_{m,tot}}{\dot{D}_m} \quad (17)$$

The reactor length was determined from an iterative study having as main goal the evaluation of the regeneration temperature required for feed vaporization. The values of the geometrical characteristics of the circulating-bed reactor, as well as the physical properties and other data used in the simulation are presented in Table 3.

The value of the regeneration temperature determined by iterative calculations is 645 °C, value that ensure the efficient catalyst regeneration, being close to the ones implemented in the hydrocarbon catalytic cracking process.

The reactor simulation results in terms of glycerol conversion, temperature profile, selectivity in acrolein and coke concentration is presented in Fig. 3. Results evidence a total glycerol conversion at the reactor outlet (Fig. 3a) as well as a good selectivity in acrolein (around 44 %). Due to the reaction endothermicity, the reactor temperature is decreasing from the inlet to the outlet by 100 °C. The calculated coke concentration on the catalyst is relatively low (1.1 %), but even this small amount is sufficient to acquire the autothermal regime inside the reactor.

3.2. Design of the separation section

The design and performance evaluation of the separation section for the acrolein synthesis plant was performed in Aspen Plus environment. The proposed process flowsheet is presented in Fig. 4. To design the separation equipments, the components were ordered by their boiling points (Table 4), and the potential outlet streams were grouped into products (acrolein) and by-products (gases, carbonyl compounds).

Table 3. Reactor simulation data

| Data | Symbol | Value | Unit | References and observations |
|---|------------------|--------|-------------------------------------|--|
| Catalyst to oil ratio | COR | 5.4 | kg kg ⁻¹ | Average value from Corma et al. (2008) |
| Glycerol feed flowrate | $D_{m,sol}$ | 18 | kg s ⁻¹ | Calculated |
| Dispersion steam flowrate | $D_{m,steam}$ | 1.8 | kg s ⁻¹ | Calculated |
| Catalyst density | ρ_{cat} | 720 | kg m ⁻³ | ZSM-5 catalyst density |
| Reactor diameter | D | 0.3 | m | Calculated |
| Reactor height | L | 10 | m | Calculated |
| Void fraction | ε | 0.75 | - | Proposed value |
| Preexponential factor for deactivation constant | a_0 | 59100 | s ⁻¹ | Ahari et al. (2008) |
| Catalyst deactivation activation energy | E_{cat} | 67210 | kJ kmol ⁻¹ | Ahari et al. (2008) |
| Catalyst specific heat | $c_{s,cat}$ | 1.2 | kJ kg ⁻¹ K ⁻¹ | Nakasaka et al. (2012) |
| Air specific heat | $c_{s,aer}$ | 1 | kJ kg ⁻¹ K ⁻¹ | Reid et al. (1987) |
| Air temperature at regenerator inlet | T_a | 250 | °C | Proposed value |
| Coke conversion in regenerator | X_{coke} | 90 | % | Proposed value |
| Carbon combustion enthalpy | $\Delta H_{c,C}$ | 31500 | kJ kg ⁻¹ | Corma et al. (2008) |
| Hydrogen combustion enthalpy | $\Delta H_{c,H}$ | 115000 | kJ kg ⁻¹ | Corma et al. (2008) |
| Glycerol vaporization enthalpy | $\lambda_{V,G}$ | 635 | kJ kg ⁻¹ | Aspen Hysys V 8.4 database |
| Water vaporization enthalpy | $\lambda_{V,W}$ | 900 | kJ kg ⁻¹ | Aspen Hysys V 8.4 database |
| Glycerol specific heat | $c_{s,GL}$ | 4.1 | kJ kg ⁻¹ K ⁻¹ | Aspen Hysys V 8.4 database |
| Water specific heat | $c_{s,W}$ | 6.9 | kJ kg ⁻¹ K ⁻¹ | Aspen Hysys V 8.4 database |

Table 4. Reaction products destination and boiling points

| Compound | Boiling point, °C | Destination |
|--|-------------------|-------------|
| Hydrogen | -252.87 | by-product |
| Carbon monoxide | -191.5 | by-product |
| Hydrocarbons (C ₂ H ₄) | -103.7 | by-product |
| Carbonyl compounds (C ₂ H ₄ O) | 20.2 | by-product |
| Acrolein | 53 | product |
| Water | 100 | recycle |
| Glycerol | 290 | recycle |

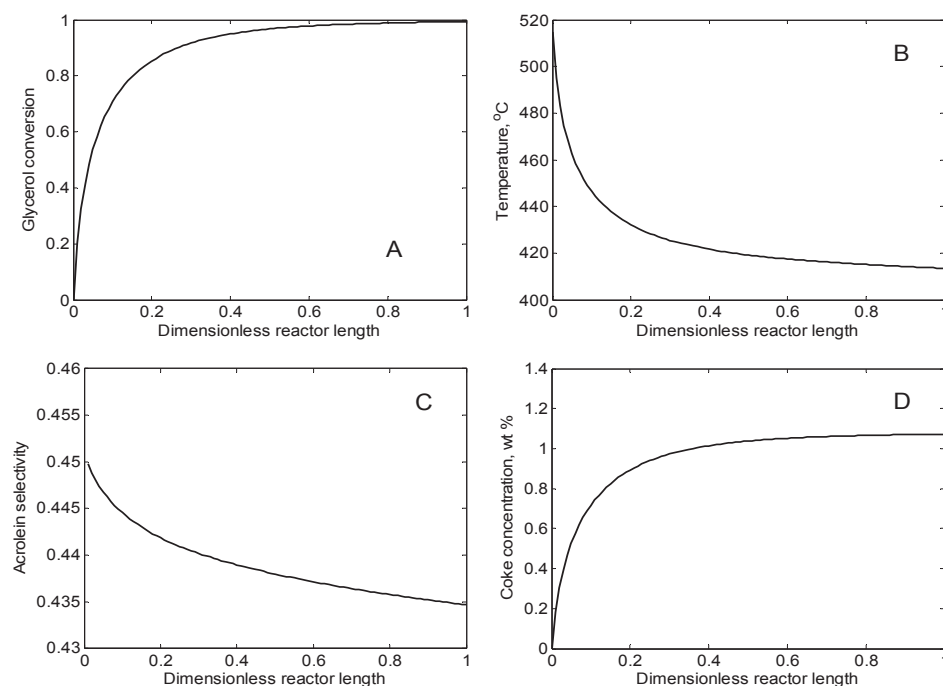


Fig. 3. Reactor simulation results

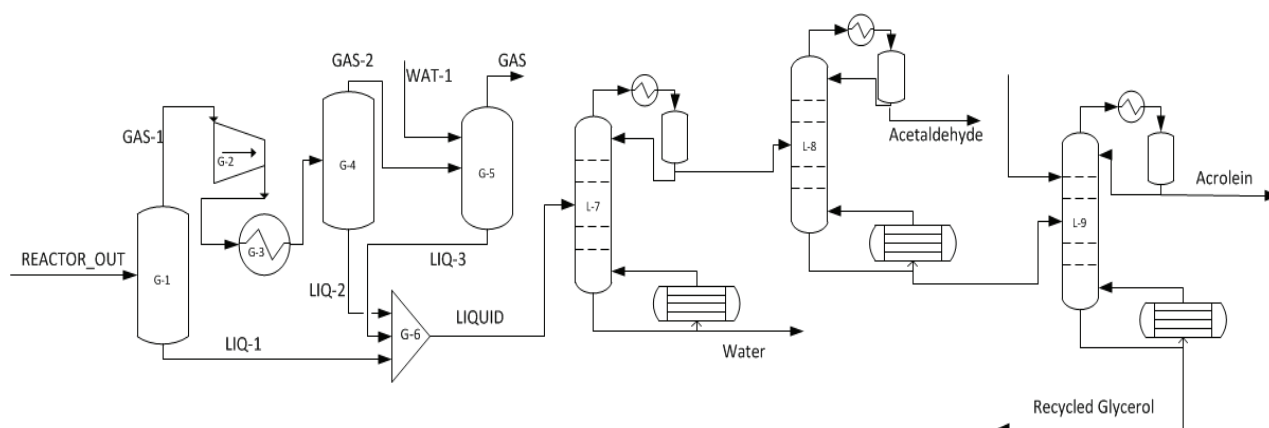


Fig. 4. Separation section flowsheet

In order to separate the gaseous components from the reactor effluent, a gas-liquid split section was proposed. Due to the low boiling point of the carbonyl compound present in the mixture, a compressor (G-3) is used to raise the operating pressure up to 10 bars, to ensure a separation of the acetaldehyde from the gaseous stream.

After a second high-pressure flash-separation, to acquire the complete removal of the gaseous components from the LIQUID stream, an adsorption column is used, with water as the adsorbent. The mass balance for the gas-separation section is presented in Table 5. The data emphasize the efficiency of the gas-separation, the LIQUID stream containing more than 95 % (acrolein, acetaldehyde) of the compounds of interest coming out from the reactor.

The separation of liquid phase was carried out in a series of distillation columns, where the components are separated by the "lights out first" rule. The column L-7 separates the heavy component

(water) from the LIQUID stream, the distillate stream consisting in mainly acrolein and acetaldehyde. The second distillation column (L-8) is removing the light component (acetaldehyde) in the distillate stream, with a purity of over 99 %.

The challenge in the proposed separation section remains the separation of the acrolein-water azeotrope that is to be broken in the distillation column L-9.

To achieve this separation, an extractive distillation is implemented, using pure glycerol as extracting phase, given the fact that the azeotrope glycerol-water is more stable than the previous one. The advantage of using this technique is the subsequent use of the glycerol-water solution resulting as the bottom stream in the distillation column L-9, as a feed for the dehydration reactor. The resulting top stream contains over 98 % acrolein as pure compound. In order to emphasize the efficiency of the liquid separation section, the mass balance for the main streams is presented in Table 6.

Table 5. Mass balance for gas-separation section

| <i>Property</i> | <i>Reactor-out</i> | <i>Gas</i> | <i>Liquid</i> | <i>Wat-1</i> |
|-----------------------------------|--------------------|------------|---------------|--------------|
| Temperature, °C | 410 | 34.4 | 23.7 | 20 |
| Pressure, bar | 1 | 10 | 10 | 10 |
| Total mass flow, kg/hr | 67768.40 | 6947.02 | 66225.9 | 5404.58 |
| Components mass flow kg/hr | | | | |
| Glycerol | 326.33 | | 326.33 | |
| Carbonyl compounds | 9461.56 | 288.54 | 9173.02 | |
| Acrolein | 13623.59 | 124.66 | 13498.9 | |
| H ₂ | 628.54 | 620.04 | 8.495 | |
| Water | 37473.22 | 50.75 | 42827.0 | 5404.58 |
| CO | 6121.84 | 5736.51 | 385.32 | |
| Hydrocarbons | 133.31 | 126.50 | 6.807 | |

Table 6. Mass balance for the liquid separation section

| <i>Property</i> | <i>Separation in</i> | | | | <i>Separation out</i> | | | |
|-----------------------------------|----------------------|--------------|----------------|--------------------------|-----------------------|-----------------|--------------|--------------|
| | <i>REACTOR_OUT</i> | <i>WAT-1</i> | <i>ADS_GLY</i> | <i>Recycled glycerol</i> | <i>Acetaldehyde</i> | <i>Acrolein</i> | <i>Gases</i> | <i>Water</i> |
| Temperature, °C | 410 | 20 | 80 | 115.5 | 23.8 | 51.9 | 33.3 | 148.5 |
| Pressure, bar | 1 | 10 | 1 | 1 | 2 | 1 | 2 | 5 |
| Mole Flow, kmol/hr | 3076.5 | 300 | 40 | 11362 | 203.7 | 241 | 551.1 | 2307.02 |
| Total Mass Flow, kg/hr | 67768.4 | 5404.8 | 3683.7 | 5009.1 | 8955.3 | 13335.3 | 7554.4 | 42002.5 |
| Component mass flow, kg/hr | | | | | | | | |
| Glycerol | 326.3 | | 3683.8 | 3683.7 | | trace | trace | 326.3 |
| Carbonyl compounds | 9461.5 | | | trace | 8911.1 | 9.84 | 485.4 | 55.1 |
| Acrolein | 13623.5 | | | trace | 19.0 | 13243.5 | 146.4 | 214.6 |
| H ₂ | 628.5 | | | | 0.02 | | 628.519 | 0.001 |
| Water | 37473.2 | 5404.5 | | 1325.2 | 12.5 | 82.074 | 51.941 | 41406.1 |
| CO | 6121.8 | | | | 11.6 | | 6109.7 | 0.39 |
| Hydrocarbons | 133.3 | | | | 1.02 | | 132.2 | 0.003 |

A similar approach with the one presented in the literature (Zaharia et al., 2013) was implemented in our study. The design of the distillation columns was performed by using the DSTWU short-cut model from Aspen Plus (based on Underwood-Fenske and Gilliland approach). To achieve this, a minimum number of trays was specified along with the minimum reflux number. Then the rigorous distillation model “RADFRAC” was used, to adjust the values of the distillate flow rate in order to satisfy the products purities.

The column diameter has been evaluated by using the tray-sizing facility of Aspen Plus environment and the column height was calculated by considering 0.6 m tray spacing, and adding a 20 % distance to accommodate the top and bottom parts. In order to achieve the best separation efficiency with minimum investment, the tray number has been adjusted by closely inspecting the temperature profiles inside the distillation columns.

4. Economic evaluation of the acrolein synthesis plant

The total annual cost of the plant was considered to include the capital cost and energy cost, expressed by Eq. (18).

$$TAC = \frac{\text{capital cost}}{\text{payback period}} + \text{energy cost} \quad (18)$$

The payback period was considered 10 years. The capital cost includes the cost of reactor-regenerator system, mixers, gas-liquid separators, distillation columns (trays and heat exchangers) and other heat exchanging equipment. The economic evaluation was performed using literature data as well as Aspen Economic Evaluation 8.4 module.

In order to perform the evaluation of catalyst cost, an analogy with the “riser” reactor from the FCC process was taken into account, considering that the catalyst amount existent at a given time inside the reactor is about 100 t. It was also considered that the annual catalyst waste due to deactivation is 300 t.

The prices of raw materials taken from the literature are presented in Table 7. The prices of main equipment are given in Table 8.

Due to the complexity of the reactor-regenerator system, the direct cost of this equipment was evaluated by analogy with data presented in the literature (Nexant-Inc., 2006). The prices of utilities, in terms of steam, cooling water and electricity are given in Table 9. Taking into account the calculated data, the total project capital cost is $9.37 \cdot 10^8$ EUR and the utilities price is $1.9 \cdot 10^8$ EUR/yr.

Table 7. Raw materials prices

| Raw Materials | Amount (t/yr) | Price/t (EUR) | Total price |
|---------------|---------------|---------------|-------------------|
| Glycerol | 450000 | 400 | $1.80 \cdot 10^8$ |
| Water | 200800 | 0.21 | 42168 |
| Catalyst | 400 | 2200 | $8.8 \cdot 10^6$ |

Table 8. Main equipment costs

| Identifier | Operation | Total Direct Cost (EUR) | Equipment Cost (EUR) |
|------------|--------------------------------|-------------------------|----------------------|
| G-1 | Flash low pressure | 183900 | 32000 |
| G-2 | Compressor | $2.85 \cdot 10^6$ | $2.64 \cdot 10^6$ |
| G-3 | Heat exchanger | 92000 | 18800 |
| G-4 | Flash high pressure | 109700 | 19900 |
| G-5 | Adsorption column | 200900 | 55400 |
| L-2 | Water separation column | 3437500 | 2765100 |
| L-3 | Acetaldehyde separation column | 6691100 | 5498200 |
| L-4 | Acrolein separation column | 10531200 | 8357400 |
| R-1/R-2 | Reactor-regenerator system | 2400000 | 1900000 |

Table 9. Utilities prices

| Utility | Rate | Units | Rate Units | Cost per Hour (EUR h ⁻¹) |
|---------------|--------|----------------|--------------------------------|--------------------------------------|
| Electricity | 2378.4 | kW | kWh | 184.3 |
| Cooling water | 9122.5 | m ³ | m ³ h ⁻¹ | 289.1 |
| Steam | 149.8 | t | t h ⁻¹ | 2684.6 |

Using the calculated data, the production cost of acrolein was evaluated at 1.13 EUR/kg. Given that the market price is about 3.3 EUR/kg (<https://www.zauba.com/import-ACROLEIN-hs-code.html>, accessed on October 2014), this value shows the ability of the proposed technological scheme to be feasible from the economic point of view as well as to produce chemicals with high purities.

5. Conclusions

The glycerol conversion to acrolein on zeolite catalysts is a process that can be performed in a reactor-regenerator system similar with the one used in the catalytic cracking of hydrocarbons.

The evaluation of thermal balance for this reaction system has shown that it can be operated in autothermal regime, lowering in this way the energy requirements.

Given that the main issue in the separation of reaction products is the breakdown of the acrolein-water azeotrope, its separation was achieved using glycerol in an extractive distillation unit.

The advantage of using glycerol is that the reaction products will not be unpurified with compounds non-existent already in the mixture. Taking into account the hypotheses used in the design of this process, the economic evaluation of the whole plant proved the feasibility of the proposed technology, the calculated production price of glycerol being much lower than the market one.

Acknowledgements

The work has been funded by the Sectoral Operational Programme Human Resources Development 2007-2013 of

the Ministry of European Funds through the Financial Agreement POSDRU/159/1.5/S/132395.

Nomenclature

| | |
|---------------------|---|
| A_t | - reactor cross section, m ² |
| C_{coke} | - coke concentration on catalyst, wt % |
| c_s | - specific heat, J kg ⁻¹ K ⁻¹ |
| \dot{D}_m | - mass flow rate, kg s ⁻¹ |
| \dot{D}_m | - specific mass flow rate, kg s ⁻¹ m ⁻² |
| D_A | - diffusion coefficient of MMA in air, m ² s ⁻¹ |
| ΔH_R | - reaction enthalpy (heat of reaction), J kg ⁻¹ |
| $\Delta H_{R,coke}$ | - coke combustion reaction enthalpy, J kg ⁻¹ |
| k | - reaction rate constant, kmol ⁻¹ ·kg ⁻¹ ·s ⁻¹ |
| p | - reactor pressure, bar |
| Q_{react} | - reaction thermal effect, kJ/kg |
| $ro2$ | - correlation coefficient; |
| R_G | - the constant of ideal gas, J·mol ⁻¹ ·K ⁻¹ |
| t_0 | - residence time, s |
| T_a | - temperature of air at the regenerator inlet, K |
| $T_{e,r}$ | - temperature of the catalyst at the reactor, outlet, K |
| T_{go} | - glycerol solution feed temperature, K |
| $T_{i,reg}$ | - temperature of the catalyst at the regenerator inlet, K |
| T_r | - reactor temperature, K |
| T_{reg} | - catalyst regeneration temperature, K |
| T_s | - dispersion steam temperature, K |
| T_{vap} | - glycerol solution vaporization temperature, K |
| v_R | - reaction rate, kmol·kg ⁻¹ ·s ⁻¹ |
| W | - weighting factors, |
| x | - dimensionless coordinate |

Greek Letters

| | |
|---------------|--|
| ε | - void fraction of the catalyst bed; |
| ξ_m | - reaction extent, kmol s ⁻¹ kg ⁻¹ |

Subscripts

| | |
|------------|---------------------|
| A | - acrolein |
| $carbonyl$ | - carbonyl compound |

| | |
|------------|--|
| <i>cat</i> | - catalyst |
| <i>C</i> | - coke |
| <i>g</i> | - gas phase mixture inside the reactor |
| <i>G</i> | - glycerol |
| <i>GL</i> | - liquid phase glycerol |
| <i>GV</i> | - vapour phase glycerol |
| <i>hc</i> | - hydrocarbons |
| <i>sol</i> | - glycerol solution |
| <i>W</i> | - water |
| <i>WL</i> | - liquid phase water |
| <i>WV</i> | - vapour phase water |

References

- Ahari J.S., Farshi A., Forsat K., (2008), A mathematical modeling of the riser reactor in industrial FCC unit, *Petroleum & Coal*, **50**, 15-24.
- Bozga E.R., Plesu V., Bozga G., Bildea C.S., Zaharia E., (2011), Conversion of Glycerol to Propanediol and Acrolein by Heterogeneous Catalysis, *Revista de Chimie*, **62**, 646-654.
- Chai S.-H., Wang H.-P., Liang Y., Xu B.-Q., (2009), Sustainable production of acrolein: Preparation and characterization of zirconia-supported 12-tungstophosphoric acid catalyst for gas-phase dehydration of glycerol, *Applied Catalysis A: General*, **353**, 213-222.
- Corma A., Huber G., Sauvanaud L., Oconnor P., (2008), Biomass to chemicals: Catalytic conversion of glycerol/water mixtures into acrolein, reaction network, *Journal of Catalysis*, **257**, 163-171.
- Dimian A.C., Bildea C.S., (2008), *Chemical Process Design*, Wiley-VCH Verlag GmbH & Co. KGaA, Weinheim.
- Dimian A.C., Bildea C.S., Kiss A., (2014), *Integrated design and simulation of chemical processes*, Second edition., Elsevier B.V., Amsterdam, Netherlands.
- Gu Y., Cui N., Yu Q., Li C., Cui Q., (2012), Study on the influence of channel structure properties in the dehydration of glycerol to acrolein over H-zeolite catalysts, *Applied Catalysis A: General*, **429-430**, 9-16.
- McNeil J., Day P., Sirovski F., (2012), Glycerine from biodiesel: The perfect diesel fuel, *Process Safety and Environmental Protection*, **90**, 180-188.
- Nakasaka Y., Tago T., Konno H., Okabe A., Masuda T., (2012), Kinetic study for burning regeneration of coked MFI-type zeolite and numerical modeling for regeneration process in a fixed-bed reactor, *Chemical Engineering Journal*, **207-208**, 368-376.
- Nexant-Inc., (2006), *Equipment Design and Cost Estimation for Small Modular Biomass Systems, Synthesis Gas Cleanup, and Oxygen Separation Equipment; Task 1: Cost Estimates of Small Modular Systems*, San Francisco, California, On line at: <http://www.osti.gov/scitech/biblio/882499>, last accessed oct 2014.
- Nogueira L.A.H., (2011), Does biodiesel make sense?, *Energy*, **36**, 3659-3666.
- Olivieri G., Guida T., Salatino P., Marzocchella A., (2013), A techno-economic analysis of biodiesel production from microalgae, *Environmental Engineering and Management Journal*, **12**, 1563-1573.
- Puau J.P., Banu I., Nagy I., Bozga G., (2007), A study of L-lactide ring-opening polymerization kinetics, *Macromolecular Symposia*, **259**, 318-326.
- Reid R.C., Prausnitz J.M., Poling B.E., (1987), *The Properties of Gases and Liquids*, 4th edition, McGraw-Hill Book Company, New York.
- Sabater-Prieto S., (2007), *Optimization of the dehydration of glycerol and a scale up in a pilot plant*, PhD Thesis, Rheinisch-Westfälischen Technischen Hochschule Aachen, Germany.
- Talebian-Kiakalaieh A., Amin N.A.S., Hezaveh H., (2014), Glycerol for renewable acrolein production by catalytic dehydration, *Renewable and Sustainable Energy Reviews*, **40**, 28-59.
- Tan H.W., Abdul-Aziz A.R., Aroua M.K., (2013), Glycerol production and its applications as a raw material: A review, *Renewable and Sustainable Energy Reviews*, **27**, 118-127.
- Yadav G.D., Sharma R.V., Katole S.O., (2013), Selective dehydration of glycerol to acrolein: development of efficient and robust solid acid catalyst MUICaT-5, *Industrial & Engineering Chemistry Research*, **52**, 10133-10144.
- Zaharia E., Bildea C.S., Bozga G., (2013), Conceptual design of glycerol hydrogenolysis plant, *Journal of Chemistry (Revista de Chimie)*, **64**, 430-434.



"Gheorghe Asachi" Technical University of Iasi, Romania



INFLUENCE OF NANOPOROUS MATERIALS ON THE CHEMICAL COMPOSITION OF MERLOT AND CABERNET SAUVIGNON WINES

**Camelia Elena Luchian¹, Valeriu V. Cotea^{1*}, Lucia Cintia Colibaba¹, Catalin Zamfir²,
Maria Codreanu¹, Marius Niculaua², Antoanela Patraș¹**

¹The University of Agricultural Sciences and Veterinary Medicine, 3 Mihail Sadoveanu Alley, 700490 Iași, Romania

²Oenological Research Center - Romanian Academy, 8, Carol I Bvd., 700505 Iasi, Romania

Abstract

The variation of the content of 12 phenolic compounds from 5 months aged Cabernet Sauvignon and Merlot wine samples treated with siliceous and aluminosiliceous porous materials was analysed through a HPLC method. The standard physical-chemical analyses (alcoholic concentration, total acidity, volatile acidity, relative density, reductive sugars, total dry extract, non-reductive extract, free SO₂, total SO₂, pH) were registered. The used nanomaterials: SBA-15, Al-MCM-41, KIT-6 were synthesized in the laboratory and were structurally characterized through the BET and SEM methods. The obtained results are in accordance to literature findings. The experimental results are proof that the maturation of wine, specifically Cabernet Sauvignon and Merlot, in the presence of porous materials modifies the physical-chemical composition as well as the phenolic content of wines.

Key words: adsorption, nanomaterial, phenolic compound, wine

Received: November, 2014; Revised final: March, 2015; Accepted: March, 2015

1. Introduction

Red wines are alcoholic beverages, their composition being influenced by many and diverse factors corresponding to the specific production area, such as grape variety, soil and climate, culture, yeast, winemaking practices, transport and storage.

Every winemaker knows the important role played by polyphenols in the visual and gustative quality of red wines and their importance during aging. Consumers are increasingly demanding highly coloured wines, with a good structure and roundness, meaning that polyphenol content should be as high as possible to ensure colour intensity and stability during aging. The exploration of compositions and structures for micro and mesoporous materials in view of specific applications in the oenological area as sorption and separation support, has led to considerable results, reported in literature (Cotea et al., 2011; Luchian et al., 2011).

Studies were continued by focusing on the time-based influence of these innovative materials with different samples structures of Cabernet Sauvignon and Merlot samples. The wines were bottled and stored for 5 months in contact with the micro- and mesoporous materials and then analyses were performed.

The synthesis of nanoporous materials is an active segment of research. The ordered mesoporous silica materials contain a homogeneous distribution of mesopores ($2 \text{ nm} < d_p < 50 \text{ nm}$) which are characterized by a very narrow pore size distribution. The pore size and pore volume of these materials make them suitable potential matrices to incorporate and then release a large variety of molecules. Highly ordered hexagonal mesoporous silica structure SBA-15 has been synthesized by using commercially available block-copolymer surfactants in strong acid media (Zhao et al., 1998). SBA-15 possesses a hexagonal array of mesopores, approximately 6.0 nm

* Author to whom all correspondence should be addressed: e-mail: vcotea@uaiasi.ro; Phone/Fax.: 0232407519

in diameter. The textural properties of the mesoporous MCM-41, which have been extensively studied, are determined by the regular array of hexagonally shaped pores. The introduction of aluminum and others transitional metals in the structure of the mesoporous material leads to an increase of acidity and of specific catalytic activity. Creation of Al-O(H)-Si bridges generates Brønsted acidity (Corma et al., 1994, Corma et al., 1995).

In literature it was reported the synthesis of other mesoporous materials with larger pores, KIT-6, with Ia3d cubic type structure and a network of interconnected channels. The siliceous material KIT-6, has numerous applications in adsorption and catalysis, thanks to unique 3-D structures (Xiaoying et al., 2002).

In this study, in the treatment of wine samples we used a natural zeolite - clinoptilolite, which was collected from Mârşid, Romania (obtained from volcanic eruptions). Clinoptilolite is a natural zeolite with a complex formula: $(\text{Na}, \text{K}, \text{Ca})_{2-3}\text{Al}_3(\text{Al}, \text{Si})_2\text{Si}_{13}\text{O}_{36} \cdot 12\text{H}_2\text{O}$, comprising a microporous arrangement of silica and alumina tetrahedra. Natural zeolites are aluminium silicate minerals with high cation exchange capacities (CECs) and high selective adsorption properties (Copcica et al., 2010; Apreutesei et al., 2008).

The aim of this research is to investigate the impact of SBA-15, AIMCM-41, KIT-6 and clinoptilolite materials on the chemical composition and phenolic compound content of Merlot and Cabernet sauvignon red wines, harvested in 2013. The used methods for wine analysis are in accordance with OIV specifications (OIV, 2013).

2. Materials and method

2.1. Chemicals

Amphiphilic nonionic triblock copolymer Pluronic P123 ($\text{EO}_{20}\text{PO}_{70}\text{EO}_{20}$, molecular weight 5800, Aldrich) as structure directing agent (SDA), tetraethylortosilicate (TEOS 98%, Merck) as silica source, hydrochloric acid (37%, Merck) were used in the synthesis of mesoporous material SBA-15.

No modifications were brought to the following reagents used for the Al-MCM-41 synthesis: cetyltrimethylammonium bromide ($\text{C}_{16}\text{H}_{33}(\text{CH}_3)_3\text{N}^+\text{Br}$, Aldrich) for structure directing reagent, tetraethylorthosilicate (TEOS, 98% Merck) as silica source, aluminum isopropoxide ($\text{Al}[\text{O}-\text{CH}(\text{CH}_3)_2]_3$, Merck) to generate aluminum cations, tetraethylammonium hydroxide ($(\text{C}_2\text{H}_5)_4\text{NOH}$ 10%, Merck) as mineralizing agent.

No changes were applied to the tetraethylortosilicate (TEOS 98%, Merck) as silica source, amphiphilic nonionic triblock copolymer Pluronic P123 ($\text{EO}_{20}\text{PO}_{70}\text{EO}_{20}$, molecular weight 5800, Aldrich) as structure directing reagent, hydrochloric acid (37%, Merck), n-butanol (99.4%, Aldrich) used in the synthesis of KIT-6. Other chemicals necessary for the normal physical-

chemical and HPLC analyses were purchased from Merck. All chemicals were used as received without further purification.

2.2. Grape and wine samples

Grapes of the Cabernet Sauvignon and Merlot varieties were harvested from Târgu Bujor vineyard in September 2013. *Saccharomyces cerevisiae* (Fermol Grand Rouge®, Spindal, 30g/100L) was used for wine fermentation. After stabilization, the wine was mixed with prepared porous materials (about 4 g/L) and stored in glass bottles for 5 months. The samples were then filtered and analysed.

2.3. Synthesis of mesoporous silica SBA-15

The mesoporous silica SBA-15 was synthesized using Pluronic P123 by method found in specific literature (Zhao et al., 1998) with changes. The molar ratio of the components was as follows: $1\text{SiO}_2 : 0.017 \text{ P123} : 5.87 \text{ HCl} : 194 \text{ H}_2\text{O}$. The process to obtain solid powder SBA-15 involves dissolving of P123 (4 g) in acidic solution (HCl, 2M) (150 mL) under stirring, adding drop-wise TEOS – as silica source (9.6 mL). The mixed solution was aged at 45 °C for 8 hours and finally the sol-gel suspension was heated up to 80 °C for 5 hours in a conventional oven. The white solid was filtered off, washed several times with deionized water, dried at room temperature and finally calcined at 550 °C for 6 hours (heating rate of 1°C/min) in air in a programmable furnace.

2.4. Synthesis of mesoporous silica KIT-6

The synthesis of mesoporous KIT-6 silica was performed according to procedures found in literature (Xiaoying et al., 2002). Typically, 5 g of Pluronic P123 was dissolved in 180 g of distilled water and 9.9 g of HCl solution (35 %) under vigorous stirring at 35 °C. After complete dissolution, 5 g of n-butanol (99.4 %) were added. Following further stirring for 1 h, 10.75 g of TEOS was immediately added. The molar ratio of the gel was:

$0.017 \text{ P123} : 1.3 \text{ TEOS} : 1.31 \text{ BuOH} : 1.83 \text{ HCl} : 195 \text{ H}_2\text{O}$

The mixture was left stirring at 35 °C for 24 h and transferred into autoclave, which, in turn, was sealed and maintained at 100 °C for 24 h. The resulting solid product was filtered and dried at 100°C overnight. After a brief ethanol/HCl washing, the final sample was dried at 70 °C and calcined at 550 °C for 6 h in air.

2.5. Synthesis of Al-MCM-41

For the synthesis of mesoporous material Al-MCM-41 ($\text{Si}/\text{Al} = 16$), 22.3 mL (1 mol) of TEOS was mixed with 0.68 g (0.033 mol) of aluminium

isopropoxide. The obtained solution was stirred for 30 min at 250 rpm and tetraethylammonium hydroxide solution (10% water) was added with continues stirring for another 30 min at a speed of 250 rpm until the formation of the gel (pH = 11). 7.2 g (0.2 mol) of CTAB was added dropwise (30 mL / h). The gel became suspension. After further stirring for 1 h, the resulting gels of composition: $1\text{SiO}_2 : 0.033\text{Al}_2\text{O}_3 : 0.2\text{C}_{16}\text{TMABr} : 100\text{H}_2\text{O}$ was transferred into a teflon steel autoclave and heated to 150 °C for 48 h. After cooling, the sample was recovered by filtration. The obtained solid was washed with distilled water plus ethanol, and then dried in air at 70 °C for 1 h and finally calcined in flowing air at 540 °C for 6 h (Stein and Holland, 1996).

2.6. Clinoptilolite preparation

Clinoptilolite was collected from Mârşid Romania subsoil assets (obtained from volcanic eruptions). It was crushed and sieved to obtain the fractions of 0.1 and 1.0 mm.

Natural zeolite was subjected to an acidic treatment, with the aim of improving its ionic exchange property and also for usage in the wine industry. Oxalic acid was used for this treatment - $\text{H}_2\text{C}_2\text{O}_4$ (1 M concentration), liquid solid ratio of 5:1. After treatment, the samples were filtered, washed with distilled water for a few times and dried at 105 °C for 6 hours. After drying, the samples were calcinated at a temperature of 550 °C (Copia et al., 2010).

2.7. Characterization

N₂ sorption

The textural properties of SBA-15, AIMCM-41 and KIT-6 were determined with a NOVA 2200 Quanta Chrome Inc.) sorption apparatus. The sample was degassed at 300 °C for 3 hours before the measurement was taken. Pore size distribution was determined based on the Barret-Joyner-Halenda (BJH) adsorption curve.

Scanning Electron Microscopy (SEM) was carried out on a SEM VEGA II LSH TESCAN with EDX detector tip QX2 (Bruker/ Roentex).

X-ray diffraction

The clinoptilolite samples were characterized by analyzing the X rays diffraction (DRX) using a Philips PW 3710 diffractometre with $\text{CuK}\alpha$ diffraction. The X rays tube voltage was 40V and the current intensity was 30 mA, the 2θ angle was between 5° and 70° with a step size of 0.02°.

Standard chemical analysis of wine according to OIV methods

Each wine was decarbonated and then analysed for: volatile acidity OIV-MA-AS313-02, total acidity OIV-MA-AS313-01, alcoholic strength by frequency oscillator OIV-MA-AS312-01A,

reducing substances OIV-MA-AS311-01A, pH OIV-MA-AS313-15, total dry matter and non-reducing substances OIV-MAAS2-03B were done according to present standards (OIV, 2013) and specific literature (Ribéreau-Gayon et al., 2006).

Wine phenolic compounds analysis.

Phenolic compounds were identified and quantitatively determined with high-performance liquid chromatograph (HPLC) Shimadzu. This unit is equipped with two chromatographic columns Merck Chromolith Performance RP-18 (Castellari et al., 2002; Bodîrlău et al., 2009).

3. Results and discussion

3.1. Physical adsorption, BET

Fig. 1 exhibits the N_2 adsorption – desorption isotherm at -196 °C for calcined silica-SBA-15. Typical silica-SBA-15 isotherm is of Type IV with a hysteresis loop Type H1, a characteristic of mesoporous solids, according to the IUPAC classification (Kruk et al., 2000; Kruk and Jaroniec, 2001). The specific surface area of calcined silica-SBA-15 was calculated using the multiple point BET method and BET equation - $S_{\text{BET}} = 775 \text{ m}^2/\text{g}$. The pore size distribution curve (inside Fig. 1) was computed based on the BJH model and the pore size estimated from the peak position in BJH curve - $D_{\text{BJH}} = 6.62 \text{ nm}$. The total pore volume ($0.942 \text{ cm}^3/\text{g}$) was obtained from the volume of N_2 adsorbed at a relative pressure $p/p_0 = 0.955$.

Fig. 2 represents the adsorption - desorption isotherm of N_2 at a temperature of -196 °C, for the calcined KIT-6 material, synthesized by classical method. The typical isotherm for this material is a type IV, characteristic for mesoporous solids, in accordance with IUPAC classifications. The textural characteristics of the synthesized material are: specific BET surface calculated through BET method is $644,5 \text{ m}^2/\text{g}$, pore diameter calculated through BJH method is $8,34 \text{ nm}$, total pore volume at $p/p_0 = 0.97$ is of $0.761 \text{ cm}^3/\text{g}$.

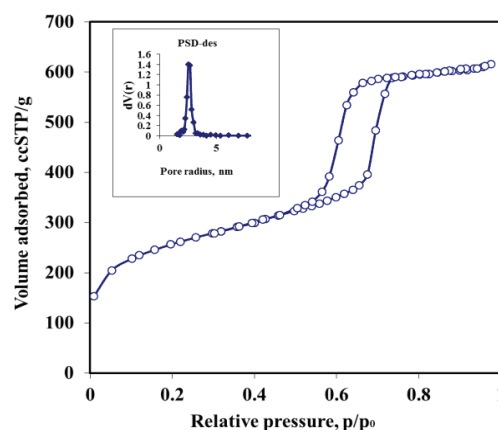


Fig. 1. The N_2 adsorption – desorption isotherm at -196 °C of calcined silica-SBA-15. Inset: the pore size distribution (PSD)

Fig. 3 indicates the allure of the absorption - desorption isotherm of N₂ for the calcined AIMCM-41 material.

The AIMCM-41 has a specific BET surface of 2098 m²/g and a total pore volume of 0.691 cm³/g (at $p/p_0 = 0.94$). The distribution of pores according to rays is quite tight, the diameter of pores being 3.92 nm.

3.2. SEM analysis of mesoporous materials

Fig. 4 shows the SEM images of the calcined sample.

3.3. X-ray diffraction analysis

The analysis of XRD diffractograms of natural and modified clinoptilolite tuff indicates a small change in the peak position and peak intensity caused by the removal of additional species as well as the dealumination of zeolite (hydrolysis of Al-O-Si bonds) as presented in Fig. 5.

Moreover, during the acid or alkaline treatment, the removal of cations Na⁺, Ca²⁺, K⁺, Mg²⁺ and Fe³⁺ takes place, as well as the change in pore dimension and pore distribution, corresponding to clinoptilolite in H⁺ form, respectively in Na⁺ form.

3.4. Standard chemical analysis of wine

Ethanol, relative density, pH, total acidity, volatile acidity, sugars, total dry extract (TDE), total and free SO₂ of the wine sample were analysed by the recommended methods of International Organisation of Vine and Wine (OIV) (Table 1). Analysing the results presented in Table 1, it can be seen that the use of meso- and microporous materials used as wine treatments, influences its physical-chemical composition. Both in the case of Cabernet Sauvignon and Merlot wine samples, the alcoholic concentration changes, as follows: clinoptilolite and Kit-6 lead to its significant increase for Merlot samples, it increases from 11.83% (M) to 12% (M3) respectively 12.15% (M4); for Cabernet Sauvignon samples, it increases from 13.23% (CS) in the control sample to 13.41% (CS3) and 13.39% (CS4).

In the case of total acidity, small variations are registered in the case of samples treated with clinoptilolite and KIT-6 as well (M3, CS3 and CS4). The volatile acidity increases in Merlot samples treated with AIMCM-41 (M2) and clinoptilolite (M3); it decreases in Cabernet sample treated with AIMCM-41 (CS2). Total and free SO₂ have decreasing values in all wine samples. The other indices show no significant changes.

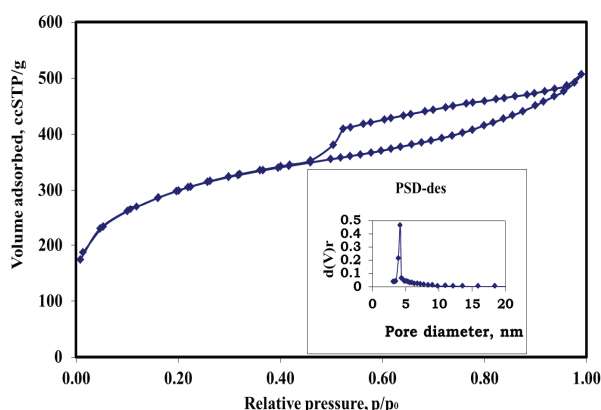


Fig. 2. The N₂ adsorption – desorption isotherm at -196 °C of calcined KIT-6. Inset: the pore size distribution (PSD)

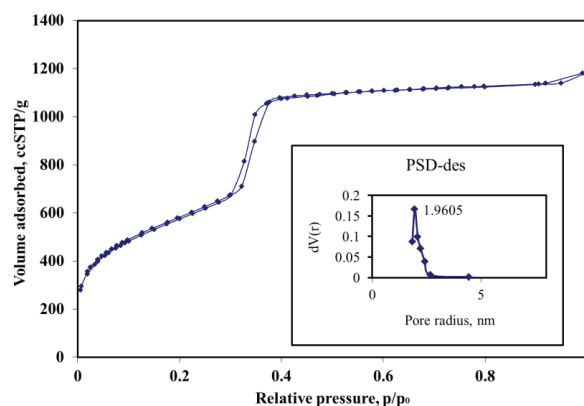


Fig. 3. The N₂ adsorption – desorption isotherm at -196 °C of calcined AIMCM-41. Inset: the pore size distribution (PSD)

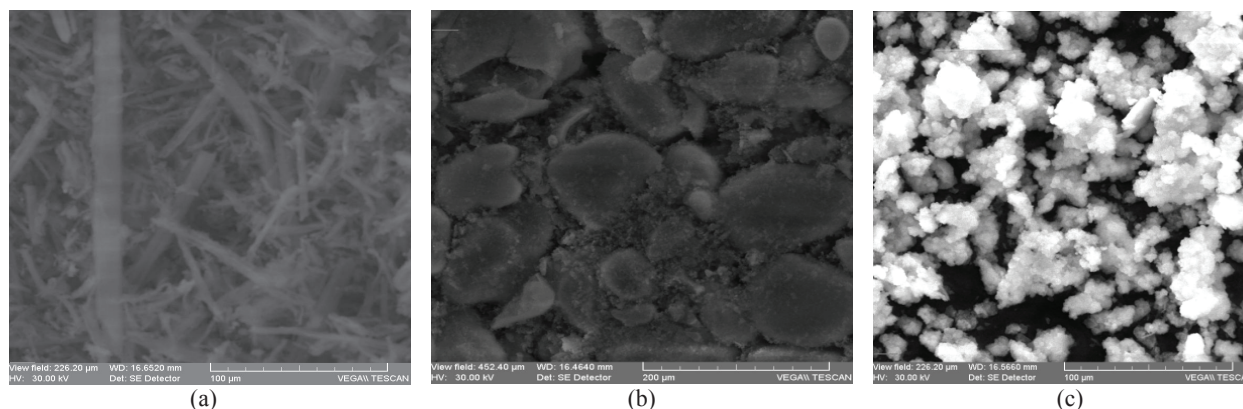


Fig. 4. SEM micrograph of calcined AIMCM-41 (a), SBA-15 (b) and KIT-6(c) samples

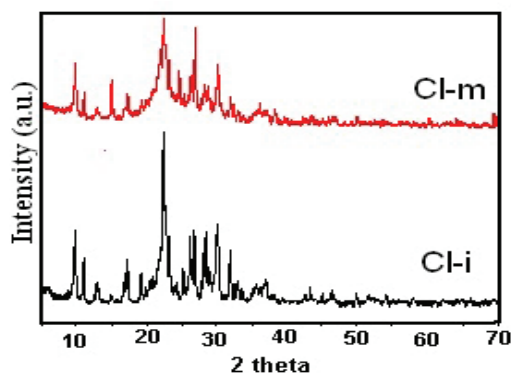


Fig. 5. XRD spectra for natural clinoptilolite tuff samples (Cl-i) and modified (Cl-m)

All analyses were repeated three times and the mean value was registered.

3.5. Wine phenolic compounds analysis

Identification of the phenolic compounds from treated wines was carried out using a HPLC method. In this case wine samples were analysed after a preliminary microfiltration. The separation optimization of these compounds was achieved after

experimenting with various gradient profiles and mobile phase flow rates. The HPLC method used to identify the adsorbed species involved an elution program. One of the eluents contains an aqueous solution of 1% methanol acidulated with TFA and the other, an aqueous solution of 50% methanol. The quantitative identification of phenolic components is based on their retention time and spectral characteristic (Table 2). The chromatographic analysis of samples registers a modified phenolic composition compared to the control wine samples. Salicylic acid present in the control sample in Cabernet sauvignon (0.42 mg/L) is under the detection limit in the wine sample treated with SBA-15.

Quercitine is under the detection limit in the control Merlot sample, while in the variants treated with clinoptilolite and KIT 6 the values are of 0.08 mg/L and 0.22 mg/L. Moreover, the rutin trihydrate concentration increases in all treated Cabernet Sauvignon samples and in the Merlot variants where SBA-15 and AlMCM-41 were used. The concentration of caffeic acid is double in the treated Cabernet Sauvignon wine samples. All analyses were repeated three times and the mean value was registered.

Table 1. Traditional analysis of Cabernet Sauvignon and Merlot treated wines

| Variants | Physical-chemical characteristics | | | | | | | | | |
|---------------------------|-----------------------------------|----------------------------------|-------------------------------------|---------------------------------------|-----------------------|-----------|----------|--------------------|---------------------|------|
| | Alcohol strength (%) | Total acidity (g/L $C_4H_6O_6$) | Volatile acidity (g/L $C_2H_4O_2$) | Relative density (g/cm ³) | Reductive sugar (g/L) | EST (g/L) | EN (g/L) | Free SO_2 (mg/L) | Total SO_2 (mg/L) | pH |
| Merlot | | | | | | | | | | |
| M | 11.83 | 5.54 | 0.40 | 0.9923 | 1.99 | 19.80 | 17.81 | 37.56 | 95.47 | 3.42 |
| M1(SBA-15) | 11.69 | 5.54 | 0.46 | 0.9925 | 2.01 | 21.90 | 19.89 | 30.66 | 85.47 | 3.44 |
| M2 (Al-MCM-41) | 11.77 | 5.54 | 0.54 | 0.9925 | 2.05 | 22.22 | 20.15 | 35.61 | 91.35 | 3.42 |
| M3 (Clinoptilolite) | 12.00 | 5.78 | 0.61 | 0.9920 | 1.65 | 20.30 | 18.65 | 28.18 | 80.21 | 3.43 |
| M4 (KIT-6) | 12.15 | 5.69 | 0.45 | 0.9921 | 1.79 | 20.90 | 19.14 | 25.7 | 82.06 | 3.41 |
| Cabernet Sauvignon | | | | | | | | | | |
| CS M | 13.23 | 5.48 | 0.46 | 0.9910 | 2.48 | 21.40 | 18.92 | 28.89 | 70.30 | 3.17 |
| CS 1(SBA-15) | 13.38 | 5.48 | 0.45 | 0.9912 | 2.42 | 21.90 | 19.48 | 23.23 | 70.61 | 3.28 |
| CS 2 (Al-MCM-41) | 13.33 | 5.43 | 0.39 | 0.9913 | 2.42 | 21.60 | 19.18 | 17.96 | 60.08 | 3.23 |
| CS 3 (Clinoptilolite) | 13.41 | 5.43 | 0.45 | 0.9914 | 2.47 | 21.90 | 19.43 | 18.89 | 68.13 | 3.27 |
| CS 4 (KIT-6) | 13.39 | 5.64 | 0.46 | 0.9912 | 2.42 | 20.90 | 18.48 | 24.46 | 70.08 | 3.26 |

EST(g/L)-Total dry extract; EN(g/L)-Non-reductive extract

Table 2. Polyphenolic constituents (mg/L) in Cabernet Sauvignon and Merlot treated samples

| | Gallic acid | Protocatechic acid | Gentisic acid | Catechin | Vanillic acid | Caffeic acid | Chlorogenic acid | Salicylic acid | Epicatechin | Sinapic acid | trans Resveratrol | Rutin trihydrate | Quercitin |
|------|-------------|--------------------|---------------|----------|---------------|--------------|------------------|----------------|-------------|--------------|-------------------|------------------|-----------|
| M | 7.36 | 1.51 | 5.48 | 6.42 | 1.15 | 1.64 | 1.11 | 0.67 | 1.56 | 0.03 | 0.17 | 1.65 | 0 |
| M 1 | 7.33 | 1.58 | 5.33 | 7.23 | 1.23 | 1.61 | 1.15 | 0.58 | 1.49 | 0.03 | 0.18 | 2.72 | 0 |
| M 2 | 7.34 | 1.69 | 5.14 | 7.42 | 1.41 | 1.59 | 1.08 | 1.05 | 0.83 | 0.06 | 0.18 | 2.85 | 0 |
| M 3 | 7.32 | 2.16 | 5.30 | 9.25 | 1.58 | 1.50 | 0.99 | 0.81 | 9.41 | 0.08 | 0.18 | 1.52 | 0.08 |
| M 4 | 7.10 | 2.11 | 5.02 | 7.57 | 1.07 | 1.20 | 0.81 | 0.13 | 1.06 | 0.06 | 0.13 | 1.18 | 0.22 |
| CS | 10.60 | 5.79 | 37.69 | 8.36 | 2.67 | 0.99 | 4.25 | 0.42 | 4.91 | 0.08 | 0 | 1.54 | 0.08 |
| CS 1 | 10.5 | 5.68 | 39.32 | 8.31 | 2.70 | 1.90 | 7.37 | 0 | 5.85 | 0.4 | 0.18 | 2.35 | 0.18 |
| CS 2 | 10.46 | 5.64 | 38.15 | 8.19 | 2.64 | 1.78 | 7.38 | 4.51 | 2.24 | 0.27 | 0.12 | 1.73 | 0.16 |
| CS 3 | 9.99 | 5.46 | 39.37 | 1.08 | 2.81 | 1.98 | 7.24 | 4.62 | 2.25 | 0.45 | 0.18 | 2.33 | 0.32 |
| CS 4 | 9.91 | 5.29 | 38.73 | 0.29 | 2.67 | 1.97 | 7.15 | 4.36 | 2.28 | 0.45 | 0.17 | 2.24 | 0.96 |

4. Conclusions

SBA-15, AIMCM-41, KIT-6 materials, all synthesized in the laboratory, were characterized from a structural and morphological point of view and are in accordance with the data in specific literature. Clinoptilolite, natural zeolite, was treated with oxalic acid, in order to bring it in H form and was then analysed by X-ray diffraction.

The physical-chemical characteristics of treated wines are changed, a higher influence being observed in the clinoptilolite and KIT-6.

The chromatographic analysis shows that the applied treatments modify selectively the phenolic compounds' content in wines matured for 5 months.

Acknowledgments

The research was funded by the grant no. 5525/ 25.04.2013 of USAMV Iasi and by the PN-II-RO-CY-2013-1 project, nr. 764/2014.

The authors would also like to thank the staff of Arheoinvest Research Platform for their support for EDX analysis.

References

- Apuretesei R.A., Catrinescu C., Teodosiu C., (2008), Surfactant-modified natural zeolites for environmental applications in water purification, *Environmental Engineering and Management Journal*, **7**, 149-161.
- Bodîrlău R., Spiridon I., Teacă C.A., Anghel N., Ichim M., Colceru S., Armatu A., (2009), Anti-inflammatory constituents from different plant species, *Environmental Engineering and Management Journal*, **8**, 785-792.
- Castellari M., Sartini E., Fabiani A., Arfelli G., Amati A., (2002), Analysis of wine phenolics by high-performance liquid chromatography using a monolithic type column, *Journal of Chromatography A*, **973**, 221-227.
- Copcia V.E., Luchian C.E., Bilba N., (2010), Ammonium ions removal from aqueous solution using mesoporous (Al)Si-MCM-41, *Environmental Engineering and Management Journal*, **9**, 1243-1250.
- Corma A., Fornés V., Navarro M.T., Perez-Pariente J., (1994), Acidity and stability of MCM-41 crystalline aluminosilicates, *Journal of Catalysis*, **148**, 569-574.
- Corma A., Martinez A., Martinez-Soria V., Monton J.B., (1995), Hydrocracking of Vacuum Gasoil on the Novel Mesoporous MCM-41 Aluminosilicate Catalyst, *Journal of Catalysis*, **153**, 25-31.
- Cotea V.V., Luchian C., Bilba N., Niculau M., (2011), Mesoporous silica SBA-15, a new adsorbent for bioactive polyphenols from red wine, *Analytica Chimica Acta*, **732**, 180-185.
- Kruk M., Jaroniec M., Ko C.H., Ryoo R., (2000), Characterization of the porous structure of SBA-15, *Chemistry of Materials*, **12**, 1961-1968.
- Kruk M., Jaroniec M., (2001), Gas adsorption characterization of ordered organic-inorganic nanocomposite materials, *Chemistry of Materials*, **13**, 3169-3183.
- Luchian C., Cotea V.V., Sandu I., Copcia V., Bilba N., (2011), Removal of Mn(II), Ni(II) and Cu(II) ions from white wine through ion exchange in microporous mordenite and mesoporous Al-MCM-41, *Revista de Chimie*, **62**, 782-786.
- Stein A., Holland B., (1996), Aluminum-containing mesostructural materials, *Journal of Porous Materials*, **3**, 83-92.
- Ribèreau-Gayon P., Glories Y., Maujean A., Dubourdieu D., (2006), *Handbook of Enology*, The Chemistry of Wine Stabilization and Treatments, 2nd Edition, John Wiley & Sons, New York.
- Xiaoying L., Bozhi T., Chengzhong Y., Feng G., Songhai X., Bo T., Renchao C., Lian-Miao P., Dongyuan Z., (2002), Room-Temperature Synthesis in Acidic Media of Large-Pore Three-Dimensional Bicontinuous Mesoporous Silica with Ia3d Symmetry, *Angewandte Chemie*, **114**, 4032-4034.
- Zhao D.Y., Feng J.L., Huo Q.S., Melosh N., Fredrikson G.H., Chmelka B.F., Stucky G.D., (1998), Triblock copolymer syntheses of mesoporous silica with periodic 50 to 300 angstrom pores, *Science*, **279**, 548-552.



"Gheorghe Asachi" Technical University of Iasi, Romania



CELLULOSE CELLETS AS NEW TYPE OF ADSORBENT FOR THE REMOVAL OF DYES FROM AQUEOUS MEDIA

Daniela Suteu^{1*}, Gabriela Biliuta², Lacramioara Rusu³, Sergiu Coseri², Gabriela Nacu¹

¹"Gheorghe Asachi" Technical University of Iasi, Faculty of Chemical Engineering and Environmental Protection,
73 Prof. Dr. docent Dimitrie Mangeron Str., 700050 Iasi, Romania

²"Petru Poni" Institute of Macromolecular Chemistry of Romanian Academy, Iasi,
41A Gr. Ghica Voda Alley, 700487 Iasi, Romania

³"Vasile Alecsandri" University of Bacau, Faculty of Engineering, 157 Calea Mărășești, 600115 Bacau, Romania

Abstract

In the current study, the structural and adsorptive properties of the micro crystalline cellulose beads, Cellets 200 and 350, as well as the possibility to use them as adsorbents for removal of reactive dye Brilliant Red HE-3B and cationic dye Methylene Blue from aqueous solutions have been investigated. Batch experiments were conducted to study the effect of adsorbent particles size (200-500 μm), initial solution pH (1-11), adsorbent dose, dye concentration, temperature (2-45 $^{\circ}\text{C}$) and contact time (30 min – 24 hours). It was observed that the optimum values of experimental parameters and the maximum amount of dye adsorbed onto cellulose were dependent on the type of dye. The results of the study suggest the adsorption capacity of the investigated materials for removal of dyes from aqueous environment strongly depends on the structure of dyes and the working conditions. At the same time, further research regarding the study of adsorption equilibrium is encouraged in order to gain useful information for extending the process at a large scale, and also for applying the process for adsorption of some inorganic species, such as metallic ions.

Key words: adsorption, aqueous medium, cationic dye, cellulose CELLETS, operating variables, reactive dye

Received: November, 2014; Revised final: March, 2015; Accepted: March, 2015

1. Introduction

Removal of textile dyes from wastewater constitutes an important topic of study for environmental protection specialists, considering the impact of these pollutants on the waters where they are discharged. Thus, the presence of dyes in surface waters leads to problems related to esthetics, inhibition of aquatic flora and fauna development, occurrence of different byproducts with carcinogenic effect formed by dyes degradation.

Different techniques have been developed and applied for treatment of textile wastewater, which is characterized by color, high values of pH, considerable amounts of suspended solids, different and unacceptable COD levels, and the presence of

non-biodegradable chemical compounds (Ding et al., 2010; Pereira and Alves, 2012; Sulak and Yatmaz, 2012; Zaharia and Suteu, 2012). Physical methods, such as mechanic separation (coagulation, flocculation, precipitation) or membrane processes, physico-chemical processes (adsorption, chemical precipitation, coagulation-flocculation, and ionic exchange), chemical process (advanced oxidation with ozone, H_2O_2 , UV), biological process (biological processes in connection with the activated sludge processes and membrane bioreactors) or combination of those can be applied in order to ensure the efficiency of dye containing wastewater treatment process (Allen and Koumanova, 2005; Anjaneyulu et al., 2005; Ding et al., 2010; Kanawade, 2014; Kasperchik et al., 2012; Kharub,

* Author to whom all correspondence should be addressed: e-mail: danasuteu67@yahoo.com

2012; Latif et al., 2011; Mohamed et al., 2014; Ozdenir et al., 2011; Ramesh et al., 2007; Saraswathy et al., 2013; Suteu et al., 2009a; Zaharia et al., 2009, 2012; Zaharia and Suteu, 2012). Adsorption remains one of the techniques that have been successfully applied for dyes removal (Kanawade, 2014; Rashed, 2013). This is the result of the fact that adsorption is an easy and feasible technology that can use a variety of materials as adsorbents. These materials can be classified as follows (Abbas, 2013; Bharathi and Ramesh, 2013; Kyzas et al., 2013; Ouasif et al., 2013; Sharma et al., 2011; Suteu et al., 2009b, 2012; Sulak and Yatmaz, 2012):

a) *synthetic and engineered materials*, including synthetic resins, polyamides, ion exchange (celluloses, functionalized polymers (with chelating group, textile dyes), activated charcoal and ash;

(b) *unconventional materials*, such as: (b1) synthetic, (ashes, different charcoals both in the presence or absence of biodegradable polymers such as polyelectrolytes); (b2) natural, cellulosic and/or lignocellulosic materials (pumpkin core, hemp fibres, cellolignin, sawdust, peat); (b3) agriculture and seafood industry wastes.

Recently, researches regarding the materials used as adsorbents for textile dyes have been focused again on synthetic and engineered materials probably due to several advantages that include (1) ease of use in dynamic systems, (2) increased adsorption efficiency, (3) possibility of being employed in several consecutive cycles of adsorption - desorption and (4) high performance in terms of degree of discoloration and treatment of aqueous effluents (Greluk and Hubicki, 2011; Suteu et al., 2014; Wawrzkiwicz and Hubicki, 2010).

Cellets represents a versatile product of cellulose type, which combines different properties such as perfect sphericity, narrow particle size distribution, low friability, low solubility and inertness. Cellulose, a natural carbohydrate polymer consisting of β -D-glucose repeating units (Klemm et al., 2005) is considered the most abundant renewable polymer resource available on Earth (Kaplan, 1998). Depending on the technological process used to produce them, celluloses may be found in many forms and types ranging from fibers, linters, microcrystalline powders, softwood pulp, bacterial cellulose and many others.

Cellets are microcrystalline cellulose beads, produced exclusively by microcrystalline cellulose and purified water, without any additive. They possess high spherical starter cores with extreme stability and low friability.

The aim of this paper is to investigate the structural and adsorptive properties of Cellets 200 and 350 and the possibility to use them as adsorbents in order to remove reactive dye *Brilliant Red HE-3B* (BRed) and cationic phenothiazine dye *Methylene Blue* (MB) from aqueous solutions under batch conditions. The dyes adsorption potential of *Cellets 200* and *350* was evaluated as a function of adsorbent particles size, initial solution pH, adsorbent dose, dye

concentration, temperature and contact time. The results confirm the moderate adsorption capacity of studied celluloses beads -*Cellets 200* and *350*- and suggest the necessity to complete the data with equilibrium, thermodynamic and kinetic studies in order to elucidate the mechanism and the rate-limiting step.

2. Experimental

2.1. Materials

2.1.1. Adsorbent types

Two sorts of Cellets, differing on their particle size, namely Cellets 200 and Cellets 350 were used in our work. Table 1 shows the main physical and chemical characteristics of Cellets.

Table 1. Physical and chemical parameters of microcrystalline cellulose spheres

| | <i>Cellets 200</i> | <i>Cellets 350</i> |
|-------------------------------------|--|--|
| <i>Particle size distribution</i> | <i>200 – 355 μm</i> ($\geq 85\%$) | <i>350 – 500 μm</i> ($\geq 85\%$) |
| Loss on drying | $\leq 7.0\%$ | |
| Bulk density (g cm^{-3}) | $0.80 \pm 5\%$ | |
| Sphericity degree (average) | 0.90 ± 0.05 | |
| Degree of polymerization | ≤ 350 | |
| pH value | $5.0 - 7.0$ | |
| Conductivity/ $\mu\text{S cm}^{-1}$ | ≤ 75 | |

2.1.2. Dye

Methylene Blue (Fig. 1a), and *Brilliant Red HE-3B* (Fig.1b) were selected as dyes for experimental studies. The selected dyes were used as commercial salts and are characterized in Table 2. The working solutions were obtained by appropriate dilution of a stock solution.

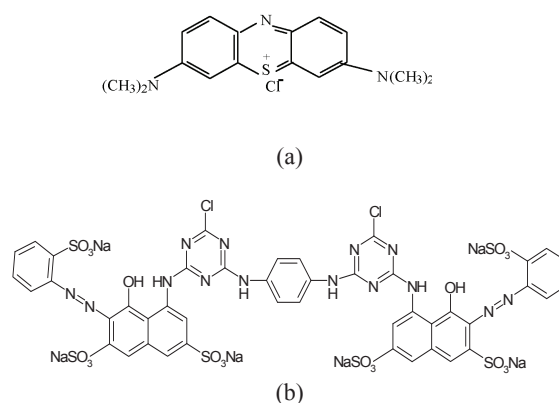


Fig. 1. (a) Structure of the Methylene Blue dye; (b) Structure of the Brilliant Red HE-3B dye

2.2. Dye adsorption procedure

The adsorption experiments were performed through batch method by contacting different amounts of adsorbent with 25 mL of solution containing various amounts of dye.

Table 2. Summary data on dyes studied

| Name | Classification | C.I. | MW, g/mol | λ_{max} nm | Concentration of solutions, mg/L | |
|--|---------------------------|-------|--------------|-----------------------|----------------------------------|----------|
| | | | | | Stock | Working |
| Brilliant Red HE-3B (Procion Red HE-3B ; Reactive Red 120; C.I. 25810) | anionic reactive | 25810 | 1463 | 530 | 500 | 25 - 400 |
| Methylene Blue (Basic Blue 9; C.I. 52015) | cationic phenothiazine | 52015 | 319.85 | 660 | 320 | 19 -102 |

Note. Abbreviations: BRed - Brilliant Red HE-3B; MB- Methylene Blue

The pH of the solution was adjusted to the required value using NaOH and HCl aqueous solutions (1N and 0.1 N, respectively). Concentrations were measured with a RADELKIS OP-271 pH/Ion analyzer. The system was maintained at constant temperature in a thermostatic bath, under stirring. After reaching the equilibrium time (24 hours), the amount of unretained dye was determined using a spectrophotometric method. The adsorption capacities of the cellulosic adsorbent were evaluated by means of the amount of dyes adsorbed according to Eq. (1) and by percent of dye removal (Eq. 2), where: C_0 and C are initial and the equilibrium concentration of dye in solution in mg/ L, G is the amount of cellulose (g) and V is the volume of solution (L).

$$q = \frac{C_0 - C}{G} \cdot V \quad (1)$$

$$R, \% = \frac{(C_0 - C) \cdot 100}{C_0} \quad (2)$$

2.3. Analytical methods for quantitative determinations and physicochemical characterization

The concentrations of unretained dyes were determined spectrophotometrically at the maximum wavelengths (Table 1) and using a JK-VS-721N VIS spectrophotometer.

2.3.1. Fourier transforms infrared spectroscopy (FTIR)

The FT-IR spectra for the Cellets, the studied dye and the dye attached to the Cellets beads were obtained using a Bruker Vertex 70 instrument with 4 cm⁻¹ resolution in KBr pills.

2.3.2. Environmental Scanning Electron Microscopy (ESEM)

The structural characterization of the microcrystalline cellulose spheres, before and after dye attaching, was performed by environmental scanning electron microscopy (ESEM). The ESEM studies were performed on Quanta 200 instrument. Samples were fixed by means of colloidal silver on copper supports.

The samples were covered with a thin layer of gold, by sputtering (EMITECH K 550x). The coated surface was examined by using an Environmental

Scanning 200, operating at 5 KV with secondary electrons in High Vacuum Mode.

3. Results and discussion

3.1. Characterization of the CELLETS celluloses beads before dyes adsorption

Before the adsorption experiments, the Cellets beads were structurally and morphologically characterized by using FTIR and SEM analyzes. The FTIR spectrum of Cellets beads consist on absorption bands characteristic for any cellulosic materials: a broad band in the 3600 – 3100 cm⁻¹ region due to the OH-stretching vibration and a sharp band at 2922 cm⁻¹ which corresponds to the C-H stretching vibration.

The band from 1645 cm⁻¹ is attributed to the OH bending of absorbed water, since the region between 1200 – 1000 cm⁻¹ summarizes the totality of the C-O-C symmetric stretching, OH plane deformation, C-O-C asymmetrical stretching, and as well as the C-C, C-OH, C-H ring and side group vibrations. The cellulosic materials exhibit both weak base and weak acid components bound to the same matrix and, depending on solution pH, they can remove cationic and/or anionic species. The morphology and surface of Cellets beads were also investigated by means of ESEM microscopy (Fig. 2).

The structure of the original cellulose beads, presented in Fig. 2, consists on small size spheroids, in the range of 200 – 350 µm for Cellets 200 and 350 – 500 µm for Cellets 350 respectively.

3.2. Effect of solution pH and type of cellulose on adsorption efficiency

The pH value determines the surface charge of the adsorbent and the ionic form of the dyes molecules, both influencing the amount of dye adsorbed by unit weight of adsorbent. The surface charge of the adsorbent is a function of the solution pH. The solution characteristic pH value is in the range 5-7 (Table 1). At pH values lower than this range, the adsorbent surface is positively charged, exhibiting affinity for anionic dye. At pH higher than 7, the surface of Cellets is negatively charged and this is available to electrostatic interactions with cationic dyes. The effect of initial solution pH on the adsorption of dyes onto microcrystalline cellulose beads (Cellets) was examined and the results are presented in Fig. 3.

The variation of dyes uptake (q , mg/g) as a function of initial pH of solution, presented in Fig. 3, shows that the anionic dye is adsorbed from acidic media with pH of about 1.3 (lower than 5), while cationic dye is adsorbed from basic solutions with pH of about 11.5 (higher than 7). This behaviour may be the consequence of the availability of dyes exchange positions and also of the variation of the adsorbent surface charge as a function of the solution pH.

Thus, when the cellulose surface is positively charged, it is susceptible to electrostatic interactions with the polar fractions of Brilliant Red HE-3B (reactive dye) molecule (dissociated sulphonic

groups), whereas when the surface is negatively charged, it is not able to bind anionic dyes, but is available to electrostatic interactions with Methylene Blue (cationic dye) molecules.

3.3. Effect of adsorbent dose and dye structure on adsorption efficiency

Aiming at establishing the optimum dose of the microcrystalline cellulose beads, different amounts of material were contacted with solutions containing the studied dyes in certain concentrations, at the selected initial pH, for 24 hours.

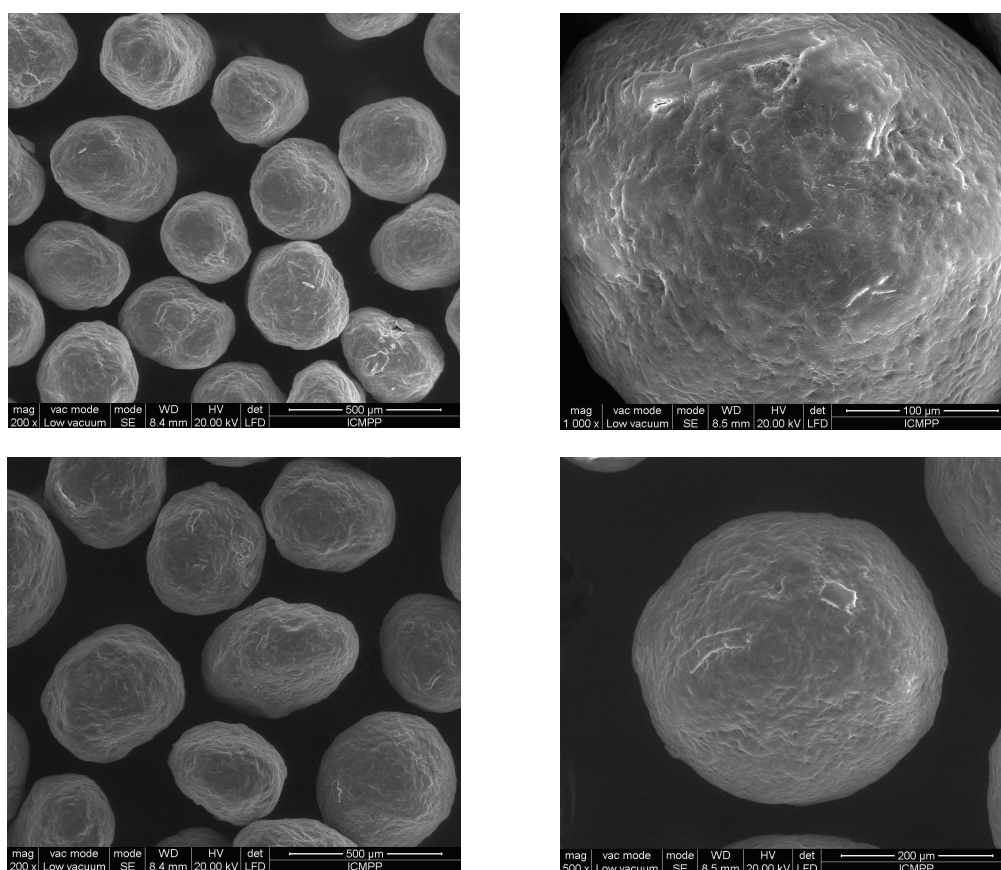


Fig. 2. ESEM images for Cellets 200 (top) and Cellets 350 (bottom)

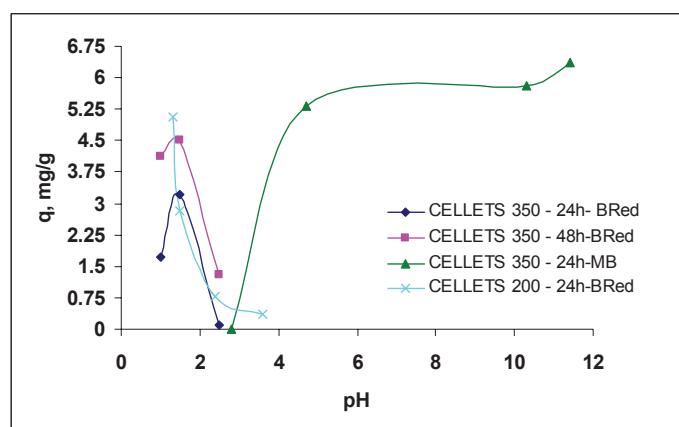


Fig. 3. Effect of pH and type of celluloses on the adsorption of BRed dye onto microcrystalline cellulose pellets: $C_0 = 50$ mg/L; adsorbent dose- 2 g/L, 24 h, $T = 25^\circ\text{C}$ and MB dye: $C_0 = 51.2$ mg/L; adsorbent dose- 2 g/L, 24 h, $T = 25^\circ\text{C}$

The results presented in Fig. 4, show that the dye uptake decreases with the increase in adsorbent dose (from 1.682 mg/g to 1.517 mg/g for BRed and from 10.69 mg/g to 3.8 mg/g for MB). At the same time, the percent of dye removal increases from 7.26 % to 25.8 % in the case of MB, and from 41.76 % to 61.45 % in the case of BRed. The adsorbent dose which results in a higher removal percent is dependent on size of dye molecule: 2 g/L for Methylene Blue and 4 g/L Brilliant Red HE-3B.

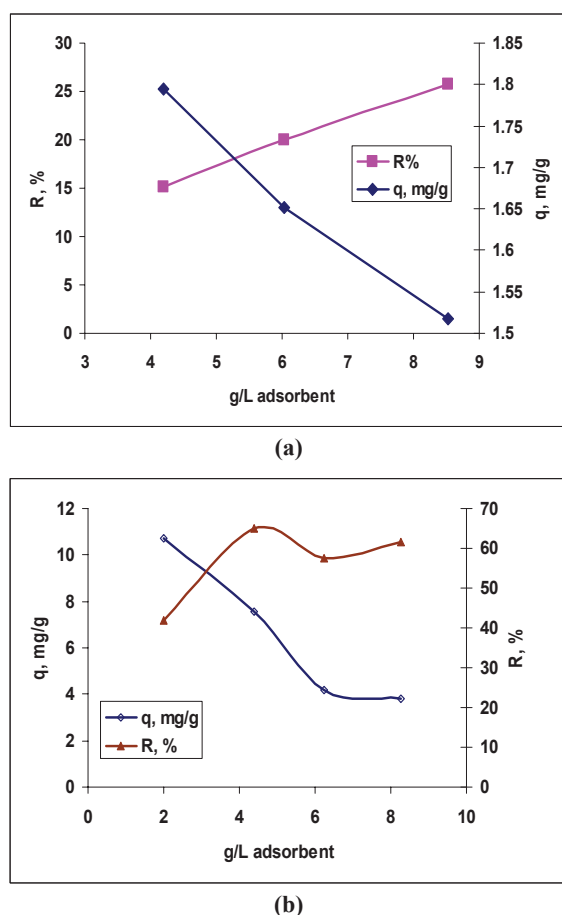


Fig. 4. Effect of adsorbent dose on the adsorption of dye onto microcrystalline cellulose pellets Cellets 350: (a) BRed - $C_0 = 50 \text{ mg/L}$; $\text{pH} = 1.5$; 24 h, $T = 25^\circ\text{C}$; (b) MB - $C_0 = 51.2 \text{ mg/L}$; $\text{pH} = 11.4$; 24 h, $T = 25^\circ\text{C}$

Moreover, the results show a completely different behaviour of the celluloses toward the studied dyes. It is obvious that the material has a much greater affinity for MB dye compared with BRed dye, fact which could be explained by the reduction of dispersion inside the solid powder mass due to the dye steric effect and preservation of anionic dye with more voluminous molecule only at the outside of the adsorbent.

3.4. Effect of temperature and initial dye concentration on adsorption efficiency

Adsorption of Brilliant Red HE-3B dye onto cellulose powder is dependent on the solution

temperature. In order to assess this influence, experiments were performed using aqueous solutions of dyes with concentration of 50 mg/L which were contacted with a dose of 4 g/L adsorbent materials at $\text{pH} = 1.5$ and at three temperature values (2, 20 and 45°C). The experiments reveal that the dyes adsorption onto microcrystalline cellulose beads depends on temperature value.

Adsorption capacity decreased with increase of temperature from 2.984 mg/L at 2°C to 1.49 mg/L at 45°C (for Brilliant Red HE-3B dye), suggesting an exothermic process in which the lower temperatures favors the dyes molecules diffusion in the internal porous structure of adsorbent.

3.5. Effect of contact time on adsorption efficiency

The influence of phases contact time on the dyes adsorption upon microcrystalline cellulose has been investigated for solution with 50 mg/L BRed dye, at $\text{pH} = 1.5$ and 20°C .

The experimental data from Figs. 3 and 5 show that dye removal rate has increased with time up to 2000 min, after that remaining constant as a result of the fact that the equilibrium was reached.

The extent of adsorption could be expressed by the fractional attainment of equilibrium, F , according to Eq. (3), where q_t and q_e (mg/g) are the amounts of dye adsorbed at time t and at equilibrium (24 h).

$$F = q_t / q_e \quad (3)$$

The $t_{50\%}$ ($F = 0.5$) values correspond to about 250 min for an initial dye concentration of 50 mg/L.

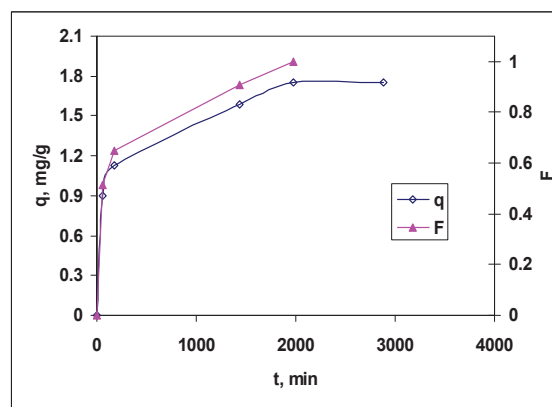


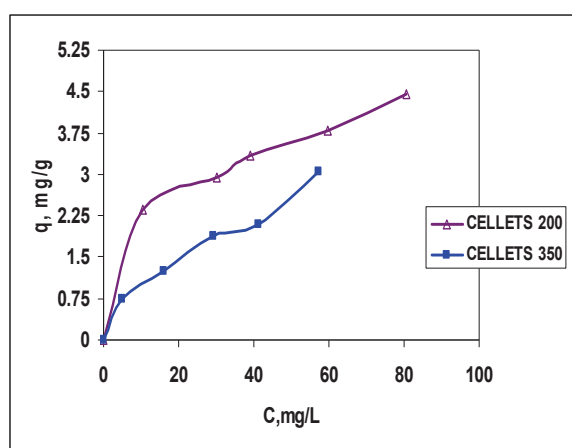
Fig. 5. Effect of contact time on BRed dye adsorption onto microcrystalline cellulose Cellets 350: $C_0 = 50 \text{ mg/L}$; 4g adsorbent/L, 24h, $T = 20^\circ\text{C}$

3.6. Effect of initial dye concentration, type of cellulose and dye structure on adsorption efficiency

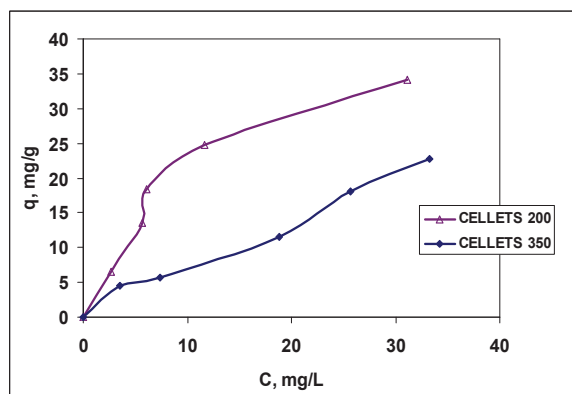
The adsorption capacity of cellulose beads for selected dyes was determined in solutions with different initial dyes concentrations and corresponding values of pH. The results presented in Fig. 6 a, b show that the dyes uptake ($q, \text{mg/g}$)

increases with the increase in initial dye concentration. Therefore, for BRed adsorption onto *Cellets* 350, the dye uptake has increased from 2.35 mg/g to 4.455 mg/g when the dye initial concentration increased from 8 to 100 mg/L. At the same time, increase in the initial MB dye concentration from 13.6 mg/L to 81.6 mg/L led to increase in adsorption capacity of the celluloses from 6.49 mg/g to 34.1 mg/g.

The relative low value of adsorption capacity for BRed may be attributed to the large size of dye molecule, which inhibits adsorption in the porous structure of adsorbent. Also, one can observe a different behavior of the two celluloses. This can be attributed to the different pore size: the smaller pore size in case of *Cellets* 200 provides a higher specific surface area (up to 75%) and therefore a higher adsorption capacity.



(a)



(b)

Fig. 6. The effect of initial dye concentration on dye adsorption on microcrystalline cellulose: (a) BRed - pH=1.5; adsorbent dose- 4 g/L, 24 h, $T = 25^{\circ}\text{C}$; (b) MB - pH=11.5; adsorbent dose- 2 g/L, 24 h, $T = 25^{\circ}\text{C}$

The greater adsorption capacity of the adsorbent in the case of MB dye (Molecular weight = 320 g/moles) may be a consequence of smaller size of the dye molecule, compared with BRed (Molecular weight = 1460 g/mole), whose larger molecules inhibit the adsorption process onto the material with relatively small pores.

3.7. Characterization of celluloses after dyes adsorption

The FT-IR spectra of the original *Cellets* beads (C200 μm), but also of the beads modified with dyes (BRed and MB) are shown in Fig. 7. These spectra are different in a small extent, with representative peaks of the cellulosic structures located around $4000 - 2995\text{ cm}^{-1}$ (hydrogen-bonded OH stretching), and 2891 cm^{-1} (CH stretching mode). The differences are visible in the spectra of *Cellets*-MB and *Cellets*-BRed, especially in the range of $1000 - 2000\text{ cm}^{-1}$, when a shoulder peak located around 1780 cm^{-1} appears after adsorption processes. Also, there are some shifts and reduction of the intensity of the peaks originated from cellulose structure, located at 1645 cm^{-1} . These changes clearly evidenced the dye adsorption on the cellulose structure.

Microphotographs of the original and modified *Cellets* reveal that they have regular spherical shapes, with a compact structure within the size range of $200 - 350\text{ }\mu\text{m}$, as Fig. 3 shows. The modified samples reveal insignificant modification as compared with the original materials, (Fig. 8). One can assume that the dyes structures have no effect on the cellulose structure.

Even at the surface level, there are not visible any damages or defects of the *Cellets* beads after adsorption, therefore the cellulosic materials might be suitable for being used for multiple adsorption stages.

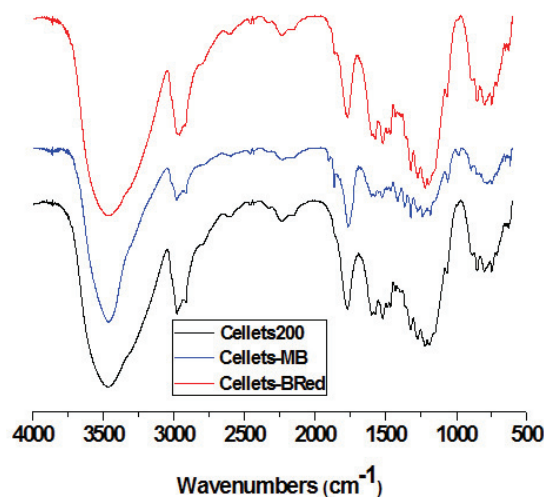


Fig. 7. FT-IR spectra of starting (C200 μm) and modified (B and R) materials (spectra were vertically shifted for better comparison)

4. Conclusions

Adsorption of both Brilliant Red HE-3B reactive dye and Methylene Blue cationic dye from aqueous environment onto microcrystalline cellulose was investigated as a function of initial solution pH, cellulose dose, dye concentration, temperature, contact time, dye structure and cellulose type.

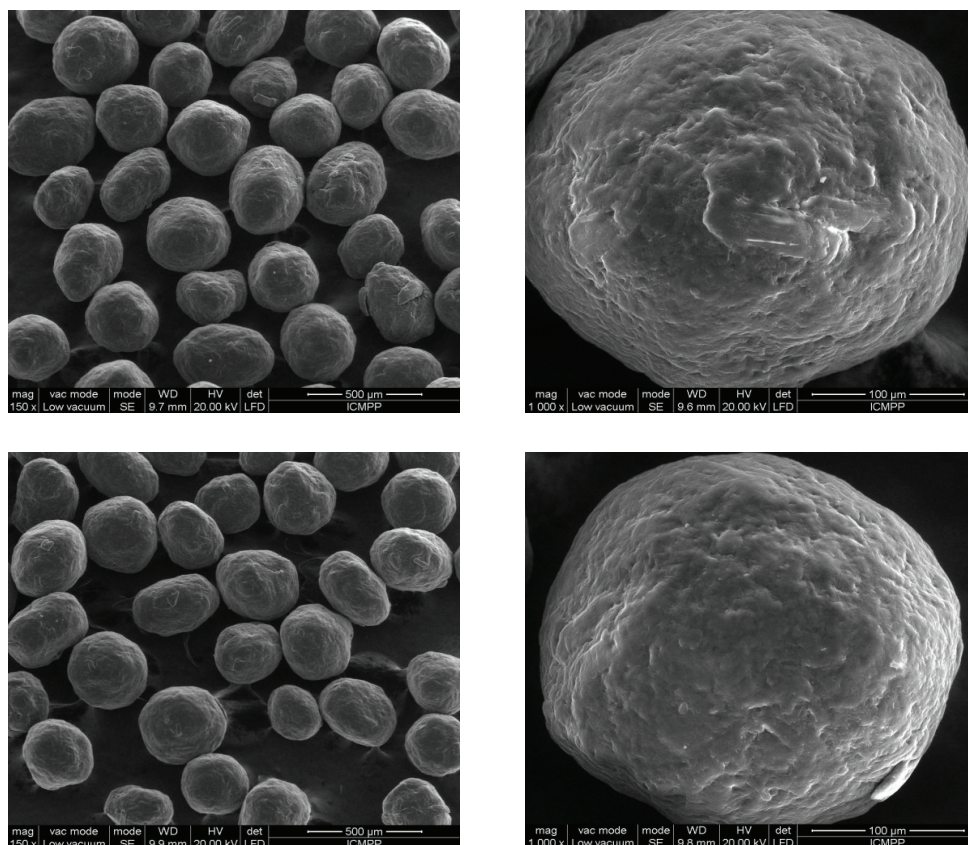


Fig. 8. ESEM images of MB adsorbed on Cellets 200 μm (top), and BRed adsorbed on Cellets 200 μm (bottom)

The results indicated that adsorption depends on the dye structure (molecular weight) and cellulose type (pore size distribution). Moreover, the adsorption capacity increases with increase in dye concentration, adsorbent dose, contact time and decreases with increase in temperature. The initial solution pH is an important factor and the selection of the optimum value depends upon the dye type: anionic or cationic.

The results lead to conclusion that the microcrystalline cellulose, cellets, can be considered as a new and valuable adsorbent for the removal of dyes with relatively low molecular weight from aqueous solutions. Further studies should be performed regarding the equilibrium, thermodynamics and kinetics of the adsorption process in order to determine the quantitative characteristic parameters, thermal effect, rate limiting step and to assess the mechanism of adsorption.

References

- Allen S.J., Koumanova B., (2005), Decolourisation of water/wastewater using adsorption (review), *Journal of the University of Chemical Technology and Metallurgy*, **40**, 175-192.
- Anjaneyulu Y., Sreedhara Chary N., Samuel Suman Raj, D., (2005), Decolourization of industrial effluents – available methods and emerging technologies – a review, *Reviews, Environmental Science and Bio/Technology*, **4**, 245-273.
- Abbas F.S., (2013), Dyes removal from wastewater using agricultural waste, *Advances in Environmental Biology*, **7**, 1019-1026.
- Bharathi K.S., Ramesh S.T., (2013), Removal of dyes using agricultural waste as low cost adsorbents: A review, *Applied Water Science*, **3**, 773-790.
- Ding S., Li Z., Rui W., (2010), Overview of dyeing wastewater treatment technology, *Water Resource Protection*, **26**, 73-78.
- Greluk M., Hubicki Z., (2010), Comparison of the gel anion exchangers for removal of Acid Orange 7 from aqueous solution, *Chemical Engineering Journal*, **162**, 919-926.
- Kanawade S.M., (2014), Treatment on dye industrial wastewater by using adsorption, *International Journal of Chemistry and Material Science*, **2**, 059-067.
- Kasperchik V.P., Yasevich A.L., (2012), Wastewater treatment for removal of dyes by coagulation and membrane processes, *Petroleum Chemistry*, **52**, 545-556.
- Kaplan D.L., (1998), *Introduction to Biopolymers from Renewable Resources*, In: *Biopolymers from Renewable Resources*, Kaplan D.L. (Ed.), Springer Publishing, Berlin, 1-29.
- Kharub M., (2012), Use of various technologies, methods and adsorbents for removal of dye, *Journal of Environmental Research and Development*, **6**, 879-883.
- Klemn D., Heublein B., Fink H.P., Bohn A., (2005), Cellulose: fascinating biopolymer and sustainable raw material, *Angewandte Chemie (International Edition in English)*, **44**, 3358-3393.

- Kyzas G.Z., Fu J., Matis K.A., (2013), The change from past to future for adsorbent materials in treatment of dyeing wastewater, *Materials*, **6**, 5131-5158.
- Latif A., Noor S., Sharif Q.M., Najeibullah M., (2010), Different techniques recently used for the treatment of textile dyeing effluents: A review, *Journal of Chemical Society of Pakistan*, **32**, 115-122.
- Mohamed R.M.S.R., Nanyan N.Mt., Rahman N.A., Kutty M.A.I., Kassim A.H.M., (2014), Colour removal of reactive dye from textile industrial wastewater using different types of coagulants, *Asian Journal of Applied Science*, **2**, 650-657.
- Ouasif H., Yousfi S., Bouamrani M.L., El Kouali M., Benmokhtar S., Talbi M., (2013), Removal of cationic dye from wastewater by adsorption onto natural adsorbents, *Journal of Materials and Environmental Science*, **4**, 1-10.
- Ozdemir C., Oden M.K., Sahinkaya S., Kalipci E., (2011), Color removal from synthetic textile wastewater by sono-fenton process, *Clean – Soil, Air, Water*, **39**, 60-67.
- Pereira L., Alves M., (2012), *Dyes – Environmental Impact and Remediation*, In: *Environmental Protection Strategies for Sustainable Development*, Malik A., Grohmann E. (Eds.), Springer Science Business, 111-162.
- Rashed M.N., (2013), *Adsorption Techniques for the Removal of Organic Pollutants from Water and Wastewater*, In: *Organic Pollutants – Monitoring, Risk and Treatment*, Nageeb Rashed M. (Ed.), INTECH Publisher, Rijeka, Croatia, 167-194.
- Ramesh Babu B., Parande A.K., Raghu S., T. Prem Kumar, (2007), Textile technology - cotton textile processing: waste generation and effluent treatment, *The Journal of Cotton Science*, **11**, 141-153.
- Sharma P., Kaur H., Sharma M., Sahore V., (2011), A review on applicability of naturally available adsorbents for the removal of hazardous dyes from aqueous waste, *Environmental Monitoring and Assessment*, **183**, 151-195.
- Saraswathy T., Singh A., Ramesh S.T., (2013), New trends in electrocoagulation for the removal of dyes from wastewater: A review, *Environmental Engineering Science*, **30**, 333-349.
- Sulak M.T., Yamaz H.G., (2012), Removal of textile dyes from aqueous solution with eco-friendly biosorbent, *Desalination & Water Treatment*, **37**, 169-177.
- Suteu D., Zaharia C., Bilba D., Muresan R., Popescu A., (2009a), Decolorization of textile wastewaters – chemical and physical methods, *Textile Industry (Industria Textila, Bucharest)*, **60**, 254-263.
- Suteu D., Zaharia C., Muresan A., Muresan R., Popescu A., (2009b), Using of industrial waste materials for textile wastewater treatment, *Environmental Engineering and Management Journal*, **8**, 1097-1102.
- Suteu D., Bilba D., Aflori M., Doroftei F., Lisa G., Badeanu M., Malutan T., (2012), The seashell wastes – A new biosorbent for reactive dye removal from textile effluents, *CLEAN - Soil, Air, Water*, **40**, 198-205.
- Suteu D., Bilba D., Coseri S., (2014), Macroporous polymeric ion exchangers as adsorbent for removal of cationic dye Basic Blue 9 from aqueous solution, *Journal of Applied Polymer Science*, **131**, DOI: 10.1002/app.39620.
- Zaharia C., Suteu D., Muresan A., Muresan R., Popescu A., (2009), Textile wastewater treatment by homogenous oxidation with hydrogen peroxide, *Environmental Engineering and Management Journal*, **8**, 1359-1369.
- Zaharia C., Suteu D., Muresan A., (2012), Option and solutions for textile effluent decolorization using some specific physico-chemical treatment steps, *Environmental Engineering and Management Journal*, **11**, 493-509.
- Zaharia C., Suteu D., (2012), *Textile Organic Dyes – Characteristics, Polluting Effects, and Separation/Elimination Procedures from Industrial Effluents. A Critical Overview*, In: *Organic Pollutants Ten Years after the Stockholm Convention – Environmental and Analytical Update*, INTECH Publisher, Rijeka, Croatia, 55-86.
- Wawrzekiewicz M., Hubicki Z., (2010), Kinetics, isotherm and thermodynamic studies of Reactive Black 5 removal by acid acrylic resins, *Chemical Engineering Journal*, **157**, 29-34.



“Gheorghe Asachi” Technical University of Iasi, Romania



SEPARATION OF SUCCINIC ACID FROM FERMENTATION BROTHS. MODELLING AND OPTIMIZATION

Elena-Niculina Dragoi¹, Silvia Curteanu^{1*}, Dan Cascaval^{1*}, Anca Irina Galaction²

¹*“Gheorghe Asachi” Technical University of Iasi, Faculty of Chemical Engineering and Environmental Protection,
73 Prof. dr. docent Dimitrie Mangeron Str., 700050 Iasi, Romania*

²*“Gr. T. Popa” University of Medicine and Pharmacy, Faculty of Bioengineering,
9-13 Mihail Kogalniceanu Str., 700454 Iasi, Romania*

Abstract

Succinic acid is widely used in different industries, its demand increasing each year. Therefore, efficiently producing it (especially from bio-regenerable sources) is an aspect that researchers try to solve thorough different methods, one of the approaches consisting in using process models for generating predictions and improving production by process optimization. In this work, a combination of two bio-inspired algorithms represented by Artificial Neural Networks and Clonal Selection was employed for determining optimal models for the separation of succinic acid from fermentation broths. Since these two algorithms cannot be naturally combined, a direct, real-value encoding for the most important model parameters was employed. In order to improve the performance of the general algorithm, a local hybrid search method based on Random Search and Back-Propagation was introduced into the optimization procedure. The results obtained showed that the algorithm improvements are translated into performance improvements.

Key words: back-propagation, clonal selection, neural network, random search, succinic acid

Received: November, 2014; Revised final: March, 2015; Accepted: March, 2015

1. Introduction

Models are adequate tools for system exploration, predictions, guidance, and optimization and, therefore, their use in solving real-life problems can help saving money and time (through reduction of materials required and experimental setups) (WU et al., 2008). Since a majority of the systems encountered in chemical engineering are non-convex, non-linear, and with constrained parameters, the classical approaches based on the chemical and physical laws often do not provide the required level of accuracy in the modelling attempt.

In this context, due to their interesting characteristics - capability of modelling non-linear relation, parallel processing, learning and fault tolerance -, neural networks (NNs) represent one of most used methods for replacing the

phenomenological models, various studies on different chemical engineering aspects being performed (Curteanu and Cartwright, 2012; Curteanu et al., 2014; Dragoi et al., 2014; Gholikandi et al., 2014; Himmelblau, 2000; Suditu et al., 2013; Woinaroschy and Radu, 2014). Different types of networks were applied, the majority of works employing feed forward multiplayer perceptron (MLP) because it has a simple structure (simple interconnected neurons organized in layers) and can be applied to approximate virtually any smooth, measurable function. Consequently, the MLP neural network was used in this work for modelling an important bio-chemical process.

Although simple and easy to use, the NNs have a critical shortcoming related to the lack of robustness when improper architecture, training and validation procedures are used (Noor et al., 2010). In

* Author to whom all correspondence should be addressed: e-mail: silvia_curteanu@yahoo.com; dancasca@ch.tuiasi.ro

order to solve this problem and to overcome the gradient descent based training shortcomings, neuro-evolution (evolving neural networks with evolutionary algorithms) can be applied. In this work, the idea of neuro-evolution is taken further, the alteration and optimization of neural networks being performed with an Artificial Immune System (AIS) algorithm represented by Clonal Selection (CS).

The AIS algorithms can be applied to various types of problems, the domains where is most used, ordered descending based on the number of applications are: clustering/classification, anomaly detection, computer security, numeric function optimization, combinatorial optimization, learning, bio-informatics, image processing, robotics, control, virus detection, web mining (Hart and Timmis, 2005). Other applications are represented by: pattern recognition, scheduling control, machine learning, reasoning, emergent behavior (Khilwani et al., 2008; Tan et al., 2008).

Regarding the applications of AIS in the chemical engineering field, there are only a few works, in the latest years, a rising use trend being observed. For example, Hu and Yan (2009) used the principles of the artificial immune system to auto-adapt the parameters of the differential evolution algorithm, the combination being applied for the kinetic parameters estimation of the homogenous mercury oxidation. Similarly, a hybridization of a fuzzy –based adaptive genetic algorithm with a new variant of AIS - fuzzy theory, is applied for parameter estimation of a reaction dynamic model of the low temperature SO₂ oxidation, using Cs-Rb-V sulfuric acid catalyst (Yang and Yan, 2011). Another combination of algorithms (AIS and dynamic time warping) was used for the diagnosis of batch chemical process faults (Dai and Zhao, 2011).

In Guzella et al. (2007), a Dynamic Effector Regulatory Algorithm was applied for fault and anomaly detection in case of a sugar factory from Poland. Other applications are: chemical sensor drift mitigation (Martinelli et al., 2013), charge state assignment of small molecule mass spectra (Kilgour et al., 2012).

The real-life case study considered for this work is represented by the separation of succinic acid from the fermentation broths. Succinic acid, a water soluble, colorless crystal is emerging as one of the most competitive new bio-based chemicals, its production from petroleum based products being replaced with renewable feedstock through a fermentation process. Due to the fermentation process, different chemical compounds are encountered in the broth, and therefore, a separation step must be performed. A set of anterior experiments indicated that separation of this acid by pertraction from the mixture obtained in fermentation is possible (Wang et al., 2010). But this process is difficult to perform and, to model because the inner workings are not fully know and understood. Consequently, the application of a CS optimized NN is an efficient way to model the system.

2. Clonal selection

Although based on different biological inspiration theories, the Clonal Selection and the Evolutionary Algorithms (EAs) are very similar because they are population-based search and optimize algorithms (Dasgupta and Nino, 2009). Also, the two central processes which are involved in antibodies production, genetic recombination and mutation, are the same as the ones used for the evolution of species reproduction. The same mechanism (that provides the variation on which natural selection is based) has the role of fitting the organism into the environment (de Castro and Von Zuben, 2000). Except for the inspiration source, the nomenclature, operators, and the specific adaptive mechanisms (Brownlee, 2007) represent other differences between CSs and EAs.

Multiple algorithms belonging to CS class can be encountered in literature, most of them having the same features (de Castro and Von Zuben, 2000): i) population initialization; ii) selection of the best individuals; iii) reproduction (cloning); iv) hyper-mutation of the clones and reselection of improved clones; and v) replacement of some of the antibodies from the population with novel ones (diversity introduction), operation which is called Receptor editing.

Initialization represents the first step of the algorithm, and it is recommended that the antibodies should be scattered uniformly over the feasible search space (Gong et al., 2010). The classical approach is represented by a random generation of antibodies (which are the B cells of the biological immune system (Cutello et al., 2004)) with a uniform distribution probability (Swain et al., 2011). In order to obtain better results, researchers applied a series of methods to improve the initialization step so that the search starts from a better pool of solutions (Dasgupta and Nino, 2009; Gong et al., 2010).

After that, the population is evaluated using affinity function. Each antibody has an associated affinity value, and, based on this information, some of them are selected for cloning. The affinity is computed using different measures, such as: crowding distance value (Chen et al., 2010), Euclidian distance (Zhang, 2011), and arithmetic expressions (Gan et al., 2009).

In the next step, a percent or a fixed number of the best affinity individuals are selected for cloning, which is the process of creating new antibodies from a single common ancestor (Chen et al., 2010). The number of clones is usually generated using one of the two principles: i) static cloning (a predefined number of clones is created for each selected antibody) and ii) proportional cloning (the number of clones is proportional to the antigenic affinities) (Cutello et al., 2004). After cloning, the clones are matured, in order to improve their affinity. This is a process of variation and selection achieved by somatic hyper-mutation (which performs the local search) and selection of the better matched

antibodies (which performs the global search) (Dasgupta and Nino, 2009). The hyper-mutation operator explores the search space by introducing innovation in the potential solution population (Cutello et al., 2004). When considering the mutation potential, the following variants of hyper-mutation operators exist: static, proportional, inversely proportional, hyper-macromutation and hybridizations (Cutello et al., 2004). Concerning the modality of introducing the hyper-mutation, the variants are: somatic hyper-mutation (Simoes and Costa, 2003), tangent vector (de Mello Honorio et al., 2007), Jacobian vector (de Mello Honorio et al., 2007), adaptive Gaussian (Goncalves et al., 2007), adaptive (Goncalves et al., 2007), two phase mutation process (Mobini et al., 2011).

After the clones are hyper-mutated, the affinity of the cloned population is computed, the individuals with the higher affinities being selected for introduction in the population.

3. hCS-NNm

The hCS-NNm algorithm proposed in this work is based on a previous CS-NN version (Dragoi et al., 2012), where CS is used to simultaneously optimize the topology and the inner parameters of the neural model. The parameters considered for optimization are: number of hidden layers, number of neurons in the hidden layers, weights, and bias, activation function and parameter of the activation function (whenever is the case). During the optimization, each neuron can have one of the following activation functions: Linear, Hard Limit, Bipolar Sigmoid, Logistic Sigmoid, Tangent Sigmoid, Sinus, Radial Basis and Triangular Basis. Another limitation imposed to the network is related to the number of hidden layers. As the majority of known processes can be modeled with a two hidden layer network, a limitation related to this parameter was set and each determined model can have none, one or two hidden layers.

As mentioned in the previous section, from a structural point of view, CS is similar to an EA, a set of potential solutions called antibodies being evolved through generations by the application of cloning, hyper-mutation, and receptor editing (similar to selection). A specific characteristic of the CS-NN algorithm is represented by a hybrid hyper-mutation approach in which one of the three types of hyper-mutation (Gaussian, non-uniform, and pair wise) is used, based on random parameter.

In its natural form, the NN cannot be optimized using CS, and therefore, an encoding procedure was applied to create a working inter-relation between the two algorithms. From the multitude of encoding approaches, a direct real value variant was chosen, not only for its simplicity, but also for the low computational cost it utilizes when performing encoding - decoding actions, at each iteration and for each antibody, at least one of this actions being performed.

As the antibodies used in CS-NN are representation of different NNs acting as models for the considered process, it is possible to include a back-propagation (BK) procedure as local search. The Random Search (RS) approach was alternatively applied to improve the best solution at the end of each generation because, during the evolution, the best solution may not change as often as desired and BK is helpful only when applied to a limited population (as it requires considerable computational resources when used for a high number of models). This combination of BK and RS applied as a local search procedure, along with its application in a real case study (which to the author's knowledge was never modelled with a clonal-neural approach) represents the novelty of this work.

A simplified schema of the proposed hCS-NNm algorithm, where stop condition is represented by the number of generations reaching a specific maximum limit, is presented in Fig. 1.

In this figure, N_c represents the number of individuals which will be cloned, Ma is the medium affinity of the population (computed as the average affinity of all the individuals from the population at the specific generation) and bs represents the best solution.

4. Database for the separation of succinic acid

The succinic acid, which is also known as amber acid or butandioic acid, is widely used in many areas, the production of this compound from renewable resources being more cost-effective than from petroleum based products (Song and Lee, 2006). Consequently, determining good succinate production hosts and optimal conditions which lead to maximum efficiency are problems which must be solved in order to obtain applicable workflows in large scale equipments.

Succinic acid is a dicarboxylic acid with numerous applications in chemical industry (reagents, synthetic resins, biodegradable polymers, electroplating, green solvents, detergents, inks), agriculture (pesticides, growth regulators and stimulants), pharmaceutical and food industries (amino acids, antibiotics, vitamins, surfactants, additives) (Liu et al., 2008; Song and Lee, 2006; Zeikus et al., 1999).

This acid is industrially produced using liquefied petroleum gas, namely butane, by chemical synthesis *via* maleic anhydride. The cost of this technology varies between 4.1 to 6.3 EUROS kg^{-1} succinic acid, depending on the acid's final purity, the contribution of raw materials to this cost being of 1 EURO kg^{-1} succinic acid (Song and Lee, 2006; Zeikus et al., 1999). Due to the difficulties of the chemical synthesis, succinic acid production by fermentation of *Actinobacillus succinogenes* or *Actinobacillus succiniproducens* have been considered as important alternative (Corona-Gonzalez et al., 2008; Dorado et al., 2009; Galaction et al., 2012; Li et al., 2010).

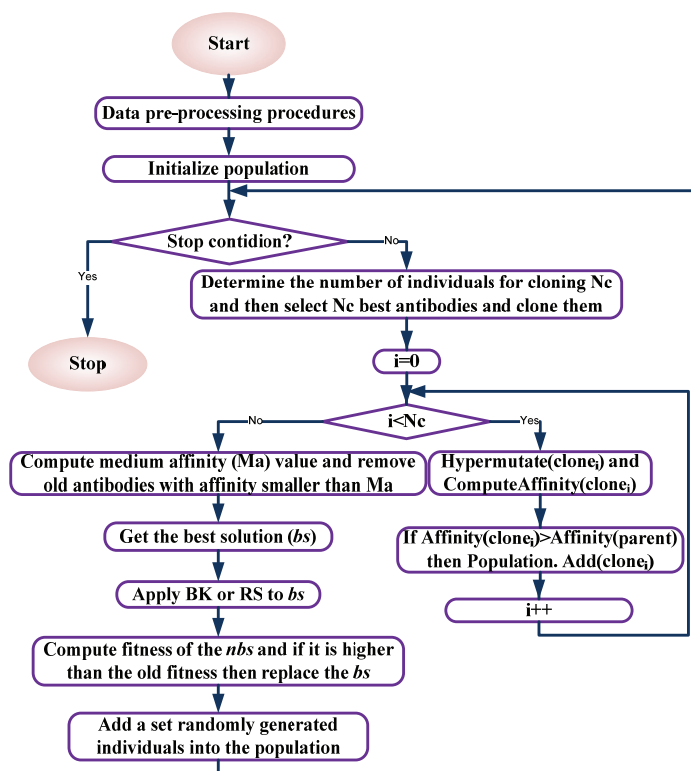


Fig. 1. The simplified schema of the hCS-NNm algorithm

However, the separation of succinic acid from the fermentation broths is difficult, especially due to the presence of other carboxylic acids, the most important being formic and acetic acids.

A series of previous experiments indicated that the selective separation of these acids by facilitated pertraction with tri-*n*-octylamine (TOA) of formic, acetic and succinic acid from their mixture obtained by *A. succinogenes* fermentation is possible (Galaction et al., 2013). Thus, formic and acetic acids can be transferred from the feed phase through liquid membrane to the stripping phase, while succinic acid remains in the feed phase. Superior values of selectivity factors can be obtained by combining the effects of pH-gradient between the aqueous phases, carrier concentration and mixing intensity on pertraction of carboxylic acids obtained by succinic acid fermentation.

In this context, the aim of applying a neural network optimizer as Clonal Selection is to establish the model describing the influences of the considered parameters on the pertraction selectivity. In the same time, the goal of the optimization is to find the operating conditions corresponding to the maximum selectivity factor.

The database used for modelling the separation of succinic acid from the fermentation broths is composed from experimental data. The experiments have been carried out using the pertraction equipment that allows obtaining and maintaining easily the solvent layer between the two aqueous phases (free liquid membrane).

The pertraction cell consists in a U-shaped glass pipe having an inner diameter of 45 mm and a total volume of 450 mL, the volume of each compartment being of 150 ml (Galaction et al., 2008). The aqueous solutions and the solvent phase have been independently mixed by means of double blade impellers with 6 mm diameter and 3 mm height. For the two aqueous phases, the rotation speed of the impellers varied between 0 and 800 rpm. The membrane phase has been mixed at 500 rpm. The area of mass transfer surface, both for extraction and for re-extraction, was of $1.59 \times 10^{-3} \text{ m}^2$. The interfaces between the phases remained flat, and, hence, the interfacial area constant, for entire rotation speed domain used.

The experiments have been carried out in a pseudosteady-state regime, at steady-state conditions related to the aqueous phases and unsteady-state mode related to the membrane phase. The aqueous solutions have been separately fed with a volumetric flow of 2.5 L h^{-1} . The liquid membrane phase consisted of dichloromethane in which has been separately dissolved the carrier TOA, its concentration varying between 5 and 300 g L^{-1} ($0.014 - 0.85 \text{ M}$).

The feed phases were aqueous solutions respecting the composition obtained by succinic fermentation with *A. succinogenes*: 33 g L^{-1} (0.28 M) succinic acid, 4 g L^{-1} (0.087 M) formic acid and 10 g L^{-1} (0.17 M) acetic acid, respectively (Dorado et al., 2009). The pH-value of the feed phase varied between 1 and 7, the pH adjustment being made with

solution of 3% sulfuric acid or 3% sodium hydroxide, function on the prescribed pH-value.

The stripping phases consisted of solutions of sodium hydroxide with pH = 7 - 12. The pH-values of both aqueous phases were determined using a digital pH-meter of Consort C836 type and have been recorded throughout each experiment. Any pH change was recorded during the extraction experiments.

The pertraction process was analyzed by means of the selectivity factor. For calculating this parameter, the acids concentrations in the feed and stripping phases have been measured and the mass balance for the pertraction system has been used. Succinic, formic, and acetic acids concentrations have been determined by high performance liquid chromatography technique (HPLC, Star Varian Chromatography Workstation) with a PL Hi-Plex H column (7.7 mm diameter, 300 mm length, 8 μ m porous particle), provided with UV Prostar 330 PDA detector (Galaction et al., 2013). The mobile phase was a solution of 0.1% trifluoroacetic acid with a flow rate of 0.6 mL min⁻¹. The analysis has been carried out at 60°C.

A series of multiple experiments with varying parameters were performed, the final database having a set of 2370 data. For modeling purpose, 75% of data was used in the training phase and 25% in the testing phase. In addition, a normalization procedure was applied, to reduce the difference between the maximum and minimum values of each parameter.

4. Results and discussion

After data describing, the process was gathered and worked using a normalization procedure, various simulations with the hCS-NNm are performed in order to determine the algorithm's performance concerning model determination for the separation of succinic acid from mixtures of succinic, acetic, and formic acids formed in the fermentation broths. The main parameters considered for modelling the pertraction process were: pH value of feed phase (pH_f), pH value of stripping phase (pH_s), the TOA concentration (CTOA, g L⁻¹), and the impeller speed (N, rpm).

The architecture of the models (the CS work with) influences the computational resources. A direct dependency between how big the network is (in terms of number of hidden layer and neurons in each hidden layer) and the dimension of the corresponding encoding exists. Consequently, a set of limitation to the model architecture were imposed. For the majority of processes, it was observed that a network with a maximum of 2 hidden layers can provide acceptable results.

Therefore, a network modelling the separation of succinic acid from fermentation broths can have maximum 2 hidden layers. On what concerns the maximum number of neurons in the two hidden layers, a set of 30 and respectively 20 was considered sufficient.

A set of five best results obtained with the proposed hCS-NNm algorithm are presented in Table 1, where a 'inputs: no_neurons_first_layer: no_neurons_second_layer: outputs' notation is used to represent the network topology. In order to determine the effectiveness of the proposed hCS-NNm algorithm, a comparison with an earlier version CS-NN (Dragoi et al., 2012) was performed. The best model determined with CS-NN had a topology of 4:8:1:1, with a mean squared error (of the normalized data) in the training phase of 0.0414 and of 0.0696 in the testing phase.

Also, the average relative error (ARE) for the best models obtained with the best algorithms were computed (Table 2). As it can be observed, after the data is de-normalized, the error in the training and testing phases are still lower for the hCS-NNm.

For a representative set from the training and testing data, a comparison between experimental data, predicted data with hCS-NNm and CS-NN is given in Figs. 2 and 3. As the curve of hCS-NNm is closer to the experimental data than the one of CS-NN, it was concluded that hCS-NNm works better.

Table 1. Results obtained with the hCS-NNm algorithm

| Neural network topology | Training mean squared error | Testing mean squared error |
|-------------------------|-----------------------------|----------------------------|
| 4:16:2:1 | 0.0405 | 0.0601 |
| 4:10:1 | 0.0409 | 0.0662 |
| 4:29:3:1 | 0.0430 | 0.0686 |
| 4:29:1 | 0.0431 | 0.0601 |
| 4:15:10:1 | 0.0445 | 0.0702 |

Table 2. The average relative error for the best models

| Algorithm | Model | Training ARE | Testing ARE |
|-----------|----------|--------------|-------------|
| hCS-NNm | 4:16:2:1 | 14.59% | 15.04% |
| CS-NN | 4:8:1:1 | 30.87% | 36.73% |

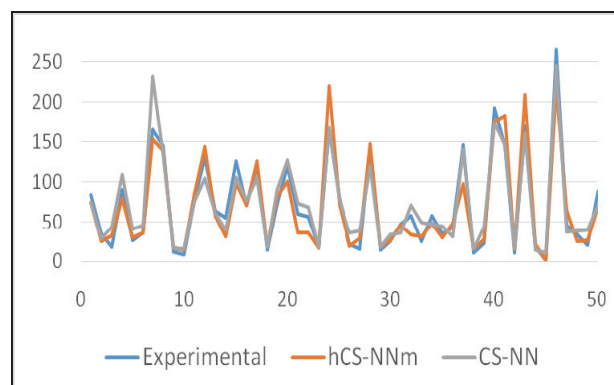


Fig. 2. Expected and neural network predictions for a representative set from the training data

5. Conclusions

In this work, the successful modelling of the succinic acid separation from fermentation broths was performed using a new hybrid combination of ANNs, CS, BK, and RS, called hCS-NNm.

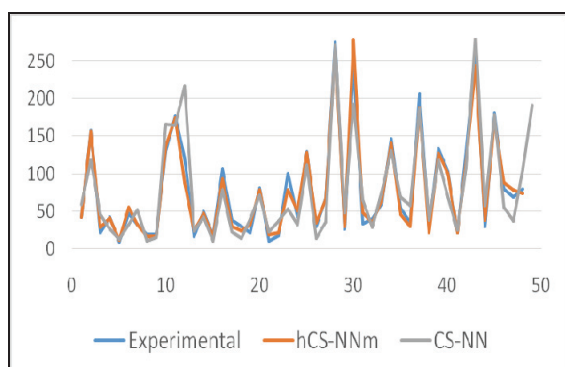


Fig. 3. Expected and neural network predictions for a representative set from the testing data

In this combination, ANN modeled the process, while the CS is the optimizer used to modify the model's parameters in order to minimize the error between predicted and experimental data.

In addition, BK and RS were applied (based on a random number generator) for the improvement of the best solution found so far. In this manner, the performance was further improved, as it was demonstrated by the application of hCS-NNm for modelling the succinic acid separation from fermentation broths, where it proved to be an efficient and reliable tool.

Acknowledgments

This work was supported by the "Partnership in priority areas – PN-II" program, financed by ANCS, CNDI - UEFISCDI, project No. 23/2012.

References

- Brownlee J., (2007), *Clonal Selection Algorithms*, CIS Technical Report 070209A, 1-13, Swinburne University of Technology, Melbourne, Australia, On line at: <http://researchbank.swinburne.edu.au>.
- Chen J., Lin Q., Ji Z., (2010), A hybrid immune multiobjective optimization algorithm, *European Journal of Operational Research*, **204**, 294-302.
- Corona-Gonzalez R.I., Borjes A., Gonzalez-Alvarez V., Pelayo-Ortiz C., (2008), Kinetic study of succinic acid production by *Actinobacillus succinogenes* ZT-130, *Process Biochemistry*, **43**, 1047-1053.
- Curteanu S., Cartwright H., (2012), Neural networks applied in chemistry. I. Determination of the optimal topology of multilayer perceptron neural networks, *Journal of Chemometrics*, **25**, 527-549.
- Curteanu S., Suditu G., Buburuzan A.M., Dragoi E.N., (2014), Neural networks and differential evolution algorithm applied for modelling the depollution process of some gaseous streams, *Environmental Science and Pollution Research*, **21**, 12856-12867.
- Cutello V., Nicosia G., Pavone M., (2004), *Exploring the Capability of Immune Algorithms: A Characterization of Hypermutation Operators*, Berlin, Springer-Verlag Berlin.
- Dai Y., Zhao J., (2011), Fault diagnosis of batch chemical processes using a Dynamic Time Warping (DTW)-based Artificial Immune System, *Industrial & Engineering Chemistry Research*, **50**, 4534-4544.
- Dasgupta D., Nino F., (2009), *Immunological Computation, Theory and Applications*, CRC Press, New York.
- de Castro L.N., Von Zuben F., (2000), *The Clonal Selection Algorithm with Engineering Applications*, GECCO 2000 - Workshop on Artificial Immune Systems and Their Applications, Las Vegas, USA, 36-37, On line at: http://www.dca.fee.unicamp.br/~vonzuben/research/lnunes_dout/artigos/gecco00.pdf.
- de Mello Honorio L., da Silva A., Barbosa D., (2007), *A Gradient-Based Artificial Immune System Applied to Optimal Power Flow Problems*, In: *Artificial Immune Systems*, de Castro L., Von Zuben F., Knidel H. (Eds.), Springer Berlin Heidelberg, Vol. 4628, 1-12.
- Dorado M.P., Lin S.K.C., Koutinas A., Du C., Wang R., Webb C., (2009), Cereal-based biorefinery development: Utilisation of wheat milling by-products for the production of succinic acid, *Journal of Biotechnology*, **143**, 51-59.
- Dragoi E.N., Suditu G.D., Curteanu S., (2012), Modeling methodology based on artificial immune system algorithm and neural networks applied to removal of heavy metals from residual waters, *Environmental Engineering and Management Journal*, **11**, 1907-1914.
- Dragoi E.N., Horoba C.A., Mamaliga I., Curteanu S., (2014), Grey and black-box modelling based on neural networks and artificial immune systems applied to solid dissolution by rotating disc method, *Chemical Engineering and Processing: Process Intensification*, **83**, 173-184.
- Galaction A.I., Cascaval D., Nicuta N., (2008), Selective removal of Gentamicin C1 from biosynthetic Gentamicins by facilitated pertraction for increasing antibiotic activity, *Biochemical Engineering Journal*, **42**, 28-33.
- Galaction A.I., Kloetzer L., Turnea M., Webb C., Vlysidis A., Cașcaval D., (2012), Succinic acid fermentation in a stationary-basket bioreactor with a packed bed of immobilized *Actinobacillus succinogenes*: 1, Influence of internal diffusion on substrate mass transfer and consumption rate, *Journal of Industrial Microbiology and Biotechnology*, **39**, 877-888.
- Galaction A.I., Postaru M., Cascaval D., Kloetzer L., (2013), Selective separation of carboxylic acids obtained by succinic acid fermentation using facilitated pertraction, *Solvent Extraction and Ion Exchange*, **31**, 171-183.
- Gan Z., Chow T.W.S., Chau W.N., (2009), Clone selection programming and its application to symbolic regression, *Expert Systems with Applications*, **36**, 3996-4005.
- Gholikandi G.B., Jamshidi S., Hazrati H., (2014), Optimization of anaerobic baffled reactor (ABR) using artificial neural network in municipal wastewater treatment, *Environmental Engineering and Management Journal*, **13**, 95-104.
- Goncalves R.A., de Almeida C.P., Delgado M.R., Goldbarg E.F., Goldbarg M.C., (2007), *A Cultural Immune System for Economic Load Dispatch with Non-smooth Cost Functions*, In: *Artificial Immune Systems*, de Castro L., Von Zuben F., Knidel H. (Eds.), Springer, Berlin, Heidelberg, 382-394.
- Gong M., Jiao L., Liu F., Ma W., (2010), Immune algorithm with orthogonal design based initialization, cloning, and selection for global optimization, *Knowledge and Information Systems*, **25**, 523-549.

- Guzella T., Mota-Santos T., Caminhas W., (2007), *A Novel Immune Inspired Approach to Fault Detection*, In: *Artificial Immune Systems*, de Castro L., Von Zuben F., Knidel H. (Eds.), Springer Berlin, Heidelberg, 107-118.
- Hart E., Timmis J., (2005), *Application Areas of AIS: The Past, The Present and The Future*, In: *Artificial Immune Systems*, Jacob C., Pilat M.L., Bentley P.J., Timmis J.I. (Eds.), Springer Berlin, Heidelberg, 483-497.
- Himmelblau D., (2000), Applications of artificial neural networks in chemical engineering, *Korean Journal of Chemical Engineering*, **17**, 373-392.
- Hu C., Yan X., (2009), An immune self-adaptive differential evolution algorithm with application to estimate kinetic parameters for homogeneous mercury oxidation, *Chinese Journal of Chemical Engineering*, **17**, 232-240.
- Khilwani N., Prakash A., Shankar R., Tiwari M.K., (2008), Fast clonal algorithm, *Engineering Applications of Artificial Intelligence*, **21**, 106-128.
- Kilgour D.P., Mackay C.L., Langridge-Smith P.R., O'Connor P.B., (2012), Use of an artificial immune system derived method for the charge state assignment of small-molecule mass spectra, *Analytical Chemistry*, **84**, 7436-7439.
- Li J., Jiang M., Chen K., Shang L., Wei P., Ying H., Ye Q., Ouyang P., Chang H., (2010), Enhanced production of succinic acid by *Actinobacillus succinogenes* with reductive carbon source, *Process Biochemistry*, **45**, 980-985.
- Liu Y.P., Zheng P., Sun Z.H., Ni Y., Dong J.J., Zhu L.L., (2008), Economical succinic acid production from cane molasses by *Actinobacillus succinogenes*, *Bioresource Technology*, **99**, 1736-1742.
- Martinelli E., Magna G., De Vito S., Di Fuccio R., Di Francia G., Vergara A., Di Natale C., (2013), An adaptive classification model based on the Artificial Immune System for chemical sensor drift mitigation, *Sensors and Actuators B: Chemical*, **177**, 1017-1026.
- Mobini M., Mobini Z., Rabbani M., (2011), An Artificial Immune Algorithm for the project scheduling problem under resource constraints, *Applied Soft Computing*, **11**, 1975-1982.
- Noor R.A.M., Ahmad Z., Don M.M., Uzir M.H., (2010), Modelling and control of different types of polymerization processes using neural networks technique: A review, *The Canadian Journal of Chemical Engineering*, **88**, 1065-1084.
- Simoes A., Costa E., (2003), *An Immune System-Based Genetic Algorithm to Deal with Dynamic Environments: Diversity and Memory*, Proc. of the Sixth International Conference on Neural Networks and Genetic Algorithms (ICANNGA'03), Pearson D.W., Steele N.C., Albrecht R.F. (Eds.), Springer-Verlag, 168-175.
- Song H., Lee S.Y., (2006), Production of succinic acid by bacterial fermentation, *Enzyme and Microbial Technology*, **39**, 352-361.
- Suditu G.D., Piuleac C.G., Bulgariu L., Curteanu S., (2013), Application of a neuro-genetic technique in the optimization of heavy metals removal from wastewaters for environmental risk reduction, *Environmental Engineering and Management Journal*, **12**, 167-174.
- Swain R.K., Barisal A.K., Hota P.K., Chakrabarti R., (2011), Short-term hydrothermal scheduling using clonal selection algorithm, *International Journal of Electrical Power & Energy Systems*, **33**, 647-656.
- Tan K.C., Goh C.K., Mamun A.A., Ei E.Z., (2008), An evolutionary artificial immune system for multi-objective optimization, *European Journal of Operational Research*, **187**, 371-392.
- Wang Y.N., Wu L.H., Yuan X.F., (2010), Multi-objective self-adaptive differential evolution with elitist archive and crowding entropy-based diversity measure, *Soft Computing*, **14**, 193-209.
- Woinaroschy A., Radu A.D., (2014), Sensitivity analysis for uranium soils decontamination using a Monte Carlo simulation, *Environmental Engineering and Management Journal*, **7**, 1817-1826.
- Wu Y., Lu J., Sun Y., (2008), An improved differential evolution for optimization of chemical process, *Chinese Journal of Chemical Engineering*, **16**, 228-234.
- Yang C., Yan X., (2011), A Fuzzy-based Adaptive Genetic Algorithm and Its Case Study in Chemical Engineering, *Chinese Journal of Chemical Engineering*, **19**, 299-307.
- Zeikus J.G., Jain M.K., Elankovan P., (1999), Biotechnology of succinic acid production and markets for derived industrial products, *Applied Microbiology and Biotechnology*, **51**, 545-552.
- Zhang Z., (2011), Artificial immune optimization system solving constrained omni-optimization, *Evolutionary Intelligence*, **4**, 203-218.



“Gheorghe Asachi” Technical University of Iasi, Romania



EQUILIBRIUM PERFORMANCES OF *CRYSTAL-RIGHT™ CR100* ZEOLITE USED IN WATER SOFTENING PROCESS

Liliana Lazar^{1*}, Bogdan Bandrabur², Ramona-Elena Tataru-Fărnuș¹,
Mioara Drobota³, Silviu-Gabriel Stroe⁴, Gheorghe Gutt⁴

¹“Gheorghe Asachi” Technical University of Iasi, Faculty of Chemical Engineering and Environmental Protection,
Department of Chemical Engineering, 73 Prof. dr. docent Dimitrie Mangeron Str., 700050 Iasi, Romania

²Hach Lange SRL, 3 Căminului Str., 021741 Bucharest, Romania

³“Petru Poni” Institute of Macromolecular Chemistry, Department of Polymer Materials Physics,
41A Gr. Ghica Voda Alley, 700487 Iasi, Romania

⁴“Stefan cel Mare” University of Suceava, Faculty of Food Engineering, 13 University Str., 720229 Suceava, Romania

Abstract

The present work investigates the performance of *Cristal-Right™ CR100* zeolite based on the equilibrium and thermodynamics water softening process. The commercial zeolite was characterized by scanning electron microscopy combined with energy dispersive X-ray spectroscopy and FT-IR spectroscopy. The equilibrium performances of zeolite were evaluated by the sorption capacity of calcium cations from calcium chloride solutions varying the calcium concentrations corresponding to moderate, hard and very hard waters. Experiments were carried in batch mode out as a function of temperature (278, 298, 318 and 338 K) and in fixed optimum conditions for soption process (pH, zeolite dose and contact time). Equilibrium sorption data were analysed using Langmuir, Freundlich and Dubinin-Radushkevich isotherm models to obtain the characteristic parameters of each model. Sorption equilibrium data fitted very well to the Langmuir model that confirmed the monolayer sorption with high correlation coefficients. According to the evaluation using the Langmuir isotherm, the maximum sorption capacities of calcium cations onto *Cristal-Right™ CR100* zeolite were 31.45 mg/g for 298 K. The thermodynamic parameters values indicate the spontaneous and endothermic nature of the sorption process by ambient temperature. The sorption energy fell in the range of physisorption.

Key words: isotherms, permanent hard water softening, sodium-zeolite, sorption capacity, thermodynamics

Received: November, 2014; Revised final: March, 2015; Accepted: March, 2015

1. Introduction

Water with a high level of hardness caused by calcium (Ca^{2+}) and magnesium (Mg^{2+}) cations is an important operational costs increase factor in most of its application fields (Gray, 2010; Ștefanache et al., 2015). Most of the water sources require treatment processes before being used as a raw material or as technological water. Water softening is a treatment process where the calcium and magnesium cations are removed from water. The most widespread industrial scale method employed for partly or total removing of permanent hard water caused by calcium

and magnesium salts that do not precipitate is based on the ion exchange procedure (Smith et al., 2008; Zagorodni, 2007). The ion exchange materials used consisting of polymeric resins (Bandrabur et al., 2012; Hoffmann and Martinola, 1988; Lazar et al., 2014) and zeolites (Shoumkova, 2011; Wang and Peng, 2010).

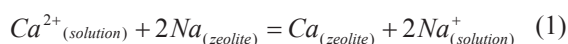
Zeolite both as natural and as produced synthetic are widely used nowadays in various water and treatment processes due to low cost, high ion exchange and adsorption potential, selectivity, high surface area distributed throughout pores with several diameters (Zagorodni, 2007). This advantage in

* Author to whom all correspondence should be addressed: e-mail: lillazar@ch.tuiasi.ro

economic aspect of zeolite has been reported in several works that was investigated and applied to remove cation contaminants in water and wastewater, such as:

(1) *water softening* – removal of permanent hard water for drinking or industrial water preparation (Arrigo et al., 2007; Cinar and Beler-Baykal, 2005; Coker and Rees, 2005; Qin et al., 2010a, 2010b; Sivasankar and Ramachandramoorthy, 2011; Xue et al., 2014; Zhao et al., 2009);

(2) *water purification* – removal of *heavy metal cations*: Fe^{3+} (Al-Anber and Al-Anber, 2008); Cu^{2+} , Zn^{2+} , Mn^{2+} , Ni^{2+} , Cd^{2+} , Pb^{2+} (Doula, 2009; Ibrahim et al., 2010; Jamil et al., 2010; Nibou et al., 2010; Ören and Kaya, 2006), As^{3+} , As^{5+} (Baskan and Pala, 2011; Noroozifar et al., 2014), Ce^{+} (Shahwan et al., 2005). Zeolites used for water softening process are mostly charged with sodium (Na^{+}) or potassium (K^{+}) cations that will be exchanged with Ca^{2+} and Mg^{2+} cations from the raw hard water passing through the crystalline structure (Loiola et al., 2012; Lühns et al., 2012; Shoumkova, 2011; Wang and Peng, 2010). For example, sodium-zeolite removes Ca^{2+} cations from water by exchange with sodium as illustrated by Eq. (1).



Zeolite softening will also remove other soluble cation species such as iron and manganese present in the raw water and will mechanically retain small suspended solids. When zeolite for water softening is saturated with Ca^{2+} , Mg^{2+} , Fe^{3+} , Mg^{2+} cations, it may be backwashed with a sodium chloride solution to remove the calcium and used again (Zagorodni, 2007). Typically, the operating cycle of an ion exchanger consists of three stages: (I) cations removal, (II) column regenerations and (III) column washing (Górka et al., 2008).

The ion exchange process in zeolites is influenced by several factors such as concentration and nature of cations and anions in the initial aqueous solution, initial pH value of solution, the ratio zeolite mas/ solution volume (dose), temperature, phase contact time and crystal structure of the zeolite (Al-Anber and Al-Anber, 2008; Jamil et al., 2010; Nibou et al., 2010; Ören and Kaya, 2006). Optimal design of the process operating in dynamic process requires preliminary knowledge on both the ion exchange equilibrium and kinetics models (Górka et al., 2008; Zhao et al., 2009).

Sorption equilibrium analysis is fundamental in supplying the essential information required for understanding of phenomena at the solid-liquid interface and design of the sorption process. In this perspective, equilibrium relationships between zeolite (sorbent) and calcium cations from aqueous solution (sorbate) are describe by sorption isotherms obtained in batch system at fixed temperature (Foo and Hameed, 2010). The quantity of a solute adsorbed can be given conventionally in terms of

moles of volume (for adsorption) or ion-equivalents (for ion exchange) per unit mass of volume of zeolite (Douglas et al., 2008).

The present work consists in experimental studying the performances at equilibrium of a commercial *Cristal-Right™ CR100* zeolite recommended for water softening. Equilibrium studies in sorption process gave the capacity of the zeolite. Accordingly, the objectives of the work are: (1) study of the equilibrium isotherms on the calcium cations from calcium chloride solution sorption onto zeolite and (2) evaluation of the application of sorption isotherms and analysing of the sorption mechanism. The equilibrium isotherm for sorption of calcium cations on zeolite is evaluated using Langmuir, Freundlich and Dubinin-Radushkevich models. The thermodynamic parameters were also determined from the temperature dependence.

2. Experimental

2.1. Materials and characteristics

Cristal-Right™ CR100 is a modified natural zeolite produced by *Mineral Right® Inc.* company (USA), relatively recently introduced in the Romanian market, delivered in the form of aluminosilicate crystals and which has ion exchange properties due to its sodium cations content. It is recommended for the use in the domestic and industrial water softening at the same time with the retention of ammonia, iron, manganese cations removal, and the rise of the pH of some low acidic waters. In addition, *Crystal-Right™ CR100* zeolite is impervious to chlorine and so it can be used with self-chlorinating, automated sanitizing systems.

The particles with average diameters 0.85 mm were tested (Gruett, 2003). The structural and morphological characteristics of the *Crystal-Right™ CR100* zeolite in delivery form are examined through scanning electron microscopy combined with energy dispersive X-ray spectroscopy (SEM-EDX) and Fourier transforms infrared spectroscopy (FT-IR). SEM micrographs of the zeolite were recorded on a 30 kV VEGA Tescan microscope. Fig. 1 showed the SEM image of zeolite particle from a 30 keV with 150X magnification.

The nonuniform macro crystals distribution from the dimensional and shape point of view and the irregular surface confirm the natural origins of the material. The surface elemental analysis recorded with Quanta 200 instrument indicates that the material is a sodium alumina-silicate type with a molar ratio Si : Al = 3.2 (Table 1). The FT-IR spectra of zeolite was obtained at room temperature, were performed on a Bruker Vertex 70 spectrometer with 400 – 4000 cm^{-1} spectral range and a 4 cm^{-1} resolution in transmission technique using the KBr pellet and the Opus 5 FTIR Software. In Fig. 2 is presented the FT-IR spectra of *Crystal-Right™ CR100* zeolite in delivery form.

Table 1. Crystal-Right™ CR100 zeolite surface elemental analysis for the delivery form from the SEM-EDX analysis results

| Element | Si | Al | O | Na | Ca | K | Au | Cl |
|---------------|-------|------|-------|------|------|------|------|------|
| Value (% w/w) | 30.25 | 9.27 | 52.02 | 5.13 | 2.43 | 0.66 | 0.44 | 0.29 |

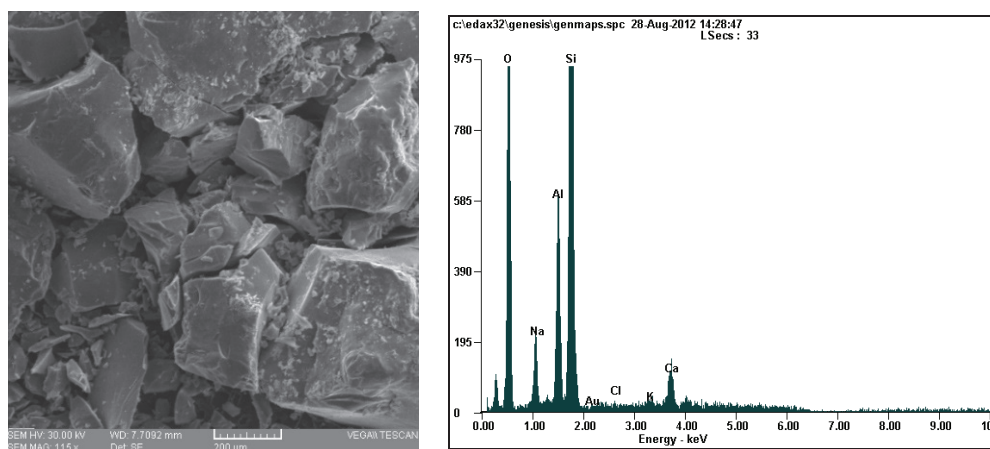


Fig. 1. SEM image and EDX spectra for the Crystal-Right™ CR100 zeolite in the delivery form

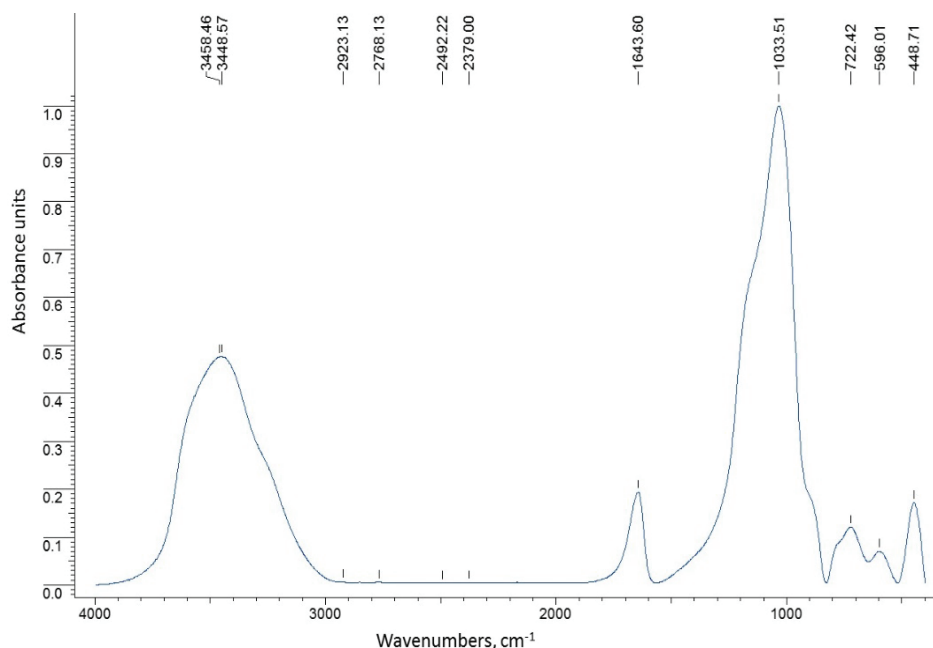


Fig. 2. FT-IR spectra of Crystal-Right™ CR100 commercial zeolite

According with literature (Breck, 1974; Korkuna et al., 2006; Qin et al., 2010a; Loiola et al., 2012; Sivasankar and Ramachandramoorthy, 2011), the bands at 1200 – 450 cm^{-1} are known to be assigned to Si–O–Al, Si–O–Si, Si–O, and Al–O species. The most well pronounced band in the spectrum is the one present at 1033 cm^{-1} , being attributed to the asymmetric vibrations of the SiO_4 tetrahedral structure or to the Si–O bonds.

We can detect a small peak at 1643 cm^{-1} together with the 3448 cm^{-1} peak which is a harmonic (overtone) attributed characteristic the HO bonds. This evolution is due to the formation of hydrogen bonds, which confirm some molecules of water are kept in the cages and channels inside the zeolite

structure. The peaks at 596 and 722 cm^{-1} are of Al–OH translation type. The peak at 448 cm^{-1} is attributed to Al–O type bonds.

2.2. Batch sorption experiments

All the experiments were realised using the Crystal-Right™ CR100 zeolite in the delivery form, according to the instructions provided by their producers. The data interpreting and analysis is always reported to the dry state of the zeolite. The equilibrium sorption capacity of the zeolite of the calcium cations used to express the zeolite performance was evaluated in batch technique at contact time equal with 24 hours, from the point of

view of the following sorption process specific experimental factors: temperature and concentration of calcium cations in the aqueous solutions to be treated. Sorption results show that a 24 hours equilibrium-period was sufficient to establish steady state or equilibrium.

The experiments for equilibrium sorption of calcium cations from calcium chloride solution were performed at constant zeolite amount of 8 g/L and various initial calcium concentrations between 44.5 to 230.5 mg Ca²⁺/L, corresponding to moderate hard and hard waters. The optimum zeolite dose equal with 8 g/L was selected based on the preliminary studies and was maintained in all experiments. During all the experiments at constant pH 6.75, the value was adjusted as it was varying more than ± 0.1 unit by small addition of 0.1 M NaOH aqueous solution. Erlenmeyer flasks were used for the 50 mL CaCl₂ solution and the zeolite dose. All flasks were kept under agitation at a constant speed of 100 rpm. The effect of temperature on the calcium cations sorption was investigated at different value of temperature: 278, 298, 313 and 338 K with ± 1 K. The initial and final calcium cations concentrations analysis was performed using the EDTA method (SR ISO 6058, 2008). An automatic titrator and specific titration end-point indicators for water hardness analysis from Hach Company were used. The indicator used in experiments is based on Murexide, specially modified to facilitate the highlighting of equivalence point, both in low and high concentrations calcium range. All the experimental solutions were prepared using analytical grade reagents from Merck or Sigma Aldrich dissolved in ultrapure water.

The performance of the sorbent usually means its uptake capacity (Volesky, 2003). The amount of calcium cations sorbed at equilibrium by the zeolite (equilibrium sorption capacity in mg/g – q_e) was calculated according to Eq. (2).

$$q_e = \frac{(C_0 - C_e) \cdot V_{sol}}{m_{zeo}} \quad (2)$$

The softening process efficiency was qualitatively evaluated by using the calcium sorption degree, R (%), calculated with the Eq. (3), where C_0 is the initial calcium concentration of CaCl₂ solution (mg/L); C_e is the equilibrium calcium concentration (mg/L); V_{sol} is the volume of solution to be softened (L); m_{zeo} is the weight of the zeolite used in the experiment in dry state, (g).

$$R = \frac{C_0 - C_e}{C_0} \quad (3)$$

2.2. Equilibrium isotherms

The equilibrium performances of the *Cristal-RightTM CR100* zeolite for sorption of calcium cations were investigated using the isotherm (equilibrium

sorption capacity versus equilibrium concentration of calcium cations in calcium chloride solution). The most common isotherms frequently used in literature for sorption equilibrium are the Langmuir, Freundlich and Dubinin-Radushkevich models (Foo and Hammed, 2010; Volesky, 2003).

The experimental data were fitted to the Langmuir, Freundlich and Dubinin-Radushkevich isotherms calculated by linear regression to obtain the characteristic parameters of each model.

The Langmuir isotherm model is based on the monolayer sorption onto homogeneous surface. This model assumed that adsorption forces are similar to the forces in chemical interactions, and can be used to estimate the maximum sorption capacity (q_{max} , mg/g), upon complete saturation of the adsorbent surface. The empirical Freundlich model which indicates the surface heterogeneity of the adsorbent, was chosen to estimate the sorption intensity of the adsorbate towards adsorbent. The Dubinin-Radushkevich isotherm model, which is based on the Polanyi theory, is more general than the Langmuir isotherm, because it does not assume a homogeneous surface or constant sorption potential. It is used to estimate the apparent free energy of adsorption as well as to make a difference between physical and chemical adsorption process (Douglas et al., 2008; Foo and Hammed, 2010; Volesky, 2003).

Langmuir, Freundlich and Dubinin-Radushkevich isotherm models can be expressed by Eqs. (4-6), respectively, where q_e represents a maximum amount of the calcium cations at the equilibrium per unit weight of the zeolite to form a complete monolayer on the surface bound at high (mg/g, or mol/g); q_{max} is the practical limiting sorption capacity when the surface is fully covered with calcium and assists in the comparison of sorption performance, particularly in cases where the zeolite did not reach its full saturation in experiments (mg/g or mol/g); C_e is the equilibrium calcium concentration (mg/L); K_L is the Langmuir isotherm constant (L/mg) related to the affinity of the binding sites; K_F is the Freundlich constant is an indicator of the sorption capacity (mg/g); n represents a constant that characterizes the affinity of the calcium for the zeolite; β is a constant related to the sorption energy (mol²/J²); ε is the Polanyi potential, calculated according to Eq. (7) (where R is the universal gas constant, (8.314 J/mol K) and T is temperature (K)).

$$q_e = q_{max} \frac{K_L C_e}{1 + K_L C_e} \quad (\text{mg/g}) \quad (4)$$

$$q_e = K_F (C_e)^{1/n} \quad (\text{mg/g}) \quad (5)$$

$$q_e = q_{max} \cdot \exp(-\beta \cdot \varepsilon^2) \quad (\text{mol/g}) \quad (6)$$

$$\varepsilon = RT \ln \left(1 + \frac{1}{C_e} \right) \quad (7)$$

For determining the best-fitting isotherms the linear regression is frequently used. The linear least-squares method with linearly transformed isotherm equations has also been widely applied to confirm experimental data and isotherms using coefficients of determination (Douglas et al., 2008; Foo and Hammed, 2010; Volesky, 2003). The linearized forms of Langmuir, Freundlich and Dubinin-Radushkevich nonlinear equations are given by Eqs. (8 – 10).

$$\frac{1}{q_e} = \frac{1}{q_{max}} + \frac{1}{q_{max}K_L} \cdot \frac{1}{C_e} \quad (8)$$

$$\lg q_e = \lg K_F + \frac{1}{n} \lg C_e \quad (9)$$

$$\ln q_e = \ln q_{max} - \beta \cdot \varepsilon^2 \quad (10)$$

3. Results and discussion

3.1. Effect of initial calcium concentration and temperature on the sorption capacity of calcium cations

The equilibrium sorption process is a function of temperature and calcium concentration of initial solution. Equilibrium sorption capacity of calcium cations on Crystal-Right™ CR100 zeolite were investigated out by varying the initial concentration of the calcium from 44.5 to 230.5 mg/L at different sorption temperatures of 278, 298, 318 and 333 K. The experimental data showed that the equilibrium sorption capacity of zeolite increased with the increase of temperature and initial calcium cations concentration (Fig. 3), thereby indicating the process to be endothermic.

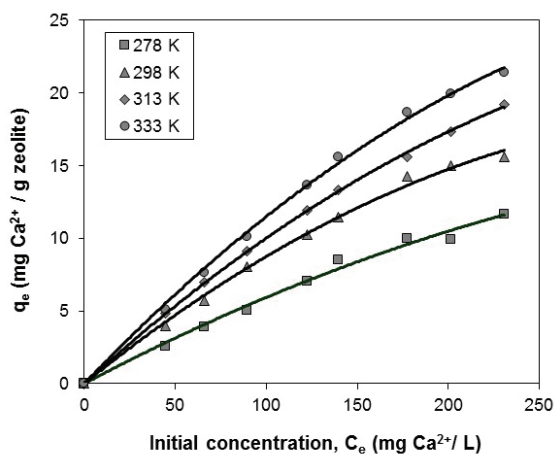


Fig. 3. Effect of initial concentration on the sorption equilibrium onto Crystal-Right™ CR100 zeolite at different temperatures (pH = 6.75, $m_{zeo} = 8$ g/L, time = 24 hours)

This behaviour is explained in literature by the migration of calcium cations from the external surface to the internal micro-phase of the zeolite

within a given contact time and at higher initial concentration (Bulgariu et al., 2012; Ceica et al., 2011; Sepehr et al., 2013).

The calcium cations could exchange with sodium cations not only on the surface of the zeolite but also on the internal surface of the zeolite. This suggests that zeolite has strong calcium sorption ability at higher temperature. At higher temperature, calcium cations are moving faster and cations become smaller because solvation is reduced. This reduction effect allows cations to diffuse in the inner part of the pore system of the zeolite. Increasing the temperature may produce a swelling effect within the internal structure of zeolite enabling calcium cations to penetrate further.

3.2. Calcium sorption isotherms

The sorption isotherms of calcium cations on Crystal-Right™ CR100 zeolite were plotted between the equilibrium sorption capacity (q_e , mg/g) and the amount of calcium cations left in equilibrium solution, C_e (mg/L) at different temperature (Fig. 4). As can be seen from Fig. 4 the isotherms are regular, positive, and concave to the concentration axis. The temperature increase was observed to occur in two stages. The sorption equilibrium occurs rapidly at lower calcium concentration, for all studied temperatures and becomes relatively constant at higher concentrations. On the basis of these considerations, the studied resin could be efficiently used at ambient temperature, avoiding the high temperatures, which are not economically justified.

The performances of the Crystal-Right™ CR100 zeolite at the equilibrium and isotherm parameters were evaluated using Langmuir, Freundlich and Dubinin–Radushkevich models.

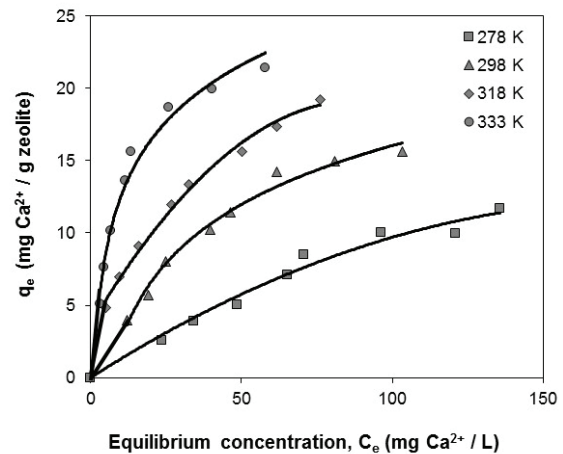


Fig. 4. Effect of temperature on the calcium sorption isotherm on Crystal-Right™ CR100 zeolite (pH = 6.75, $m_{zeo} = 8$ g/L, 298 K; time = 24 hours)

These isotherms are useful tools for describing the distribution of calcium cations (sorbate species) between the zeolite and the batching calcium chloride solution. The Langmuir, Freundlich and Dubinin–Radushkevich isotherms for the

sorption of calcium cations of calcium chloride solution are illustrated in Fig. 5.

The straight lines obtained for the three isotherms indicate that the sorption of both cations fit with the three investigated isotherms models. The value of three isotherm parameters and the correlation coefficient were calculated from the slope and the intercept of the linear plots: $1/q_e$ vs. $1/C_e$ (for Langmuir model – Fig. 5a), $\lg q_e$ vs. $\lg C_e$ (for Freundlich model– Fig. 5b) and $\ln q_e$ vs. ϵ^2 (for Dubinin–Radushkevich model – Fig. 5c).

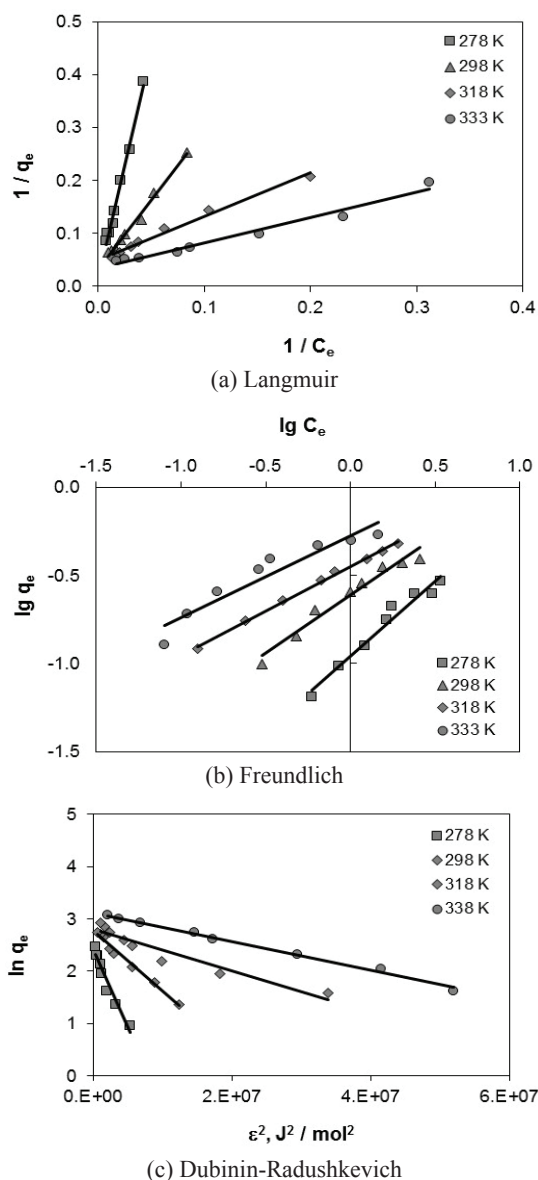


Fig. 5. The linearized Langmuir (a), Freundlich (b) and Dubinin-Radushkevich (c) isotherm of calcium onto *Crystal-Right™ CR100* zeolite at different temperatures (pH = 6.75; $m_{zeo} = 8$ g/L; time = 24 hours)

The corresponding Langmuir, Freundlich and Dubinin–Radushkevich parameters along with correlation coefficients are given in Table 2. The best-fit equilibrium model was established based on the linear regression correlation coefficients (R^2). The Langmuir model fitted the data ($R^2 = 0.97 -$

0.99) better than the Freundlich model ($R^2 = 0.90 - 0.99$) and Dubinin–Radushkevich model ($R^2 = 0.94 - 0.96$).

The simple Langmuir isotherm equation for adsorption of a single adsorbate on a single-site surface is still frequently applied to sorption process. The essential features of a Langmuir isotherm can be expressed in terms of a dimensionless constant separation factor or equilibrium parameter (Foo and Hammed, 2010; Volesky, 2003), that is used to predict if an sorption system is favourable ($0 < R_L < 1$) or unfavourable ($R_L > 1$), linear ($R_L = 1$) or irreversible ($R_L = 0$). The separation factor, R_L is calculated by Eq. (11), where C_0 is initial concentration (mg/L), K_L is Langmuir constant (L/mg).

$$R_L = \frac{1}{1 + K_L \cdot C_0} \quad (11)$$

For the temperature range studied, all R_L values obtained using Eq. (11) are given in Fig. 6. The R_L value indicate that sorption of calcium cations onto *Crystal-Right™ CR100* zeolite is more favourable for the higher initial calcium ion concentrations than for the lower ones.

A plot of $\lg q_e$ in function of $\lg C_e$, yielding a straight line, indicated the confirmation of the Freundlich sorption isotherm. Although the Langmuir and Freundlich constants q_{max} and K_F have different meanings, they led to the same conclusion about the correlation of the experimental data with the sorption model. The Langmuir isotherm assumes sorption free energy independent of both the surface coverage and the formation of monolayer whereas the solid surface reaches saturation while the Freundlich isotherm does not predict saturation of the solid surface by the sorbate, and therefore, the surface coverage being mathematically unlimited.

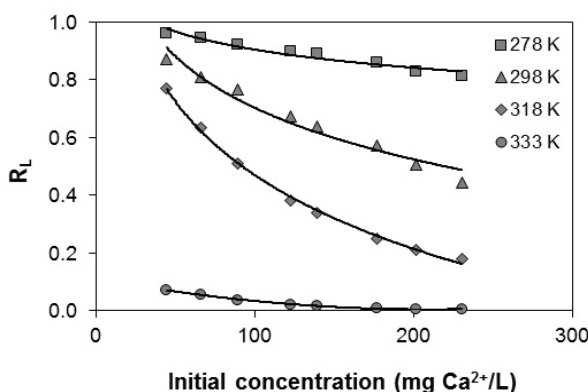


Fig. 6. Plot of dimensionless constant separation factor R_L against initial calcium ion concentration (pH = 6.75; $m_{zeo} = 8$ g/L; time = 24 hours)

For example, the experimental results for 298 K of Langmuir model indicate the monolayer sorption capacity value q_{max} of 31.447 mg/g zeolite and constant related to the energy of sorption value K_L of 0.0121 L/mg, whereas the Freundlich model indicate the relative sorption capacity K_F of 1.5361 mg/g with the sorption intensity n of 1.5361.

Table 2. Isotherm sorption parameters for removal of calcium cations from aqueous solution onto *Crystal-Right™ CR100 zeolite* (pH = 6.75; $m_{zeo} = 8$ g/L; time = 24 hours)

| Isotherm | Parameters | Temperature, K | | | |
|----------------------|---|----------------------|---------|--------|--------|
| | | 278 | 298 | 318 | 338 |
| Langmuir | q_{max} , mg/g | 68.0272 | 31.447 | 20.284 | 30.303 |
| | K_L , L/mg | 0.00171 | 0.0121 | 0.0598 | 0.0687 |
| | R^2 | 0.9883 | 0.9906 | 0.9840 | 0.9730 |
| | S_0 , m ² /g | 31.534 | 14.5772 | 9.399 | 14.014 |
| Freundlich | K_f , mg/g | 0.1099 | 0.2442 | 0.3475 | 0.5320 |
| | n | 1.1724 | 1.5361 | 2.0597 | 2.1542 |
| | R^2 | 0.9654 | 0.9487 | 0.9894 | 0.9058 |
| Dubinin–Radushkevich | q_{max} , mg/g | 11.003 | 15.991 | 16.425 | 22.594 |
| | β , mol ² /kJ ² | $2.98 \cdot 10^{-3}$ | 0.1166 | 0.0400 | 0.0276 |
| | E , kJ/mol | 0.0130 | 2.0712 | 3.5338 | 4.2530 |
| | R^2 | 0.9559 | 0.9633 | 0.9401 | 0.9581 |

However, the value of sorption intensity of calcium cations on zeolite surface is greater than 1.0 at temperatures above 298 K, indicating that calcium ion is favourable adsorbed by zeolite, even at higher calcium concentration.

Fig. 7 shows plots comparing the experimental data with theoretical Langmuir isotherm and empirical Freundlich isotherm. The equation shows an excellent fit with the experimental data for the Langmuir isotherm. Assumption of a value for the surface area covered per molecule (plateau on each isotherm) could allow computation of the active specific surface area of the sorbent using Avogadro's number (Volesky, 2003).

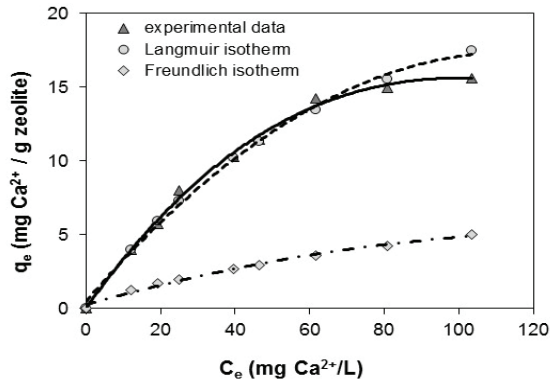


Fig. 7. Isotherm of calcium cations sorbed on *Crystal-Right™ CR100 zeolite* (pH = 6.75; $m_{zeo} = 8$ g/L; time = 24 hours, temperature = 298 K)

For the ultimate sorptive capacity (q_{max}) when the zeolite surface is fully covered with calcium cations (corresponds to monolayer coverage), can be calculated the specific surface area occupied by calcium cations (S_0 in m²/g zeolite) using Eq. (12), where q_{max} is monolayer sorption capacity (g/g); N is Avogadro number ($6,023 \cdot 10^{23}$); A is cross sectional area of calcium ion (m²); M is molecular weight of calcium ion (g/mol). For calcium ion, the molecular weight is 40 g/mol and the cross sectional area have been determined to 3.08 Å² (radius is 0.99 Å, Cruceanu et al., 1986) in a close packed monolayer.

The results are shown in Table 2. The magnitude of sorption energy (E) determined in the Dubinin-Radushkevich equation can be related to the nature of the sorption mechanism in this system (Foo and Hammed, 2010).

$$S = q_{max} \frac{N \cdot A}{M} = q_{max} \frac{N \cdot (\pi r_{Ca}^2)}{M} \quad (12)$$

The mean free energy of sorption (E), is defined as the free energy change when one mole of ion is transferred to the surface of the solid from infinity in the solution, and was calculated from the constant related to the sorption energy value (β) using the Eq. (13):

$$E = (-2\beta)^{-1/2} \quad (13)$$

According with literature (Cruceanu et al., 1986; Zagorodni, 2007) the magnitude of E gives the information about the type of sorption process: physical (< 8 kJ/mol), ion exchange (8 – 16 kJ/mol) and chemical (> 16 kJ/mol). For present experimental data, the values of mean free energy, E , of calcium sorption decrease in the range 0.1166 to 0.0276 kJ/mol with increasing temperature from 298 K to 333 K. These values indicate that the physical forces may affect the sorption mechanism and calcium cations sorption of *Crystal-Right™ CR100 zeolite* could be considered physisorption in nature.

3.3. Thermodynamic parameters

Based on the sorption constant K_L in the Langmuir isotherm (Volesky, 2003), thermodynamic parameters (ΔG^0 – free Gibbs energy, ΔH^0 – standard enthalpy and ΔS^0 – standard entropy) changes were also calculated using Eqs. (14 – 16), where R is the gas constant and T is the absolute temperature. The plot of $\ln K_L$ vs. $1/T$ gives the straight line from which ΔH^0 and ΔS^0 was calculated from the slope and intercept of the linearised form.

$$\Delta G^0 = -RT \cdot \ln K_L \quad (14)$$

$$\ln K_L = \frac{\Delta S^0}{R} - \frac{\Delta H^0}{R} \cdot \frac{1}{T} \quad (15)$$

$$\Delta S^0 = \frac{\Delta H^0 - \Delta G^0}{T} \quad (16)$$

Table 3 shows the values of thermodynamic parameters of calcium cations sorption onto *Crystal-Right™ CR100* zeolite.

Table 3. Thermodynamic parameters of calcium sorption onto *Crystal-Right™ CR100* zeolite (pH = 6.75; $m_{zeo} = 8$ g/L; time = 24 hours)

| Temperature, K | ΔG^0 , kJ/mol | ΔH^0 , kJ/mol | ΔS^0 , J/mol.K |
|-------------------|--------------------------|--------------------------|---------------------------|
| 278 | 1.986 | 54.184 | 187.764 |
| 298 | -1.770 | | |
| 318 | -5.525 | | |
| 333 | -8.341 | | |

As seen that of low temperature below 278 K the sorption process of calcium cations is not spontaneous. For range of temperature 298 – 333 K, the sorption is spontaneous with the negative values of ΔG^0 . It was also observed that with increase in temperature ΔG^0 became more negative, which justify that sorption is favoured by an increasing temperature. The positive value of ΔH^0 for the sorption of calcium cations on zeolite indicates that the process is endothermic in nature. The positive ΔS^0 value corresponds to an increase disorder at the zeolite – calcium solution interface during the sorption of calcium cations. The positive value of the ΔS^0 indicates the partial dehydration of the calcium cations before sorption, thus increasing the spontaneity.

The sorption increases randomness at the zeolite/solution interface with some structural changes in the zeolite and calcium cations and an affinity of the zeolite.

4. Conclusions

In this study were investigated of the performances of *Crystal-Right™ CR100* zeolite to calcium cations form calcium chloride solution at equilibrium at temperatures of 278, 298, 318 and 338 K. The equilibrium sorption study is important for an estimation of the practical sorption capacity and optimization of the design of water softening process. The *Crystal-Right™ CR100* zeolite presents a good equilibrium sorption capacity for calcium cations for the experimental conditions.

The equilibrium sorption study increased with initial calcium cations concentration of solution and temperature increased. For example, at initial concentration of calcium cations equal with 139.478 mg/L (equivalent with 19 degree German), the

experimental equilibrium sorption capacity are respectively: 8.492 mg/g for 278 K (R = 49.43 %), 11.426 mg/g for 298 K (R = 66.67 %), 13.323 mg/g for 318 K (R = 76.72 %) and 15.607 mg/g for 333 K (R = 90.34 %).

The equilibrium and thermodynamic studies show that the sorption of calcium cations is feasible at ambient temperature when the process is endothermic ($\Delta H^0 > 0$) and is spontaneous ($\Delta G^0 < 0$). The equilibrium $q_e - C_e$ data have been analysed against Langmuir, Freundlich and Dubinin-Radushkevich models and the characteristic parameters for each isotherm have been determined. The results from this study indicated that the sorption described by the theoretical Langmuir isotherm.

The correlation coefficients for fitting the Langmuir model were significantly better than the coefficients for Freundlich or Dubinin-Radushkevich models. The energy of activation for calcium sorption to zeolite is lower and takes place predominantly by physical sorption mechanism. This finding suggests a better orientation of calcium cations to zeolite surface.

Acknowledgments

This research was supported by the project “*Knowledge provocation and development through doctoral research PRO-DOCT*”, project co-funded by the European Social Fund in Romania, under the responsibility of the Managing Authority for the Sectorial Operational Programme for Human Resources (no. POSDRU/88/1.5/S/52946).

References

- Al-Anber M., Al-Anber Z.A., (2008), Utilization of natural zeolite as ion-exchange and sorbent material in the removal of iron, *Desalination*, **225**, 70–81.
- Arrigo I., Catalfamo P., Cavallari L., Di Pasquale S., (2007), Use of zeolitized pumice waste as a water softening agent, *Journal of Hazardous Materials*, **147**, 513–517.
- Baskan M.B., Pala A., (2011), Removal of arsenic from drinking water using modified natural zeolite, *Desalination*, **281**, 396–403.
- Bandrabur B., Lazăr L., Tataru-Fărnuș R.-E., Bulgariu L., Gutt G., (2012), Permanent hard water softening using different cation exchange resins, *Bulletin of the Polytechnic Institute of Iasi, Section Chemistry and Chemical Engineering*, **58**, 141–150.
- Breck D.W., (1974), *Zeolite Molecular Sieves – Structure Chemistry and Use*, Wiley Interscience, New York.
- Bulgariu L., Ceica A., Lazar L., Crețescu I., Balasanian I., (2012), Equilibrium and kinetics study of nitrate removal from water by Purolite A520-E resin, *Environmental Engineering and Management Journal*, **11**, 37–45.
- Ceica A., Bulgariu L., Lazar L., Crețescu I., Balasanian I., (2011), Influence of parameters to nitrate removal from water by Purolite A-520E, *Environmental Engineering and Management Journal*, **10**, 1553–1559.
- Cinar S., Beler-Baykal B., (2005), Ion exchange with natural zeolites: an alternative for water softening?, *Water Science and Technology*, **51**, 71–77.
- Coker E.N., Rees L.V.C., (2005), Kinetics of ion exchange in quasi-crystalline aluminosilicate zeolite precursors,

- Microporous and Mesoporous Materials*, **84**, 171–178.
- Cruceanu M., Popovici E., Balba N., Naum N., Vladescu L., Russu R., Vasile A., (1986), *Zeolite Molecular Sieves*, Scientific and Encyclopedic Publishing House, Bucharest, Romania.
- Douglas LeVan M., Carta G., Yon C.M., (2008), *Adsorption and Ion Exchange*, In: *Perry's Chemical Engineers' Handbook*, 8th Edition, Perry R.H., Green D.N. (Eds.), McGraw-Hill Companies, Inc., New York, 16:1 – 16:16.
- Doula M.K., (2009), Simultaneous removal of Cu, Mn and Zn from drinking water with the use of clinoptilolite and its Fe-modified form, *Water Research*, **43**, 3659–3672.
- Foo K.Y., Hameed B.H., (2010), Insights into the modeling of adsorption isotherm systems – Review, *Chemical Engineering Journal*, **156**, 2–10.
- Górka A., Bochenek R., Warchoń J., Kaczmarski K., Antos D., (2008), Ion exchange kinetics in removal of small ions. Effect of salt concentration on inter- and intraparticle diffusion, *Chemical Engineering Science*, **63**, 637–650.
- Gray N.F., (2010), *Water Technology an Introduction for Environmental Scientists and Engineers*, Second Edition, Elsevier.
- Gruett K., (2003), *The art of zeolite application. A complete guide to zeolite use for a host of water treatment problems*, Water Technology, Applying Crystal-Right – Water Right, Inc., 1–5.
- Hoffmann H., Martinola F., (1988), Selective resins and special processes for softening water and solutions; A review, *Reactive Polymers, Ion Exchangers, Sorbents*, **7**, 263–272.
- Ibrahim H.S., Jamil T.S., Hegazy E.Z., (2010), Application of zeolite prepared from Egyptian kaolin for the removal of heavy metals: II. Isotherm models, *Journal of Hazardous Materials*, **182**, 842–847.
- Jamil T.S., Ibrahim H.S., Abd El-Maksoud I.H., El-Wakeel S.T., (2010), Application of zeolite prepared from Egyptian kaolin for removal of heavy metals: I. Optimum conditions, *Desalination*, **258**, 34–40.
- Korkuna O., Lebeda R., Skubiszewska-Zieba J., Vrublevsky`ka T., Gun'ko V.M., Ryczkowski J., (2006), Structural and physicochemical properties of natural zeolites: clinoptilolite and mordenite, *Microporous and Mesoporous Materials*, **87**, 243–254.
- Lazar L., Bandrabur B., Tataru-Fărnuș R.-E., Droboță M., Bulgariu L., Gutt G., (2014), FTIR analysis of ion exchange resins with application in permanent hard water softening, *Environmental Engineering and Management Journal*, **13**, 2145–2152.
- Loiola A.R., Andrade J.C.R.A., Sasaki J.M., Da Silva L.R.D., (2012), Structural analysis of zeolite NaA synthesized by a cost-effective hydrothermal method using kaolin and its use as water softener, *Journal of Colloid and Interface Science*, **367**, 34–39.
- Lühns H., Derr J., Fischer R.X., (2012), K and Ca exchange behavior of zeolite A, *Microporous and Mesoporous Materials*, **151**, 457–465.
- Nibou D., Mekatel H., Amokrane S., Barkat M., Trari M., (2010), Adsorption of Zn²⁺ ions onto NaA and NaX zeolites: Kinetic, equilibrium and thermodynamic studies, *Journal of Hazardous Materials*, **173**, 637–646.
- Noroozifar M., Khorasani-Motlagh M., Naderpour H., (2014), Modified nanocrystalline natural zeolite for adsorption of arsenate from wastewater: Isotherm and kinetic studies, *Microporous and Mesoporous Materials*, **197**, 101–108.
- Ören A.H., Kaya A., (2006), Factors affecting adsorption characteristics of Zn²⁺ on two natural zeolites, *Journal of Hazardous Materials*, **131**, 59–65.
- Qin C., Wang R., Ma W., (2010a), Characteristics of calcium adsorption by Ca-Selectivity zeolite in fixed-pH and in a range of pH, *Chemical Engineering Journal*, **156**, 540–545.
- Qin C., Wang R., Ma W., (2010b), Adsorption kinetic studies of calcium ions onto Ca-Selective zeolite, *Desalination*, **259**, 156–160.
- Sepehr M.N., Zarrabi M., Kazemian H., Amrane A., Yaghmaian K., Ghaffari H.R., (2013), Removal of hardness agents, calcium and magnesium, by natural and alkaline modified pumice stones in single and binary system, *Applied Surface Science*, **274**, 295–305.
- Shahwan T., Akar D., Eroğlu A.E., (2005), Physicochemical characterization of the retardation of aqueous Cs⁺ ions by natural kaolinite and clinoptilolite minerals, *Journal of Colloid and Interface Science*, **285**, 9–17.
- Shoumkova A., (2011), Zeolites for water and wastewater treatment: An overview, *Research Bulletin of the Australian Institute of High Energetic Materials, Special Issue on Global Fresh Water Shortage*, **2**, 10–70.
- Sivasankar V., Ramachandramoorthy T., (2011), Water softening behaviour of sand materials – Mimicking natural zeolites in some locations of Rameswaram Island, India, *Chemical Engineering Journal*, **171**, 24–32.
- Smith R., Kim J.K., Kleme J., (2008), *Handbook of Water and Energy Management in Food Processing*, Hardcover, Woodhead Publishing Ltd.
- SR ISO 6058, (2008), Water quality – Determination of calcium content – EDTA titrimetric method, ASRO, Bucharest, Romania.
- Ștefanache A., Mihăilescu E., Stan C., (2015), Forecasting the presence of Ca²⁺ and Mg²⁺ cations in mineral waters. A model based on fuzzy logic, *Environmental Engineering and Management Journal*, **14**, 223–232.
- Volesky B., (2003), *Sorption and Biosorption*, Bv Sorbex, Inc., Canada.
- Wang S., Peng Y., (2010), Natural zeolites as effective adsorbents in water and wastewater treatment, *Chemical Engineering Journal*, **156**, 11–24.
- Xue Z., Li Z., Ma J., Bai X., Kang Y., Hao W., Li R., (2014), Effective removal of Mg²⁺ and Ca²⁺ ions by mesoporous LTA zeolite, *Desalination*, **341**, 10–18.
- Zagorodni A.-A., (2007), *Ion Exchange Materials: Properties and Applications*, Elsevier Science, Oxford, UK.
- Zhao H., Vance G.F., Urynowicz M.A., Gregory R.W., (2009), Integrated treatment process using a natural wyoming clinoptilolite for remediating produced waters from coal bed natural gas operations, *Applied Clay Science*, **42**, 379–385.



"Gheorghe Asachi" Technical University of Iasi, Romania



ADSORPTION OF ENDOCRINE DISRUPTORS ON EXFOLIATED GRAPHENE NANOPATELETS

Elena Radu¹, Alina Catrinel Ion^{2*}, Florinela Sirbu³, Ion Ion²

¹National Research & Development Institute for Chemistry and Petrochemistry ICECHIM,
202 Splaiul Independentei Str., 060021 Bucharest, Romania

²University POLITEHNICA of Bucharest, 313 Splaiul Independentei Str., 060042 Bucharest, Romania

³"Ilie Murgulescu" Institute of Physical Chemistry of Romanian Academy,
202 Splaiul Independentei Str., 060021 Bucharest, Romania

Abstract

Drinking water treatment using activated carbon (AC) decontamination offers effective methods for removing some organic compounds, tastes and odors, but it is not so efficient for metals, nitrates, microbial contaminants and other organic and inorganic contaminants. In the last years, nanotechnologies introduced several types of nanomaterials for organic, inorganic and biological removal of contaminants in drinking water, such as: sorption, filtrations and catalytic processes. In this work, exfoliated graphite nanoplatelets (xGnP) were used as bisphenol A (BPA) adsorbents, their potential of removing this endocrine disruptor being investigated. The effect of the following parameters such as: contact time, initial BPA concentration, temperature, ionic strength and pH over the sorption behavior of xGnP was studied. In these experiments, it was found that the maximum adsorption capacity of xGnP at 298.15 K is 850 mg/g and the adsorption process most closely fits to the Langmuir isotherm. The results also showed a decrease in the affinity of BPA molecule for the xGnP binding sites by increasing the temperature.

Key words: decontamination, endocrine disruptor, exfoliated graphite nanoplatelets, sorption

Received: November, 2014; Revised final: March, 2015; Accepted: March, 2015

1. Introduction

In water purification, high adsorption capacity of the adsorbents is mandatory. Based on this, the lifetime of the system was observed to be substantially improved (Pan et al., 2010). Carbon based nanomaterials can offer promising applications in drinking water treatment, extensive reviews on the adsorption of metal contaminants, organics and biological contaminants already existing in the literature.

Several studies present Carbon Nanotubes (CNTs) as adsorbents for organic chemicals in water treatment by comparison with activated carbon (Su and Lu, 2007; Wang et al., 2008), the understanding of organic chemical-CNT interactions providing important information on their possible applications

and environmental risks. Organizing individual nanotubes into hierarchical structures represents a new strategy to scale up nanomaterials for macroscopic engineering applications. These structures are more effectively separated from water using gravitational sedimentation, magnetic attraction, and membrane filtration while having the ability to perform adsorption, disinfection, and catalytic degradation of contaminants (Pyrzynska et al., 2007).

The researchers showed that these hierarchical structures are as good as CNTs for removing contaminants from water as adsorbents, disinfectants, and catalyst and they can be separated more effectively using common techniques such as gravitational sedimentation, magnetic attraction, and membrane filtration. For water purification, the

* Author to whom all correspondence should be addressed: e-mail: ac_ion@yahoo.com; Phone: +40723295334; Fax: +40214023904

challenge is how to connect these two worlds (nanotechnology and water chemistry) on the dimension ladder.

Since its discovery, graphene has become a spotlight nanomaterial. In the last few years, there are investigations focused on the applications of graphene, pristine, functionalized, or composites in removal different water pollutants (Wang et al., 2013), due to its flexibility in introducing functional groups and to its easy operation (Ji et al., 2009; Maliyekkal et al., 2013; Pavaghadi et al., 2013).

Endocrine disruptors as environmental contaminants can generate severe health risks (Shi et al., 2013). Among them, bisphenol A (BPA; 2, 2-bis(4-hydroxyphenyl)propane) is an organic compound present in food containers, industrially used in the production of polycarbonates. It can be discharged as a waste product into the water system, ground, surface and drinking water (Santhi et al., 2012). BPA is an endocrine disruptor, the risks of BPA pollution leading to obligatory control and detection of BPA in the environment (EU, 2011). It is an endocrine disruptor linked to prostate cancer, obesity and hypertension (Vandenberg et al., 2007).

Exfoliated graphite nanoplatelets (xGnP) represent a new effective adsorbent material with high adsorption capacity, good stability and fast adsorption, with thicknesses of the platelets in the nano range, but areas in the micrometer range (Ion et al., 2011a, 2011b). Additionally, xGnP can be easily obtained from cheap, natural graphite, in large quantities, without any need for dimensional increasing for their use in water purification. These materials are less expensive than CNTs, possible to be incorporated into water treatment processes and facile to remove or to regenerate after. There were several computational studies on the interaction energies of systems formed upon the adsorption of BPA on single-walled carbon nanotubes (SWCNTs) and graphene (Zaib et al., 2012).

Various models have been used to explain the adsorption of organic molecules on carbon based nanomaterials, such as Freundlich (Agnihotri et al., 2005; Liu et al., 2004; Pyrzyńska et al., 2007), Langmuir (Brichka et al., 2006; Lu et al., 2007) and Polanyi-Manes (Yang et al., 2006; Yan et al., 2008) models, all suggesting a heterogeneous adsorption. Multilayer adsorption occurs when organic chemicals are adsorbed on carbon based materials surfaces, the first layers interacting with the surface and other molecules interact with each other (Gotovac et al., 2006, 2007). These factors indicate distributed adsorption energy of adsorption sites and a possible

concentration - dependent thermodynamics in aqueous solutions (Agnihotri et al., 2008). Recently, Xu et al. (2012) used graphene for removing BPA from water, obtaining better adsorption capacities in comparison with modified carbon nanotubes and porous carbon.

Different mechanisms have been proposed to explain the interactions between organic chemicals and carbon-based nanomaterials, like π - π interactions between the surface and organic molecules with C=C double bonds or benzene rings, hydrogen bonds and electrostatic interactions (Chen et al., 2008; Lin and Xing, 2008). It must be also emphasized that the change of environmental conditions affects the contribution of each individual mechanism over the overall adsorption of the organic chemicals. Several analyses led to the proposal of an adsorption mechanism for BPA on graphene involving π - π electron coupling between the π -electrons of the benzene rings of BPA and graphene and the hydrogen bond interactions between the hydroxyl groups of BPA and the functional groups on the graphene surface.

In this work, exfoliated graphite nanoplatelets (xGnP) were used as BPA adsorbents, their potential of removing this endocrine disruptor being investigated. The effect of several parameters such as: contact time, initial BPA concentration, temperature, ionic strength and pH of the batch sorption solutions were studied, various isotherm equations being used to assess the best isotherm equation which represents the correlation of the experimental data.

2. Experimental

2.1. Chemicals

Commercial exfoliated graphite nanoplatelets (xGnP) were purchased as powder from XG Sciences, Inc, Michigan, US. xGnP (with average diameter of 15 μ m and average length < 0.01 μ m) were provided from XG Sciences, Inc. East Lansing, MI 48823. Detailed information on fabrication, geometrical and surface characteristics of this material can be found elsewhere (Kalaitzidou et al., 2007). Bisphenol A (BPA) >99.9% purity, was purchased from Sigma, Germany and was dissolved in methanol for the stock solution (1000 mg/L), being further diluted with large amount of water till the required concentrations (Table1). All other chemicals were analytical reagent grade.

Table 1. Graphene-based materials as adsorbents for the removal of pollutants in water

| <i>Materials</i> | <i>Adsorbate</i> | <i>Adsorption capacity (mg/g)</i> | <i>References</i> |
|----------------------|------------------|-----------------------------------|---------------------|
| Graphene | Methylene blue | 153.85 | Liu et al. (2012) |
| Graphene | Bisphenol A | 182 | Xu et al. (2012) |
| Sulphonated graphene | 1-Naphthol | ~6.4 | Zhao et al. (2011a) |
| Sulphonated graphene | Naphthalene | ~297 | Zhao et al. (2011b) |

2.2. Methods

The chromatographic separation of bisphenol A was achieved at 25°C, using an Agilent 1100 series HPLC system with UV detection at variable wavelengths. A Kromasil 100-5C18 column 150 mm x 4.6 i.d., 5µm was used. BPA elution was carried out using a mobile phase consisting of 20% water and 80% methanol, using a flow rate of 0.5 mL/min. The column was equilibrated for 30 minutes before injection. The injected sample volume was 10 µL, and UV detection operates at 280 nm.

2.3. Adsorption procedure

Adsorption experiments were performed in sealed 100 ml bottles in an ultrasound bath (Elma P-30H Ultrasonic) operated at a 37 Hz frequency at 25°C. Each bottle contained between 0.1 and 0.5 mg graphene and 100 ml of 1-10 mg/L BPA. The concentration of BFA was measured after 30 minutes. The adsorption kinetic study was carried out at 1 mg L⁻¹ initial BPA concentration at three different temperatures: 293.15 K, 298.15 K and 303.15 K, pH 5.5-6.15 in order to determine the minimum time required to reach the adsorption equilibrium. The concentrations of BPA were measured at different time intervals from 10 to 80 minutes. The influence of the pH over the adsorption of BPA was studied at an initial BPA concentration of 1 mg L⁻¹ in a pH range of 2 to 10 at 298.15 K, adjusted with appropriate volumes of 0.1 M HCl or 0.1 M NaOH. The influence of ionic strength on the adsorption of BPA was studied by adding by adding NaCl to a 1 mgL⁻¹ BPA solution in a concentration range from 0.01 to 0.375 M at 298.15 K and pH 6.

After adsorption experiments, the suspensions were filtered through 0.45 µm membrane filters. The concentration of BPA was determined by a high-performance liquid chromatography (HPLC, Agilent Technologies Inc.) and a UV absorbance detector operated at 280 nm. The mobile phase was 0.5 mL/min of 80% methanol and 20% deionized water.

3. Results and discussion

3.1. Characterization of the nanomaterial

xGnP possesses the smallest particle size (X-Y dimension 2 micron, thickness 2 nm) and largest specific surface (720 m²/g), BET surface (771 m²/g), possibly due to dry powder aggregation. The particles are irregular in shape and planar with intermittent folds. Carbon sp² is the most abundant because of the conjugated π system, but carbon sp³ also exists due to the C-C bonds with incomplete benzene structures. There can be also present rests of hydroxyl, ether, carbonyl and carboxyl groups (Figs. 1-2). The tested nanomaterials were fully characterized by Vandenberg et al. (2007).

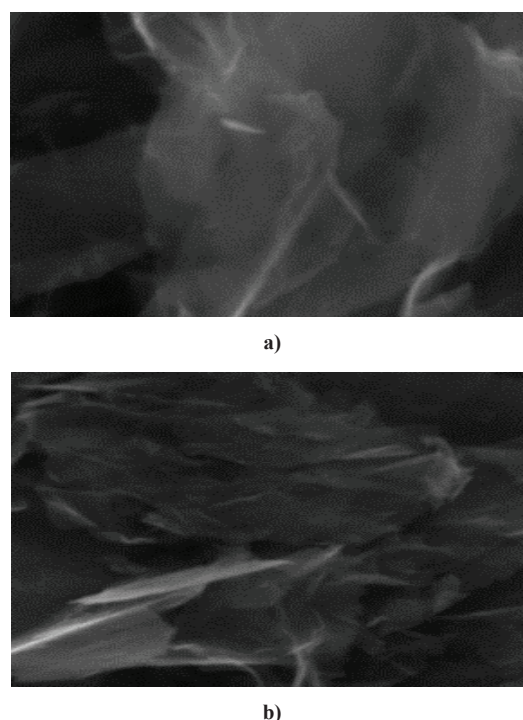


Fig. 1. Scanning electron microscopy (SEM) images of xGnP; a) as grown before adsorption; b) after adsorption of BPA

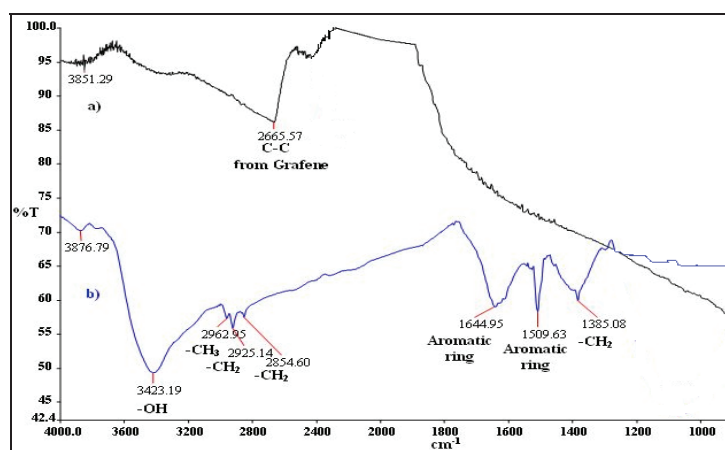


Fig. 2. FT-IR spectra; a) xGnP; b) xGnP after adsorption of BPA

3.2. BPA sorption kinetics

Pseudo-first and second order models and intraparticle diffusion one were used to test the experimental data in order to understand the kinetics of the adsorption process. The equations of these kinetic models are presented in Table 2. There were three configurations found on the physisorption of BPA on pristine graphene (Cortes-Arriagada et al., 2013).

Table 2. The equations of several kinetic models

| Kinetic Models | Functional Form |
|--|--------------------------------------|
| Lagergren model | $\frac{dq}{dt} = k(q_e - q_t)$ (1) |
| Kavitha and Namasivayam model | $q = k_i t^{1/2} + C$ (2) |
| Pseudo-second order model | $\frac{dq}{dt} = k(q_e - q_t)^2$ (3) |
| Variables in the kinetics equations: q_e - amount of solute adsorbed at equilibrium, (mg/g) q_t - amount of solute adsorbed at any given time t , (mg/g) C - concentration of sorbate in the solution at any given time t | |

In the first one, BPA interacts with the graphene bulk at a distance of 2.36 \AA , maximizing the π - π interactions with the phenol ring. In the second one the distance between the BPA and the graphene surface is of 2.76 \AA , the phenol ring being perpendicular to the surface and van der Waals interactions are reduced. In the third one, the distance between the BPA and graphene surface is of 2.69 \AA , while the angle between the phenols increased in comparison with the other two configurations. Here, the physisorption is increased, because it maximized the π - π stacking and the dispersion forces between adsorbent and adsorbate.

The effect of the contact time on the adsorption of BPA on xGnP is presented in Fig. 3. It was observed that the adsorption capacity increased in the first 30 minutes and then it decreased rapidly in the next 30 minutes.

Based on these results a contact time of 30 minutes was used in the experiments. The kinetic parameters are presented in Table 3. It can be observed that the experimental adsorption capacity $q_e \text{ exp}$ was in a better accordance with the calculated one based on the pseudo-second order model.

There are several mechanisms that govern the adsorption kinetics: external diffusion, boundary layer diffusion and intraparticle diffusion (Guibal et al., 2003), the last one being the most important limiting step of this process (Özkan and Özcan, 2005).

The lying-down configuration of BPA is conserved during the production step and it determines an increase in the adsorption energy, graphene being a strong electron acceptor, due to its large π system, favoring a configuration that allows the interaction with the negatively charged sites of BPA. In addition with the van der Waals interactions, charged controlled interactions contribute to the physisorption of BPA on graphene, the chemisorption being less important on pristine xGnP.

3.3. BPA sorption isotherms

Equilibrium data are necessary in developing an equation that models the results in order to design adsorption systems. In this study, Langmuir, Freundlich, Harkin-Jura and Temkin isotherms were used to describe equilibrium adsorption and are presented in Table 4.

The adsorption isotherm models are used to indicate the interactions between the adsorbate and the adsorbent when the adsorption process reaches equilibrium. In Fig. 4, there are presented the adsorption isotherms of BPA on xGnP at different temperatures, 293.15, 298.15, 303.15.

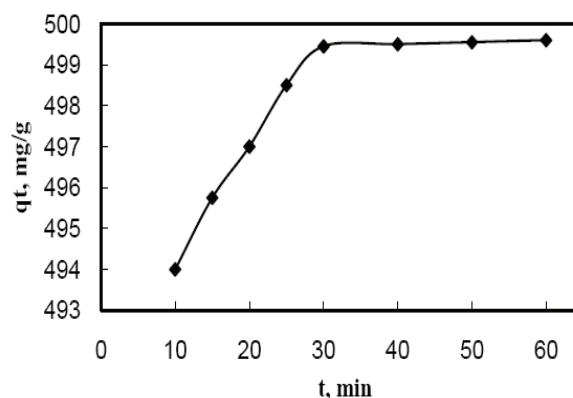


Fig. 3. Effect of contact time on the adsorption of BPA by xGnP (0.1 mg of xGnP and 50 mL of 1 mg/L BPA at 298.15 K, pH=5.5)

Table 3. Kinetic parameters for adsorption of BPA onto xGnP (1, 5, 10 mg/L)

| Model | Pseudo-first order | Pseudo-second order | Intra-particle diffusion |
|---|---|---------------------------------------|---------------------------------|
| Equation | $\log(q_e - q_t) = \log q_e - (k_1/2.303)t$ (4) | $t/q_t = (1/k_2 q_e^2) + (t/q_e)$ (5) | $q = k_i t^{1/2} + C$ (6) |
| $q_e \text{ exp (mg/g)}$ | 850 | 850 | 850 |
| $q_e \text{ (mg/g)}$ | 1071 | 725 | $C=7.25$ |
| $K, (g \text{ mg}^{-1} \text{ min}^{-1})$ | 0.049 | 0.024 | 10 |
| R^2 | 0.9878 | 0.9824 | 1 |

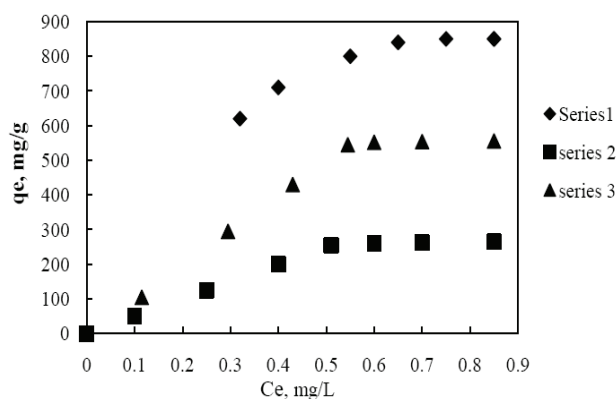


Fig. 4. Adsorption isotherms of BPA by xGnP at three different temperatures (0.1 mg of xGnP and 50 mL of 1-10 mg/L BPA at 293.15 K (■), 298.15 K (▲), 303.15 K (◆), pH=5.5, contact time 30 minutes)

Table 4. Functional equations of different sorption models used in this study

| Isotherm | Functional form |
|-------------|---|
| Freundlich | $q_e = K_F C_e^{1/n}$ (7) |
| Langmuir | $q_e = q_{\max} \frac{K_L C_e}{1 + K_L C_e}$ (8) |
| Temkin | $q_e = \frac{RT}{b} \ln(a C_e)$ (9) |
| Harkin-Jura | $1/q_e^2 = (A/B) - (1/A) \log C_e$ (10) |
| Halsey | $q_e = \left(\frac{K_H}{C_e}\right)^{1/n_H}$ (11) |

C_e – equilibrium concentration; C_s – adsorbate solubility at a given temperature; E_0 – solid characteristic energy towards a reference compound; q_e – adsorbed amount; q_{\max} – saturated monolayer sorption capacity; K_F – Freundlich constant, mg/g; $1/n$ – Freundlich constant indicating adsorption intensity; K_L – Langmuir constant, L/mg; a – Temkin constant, L/mg; b – Temkin constant related to adsorption heat; A , B – Harkins-Jura constants indicating the multilayer adsorption; K_H – Halsey constant.

It can be observed from Fig. 4, that the adsorption capacity of xGnP increased by increasing temperature and by increasing BPA concentration till the maximum value by reaching a plateau. In Table 5, the isotherm parameters of Langmuir, Freundlich, Temkin, Harkins-Jura and Halsey simulations for different temperatures are presented. The adsorption capacities increased by increasing the BPA concentration and reached almost constant final values, which represent the maximum adsorption capacity.

The maximum adsorption capacities of xGnP at 293.15 K, 298.15 K, 303.15 K are 250, 850 and 550 mg/g. Based on a comparison of the R^2 values from the table, the adsorption of BPA on xGnP most closely fits to Langmuir isotherm, suggesting a monolayer adsorption system on the surface. The results showed a decrease of the affinity of BPA for the xGnP binding sites as temperature increases. The sub-unity value of R_L confirms a favorable adsorption.

3.4. Adsorption thermodynamic study

The thermodynamic parameters give indications about internal energy changes during the adsorption process and can be calculated using Eq. (18), where K_L is the Langmuir equilibrium constant (L/mol), R is the gas constant (8.314×10^{-3} kJ/molK) and T is the absolute temperature (K). ΔH^0 and ΔS^0 were determined from the slope and the intercept of the van't Hoff plot of $\ln(K)$ vs. $1/T$ (Fig. 5). The calculated values are indicated in Table 6.

$$\Delta H^0 - \Delta T^0 = -RT \ln K_L \quad (18)$$

A positive value of the heat of adsorption indicates a chemisorption process together with the physisorption one at the surface of the exfoliated graphite nanoplatelets. The value of ΔH^0 (kJ mol $^{-1}$) indicates an exothermic process, supported also by the decrease of the adsorption capacity by increasing the temperature. As it can be observed from Table 7, the negative standard free energy ΔG^0 indicates a spontaneous process (kJ mol $^{-1}$), the ΔG^0 value being more negative by increasing the temperature, a temperature of 298.15 K representing the optimum value for a facilitated adsorption process. The negative value of ΔH^0 (kJ mol $^{-1}$) indicates an exothermic nature of the process. Similar observations were done before by Özcan and Özcan (2005).

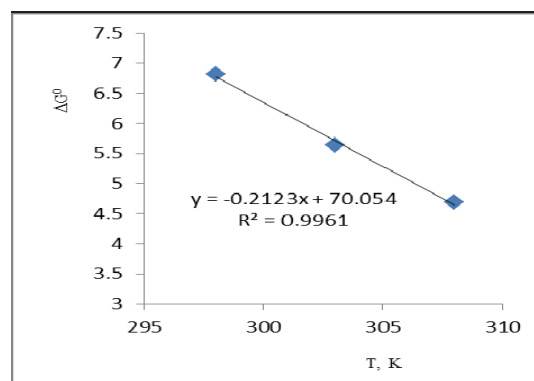


Fig. 5. Van't Hoff plot for the adsorption of BPA onto xGnP

3.5. Effect of the solution pH and ionic strength

The effect of solution pH over BPA removal was investigated over the entire pH range. When the value of pH is below 4, due to protonation of the negative charge of xGnP surface, it was observed that the adsorption of BPA decreases (Gong et al., 2007). Above a 10 value of the pH, the hydrophobic interactions between the π electrons of the graphite surface and the π electrons of the C=C double bonds of BPA decrease because of the deprotonation of BPA and the adsorption of BPA on the xGnP surface decreases in consequence.

Table 5. Langmuir, Freundlich, Temkin, Harkin-Jura and Halsey isotherm parameters for BPA removal by xGnP

| Equation | Parameter | | | |
|--|---------------------------|--------------------------|--------------|------------|
| Langmuir 1 $C_e/q_e = 1/Kq_m + C_e/q_m$ (12) | $q_m(\text{mg/g})=526.31$ | $K_L(\text{L/mg})=0.015$ | $R^2=0.9935$ | $R_L=0.06$ |
| Langmuir 2 $1/q_e = 1/q_m + 1/Kq_m C_e$ (13) | $q_m(\text{mg/g})=555.5$ | $K_L(\text{L/mg})=0.016$ | $R^2=0.9095$ | |
| Freundlich $\ln q_e = \ln K_F + 1/n \ln C_e$ (14) | $K_F(\text{mg/g})=38$ | $n=3.01$ | $R^2=0.9761$ | |
| Temkin $q_e = B \ln A + B \ln C_e$ (15) | $A=3.50$ | $B=24.39$ | $R^2=0.9863$ | |
| Harkins-Jura $1/q_e = A/B - (1/A) \log C_e$ (16) | $A=9.89$ | $B=0.03$ | $R^2=0.9626$ | |
| Halsey $\ln q_e = [(1/n) \ln K] - (1/n) \ln C_e$ (17) | $n=7.50$ | $k=1.71$ | $R^2=0.9761$ | |

Table 6. Adsorption capacity of BPA by graphene in comparison to other literature values

| Adsorbent | pH | T (K) | q_{\max} (mg/g) | Reference |
|---|-----|--------|-------------------|---------------------|
| graphene | 6.0 | 302.15 | 181.6 | Xu et al. (2012) |
| porous carbon produced at 400°C from Moso bamboo | NA | 296.15 | 2.1 | Asada et al. (2004) |
| AC purchased from Wako | NA | 296.15 | 56.5 | Lin and Xing (2008) |
| carbonaceous material produced at 600°C from wood chips | NA | 298.15 | 4.2-18.2 | Chen et al. (2008) |
| as-grown CNTs | 6.0 | 280.15 | 61.0 | Kuo (2009) |
| modified CNTs | 6.0 | 280.15 | 70.0 | Chen et al. (2008) |

NA=data not available; q_{\max} = maximum adsorption capacity

Table 7. Thermodynamic parameters for adsorption of BPA onto xGnP

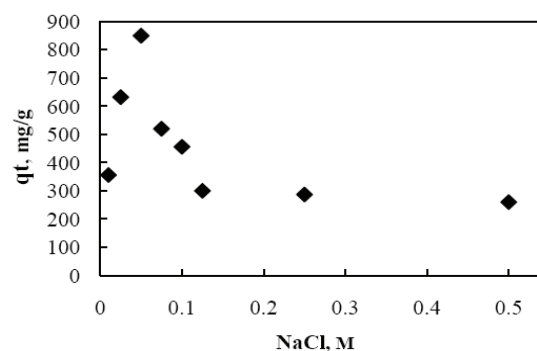
| Thermodynamic parameter | ΔH^0 (kJ mol ⁻¹) | ΔS^0 (J mol ⁻¹ K ⁻¹) | ΔG^0 (kJmol ⁻¹) | | |
|-------------------------|--------------------------------------|---|-------------------------------------|---------------------|---------------------|
| BPA | -70.25 | -212.3 | -6.82 (293.15 K) | -5.64 (298.15 K) | -4.69 (303.15 K) |

It was noticed that in the conditions of (0.1 mg of xGnP and 50 mL of 1-10 mg/L BPA at 298.15 K, pH = 5.5, contact time 30 minutes, by increasing pH from 3 to 7, the adsorption of BPA slightly increased, than it begins to decrease between 7 and 9. Based on these results, in the experiments pH values between 5.5 and 7 were maintained during investigating the effects of the studied sorption parameters.

The effect of ionic strength of the working solutions over removal of organic pollutants was also studied in previous papers (Güven et al., 2012). The adsorption process of BPA on xGnP surface is improved in the presence of salts and natural organic matter.

In our experiment it was found that the optimum value of the concentration of NaCl in aqueous solution is 0.037 M (Fig. 6). Adsorption of BPA with nonplanar and flexible structure significantly increases at small concentrations of NaCl in solution and it begins to decrease at higher ones. This behavior might be explained by the distribution of the Na⁺ and Cl⁻ ions between the negatively charged graphite platelets, producing a screening effect and favoring the adsorption of BPA molecules. The presence of NaCl in solution decreases the solubility of BPA and enhances its adsorption on the xGnP. The “butterfly”, or lying-down configuration of BPA (Güven et al., 2012) could facilitate the occupation of the more available

adsorption sites due to the presence of Na⁺ and Cl⁻ ions. This is more stable, in comparison with that one with one of the phenol rings oriented perpendicular to the surface and Van der Waals interactions are reduced. It was observed that at concentrations over 0.05 M, the adsorption capacity decreased, probably because of the competition between the species involved in the process.

**Fig. 6.** Effect of ionic strength on the adsorption of BPA by xGnP (0.1 mg of xGnP and 50 mL of 1 mg/L BPA at 298.15 K, pH=5.5)

4. Conclusions

In this study, commercially available exfoliated graphite nanoplatelets (xGnP) were evaluated for their sorption performance over

bisphenol A (BPA). The risks of this endocrine disruptor pollution lead to obligatory control and removal of BPA from the environment.

The influence of several parameters was studied such as: contact time, initial BPA concentration, temperature, ionic strength, and pH. Several equations of different sorption models were used in order to assess the best isotherm equation which represents the correlation of the experimental data (contact time 30 minutes, BPA concentration range between 1 and 10 mg L⁻¹, xGnP amount 0.1 mg in 10 mL, temperature range between 293.15 K and 303.15 K, ionic strength 0.037 M NaCl).

The maximum adsorption capacities of xGnP at 293.15 K, 298.15 K, 303.15 K are 250, 850 and 550 mg/g. Based on a comparison of the R² values, the adsorption of BPA on xGnP most closely fit to Langmuir isotherm, suggesting a monolayer adsorption system on the surface.

References

- Agnihotri S., Rood M.J., Rostam-Abadi M., (2005), Adsorption equilibrium of organic vapors on SWCNTs, *Carbon*, **43**, 2379-2388.
- Agnihotri S., Kim P., Zheng Y., Mota J.P.B., Yang L.C., (2008), Regioselective competitive adsorption of water and organic mixtures on pristine SWCNTs bundles, *Langmuir*, **24**, 5746-5754.
- Asada T., Oikawa K., Kawata K., Ishihara S., Iyobe T., Yamada A., (2004), Study of removal effect of bisphenol A and beta-estradiol by porous carbon, *Journal of Health Science*, **50**, 588-593.
- Brichka S.Y., Belyakova L.A., Prikhod'ko G.P., Roik N.V., (2006), Surface structure and adsorption properties of MWCNTs, *Russian Chemistry Bulletin*, **55**, 1775-1779.
- Chen W., Duan L., Wang L., Zhu D.Q., (2008), Adsorption of hydroxyl- and amino-substituted aromatics to carbon nanotubes, *Environmental Science and Technology*, **42**, 6862-6868.
- Cortes-Arriagada D., Sanhueza K., Santander-Nelli M., (2013), Modeling the physisorption of bisphenol A on graphene and graphene oxide, *Journl of Molecular Model*, **19**, 3569-3580.
- EU, (2011), Commission Directive 2011/8/EU of 28 January 2011 amending Directive 2002/72/EC as regards the restriction of use of bisphenol A in plastic infant feeding bottles, *Official Jurnal of the European Union*, **L26**, 11-14.
- Gong R., Hu Y., Chen J., Chen F., Liu Z., (2007), A cellulose based carbonyl cotton chelating agent having citric acid as an anchor ligand, *Microchimica Acta*, **158**, 315-320.
- Gotovac S., Hattori Y., Noguchi D., Miyamoto J., Kanamaru M., Utsumi S., Kanoh H., Kanedo K., (2006), Phenantrene adsorption from solution on single carbon nanotubes, *Journal of Physical Chemistry. B*, **110**, 16219-16224.
- Gotovac S., Song L., Kanoh H., Kaneko K., (2007), Assembly structure control of SWCNTs with liquid phase naphthalene adsorption, *Colloids and Surfaces A*, **300**, 117-121.
- Guibal E., McCarrick P., Tobin J.M., (2003), Comparison of the adsorption of anionic dyes on activated carbon and chitosan derivatives from dilute solutions, *Separation Science and Technology*, **38**, 3049-3073.
- Guyen Apul O., Wang Q., Zhou Y., Karanfil T., (2013), Adsorption of aromatic organic contaminants by graphene nanosheets: Comparison with carbon nanotubes and activated carbon, *Water Research*, **47**, 1648-1654.
- Ion A.C., Alpatova A., Ion I., Culetu A., (2011a), Study on phenol adsorption in aqueous solution on exfoliated graphite nanoplatelets, *Materials Science and Engineering B*, **176**, 588-595.
- Ion A.C., Ion I., Culetu A., (2011b), Lead adsorption onto exfoliated graphite nanoplatelets in aqueous solutions, *Materials Science and Engineering B*, **176**, 504-509.
- Ji L., Chen W., Duan L., Zhu D., (2009), Mechanisms for strong adsorption of tetracycline to carbon nanotubes: A comparative study using activated carbon and graphite as adsorbent, *Environmental Science and Technology*, **43**, 2322-2327.
- Kalaitzidou K., Fukushima H., Drzal L.T., (2007), Mechanical properties and morphological characterization of exfoliated graphite-polypropylene nanocomposites, *Composites: Part A*, **38**, 1675-1682.
- Kuo C.Y., (2009), Comparison with as-grown and microwave modified carbon nanotubes to removal aqueous bisphenol A, *Desalination*, **249**, 976-982.
- Lin D.H., Xing B.S., (2008), Adsorption of phenolic compounds by carbon nanotubes: Role of aromaticity and substitution of hydroxyl groups, *Environmental Science and Technology*, **42**, 7254-7259.
- Liu G.H., Wang J.L., Zhu Y.F., Zhang X.R., (2004), Application of MWCNTs in solid - phase extraction sorbent for chlorobenzene, *Analytical Letters*, **37**, 3085-3104.
- Liu T., Li Y., Du Q., Sun J., Jiao Y., Yang G., et al., (2012), Adsorption of methylene blue from aqueous solution by grapheme, *Colloids Surface B*, **90**, 197-203.
- Lu C.S., Chung Y.L., Chang K.F., (2006), Adsorption thermodynamic and kinetic studies of trihalomethanes on MWCNTs, *Journal of Hazardous Materials*, **138**, 304-310.
- Maliyekkal S.M., Sreeprasad T.S., Krishnan D., Kouser S., Mishra A.K., Waghmare U.V., Pradeep T., (2013), Graphene: a reusable substrate for unprecedented adsorption of pesticides, *Small*, **9**, 273-283.
- Özcan A., Özcan A.S., (2005), Adsorption of acid red 57 from aqueous solutions onto surfactant-modified sepiolite, *Journal of Hazardous Materials*, **125**, 252-259.
- Pan B., Sun K., Xing B., (2010), Adsorption kinetics of 17 α -ethynil estradiol and bisphenol A on carbon nanomaterials, *Journal of Soils and Sediments*, **10**, 838-844.
- Pavaghadi S., Tang A.I.L., Sathishkumar M., Loh K.P., Balasubramanian R., (2013), Removal of microcystin-LR and microcystin-RR by graphene oxide: Adsorption and kinetic experiments, *Water Research*, **47**, 4621-4629.
- Pyrzynska K., Stafiej A., Biesaga M., (2007), Sorption behavior of acidic herbicides on carbon nanotubes, *Microchimica Acta*, **159**, 293-298.
- Santhi V.A., Sakai N., Ahmad E.D., Mustafa A.M., (2012), Occurrence of bisphenol A in surface water, drinking water and plasma from Malaysia with exposure assessment from consumption of drinking water, *Science of the Total Environment*, **427-428**, 332-338.

- Shi J., Liu X., Cao J., Bo T., Li Y., (2013), Occurrence and risk assessment of estrogens and anti-inflammatories in Baiyangdian lake North China, *Environmental Engineering and Management Journal*, **12**, 1437-1445.
- Su F.S., Lu C.S., (2007), Adsorption kinetics, thermodynamics and desorption of natural dissolved organic matter by MWCNTs, *Journal of Environmental Science and Health Part A*, **42**, 1543-1552.
- Vandenberg L.N., Hauser R., Marcus M., Olea N., Weshons W.V., (2007), Human exposure to bisphenol A (BPA), *Reproductive Toxicology*, **24**, 139-177.
- Wang X., Lu J., Xing B., (2008), Sorption of organic contaminants by carbon nanotubes: Influence of adsorbed organic matter, *Environmental Science & Technology*, **42**, 3207-3212.
- Wang S., Sun H., Ang H.M., Tade M.O., (2013), Adsorption remediation of environmental pollutants using novel graphene-based nanomaterials, *Chemical Engineering Journal*, **226**, 336-347.
- Xu J., Wang L., Zhu Y., (2012), Decontamination of bisphenol A from aqueous solution by graphene adsorption, *Langmuir*, **28**, 8418-8425.
- Yan X.M., Shi B.Y., Lu J.J., Feng C.H., Wang D.S., Tang H.X., (2008), Adsorption and desorption of atrazine on carbon nanotubes, *Journal of Colloid and Interface Science*, **321**, 30-38.
- Yang K., Zhu L.Z., Xing B.S., (2006), Adsorption of PAHs by carbon nanomaterials, *Environmental Science and Technology*, **40**, 1855-1861.
- Zaib Q., Khan I., Saleh N., Flora J.V., Park Y.G., Yoon Y., (2012), Removal of bisphenol A and 17 β -estradiol by single-walled carbon nanotubes in aqueous solution: adsorption and molecular modeling, *Water, Air, and Soil Pollution*, **223**, 3281-3293.
- Zhao G., Li J., Wang X., (2011a), Kinetic and thermodynamic study of 1-naphthol from aqueous solution to sulfonated graphene nanosheets, *Chemical Engineering Journal*, **173**, 185-190.
- Zhao G., Jiang L., He Y., Li J., Dong H., Wang X., Hu W., (2011b), Sulfonated graphene for persistent aromatic pollutant management, *Advanced Materials*, **23**, 3959-3963.



"Gheorghe Asachi" Technical University of Iasi, Romania



EVOLUTION OF TROPHIC PARAMETERS FROM AMARA LAKE

**Ofelia Axinte¹, Iulia Simona Bădescu¹, Cristina Stroe², Valeria Neacsu³,
Laura Bulgariu¹, Dumitru Bulgariu^{4,5*}**

¹Gheorghe Asachi Technical University of Iasi, Faculty of Chemical Engineering and Environmental Protection,
Department of Environmental Engineering and Management, 73 Prof. dr. docent Dimitrie Mangeron Str., 7000050 Iasi, Romania

²Environmental Protection Agency Ialomita, 1 Mihai Viteazu Str., 920083 Slobozia, Romania

³Department of Water Resources Management, The Water Resources of the Water Management System Buzau-Ialomita,
20 bis Bucegi Str., 120208 Buzău, Romania

⁴"Al.I.Cuza" University, Faculty of Geography and Geology, Department of Geology, 20 A Carol I Str., 700506 Iasi, Romania

⁵Romanian Academy, Branch of Iasi, 18 Carol I Str., 700506 Iasi, Romania

Abstract

The transformation of lentic ecosystems in other types of ecosystems (plain, forest) is a part of normal process of ecological succession that occurs slowly, at geological scale. The filling of cuvette with eroded material transported by precipitations, air masses or detritus produced *in situ*, start from the moment when the body of water lakes is formed and has different rates depending on many factors: geographical location, geological substrate type, types of existing uses in the basin. Nutrient pollution, especially those originating from human activity, leads to water eutrophication, which accelerates the aging process of lakes. This is the case of Lake Amara, whose body of water has decreased considerably in recent years, large areas being now covered reed. Amara Lake, located in south-eastern Romania, is one of the five lakes in the country where they form mud exploited for therapeutic purposes. The importance of the lake derives both from the position of spa tourism, and the status of special protection avifaunistic area. These functions depend on maintaining constant parameters lacustrine ecosystem, the preservation of the current status and finding ways of halting and reversing the processes of nutrient pollution, so the process of eutrophication. From this reason, Amara Lake is constantly monitored in terms of trophic parameters, for that the measures to stop the eutrophication to be applied at time. In this paper, are presented the actual trophic status of Amara Lake and his evolution in the last decennium. This study can gives useful information for the management decisions that to allowing the sustainable development of this area.

Key words: aqvifaunistic area, ecological succession, eutrophication, trophic parameters

Received: November, 2014; Revised final: March, 2015; Accepted: March, 2015

1. Introduction

Ecological succession is a process that takes place with different rates depending on a variety of factors of which some can be listed: geographic position, geological substrate type etc. In lentic ecosystems, this process consists in filling the basin, covering the following phases: shallow lake, marsh reed long, plain. Field can be covered by shrubs and trees, turning into forest ecosystem. This transformation does not necessarily have a negative

impact, excepting the point of view of human use, and can seriously affect types of resources of natural capital to which the population has access, with economic and social repercussions. The unbalance of these factors influences the rate of ecological succession and leads to its acceleration (Andersen et al., 2006).

Increasing the amount of nutrients in lake water causes an explosive growth of aquatic plants in the first phase, then unbalancing the entire trophic network of ecosystem, with more or less severe

* Author to whom all correspondence should be addressed: e-mail: dbulgariu@yahoo.com

effects, depending on the type of nutrients found in excess, on the opportunistic algal associations or time for self adjustment (Thomas, 1969).

Eutrophication means the enrichment of water in nutrients, especially by nitrogen and phosphorus compounds, which cause an accelerated growth of algae and superior forms of vegetable life, producing an undesirable disturbance of the balance of organisms present in water and of waters quality (Parvu, 1999). In other words, eutrophication is a process of ecosystem degradation caused by the existence of large amounts of nutrients, and this process can be: natural - when done in a long time, or anthropogenic, due to human activities - when its evolution is rapid (Vadineanu et al., 1999). Phenomena and processes described for a lentic ecosystem do not overlap exactly one another because of differences in morphological, climatic and anthropogenic use. The status of a eutrophic lake can be established only when compared to its previous state or a reference lake (similar as geographic location etc.) (Rougé et al., 2013). Eutrophication of freshwater bodies (but not only, since it has been observed blooms in Black Sea, marine bays and estuaries) is currently the main problem of interest for researchers and political and economical decisions makers (Carpenter et al., 1999; Yang et al., 2008).

In Romania, the requirement of monitoring trophic status of water bodies lies with the National Administration Romanian Waters, in the view of complying with regulations and European standards for collection, analysis and interpretation of physical-chemical and biological samples. Evolution of trophic lakes is studied based on investigative methods developed by ICIM - Environmental Engineering Research Institute in 1984 (ICIM, 1995).

The importance of the Amara Lake derives both from its position for tourism and from its special status as protected aqvi-faustic area for 54 bird species. Amara Lake is a shallow lake, very sensitive to nutrient pollution because it is surrounded by farmland steppe and the climate is favourable for wind transport phenomena and the leaching of nutrients from the sides toward the water. Also, being a lake used for tourism and treatment, it supports a high pressure of human factors, especially in the summer. The influence of these factors have

determined the gradual reduction of water surface, since large areas, especially those of shallow bay types are already covered with reeds (Fig. 1).

In consequence, a constant monitoring of Amara Lake in terms of trophic parameters is required, in order to implement timely measures to stop eutrophication.

In this study we presented both the actual trophic status of Amara Lake and its evolution in the last decade. The study offers useful information for the management decisions for allowing the sustainable development of this area.

2. Experimental

The evaluation of water quality and its compliance with quality classes was done by collecting and analyzing water samples from 13 sampling points (Table 1), determined after plotting transects on the lake map (Fig. 2), during of 2002 – 2013 period.

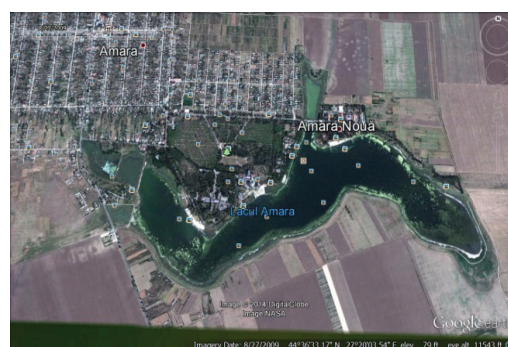
In all these points an ecological monitoring program was conducted, six of them being additionally supervised for vulnerability to nutrients (points 4, 5, 8, 9, 10 and 13), while 5 points (5, 8, 9, 10, 13) being monitored for fish life. Since 2007, four annual monitoring campaigns have been achieved, and the number of monitoring points was reduced to one (2007, 2008, 2009, 2010- Middle lake - position 7 in Table 1), maximum two (2008, 2011, 2012, 2013- Middle lake and Perla Complex - out lake – positions 7 and 12 in Table 1).

In 2008, the Middle lake point and the profile „photic zone limit” were monitored. The 13 sampling points were monitored discontinuously, most recordings being focused on the Middle lake point (code 1120340), and while the fewest records were those for Tail Lake (code 1120310) and Wharf points (code 1120320).

In Table 2 it is summarized the frequency of water quality monitoring, at collection points set out in sections of Amara Lake. None of the sections did benefit from constant monitoring over the 10 years referred in to the study. The monitoring program was established by SGA Buzau-Ialomița, which, for administrative reasons, political, financial or climate (flooding) reasons have ranged and the number of sampling campaigns per calendar year.



(a)



(b)

Fig. 1. Satellite image of Amara Lake in 2009 (a) and 2013 (b) (Google Earth)

The year with the most campaigns was 2006 – with 9 campaigns in 6 points from the 13 sampling points established. During the period 2002-2005 4 annual campaigns were conducted (one in each spring and autumn and 2 in each summer) in 12 points by 13 points. Between 2008-2010 there were four campaigns covering only two sampling points from 13, while four campaigns were scheduled in 2007, but in one monitoring point - Middle lake (code 1120340) (Table 2). The main eutrophication parameters monitored in sampling points established on Amara Lake are: transparency, suspended solids, total phosphorus, total nitrogen and total phytoplankton biomass.



Fig. 2. Amara Lake – sampling points location

Table 1. The coordinates of sampling points from Amara Lake, used for monitoring in 2002-2013 period

| No. | Section name/ Sampling point | Code | Eastern longitude | Northern latitude | Layering | Monitoring Program ¹ |
|-----|---|-----------|----------------------|----------------------|---------------------|------------------------------------|
| 1 | Lake tail (Center) / 0 m | 112031010 | 27°21'27" | 44°36'10" | unlayered | ES ¹ |
| 2 | Lake tail (Center) /2.5 m | 112031020 | 27°21'27" | 44°36'10" | unlayered | ES |
| 3 | Lake tail (Mircești)/ surface | 112032010 | 27°21'27" | 44°36'10" | unlayered | ES |
| 4 | Lake tail (Mircești) / photic zone | 112032020 | 27°21'27" | 44°36'10" | unlayered | ES,VN ² |
| 5 | Dock /0m | 112033010 | 27°21'10" | 44°36'25" | unlayered | ES,VN, FL ³ |
| 6 | Dock / 2.5m | 112033020 | 27°21'10" | 44°36'25" | unlayered | ES |
| 7 | Middle lake/surface | 112034010 | 27°20'42" | 44°36'33" | layered epilimnion | ES |
| 8 | Middle lake/photic zone | 112034020 | 27°20'42" | 44°36'33" | layered epilimnion | ES,VN, FL |
| 9 | Middle lake photic zone limit | 112034030 | 27°20'42" | 44°36'33" | layered hipolimnion | ES,VN, FL |
| 10 | U.G.S.R. ⁴ /0m | 112035010 | 27°20'12" | 44°36'39" | unlayered | ES,VN, FL |
| 11 | U.G.S.R./2.5m | 112035020 | 27°20'12" | 44°36'39" | unlayered | ES |
| 12 | Perla Complex (lake outlet)/surface | 112036010 | 27°19'09" | 44°36'23" | layered epilimnion | ES |
| 13 | Perla Complex (lake outlet) /photic zone | 112036020 | 27°19'09" | 44°36'23" | unlayered | ES,VN, FL |

¹ES = ecological surveillance; ²VN= vulnerability to nutrient; ³FL = fish life; ⁴U.G.S.R= former name meaning „General Union of Trade Unions of Romania”

Table 2. The sampling frequency for Lake Amara monitoring, in period 2002-2013

| Section name/ Sampling point/year/ number of campaigns | 2002 | 2003 | 2004 | 2005 | 2006 | 2007 | 2008 | 2009 | 2010 | 2011 | 2012 | 2013 |
|--|------|------|------|------|------|------|------|------|------|------|------|------|
| 1 Lake tail (Center) / 0 m | 4 | 4 | 4 | 4 | - | - | - | - | - | - | - | - |
| 2 Lake tail (Center) /2.5 m | 4 | 4 | 4 | 4 | - | - | - | - | - | - | - | - |
| 3 Lake tail (Mircești)/ surface | 4 | 4 | 4 | 4 | 9 | - | - | - | - | - | - | - |
| 4 Lake tail (Mircești) / photic zone | 4 | 4 | 4 | 4 | 9 | - | - | - | - | - | - | - |
| 5 Dock /0m | 4 | 4 | 4 | 4 | - | - | - | - | - | - | - | - |
| 6 Dock / 2.5m | 4 | 4 | 4 | 4 | - | - | - | - | - | - | - | - |
| 7 Middle lake/ surface | 4 | 4 | 4 | 4 | 9 | 4 | 4 | - | - | - | - | - |
| 8 Middle lake/ photic zone | 4 | 4 | 4 | 4 | 9 | - | 4 | - | - | - | - | - |
| 9 Middle lake photic zone limit | - | - | - | - | 9 | - | - | - | - | - | - | - |
| 10 U.G.S.R. ⁴ /0m | 4 | 4 | 4 | 4 | - | - | - | - | - | - | - | - |
| 11 U.G.S.R./2.5m | 4 | 4 | 4 | 4 | - | - | - | - | - | - | - | - |
| 12 Perla Complex (lake outlet) /surface | 4 | 4 | 4 | 4 | 9 | - | - | - | - | 4 | 4 | 4 |
| 13 Perla Complex (lake outlet) /photic zone | 4 | 4 | 4 | 4 | - | - | - | 4 | 4 | - | - | - |

Each of this parameter has been analyzed according with the standard procedures (Fresenius et al., 1988; ICIM, 1995), and on the basis on their determined values, the evolution of trophic state of Amara Lake has been discussed.

3. Results and discussion

3.1. Monitoring of suspended matter and water transparency

Light affects photosynthesis through radiation with a wavelength between 390-710 nm, which represents 46-48% of the incident solar radiation (Buruian, 2002). Regarding Amara Lake whose water surface is not shaded by tall slopes, lake photo-autotrophies are influenced by the number of days of sunshine and water transparency. The amount of the incident light has also seasonal variations (with a minimum in winter and maximum in summer) and diurnal variations. Water transparency depends on a number of factors related to climatic peculiarities of the area, morpho-geology of basin, hydrological regime and the type and intensity of biological processes.

Depending on transparency and hence the percentage of light incident radiation which is reflected in the water body, two layers are defines: *photic or trophogenic zone* (intake of > 1% of the amount of light) and the *aphotic or tropholitic zone* (input <1% of the light) between which a compensation area exists (Brezeanu and Simion-Gruia, 2002). Transparency index, as the ratio between transparency and depth (T/A) is associated with the development of macrophytes. At a ratio lower than 0.20, there are not conditions for photosynthesis of organic substances in lake water (Yang et al., 2014), and this significantly influence the eutrophication of water.

Shallow lakes usually have a low transparency because moving air masses causes the waves and currents, which leads to the entrainment of deposits from the bottom of the basin, leading to an increase in the amount of suspended solids in the water.

In Table 3 there are presented the limits of photic zone for sampling point “Middle lake” (code 112034030) correlated with the amount of suspended matter and water transparency index, for one year taken as example – 2009.

Increasing the amount of suspended matter, in samples obtained during harvesting campaigns, reduces the limit of photic zone, but transparency index values do not falls below 0.20, which is proved by the presence of some macrophytes such as: *Phragmites australis*, *Potamogeton pectinatus*, *Chara vulgaris*, *Cladophora glomerata*, *Spyrogira sp.*, *Filamentous algae*) in water samples.

Fig. 3 illustrates the variation of the amount of suspended matter (mg/L) in water samples from different sampling points, during of 2004 – 2013 period. It can be observed that in the studied period, the value of this parameter increases very little with the depth, due to sedimentation processes. Also, the experimental measurements highlight that, in the last three years a stabilization of the amount of suspended matter occurs, which increases the photic zone depth (Table 4). The values summarized in Table 4 show that the lake water transparency is lower in the summer period, when the algae growth is favored and when the amount of exogene dust transported by wind is higher, in comparison with autumn period, when these factor and less important.

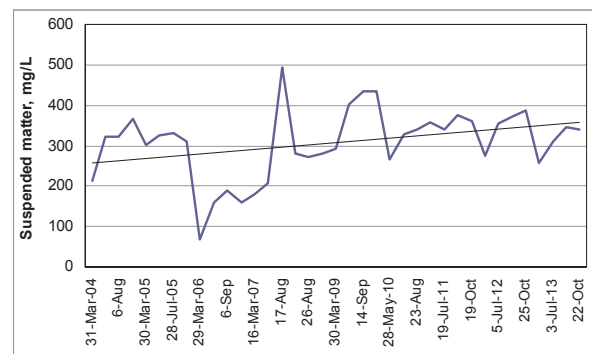


Fig. 3. Variation of amount of suspended matter in Amara Lake, in 2004 – 2013 period

Table 3. Transparency index of water from Amara lake – “Middle lake” sampling point, 2009

| Date | 03/30 | 06/20 | 09/14 | 12/02 |
|--------------------------------------|-------|-------|-------|-------|
| Limit of photic zone (m) | 2.80 | 2.90 | 2.30 | 1.50 |
| Suspended matter (mg/L) | 304.0 | 423.0 | 506.5 | 474.5 |
| Index of transparency ($A = 4.1$ m) | 0.68 | 0.70 | 0.56 | 0.36 |

Table 4. Transparency of Amara Lake in 2010 – 2013 period

| Year | Date | Middle lake | Lake tail | Year | Date | Middle lake | Lake tail |
|------|-------|-------------|-----------|------|-------|-------------|-----------|
| 2010 | 05/28 | 250 | 220 | 2011 | 05/03 | 100 | 110 |
| | 06/23 | 150 | 70 | | 06/19 | 280 | 260 |
| | 08/23 | 150 | 110 | | 08/29 | 200 | 250 |
| | 09/27 | 150 | 110 | | 10/19 | 70 | 70 |
| 2012 | 05/08 | 280 | 210 | 2013 | 04/26 | 220 | 230 |
| | 06/05 | 110 | 110 | | 06/03 | 350 | 325 |
| | 09/17 | 80 | 85 | | 08/16 | 300 | 180 |
| | 10/25 | 200 | 200 | | 10/22 | 130 | 250 |

3.2. Monitoring of phosphorus content

The dissolved organic phosphorus is mineralized by specific bacteria and transformed in inorganic phosphorus that can be metabolized by algae, and this process is significantly influenced by temperature (Ludwig et al., 2003; Macoveanu et al., 2005). The phosphorus concentration in water depends on the concentration of organic substances, temperature and intensity of bacterial activity. The wastewater with high content of organic matter increases the phosphorus level, increasing the risk of eutrophication. There are two major anthropogenic sources of phosphorus: domestic wastewater loaded with detergents and organic substances (watery faeces) and animal manure from livestock farms (Arnaldos and Pagilla, 2010; Qin et al., 2015).

In case of Amara Lake, the annual average of total phosphorus content, plotted in Fig. 4, shows that for the last four years a stabilization of values without sudden positive or negative changes occurred, which suggests is a tendency toward balancing processes in the lake.

3.3. Monitoring of nitrogen content

Nitrogen is an essential element for life in the biosphere because it is included in the structure of all proteins, nucleic acids, chlorophyll, vitamins and hormones. Atmospheric diatomic nitrogen (N_2) is an inaccessible gas for most of biologic systems, and therefore is converted at fix forms (NH_4^+ , NO_3^- , NO_2^-) (He et al., 2015; Mihaescu et al., 2007). Molecular nitrogen penetrates quite easily from atmosphere into water, diffuses to the depths. In this form, the nitrogen can be used only by fixing bacteria and by some blue algae (Bouwman et al., 2009). After the mineralization which ensure the conversion in utilizable inorganic forms, the nitrogen becomes available and for other plants and microorganisms, and this process is essential for the cycle of this element in nature (Berca, 2000).

The annual average of total nitrogen content is illustrated in Fig. 5. The average obtained values shows that in case of Amara Lake significant fluctuations appear, during of studied period. These fluctuations are influenced by the hydrological regime of the area, the ascending curves being corresponding to the rainy years.

3.4. Monitoring of phytoplankton biomass

The dominant species of phytoplankton biomass in Amara Lake, during of 2002 – 2013 period were: Cyanophyta-*Aphanizomenon flos-aquae*, *Microcystis aeruginosa*, *Merismopedia elegans*, *Synechocystis* sp., *Gloeocapsa minima*, Bacillariophyta- *Cocconeis pediculus*, *Cyclotella meneghiniana*, *Fragillaria crotonensis*, *Stauroneis anceps*, *Anomoconeis sphaerophora*, *Nitzschia closteriu*, *N. Sigmoidea*, *Cryptophyta- Chroomonas*

caudata, *Chroomonas acuta*, Chlorophyta-*Cosmarium leave*, *Scenedesmus quadricauda*, *Chlamydomonas* sp., *Ankistrodesmus minutissima*, *Oocystis submarina*, *Ankira* sp., Euglenophyta-*Monomorphina pyrum*, *Phacus longicauda* and *Euglena viridis*. All these species have been periodically measured and expressed as total phytoplankton biomass. The evolution of the total phytoplankton biomass for Amara Lake, in the last decade is presented in Fig. 6.

It can be observed that the total phytoplankton biomass altered between periods with high microalgae production (for years 2005 and 2012) and clear water phase of Amara Lake (where the average value of total phytoplankton biomass is not higher than 3.0 mg/L).

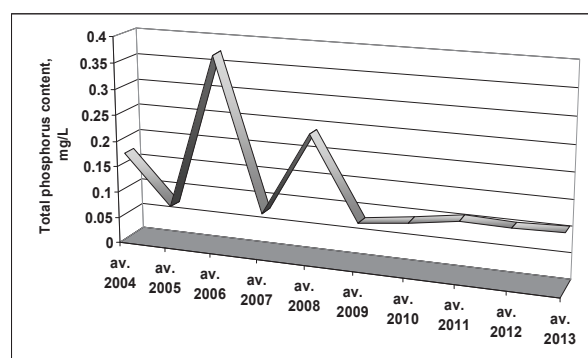


Fig. 4. Annual average of total phosphorus content in water of Amara Lake, in 2004 – 2013 period

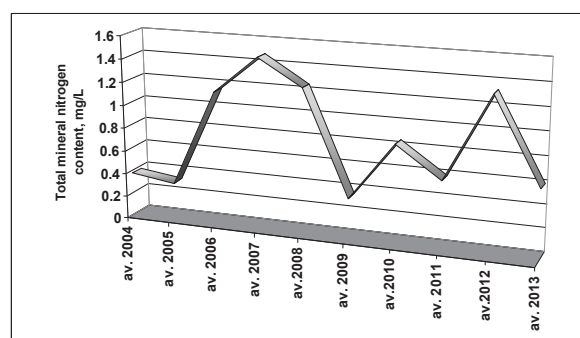


Fig. 5. Annual average of total mineral nitrogen content in water of Amara Lake, in 2004 – 2013 period

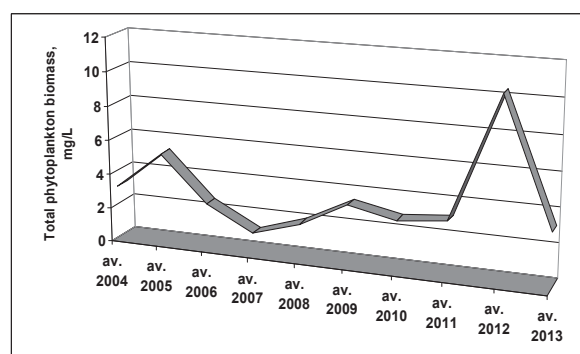


Fig. 6. Annual average of total phytoplankton biomass in water of Amara Lake, in 2004 – 2013 period

Table 5. Framing in quality class of Amara Lake, for 2002 – 2013 period

| Year | 2002 | 2003 | 2004 | 2005 | 2006 | 2007 | 2008 | 2009 | 2010 | 2011 | 2012 | 2013 |
|-----------------------------|---------------|------|------|------|------|------|------|------|------|------|------|------|
| Indicator | Quality class | | | | | | | | | | | |
| Total phosphorus | E | H | H | E | H | E | E | E | H | E | E | E |
| Total mineral nitrogen | U | U | O | O | E | E | E | O | O | O | E | E |
| Total phytoplankton biomass | E | M | M | E | O | O | O | M | E | O | M | E |
| Global quality class | E | E | E | E | H | E | M | E | H | E | E | E |
| Conventional number | 4 | 4 | 4 | 4 | 5 | 4 | 3 | 4 | 5 | 4 | 4 | 4 |

Notations: "U" – ultraoligotroph (cn = 1); "O" – oligotroph (cn = 2); "M" – mesotroph (cn = 3); "E" – eutroph (cn = 4); "H" – hypertroph (cn = 5); cn – conventional number

These fluctuations are mainly determined by the climatic regime of the year, in special during of summer. Thus, in warmest years (such as 2005 and 2012), the high nutrient concentrations and warm temperatures stimulated the phytoplankton growth. In the years where the summer temperatures were not so high (such as 2007), the microalgae biomass is strongly reduced, and in consequence the phytoplankton growth is lower. It should be also noted that the fluctuations of total phytoplankton biomass are offset because of the time necessary for carrying out biological processes.

3.5. Quality class of Amara Lake

Considering the global quality classification as a function of main indicators of eutrophication (www.daib.rowater.ro), the Amara Lake can be still included in E category, which demonstrates an equilibrium state of these indicators (Table 5).

For a complete picture of the state of the lake in terms of eutrophication, we compared the evolution of the main indicators (total phosphorus, total mineral nitrogen, total phytoplankton biomass) in Amara Lake, for 2004 – 2013 period, which is presented in Fig. 7.

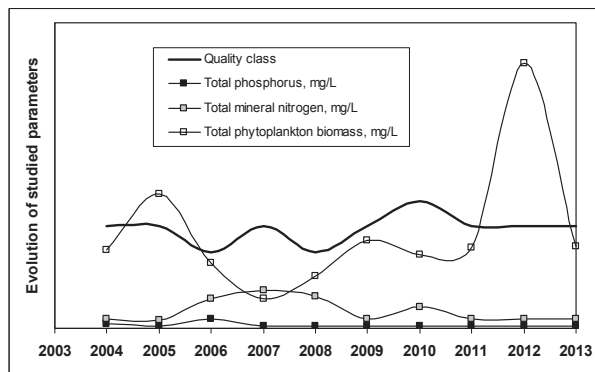


Fig. 7. Parameters of eutrophication degree and quality class of Amara Lake, in 2004 – 2013 period

It can be observed that, with exception of total phytoplankton biomass, whose variations could be correlated with other physical and chemical factors (temperature, pH, diversity index etc.), all the other indicators have insignificant variations during the last three years. This indicates that the Amara Lake is in a self-regulation stage of biological and physicochemical processes.

4. Conclusions

The functions of Amara Lake depend on the the possibilities of maintaining constant various parameters of lacustrine ecosystem, the preservation of the current status and finding ways of halting and reversing the processes of nutrient pollution, such as the process of eutrophication.

In this paper, it is presented the evolution of some parameters responsible for the eutrophication process of Amara Lake. The obtained average values of studied parameters (suspended matter, water transparency, total phosphorus, total mineral nitrogen, total phytoplankton biomass) have shown insignificant variations for the last three years, which suggest that the Amara Lake is in a self-regulation stage of biological and physicochemical processes.

The current trophic status of the lake and its evolution in the last decade can give useful information and support for management decisions that to allowing the sustainable development of this area.

Acknowledgments

The financial support of this study was ensured by The Water Resources of the Water Management System Buzau-Ialomita and Environmental Protection Agency.

References

- Andersen H.E., Kronvang B., Larsen S.E., Hoffmann C.C., Jensen T.S., Rasmussen E.K., (2006), Climate-change impacts on hydrology and nutrients in a Danish lowland river basin, *Science of the Total Environment*, **365**, 223–237.

- Arnaldos M., Pagilla K., (2010), Effluent dissolved organic nitrogen and dissolved phosphorus removal by enhanced coagulation and microfiltration, *Water Research*, **44**, 5306–5315.
- Berca M., (2000), *General Ecology* (in Romanian), Ceres Publishing House, Bucharest, Romania.
- Bouwman A.F., Beusen A.H.W., Billen G., (2009), Human alteration of the global nitrogen and phosphorus soil balances for the period 1970–2050, *Global Biogeochemistry Cycles*, **23**, 88–97.
- Brezeanu G., Simion-Gruiță A., (2002), *General Limnology*, H*G*A Publishing House, Bucharest, Romania.
- Burian P.V., (2002), *The Lake: Bioassay*, University of Medicine and Pharmacy Press, Targu-Mures, Romania.
- Carpenter S.R., Ludwig D., Brock W.A., (1999), Management of eutrophication for lakes subject to potentially irreversible change, *Ecological Applications*, **9**, 751–771.
- Fresenius W., Quentin K.E., Schneider W., (1988), *Water Analysis*, Springer-Verlag, Berlin.
- ICIM, (1995), Methodological Guidelines for surveillance trophic evolution of reservoirs and natural lakes, Bucharest, 1995.
- He H., Kang Y., Liu Z., (2015), Nitrogen inputs enhance phytoplankton growth during sediment resuspension events: a mesocosm study, *Hydrobiologia*, **744**, 297 – 305.
- Ludwig D., Carpenter S., Brock W., (2003), Optimal phosphorus loading for a potentially eutrophic lake, *Ecological Applications*, **13**, 1135–1152.
- Macoveanu M., Gavrilescu M., Ungureanu F. Cojocaru C., (2005), *Processes Modeling and Simulation in Environmental Engineering* (in Romanian), Vol. I, Ecozone Publishing House, Iasi, Romania.
- Mihaescu G., Chifiriuc C., Ditu L.M., (2007), *General Microbiology* (in Romanian), University of Bucharest Publishing House, Bucharest, Romania.
- Parvu C., (1999), *General Ecology* (in Romanian), Tehnical Publishing House, Bucharest, Romania.
- Qin C., Liu H., Liu L., Smith S., Sedlak D.L., April Z.G., (2015), Bioavailability and characterization of dissolved organic nitrogen and dissolved organic phosphorus in wastewater effluents, *Science of the Total Environment*, **511**, 47–53.
- Rougé C., Mathias J.D., Deffuant G., (2013), Extending the viability theory framework of resilience to uncertain dynamics, and application to lake eutrophication, *Ecological Indicators*, **29**, 420–433.
- Thomas A.E., (1969), *The Process of Eutrophication in Central European Lakes*, In: *Eutrophication: Causes, Consequences, Correctives*, Proceedings of Symposium, National Academy of Sciences, Washinton D.C., 23–28.
- Vadineanu A., Negrei C., Lisievici P., (1999), *Sustainable Development, Theory and Practice, Mechanisms and Instruments* (in Romanian), Vol. I, University of Bucharest Publishing House, Bucharest, Romania.
- Yang L., Zhao X., Peng S., Zhou G., (2014), Integration of Bayesian analysis for eutrophication prediction and assessment in a landscape lake, *Environmental Monitoring and Assessment*, **187**, 41–69.



“Gheorghe Asachi” Technical University of Iasi, Romania



A NEW STRATEGY FOR PENTACHLOROPHENOL MONITORING IN WATER SAMPLES USING ULTRA-HIGH PERFORMANCE LIQUID CHROMATOGRAPHY - MASS SPECTROMETRY TANDEM

Yassine Kadmi^{1,2}, Lidia Favier^{1,2*}, Maria Harja³, Andrei Ionut Simion⁴,
Lacramioara Rusu⁴, Dominique Wolbert^{1,2}

¹Ecole Nationale Supérieure de Chimie de Rennes, CNRS, UMR 6226, 11 Allée de Beaulieu, CS 50837,
35708 Rennes Cedex 7, France

²Université Européenne de Bretagne, France

³“Gheorghe Asachi” Technical University of Iasi, Faculty of Chemical Engineering and Environmental Protection,
Department of Environmental Engineering and Management, 73 Prof. dr. docent Dimitrie Mangeron Str., 700050 Iasi, Romania

⁴“Vasile Alecsandri” University of Bacau, Faculty of Engineering, Department of Chemical and Food Engineering,
157 Calea Marasesti, 600115 Bacau, Romania

Abstract

A novel sensitive and rapid analytical approach based on ultra-high performance liquid chromatography - mass spectrometry (UHPLC/MS/MS) tandem was developed for the monitoring of pentachlorophenol in water samples. Chromatographic separation was carried out on Acquity BEH C18 (100 x 2.1 mm, 1.7 μ m) column under gradient mode using a mobile phase consisting of acetonitrile/ultrapure water/formic acid. Quantification of pentachlorophenol was performed on a triple-quadrupole tandem mass spectrometer under multiple reaction monitoring (MRM) mode, via a negative electrospray ionization (ESI⁻). The limit of quantification of the developed instrumental method was 0.3 μ g L⁻¹. The linearity was validated within the concentration range 0.1-100 μ g L⁻¹ with a correlation coefficient (R^2) of 0.998. Intra-day and inter-day precision values were 99.78 and 99.12%, respectively. Moreover, for the application to real water samples, a solid phase extraction method (SPE) was proposed for the extraction and preconcentration of analyte. Some of the main factors involved in the SPE extraction process such as solid phase material, elution solvent and sample volume were investigated and optimized in order to maximize the extraction efficiencies. Oasis HLB cartridges showed the best results in terms of extraction recovery. High analyte recoveries (between 98.2% and 100.18%) were achieved with the proposed SPE procedure and the extraction RSD was less than 3.1%. In addition, the whole new analytical strategy (SPE-UHPLC/MS/MS) was then successfully applied for pentachlorophenol quantification in natural waters at low part per trillion levels.

Key words: pentachlorophenol, solid phase extraction, tandem mass spectrometry, ultra-high performance liquid chromatography, water analysis

Received: November, 2014; Revised final: March, 2015; Accepted: March, 2015

1. Introduction

Phenols and their derivative compounds commonly exist in the environment due to various industrial activities. Among the hazardous compounds included in the family of chlorophenols, pentachlorophenol (PCP) is considered as the most

toxic and was identified as environmental endocrine disruptor (EED) (Yang et al., 2005). Some studies revealed potential possibility to cause decreases in thyroid hormone levels of neonates, neurological disorders, immunodeficiency, or acute pancreatitis (Dallaire et al., 2009; Yang et al., 2006). This organic molecule has been widely used as wood preservative

* Author to whom all correspondence should be addressed: e-mail: lidia.favier@ensc-rennes.fr; Phone: +33223238135; Fax: +33223238020

in industry, as broad spectrum herbicide and germicide in agriculture and as an intermediate in pharmaceuticals. Moreover, this compound can be formed from phenols during the drinking water disinfection with chlorine affecting the taste and odor of distributed water (Kadmi et al., 2015). All these applications often lead to wastewater, groundwater and even to drinking water contamination.

During the last decades, PCP has drawn a significant scientific attention, due to its high toxicity, hydrophobicity and long environmental persistence related to its stable aromatic ring system and high chloride content (Dudal et al., 2004; Ge et al., 2007; Zheng et al., 2012). The reported toxic effects on human health are related to its estrogenic, mutagenic and carcinogenic properties (Gavrilescu, 2009; Michalowicz and Duda, 2007). The International Agency for Research on Cancer (IARC) classified PCP as group 2B carcinogen (IARC, 1991), possibly carcinogenic to humans. Based on its toxicity and widespread distribution in the environment PCP has been included in both U.S. Environmental Protection Agency and European Union List of priority pollutants and strict restrictions on the maximum admissible concentrations (MAC) in drinking water have been fixed ($0.5 \mu\text{g L}^{-1}$ for total phenols and $0.1 \mu\text{g L}^{-1}$ for individual compounds) (EPA, 2004; Jakab et al., 2013; Jakab et al., 2014; Wennrich et al., 2000). The MAC value for PCP in inland and other surface waters the set to $1 \mu\text{g L}^{-1}$.

Generally, the concentration of PCP is very variable and depends on the type of water. For example, higher levels (in the $\mu\text{g L}^{-1}$ range) were found in landfill leaches (Ho et al., 2008; Wei and Jen, 2002). However, lower levels (in the ng L^{-1} range) have been reported in China's rivers by Gao et al. (2008). Hence, it is of great interest in the environmental field to develop fast and sensitive analytical methods for the monitoring of trace and ultra-trace levels of PCP in water samples. The major challenge in the analysis of such molecule is to attain the high sensitivity required for determination of trace levels in environmental samples.

Over the last decade, a variety of analytical methods including liquid chromatography (LC), gas chromatography (GC), high performance liquid chromatography (HPLC) and thin layer chromatography (TLC) in combination with selective detectors such as electron capture, diode array, mass spectrometer and flame ionization have developed for detection and quantification of PCP and congeners in different samples (Barták et al., 2000; Callejon et al., 2007; Favaro et al., 2008; Gremaud and Tureski, 1997; Pugliese et al., 2004). Among these methods, those based on gas chromatography are the most commonly used due to their high sensitivity and good resolution (Bagheri and Sajari, 2001; Padilla-Sánchez et al., 2011). Additionally, for the GC and GC/MS determinations a derivatisation step (by methylation, pentafluorobenzoylation or acetylation) is generally needed to improve the signal detection and peak resolution (Korenman et al., 2003;

Llompart et al., 2002) requiring additional time consuming steps and the use harmful reactive chemical agents.

All these reasons pointed out, the interest in the development of more environmentally friendly analytical techniques for the detection of this persistent pollutant. Recently, ultra-high performance liquid chromatography combined with triple quadrupole tandem mass spectrometry (UHPLC/MS/MS) in multiple reaction monitoring mode (MRM) has become a promising analytical tool in the domain of environmental analysis. Such technique could provide high sensitivity, efficiency and molecular weight data for the analytes identification. In this sense, UHPLC/MS/MS appear as suitable techniques for the analysis traces of PCP in environmental water samples.

Nevertheless, due to the low concentration levels of PCP in environmental matrices sample pretreatment is normally required prior to instrumental analysis in order to isolate, clean-up and preconcentrate the target analyte from the matrix and to obtain the required instrumental detection limits. Several sample-handling techniques such as the conventional liquid-liquid extraction (LLE), solid phase microextraction (SPME) and stir bar sorptive extraction (SBSE) are have been reported for the extraction of chlorophenols (Domeno et al., 2005; Llompart et al., 2002; Llorca-Porcel et al., 2009). However, some of these techniques have limitations because they are time-consuming and require high amount of organic solvents. Solid phase extraction (SPE) is one of the most widely used methods for the sample pretreatment in environmental analysis.

In this study, a new analytical strategy coupling solid phase extraction with ultra high performance liquid chromatography tandem mass spectrometry was developed for the quantification of PCP in water samples at low ng L^{-1} level. This work aims to prove the utility and reliability of such analytical strategy for the monitoring of pentachlorophenol in water samples. Several factors affecting the SPE extraction efficiency were studied and optimized in order to improve the target analyte extraction recovery.

The main advantage of the proposed methodology compared with existing methods from the literature (with or without derivatization) is the substantial improvement of its sensitivity for the detection of PCP. Thus it could be a promising analytical tool for the PCP monitoring in real water samples. To our knowledge, this is the first work reporting the analysis of this hazardous organic compound by SPE-UHPLC/MS/MS.

2. Experimental

2.1. Reagents and samples

2.1.1. Reagents

The target compound studied here is pentachlorophenol, obtained from Sigma Aldrich

GmbH (Steinheim, Germany). All chemicals (reagents and solvents) used in this study were of the highest analytical purity grade. Acetonitrile and formic acid were supplied by J.T. Baker (Deventer, Netherlands). Methanol and dichloromethane were obtained from Fischer Scientific-Bioblock (Illkirch, France). Acetic acid, ethyl acetate, diethyl ether and sodium hydroxide were purchased from Acros Organics (Noisy-le-Grand, France).

2.1.2. Preparation of standard solutions and water samples

A stock standard solution (1000 mg L^{-1}) of pentachlorophenol was prepared by dissolving accurate amount in methanol. The working solutions were freshly prepared by appropriate dilutions (to reach the working concentration range) of the stock standard solution in acetonitrile/ultrapure water (55/45, v/v). This composition ensured good stability of the chlorophenols in water samples. The ultrapure water (with a resistivity of $18 \text{ M}\Omega$ and a DOC value less than 0.1 mg L^{-1}) used for the preparation of the samples was obtained with an Elga Option-Q DV-25 water purification system (Antony, France). All solutions were stored in glass bottles in the dark at -20°C . To demonstrate the applicability of the developed method real water samples including river water were used in this work.

The samples were collected in October 2013 and January 2014, from different locations (from Brittany region, France). All samples were collected in baked glass 10-L amber bottles with Teflon lined caps to ensure sample integrity, filtered through a $0.45 \mu\text{m}$ cellulose membrane and then stored in the dark at 4°C until their analysis (within one week of collection).

2.2. Apparatus and analytical conditions

The UHPLC/MS/MS system comprised a Waters® Acquity™ UHPLC H-Class system, coupled to a Waters Quattro Premier™ Triple Quadrupole mass spectrometer (Saint-Quentin en Yvelines, France). The chromatographic system contain a binary pump, an auto-sampler and a thermostated column compartment (Waters, Saint-Quentin en Yvelines, France). Chromatographic conditions that directly affect chromatographic separation such as chromatographic column, elution mode, mobile phase composition and additives were studied and optimized in this work.

Analyte separation was carried out with a Ethylene Bridged Hybrid (BEH) C18 column ($100 \times 2.1 \text{ mm}$, $1.7 \mu\text{m}$; particles, Waters, Ireland) protected by an in-line filter purchased from Waters (Saint-Quentin en Yvelines, France). The analytical column compartment was maintained at 45°C and the auto-sampler at 5°C . The flow rate was 0.4 mL min^{-1} and the injection volume $5 \mu\text{L}$. Mobile phases were acetonitrile (A) and ultrapure water (B) containing 0.1% (v/v) formic acid (pH 3). Elution was done in gradient mode. Details on the optimized

UHPLC/MS/MS conditions are presented in Section 3.1.

2.3. Solid-phase extraction (SPE) conditions

The extraction of PCP from water samples was performed by off-line SPE. Oasis HLB cartridges (6 cc, 200 mg) from Waters (Guyancourt, France) were used for the SPE experiments. A 12-port Visiprep SPE vacuum manifold obtained from Supelco (Bellefonte, PA, USA) was used for sample extraction. Within this study, Oasis HLB (Hydrophilic-Lipophilic Balanced) cartridges (6cc, 200 mg, Waters, Milford, MA) containing a macroporous poly(divinylbenzene-co-N-vinylpyrrolidone) copolymer were selected for the development and optimization of the SPE method. The developed SPE procedure was carried out as follows: Oasis HLB cartridges were conditioned using $2 \times 2 \text{ mL}$ acetonitrile, and $2 \times 2 \text{ mL}$ methanol and then equilibrated with $2 \times 2 \text{ mL}$ of ultrapure water acidified with formic acid (0.1%) at a flow rate of 5 mL min^{-1} . The analyte was spiked into a water sample of 250 mL. The water samples were immediately loaded on the SPE cartridges at 5 mL min^{-1} . After the loading step, the cartridges were cleaned with ultrapure water adjusted to pH 3 with formic acid ($2 \times 2 \text{ mL}$). The analyte was then eluted successively with $2 \times 2 \text{ mL}$ of methanol at a flow rate of 3 mL min^{-1} .

The eluates were transferred to a clean conical graduated glass Pyrex® tube (VWR, Fontenay-sous-Bois, France) and concentrated by evaporation under a nitrogen stream to a final volume of 0.1 mL (concentration factor of 2.500). The obtained extracts are then reconstituted using acetonitrile/ultrapure water (55/45, v/v) and transferred to injection vials. Finally, the extracts were stored at 4°C until further analysis.

2.4. Quality parameters

2.4.1. Linearity, limit of detection and limit of quantification

The linearity of the method was studied from the calibration curves prepared from spiked ultrapure water samples at seven pentachlorophenol concentrations ranging from 25 to $200 \mu\text{g L}^{-1}$. Each solution was analysed in triplicate. The calibration curves were plotted by the peak area versus the concentration of analyte. The linearity was evaluated by linear regression analysis determined by the least squares regression method.

This method was used to determine the slope, intercept, and correlation coefficient (R^2) of the linear regression equation. The instrumental limit of detection (ILD) is the lowest concentration of analyte that gives a measurable response (signal to noise ratio (S/N) of 3), while the instrumental quantification limit (IQL) is the lowest concentration of analyte which can be accurately quantified (S/N of 10).

2.4.2. Precision and accuracy

The precision of the proposed instrumental method was evaluated in terms of repeatability (intra-day and inter-day precision). The repeatability values were expressed as relative standard deviation (RSD, %). It was determined by analyzing six replicates (n=6) of IQL samples. The intra-day precision was assessed by analyzing the IQL samples six times within a single day and the inter-day precision was calculated by determining the IQL samples over three days.

2.4.3. Extraction recovery and matrix effect

SPE recoveries were determined quantitatively at low and high concentration levels. The extraction recoveries (R, %) were assessed by comparing the analytical results obtained for an extracted sample using the developed SPE procedure to an unextracted pure standard. Thus, the extraction recovery of pentachlorophenol was calculated as ratio of the peak areas of the extracted and unextracted samples.

The matrix effect (ME = C/D, %) was determined as described previously by Kadmi et al. (2014). It was evaluated by comparing the peak areas obtained from the analyte in the presence of the matrix (C: samples spiked for extraction) to the one in absence of the matrix (D: pure standard solution). In this study, the matrix effect was evaluated by using a real water samples. Then, the relative standard deviations (RSD, %) were also calculated.

3. Results and discussion

3.1. Optimization of UHPLC/MS/MS conditions

The primary aim of this work was to evaluate the potential of UHPLC system for the analysis of pentachlorophenol in water samples. The UHPLC system takes full advantage of chromatographic separation with high resolution and rapid analysis

time by using columns packed with smaller particles (1.7 μm). Chromatographic conditions such as stationary phase, mobile phase composition and pH and elution mode were optimized in this study through several tests in order to obtain a good resolution, increase the signal of PCP in water samples and short run time. Several reversed phase columns such as Acquity BEH HSS T3 (100 x 2.1 mm, 1.7 μm), Acquity BEH C8 (100 x 2.1 mm, 1.7 μm) column and Acquity BEH C18 column (100 x 2.1 mm, 1.7 μm) were carefully tested in order to obtain optimal efficiency, selectivity, symmetric peak shape and reduced retention time. The Acquity BEH C18 (100 x 2.1 mm, 1.7 μm) was finally chosen in this work because it gives good peak shape and sensitivity. Different compositions of binary mixtures (of acetonitrile-ultrapure water and methanol-ultrapure water with different additives such as acetic or formic acid), were investigated as eluting solvents in both isocratic and gradient modes to achieve good separation in minimum run time for the target analyte. It was found that acetonitrile gave the better chromatographic separations (data not shown) under gradient mode. Moreover, it was observed that the addition of formic acid (0.1% v/v) remarkably improve the peak symmetry and the ionization of the target molecule (Table 1).

Therefore, a mobile phase of acetonitrile-water with formic acid (0.1%, v/v) was selected in this work for PCP separation and quantification. Elution was done in gradient mode performed as follows: by increasing linearly the content of organic modifier from 5% (initial) to 55% within 2 min, then, the percentage of A was increased linearly up to 100% between 2-4 min and then return to initial conditions 5% (A) for a 1.5 min (Table 1). Under optimized chromatographic conditions the obtained retention time for PCP was 3 min (Fig. 1). In addition, blanks were periodically run during the analysis to confirm the absence of contamination.

Table 1. Optimized conditions of UHPLC and MS/MS for the pentachlorophenol analysis

| <i>UHPLC conditions</i> | |
|--|--|
| Column | Waters Acquity BEH C18 (100 x 2.1 mm, 1.7 μm) |
| Column temperature ($^{\circ}\text{C}$) | 45 |
| Mobile phase | Acetonitrile (A) and ultrapure water (B) containing 0.1% (v/v) formic acid (pH 3) |
| Gradient program | 5-55% (A) within 0-2 min; 55-100% (A) within 2-4 min; return to the initial conditions of 5% (A) for a 1.5 min |
| Flow rate of the mobile phase | 0.4 mL min ⁻¹ |
| Injection volume | 5 μL |
| <i>MS/MS conditions</i> | |
| Source temperature ($^{\circ}\text{C}$) | 120 |
| Capillary voltage (kV) | 3.0 |
| Desolvation temperature ($^{\circ}\text{C}$) | 350 |
| Desolvation gas flow (L h ⁻¹) | 750 |
| Cone gas flow (L h ⁻¹) | 75 |
| Quantification transition, m/z | 263.0 > 35.5 |
| Confirmation transition, m/z | 263.1 > 263.5 |
| Cone voltage (V) | 25 |
| Collision energy (eV) | 10 |

Atmospheric pressure chemical ionization (APCI) and ESI (electrospray ionization) interfaces with positive and negative ionization were evaluated in order to get the optimal analytical conditions for the determination of PCP.

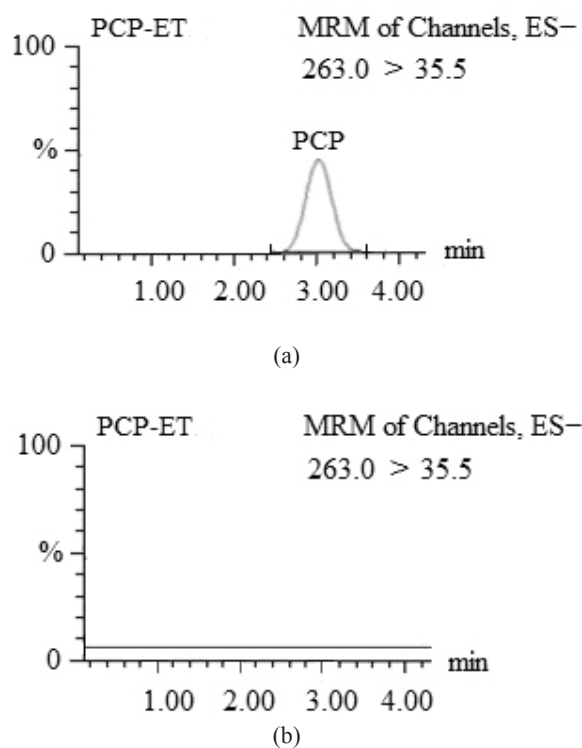


Fig. 1. Representative MRM chromatogram obtained from UHPLC/MS/MS analysis: (a) ultrapure water sample spiked with a standard solution of pentachlorophenol (concentration level IQL); (b) ultrapure water sample (blank)

Obtained results revealed that the optimal conditions for analyte quantification were achieved with ESI interface functioning in negative mode due to its high sensitivity. The different mass spectrometric parameters of the interface were optimized by direct injection of standard solution of analyte ($50 \mu\text{g L}^{-1}$) into the mass spectrometer. The selected parameters are as follows: source temperature, 120°C ; desolvation temperature, 350°C and a capillary voltage, 3 kV . Nitrogen was used as desolvation gas (750 L h^{-1}) and as cone gas (75 L h^{-1}).

Optimization of cone voltage was carried out by scanning the voltage from 10 to 120V with the full scan mode and a scan time of 1s. No additional molecular fragment was observed by increasing voltage and finally a cone voltage of 25V was established to be sufficient for analyte detection because this provided very good sensitivity for PCP. The MS/MS parameters selected for the determination of considered molecule were detailed in Table 1. Thus, these parameters remained fixed during a single analysis.

Moreover, in this study, two sensitive MRM transitions were selected for analyte determination. Indeed, two transitions have to be recorded for the considered compound in order to get a sufficient number of identification points for a suitable confirmation. Thus, in this work, the peak area of the most intense transition was used for quantitative purposes and the less intense transition was used for the confirmation of each analyte. The selected multiple reaction monitoring transitions PCP analysis are presented in Table 1.

3.2. Analytical performance of the UHPLC/MS/MS method

Once optimized, the instrumental method was characterized in terms of limit of detection, limit of quantification, precision, accuracy, and extraction recovery. The tests were carried out without organic interfering species (ultrapure water). The obtained results are summarized in Table 2. External calibration curve (6 levels and 1 blank) was established by plotting the peak areas against analyte concentration. Linear range of pentachlorophenol was obtained in the range of $0.1 - 100 \mu\text{g L}^{-1}$. The slope and intercept value for calibration curve was $y = 409.63x + 85.01$. The results show excellent correlation between the peak area and concentration of PCP ($R^2 = 0.998$). As stated previously, the instrumental limits of detection and quantification (IDL and IQL) of the proposed method were calculated based on a signal to noise ratio (S/N) of 3 and 10 respectively.

The instrumental IDL and IQL were found to be 0.1 and $0.3 \mu\text{g L}^{-1}$, respectively. The precision of the proposed instrumental method was expressed as intra-day and inter-day relative standard deviations (RSDs). It was assessed by replicate ($n=6$) analysis of ultrapure water samples spiked with PCP at a concentration level of $10 \mu\text{g L}^{-1}$. The obtained intra-day and inter-day RSDs values were 99.78% and 99.12%, respectively. These results highlight the good performance of the new developed instrumental method.

Table 2. Performance data of the optimized instrumental UHPLC/MS/MS method for the analysis of pentachlorophenol in water

| Compound | Value |
|---|-----------------------|
| Linear range ($\mu\text{g L}^{-1}$) | 0.1 - 100 |
| Calibration curve | $y = 409.63x + 85.01$ |
| Regression coefficient (R^2) | 0.998 |
| IDL ^a ($\mu\text{g L}^{-1}$) | 0.1 |
| IQL ^a ($\mu\text{g L}^{-1}$) | 0.3 |
| Intra-day precision (mean \pm RSD ^b , $\mu\text{g L}^{-1}$) | 99.78 |
| Inter-day precision (mean \pm RSD ^b , $\mu\text{g L}^{-1}$) | 99.12 |

^aInstrumental detection and quantification limit

^bRSD, relative standard deviation expressed in percentage. Calculated for six samples ($n=6$) spiked at $10 \mu\text{g L}^{-1}$

3.3. Extraction recovery

In order to have a more sensitive method for the quantification of pentachlorophenol in water samples, an extraction-preconcentration step prior to chromatographic analysis is necessary. As stated below, in order to decrease the limit of detection and quantification of PCP in water sample an off-line solid phase extraction methodology was developed in this work. SPE experiments were carried out after the optimization of UHPLC/MS/MS conditions. The optimization of the extraction process was performed in order to attain excellent recoveries for the target compound in a single extraction step. According to literature data, Oasis HLB cartridges are one of the most used, because they are able to retain a large list of organic pollutants (acidic, neutral and basic molecules) through its unique ratio of hydrophilic N-vinylpyrrolodone and lipophilic divinylbenzene sorbent (de Almeida et al., 2000). Thus, Oasis HLB cartridges were selected and used in this work.

The performance of the proposed SPE protocol was investigated through extraction recoveries obtained for six replicates in spiked ultrapure water samples at three quality control concentrations (10, 20 and 100 $\mu\text{g L}^{-1}$). Examination of results obtained by using the optimized SPE procedure showed very good recoveries for PCP (Table 3). Indeed, the calculated extraction recoveries were within the range of 2.4% and 3.15% at all quality control levels (Table 3).

On the other hand, the instrumental detection limits of the developed method were 0.1 $\mu\text{g L}^{-1}$; while detection limits obtained with the overall SPE-UHPLC/MS/MS method was 0.04 ng L^{-1} . These results are better than those previously reported in the literature for SPE-LC analysis (Opeolu et al., 2010) and are below the legal tolerance level for each chlorophenol in drinking water (100 ng L^{-1}) according to the European Community Directive

(Elci et al., 2011). The proposed SPE-UHPLC-MS/MS method therefore allowed quantification limits in the range of ng L^{-1} and an enrichment factor of 2500 for the both phenolic compounds (sample volume, 250 mL to 0.1 mL).

3.4. Analysis of real water samples

The developed SPE-UHPLC/MS/MS method was then applied for the determination of extraction recoveries from different real water samples (river water) collected from different locations situated in the Brittany region (France) in order to test the possible effects of the water matrix constituents and also the applicability of the proposed analytical methodology for environmental use.

The matrix effect is a phenomenon with great influence in liquid chromatography associated to mass spectrometry. Indeed, a such phenomenon disturb the ionization of analytes leading generally to an enhancement or an inhibition of compound signal (Kasprzyk-Horden et al., 2008).

In this study the matrix effects were studied in three surface water samples (used to supply drinking water treatment plant) spiked before extraction with a standard solutions of PCP at two levels of concentration (10 and 50 $\mu\text{g L}^{-1}$). All experiments were performed in six replicates ($n=6$). The extraction recoveries obtained with real water (surface water) samples are summarized in Table 4.

Extraction recoveries obtained with HLB cartridges were between 97.87% and 101.31% with relative standard deviations less than 4.5%. The obtained results are very close with the ones obtained in ultrapure water. Moreover, the signal obtained by the analysis of extracts at two concentration levels was compared to that obtained with pure standard solutions injected six times onto the chromatographic system.

Table 3. Recovery results and relative standard deviations (RSD, %) obtained with Oasis HLB cartridges after the extraction of 250 mL ultrapure water sample spiked at three concentration levels

| <i>Samples</i> | <i>Sample (A)</i> | <i>Sample (B)</i> | <i>Sample (C)</i> |
|---|-------------------|-------------------|-------------------|
| Concentration of blank ($\mu\text{g L}^{-1}$) | n.d. ^a | n.d. ^a | n.d. ^a |
| Spiked concentration ($\mu\text{g L}^{-1}$) | 10 | 20 | 100 |
| Founded ($\mu\text{g L}^{-1}$) | 0.982 | 9.979 | 50.09 |
| Recovery (%) | 98.20 | 99.79 | 100.18 |
| RSD (%; $n=6$) | 2.8 | 3.15 | 2.4 |

^an.d. referred to not detected.

Table 4. Recovery study of the developed method for PCP analysis performed using real samples (water river) spiked at two concentrations levels (10 and 50 $\mu\text{g L}^{-1}$)

| <i>Real sample</i> | <i>Conc. spiked ($\mu\text{g L}^{-1}$)</i> | <i>Conc. measured ($\mu\text{g L}^{-1}$)</i> | <i>Recovery (%)</i> | <i>RSD (%; $n = 6$)</i> |
|--------------------|---|---|---------------------|------------------------------------|
| Water R1 | 10 | 9.787 | 97.87 | 3.50 |
| | 50 | 49.72 | 99.44 | 3.10 |
| Water R2 | 10 | 10.13 | 101.31 | 4.25 |
| | 50 | 49.84 | 99.68 | 3.78 |
| Water R3 | 10 | 9.908 | 99.08 | 3.63 |
| | 50 | 49.11 | 98.22 | 4.39 |

Under these conditions no suppression or enhancement of the analyte signal was observed. Thus, no detectable matrix effect was observed. These results clearly demonstrate that the developed SPE-UHPLC/MS/MS methodology is not influenced by the water quality and the extraction recoveries obtained in ultrapurewater are transposable to real water samples. Therefore, the proposed analytical strategy is feasible to be used for the PCP monitoring at ultra trace levels in environmental water samples.

5. Conclusions

A new highly sensitive UHPLC/MS/MS method for the determination of ultra-trace levels of PCP in water samples was developed in this study. Good linearity, precision, accuracy, lower limits of detection, and limits of quantification were obtained. The proposed SPE methodology led to satisfactory extraction recoveries and high pre-concentration factors of the considered target analyte in different environmental water samples. In addition, in the described conditions, no significant matrix effect influences the PCP quantification under real analysis conditions.

To the best of our knowledge this is the first analytical strategy allowing highly sensitive quantification of this hazardous organic compound in environmental water samples.

In conclusion, this simple, rapid, low-cost, and reliable method can be applied for routine quantitative analysis of the target analytes at ultra-trace concentration levels (ng L^{-1}) in different types of water samples. This method can be a useful analytical tool for future toxicological and water quality surveillance studies or for the evaluation of the water disinfection processes.

References

- Bagheri H., Saraji M., (2001), New polymeric sorbent for solid phase extraction of chlorophenols from water samples followed by gas chromatography-electron-capture detection, *Journal of Chromatography A*, **910**, 87-93.
- Barták P., Frnková P., Cáp L., (2000), Determination of phenols using simultaneous steam distillation extraction, *Journal of Chromatography A*, **867**, 281-287.
- Callejon R.M., Troncoso A.M., Morales M.L., (2007), Analysis of chloroanisoles and chlorophenols in cork by stir bar sorptive extraction and gas-chromatography-mass spectrometry, *Talanta*, **71**, 2092-2097.
- Dallaire R., Muckle G., Dewailly E., Jacobson S.W., Jacobson J.L., Sandanger T.M., Sandau C.D., Ayotte P., (2009), Thyroid hormone levels of pregnant Inuit women and their infants exposed to environmental contaminants, *Environmental Health Perspectives*, **110**, 411-417.
- de Almeida A.D., Lacorte S., Vinas T., Viana P., Barcelo D., (2000), Monitoring of priority pesticides and other organic pollutants in river water from Portugal by gas chromatography-mass spectrometry and liquid chromatography-atmospheric pressure chemical ionization mass spectrometry, *Journal of Chromatography A*, **879**, 13-26.
- Domeno C., Munizza G., Nerin C., (2005), Development of a solid-phase microextraction method for direct determination of pentachlorophenol in paper and board samples: comparison with conventional extraction method, *Journal of Chromatography A*, **1095**, 8-15.
- Dudal Y., Jacobson A.R., Samson R., Deschenes L., (2004), Modelling the dynamics of pentachlorophenol bioavailability in column experiments, *Water Research*, **38**, 3147-3154.
- Elci L., Kolbe N., Elci S.G., Anderson J.T., (2011), Solid phase extractive pre-concentration coupled to gas chromatography-atomic emission detection for the determination of chlorophenols in water samples, *Talanta*, **85**, 551-555.
- EPA, (2004), List of drinking water contaminants & MCLs: On line at: <http://www.epa.gov/safewater/mcl.html>.
- Favaro G., Leo D.D., Pastore P., Magno F., Ballardini A., (2008), Quantitative determination of chlorophenols in leather by pressurized liquid extraction and liquid chromatography with diode-array detection, *Journal of Chromatography A*, **1177**, 36-42.
- Gao J., Liu L., Liu X., Zhou H., Huang S., Wang Z., (2008), Levels and special distribution of chlorophenols – 2,4-Dichlorophenol, 2,4,6-trichlorophenol, and pentachlorophenol in surface water of China, *Chemosphere*, **71**, 1181-1187.
- Gavrilescu M., (2009), Behaviour of persistent pollutants and risks associated with their presence in the environment – integrated studies, *Environmental Engineering and Management Journal*, **8**, 1517-1531.
- Ge J., Pan J., Fei Z., Wu G., Giesy J.P., (2007), Concentrations of pentachlorophenol (PCP) in fish and shrimp in Jiangsu Province, China, *Chemosphere*, **69**, 164-169.
- Gremaud E., Turesky R.J., (1997), Rapid analytical methods to measure pentachlorophenol in wood, *Journal of Agricultural and Food Chemistry*, **45**, 1229-1233.
- Ho H.P., Lee R.J., Lee M.R., (2008), Purge-assisted headspace solid-phase microextraction combined with gas chromatography-mass spectrometry for determination of chlorophenols in aqueous samples, *Journal of Chromatography A*, **1213**, 245-248.
- IARC, (1991), Summaries & Evaluations, Pentachlorophenol, International Agency for Research on Cancer, Lyon, France, **53**, 371.
- Jakab A., Manea F., Bantas C., Remes A., Pop A., Pode R., Schoonman J., (2013), Unmodified/TiO₂-modified carbon nanotubes composite electrodes for pentachlorophenol detection from water, *Environmental Engineering and Management Journal*, **12**, 999-1005.
- Jakab A., Pop A., Orha C., Manea F., Pode R., (2014), Electrochemical degradation and determination of pentachlorophenol from water using TiO₂-modified zeolite-carbon composite electrodes, *Environmental Engineering and Management Journal*, **13**, 2159-2165.
- Kadmi Y., Favier L., Soutrel I., Lemasle M., Wolbert D., (2014), Ultratrace-level determination of N-Nitrosodimethylamine, N-Nitrosodiethylamine, and N-Nitrosomorpholine in waters by solid-phase extraction

- followed by liquid chromatography-tandem mass spectrometry, *Central European Journal of Chemistry*, **12**, 928-936.
- Kadmi Y., Favier L., Wolbert D., (2015), N-nitrosamines, emerging disinfection by-products of health concern: an overview of occurrence, mechanisms of formation and analysis in water, *Water Science and Technology: Water Supply*, **15**, 11-25.
- Kasprzyk-Hordern B., Dinsdale R. M., Guwy A.J., (2008), The effect of signal suppression and mobile phase composition on the simultaneous analysis of multiple classes of acidic/neutral pharmaceuticals and personal care products in surface water by solid-phase extraction and ultra performance liquid chromatography-negative electrospray tandem mass spectrometry, *Talanta*, **74**, 1299-1312.
- Korenman Y.I., Grudzev I.V., Kondratenok B.M., Fokin V.N., (2003), Determination of chlorophenols in potable water : preconcentration by solvent extraction, derivatization of the extract, and chromatographic analysis of the derivatives, *Journal of Analytical Chemistry*, **58**, 635.
- Llompert M., Lourido M., Landín P., Garcá-Jares C., Cela R., (2002), Optimization of a derivatization solid-phase microextraction method for the analysis of 30 phenolic pollutants in water samples, *Journal of Chromatography A*, **963**, 137-140.
- Llorca-Porcel J., Martinez-Parreno M., Martinez-Soriano E., Valor I., (2009), Analysis of chlorophenols, bisphenol A, 4-tert-octylphenol and 4-nonylphenols by means of ultra sonic solvent extraction and stir bar sorptive extraction with *in situ* derivatisation, *Journal of Chromatography A*, **1216**, 5955-5961.
- Michalowicz J., Duda W., (2007), Phenols – Sources and Toxicity, *Polish Journal of Environmental Studies*, **16**, 347-362.
- Opeolu B.O., Fatoki O.S., Odendaal J., (2010), Development of a solid-phase extraction method followed by HPLC-UV detection for the determination of phenols in water, *International Journal of the Physical Sciences*, **5**, 576-581.
- Padilla-Sánchez J.A., Plaza-Bolaños P., Romero-González R., Barco-Bonilla N., Martínez-Vidal J.L., Garrido-Frenich A., (2011), Simultaneous analysis of chlorophenols, alkylphenols, nitrophenols and cresols in wastewater effluents, using solid phase extraction and further determination by gas chromatography-tandem mass spectrometry, *Talanta*, **85**, 2397-2404.
- Pugliese P., Molto J.C., Damiani P., Marin R., Cossignani R., Manes J., (2004), Gas chromatographic evaluation of pesticide residue contents in nectarine after non-toxic washing treatments, *Journal of Chromatography A*, **1050**, 185-191.
- Wei M.-C., Jen J.-F., (2002), Determination of aqueous chlorophenols by microwave-assisted headspace solid-phase microextraction and gas chromatography, *Chromatographia*, **55**, 701-706.
- Wennrich L., Popp P., Moder M., (2000), Determination of chlorophenols in soils using accelerated solvent extraction combined with solid-phase microextraction, *Analytical Chemistry*, **72**, 546-551.
- Yang S., Han X., Wei C., Chen J., Yin D., (2005), The toxic effects of pentachlorophenol on rat Sertoli cells in vitro, *Environmental Toxicology and Pharmacology*, **20**, 182-187.
- Yang C.F., Lee C.M., Wand C.C., (2006), Isolation and physiological characterization of the pentachlorophenol degrading bacterium *Sphingomonas chlorophenolica*, *Chemosphere*, **62**, 709-714.
- Zheng W.W., Yu H., Wang X., Qu W.D., (2012), Systematic review of pentachlorophenol occurrence in environment and in humans in China: not a negligible health risk due to the re-emergence of schistosomiasis, *Environment International*, **42**, 105-116.



“Gheorghe Asachi” Technical University of Iasi, Romania



COMPARATIVE STUDIES ON KINETICS OF ANAEROBIC AND AEROBIC BIODEGRADATION OF LIPIDS FROM OLIVE OIL MILL WASTEWATERS WITH MIXTURE OF *Bacillus spp.* CELLS

Ramona-Mihaela Matran¹, Alexandra-Cristina Blaga¹, Dan Cașcaval^{1*},
Alexandra Tucaliuc¹, Anca-Irina Galaction²

¹“Gheorghe Asachi” Technical University of Iasi, Faculty of Chemical Engineering and Environmental Protection,
73 Prof. dr. docent Dimitrie Mangeron Str., 700050 Iasi, Romania

²“Grigore T. Popa” University of Medicine and Pharmacy of Iasi, Faculty of Medical Bioengineering,
9-13 M. Kogalniceanu Str., 700454 Iasi, Romania

Abstract

The experiments on the olive oil mill wastewater treatment for removing the lipids by anaerobic and aerobic biodegradation with mixed *Bacillus spp.* culture indicated that the rate of the aerobic process is up to two times higher than that of the anaerobic one. In this context, it was found that the influence of the dissolved oxygen concentration on the lipids biodegradation process is significant, but the kinetic model given in literature does not consider this parameter. Therefore, using the dependence between the ratio of specific rates, for aerobic and anaerobic processes, and the concentration of oxygen dissolved in medium, the new model $-\frac{dC_{TL}}{dt} = k_d \cdot C_{O_2}^{0.62} \cdot C_{TL}$ was established for describing the kinetics of aerobic biodegradation with *Bacillus spp.* This model is more adequate for the studied systems of lipids-rich wastewaters bacterial treatment, offering the maximum error of 12.6% and the average one of $\pm 6.84\%$.

Key words: *Bacillus spp.*, biodegradation, kinetics, lipids, specific rate

Received: November, 2014; Revised final: March, 2015; Accepted: March, 2015

1. Introduction

Lipids are organic water insoluble biomolecules produced in different amounts by microbial, vegetal, and animal cells. Among the complex lipids, a particular class includes the triglycerides, namely fats and oils.

According to the Global Industry Analysts Report, the worldwide production of vegetable oils increased from 130 millions tonnes in 2010 to 144 millions tonnes in 2011, being estimated at 169 millions tonnes for 2015 (GIA, 2010). This evolution is related to the population and, implicitly, consumption increase, as well as to the

diversification of the vegetable oils utilization from food to chemical industry.

The producers of vegetable oils are important sources of wastewaters, the characteristics of pollutants depending on the used raw materials and technologies. The olive oil represents about 3% from the worldwide production of vegetable oils, most of this quantity being consumed in Europe. The wastewaters resulted from olive oil mills are important pollutants, due to their high organic content (lipids 0.2-1%, carboxylic acids 0.5-1.5%, sugars 1-8%, polyphenols and pectins 1-1.5%, tannins, polyalcohols etc.) (Azbar et al., 2004; Benitez et al., 1997). Most of the difficulties

* Author to whom all correspondence should be addressed: e-mail: dancasca@ch.tuiasi.ro; Fax: 0040232271311

associated with the pollution generated by olive oil mills wastewaters are related to the insoluble organic biopolymers, mainly lipids, and polyphenols, because these compounds affect drastically the activity of aquatic microorganisms or organisms (Aggelis et al., 2003; Mekki et al., 2007).

Several physical and chemical methods (decantation, concentration by evaporation, filtration and ultrafiltration, reverse osmosis, flotation, adsorption, oxidation and photo-oxidation etc.) (Camarota and Freire, 2006; Deschamps et al., 2003; Khoufi et al., 2007; Mameri et al., 2000; Moazed and Viraraghavan, 2005; Mysore et al., 2005; Sun et al., 2002), as well as biological or enzymatic ones (Aggelis et al., 2003; Asses et al., 2009; Benitez et al., 1997; Daims et al., 2006; Galaction et al., 2014; Gavrilescu and Chisti, 2005; Lan et al., 2009; Martinez-Garcia et al., 2009; Mechri et al., 2010; Peixoto et al., 2008; Ucisik and Henze, 2008; Zeeman and Sanders, 2001) have been tested for the treatment of lipids-rich wastewaters. The biotreatment is based on aerobic or non-aerobic processes using free or immobilized bacteria (*Burkholderia cepacia*, *Phormidium* spp., *Oscillatoria* spp., *Chroococcus* spp., *Enterobacter aerogenes*, *Mucor racenosus*), yeasts (*Candida oleophila*, *Candida tropicalis*, *Yarrowia lipolytica*), fungus (*Apergillus niger*, *Phanerochaete cryosporium*, *Lentinus edodes*, *Pleorotus ostreatus*, *Funalia trogii*, *Geotrichum candidum*, *Mucor rouxii*, *Absidia coerulea*, *Penicillium restrictum*, *Penicillium verucosum*) or enzymes (*lipases*). In the biological systems, the triglycerides are bioconverted to long chain fatty acids, which are finally oxidated to acetate or propionate and used for energy production or biomass growth (Chipasa and Medrzycka, 2006; Galaction et al., 2014; Gavrilescu and Chisti, 2005; Rinzema, 2003; Zeeman and Sanders, 2001). Because the lipids are water insoluble and, implicitly, inaccessible for the microorganism metabolism, they are initially hydrolyzed to low molecular weight compounds (fatty acids) by the microbial enzymes. These enzymes secretion is induced after the contact with the pollutants. Generally, the lipids are more rapidly consumed in the presence of oxygen, but the choice of aerobic vs. anaerobic operating conditions for wastewaters treatment at industrial scale depends on the costs of equipments and energy for aeration.

Although most of bacteria are able to use a large spectrum of natural compounds or pollutants as carbon and energy sources, one single bacterial culture does not possess the ability to metabolize all pollutants existing in the wastewater. However, the mixed cultures exhibit an amplified biodegradative potential against the xenobiotic compounds (Fritsche and Hofrichter, 2000). The use of active sludge for wastewaters treatment is more convenient from the point of view of operating cost. But, in this case, the phenomenon of flotation cannot be avoided, due to the adsorption of lipids in sludge, its intensity becoming important at high oils content (Chipasa and Medrzycka, 2006; Rinzema, 2003).

This phenomenon affects the efficiency of biological treatment. For this reason, although they are rather expensive, the treatments systems for wastewaters containing lipids with selected microorganisms or enzymes become more and more preferred, owing to their superior efficiency and productivity (Caşcaval et al., 2012).

The bacterial biodegradation of lipids can be kinetically described by the model developed by Pavlostathis and Giraldo-Gomez, 1991. This model is rather simple, being related only to the lipids concentration in the media. For this reason, its relevance for the aerobic processes is limited, due to the significant influence of oxygen content on the lipids biodegradation rate.

In this context, our studies are focused on the analysis of the performances of the anaerobic and aerobic biological treatments of olive oil mill wastewaters using mixed *Bacillus* spp. culture. By means of the experimental results, a new and more complex kinetic model for aerobic bacterial bioconversion of lipids has been proposed and compared with that from literature.

2. Experimental

The experiments were carried out in 2 L laboratory stirred bioreactor (Fermac, Electrolab), provided with computer-controlled and recorded parameters. The bioreactor mixing system consists of one turbine impeller and three baffles. The bioreactor and impeller characteristics are given in a previous paper (Caşcaval et al., 2012).

For the anaerobic biodegradation process, the dissolved oxygen amount from medium was not controlled during the process, varying free from its initial value of 1.6 mg/L. For the aerobic process, the bioreactor was provided with the sparging system consisting of a perforated tube with 7 mm diameter, placed at 15 mm from the vessel bottom, having 4 holes with 1 mm diameter. The air volumetric flow rate was varied between 5 and 30 L/h, in order to maintain the dissolved oxygen concentration at a prescribed constant value in the domain of 1.6 - 5.9 mg/L. The rotation speed was maintained at 150 rpm.

The bioreactor contained 1 L of olive oil - water emulsion (the oil concentration was 10 mg/L emulsion). According to the previous studies on olive oil biodegradation with *Bacillus* spp. cells (Caşcaval et al., 2012), the pH and temperature have been adjusted and maintained at the optimum values, namely 8 and 40 °C, respectively.

In the experiments, mixture of *Bacillus* spp. has been used (*Bacillus subtilis*, *Bacillus megaterium*, *Bacillus licheniformis*, and *Bacillus ortoliquefaciens* in equal ratios). The concentration of bacteria cells was 1 g d.w./100 ml medium. The fermentation end has been considered when either the olive oil was completely consumed or its concentration remained constant for 12 h. The process evolution has been analyzed by means of the

variation of total lipids, using the spectrophotometric method with triolein (Levy, 1972).

3. Results and discussion

The variation of total lipids concentration from wastewater during the anaerobic and aerobic biodegradation process with free *Bacillus spp.* cells is plotted in Fig. 1.

It can be observed that the concentration of lipids is more rapidly decreased in the aerobic process, the rate of lipids consumption being accelerated by increasing the concentration of oxygen in the medium. Therefore, for the anaerobic biodegradation, the total lipids content is reduced to 1.3 g/L after 60 h, while for aerobic process it is possible to become 0 g/L after 40 h, depending on the oxygen concentration.

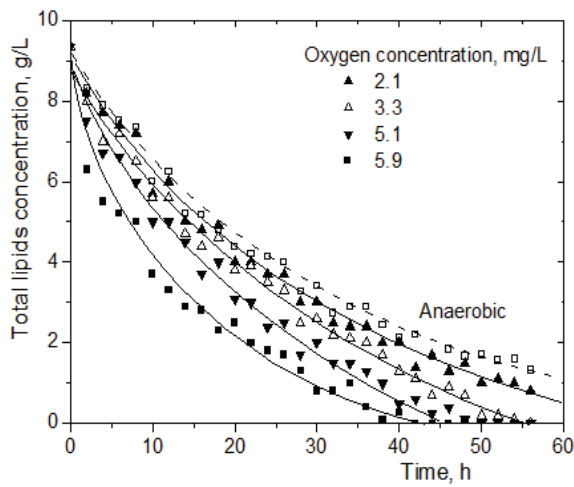


Fig. 1. Variation of total lipids concentration during their anaerobic and aerobic bacterial biodegradation

These results can be suggestively underlined by plotting in Fig. 2 the dependence between the average rate of lipids biodegradation and the value of dissolved oxygen concentration. The average rate of process is defined by (Eq. 1).

$$\bar{r}_d = \frac{C_{TL0} - C_{TL}}{t} \quad (1)$$

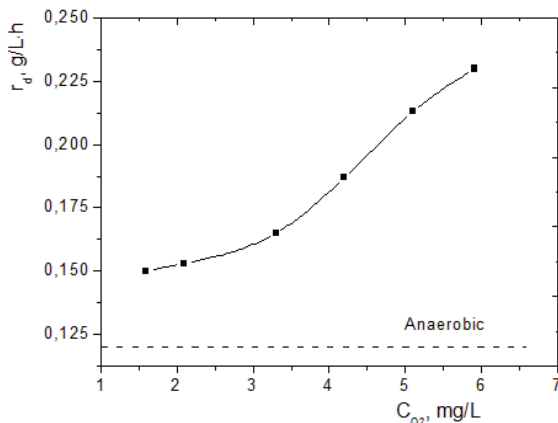


Fig. 2. Influence of oxygen concentration on average rate of lipids bacterial biodegradation

By increasing the concentration of oxygen dissolved in medium from 1.6 to 5.9 mg/L, Fig. 2 indicates that the average rate is accelerated for about 1.5 times. Compared to the anaerobic process, at 5.9 mg/L oxygen concentration the average biodegradation rate becomes for over 1.9 times higher.

The kinetic analysis of the lipids bacterial biodegradation under anaerobic conditions considers initially the model proposed by Pavlostathis and Giraldo-Gomez, 1991 (Eq. 2).

$$-\frac{dC_{TL}}{dt} = k_d \cdot C_{TL} \quad (2)$$

For establishing the value of the specific biodegradation rate for the anaerobic process, k_d , the straight line resulted by solving Eq. (2) has been plotted in Fig. 3.

$$\ln \frac{C_{TL0}}{C_{TL}} = k_d \cdot t \quad (3)$$

In the case of aerobic consumption of lipids, Eq. (2) was adapted by including the modified specific rate, k_d' , which is a function on oxygen concentration (Eq. 4).

$$-\frac{dC_{TL}}{dt} = k_d' \cdot C_{TL} \quad (4)$$

Because the oxygen concentration inside the medium is controlled and maintained at a constant level during the aerobic biodegradation process, the value of k_d' could be calculated at different oxygen concentrations similarly to the above presented algorithm, by plotting the corresponding straight lines (Fig. 3).

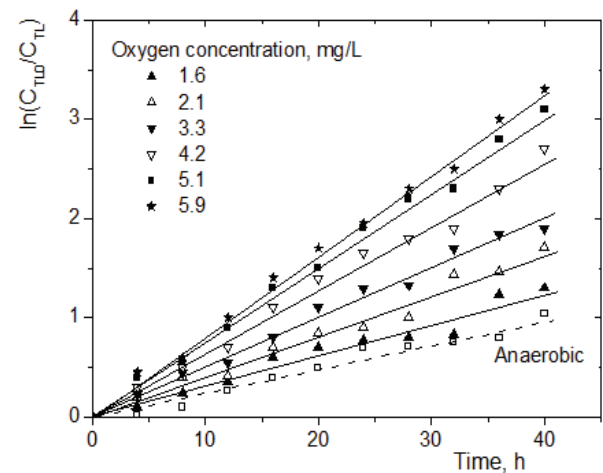


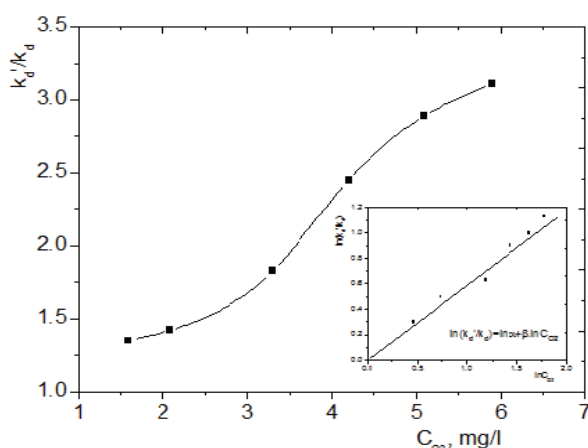
Fig. 3. Graphical calculation of specific biodegradation rate (for anaerobic process) and apparent specific biodegradation rate (for aerobic process)

The values of specific rate and modified specific rates at different concentrations of oxygen in medium are given in Table 1.

Table 1. Values of specific rate, k_d , and modified specific rate, k_d' , of lipids biodegradation with cells of *Bacillus spp.*

| C_{O_2} , mg/L | Anaerobic | 1.6 | 2.1 | 3.3 | 4.2 | 5.1 | 5.9 |
|--|-----------|------|-----|------|-----|------|------|
| k_d , $k_d' \times 10^2$, h ⁻¹ | 2.61 | 3.53 | 3.7 | 4.76 | 6.4 | 7.55 | 8.12 |

For quantifying the influence of aerobic conditions on the rate of lipids biodegradation with *Bacillus spp.*, it was analyzed the variation of the ratio k_d'/k_d with the increase of oxygen concentration. This dependence, plotted in Fig. 4, suggests the following exponential correlation (Eq. 5). The values of coefficient α and exponent β can be calculated graphically by linearizing the Eq. (5), according to Fig. 4. Therefore, Eq. (5) becomes Eq. (6). Consequently, the aerobic degradation of lipids from olive oil using *Bacillus spp.* can be described by the kinetic model expressed by Eq. (7).

**Fig. 4.** Influence of oxygen concentration on ratio k_d'/k_d

$$\frac{k_d'}{k_d} = \alpha \cdot C_{O_2}^\beta \quad (5)$$

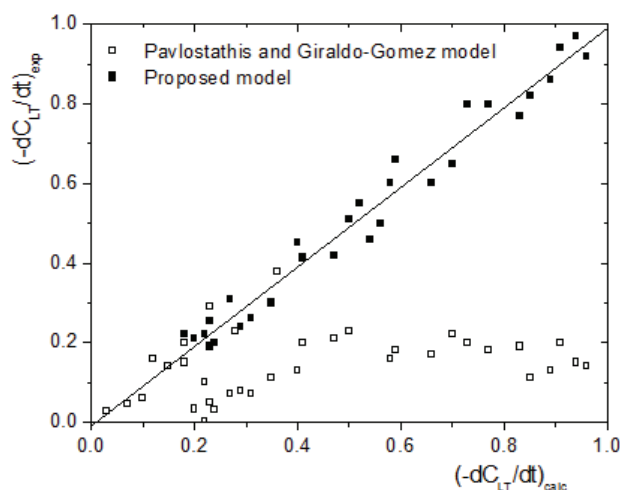
$$\frac{k_d'}{k_d} = C_{O_2}^{0.62} \quad (6)$$

$$-\frac{dC_{TL}}{dt} = k_d \cdot C_{O_2}^{0.62} \cdot C_{TL} \quad (7)$$

The comparison between the experimental values of lipids biodegradation rate and those calculated with Pavlostathis and Giraldo-Gomez model and the proposed Eq. (7) is presented in Fig. 5, which indicates that the model proposed by Pavlostathis and Giraldo-Gomez is adequate for the anaerobic process, when the biodegradation occurs slowly. For the aerobic biodegradation, which corresponds to higher rate of process, the use of this kinetic model leads to important deviations from the experimental data, the calculated values being considerable lower than the real ones.

The kinetic model which considers also the dissolved oxygen concentration describes properly the aerobic biodegradation of lipids. Therefore, from Fig. 5 it can be observed the good concordance between the experimental values of aerobic process

rate and those calculated by means of Eq. (7), the average deviation being $\pm 6.84\%$.

**Fig. 5.** Comparison between the experimental and calculated values of lipids biodegradation rate with *Bacillus spp.*

4. Conclusions

The studies on the biodegradation of lipids from olive oil mill wastewater with *Bacillus spp.* cells under anaerobic and aerobic conditions indicated that the aerobic process could be twice as fast.

Although the dissolved oxygen concentration in the medium exhibits an important influence on efficiency of biodegradation of lipids, the kinetic model proposed in literature does not include any term related to the oxygen concentration. Consequently, by means of the correlation between the modified specific rate, which includes the influence of oxygen concentration, specific rate, for the anaerobic biodegradation, and oxygen concentration, it was established a new kinetic model adequate for aerobic process.

This model offers a good concordance with the experimental results, the average deviation of the calculated values of lipids biodegradable rate from the experimental ones being $\pm 6.84\%$.

Notations

| | |
|-----------|---|
| C_{O_2} | dissolved oxygen concentration, mg/L |
| C_{TL} | total lipids concentration in wastewater, g/L |
| C_{TL0} | initial total lipids concentration in wastewater, g/L |
| k_d | specific rate of lipids biodegradation process, h ⁻¹ |
| k_d' | modified specific rate of lipids biodegradation process considering the dissolved oxygen concentration, h ⁻¹ |
| t | time, h |

References

- Aggelis G., Iconomou D., Christou M., Bokas D., Kotzailia, S., Christou G., Tsagou V., Papanikolaou S., (2003), Phenolic removal in a model olive oil mill wastewater using *Pleurotus ostreatus* in bioreactor cultures and biological evaluation of the process, *Water Research*, **37**, 3897-3904.
- Asses N., Ayed L., Bouallagui H., Ben Rejeb I., Gargouri M., Hamdi M., (2009), Use of *Geotrichum candidum* for olive mill wastewater treatment in submerged and static culture, *Bioresource Technology*, **100**, 2182-2188.
- Azbar N., Bayram A., Ayes F., Ayesn M., Fusun S., Ozer A., (2004), A review of waste management options in olive oil production, *Critical Reviews in Environmental Science and Technology*, **34**, 209-247.
- Benitez J., Beltran-Heredia J., Torregrosa J., Acero J.L., Cercas V., (1997), Aerobic degradation of olive mill wastewaters, *Applied Microbiology and Biotechnology*, **47**, 185-188.
- Cammarota M.C., Freire D.M.G., (2006), A review on hydrolytic enzymes in the treatment of wastewater with high oil and grease content, *Bioresource Technology*, **97**, 2195-2210.
- Caşcaval D., Galaction A.-I., Turnea M., Lupăşteanu A.-M., (2012), Biodegradation of lipids from olive oil mill wastewaters in a stationary basket bioreactor with immobilized *Bacillus spp.* cells – Influence of internal diffusion, *Water Science and Technology*, **65**, 920-926.
- Chipasa K.B., Medrzycka K., (2006), Behavior of lipids in biological wastewater treatment process, *Journal of Industrial Microbiology & Biotechnology*, **33**, 635-645.
- Daims H., Taylor M.W., Wagner M., (2006), Wastewater treatment: a model system for microbial ecology, *Trends in Biotechnology*, **24**, 483-489.
- Deschamps G., Caruel H., Borredon M.E., Bonnin C., Vignoles C., (2003) Oil removal from water by selective sorption on hydrophobic cotton fibres. I. Study of sorption properties and comparison with other cotton fibre-based sorbents, *Environmental Science & Technology*, **37**, 1013-1015.
- Fritzsche W., Hofrichter M., (2000), *Aerobic Degradation by Microorganisms: Principles of Bacterial Degradation*, In: *Biotechnology, Environmental Processes*, vol. IIb, Rehm H.-J., Reed G., Puhler A., Stadler A. (Eds.), Wiley-VCH, Weinheim, 145-167.
- Galaction A.I., Matran R.M., Blaga A.C., Turnea M., Caşcaval D., (2014), Applications of pneumatic bioreactors in wastewaters treatment I. Mixing efficiency and distribution in split-cylinder gas-lift bioreactor for viscous media, *Environmental Engineering Management Journal*, **13**, 2653-2664.
- Gavrilescu M., Chisti Y., (2005), Biotechnology - a sustainable alternative for chemical industry, *Biotechnology Advances*, **23**, 471-499.
- GIA, (2010), Vegetable Oils Cooking and Salad Market Report, San Jose, On line at: <http://www.strategyr.com>.
- Khoufi S., Feki F., Sayadi S., (2007), Detoxification of olive mill wastewater by electrocoagulation and sedimentation processes, *Journal of Hazardous Materials*, **142**, 58-67.
- Lan W., Gang G.E., Jinbao W., (2009), Biodegradation of oil wastewater by free and immobilized *Yarrowia lipolytica* W29, *Journal of Environmental Sciences*, **21**, 237-242.
- Levy A.L., (1972), Measurement of triglycerides using nonane extraction and colorimetry, *Annals of Clinical & Laboratory Science*, **2**, 474-479.
- Mameri N., Halet F., Drouich M., Grib H., Lounici H., Pausse A., Piron D., Belhoucine D., (2000), Treatment of olive mill washing water by ultrafiltration, *The Canadian Journal of Chemical Engineering*, **78**, 590-595.
- Martinez-Garcia G., Johnson A.C., Bachmann R.T., Williams C.J., Burgoyne A., Edyvean R.G.J., (2009), Anaerobic treatment of olive mill wastewater and piggery effluents fermented with *Candida tropicalis*, *Journal of Hazardous Materials*, **164**, 1398-1405.
- Mechri B., Chehab H., Attia F., Mariem F.B., Braham M., Hammami M., (2010), Olive mill wastewater effects on the microbial communities as studied in the field of olive trees by analysis of fatty acid signatures, *European Journal of Soil Biology*, **46**, 312-318.
- Mekki A., Dhoubi A., Sayadi S., (2007), Polyphenols dynamics and phytotoxicity in a soil amended by olive mill wastewaters, *Journal of Environmental Management*, **84**, 134-140.
- Moazed H., Viraraghavan T., (2005), Removal of oil from water by bentonite organoclay, *Practice Periodical of Hazardous, Toxic, and Radioactive Waste Management*, **9**, 130-134.
- Mysore D., Viraraghavan T., Jin Y.C., (2005), Treatment of oily waters using vermiculite, *Water Research*, **39**, 2643-2653.
- Pavlostathis S.G., Giraldo-Gomez E., (1991), Kinetics of anaerobic treatment, *Water Science and Technology*, **24**, 35-59.
- Peixotoa F., Martins F., Amaral C., Gomes-Laranjo J., Almeida J., Palmeira C.M., (2008), Evaluation of olive oil mill wastewater toxicity on the mitochondrial bioenergetics after treatment with *Candida oleophila*, *Ecotoxicology and Environmental Safety*, **70**, 266-275.
- Rinzema A., (2003), Anaerobic digestion of long-chain fatty acids in UASB and expanded granular sludge bed reactors, *Process Biochemistry*, **28**, 527-537.
- Sun X.F., Sun R.C., Sun J.X., (2002), Acetylation of rice straw with or without catalysts and its characterization as a natural sorbent in oil spill cleanup, *Journal of Agricultural and Food Chemistry*, **50**, 6428-6433.
- Ucisk A.S., Henze M., (2008), Biological hydrolysis and acidification of sludge under anaerobic conditions: The effect of sludge type and origin on the production and composition of volatile fatty acids, *Water Research*, **42**, 3729-3738.
- Zeeman G., Sanders W., (2001), Potential of anaerobic digestion of complex waste(water), *Water Science and Technology*, **44**, 115-122.



"Gheorghe Asachi" Technical University of Iasi, Romania



MAGNETIC CONTAMINATION OF ENVIRONMENT – LABORATORY SIMULATION OF MIXED IRON OXIDES IMPACT ON MICROORGANISM CELLS

Lacramioara Oprica¹, Claudia Nadejde², Maria Andries², Emil Puscasu²,
Dorina Creanga^{2*}, Maria Balasoiu³

¹"Alexandru Ioan Cuza" University, Faculty of Biology, 20 Blvd. Carol I, Iasi, Romania

²"Alexandru Ioan Cuza" University, Faculty of Physics, 11 Blvd. Carol I, Iasi, Romania

³Institute of Nuclear Research, Dubna, Russian Federation

Abstract

Magnetic contamination is considered more and more as a challenging issue related to biosphere pollution with magnetic materials originating in natural and artificial sources (volcanic eruptions and respectively industrial activities that contributed to iron and other metal compounds spreading in air, water and soil). Aiming to study the impact of magnetic metal ions such as iron and cobalt on the metabolism of some environmental microorganisms, in this paper an experimental simulation of magnetic contamination was carried out based on mixed iron/cobalt oxides as source of ions. Magnetic nanoparticles were prepared following chemical route with appropriately adjusting of their surface to ensure uniform dispersion in water. Typical crystalline structure of studied nanoparticles was evidenced with X-ray diffraction, while microstructural and magnetic properties were investigated by scanning electron microscopy and respectively vibrating sample magnetometry. Increased level of peroxidase activity in a fungus mycelium has suggested microorganism adaptation to higher levels of reactive oxygen species following the supply with magnetic nanoparticles suspensions (0-10-20-30-35 mg/L, comparable with detected levels of iron in the living organism). Lipid peroxidation was evidenced also; being assigned to the increased level of hydrogen peroxide that catalase seems enable to balance - as resulted from its decreasing activity. The variations of analyzed indicators of oxidative stress were of no more than 15%, reflecting organism adaptation to environmental constraints but also possible damages of cell membrane system.

Key words: cobalt, iron, oxidative stress markers, *Phanerochaete chrysosporium*

Received: November, 2014; Revised final: March, 2015; Accepted: March, 2015

1. Introduction

Decades ago the main threats for the environment were the radioactivity impact and chemicals toxicity; more recently electromagnetic pollution and magnetic contamination came into the scientist attention. The latter is related to the large spread of magnetic materials, basically iron compounds that can be found in the Earth crust and exploited by mining or widely spread by volcanic eruptions and intense storms. Also industrial development of metal processing and especially

nanotechnologies based on magnetic nanoparticles became new sources of particulate matter released in water, air, soil – that suggested the new concept of magnetic contamination.

The biomedical use of magnetic nanoparticles in diluted suspensions includes nanosized iron oxides as contrast agents in magnetic resonance imaging, in experimental cancer treatment through hyperthermia, in magnetically targeted drug delivery, magnetic separation of biomolecules and cells etc. Magnetic nanoparticles (MNPs) designed for applications in life sciences should be supplied to biological systems

* Author to whom all correspondence should be addressed: e-mail: mdror@uaic.ro; Phone: 040232201064; Fax: 040232201150

in fluid form (magnetizable nanofluids) as they are planned to circulate toward target organs or tissues through the circulating body fluids; thus, they are fabricated with a variety of surface stabilizers which provides uniform dispersion in aqueous media. First MNPs were considered as inert factors from the viewpoint of their metabolic interaction with cells (Huang et al., 2013). More recent studies were developed with focus on the MNPs toxicity. Either coated or non-coated magnetite or maghemite nanoparticles could be internalized by endocytosis in the cells where the lysosomal degrading triggers ferric and ferrous ions release (Sing et al., 2010; Wang and Pantopoulos, 2011).

One of the main mechanisms that can influence cell metabolism is the oxidative stress associated with reactive oxygen species (ROS) which can result in lipid peroxidation - as shown by specific indicators like glutathione, malondialdehyde (MDA) (Ma et al., 2012) and others, as well as in damages of proteins, nucleic acids and polysaccharides (Halliwell and Gutteridge, 2007). Environment safety has led to experimental investigations of MNPs influence on microorganisms (Niazi and Gu, 2009) where also ROS increase was evidenced being associated with membrane system damages. Microorganisms have been even entitled as model organisms for the study of engineered nanoparticle toxicity (Kumar et al., 2012).

Few studies were dedicated to specific fungi response to MNPs impact (Navarro et al., 2008; Saucedo et al., 2011). However the uptake of metal ions with magnetic properties by environmental fungi cells was studied recently (Sepehr et al., 2014) and a mechanism of internalized metal ions impact on *Phanerochaete chrysosporium* cellulolytic fungi was proposed based on microscopy data (Murugavelh and Mohanty, 2014). In previous reports we evidenced possible utilization of magnetite colloidal nanoparticles in fungi biotechnology, based on the fact that enzymatic equipments appeared to be stimulated for low levels of magnetite aqueous or oily suspensions (Manoliu et al., 2005; Manoliu et al., 2002). In the present study cobalt ferrite nanoparticles were utilized considering their promising - and therefore widely spread - use in cancer therapy through hyperthermia (Mazario et al., 2013). Both elements i.e. iron and cobalt are naturally present in the living cells. Iron, the fourth abundant element in the Earth crust is present in several categories of biomolecules like cytochromes, haemoglobins, catalase enzymes etc. Cobalt is the active center of coenzymes called cobalamins, the most common example of which being the cyanocobalamine, i.e. B12 vitamin. In this study we searched for biological response of cellulolytic fungi relatively to environmental pollution with concentrations of magnetic nanoparticles corresponding to the order of magnitude of iron accumulation in human brain (Buzea et al., 2007).

The importance of these types of microorganisms is related to the fact that biosphere

recirculation circuits of carbon include decomposition of organic matter in general and cellulosic substrate in particular - cellulose appearing to be its most abundant organic component.

2. Experimental

2.1. Technology of nanoparticles yielding

Metal salt precursors were Merck chemicals at molar ratio 2:1 i.e. 10.866g $\text{FeCl}_3 \times 6\text{H}_2\text{O}$ and 5.648g $\text{CoSO}_4 \times 7\text{H}_2\text{O}$, each dissolved in 300 mL deionized water (Kim et al., 2003). Deionized water (18.2 M Ω /cm, Barnstead EASYPureII ultrapure water system) was used in all steps of magnetic nanoparticle suspension synthesis. Cobalt ferrite coprecipitation was produced by stirring the two stock solutions at 75 °C and by slowly pouring of 2M NaOH (150 mL). To ensure ferrite particles uniform dispersion in deionized water, 12 mL perchloric acid aqueous solution (25%) was added (under continuous stirring at 75 °C - thus modifying the MNPs surface in order to prevent their agglomeration in the presence of ubiquitous gravitational and magnetic fields (Laurent et al., 2008).

2.2. Nanoparticle characterization

The final product was a magnetizable nanofluid based on electrostatic stabilization (Gazova et al., 2012) that presented good stability over time at pH close to biological one. Rheological investigation of MNPs suspension was carried out using: semi-analytical balance type ADAM PW254 with 10^{-4} g accuracy, 5 mL picnometer, Ubelhode capillary viscosimeter, ROHR B type stalagmometer and deionized water as reference fluid. Physical characterization of colloidal particles was carried out using: Shimadzu LabX XRD-6000 diffractometer with Cu-K α radiation of $\lambda=1.54 \text{ \AA}$, Vibrating Sample Magnetometer (VSM) MicroMag model 2900/3900 at room temperature, Scanning Electron Microscopy (SEM) device type VEGA\TESCAN (SE detector, HV: 30.00 kV).

2.3. Biotechnological procedure

2.3.1. Biological material

The white rot fungal strain *Phanerochaete chrysosporium* used in this experiment was obtained from the collection of the Faculty of Biology at "Al. I. Cuza" University Iași, Romania being achieved from the Institute Scientifique de Santé Publique, Belgium (HEM no. 5772). This species is one of the microorganisms with important role in decomposing cellulose wastes from environment. The fungus was cultivated on agarized Sabouraud medium (peptone 10 g/L, glucose 35 g/L, agar 2 g/L, distilled water up to 1.0 L (Manoliu et al., 2010) in adequate Petri dishes) and kept at 28 °C. Further 6 mm mycelial plugs taken from a 7-day-old Petri dishes culture were used as inoculum for 500 mL flasks containing

liquid Sabouraud medium. MNPs were supplied to fungi culture samples in concentration of 0-15-25-30-35 mg/L equivalent with metal ion concentrations of 0-10.2-15.3-20.3-25.5 $\mu\text{g/mL}$.

2.3.2. Biochemical investigation

SOD (superoxide dismutase) activity assay in fungus mycelium was accomplished according to Winterbourn's method– measuring light absorbance at 560 nm wavelength (Artenie et al., 2008). CAT (catalase) activity was assayed through the method described by Sinha (1972). Malondialdehyde (MDA) assay (the end product of lipid peroxidation) was carried out using thiobarbituric acid (TBA) according to Hodges et al. (1999). The results were expressed relatively to protein content (the assay of soluble protein content was carried out according to Bradford (1976). Graphical plots were drawn with average values and standard deviations resulted from five repeated measurements of each biochemical parameter.

3. Results and discussion

3.1. Magnetic nanoparticles characterization

XRD investigation revealed typical spinel structure with characteristic peaks (Fig. 1) at known positions on the scale of X-ray scattering degrees (Table 1). Average value of crystallite size (of 11.5 nm) was assessed with Scherrer's formula (Eq. 1), where: K is a dimensionless factor which varies with the actual shape of the crystallite (in this case $K=0.89$), β is the half width of the (ijk) diffraction peak, λ is the X-ray wavelength and θ is the Bragg angle of the peak).

$$D_{ijk} = (k\lambda) / (\beta \cos \theta) \quad (1)$$

The results from XRD diagram processing were comparable with other results reported by different authors. Mahadevan et al. (2007) reported crystalline domains for Fe_3O_4 at 5.1 nm, while Kumar et al. (2013) reported crystalline domains for CoFe_2O_4 at 9 nm.

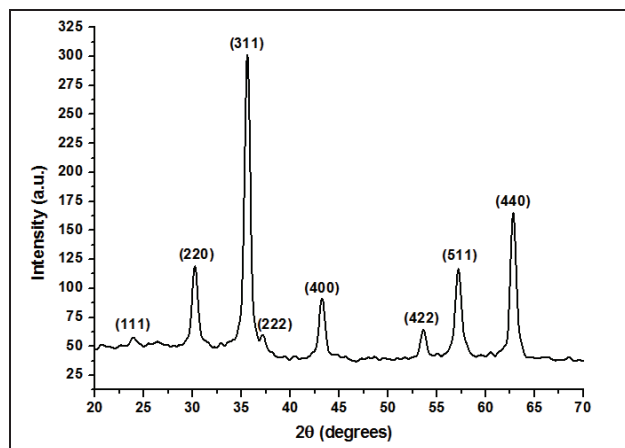


Fig. 1. X-ray diffraction investigation of MNPs

Microstructural investigation with SEM (Fig. 2) revealed quasi-uniform particles with spherical shape that tend to form associations when deposited on the sample support of SEM device following the evaporation of the dispersion liquid; average size of physical diameter was estimated at 40 nm. Magnetic properties were estimated from the magnetization curve (Fig. 3) where saturation magnetization for CoFe_2O_4 was of $M_s=58 \text{ Am}^2/\text{kg}$ corresponding to magnetic field intensity of 790 kA/m while coercive field was of 239 kA/m.

The presence of the hysteresis cycle suggests that during ferrophase synthesis both superparamagnetic and ferrimagnetic nanoparticles were precipitated that resulted in the presence of magnetic coercivity at room temperature (Kim et al., 2004). Rheological data have evidenced that CoFe_2O_4 colloidal suspension was characterized by increased average values of surface tension coefficient and viscosity coefficient comparatively with reference liquid – the deionized water: from 7.27 to 7.60 Nm^{-1} and respectively from 1002 to 2162 NSm^{-2} (from ten repeated measurements in identical ambient conditions); the results were similar with those reported for magnetite colloidal suspension stabilized with perchloric acid, according to Racuciu et al. (2010).

3.2. Biochemical assay results

Following the supply with colloidal suspension as source of magnetic metal ions for the culture medium of *P. chrysosporium* fungus, grown mycelium specimens were withdrawn and repeated measurements of biochemical parameters indicating oxidative stress action were carried out.

Table 1. Estimation of crystallite size from XRD raw data

| Miller indices | 2θ (°) | Intensity (a.u.) | β (rad) | D_{ijk} (nm) |
|----------------|---------------|------------------|---------------|----------------|
| (111) | 23.9 | 57.6 | 0.0170 | 8.2 |
| (220) | 30.2 | 118.8 | 0.0129 | 11.0 |
| (311) | 35.6 | 301.1 | 0.0122 | 11.8 |
| (400) | 43.2 | 91.3 | 0.0118 | 12.4 |
| (422) | 53.6 | 64.3 | 0.0118 | 12.9 |
| (511) | 57.2 | 116.7 | 0.0132 | 11.7 |
| (440) | 62.8 | 165.1 | 0.0125 | 12.7 |

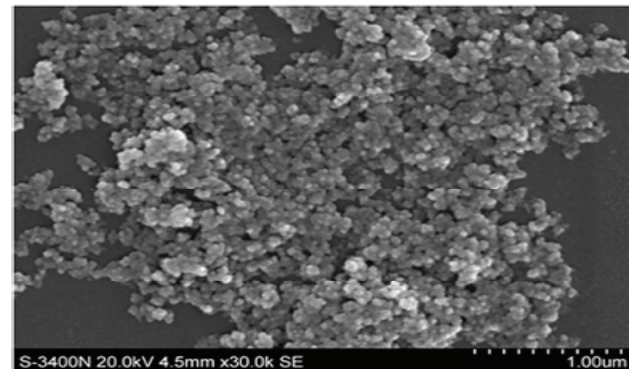
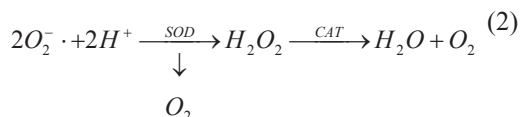


Fig. 2. Characteristic image of MNP with SEM investigation

In Fig. 4, the SOD activity in fungi mycelium is presented; the tendency of SOD increasing with up to 15% at 14 days compared to the control ($p < 0.05$) was evidenced for MNP increasing concentration - although no precise quantitative correlation could be established, at least for the 7 days situation. This could be taken as an indication on the intensified O_2^- release into the cells that further triggered the amplification of SOD biosynthesis as adaptation to the oxidative stress threatening (Eq. 2), since the enzyme neutralizes the O_2^- radical.



In the same time the increasing of SOD activity could lead to increased H_2O_2 level. Possibly, the hydrogen peroxide triggered peroxidasic reaction cascade and has caused the lipid peroxidation.

Indeed the indicator of final product of lipid peroxidation, namely MDA was found increased at 14 days (with about 13%, $p < 0.05$) in fungi mycelium (Fig. 5) – although not in 7 day old samples – this result being concordant with SOD activity variation.

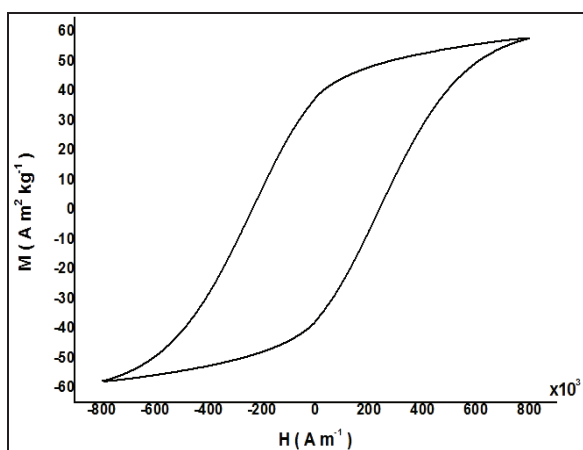


Fig. 3. Magnetization curve of MNPs sample

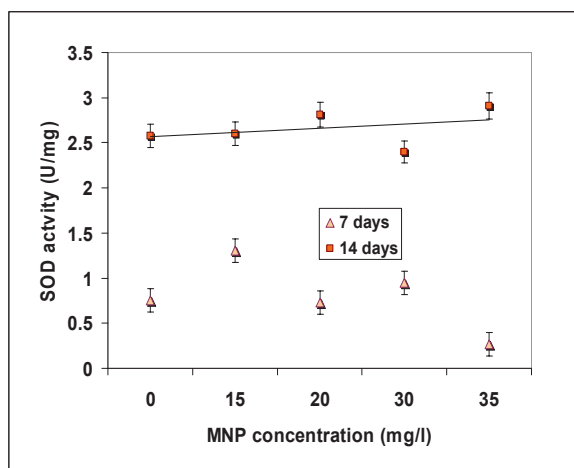


Fig. 4. SOD activity in *P. chrysosporium* samples

In the present investigation iron ions are predominant metal components so their role could be assumed to be the essential one.

The tests carried out on the effect of MNP surface coating, when supplied in equivalent amounts with those corresponding to colloidal suspensions, gave no discernible results. According to some reports (Huang et al., 2013; Singh et al., 2010; Wang and Pantopoulos, 2011), it was expected that magnetic nanoparticles were degraded and metabolized in the cellular endocytic organelles with release of free iron ions - ROS yielding intensification being the main cellular mechanism underlying the supposed toxicity of iron ions (Halliwell and Gutteridge, 2007; Ma et al., 2012; Niazi and Gu, 2009).

The hydrogen peroxide yielded by SOD action is subject of concurrent mechanisms decomposing it: the catalase action (Eq. 3):



and the iron ions Fenton reactions (Eqs. 4-5), where: H_2O_2 is transformed into hydroxyl or superoxide radicals which are highly reactive.



Presuming that cell adaptation capacity includes also catalase synthesis stimulation in the presence of increased hydrogen peroxide one would expect enhanced CAT activity evidence in the fungi samples.

However this biochemical parameter was found not increased but on the contrary – diminished in the samples where metal ions were supplied by means of magnetic nanoparticles in diluted suspension form. As one can see in Fig. 6 the catalase activity appears to be diminished with up to 10% ($p < 0.05$). This could be explained also by the presence of MNP in the cellular medium.

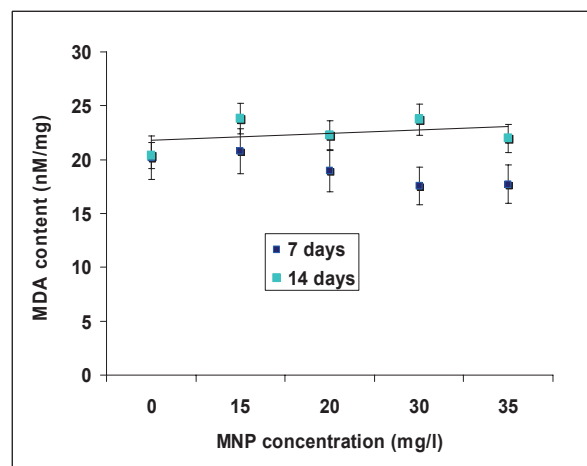


Fig. 5. MDA level in *P. chrysosporium* samples

According to some authors (Freitas et al., 2003), following MNPs supply in living mice not only the oxidative changes (lipid peroxidation) were intensified but also liver catalase activity exhibited variations that were time and MNP-concentration dependent. Other report (Doğaç and Teke, 2012) demonstrated the CAT attachment onto the MNP surface – with probable enzyme activity blockage. Thus it was presumed that concurrent processes could be elicited by MNP impact on living cells: the stimulation of CAT synthesis on a side and its inactivation on the other side.

In the present case it seems that the second one was dominating the whole picture. Cobalt is essential element to cell metabolism but, like iron, it can be also toxic. Toxicity of cobalt ions in certain concentrations was discussed by Fleury et al. (2006) based on mammals cell cultures; Kubrak et al. (2012) reported the cobalt stimulated oxidative stress in the goldfish. Cobalt ferrite MNP toxicity was reported also by Peeples et al. (2014) and Di Guglielmo et al. (2010); Drašler et al. (2013) have discussed the damaging impact of coated MNP of cobalt ferrite on the artificial lipid membranes; the observed correlation (Horev-Azaria, 2013) between the oxidative stress, caused by the presence of nanoparticulate CoFe_2O_4 , and the sensitivity of different cell types towards toxicity, suggests that oxidative stress is one possible mechanism for the toxicity of cobalt ferrite MNPs. It is assumed that Co^{2+} may enter the Fenton reactions, Co^{2+} appearing to be a better catalyst than Fe^{3+} although only limited free radical formation in the $\text{Co}^{2+}/\text{H}_2\text{O}_2$ reaction system was shown in ESR studies (Strlič et al., 2003).

Thus, in the study presented above we might have to deal with the toxicity of both metal ion types originating in the nanoparticles delivered into the culture medium of cellulolytic fungus taken as model organism.

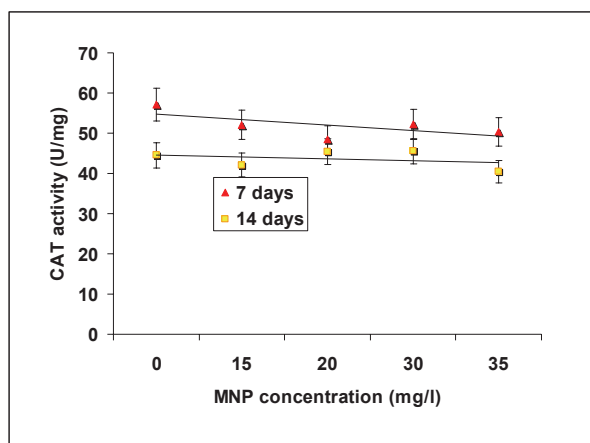


Fig. 6. CAT activity in *P. chrysosporium* samples

4. Conclusions

The increased SOD activity was assigned to ROS species yielded by metal ions supplied in *P.*

chrysosporium culture medium that led to hydrogen peroxide formation. The effect of lipid peroxidation was further evidenced by increased level of MDA in the fungus mycelium. CAT activity was found diminished which is probably due to the nanoparticulate form of the metal ion source since nanoparticles can bind to CAT molecules blocking their active site. All these results suggest that environment pollution with cobalt ferrite MNPs released from specific nanotechnologies can impede cellulolytic fungi metabolism and their ecological role of wood waste decomposing.

Acknowledgements

This study was partially supported by IUCN-UAIC cooperation grants 57/04-4-1121-2015/2017 and 56/04-4-1121-2015/2017.

References

- Artenie V., Ungureanu E., Negura A.M., (2008), *Methods of Investigation Glucidic and Lipidic Metabolism* (in Romanian), Ed. Pim, 66-67.
- Bradford M.M., (1976), A rapid and sensitive method for microgram quantities of protein utilizing the principle of protein-dye binding, *Analytical Biochemistry*, **72**, 248–254.
- Buzea C., Pacheco Blandino I.I., Robbie K., (2007), Nanomaterials and nanoparticles: Sources and toxicity, *Biointerphases*, **2**, 17–172.
- Di Guglielmo C., López D.R., De Lapuente J., Mallafre J.M., Suárez M.B., (2010), Embryotoxicity of cobalt ferrite and gold nanoparticles: a first *in vitro* approach, *Reproductive Toxicology*, **30**, 271-276.
- Doğaç, Y., Teke M., (2013), Immobilization of bovine catalase onto magnetic nanoparticles, *Preparative Biochemistry and Biotechnology*, **43**, 750-765.
- Drašler B., Drobne D., Novak S., Valant J., Boljte S., Otrin L., Rappolt M., Sartori B., Igljč A., Kralj-Igljč V., Šuštar V., Akovec D., Gyergyek S., Hočevan M., Godec M., Zupanc J., (2013), Effects of magnetic cobalt ferrite nanoparticles on biological and artificial lipid membranes, *International Journal of Nanomedicine*, **8**, 189–199.
- Fleury C., Petit A., Mwale F., Antoniou J., Zukor D.J., Tabrizian M., Huk O.L., (2006), Effect of cobalt and chromium ions on human MG-63 osteoblasts *in vitro*: morphology, cytotoxicity and oxidative stress, *Biomaterials*, **27**, 3351-3360.
- Freitas M.L.L., Silva L.P., Freitas J.L., Azevedo R.B., Lacava Z.G.M., Homem de Jittencourt P.I., Curi R., Buske N., Morais P.C., (2003), Investigation of lipid peroxidation and catalase activity in magnetic fluid treated mice, *Journal of Applied Physics*, **93**, 6709.
- Gazova Z., Siposova K., Koneracka M., Antosova A., Zavisova V., Ubovcikova M., Fedunova D., Bagelova J., Tomasovicova N., Daxnerova Z., Kopcansky P., (2012), Presence of magnetic fluids leads to the inhibition of insulin amyloid aggregation, *Acta Physica Polonica A*, **121**, 5-6.
- Halliwell B., Gutteridge J.M.C., (2007), *Free Radicals in Biology and Medicine*, New York: Oxford University Press, 125-126.
- Hodges D.M., Delong J.M., Forney C.F., Prange R.K., (1999), Improving the thiobarbituric acid reactive substances assay for estimating lipid peroxidation in plant tissue containing anthocyanin and other interfering compounds, *Planta*, **207**, 604–611.

- Horev-Azaria L., Baldi G., Beno D., Bonacchi D., Golla-Schindler U., Kirkpatrick J.C., Kolle S., Landsiedel R., Maimon O., Marche P.N., Ponti J., Romano R., Rossi F., Sommer D., Uboldi C., Unger R.E., Villiers C., Korenstein R., (2013), Predictive toxicology of cobalt ferrite nanoparticles: comparative *in vitro* study of different cellular models using methods of knowledge discovery data, *Particle and Fibre Toxicology*, **10**, 32-49.
- Huang G., Chen H., Dong Y., Luo X., Yu H., Moore Z., Bey E.A., Boothman D.A., Gao J., (2013), Superparamagnetic iron oxide nanoparticles: Amplifying ROS stress to improve anticancer drug efficacy, *Theranostics*, **3**, 116-126.
- Kim Y., Kim D., Lee C.S., (2003), Synthesis and characterization of CoFe_2O_4 magnetic nanoparticles prepared by temperature controlled coprecipitation method, *Physica B: Condensed Matter*, **337**, 42-51.
- Kubrak O., Husak V.V., Rovenko B.M., Storey J.M., Storey K.B., Lushchak V.I., (2011), Cobalt-induced oxidative stress in brain liver and kidney of gold fish *Carassius auratus*, *Chemosphere*, **85**, 983-989.
- Kumar A., Pandey A.K., Shanker R., Dhawan A., (2012), *Microorganisms: a Versatile Model for Toxicity Assessment of Engineered Nanoparticles*, In: *Nano-Antimicrobials. Progress and Prospects*, Cioffi N., Rai M. (Eds.), Springer, Berlin Heidelberg New York, XIV, 497-524.
- Kumar L., Kumar P., Narayan A., Kar M., (2013), Rietveld analysis of XRD patterns of different sizes of nanocrystalline cobalt ferrite, *International Nano Letters*, **3**, 2-12.
- Laurent S., Forge D., Port M., Roch A., Robic C., Elst L.V., Muller R.N., (2008), Magnetic iron oxide nanoparticles: synthesis, stabilization, vectorization, physicochemical characterizations, and biological applications, *Chemical Reviews*, **108**, 2064-2110.
- Ma P., Luo Q., Chen J., Gan Y., Du J., Ding S., Xi Z., Yang X., (2012), Intraperitoneal injection of magnetic Fe_3O_4 -nanoparticle induces hepatic and renal injuries via oxidative stress in mice, *International Journal of Nanomedicine*, **7**, 4809-4818.
- Mahadevan S., Gnanaprakash G., Philip J., Rao B.P.C., Jayakumar T., (2007), X-ray diffraction-based characterization of magnetite nanoparticles in presence of goethite and correlation with magnetic properties, *Physica E: Low-dimensional Systems and Nanostructures*, **39**, 20-25.
- Manoliu A., Balan M., Oprica L., Gradinaru P., (2010), The evolution of catalase and peroxidase activity in *Phanerochaete chrysosporium* grown on media containing beech and fir sawdust and under the influence of some amino acids, *Scientific Annals of Alexandru Ioan Cuza University, Iași, Genetics and Molecular Biology*, **6**, 47-52.
- Manoliu A., Olteanu Z., Oprica L., Zamfirache M.M., Creanga D., (2002), Petroleum ferrofluid influence on cellulase specific activity in *Chaetomium globosum*, *Romanian Biotechnological Letters*, **7**, 737-744.
- Manoliu A., Oprica L., Creanga D.E., (2005), Ferrofluid and cellulolytic fungi, *Journal of Magnetism and Magnetic Materials*, **289**, 473-475.
- Mazario E., Menéndez N., Herrasti P., Cañete M., Connord V., Carrey J., (2013), Magnetic hyperthermia properties of electrosynthesized cobalt ferrite nanoparticles, *The Journal of Physical Chemistry C*, **117**, 11405-11411.
- Murugavel S., Mohanty K., (2014), Mechanism of Cr(VI) bioaccumulation by *Phanerochaete chrysosporium*, *Environmental Engineering and Management Journal*, **13**, 231-492.
- Navarro E., Baun A., Behra R., Hartmann N.B., Filser J., Miao A., Quigg A., Santschi P.H., Sigg L., (2008), Environmental behavior and ecotoxicity of engineered nanoparticles to algae, plants and fungi, *Ecotoxicology*, **5**, 372-386.
- Niazi J.H., Gu M.B., (2009), *Toxicity of Metallic Nanoparticles in Microorganism – A Review*, In: *Atmospheric and Biological Environmental Monitoring*, Kim Y.J., Platt U., Gu M.B., Iwahashi H. (Eds.), Springer, Berlin Heidelberg New York, 193-206.
- Peeples B., Goornavar V., Peeples C., Spence D., Parker V., Bell C., Biswal D., Ramesh G.T., Pradhan A.K., (2014), Structural, stability, magnetic and toxicity studies of nanocrystalline iron oxide and cobalt ferrites for biomedical applications, *Journal of Nanoparticle Research*, **16**, 2290.
- Racuciu M., Creanga D., Airinei A., Chicea D., Badescu V., (2010), Synthesis and properties of magnetic nanoparticles coated with biocompatible compounds, *Materials Science-Poland*, **28**, 609-616.
- Saucedo C.G., Field J.A., Gonzalez J.O., Álvarez R.S., (2011), Low toxicity of HfO_2 , SiO_2 , Al_2O_3 and CeO_2 nanoparticles to the yeast *Saccharomyces cerevisiae*, *Journal of Hazardous Materials*, **192**, 1572-1579.
- Sepehr M. N., Zarrabi M., Amrane A., (2014), Effect of medium nutrients on Cr(III) removal by *Phanerochaete chrysosporium*, *Aspergillus niger* and *Aspergillus oryzae*, *Environmental Engineering and Management Journal*, **13**, 763-1038.
- Singh N., Jenkins G.J.S., Asadi R., Doak S.H., (2010), Potential toxicity of superparamagnetic iron oxide nanoparticles (SPION), *Nano Reviews*, **1**, 3402-5358.
- Sinha A.K., (1972), Colorimetric assay of catalase, *Analytical Biochemistry*, **47**, 389-394.
- Strlič M., Kolar J., Šelih V.S., Kočar D., Pihlar B., (2003), A comparative study of several transition metals in Fenton-like reaction systems at circum-neutral pH, *Acta Chimica Slovaca*, **50**, 619-632.
- Wang J., Pantopoulos K., (2011), Regulation of cellular iron metabolism, *Biochemical Journal*, **434**, 365-381.



"Gheorghe Asachi" Technical University of Iasi, Romania



GREEN SYNTHESIS AND CHARACTERIZATION OF GOLD NANOPARTICLES OBTAINED BY A DIRECT REDUCTION METHOD AND THEIR FRACTAL DIMENSION

**Razvan State^{1,2*}, Florica Papa², Gianina Dobrescu², Cornel Munteanu²,
Irina Atkinson², Ioan Balint², Adrian Volceanov¹**

¹University "Politehnica" of Bucharest, 313 Splaiul Independentei, Bucharest, Romania

²"Ilie Murgulescu" Institute of Physical Chemistry of the Romanian Academy, 202 Splaiul Independentei, Bucharest, Romania

Abstract

Nanoparticles are very interesting materials due to their properties which can be different than those of the bulk and they have many applications in various domains, like electronic, catalytic or biomedical. Gold is one of the most studied materials and is used in many applications that will have the human being as recipient, that's why gold nanoparticles should be obtained as environmentally friendly as possible. In this work, particles of around 50 nm were obtained in a so called "green" way by simply adding a solution containing the gold precursor (HAuCl_4) in a tannic acid solution. It was found that the amount of gold added in the tannic acid is directly proportional with the size of the obtained nanoparticles.

Key words: fractal dimension, gold nanoparticles, green synthesis

Received: November, 2014; Revised final: March, 2015; Accepted: March, 2015

1. Introduction

Due to their nanosized dimensions, nanoparticles have witnessed an increasing interest in the last decade becoming one of the most studied fields in the scientific community (Ahmad and Khan, 2013; Granmayeh Rad et al., 2011). Nanosized metal materials are the subject of many scientific researches due to their characteristic surface properties which are different from those of the bulk material. Great interest was focused on the noble metals nanoparticles (Kumari et al., 2013; Zhang et al., 1999). Gold is one of the most studied materials (Aswathy and Philip, 2012; Bratescu et al., 2013; Kyrychenko et al., 2011; Lee et al., 2007; Sárkány et al., 2008; Zabetakis et al., 2012) due to its unique optical, catalytic and spectroscopic properties.

The obtaining of Au nanoparticles becomes an important topic in different applications because the

physical and chemical properties of the particles depend on their shape and size. Generally Au nanoparticles were synthesized by reducing HAuCl_4 with different reduction agents in the presence of some stabilizers (Hamaguchi et al, 2010; Kaur et al., 2012; Peng et al., 2008; Xu et al., 2013; Zhang and Toshima, 2012; Zhou et al., 2009; Zhu et al., 2005). Greener, environmentally friendly methods for the obtaining of metal nanoparticles are nowadays goal for a vast number of scientists in modern nanotechnology field.

Tannic acid is a polyphenolic compound derived from plants. It has antioxidant, antimutagenic and anticancer properties and it also reduces triglycerides. Besides its multipurpose applications it has been used also as a reducing agent and a protective colloid in noble nanoparticle synthesis (Ahmad et al., 2013; Ahmad, 2014; Yi et al., 2011). At its natural pH, tannic acid behaves as a weak

* Author to whom all correspondence should be addressed: e-mail: rstate@icf.ro, razvan.state@yahoo.com; Phone: 0721274801

reducing agent which can induce growth of nanoparticles at room temperature. Room temperature synthesis of silver or gold nanoparticles using tannic acid has been demonstrated recently by (Sivaraman et al., 2010) and long before (Ostwald et al., 1917) showed that tannin can reduce chloroauric acid at neutral pH to form stable gold nanoparticles even if tap water is used to prepare the aqueous solutions. Thus, tannic acid can be considered as an environmentally friendly reducing agent.

The goal of this work is to carry out: (a) synthesis of gold nanoparticles with various amounts of HAuCl_4 , by a direct and environmentally friendly reduction method of the gold precursor solution with tannic acid; (b) analysis of the influences of how the gold precursor was added, on the size and shape of the obtained gold nanoparticles; (c) structural and morphologic characterization by different techniques of the synthesized gold nanoparticles.

2. Materials and methods

Chloroauric acid ($\text{HAuCl}_4 \cdot 4\text{H}_2\text{O}$) was provided by Wako Pure Chemical Industry, Ltd. and tannic acid ($\text{C}_{34}\text{H}_{28}\text{O}_{21}$) from Carl Roth GmbH. All the solutions for the synthesis of gold nanoparticles in this paper were freshly prepared using demineralised water.

The as obtained nanoparticles were characterized through XRD spectroscopy. The XRD patterns were collected by means of a Rigaku diffractometer type Ultima IV in parallel-beam geometry. The source of the X-rays was a Cu tube ($\lambda = 0.15418 \text{ nm}$) operating at 40 kV and 30 mA. Counts were collected from 10° to 80° with a step size of 0.02 and a speed of $5^\circ/\text{min}$. Rigaku's PDXL software package, connected to the ICDD database was used for the phase identification. Transmission electron microscopy (TEM) was performed on FEI Tecnai G2-F30 S-Twin field-emission gun scanning transmission electron microscope (FEG STEM) operating at 300 kV. A drop of the nanoparticles suspension was mounted on a holey carbon film copper grid allowing the solvent to evaporate at room temperature. UV-VIS spectra were performed using an Analytic Jena Specord 200 plus apparatus.

3. Experimental

Until now, the majority of the obtained materials using similar synthesis aimed particle size up to 20 nm. In this work, gold nanoparticles of around 50 nm were obtained very simple, through a direct and environmentally friendly reduction method. The gold precursor consisted in a water based solution of chloroauric acid of 0.9 mM. After obtaining of the gold precursor, it was injected in a water based solution of tannic acid of 0.9 mM according to scheme presented in Fig. 1. Firstly, two sample batches were prepared. In one of them 15 mL of the as obtained gold precursor solution was injected slowly, using a dropping funnel, in 15 mL of

tannic acid solution, sample Au1 (molar ratio Au: tannic acid 1:1) and in the second one, 35 mL of gold precursor solution was injected also slowly into 15 mL solution of tannic acid, sample Au2 (molar ratio Au: tannic acid 2.3:1).

The tannic acid solution was kept in both cases under magnetic stirring. The reduction occurs almost instantly. In the case of 1:1 ratio (Au1) the solution turns dark blue and in the second case, 2.3:1 (Au2) the solution turns in a brown-red (muddy red) color. Both solutions were kept under stirring for a better homogenization and then the synthesized nanoparticles were recovered. The recovery was made by using a 4000 RPM centrifuge device. After separation, the obtained powder was calcinated at 200°C for 2 hours. A third sample of 2.3:1 ratio was prepared following the same protocol with the exception that the gold precursor solution was injected rapidly in the tannic acid solution, sample Au3. The obtained solution was also muddy red. After recovery, all the samples were characterized through TEM and XRD analyses. UV-Vis spectra were obtained for the prepared solutions prior to nanoparticle recovery.

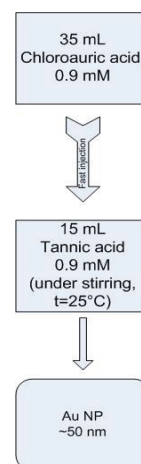


Fig. 1. Schematic representation of gold nanoparticles synthesis, sample A3

4. Results and discussion

The reduced gold solutions were analyzed by UV-Vis spectroscopy (Fig. 2), prior to nanoparticle recovery. It can easily be seen that the as obtained gold nanoparticles have a good adsorption in the visible range, with the 2.3:1 sample having a bigger adsorption than the 1:1 sample.

In order to observe the morphology, size and shape of the synthesized Au nanoparticles all 3 samples were subjected to TEM analysis. It was observed that the Au nanoparticles are faceted (Fig. 3), with a size ranging from 20 to 50 nm, depending on the amount of gold precursor added in the tannic acid solution. Unfortunately the dispersion in the first 2 samples was rather poor (Fig. 4), but this was solved in the third sample when the injection mechanism was changed.

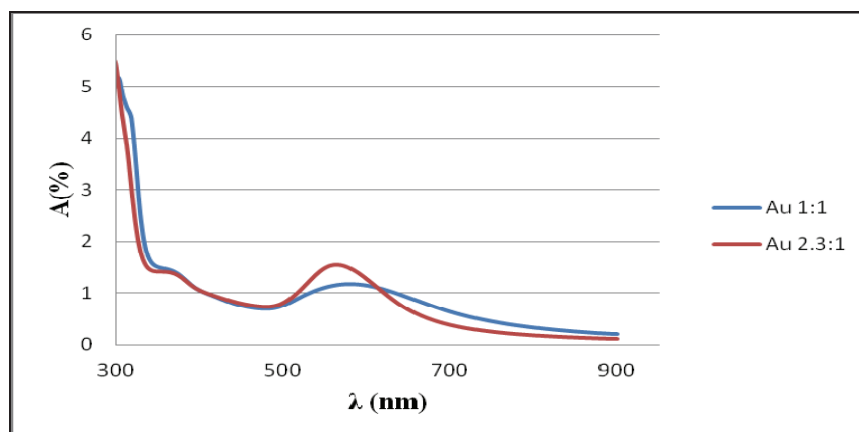


Fig. 2. UV-Vis spectra of the reduced gold solutions

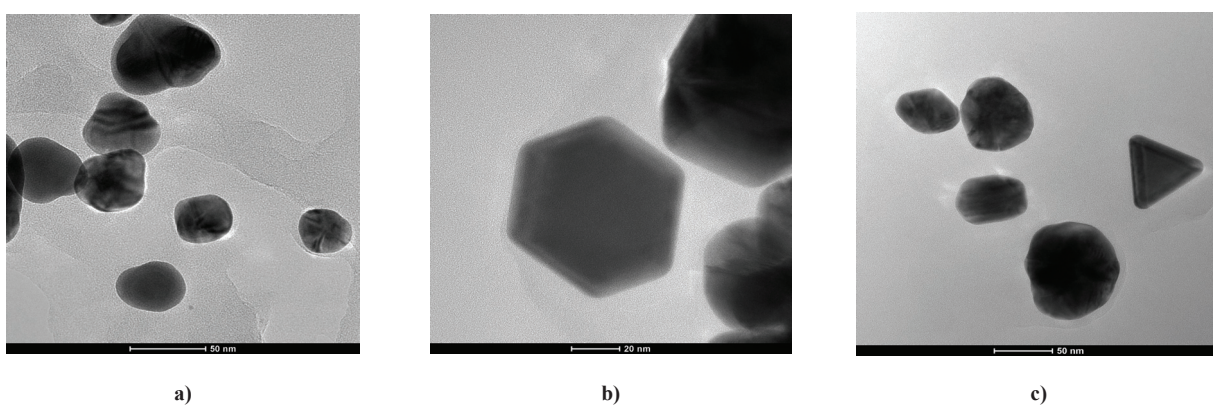


Fig. 3. TEM images of: a) Au1, b) Au2 sample and c) Au3

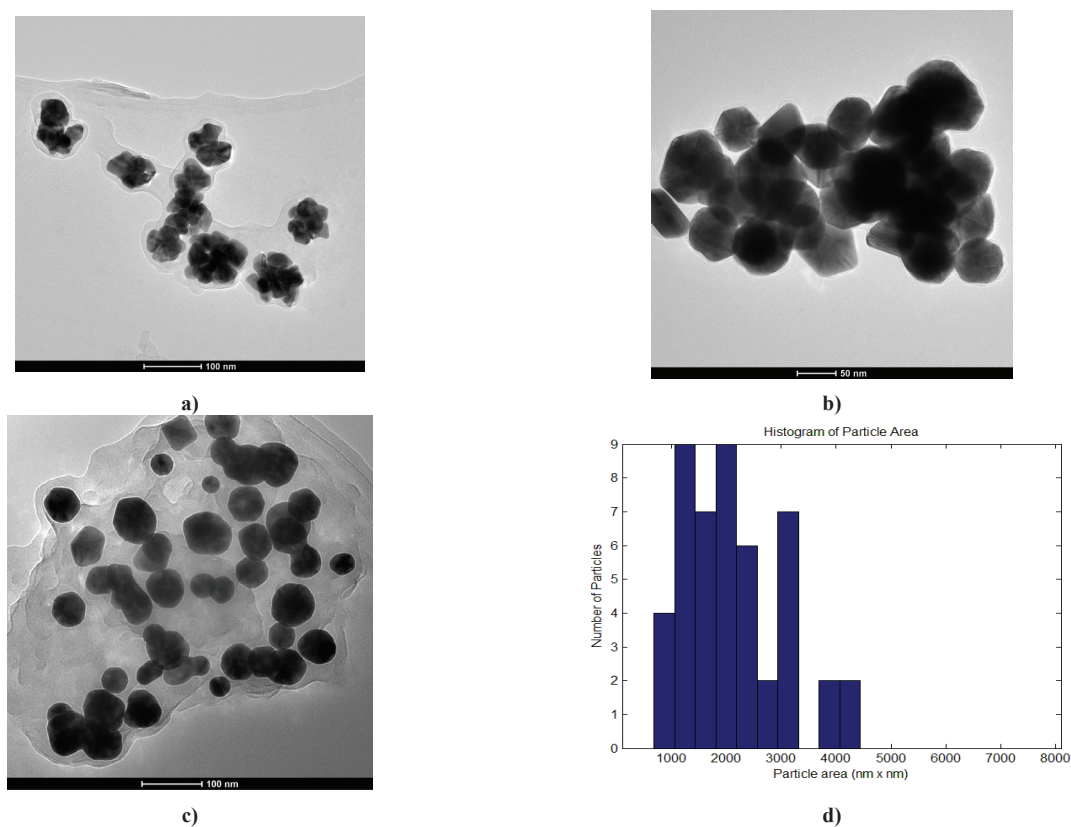


Fig. 4. TEM images showing the nanoparticle dispersion of a) Au1 sample, b) Au2 sample and c) Au3 sample. Histogram of particle area (d) of Au3 sample

In Fig 4 one can see that the dispersion is much better for the sample Au3 then in the case of the other 2 where the chloroauric solution was slowly added in the tannic acid. When analyzing the particle area one can see that the majority of the particles have a surface area between 1500 and 3000 nm², making them suitable for many applications, including catalysis. Unfortunately the shape is inconclusive. They are faceted, some of them are triangles or hexagons (Fig. 3) but the majority has an undefined shape.

TEM images were also analyzed using the fractal theory (Mandelbrot, 1977). A *fractal* is an object whose observed volume depends on the resolution (length scale) at several orders of magnitude and follows a power law behavior with a nontrivial exponent; it has the property of self-similarity. The fractal dimension was computed using three methods: the correlation function method, the variable length scale method and the box-counting method. The first two methods were carried out using personal computer codes, meanwhile the last one using Benoit Soft, version 1.31, TruSoft Int'l, Inc. Self-similarity has a mathematical description given by Eq. (1), where: D is the fractal dimension and $N(r, R)$ is the number of boxes of size r which cover the object of linear size R ; in other words, self-similarity is the property of an object to look the same when zooming in (Mandelbrot, 1977; Mandelbrot, 1982).

$$N(r/R) \sim (r/R)^{-D} \quad (1)$$

Keeping constant the maximum size of the object R , the box dimension is defined as the exponent D in Eq. (2), where: $N(r)$ is the number of boxes of linear size r necessary to cover the object in a two-dimensional plane.

$$N(r) = Ar^{-D} \quad (2)$$

For Euclidean objects, one needs a number of boxes proportional to r^{-D} , so the exponent D is the Euclidean dimension of the plane, 2. The prefactor A , sometimes named lacunarity, is a measure of how the space is filled, a measure of the gap or of the object texture (Lapuerta et al., 2010). The grey level of each image pixel was converted in height and the fractal dimension of the equivalent surface was computed using two methods: the height correlation function method and the variable length scale method. The first method (Family and Vicsek, 1985) uses the height correlation function according to Eq. (3), where: the symbol $\langle \dots \rangle$ denotes an average over x .

$$G(r) \equiv \langle [h(\vec{x}) - h(\vec{x} + \vec{r})]^2 \rangle_x \quad (3)$$

Thus the height correlation function $G(r)$ obeys the following scaling relation for a surface embedded in a 3-dimensional Euclidean space (Eq. 4).

$$G(r) \sim r^{2(3-D)}, r \ll L \quad (4)$$

The scaling range where equation (4) is valid defines the “cut-off” limits and indicates the range of self-affinity, in other words, the range where there are correlations between surface points. The second method was proposed by (Chauvy et al., 1998) and consists in computing the rms deviation of the surface. The algorithm is the following: (i) an interval of length ε in case of a profile, (or a box of size $\varepsilon \times \varepsilon$ in case of a surface) is defined; (ii) a linear (or planar) least square fit on the data within the interval is performed and the roughness is calculated; (iii) the interval (box) is moved along the profile (surface) and step (ii) is repeated; (iv) the rms deviation for multiple intervals is computed, and (v) steps (ii)-(iv) are repeated for increasing lengths (box sizes).

Rms deviation $R_{q\varepsilon}$, averaged over n_ε , the number of intervals of length ε , is defined by Eq. (5), where: z_j is the j th height variation from the best fit line within the interval i , and p_ε is the number of points in the interval ε .

$$R_{q\varepsilon} = \frac{1}{n_\varepsilon} \sum_{i=1}^{n_\varepsilon} \sqrt{\frac{1}{p_\varepsilon} \sum_{j=1}^{p_\varepsilon} z_j^2} \quad (5)$$

The log-log plot of $R_{q\varepsilon}$ versus ε gives the Hurst or roughening exponent H , and the fractal dimension D , can be calculated as given by Eq. (6), where: D_T is the topological dimension of the embedding Euclidean space ($D_T=2$ for profiles and $D_T=3$ for surfaces).

$$D = D_T - H \quad (6)$$

The variable length scale method is more suitable for higher scaling range than the correlation function method because of the necessity to have enough points in an interval $\varepsilon \times \varepsilon$ to compute rms deviation $R_{q\varepsilon}$, averaged over n_ε , meaning that ε must be high enough for a good statistic.

The last two methods describe the fractal properties of the equivalent surfaces defined by the gray-level of each pixel converted into height, meanwhile the box-counting method describes the fractal properties of an equivalent image obtained from conversion of the gray scaled image into a black and white one. The results are presented in Tables 1-3.

The samples have fractal behavior as all methods shows. The Au1 sample is characterized, as an equivalent surface, by three fractal dimensions: 2.40, 2.63 and 2.34, indicating that the nanoparticles are agglomerated in correlated clusters. The Au2 sample is also characterized by three fractal dimensions: 2.31, 2.55 and 2.15. The first two fractal dimensions indicate correlations between points on each nanoparticle, meanwhile the last one shows the

existence of a single cluster, with a global fractal behavior characterized by a low fractal dimension and strong agglomeration. The Au3 sample is characterized by two fractal dimensions: 2.48-2.58 for correlations between points on each nanoparticle and 2.30, characterizing correlations between nanoparticles themselves. The dispersion in the fractal values 2.48-2.58 is a result of some overlapping nanoparticles and of the projection of a 3-dimensional structure onto the 2-dimensional image.

The box-counting fractal dimension of the black-and-white image for the Au1 sample has two values: 1.83 at short scale and 1.35 at a large scale. The first values indicates correlations between nanoparticles in a cluster, meanwhile the second one indicates the correlation between clusters. It is very interesting to notice that the first value of 1.83 is very closed to Sutherland's simulations $D=1.85$ (Stanley, 1977; Sutherland, 1967; Sutherland, 1970; Sutherland and Goodarz-Nia, 1971).

The model was developed for colloidal aggregation and suppose that the single particles aggregate one with each other and then to form binary clusters, the binary clusters aggregate one with each other, and so on. In our case, the slowly gold precursor solution injection will favor aggregation, as diffusion is not a leading mechanism in the system. The box-counting fractal dimension of the Au2 sample is 1.87, again, very close to the Sutherland's value of 1.85. The box-counting fractal dimension of the Au3 sample is 1.79 very closed to the 1.78 value obtained from diffusion limited cluster-cluster aggregation simulations (Meakin, 1986) in the aggregation of gold colloids (Weitz and Oliveira, 1984), when rapid aggregation is involved and diffusion is a leading mechanism, the fractal dimension will lead to the 1.75 value, very close to our 1.79.

Table 1. Nanoparticle fractal dimensions of Au1 sample

| Method | Fractal dimension | Determination Coefficient | Self-similarity domain (nm) |
|------------------------------|------------------------|---------------------------|-----------------------------|
| Correlation method | 2.40±0.01 | 0.999 | 2.5-29 |
| Variable Length Scale Method | 2.63±0.01 2.34±0.02 | 0.992 0.982 | 6-20 20-55 |
| Box-Counting Method | 1.83±0.01 1.35±0.04 | 0.999 0.995 | 0.4-24 24-115 |

In order to make sure of their composition, the synthesized gold nanoparticles were subjected to X-Ray diffraction analysis. The XRD diffractograms confirms the existence of metallic gold without the presence of any other impurities for all the studied samples. Fig. 5 shows the XRD patterns of Au1-Au3 samples. The XRD patterns reveal the presence of

diffraction lines centred at 38.18°, 44.43°, 64.61° and 77.64° corresponding to (111), (200), (220) and (311) planes respectively of Au compound with cubic structure (JCPDS card no. 00-004-0784). The broad halo at around $2\theta=20^\circ$ in the diffraction patterns is the contribution of glass sample holder.

Table 2. Nanoparticle fractal dimensions of Au2 sample

| Method | Fractal dimension | Determination Coefficient | Self-similarity domain (nm) |
|------------------------------|------------------------|---------------------------|-----------------------------|
| Correlation method | 2.31±0.01 | 0.999 | 2.6-13 |
| Variable Length Scale Method | 2.55±0.03 2.15±0.03 | 0.981 0.994 | 4-13 13-56 |
| Box-Counting Method | 1.87±0.01 | 0.999 | 0.3-119 |

Table 3. Nanoparticle fractal dimensions of Au3 sample

| Method | Fractal dimension | Determination Coefficient | Self-similarity domain (nm) |
|------------------------------|------------------------|---------------------------|-----------------------------|
| Correlation method | 2.48±0.01 | 0.995 | 2-20 |
| Variable Length Scale Method | 2.58±0.01 2.30±0.01 | 0.996 0.990 | 6-17 17-89 |
| Box-Counting Method | 1.79±0.01 | 0.999 | 1-151 |

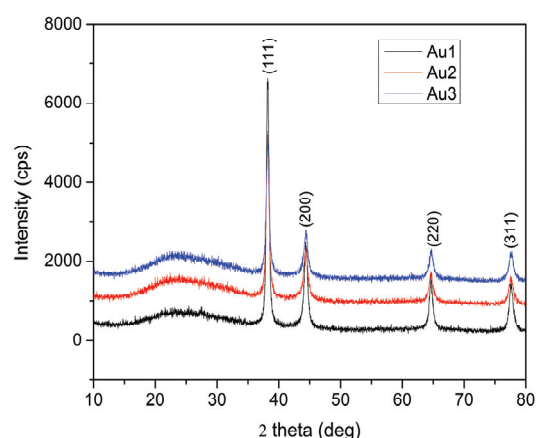


Fig. 5. XRD spectra of the synthesized gold nanoparticles

5. Conclusions

Gold nanoparticles of 20 to 50 nm were obtained using a simple and in the same time an environmentally friendly synthesis method. In the first two samples only the amount of added gold precursor is different, the synthesis mechanism being identical. It was observed that the dimension of the

obtained nanoparticles is directly proportional with the amount of gold added in the tannic acid. Because the dispersion of the synthesized nanoparticles is rather poor, a third sample was made, keeping the quantities used in the second sample but changing the injection mechanism. Thus, rapidly injecting the precursor solution in the reducing one, we obtained a better dispersion of the nanoparticles than it was obtained by slowly adding the chloroauric acid aqueous solution in the tannic acid solution. We used the proportions of the second sample because we needed to obtain nanoparticles with average size around 50 nm. Even though the shape of the as obtained particles is not homogenous, we saw from the UV-Vis spectra that all the samples adsorb in the visible range.

Fractal analysis of TEM images indicate the same behavior: the first two samples are correlated clusters of nanoparticles, with low dispersion and highly agglomerated, characterized by three fractal dimensions, meanwhile the last one consist of a self-similar structure of nanoparticles with high dispersion, and two characteristic fractal dimensions. The box-counting fractal dimension values offer some information about the synthesis mechanism: slow injection can be simulated by the colloidal aggregation; meanwhile the rapid injection is well described by the diffusion limited cluster-cluster aggregation model. Also, from the XRD spectra it was clear that all the obtained materials consist only in metallic gold.

Therefore, these nanoparticles, obtained by a so called 'green synthesis' are suitable for further analysis and testing in many applications, including catalytic and photo catalytic tests for a current worldwide problem consisting in the removal of nitrite from water (Bulgariu et al., 2012), which is the goal of our future study.

Acknowledgements

This work was supported by Project SOP HRD - PERFORM /159/1.5/S/138963, PN2 100/2012 INTEGRATREAT and PN2 46/2012 BICLEANBIOS.

References

- Ahmad T., (2014), Reviewing the tannic acid mediated synthesis of metal nanoparticles, *Journal of Nanotechnology*, ID 954206, <http://dx.doi.org/10.1155/2014/954206>.
- Ahmad T., Khan W., (2013), Size variation of gold nanoparticles synthesized using tannic acid in response to higher chloroauric acid concentrations, *World Journal of Nano Science and Engineering*, **03**, 62-68.
- Aswathy A.S., Philip D., (2012), Facile one-pot synthesis of gold nanoparticles using tannic acid and its application in catalysis, *Physica E: Low-dimensional Systems and Nanostructures*, **44**, 1692-1696.
- Bratescu MA., Takai O., Saito N., (2013), One-step synthesis of gold bimetallic nanoparticles with various metal-compositions, *Journal of Alloys and Compounds*, **562**, 74-83.
- Bulgariu L., Ceica A., Lazar L., Cretescu I., Balasanian I., (2012), Equilibrium and kinetics study of nitrate removal from water by Purolite A520-E resin, *Environmental and Management Journal*, **11**, 37-45.
- Chauvy P.F., Madore C., Landolt D., (1998), Variable length scale analysis of surface topography: characterization of titanium surfaces for biomedical applications, *Surface and Coatings Technology*, **110**, 48-56.
- Family F., Vicsek T., (1985), Scaling of the active zone in the Eden process on percolation networks and the ballistic deposition model, *Journal of Physics, A*, **18**, 1, 75-82.
- Granmayeh Rad A., Abbasi H., Hossein Afzali M., (2011), Gold nanoparticles: Synthesising, characterizing and reviewing novel application in recent years, *Physics Procedia*, **22**, 203-208.
- Hamaguchi K., Kawasaki H., Arakawa R., (2010), Photochemical synthesis of glycine-stabilized gold nanoparticles and its heavy-metal-induced aggregation behavior, *Colloids and Surfaces A: Physicochemical and Engineering Aspects*, **367**, 167-173.
- Kaur R., Pal B., (2012), Size and shape dependent attachments of Au nanostructures to TiO₂ for optimum reactivity of Au-TiO₂ photocatalysis, *Journal of Molecular Catalysis A: Chemical*, **355**, 39-43.
- Kyrychenko A., Karpushina G.V., Bogatyrenko S.I., Kryshal A.P., Doroshenko A.O., (2011), Preparation, structure, and a coarse-grained molecular dynamics model for dodecanethiol-stabilized gold nanoparticles, *Computational and Theoretical Chemistry*, **977**, 34-39.
- Lapuerta M., Martos F.J., Martin-Gonzalez G., (2010), Geometrical determination of the lacunarity of agglomerates with integer fractal dimension, *Journal of Colloid and Interface Science*, **346**, 23-31.
- Lee K.Y., Hwang J., Lee W., Kim J., Han S.W., (2007), One-step synthesis of gold nanoparticles using azacryptand and their applications in SERS and catalysis, *Journal of Colloid and Interface Science*, **316**, 476-481.
- Mandelbrot B.B., (1977), *Fractals: Form, Chance and Dimension*, Freeman, San Francisco.
- Mandelbrot B.B., (1982), *The Fractal Geometry of Nature*, Freeman, San Francisco, 14-19.
- Meakin P., (1986), *Computer Simulation of Growth and Aggregation Processes*, In: *On Growth and Form*, Stanley H.E., Ostrowsky N. (Eds.), Martinus Nijhoff Publishers, 111-135.
- Meena Kumari M., Aromal S.A., Philip D., (2013), Synthesis of monodispersed palladium nanoparticles using tannic acid and its optical non-linearity, *Spectrochimica Acta Part A: Molecular and Biomolecular Spectroscopy*, **103**, 130-133.
- Ostwald W., (1917), *An Introduction to Theoretical and Applied Colloid Chemistry*, John Wiley and Sons New York.
- Peng S., Lee Y., Wang C., Yin H., Dai S., Sun S.H.A., (2008), A facile synthesis of monodisperse Au nanoparticles and their catalysis of CO oxidation, *Nano Research*, **1**, 229-234.
- Sárkány A., Geszti O., Safran G., (2008), Preparation of Pd shell-Au core/SiO₂ catalyst and catalytic activity for acetylene hydrogenation, *Applied Catalysis A: General*, **350**, 157-163.
- Sivaraman S., Kumar S., Santhanam V., (2010), Room-temperature synthesis of gold nanoparticles – Size-control by slow addition, *Gold Bulletin*, **43**, 275-286.
- Stanley H.E., (1977), Cluster shapes at the percolation threshold: and effective cluster dimensionality and its

- connection with critical-point exponents, *Journal of Physics*, **10**, L211-L220.
- Sutherland D.N., (1967), A theoretical model of floc structure, *Journal of Colloid and Interface Science*, **25**, 373-380.
- Sutherland D.N., (1970), Chain formation of fine particle aggregates, *Nature*, **226**, 1241-1242.
- Sutherland D.N., Goodarz-Nia I., (1971), Floc simulation: The effect of collision sequence, *Chemical Engineering Science*, **26**, 2071-2085.
- Weitz D.A., Olivera M., (1984), Fractal structures formed by kinetic aggregation of aqueous gold colloids, *Physical Review Letters*, **52**, 1433-1436.
- Xu F., Zhang Q., Gao Z., (2013), Simple one-step synthesis of gold nanoparticles with controlled size using cationic Gemini surfactants as ligands: Effect of the variations in concentrations and tail lengths, *Colloids and Surfaces A: Physicochemical and Engineering Aspects*, **417**, 201-210.
- Yi Z., Li X., Xu X., Luo B., Luo J., Wu W., Yi Y., Tang Y., (2011), Green, effective chemical route for the synthesis of silver nanoplates in tannic acid aqueous solution, *Colloids and Surfaces A: Physicochemical and Engineering Aspects*, **392**, 131-136.
- Zabetakis K., Ghann W.E., Kumar S., Daniel M.-C., (2012), Effect of high gold salt concentrations on the size and polydispersity of gold nanoparticles prepared by an extended Turkevich–Frens method, *Gold Bulletin*, **45**, 203-211.
- Zhang H., Toshima N., (2012), Fabrication of catalytically active AgAu bimetallic nanoparticles by physical mixture of small Au clusters with Ag ions, *Applied Catalysis A: General*, **447-448**, 81-88.
- Zhou J., Ralston J., Sedev R., Beattie D.A., (2009), Functionalized gold nanoparticles: synthesis, structure and colloid stability, *Journal of Colloid and Interface Science*, **331**, 251-262.
- Zhu H., Pan Z., Hagaman E.W., Liang C., Overbury S.H., Dai S., (2005), Facile one-pot synthesis of gold nanoparticles stabilized with bifunctional amino/siloxy ligands, *Journal of Colloid and Interface Science*, **287**, 360-365.



“Gheorghe Asachi” Technical University of Iasi, Romania



ENHANCING THE FENTON PROCESS BY UV LIGHT APPLIED IN TEXTILE WASTEWATER TREATMENT

Vasilica-Ancuta Simion¹, Igor Cretescu^{1*}, Doina Lutic²,
Constantin Luca³, Ioannis Poullos⁴

¹“Gheorghe Asachi” Technical University of Iasi, Faculty of Chemical Engineering and Environmental Protection,
Department of Environmental Engineering and Management, 73 Prof. Dr. docent Dimitrie Mangeron Str., 700050 Iasi, Romania

²Al. I. Cuza University, Department of Materials Chemistry, 11 Carol I Blvd., 700506 Iasi, Romania

³“Gheorghe Asachi” Technical University of Iasi, Faculty of Chemical Engineering and Environmental Protection,
Department of Organic, Biochemical and Food Engineering, 73 Prof. Dr. docent Dimitrie Mangeron Str., 700050 Iasi, Romania

⁴Aristotle University of Thessaloniki, Department of Chemistry, 54124 Thessaloniki, Greece

Abstract

Nowadays, an efficient wastewater management involves the use of advanced treatment technologies able to decompose hardly biodegradable compounds with reasonable costs at the lowest possible environmental impact. In our work we used one of the most efficient advanced wastewater treatment, the Fenton reaction and its photo-assisted version. The hydrogen peroxide was the oxidizer; despite its relatively high cost, its high activity in oxidizing of a large variety of organic persistent pollutants in the presence of Fe^{3+} ions as catalyst, makes it an alternative which is worth to be considered even in practical medium scale systems. The Fenton and photo-Fenton oxidation were performed using a model dye, the xanthene-type Rhodamine 6G, widely used in a series of biotechnology applications, but having major drawbacks when released in natural water flows, mainly mutagen and carcinogen effects. Therefore, a parametric case study was performed in order to define the optimal operating parameters (the pH value, the hydrogen peroxide concentration and the iron catalyst concentration). The oxidative degradation of Rhodamine 6G by Fenton reaction was more effective when combined with UV irradiation. Each parameter of the oxidative treatment is essential for the color and TOC removal. The optimal values found for the total color degradation and mineralization of the dye were as follows: 16 ppm Fe^{3+} , 100 ppm H_2O_2 and pH of 4.5.

Key words: advanced wastewater treatment, advanced oxidation process, photo-Fenton, Rhodamine 6G, UV irradiation

Received: November, 2014; Revised final: March, 2015; Accepted: March, 2015

1. Introduction

The importance paid to an efficient wastewater management is a real label for a civilized, sustainable-oriented society. The complexity of the wastewater composition had increased a lot in the latest decades, due to the multiplication of the human activities (or the dramatic increase of their scales) requiring water as raw material: washing agent, steam production, heating and cooling agent. Up to an extent, the long-term kinds of water use are well-known and consequently, the water quality

management and the corresponding decontamination treatments have entered to a routine. The big problem nowadays is the accumulation of organic stable and toxic compounds in the wastewater (dyes, pesticides, surfactants), refractory to the biologically degradation treatments, generating a chemical composition hard to define in details and even more difficult to establish a versatile strategy to get rid of (Caliman et al., 2008; Papić et al., 2014; Yazdanbakhsh et al., 2014; Zaharia and Suteu, 2012). On another part, the reuse of domestic or industrial wastewater after the treatments is not enough

* Author to whom all correspondence should be addressed: e-mail: icre@ch.tuiasi.ro

seriously directed to a sustainable-oriented direction by the water management. There still is some work to do on this topic from cultural, legislative and economical point of view. Large masses of people tend to consider water an endless and renewable resource, so the rational water consummation sounds like an empty slogan, especially for the less educated people. The poorness and ignorance makes the regulations about the water management quite permissive in the undeveloped countries, being evident that the wastewater treatment technologies require high financial efforts (Lutic et al., 2014).

The multitude of wastewater contaminants depend on their source and starts with domestic use products (fats, waste from personal care or hygiene products, pesticides from food processing or preserving) and continues with industrial products (dyes and surfactants from textile industry, organics from oil refinery, chemicals used in food industry, biotechnologies, pharmaceuticals). An important point is the strong pollution at small scale due to research activities or to medical investigation laboratories, which use relatively small amounts of extremely toxic or stable chemicals, thus generating dangerous wastewaters. It is therefore interesting to investigate methods applicable to the small-scale wastewater treatment units, since their role is treating preliminary wastewaters before releasing them to the normal flowing course (Arsene et al., 2011; Teodosiu, 2007; Zaharia and Suteu, 2012).

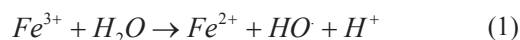
Due to the toxic nature and low biodegradability of most synthetic dyes, several groups of methods were applied: adsorption on solids followed by different oxidation procedures (Macoveanu et al., 1997; Zaharia et al., 2014a), electrochemically and/or sonic assisted oxidation procedures (Noubactepa and Schönerb, 2010; Raschitor et al., 2014; Rein, 2001). The request to decompose, not only to remove temporary by adsorption from water the POPs, especially the dyes, involved an increase interest for the employment of Advanced Oxidation Processes (AOPs). The AOPs are methods used to degrade and eventually mineralize by means of oxidation different types of rebel chemicals (named generically Persistent Organic Pollutants - POPs) from liquid effluents. The literature data agree that the key-step in the AOPs is developing a large amount of HO[•] radicals in the reaction medium. This reactive species is able to initiate a chain radical reaction in which the POPs and the oxygen participate together. The POP molecules are splitted gradually in smaller molecules and then finally mineralized to carbon dioxide and water (Amilcar et al., 2009, 2012).

An excellent candidate for the oxidation of POPs is the hydrogen peroxide, H₂O₂ (Zaharia et al., 2009). Despite its relatively high price, its non-polluting nature and high efficiency even at ambient temperature recommend it as a "green oxidizer". The Fenton reaction involves the use of ferric or ferrous ions as catalysts together with hydrogen peroxide, in order to increase the efficiency of the HO[•] radicals

production (Da Silva, 2013; Navalon et al., 2010). A restriction of this reaction is the requirement to work at low pH values, since the iron ions have a strong trend to precipitate as ferric hydroxide (solubility product $4 \cdot 10^{-38}$) (Navalon et al., 2010). Generally, at some tens of ppm ferric ions concentrations, the pH values usually involved in the Fenton reaction are comprised between 3 and 4 (Amilcar et al., 2009). Sometimes a combined homogeneous-heterogeneous procedure is applied, using a solid as the Fe³⁺ source, by the partial dissolution of its framework, under the influence of the reaction medium; this strategy also allows applying higher pH values (around 7) for the reaction (Barona et al., 2015).

The synthetic, non-degradable dyes are among the top pollutants due to their property to absorb light according to their structure. Even if not necessarily toxic, the fore-mentioned behavior leads to the modification of the aquatic environment for different living creatures and aesthetic pollution (Secula et al., 2008). The amount of iron required in this type of homogenous catalysis, could be controlled by anodic dissolution or an iron electrode, when the process is namely electro-Fenton (Petrescu et al., 2009; Priambodo et al., 2011).

The presence of UV irradiation accelerates even more the process. Moreover, the UV light promotes the oxidation of Fe²⁺ to Fe³⁺, while generating HO[•] radicals and acidifying the reaction medium (Eq. 1).



In brief, due to its high efficiency, the photo-Fenton reaction can be considered one of the most convenient, environmentally friendly and efficient method for the oxidation of POPs. (Almicar et al., 2012; Ruales-Lonfat et al., 2015; Sayid Abdullah et al., 2014). There are literature data (Chong et al., 2010) indicating the use of solar light as the UV radiation source (Muthuvel et al., 2012, 2014) or combining the photo-oxidation with electrochemical processes (Priambodo et al., 2011).

Rhodamine 6G is an intense and persistent xanthene dye, with intense pink color and green fluorescence, widely used as a tracer dye in hydrological studies as well as in laboratory investigations involved in biotechnology and genetic by microscopy, fluorescence, ELISA, etc. Its very high stability, persistence and color intensity even at concentrations around 1 ppm in solution makes it an interesting species to be studied in the oxidative mineralization (Lutic et al., 2012; Lutic et al., 2014; Zaleschi, 2014).

In this study, we investigated the degradation of dye Rhodamin 6G by the Fenton system, while UV irradiation is applied. The Fenton reaction is cited in literature as a reliable method to allow the decomposition or mineralization of several dyes (Muthuvel et al., 2012; Muthuvel et al., 2014; Peng-Sheng et al., 2009; Zaharia et al., 2014a)

2. Experimental part

The UV-vis spectrum of R6G shows a main maximum absorption peak at about 525 nm and a lower intensity peak located around 244 nm (Fig. 1). The position of the main peak is preserved constant during the photodegradation, so its intensity is trusted for the dye concentration measuring.

The experimental setup of the photo-Fenton process is displayed in Fig. 2. (Betianu et al., 2008; Lutic et al., 2012). The reactor (4) is a glass vessel of 0.5 L, covered with a lid (1), accommodating a central quartz tube (3) serving to insert an UV lamp (2). The dye solution was exposed to UV in the space between the reactor and the central tube.

The dye solution was magnetically agitated on a stirring plate (6) at about 400 rpm using a magnetic range (5). The runs were performed at ambient temperature (296 - 298K). The initial dye solution concentration was 30 ppm. Dye samples were taken at due time durations from the photoreactor and the concentration was measured by spectrophotometric measurements, on a Shimadzu UV-1700 apparatus. The Total Carbon Content (TOC) values on selected samples were measured on a SHIMADZU Total Organic Carbon Analyzer 5000A.

Ferric chloride, sulfuric acid and sodium hydroxide solutions (0.1 N) of analytical purity from Merck were used respectively as a source of Fe^{3+} ions and for the pH setting at the desired values.

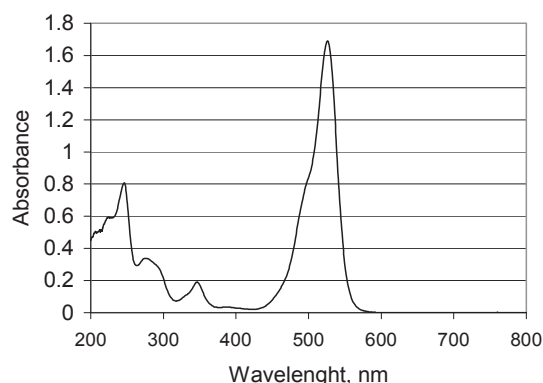


Fig. 1. The UV-Vis spectrum of Rhodamine 6G solution

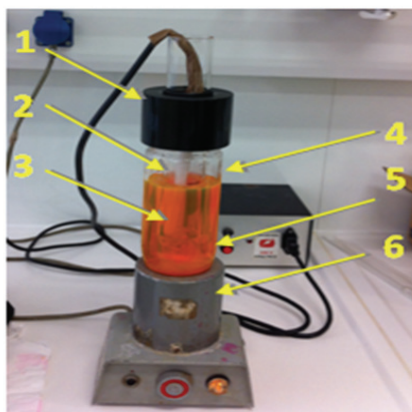


Fig. 2. Experimental setup for the advanced oxidation of Rhodamin 6G by photo-Fenton reaction

3. Results and discussion

3.1. Individual roles of the oxidation and irradiation on process effectiveness

According to a standard procedure, when investigating several factors which could give a synergetic effect on a reaction, their individual role must be highlighted before concluding (Lutic et al., 2012; Rein, 2001; Zaharia et al., 2014b). Therefore, blank experiments were performed as follows:

- if no oxidant (H_2O_2) was used and 16 mg/L Fe^{3+} was mixed in the dye solution, the decolorizing after 60 min of exposure to light reached only around 14%; this is the photolysis degree with no oxidizer;

- when 100 ppm H_2O_2 was added but no catalyst (Fe^{3+}) was introduced in the system, the conversion was below 10% in the first 30 min and finally reached around 20% after 1 hour; this is the pure role of the oxidizer;

- when only the Fenton reagents were used, without illumination, the conversion was around 11%; we concluded that the light role was essential for the degradation of the dye;

The second and third blank experiments correlated show that the addition of Fe^{3+} has a certain inhibition effect on the decolorizing.

Broad limits were taken for all the parameters to be studied, 27 - 173 ppm H_2O_2 , 0.3-30.6 ppm Fe^{3+} and pH 2.3 - 4.7.

3.2. Influence of pH value on the dye removal

This is a key parameter for the removal of organic pollutants by Fenton reaction, especially due to the iron ions solubility, but also to the activation of the dye molecule and generation of $\text{HO}\cdot$ radicals. The influence of the pH was investigated in reaction systems containing 100 ppm H_2O_2 and 16 ppm Fe^{3+} . We must outline that at ambient temperature, the spontaneous hydrogen peroxide decomposition occurs at an appreciable extent, so it is convenient to find the proper conditions able to remove the dye within some tens of minutes.

The time dependence of the decolorizing extent is displayed in Fig. 3. The results show that Fenton reaction is highly favored by the pH value of 3.5. The dye removal is extremely fast, since it had been removed almost totally within some minutes. Neither lower nor higher values of the pH worked better, but the pH value of 4.7 was much better than the low 2.3. It is important information, since usually wastewaters have pH values close to neutral and a fast reaction requires the pH adjustments. This set of experiments let us conclude that a pH value comprised between 3.5 - 4.5 is reasonable for an eventual practical application, since for both values the time reaction comprised between 15-20 minutes gave high decolorizing degrees.

A better way to express the degradation of a dye by Fenton reaction is measuring the remains of total organic matter by TOC determination, since

decolorizing is the first step in the degradation, but the final target is to mineralize as much as possible the organic matter from the wastewater.

Table 1 presents some data illustrating the removal dye degree in terms of TOC. The high pH values seem to have a net more favorable effect on the dye removal, since at pH of 4.7 the mineralization degree reaches over 66% after one hour of reaction.

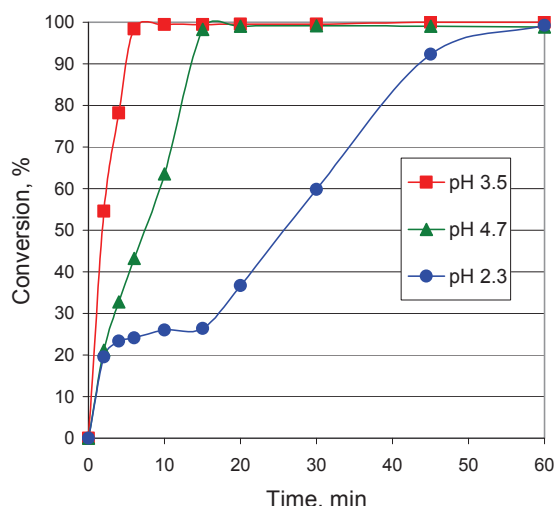


Fig. 3. The pH value influence on photo Fenton reaction advancement in terms of decolorizing

Table 1. Dye degradation extent calculated from TOC data at different pH values

| Time, min / pH value | 2.3 | 4.7 |
|----------------------|-------|-------|
| 30 | 9.8 | 34.3 |
| 60 | 36.96 | 66.32 |

3.3. Influence of the H_2O_2 concentration on the performance of dye degradation

In order to investigate the influence of the oxidizer concentration on the process, in this series of experiments, the pH value of 3.5 was chosen and the Fe^{3+} concentration was kept also at 16 ppm. As expected, the hydrogen peroxide concentration has a strong influence on the performance of the reaction.

The high values of the oxidizer concentrations involved an extremely fast decolorizing photo Fenton process, almost instantaneous, when the H_2O_2 concentration value was 173 ppm. In fact, a lot more interesting from a practical perspective is the behavior when only 27 ppm H_2O_2 was added in the system. At a thus low concentration, the total decolorizing occurs in about 10 minutes. It indicates that the presence of H_2O_2 is necessary in the initial step of the oxidation, for the initiation of HO· radicals production and for this purpose 27 ppm is enough. Later on, the reaction continues on the expense of the radicals propagated in the system and after 10 minutes the decolorizing is almost complete (Fig. 4).

The TOC values for some selected points are shown in Table 2. In this case, the behavior is very different. The presence of high amounts of H_2O_2

determines the mineralization up to 70% during the first 30 minutes, and then the mineralization degree does not grow any more in a significant extent.

For the low concentrations of the H_2O_2 , the mineralization is slower and weaker. It shows that the breakage of the chromophore chemical bondings can occur at low concentrations of the oxidizer, but the fragments resulted from the split of the entire dye molecule are transformed to carbon dioxide only in the presence of high hydrogen peroxide content. So, we could say that the photo-induced process is strictly necessary to initiate the bulk molecule split, while the oxidizer is very active for the mineralization of the smaller fragments.

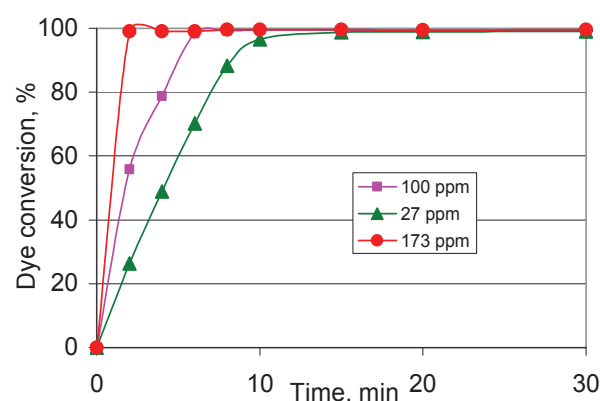


Fig. 4. The effect of H_2O_2 concentration on photo Fenton reaction – decolorizing

Table 2. Dye degradation extent calculated from TOC data at different oxidizer concentrations

| Time, min / H_2O_2 concentration | 27 | 173 |
|------------------------------------|-------|-------|
| 30 | 18.86 | 66.70 |
| 60 | 31.47 | 69.59 |

3.4. The influence of the Fe^{3+} concentration on dye removal efficiency

Three values of Fe^{3+} concentrations were tested in the R6G degradation, namely 1.5, 16 and 30.6 ppm. These experiments were run at hydrogen peroxide concentration 100 ppm and pH value of 3.5 (the corresponding saturation concentration of the Fe^{3+} ions is 70.8 ppm).

Even at the very low concentration values of Fe^{3+} , the Fenton system is working, although the decolorizing is very slow. An increase of the Fe^{3+} ions concentration to 16 ppm gives a spectacular decolorizing rate, since a reaction time of 5 minutes arises a 98% conversion degree (Fig. 5).

4. Conclusions

This research studied the performance of the Fenton system during UV irradiation on the degradation of Rhodamin 6G dye. The essential role of all components in the reaction medium was highlighted first: the oxidizer, the catalyst and the UV irradiation.

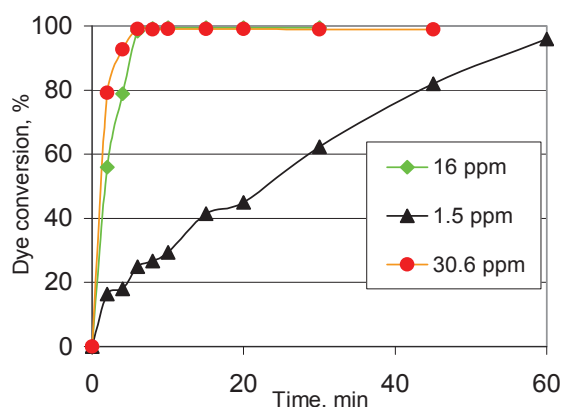


Fig. 5. Fe^{3+} concentration influence on photo Fenton reaction

A parametric study allowed defining the optimal set of working conditions judged from the point of view of dye decolorizing and its total mineralizing. The role of the oxidizer was rather to be an efficient initiator of the dye degradation, since its use at a low concentration of 27 ppm leads to the total decolorizing in several tens of minutes, while the high degrees of mineralizing required higher concentrations of oxidizer (around 100 ppm). The Fe^{3+} ions concentrations necessary for a high yield of the reaction were around 16 ppm and the pH value ranging between 3.5 and 4.7.

The possibility to enhance the performance of Fenton oxidation process of Rhodamin 6G dye in water solution in the presence of UV irradiation was proved and quantified.

Acknowledgements

This work was partly supported by the Bilateral Research Grant Romania-Greece no. 576/2012 financed in Romania by ANCS/UEFISCDI and in Greece by GSRT, Greek Ministry of Education, Lifelong Learning and Religious Affairs.

References

- Amilcar M.Jr., Oliveira S.C., Osugi M.E., Ferreira V.S., Quina F.H., Dantas R.F., Oliveira S.L., Casagrande G. A., Anaissi F.J., Silva V.O., Cavalcante R.P., Gozzi F., Ramos D.D., da Rosa A.P.P., Santos A.P.F., de Castro D.C., Nogueira J.A., (2009), *Application of Different Advanced Oxidation Processes for the Degradation of Organic Pollutants*, In: *Organic Pollutants - Monitoring, Risk and Treatment*, Nageeb Rashed M. (Ed.), InTech, Rijeka, Croatia, DOI: 10.5772/53188, 142-166.
- Amilcar M.Jr., Quina F.H., Gozzi F., Silva V.O., Friedrich L.C., Moraes J.E.F., (2012), *Fundamental Mechanistic Studies on the Photo-Fenton Reaction for Degradation of Organic Pollutants*, In: *Organic Pollutants Ten Years after the Stockholm Convention-Environmental and Analytical Update*, Puzyn T., Mostrag-Szlichtyng A., InTech, Rijeka, Croatia, DOI: 10.5772/30995, 272-285.
- Arsene D., Musteret C.P., Catrinescu C., Apopei P., Barjoveanu G., Teodosiu C., (2011), Combined oxidation and ultrafiltration processes for the removal of priority organic pollutants from wastewaters, *Environmental Engineering and Management Journal*, **10**, 1967-1976.
- Barona J.F., Morales D.F., González-Bahamón L.F., Pulgarín C., Benítez L.N., (2015), Shift from heterogeneous to homogeneous catalysis during resorcinol degradation using the solar photo-Fenton process initiated at circumneutral pH, *Applied Catalysis B: Environmental*, **165**, 620-627.
- Betianu C., Caliman A.F., Gavrilescu M., Cretescu I., Cojocaru C., Poullos I., (2008), Response surface methodology applied for Orange II photocatalytic degradation in TiO_2 aqueous suspensions, *Journal of Chemical Technology and Biotechnology*, **11**, 1454-1465.
- Caliman F.A., Curteanu, S., Betianu C., Gavrilescu M., Poullos I., (2008), Neural networks and genetic algorithms optimization of the photocatalytic degradation of Alcian Blue 8GX, *Journal of Advanced Oxidation Technologies*, **11**, 316-326.
- Chong N.M., Jin B., Chow W.K., Saint C., (2010), Recent developments in photocatalytic water treatment technology: A review, *Water Research*, **44**, 2998 - 3003.
- Da Silva L.G., Ferreira B.P., Albuquerque P.M., Silva C. C., da Silva S.A., Rodrigues M.B., de Souza J.V.B., de Souza É.S., (2013), Treatment of liquid waste produced in a small chemical laboratory using the Photo-Fenton Process, *Journal of Food Agriculture & Environment*, **11**, 1125-1128.
- Lutic D., Coromelci-Pastravanu C.G., Cretescu I., Poullos I., Stan C.D., (2012), Photocatalytic treatment of Rhodamine 6G in wastewater using photoactive ZnO , *International Journal of Photoenergy*, ID 475131, doi:10.1155/2012/475131.
- Lutic D., Simion V.A., Cretescu I., (2014), *Improving the Water Management and Protection of Natural Aquatic Resources by Using Cost-Effective Advanced Treatments of Effluents Based on Fenton Reaction*, In: *Current Topics, Concepts and Research Priorities in Environmental Chemistry*, Zaharia C. (Ed.), Al. I. Cuza University Publishing House, Iasi, Romania, 147-164.
- Macoveanu M., Teodosiu C., Duca G., (1997), *Advanced Treatment of Wastewaters Containing Non-Biodegradable Compounds* (in Romanian), Gh. Asachi Technical University Publishing House, Iasi, Romania.
- Muthuvel I., Krishnakumar B., Swaminathan M., (2012), Novel Fe encapsulated montmorillonite K10 clay for photo-Fenton mineralization of acid yellow 17, *Indian Journal of Chemistry*, **51A**, 800-806.
- Muthuvel I., Krishnakumar B., Swaminathan M., (2014), UV-A/solar light induced Fenton mineralization of Acid Red 1 using Fe modified bentonite composite, *Indian Journal of Chemistry*, **53A**, 672-678.
- Navalon S., Alvaro M., Garcia H., (2010), Heterogeneous Fenton Clays Based on Clays, Silicas and Zeolites, *Applied Catalysis B: Environmental*, **99**, 1-26.
- Noubactepa C., Schönerb A., (2010), Metallic iron for environmental remediation: Learning from electrocoagulation, *Journal of Hazardous Materials*, **175**, 1075-1080.
- Papić S., Peternel I., Krevzelj Z., Kušić H., Koprivanac N., (2014), Advanced oxidation of an azo dye and its synthesis intermediates in aqueous solution: effect of fenton treatment on mineralization, biodegradability and toxicity, *Environmental Engineering and Management Journal*, **13**, 2561-2572.

- Peng-Sheng S., Cheng-Jie L., Jian-Hui S., Shao-Hui S., Mao-Hong F., Qi Z., (2009), Decolorization of an azo dye Orange G in aqueous solution by Fenton Oxidation process: effect of system parameters and kinetic study, *Journal of Hazardous Materials*, **161**, 1052-1057.
- Petrescu S., Secula S.M., Nemțoi G., Crețescu I., (2009), Study on metal anodic dissolution, *Revista de Chimie*, **60**, 462-467.
- Priambodo R., Shih Y.-J., Huang Y.-J., Huang Y.H., (2011), Treatment of real wastewater using semi batch (Photo)-Electro-Fenton method, *Sustainable Environment Research*, **21**, 389-393.
- Raschitor A., Fernandez C.M., Crețescu I., Rodrigo M.A., Cañizares P., (2014), Sono-electrocoagulation of wastewater polluted with Rhodamine 6G, *Separation and purification technology*, **135**, 110-116.
- Rein M., (2001), Advanced oxidation processes-current status and prospects, *Proceedings of the Estonian Academy of Sciences. Chemistry*, **50**, 59-80.
- Ruales-Lonfat C., Barona J.F., Sienkiewicz A., Bensimon M., Vélez-Colmenares J., Benítez N., Pulgarín C., (2015), Iron oxides semiconductors are efficient for solar water disinfection: A comparison with photo-Fenton processes at neutral pH, *Applied Catalysis B: Environmental*, **166-167**, 497-508.
- Sayid Abdullah S.H.Y., Abu Hassan M.A., Noor Z.Z., Md Noor S.F., Aris A., (2014), Fenton and photo-fenton oxidation: a comparative study based on statistical analysis, *Environmental Engineering and Management Journal*, **13**, 531-538.
- Secula M.S., Suditu G.D., Poullos I., Cojocaru C., Crețescu I., (2008), Response surface optimization of the photocatalytic decolorization of a simulated dyestuff effluent, *Chemical Engineering Journal*, **141**, 18-26.
- Teodosiu C., (2007), Challenges for integrated water resources management in Romania, *Environmental Engineering and Management Journal*, **6**, 363-374.
- Yazdanbakhsh A.R., Mohammadi A.S., Sardar M., Godini H., Almasian M., (2014), COD removal from synthetic wastewater containing azithromycin using combined coagulation and a Fenton-like process, *Environmental Engineering and Management Journal*, **13**, 2929-2936.
- Zaharia C., Suteu D., Muresan A., Muresan R., Popescu A., (2009), Textile wastewater treatment by homogeneous oxidation with hydrogen peroxide, *Environmental Engineering and Management Journal*, **8**, 1359-1369.
- Zaharia C., Suteu D., (2012), *Textile Organic Dyes, Characteristics, Polluting Effects and Separation/Elimination Procedures from Industrial Effluents, A Critical Overview*, In: *Organic Pollutants Ten Years After the Stockholm Convention - Environmental and Analytical Update*, Puzyn T., Mostrag-Szlichtyng A., InTech, Rijeka, Croatia, InTech, DOI: 10.5772/32373, 55-82.
- Zaharia C., Amarandei V., Muresan A., (2014a), Comparative overview of different physical-chemical treatments applied for real textile effluents, *Advanced Materials Research*, **1036**, 58-64.
- Zaharia C., Fedorcea V., Beda A., Amarandei V., Muresan A., (2014b), Removal of Remazol Rosso RB dye from aqueous effluents by homogenous Fenton oxidation processes, *Chemistry Journal of Moldova. General, Industrial and Ecological Chemistry*, **9**, 74-79.
- Zaleschi L., Secula M.S., Teodosiu C., Stan C.S., Crețescu I., (2014), Removal of Rhodamine 6G from aqueous effluents by electrocoagulation in a batch reactor: assessment of operational parameters and process mechanism, *Water, Air, & Soil Pollution*, **225**, 1-14.



"Gheorghe Asachi" Technical University of Iasi, Romania



MATHEMATICAL MODELLING OF MECHANICAL BEHAVIOUR OF CELLULOSE-BASED FIBRES EXPOSED TO GAMMA RAYS AND HYDROTHERMAL TREATMENT

Angelica Olaru¹, Teodor Măluțan^{*2}, Maria Geba¹, Cristina M. Ursescu^{1*}, Corina Măluțan²

¹"Moldova" National Complex of Museums, 1 Piața Ștefan cel Mare și Sfânt Str., 700028 Iași, Romania

²"Gheorghe Asachi" Technical University of Iasi, 73 Prof. Dr. docent Dimitrie Mangeron Str., 700050 Iasi, Romania

Abstract

The deterioration of the natural polymers is a very complex process, and a problem that can be best addressed through modelling. The approach for modelling the rheological behaviour of different cellulose-based textile fibres (*cotton, hemp, flax*) when subjected to a hydrothermal treatment, followed by exposure to different doses of gamma-rays (5, 10, 15 and 25 kGy) is presented here. In order to predict the optimum radiation dose limit and hydrothermal aging time, the mathematical model was developed using MATLAB computational technique.

To study the mechanical behaviour of the tested fibres, tensile tests were carried out using a TINIUS OLSEN dynamometer H5KT according to ISO 2062 norm. The model of correlation between the mechanical properties of the fibres and the independent variables was based on a polynomial second-degree equation, with the Least-Squares fitting approach that led to the coefficients of the mathematical model.

Key words: cellulose-based textiles, gamma rays, mathematical modelling, rheological behaviour

Received: November, 2014; Revised final: March, 2015; Accepted: March, 2015

1. Introduction

As the level of environmental degradation is nowadays a rising hazard, physical treatments such as exposure to ionizing radiation (gamma rays or electron beam) prove to be the environmentally friendly methods both for reducing biological contamination and as mean of modifying polymers for different purposes. In industrial irradiators, the standard sealed sources of isotopes are subjected to national and international regulations (ASTM, 2006; ISO, 2000; ISO, 2006a; ISO, 2006b) that provide the legal basis for environmental radiation monitoring (Ionescu et al., 2012).

Although used mainly for the sterilization of medical devices and pharmaceutical products or food products decontamination, gamma-rays treatment

was taken into consideration for the last fifty years as a less noxious mass-treatment for disinfestations or micro-organisms inactivation in historical collections (Kennedy et al., 2000; Katusin-Razem et al., 2009; Van der Sluijs and Church, 2013). The main advantage in applying this treatment resides in the high penetrating power of this type of ionizing radiation, which allows a product to be treated even inside its package, while it leaves no residues on the object. As regards the conservation of textile heritage collections, the radiation dose should be selected according to the chemical and physical properties of the materials (Geba et al., 2014; Panzaru and Malutan, 2012).

The exposure to gamma rays requires thorough investigation concerning the long term effect of radiation doses (Machnowski et al., 2013;

* Author to whom all correspondence should be addressed: e-mail: thmalu@tuiasi.ro; marta_ursescu@yahoo.com

Takacs et al., 1999) on the mechanical properties of the natural fibres during aging (Olaru et al., 2013) in their future environmental conditions.

In the present study, the mechanical behaviour of cellulose-based fibres exposed to gamma rays and hydrothermal treatment was investigated, followed by empirical mathematical modelling, developed to establish the effect of both increased exposure to irradiation and hydrothermal treatment on the physical-mechanical characteristics of fibres.

2. Experimental

2.1. Materials

This study was carried out on fibres from commercial fabrics made of *cotton*, *flax* and *hemp*. Textile samples subjected to a hydrothermal treatment and irradiated at increasing doses of gamma radiation were analysed.

2.2. Weathering procedure

The tested fibres were placed in a laboratory chamber (Angellantonio Ind., Italy) and exposed to the hydrothermal treatment, to climatic conditions set at 40°C and 60 % R.H., in order to reproduce the influence of the main agents of deterioration within the museum environment. The samples were kept in the climatic chamber for 0, 24, 48 and 120 hours.

2.3. Irradiation procedure

The Technological Radiation Centre IRASM/IFIN-HH in Magurele, Ilfov, Romania provided the exposure to gamma-rays doses of: 5, 10, 15 and 25 kGy, with a Dmax/Dmin=1.14 dose uniformity, in an SVST Co-60/B type irradiator.

2.4. Tensile tests

Tensile tests were carried out using a TINIUS OLSEN dynamometer H5KT, according to ISO 2062 norm. The main tensile properties, namely breaking force (inN) and relative elongation (%) were analyzed.

3. Results and discussion

The behavior of the tested samples of cotton, flax and hemp under the radiation treatment may be different from the pure cellulose, due to the changes

already induced through fibers manufacturing (i.e. temperature, chemicals, stretching, raw materials type as cellulose source for processing the fibers) and the exposure to or the fluctuation of environmental agents (i.e. temperature, light, relative humidity). Using an appropriate mathematical model in studying the rheological behaviour of the tested textiles, one can estimate the optimum domain of the radiation doses, as well as the durations of the hydrothermal treatment that should lead to the adequate physical-mechanical characteristics. In order to establish the effect of both increased exposure to irradiation and hydrothermal treatment on the physical-mechanical characteristics of the cellulose-based fibres, an empirical mathematical second order rotational model was developed (Măluțan, 2009). Therefore, results on physical-mechanical tensile tests were subjected to mathematical modelling by means of the Least-Squares fitting approach, for the purpose of obtaining a correlation equation.

The independent variables considered in the proposed model were: time of exposure to hydrothermal treatment and gamma radiation dose. The dependent variables taken into account were the values of the measured mechanical characteristics: breaking work, breaking force and relative elongation. The model of correlation between the mechanical properties of the fibres and the independent variables was based on polynomial second-degree equations such as Eq. (1).

$$y(x) = b_0 + b_1x_1 + b_2x_2 + b_{11}x_1^2 + b_{12}x_1x_2 + b_{22}x_2^2 \quad (1)$$

The Least-Squares fitting approach and the adequate modelling of the experimental data related to physical-chemical characteristics of the cellulose-based textile materials led to the coefficients of correlation in Table 1. The different local forms in modelling the real response surfaces $Y = f(X_1, X_2)$ are shown in Figs. 1-9.

For the *cotton* samples exposed to hydrothermal treatment and radiation, the evolution of the breaking force leads to the conclusion that, under hydrothermal treatment of the same duration, the value for the breaking force decreases when the radiation dose increases. This trend is more obvious for doses higher than 15 kGy. The hydrothermal treatment up to 60 hours leads to the decrease of elongation with the increase of radiation dose to 25 kGy.

Table 1. Coefficients of correlation for the mathematical model

| Coefficients | Cotton | | | Flax | | | Hemp | | |
|--------------|-------------------|---------------|------------------|-------------------|---------------|------------------|-------------------|---------------|------------------|
| | Breaking force, N | Elongation, % | Breaking work, J | Breaking force, N | Elongation, % | Breaking work, J | Breaking force, N | Elongation, % | Breaking work, J |
| b_0 | 2.481 | 2.8948 | 0.0039 | 26.6931 | 3.3382 | 0.0395 | 20.5696 | 3.6842 | 0.0314 |
| b_1 | -0.013 | -0.0014 | -5.89e-6 | -0.2776 | -0.0566 | -0.0010 | -0.0983 | 0.0046 | -5.14e-4 |
| b_2 | -0.006 | 0.0187 | 1.142e-5 | -0.0374 | 0.0127 | 7.895e-5 | 0.3255 | 0.0287 | 5.16e-4 |
| b_{11} | -1.16e-4 | -0.0011 | -1.87e-6 | 0.0048 | 0.0015 | 2.042e-5 | -0.0069 | -0.0003 | -3.15e-6 |
| b_{12} | 8.22e-6 | 4.248e-4 | 4.664e-7 | 0.0003 | 0.0001 | -2.51e-6 | -0.0015 | 0.0004 | 3.98e-6 |
| b_{22} | 4.81e-5 | -1.35e-4 | -7.48e-8 | 0.0001 | -0.0001 | -5.03e-7 | -0.0022 | -0.0002 | -3.71e-6 |

After 120 hours of exposure, the elongation is increasing while breaking force is decreasing, which proves a pronounced deterioration of the cellulose-based material. These tendencies correlate to the evolution of the work at break, with similar trend up to 60 hours of hydrothermal treatment (Figs. 1-3).

For the *flax* fibres exposed to hydrothermal treatment and radiation, under hydrothermal treatment of the same duration the breaking force decreases when the radiation dose is increasing for the entire 0-25 kGy range of doses.

Studying the elongation, the conclusion is that under a hydrothermal treatment up to 60 hours, the elongation reaches a maximum value when the radiation dose belongs to an exposure to 10-15 kGy and the duration of the hydrothermal treatment is between 30 and 80 hours. For other values of radiation or durations of treatment, the elongation decreases (Figs. 4-6).

When exposing to hydrothermal treatment and radiation the *hemp* fibres the breaking force is continuously decreasing, in the whole gamma-rays exposure domain (0-25 kGy) and at the same duration for the exposure at hydrothermal treatment.

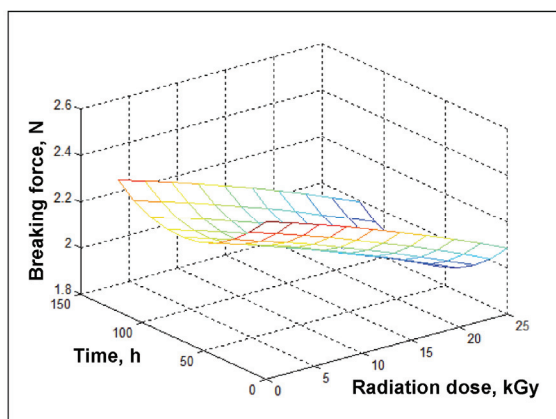


Fig. 1. Surface plot for the variation of the breaking force as a function of duration of the hydrothermal treatment and radiation dose in *cotton* samples

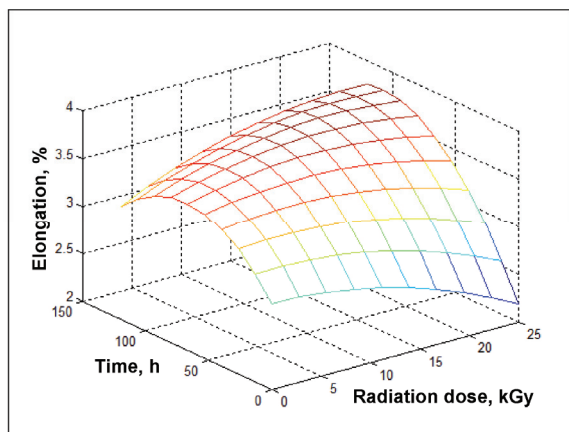


Fig. 2. Surface plot for the evolution of the elongation as a function of duration of the hydrothermal treatment and radiation dose in *cotton* samples

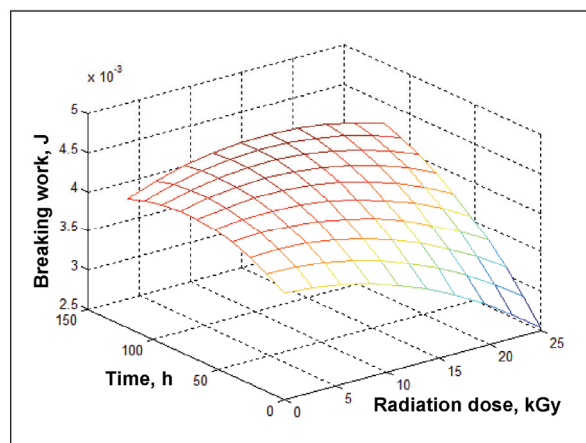


Fig. 3. Surface plot for the evolution of the breaking work as a function of duration of the hydrothermal treatment and radiation dose in *cotton* samples

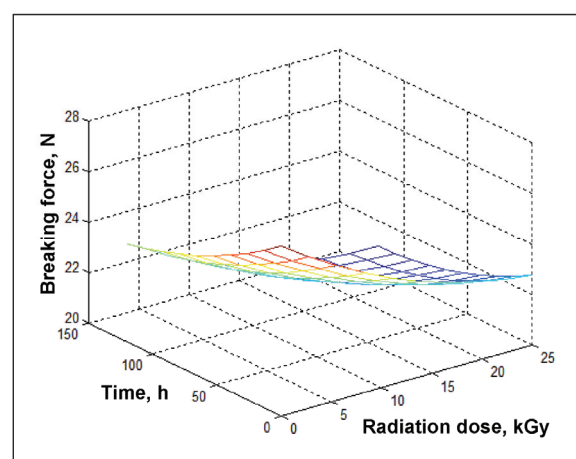


Fig. 4. Surface plot for the variation of the breaking force as a function of duration of the hydrothermal treatment and radiation dose in *flax* samples

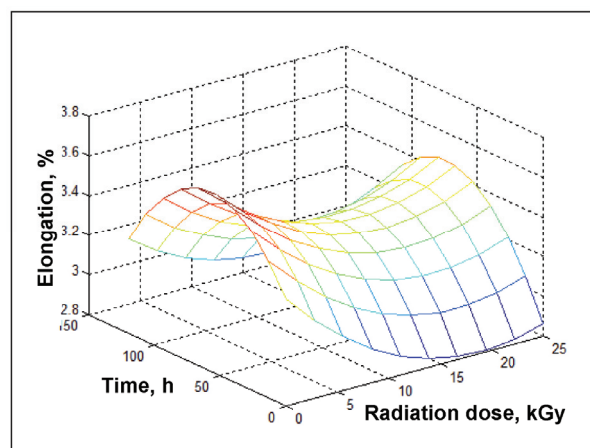


Fig. 5. Surface plot for the evolution of the elongation as a function of duration of the hydrothermal treatment and radiation dose in *flax* samples

The elongation is depicting a maximum gain at around 30–80 hours of hydrothermal exposure for

an irradiation dose between 10 and 15 kGy. For the overall domain of ionizing radiation or hydrothermal exposure, the elongation seem to be decreasing (Figs. 7-9).

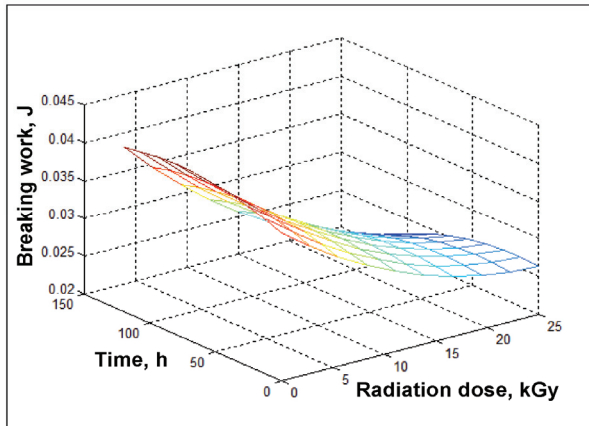


Fig. 6. Surface plot for the evolution of the breaking work as a function of duration of the hydrothermal treatment and radiation dose in *flax* samples

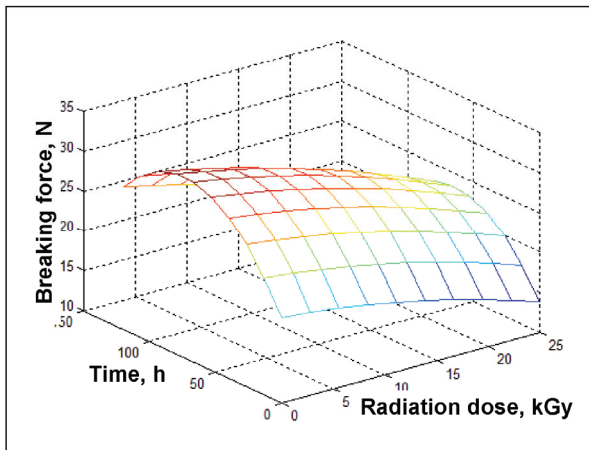


Fig. 7. Surface plot for the variation of the breaking force as a function of duration of the hydrothermal treatment and radiation dose in hemp samples

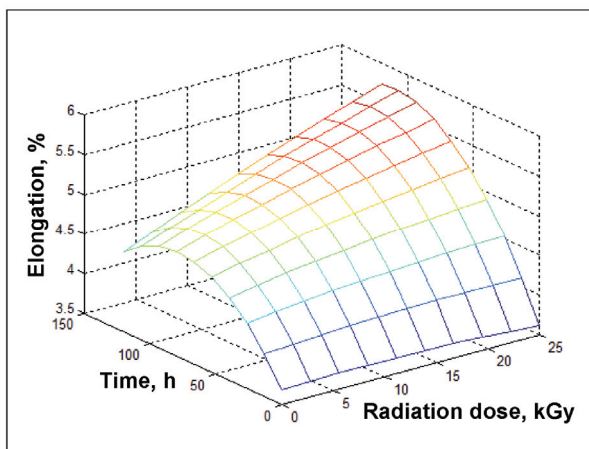


Fig. 8. Surface plot for the evolution of the elongation as a function of duration of the hydrothermal treatment and radiation dose in hemp samples

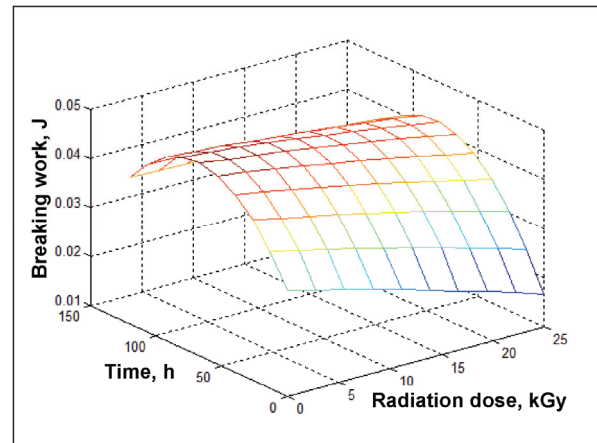


Fig. 9. Surface plot for the evolution of the breaking work as a function of duration of the hydrothermal treatment and radiation dose in hemp samples

4. Conclusions

Ongoing research performed to assess the impact of gamma-ray treatments on historical materials is essential, in order to determine the lowest possible dose that provides decontamination with minor side effects on the cultural heritage objects, stored in the most appropriate environmental conditions.

According to mechanical tests results on dose-dependency effects, low impact on the tested natural fibres was found at radiation doses below 15 kGy.

Along with experimental data on changes in the physical-chemical properties, the proposed mathematical model may lead to the proper selection of the maximum radiation dose allowed for the treatment in the particular case of historical textile objects.

Acknowledgements

Part of this work was supported by the Romanian Executive Agency for Higher Education, Research, Development and Innovation Funding (UEFISCDI) through the project TEXLECONS, *Improvement of Occupational Environment Quality in Cultural Heritage Deposits. Validation of Gamma Radiation Treatment of Textile and Leather Cultural Goods*, PN-II-PT-PCCA-2011-3-1742, contract no. 213/2012.

References

- ASTM, (2006), *Standard Guide for Selection and Calibration of Dosimetry Systems for Radiation Processing*, ISO/ASTM 51261, Annual Book of ASTM Standards, American Society for Testing and Materials, 970-988, USA, New York.
- Geba M., Lisa G., Ursescu C. M., Olaru A., Spiridon I., Leon A. L., Stanculescu I., (2014), Gamma irradiation of protein-based textiles for historical collections decontamination, *Journal of Thermal Analysis and Calorimetry*, **118**, 977-985.
- Ionescu C., Sbirna L.S., Mateescu M.D., Moldovan C.S., Sbirna S., (2012), Evaluation of gamma radiation doses in soil using the Monte Carlo simulation,

- Environmental Engineering and Management Journal*, **11**, 1355-1361.
- ISO, (2000), Sterilization of Medical Devices – General Requirements for Characterization of a Sterilizing Agent and the Development, Validation and Routine Control of a Sterilization Process for Medical Devices, ISO-14937(E), International Organization for Standardization, Geneva, Switzerland.
- ISO, (2006a), Sterilization of Health Care Products – Radiation – Part 1: Requirements for the Development, Validation and Routine Control of a Sterilization Process for Medical Products, ISO 11137-1, International Organization for Standardization, Geneva, Switzerland.
- ISO, (2006b), Sterilization of Health Care Products – Radiation – Part 2: Establishing the Sterilization Dose, ISO 11137-2, International Organization for Standardization, Geneva, Switzerland.
- Katušin-Ražem B., Ražem D., Braun M., (2009), Radiation treatment for the protection and conservation of cultural heritage artefacts in Croatia, *Radiation Physics and Chemistry*, **78**, 729-731.
- Kennedy J.F., Hassan W.H.W., Robson M., (2000), The induction and control of biodeterioration of cellulosic materials in worldwide heritage, *Cellulose Chemistry and Technology*, **34**, 253-260.
- Machnowski W., Gutarowska B., Perkowski J., Wrzosek H., (2013), Effects of gamma radiation on the mechanical properties of and susceptibility to biodegradation of natural fibers, *Textile Research Journal*, **83**, 44-55.
- Măluțan T., (2009), *Analysis, Modeling and Synthesis of Processes* (in Romanian), On line at: <http://omicron.ch.tuiasi.ro/~thmalu/asmp.htm>.
- Olaru A., Leon A.L., Geba M., Ursescu C.M., Lisă G., Cioviță S., (2013), Changes in cellulosic materials from heritage textiles during ageing treatments, *European Journal of Science and Theology*, **9**, 179-188.
- Panzaru A.E., Malutan T., (2012), Flowthrough acid hydrolysis of rapeseed stalks, *Environmental Engineering and Management Journal*, **11**, 2313-2318.
- Takacs E., Wojnarovits L., Borsa J., (1999), Effect of gamma-radiation on cotton-cellulose, *Radiation Physics and Chemistry*, **55**, 663-666.
- Van der Sluijs M.H.J., Church J.S., (2013), The effect of quarantine-level gamma radiation on cotton fibre and its subsequent textile processing performance, *Textile Research Journal*, **83**, 197-207.



"Gheorghe Asachi" Technical University of Iasi, Romania



PNiPAM-FUNCTIONALIZED MESOPOROUS CARBON FOR THE ADSORPTION OF VITAMIN B2

**Maria Ignat^{1,2*}, Maria Emiliana Fortuna¹, Liviu Sacarescu¹
Mirela-Fernanda Zaltariu¹, Valeria Harabagiu¹**

¹"Petru Poni" Institute of Macromolecular Chemistry, Department of Inorganic Polymers, 41A Grigore Ghica Voda Alley,
700487 Iasi, Romania

²"Alexandru Ioan Cuza" University of Iasi, Department of Chemistry, 11 Carol I Bvd., 700506 Iasi, Romania

Abstract

The present research reports the synthesis of poly-N-isopropylacrylamide / mesoporous carbon composites, prepared by radical polymerization of N-isopropylacrylamide inside mesoporous carbon pores functionalized with carboxylic groups. The deposition of poly-N-isopropylacrylamide on mesoporous carbon was confirmed by FT-IR spectroscopy, TEM, N₂-sorption measurements. The mesoporous carbon material was found to adsorb vitamin B2 from aqueous solution at room temperature. The obtained composite, poly-N-isopropylacrylamide / mesoporous carbon, exhibited a higher adsorption capacity for vitamin B2 as compared to un-functionalized mesoporous carbon sample, due to hydrogen bonding between carbonyl groups of poly-N-isopropylacrylamide immobilized on the mesoporous carbon surface and amino groups of vitamin B2 molecules.

Key words: mesoporous carbon (MC), poly-N-isopropylacrylamide, polymer-functionalized MC, vitamin B2

Received: November, 2014; Revised final: March, 2015; Accepted: March, 2015

1. Introduction

Uniform nanoporous polymers have attracted considerable attention for a long time in materials science (David et al., 2008). There are lots of reports on the synthesis of nanoporous polymers, but one of the disadvantages is that such structures are lower in mechanical strength and resistance to chemical treatments.

Recently, the attention have been focused on the synthesis of mesoporous carbon (MC) materials due to their physico-chemical properties, high specific surface area, tunable pore sizes, easiness for functionalization their mesopores (Liang et al., 2008; Nastas et al., 2013), these futures being of great interest in many applications as separation, catalysis, energy storage and conversion (Vinu et al., 2003).

Actually, the randomly porous carbons (active carbon) (Gerçel, 2015) are the product of

conventional synthesis and their performance in the adsorption of giant organic molecule is not optimal because of their disordered pore structure, low specific pore volume, and significant amount of micropores, which only allows the adsorption of relatively small molecules from gas or liquid phases (Bansal et al., 1998; Shen et al., 2003). On the other hand, large biomolecules such as vitamins, amino acids and proteins (Ramos et al., 2004; Vinu et al., 2006; Vinu et al., 2007), should be adsorbed by a mesoporous material, because this allows the adsorption of molecules that are too large to enter micropores. Therefore, a significant effort has been done to develop mesoporous carbon materials with a sufficiently porous matrix to accommodate macromolecules. Actually, its surface chemistry, specific area and pore structure determines its applications (Wenzhong et al., 2008). Over time, many novel ways, as arc discharge, chemical vapor

* Author to whom all correspondence should be addressed: e-mail: ignat.maria@icmpp.ro; Phone: 0746505227

deposition, laser ablation, and template synthesis techniques (Kyotani et al., 2000; Kyotani et al., 2003; Olson et al., 2008; Zhang et al., 2002) to precisely control the pore size and structure of different types of porous carbons have been proposed. The properties of such mesoporous carbons are determined by the nature of the precursor used in the template synthesis method to produce novel forms of carbon with unusual properties (Goncalves et al., 2000; Sakintuna and Yurum, 2005). For example, glycerol (Ignat and Popovici, 2011) when carbonized inside mesoporous silica pores, yielded template carbon. This shows that the confined environment (pore) can control the process of carbonization at molecular level. This method is easy, inexpensive and can be suitable adapted for large-scale production.

In this regard, a simple and reversible delivery system can be envisaged. This system is based on a combination of the MC material with a stimuli-responsive or “smart” polymer. Thus, the access to the pores is controlled by application of a stimulus, such as a change in pH, ionic strength, or temperature. Therefore, poly-N-isopropylacrylamide (PNiPAM) was selected to improve the adsorption capacity of the templated MC material, which will lead to unusually intimate interactions between the polymer and the inorganic phase (Mark et al., 2006; Winey et al., 2006). The PNiPAM/MC composite mesoporous material exhibit the same chemical properties of the used polymer, whereas the specific surface area and the stability of the pores against mechanical compression, thermal and chemical treatments is greatly enhanced. As result, the resultant composite exhibits surface properties of the polymer.

Vitamin B2 (VB2) is a water-soluble B-complex, which plays an important role in the oxidation and reduction reactions of fats, proteins and carbohydrates, promoting regular patterns of growth and development. Vitamin B2 assists the energy release from food and is part of the electron transport mechanism involved in this process. When vitamin B2 deficiency in human body occurs, a supplement administration is always requested.

Adsorption of vitamin B2 on solid surfaces has attracted the attention due to its importance for the food industry and medicine. Vadi and Hadipour (2011) have recently reported the adsorption of vitamin B2 on carbon nanotubes. They found that the adsorption of vitamin B2 on carbon nanotubes is of higher efficiency and the adsorption process obeys the Freundlich isotherms.

In this study the polymer-functionalized MC was obtained by a combination of simple surface modification of the MC material and in situ internal polymerization of PNiPAM. The formation of the PNiPAM inside the mesoporous carbon was confirmed by Fourier Transform-Infrared Spectroscopy, Transmission electron microscopy and N₂ adsorption-desorption measurements. Polymer-modified adsorbents and MC have been used for

separation of the VB2 from solutions and the equilibrium adsorption isotherms have been studied.

2. Experimental

2.1. Chemicals materials

All reagents (Analytical Grade) used in the experiment were purchased from Aldrich and Acros Organics: tetraethyl orthosilicate (Si(OC₂H₅)₄) and tri-block copolymer poly (ethylene glycol)-block-poly (propylene glycol)-block-poly(ethylene glycol) (Pluronic P123, molecular weight = 5800, EO₂₀PO₇₀EO₂₀), glycerol (C₃H₅(OH)₃), N-isopropylacrylamide (NiPAM), 2,2'-azobisisobutyronitrile (AiBN), N,N'-methylene bisacrylamide, ethanol, chloroform, vitamin B2. All products were used as received. The distilled water requested for experiments was prepared with an ELGA Purelab water system.

2.2. Synthesis of mesoporous carbons

The mesoporous carbon sample was prepared by a hard-template method, reported by Ignat and Popovici (2011), using the ordered mesoporous silica (SBA-15 type) as template (Ryoo et al., 1999) and glycerol as carbon source. The silica template has been synthesized using a tri-block copolymer (Pluronic P123) by a sol-gel method described by Ryoo in 1999.

In a typical synthesis of ordered mesoporous carbon, the SBA-15 silica was loaded with 10% glycerol solution by dry impregnation method. The resulted mixture was then subjected to polymerization and the polymer-silica composite have been pyrolyzed in a nitrogen flow at 800 °C. Afterward, the SBA-15 silica framework was leached with HF solution in order to separate the carbon structure. The obtained powdered sample was labelled as MC.

2.3. Synthesis of PNiPAM-functionalized MC

N-isopropylacrylamide, 0.25g, have been dissolved in 2 ml ethanol. Then, 0.01g of 2,2'-azoisobutyronitrile (AiBN), as free radical initiator, together with 0.02g of N,N' – methylene bisacrylamide (BIS) were added to the prepared solution and stirred at ambient temperature until a clear solution is obtained. Further, 0.1 g of mesoporous carbon material (MC) was impregnated with the above prepared mixture. After 2h of impregnation, the black solid was air-dried at room temperature to remove the alcohol.

Afterwards, the polymerization step was performed in a heating oven at 80 °C for 24 h. The resulted powdered sample was washed twice with chloroform and ethanol to remove unreacted chemicals. The obtained product was then dried overnight at 80 °C and the final sample was labeled as PNiPAM/MC composite.

2.4. Adsorption of vitamin B2

For the adsorption tests, a series of standard vitamin B2 solutions with concentrations ranging from 3 to 100 mg/L was prepared first by dissolving it in distilled water. In each adsorption experiment, 0.01 g of different mesoporous carbon based adsorbents was suspended overnight in 10 mL of the vitamin B2 solution. The resulting mixture was continuously magnetically stirred at room temperature until equilibrium was reached (typically 12 h). The amount of vitamin B2 adsorbed was determined by UV-Vis spectroscopy, at 263.5 nm, subtracting the amount found in the supernatant solution after adsorption process from the initial found amount of vitamin B2 in that solution. Calibration experiments were done separately before each set of measurements with vitamin B2 solution of different concentrations in distilled water. Filtration prior to the measurements was used to avoid potential interference from suspended scattering particles in the UV-vis analysis.

2.5. Characterization

FT-IR absorption spectra were recorded using a Bruker Vertex 70 FTIR spectrometer in order to investigate the surface chemistry of the synthesized materials. Registrations were performed in transmission mode within 400–4000 cm^{-1} range with a resolution of 2 cm^{-1} at room temperature on samples dissolved in KBr pellets.

N_2 -sorption measurements of the prepared samples were performed on a Quantachrome Nova 2200 Instrument & Pore Size Surface Area Analyzer using nitrogen as adsorbate at -196°C . Before analysis, all samples have been outgassed under vacuum for 10 hours at room temperature. The specific surface area was calculated using the formula of the BET equation. The total pore volume was taken from the adsorption-desorption isotherm at $P/P_0 = 0.95$. Pore size distributions (PSDs) were determined using Barrett-Joyner-Halenda equation (Barrett et al., 1951).

TEM images were collected on a Hitachi High-Tech HT7700 electron microscope (Hitachi High-Technologies Corporation, Tokyo, Japan) operated at 120 kV, using copper grids (300 mesh) coated with ultrathin carbon film on holey carbon support film (Ted Pella, Redding, CA).

The concentration of the vitamin B2 in solutions was monitored at 263.5 nm wavelength with a Shimadzu UV-1700 PharmaSpec spectrophotometer.

3. Results and discussion

FT-IR spectra of PNiPAM/MC, PNiPAM/MC-VB2, MC-VB2, VB2 and pristine MC solid samples are shown in Figs. 1a and 1b. The FT-IR spectra show the H-bonding between vitamin and PNiPAM/MC composite by the presence of the peak

centered at 3400 cm^{-1} . Although, N-H and O-H bonds are also involved in the hydrogen bonding, each individual O-H bond have a slightly different vibrational frequency, causing a broad peak aspect.

It is important to note that the adsorption capacity of PNiPAM/MC composite for vitamin B2 is higher as compared to un-functionalized mesoporous carbon. This happens most probably due to the formation of hydrogen bonds between carbonyl and amino groups ($\text{C}=\text{O}\cdots\text{H}-\text{N}$) from both the PNiPAM-coated mesoporous carbon surface and vitamin B2 molecules. Also, when vitamin B2 is adsorbed on mesoporous materials, a broad peak in the “fingerprint” region (below $\sim 1500\text{ cm}^{-1}$) of both MC-VB2 and PNiPAM/MC-VB2 spectra could be observed. Vibrations that occur in this region are very complex and are hard to assign to a specific functional group.

Figs. 2 and 3 show the N_2 adsorption/desorption isotherms of MC and PNiPAM/MC samples in comparison to the same adsorbents after adsorption of vitamin B2 from aqueous solutions. The isotherm of MC and PNiPAM/MC samples are of type IV according to the IUPAC classification and exhibits a H1 hysteresis loop, whereas MC-VB2 and PNiPAM/MC-VB2 samples exhibit a type IV isotherm without hysteresis. As is evident from Figs. 2 and 3, the isotherms of MC featured a large capillary condensation step, indicating different sized mesopores, while the isotherm of PNiPAM/MC sample a narrow capillary condensation step, localized at lower relative pressures, indicating narrowed mesopores. The adsorption isotherms of MC-VB2 and PNiPAM/MC-VB2 samples are of type I isotherm, which is characteristic for a microporous material. The textural properties of the mesoporous carbon-based adsorbents before and after adsorption of vitamin B2 are collected in Table 1. As expected, the specific surface area of MC carbon sample (1319 m^2/g) is higher than the specific surface area of PNiPAM/MC (678 m^2/g), due to the pore blocking by polymer particles. As well, the specific pore volume of mesoporous carbon material is 1.26 cm^3/g , which is higher as compared to the specific pore volume of PNiPAM/MC system (0.74 cm^3/g).

As result, the amount of nitrogen adsorbed decrease with VB2 uptake from solution, leading to a decrease of the BET specific surface area (from 1319 m^2/g to 130 m^2/g for MC system, and from 678 m^2/g to 67 m^2/g for PNiPAM/MC system) and the total pore volume (from 1.26 cc/g to 0.14 cc/g for MC system, and from 0.74 cc/g to 0.08 cc/g for PNiPAM/MC system), because the pores being filled up with vitamin B2 molecules.

An evidenced difference is observed from the adsorption tests that are in line with the different pore diameter of the adsorbents. It is important to note that PNiPAM/MC composite exhibited a high amount of vitamin B2 adsorption (1554 mg/g), which is 1.5 times higher as compared to MC sample (954 mg/g). In fact, the BET specific surface area of the adsorbent

is a crucial factor which determines the adsorption capacities of carbon adsorbents (Noll et al., 1992). Contrariwise, the adsorption capacity of the carbon-based adsorbents increases in the following order, $MC < PNiPAM/MC$, although MC carbon sample has a higher specific surface area as compared to PNiPAM/MC. The textural properties of the mesoporous carbon-based adsorbents other than BET specific surface area such as pore volume and pore diameter also play an important role in determining the vitamin B2 adsorption capacity. It should also be noted that, although the difference in the pore volume of MC and PNiPAM/MC is very small, there is a large difference in their amount of vitamin B2 adsorption.

Although, PNiPAM/MC system has a decreased BET specific surface area compare to MC sorbent, a reasonable explanation for the higher sorption capacity envisage the PNiPAM polymer particles deposited on the external surface of the

carbon material, confirmed by TEM (Fig. 4). Actually, PNiPAM polymer particles insert on the carbon surface functional groups that are responsible for the hydrogen bonding with vitamin B2 molecules (Fig. 1). So, in this case, the uptake of larger molecules, vitamin B2, is explained in terms of the surface functional groups inserted on the mesoporous carbon surface, not to the BET specific surface area (which normally should lead to a decreased sorption capacity).

In order to describe the absorption process of vitamin B2 on the prepared carbon materials, Langmuir, Freundlich and Temkin isotherms have been drawn (Figs. 5 and 6). All the experimental data and the calculated parameters are listed in Table 2.

Finally, could be observed that the adsorption process of vitamin B2 on MC sample obeys Temkin isotherm, reaching an $R^2 = 0.9997$, while the adsorption on PNiPAM-functionalized MC sample obeys Langmuir isotherm, reaching an $R^2 = 0.7535$.

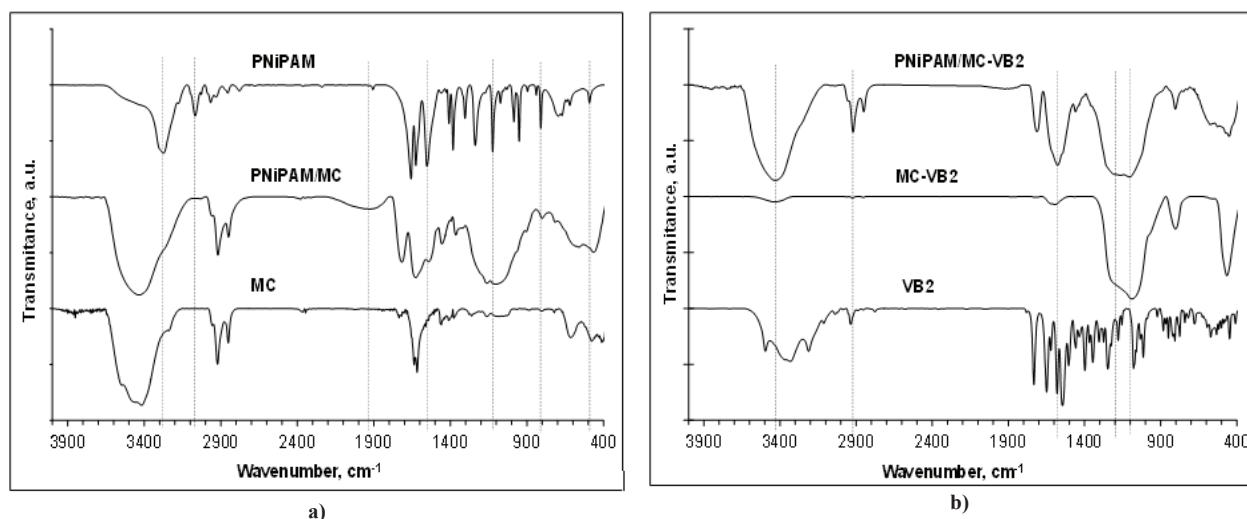


Fig. 1. FT-IR spectra of MC, PNiPAM and PNiPAM-coated MC (a) and VB2, VB2-adsorbed on simple MC and PNiPAM/MC composite (b)

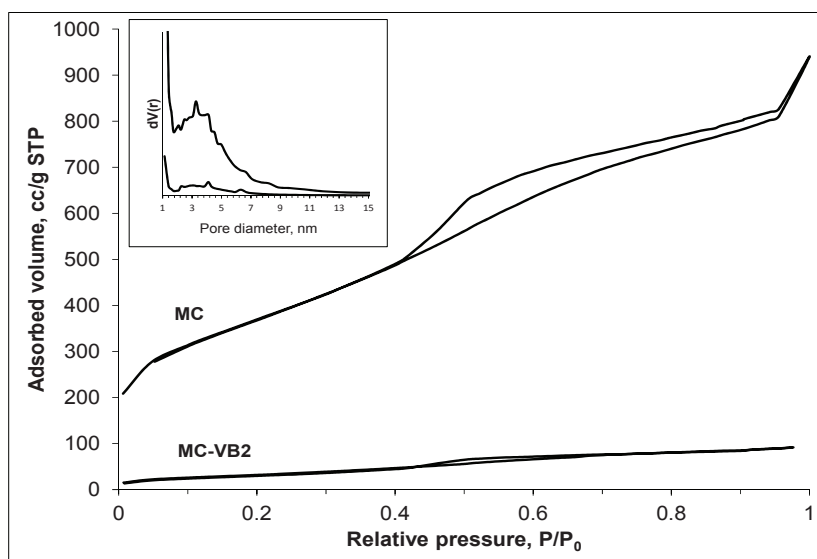


Fig. 2. Nitrogen adsorption-desorption isotherms with corresponding BJH pore size distributions (inset) of MC, MC-VB2 samples

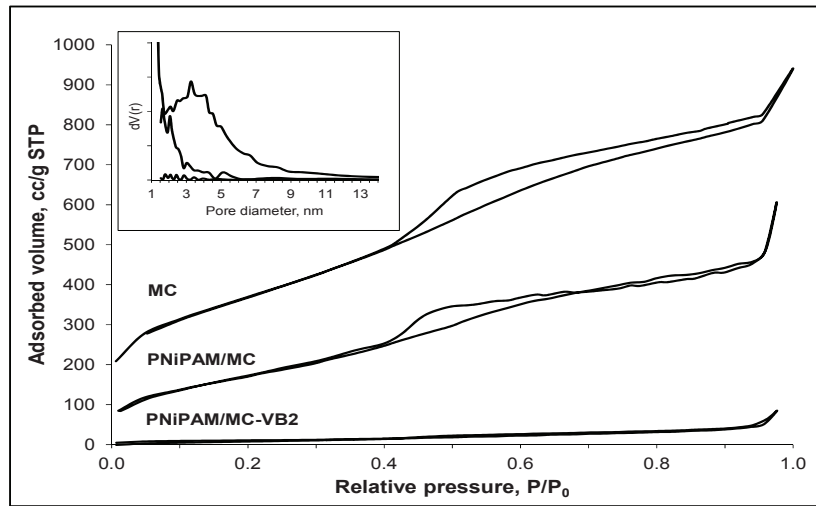


Fig. 3. Nitrogen adsorption-desorption isotherms with corresponding BJH pore size distributions (inset) of MC, PNIPAM/MC and PNIPAM/MC-VB2 samples

Table 1. Textural characteristics of the synthesized mesoporous carbon-based adsorbents

| Sample Feature* | MC | MC-VB2 | MC/PNiPAM | MC/PNiPAM-VB2 |
|---------------------------------|------|--------|-----------|---------------|
| S_{BET} , m ² /g | 1319 | 130 | 678 | 67 |
| V_{tot} , cc/g | 1.26 | 0.14 | 0.74 | 0.08 |
| V_{micro} , cc/g | 0 | 0 | 0.002 | 0 |
| S_{micro} , m ² /g | 0 | 0 | 3.93 | 0 |
| d_p , nm | 3.89 | 3.26 | 2.2 | 2.0 |

where: S_{BET} is BET specific surface area; V_{tot} - total pore volume calculated as the amount of nitrogen adsorbed at the relative pressure of $P/P_0 = 0.95$; V_{micro} - micropore volume calculated by the t-plot method; S_{micro} - micropore surface area calculated using t-plot method; d_p - average pore diameter resulted from BJH pore size distribution using adsorption branch

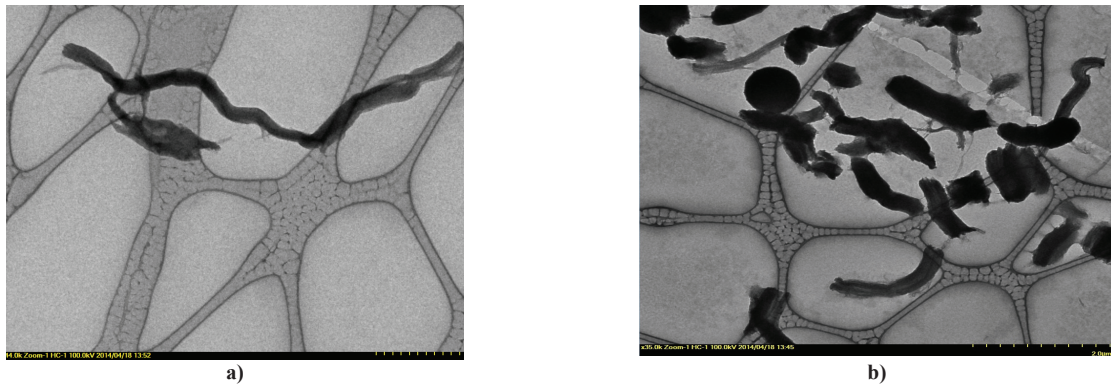


Fig. 4. TEM images of pristine MC (a) and PNIPAM/MC (b) samples

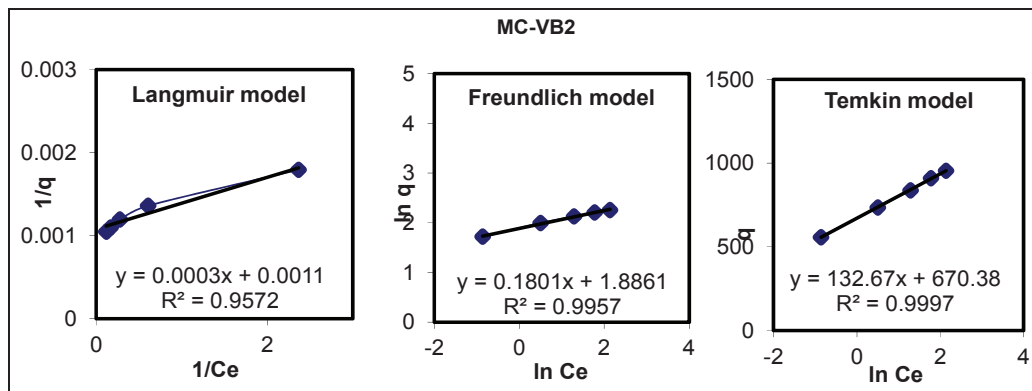
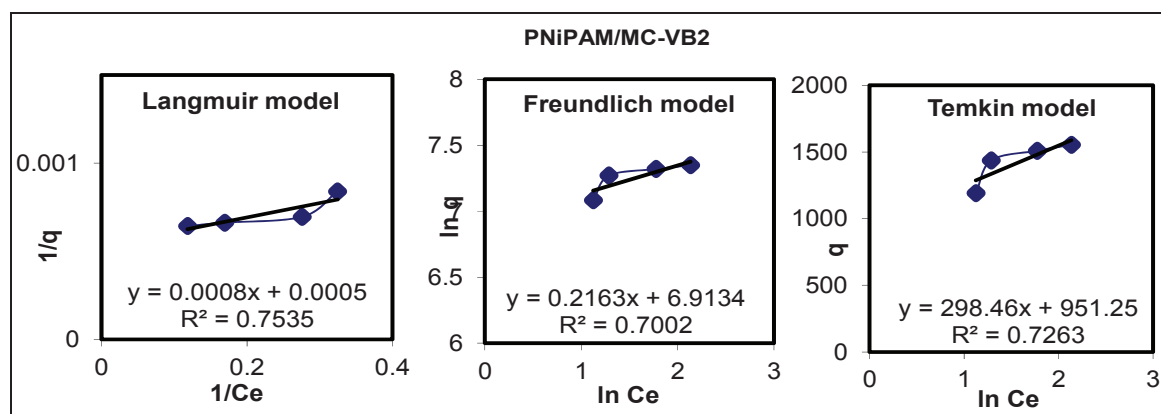


Fig. 5. Langmuir, Freundlich and Temkin isotherms for the adsorption of vitamin B2 on MC adsorbent

Table 2. Langmuir, Freundlich and Temkin parameters for adsorption of VB2 on mesoporous carbon based material

| | Post Adsorption VB2 (mg/L) | VB2 Adsorbed (mg) | | | | VB2 Adsorbed per Unit Mass of adsorbent (mg/g) | | Langmuir Data | | | | Freundlich Data | | | |
|-------|-------------------------------|----------------------|------|---------------|-----|--|--|-----------------|---------------|-----------------|---------|-----------------|---------------|------------|----------|
| | CM | CM- PNiPAM | CM | CM- PNiPAM | CM | CM- PNiPAM | | CM | CM- PNiPAM | | | CM | CM- PNiPAM | | |
| c_0 | c_e | | | | | Q | | $1/q, *10^{-2}$ | $1/c_e$ | $1/q, *10^{-3}$ | $1/c_e$ | $\log c_e$ | $\log q$ | $\log c_e$ | $\log q$ |
| 6 | 0.15 | | 5.58 | | 557 | | | 0.18 | 2.36 | | | -0.86 | 1.71 | | |
| 9 | 0.25 | | 7.35 | | 735 | | | 0.14 | 0.61 | | | 0.49 | 1.99 | | |
| 12 | 0.413 | | 8.37 | | 837 | | | 0.12 | 0.28 | | | 1.28 | 2.12 | | |
| 15 | 0.60 | 3.08 | 9.10 | 11.9 | 909 | 1191 | | 0.11 | 0.17 | 0.84 | 0.32 | 1.77 | 2.20 | 1.12 | 7.08 |
| 18 | 0.87 | 3.63 | 9.54 | 14.4 | 954 | 1437 | | 0.10 | 0.12 | 0.70 | 0.28 | 2.13 | 2.25 | 1.28 | 7.27 |
| 21 | | 5.91 | | 15.1 | | 1509 | | | | 0.66 | 0.17 | | | 1.77 | 7.31 |
| 24 | | 8.46 | | 15.5 | | 1554 | | | | 0.64 | 0.12 | | | 2.13 | 7.34 |


Fig. 6. Langmuir, Freundlich and Temkin isotherms for the adsorption of vitamin B2 on PNiPAM/MC material

4. Conclusions

Adsorption process of vitamin B2 over mesoporous carbon-based materials such as MC and PNiPAM/MC has been studied from vitamin B2 solutions with various concentrations, and the obtained results were compared. It has been observed that the vitamin B2 adsorption capacities of the adsorbents depend on the surface chemistry play an important role.

It has been found that the functionalization with PNiPAM polymer is more suitable as compared to un-functionalized mesoporous carbon to achieve high loadings of vitamin B2. The equilibrium adsorption data fitted well to all studied models, giving a better fit to the Langmuir model in the case of PNiPAM-functionalized MC sample, as was evidenced from the higher values of R^2 of 0.9997. Thus, the experimental data allowed determining the extent and degree of favorability of adsorption.

The obtained results showed that the adsorption capacity obtained for PNiPAM-functionalized mesoporous carbon (80%) is greater than the vitamin B2 adsorption on pristine mesoporous carbon (53%).

These results show that the PNiPAM-functionalized mesoporous carbon compare favorably with un-functionalized mesoporous carbon. Nitrogen adsorption-desorption data after vitamin B2 adsorption reveal that the vitamin B2 molecules entered mesopores of tested mesoporous carbon-based adsorbents.

Acknowledgements

The authors acknowledge the grants of the Romanian National Authority for Scientific Research, CNCS – UEFISCDI, project number PN-II-RU-PD-2012-3-0357, Contract 30/2013, and project number PN-II-ID-PCE-2011-3-0559, Contract 265/2011 for the financial support.

References

- Bansal C.R., Donnet J.B., Stoeckli F., (1998), *Active Carbon*, Marcel Dekker, New York.
- Gerçel O., (2015), Adsorption properties of activated carbon from wild plant prepared by chemical activation, *Environmental Engineering and Management Journal*, **14**, 129-137
- Goncalves A.B., Mangrich A.S., Zarbin A.J.G., (2000), Polymerization of pyrrole between the layers of alphan (IV) bis(hydrogen phosphate), *Synthetic Metals*, **114**, 119–24.
- Ignat M., Popovici E., (2011), Synthesis of mesoporous carbon materials via nanocasting route – comparative study of glycerol and sucrose as carbon sources, *Romanian Journal of Chemistry*, **56**, 947-952.
- Kyotani T., Tsai I.F., Tomita A., (2000), Formation of ultrafine carbon tubes by using an anodic aluminium oxide film as a template, *Journal of Materials Chemistry*, **7**, 1427-1428.
- Kyotani T., (2000), Control of pore structure in carbon, *Carbon*, **38**, 269–86.
- Kyotani T., Ma Z., Tomita A., (2003), Template synthesis of novel porous carbons using various types of zeolites, *Carbon*, **41**, 1451–1459.
- Liang C., Li Z., Dai S., (2008), Mesoporous carbon materials: synthesis and modification, *Angewandte Chemie International Edition*, **47**, 3696–3717.
- Mark J.E., (2006), Some novel polymeric nanocomposites, *Accounts of Chemical Research*, **12**, 881-888.
- Nastas R., Rusu V., Lupascu T., (2013), Copper impregnated activated carbon for the treatment of sulphurous waters, *Environmental Engineering and Management Journal*, **12**, 937-942.
- Noll K.E., Gournaris V., Hou W.S., (1992), *Adsorption technology for air and water pollution control*, Lewis Publishers: Chelsea, MI.
- Olson D.A., Chen L., Hillmyer M.A., (2008), Templating nanoporous polymers with ordered block copolymers, *Chemistry of Materials*, **20**, 869-890.
- Ramos A., Otero M., Rodrigues A.E., (2004), Recovery of vitamin B12 and cephalosporin C from aqueous solutions by adsorption on nonionic polymeric adsorbents, *Separation and Purification Technology*, **38**, 85–98.
- Ryoo R., Joo S.H., Jun S., (1999), Synthesis of highly ordered carbon molecular sieves via template-mediated structural transformation, *Journal of Physical Chemistry B*, **103**, 7743-7746.
- Sakintuna B., Yurum Y., (2005), Templated porous carbons: A review article, *Industrial & Engineering Chemistry Research*, **44**, 2893.
- Shen W.Z., Zheng J.T., Zhang Y.L., (2003), The effect of pore structure of activated carbon on the adsorption of Congo red and vitamin B12, *Studies in Surface Science and Catalysis*, **146**, 779–82.
- Vadi M., Hadipour I., (2011), Adsorption isotherm study of Vitamin B2 on carbon nanotube, *Oriental Journal of Chemistry*, **27**, 1037-1040.
- Vinu A., Streb C., Murugesan V., Hartmann M., (2003), Adsorption of Cytochrome C on New Mesoporous Carbon Molecular Sieves, *Journal of Physical Chemistry B*, **107**, 8297–8299.
- Vinu A., Hossain K.Z., Kumar G.S., Ariga K., (2006), Adsorption of l-Histidine over mesoporous carbon molecular sieves, *Carbon*, **44**, 530-536.
- Vinu A., Hossain K.Z., Srinivasu P., Miyahara M., Anandan S., Gokulakrishnan N., Mori T., Ariga K., Balasubramanian V.V., (2007), Carboxy-mesoporous carbon and its excellent adsorption capability for proteins, *Journal of Materials Chemistry*, **17**, 1807-1819.
- Wenzhong S., Zhijie L., Yihong L., (2008), Surface chemical functional groups modification of porous carbon, *Recent Patents on Chemical Engineering*, **1**, 27.
- Winey K.I., Moniruzzaman M., (2006), Polymer nanocomposites containing carbon nanotubes, *Macromolecules*, **39**, 5194-5205.
- Zhang W.H., Liang C., Sun H., Shen Z., Guan Y., Ying P. Li C., (2002), Synthesis of ordered mesoporous carbons composed of nanotubes via catalytic chemical vapor deposition, *Advanced Materials*, **14**, 1776–1778.



"Gheorghe Asachi" Technical University of Iasi, Romania



SUPERCritical FLUIDS AND ULTRASOUND ASSISTED EXTRACTIONS APPLIED TO SPRUCE BARK CONVERSION

Adina Iulia Talmaciu, Irina Volf*, Valentin I. Popa

*"Gheorghe Asachi" Technical University of Iasi, Faculty of Chemical Engineering and Environmental Protection,
73 Prof. Dr. Docent Dimitrie Mangeron Str., 700050 Iasi, Romania*

Abstract

Supercritical fluid and ultrasound assisted extractions were applied as a first step in a complex processing of spruce bark in order to recover polyphenols compounds. The aim of the study was to compare the efficiency of these "green" processes with a conventional extraction technique (ethanolic extraction). Supercritical fluid extraction was carried out in two steps: (i) static extraction for 15 min at 1000 psi with pure CO₂ and (ii) dynamic extraction for 45 min at 35, 40 and 50 °C, 1200, 2000 and 2500 psi, with CO₂ and 70% ethanol as co-solvent. UAE was carried out in an ultrasonic bath at 45, 50 and 60 °C for 5 to 75 minutes. The ethanolic extraction was performed using ethanol (70%) in a closed oven for 13 days. The extracts were characterized using Folin-Ciocalteu method for total phenolic content and quantified by high liquid performance chromatography (HPLC). The study recommend SFE and UAE instead of traditional ethanolic techniques since these provide high extraction yields, pure extracts, with a large number of polyphenolic compounds extracted and are environmentally friendly.

Key words: ethanol extraction (Eth E) spruce bark, polyphenols, supercritical fluid extraction (SFE), ultrasound assisted extraction (UAE)

Received: November, 2014; Revised final: March, 2015; Accepted: March, 2015

1. Introduction

One of the great challenges in the 21st century addresses the transition from an economy largely based on fossil origin raw materials to one based on renewable resources, processed according to sustainable development goals (Gravitis et al., 2008). Among all sustainable resources, only biomass represents an accessible source for chemicals, biomaterials, derivatives and products with energetic value (Herrero et al., 2013; Sheldon, 2011). The application of renewables based on biomass, the development of clean production and smart materials may provide the required solution for sustainability.

The main challenge is to develop innovative methods for the efficient use of biomass as it is or as wastes (livestock, industrial, agri-food, agricultural and non-recyclable fraction proceeding from waste treatment plants), (Hidalgo et al., 2014). In order to

be sustainable, biomass use will depend heavily on the successful deployment of innovative, green chemistry so as to avoid the use of toxic and/or hazardous reagents and solvents or eliminate wastes (Sheldon, 2011).

From this point of view, the biorefining concept embraces a wide range of technologies able to fractionate biomass resources into their building blocks (carbohydrates, lignin, extractives, proteins etc.), which can be converted to value added products (Cherubini, 2010). Many compounds resulting in complex biomass processing are recognized by their valuable biological properties (Bodîrlău et al., 2009; Popa, 2011; Popa, 2013). That is why, the extraction and purification processes of some biobased compounds resulted in this fractionation are essential, when they follow to be used in the preparation of dietary supplements, nutraceuticals, functional food ingredients (Volf et al., 2013), food additives,

* Author to whom all correspondence should be addressed: e-mail: iwolf@tuiasi.ro

pharmaceutical and cosmetic products, allelochemicals (Popa et al., 2008), chelating agents (Volf et al., 2012), modulators in heavy metal bioaccumulation (Stingu et al., 2011) and plant growth regulators (Tanase et al., 2013; Tanase et al., 2014). The biomass extraction results depend on various factors such as, solvents, procedures, extraction time etc., to obtain bioactive components of high quality and quantity in the crude extracts. In addition, the nature of the sample matrix and the compounds to be extracted also substantially affect the efficiency of extraction. The optimal extraction method should be simple, rapid, economical and with a large applicability (Vongsak et al., 2013)

Conventional separation techniques such as solvent extraction and distillation have the drawback of leaving trace amounts of solvents or to cause thermal degradation (Ahluwalia et al., 2013). Non-conventional methods, which are more environmental friendly due to decreased use of chemicals, reduced operational time and better yield and quality of extracts, have been developed during the last years. Thus, ultrasound, pulsed electric field, enzyme digestion, extrusion, microwave heating, ohmic heating, supercritical fluids and accelerated solvents have been studied as nonconventional methods. The ultrasound-assisted extraction (UAE), microwave assisted extraction (MAE) and supercritical fluid extraction (SFE) are probably the most applicable at pilot or industrial scale and were critically reviewed by several researchers (Azmir et al., 2013; Khoddami et al., 2013; Martins et al., 2011; Roberto et al., 2010; Vilku et al., 2008). The conventional extraction methods, such as Soxhlet is still considered as one of the reference method to compare the success of newly methodology (Azmir et al., 2013).

In this perspective, the paper presents a comparative analysis regarding technical aspects related to the two innovative and environmental friendly techniques: ultrasound-assisted extraction (UAE) and supercritical fluid extraction (SFE) in comparison with a classic solvent extraction process (EthE). These techniques were applied to isolate, from spruce bark, bioactive compounds included in polyphenols group, which are one of the most widely occurring groups of phytochemicals, described in details elsewhere (Ignat et al., 2011; Ignat et al., 2013).

The analysis takes into account the total yield in polyphenolic concentration and the qualitative extracts content highlighted by high liquid pressure chromatographic profile. The approach is appropriate even more because in Romania large amounts of bark are released as residues from forestry and woodworking processes, mainly burnt for energy recovery, without considering that as an important source of valuable chemicals. More than this, even if the presented techniques are increasingly used at laboratory and industrial level, a comparative study regarding the polyphenolic compounds extraction from spruce bark doesn't exist.

2. Materials and methods

2.1. Materials

Spruce (*Picea abies*) bark of industrial origin was provided as a waste from a wood processing Romanian company. The spruce bark was washed several times with doubly distilled water to remove impurities, dried at room temperature under normal aeration conditions and milled in a GRINDOMIX GM 2000 mill for 0.15-1.25 mm particle size. The material was stored in desiccators and was directly used without any pre-treatment. The raw material humidity was determined using a RADWARG MAX 5011 thermo-balance. The FT-IR spectrometry was used to characterize the functional groups present in biomass. The FT-IR spectra were recorded with a Bio Rad FT-IR spectrometer in 400 – 4000 cm^{-1} spectral domain, with a 4 cm^{-1} resolution and 32 scans, by KBr pellet technique.

Ethanol, Folin Ciocalteu's phenol reagent, phenols standards and other chemicals used in experiments were provided by Sigma-Aldrich and Fluka. Carbon dioxide 5.3 for supercritical extraction procedure was purchased by Linde Group. Distilled water was used for all experiments.

2.2. Ethanolic extraction (Eth E)

A classic ethanolic extraction was conducted using 50 mL ethanol/water mixture (70:30 mL, v/v) as solvent and 5 g of milled spruce bark. The extraction was performed at 40 $^{\circ}\text{C}$ in a closed reaction vessel during 13 days. The polyphenolic extraction was monitored every 24 hours in order to relieve the kinetics profile and to achieve the equilibrium (full extraction of polyphenols from biomass). The experiment was carried out in triplicate.

2.3. Ultrasound assisted extraction (UAE)

The ultrasound assisted extractions were performed in a ultrasonic bath, SONOREX RK type 100 H, (35 kHz, 320 W) produced by Bandelin Electronic GmbH & Co.KG, Berlin, Germany using 5 g of biomass in a glass vessel and 50 mL ethanol/water mixture (70%), biomass/solvent ratio of 1:10 w/v. Extractions were carried out at 45, 50 and 60 $^{\circ}\text{C}$ for 5, 10, 20, 30, 45, 60 and 75 minutes. The obtained extracts were centrifuged at 4000 rpm for 4 min in a centrifuge Hettich Rotofix 32 A type. The supernatant was collected and analyzed and all experiments were carried out in triplicate.

2.4. Supercritical fluid extraction (SFE)

Extractions were performed using a SFT 100 XW supercritical fluid extractor system in two steps: (I) static with pure CO_2 , 6 mL/min flow rate at 1000 psi constant pressure for 15 min to allow contact between the samples and the supercritical solvent;

(II) dynamic for lipophilic extraction (in the first 10–15 min at 1000 psi) followed by polyphenols extraction (30 min) with CO₂ and ethanol (70%) as co-solvent with 10:1 mL/min flow rate ratio.

The investigated conditions for the polyphenols extraction were 1200, 2000, 2500 psi at 35, 40 and 50°C. An amount of 2 g of spruce bark was used for all the experiments that were carried out in triplicate. Some inert glass balls (4 mm in diameter) were added to fill the extraction reactor.

2.5. Total phenolic content (TPC)

The total phenolic content was determined using the Folin-Ciocalteu method, based on the oxidation/reduction proprieties of phenols occurring in contact with Folin-Ciocalteu reagent. For analyses, 1 mL of diluted extract (1%) was mixed with 0.5 mL Folin-Ciocalteu reagent, 2 mL sodium carbonate for pH adjustment (10% concentration) and 5 mL distilled water.

The reaction mixture was left at rest protected from light, at room temperature for 90 min. The absorbance was measured at 765 nm using a GBS AVANTA UV-Vis spectrophotometer.

TPC was determined based on the calibration curve using gallic acid, the results being expressed as milligrams of gallic acid equivalents (GAE) per spruce bark gram (mg GAE g⁻¹), using a CINTRA software.

2.6. HPLC procedure

The extracts were fractionated by liquid-liquid extraction using ethyl acetate, then mixed with 5 mL of ultra pure methanol and filtered by a 0.45 µm diameter filter before injection in the column. The phenolic acids separation was carried out using a DIONEX Ultimate 3000 chromatographic system equipped with a DDA UV-VIS detector, at 280 nm, on a Zorbax RX C18 (4.6×250 mm, particle size 5 µm) column, using 1% acetic acid in ultra pure water as mobile phase (A) and ultra pure methanol as stationary phase (B).

The operation conditions were 30°C temperature, 1.2 mL min⁻¹ flow rate with a gradient of 10–40% B in 40 minutes. Compounds were identified by comparing their fragmentation profiles with references, run under the same experimental conditions.

2.7. Statistical analysis

All the results are expressed as mean ± standard error where $n = 3$. Comparison of the means was performed by the Fisher least significant difference (LSD) test ($p \leq 0.05$) after Statistica (Statsoft version 10.0) analysis. Sampling and chemical analyses were examined in triplicate, in order to decrease the experimental errors and to increase the experimental reproducibility.

3. Results and discussion

3.1. Chemical characterization of the biomass

Spruce bark biomass was characterized from the dry mater content, humidity and structure point of view. FTIR spectroscopy was used as tool and the spectrum (Fig. 1) displays a large number of absorption bands indicating the complex structure of the investigated biomass.

According to Chupin et al. (2013) the bands at 3400–3300 cm⁻¹ could be assigned to OH stretch vibration in phenolic and aliphatic structures. Small peaks at 2930 and 2850 cm⁻¹ originate from CH stretch vibration in aromatic methoxyl groups and in methyl and methylene groups of side chain. Peaks between 1400 and 2000 cm⁻¹ show the aromatic nature of the structure.

The wavelengths situated between 1300 and 1450 cm⁻¹ corresponds to the stretching vibrations of carbonyl groups and the deformation vibration of the C–C bonds in the phenolic groups absorb in the region 1500–1400 cm⁻¹. Signals between 1500 and 1700 cm⁻¹ may be assigned to aromatic nucleus vibrations. The signals from 1070 and 1092 cm⁻¹ are indicative for alcohol functional group, while the 1338 cm⁻¹ absorption band can be attributed to the O–H in plane deformation in polyphenols. It is a good concordance between this result and other structural characterization of spruce bark of other origin made in our research group (Ghitescu et al., 2015). The biomass used in all experiments had 10.27 % humidity.

3.2. TPC assessment of extraction procedures

3.2.1. Eth E extraction

Ethanol extractions were performed in a closed oven at 40°C for 13 days. The equilibrium concentration was reached after 6 days when a maximum concentration of TPC by 87.15 mg GAE g⁻¹ was attend (Fig. 2). After that, a slight decrease (11.2 %) of the total polyphenolic content was recorded. The decrease can be explained by the fact that after attending the equilibrium between phases, polyphenols are re-adsorbed by the biomass.

3.2.2. UAE extraction

Ultrasound assisted extraction is one of the upcoming extraction techniques offering high reproducibility in shorter times, simplified procedure and reduced energy and solvent consumption (Khan et al., 2010) based on the cavitation process involved during sonication which intensify and improve mass transfer, solvent penetration into plant tissue and capillary effects (Da Porto et al., 2013). In recent studies UAE has been applied to obtain bioactive compounds from different materials (Adam et al., 2012; Chavan et al., 2013; Dey et al., 2013; Sun et al., 2011). Time and temperature are the most important factors that have influence on UAE processes.

In this context preliminary tests were carried out at different temperatures (45, 50 and 60°C) for 5, 10, 20, 30, 45, 60 and 75 min to establish the effect of time and temperatures on polyphenols extraction. The data show a very clear influence of temperature on the extraction of polyphenols from spruce bark (Fig. 3). At 60°C the TPCs were greatly increased (42.5 mg GAE g⁻¹) comparing to the TPCs obtained at 45°C (33.48 mg GAE g⁻¹). This behavior can be explained by the higher solubility of polyphenols in the solvent, the higher diffusivities of the extracted molecules and the improved mass transfer at higher temperatures.

A rise in extraction temperature could also break the phenolic matrix bonds and influence the membrane structure of plant cells and therefore facilitate the extraction process (d'Alessandro et al., 2012). Also, it was observed that the initial rate of polyphenols extraction was faster in the first 5 to 20 min, followed by slower extraction rate approaching to an equilibrium concentration. The experiment was carried out in triplicate.

3.2.3. SFE extraction

SFE was applied for some advantages such low temperatures use, reduced energy consumption and higher product quality due to the absence of solvent in final solute phase. SFE uses the properties of fluids over their critical points to selectively extract soluble components from biomass. Supercritical carbon dioxide is recognized as an ideal solvent to extract bioactive compounds being nontoxic, non-explosive, readily available, easy to remove from the final extract, does not cause major disruptions in bio-compounds, and its biological properties can be preserved (Espinosa-Pardo et al., 2014).

A two-step SFE was performed, in triplicate, at 35, 40 and 50°C and at 1200, 2000 and 2500 psi. Experiments carried out at 35°C help us to clarify the fact that under near critical conditions lower content of polyphenols were achieved (Fig. 4). At 1200 and 2000 psi, a raising extraction temperature produced a decrease on the TPC extracted, which varied from 122.41 mg GAE g⁻¹, at 40°C, 60.12 mg GAE g⁻¹

at 50°C, due to the reduction in solvent density. On the other hand, at higher pressures 2500 psi, TPC slowly increase at 35 and 50°C despite of solvent density reduction. This behavior could be caused by the enhancement in the solute (spruce bark) of the vapor pressure with temperature, which was more significant than the reduction in the solvent density, increasing consequently the overall extraction yield as Benelli et al. (2010) reported.

3.3. Chromatographic profile of the polyphenolic extracts

Spruce bark polyphenolic extracts obtained by all three procedures were analyzed by HPLC in order to achieve a qualitative and complete characterization. The method allowed identification of seven phenolic acids (Table 1) as: catechin, gallic, vanillic, syringic, p-coumaric, ferulic and synapic acids. Their presence in spruce bark extracts was also reported in works of our research group (Hainal et al., 2011). The chromatographic profiles of spruce bark are presented in Fig. 5. The most important compounds identified in spruce bark extracts, based on their recovered amount were *p*-coumaric acid with values of 260.4073 mg L⁻¹ of extract in the case of SFE extraction and 99.4731 mg L⁻¹ of extract in UAE, followed by catechin with 171.1765 mg L⁻¹ of extract (SFE) and 112.084 mg L⁻¹ of extract (UAE), and synapic acid with 35.0534 mg L⁻¹ of extract for SFE and 13.3618 mg L⁻¹ of extract for UAE respectively. In relation to the extracts composition the retention times, peak areas and the recovered amount of each identified compound varies from an extraction technique to other.

It can be notice that by SFE and UAE extractions the numbers of the identified compounds in spruce bark tested extracts were higher compared with EthE. However, it can be observed that the extracts obtained by SFE present larger amounts of phenolic compounds in some cases (260.4073 mg L⁻¹ of extract compared to 99.4731 mg L⁻¹ of extract for *p*-coumaric acid) and lower in other (12.9180 mg L⁻¹ of extract compared to 5.1224 mg L⁻¹ of extract for syringic acid) comparing to UAE.

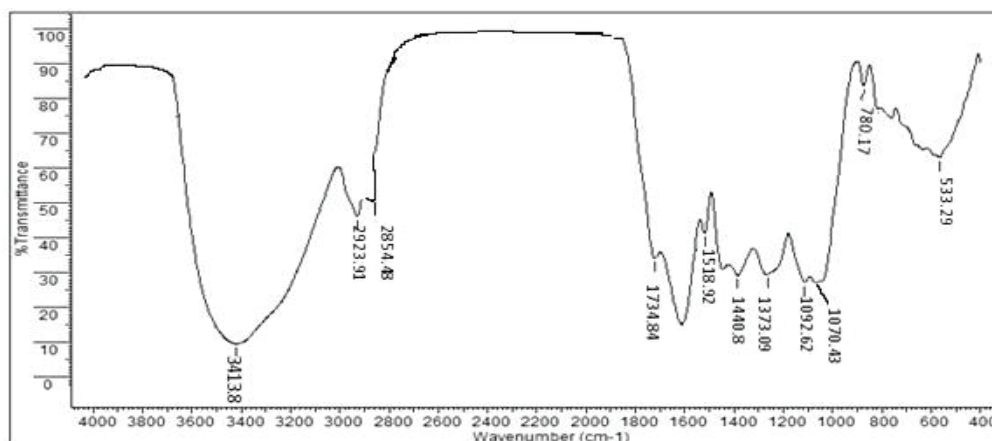


Fig. 1. FTIR spectrum of spruce bark

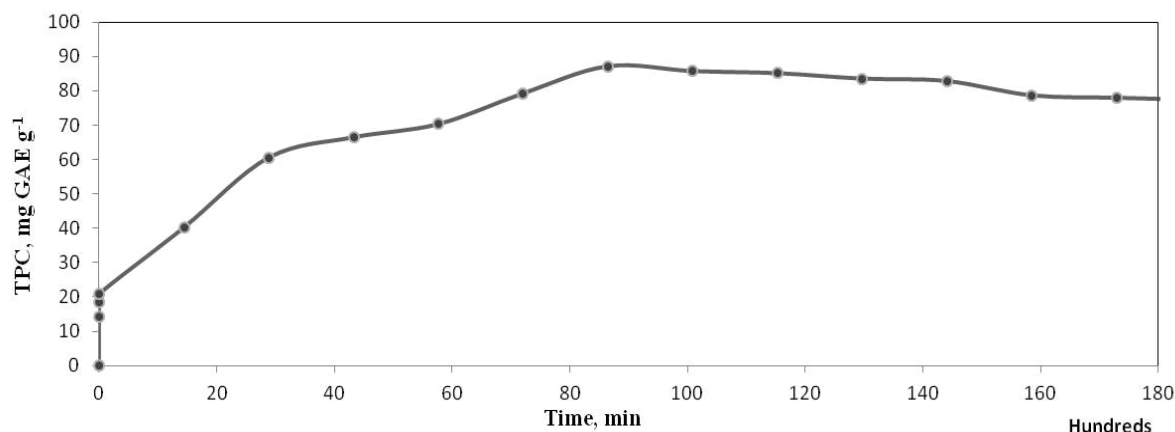


Fig. 2. Total polyphenolic content obtained by Eth E

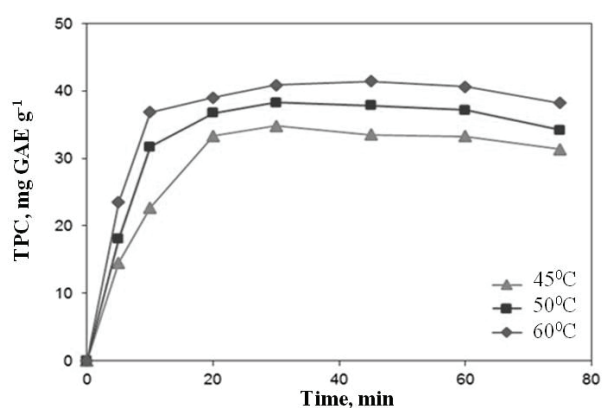


Fig. 3. Total polyphenolic content obtained by UAE

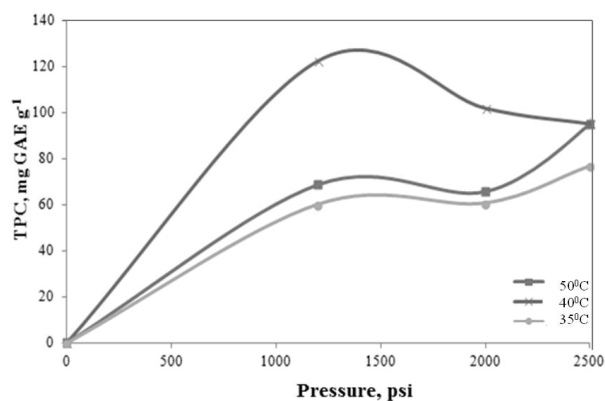


Fig. 4. Total polyphenolic content obtained by SFE

3.4. Comparative analysis

The different extraction processes applied in this study had significant effect on the TPCs extracted from spruce bark. As it was reported, the ethanolic extraction has the biggest disadvantage of a longer extraction time. To improve performances of the Eth E, ultrasounds waves and supercritical pressure of CO₂ were used to intensify the extraction process. Using UAE the total polyphenolic content increase from 14.38 mg GAE g⁻¹ spruce bark

(ethanolic extraction, 60 min) to 33.48 mg GAE g⁻¹ spruce bark and to 122.41 mg GAE g⁻¹ spruce bark in case of supercritical extraction (Fig. 6).

Increasing of phenolic compounds recover degree using ultrasound assisted extraction was also reported in the literature. d'Alessandro et al. (2012) reported a positive effect of ultrasounds on the polyphenols extraction from chokeberry (d'Alessandro et al., 2012). Also Wang et al. (2013) notice that ultrasounds are important in improving the extraction yields of polyphenols from *Sparganii rhizoma* (Wang et al., 2013).

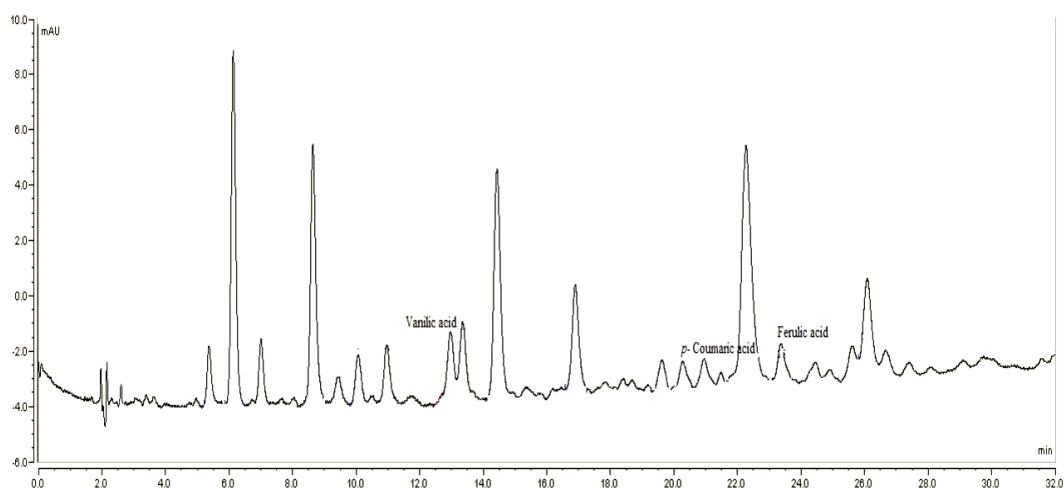
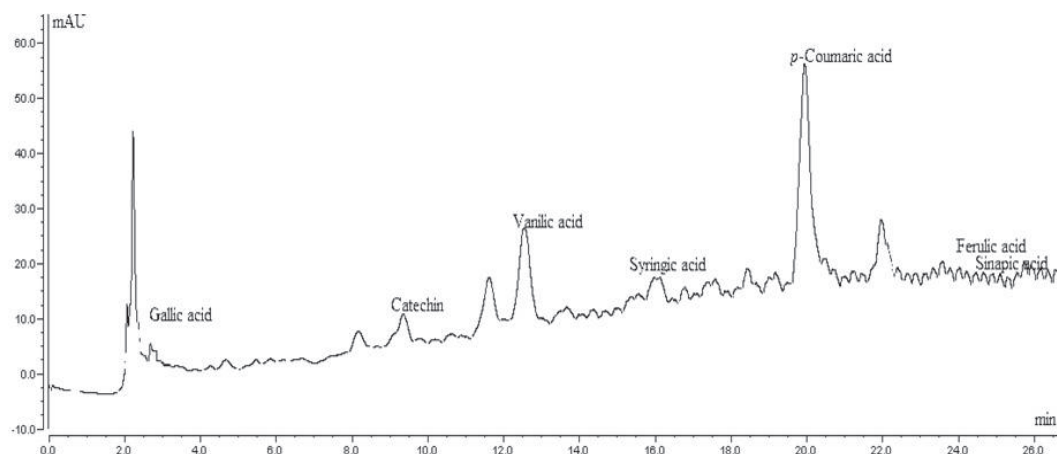
Beyond being a green technique, supercritical extraction provided extracts with better activity than the conventional extraction methods (Kazan et al., 2014) and even ultrasound assisted extraction (Roseiro et al., 2013). Data from literature sustain our research results which show that SFE offer higher total polyphenolic content extracted from spruce bark, compared with ethanolic and ultrasound assisted extraction. This can be due to the fact that SFE processes use critical points of fluids to increase the extraction yields of polyphenols from biomass (Roberto et al., 2010).

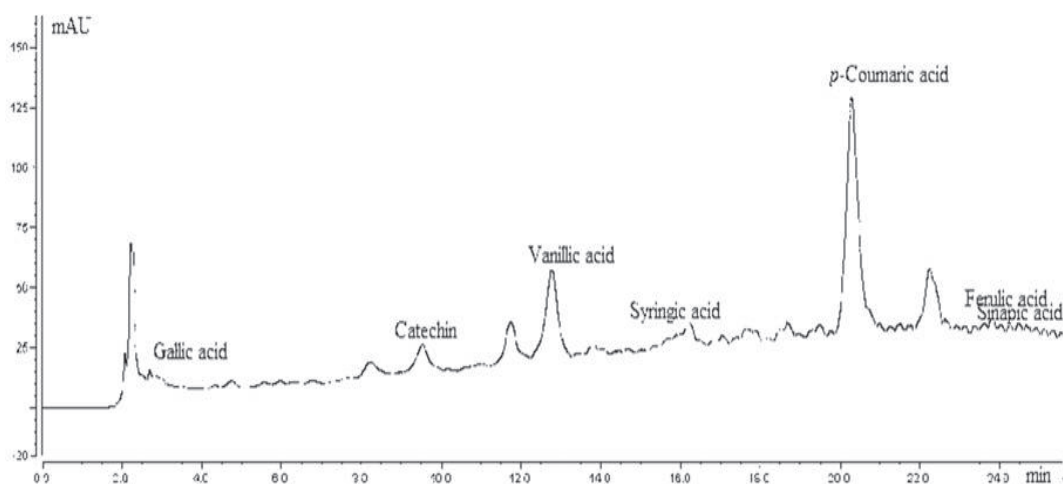
Though it is important to underline that working with mixture of solvents, in our case CO₂ - ethanol - water, the supercritical operational conditions change each one having different critical points, so the experiments could be achieved in near-supercritical conditions. Based on this study, a comparative analysis between conventional (EthE) and nonconventional extraction methods (SFE and UAE) reporting to: extraction time, quantity of solvent and biomass, total polyphenolic content and HPLC was done (Table 2). The comparison of yields (reported as mg GAE g⁻¹), times required for the extraction, volumes of solvent and selectivity for the phenolic acids (shown by HPLC) demonstrated that SFE technique is more efficient than Eth E and UAE.

The supercritical CO₂ has a higher diffusion coefficient, lower viscosity and surface tension than the liquid solvents used in UAE and Eth E, leading to easier penetration to sample matrix and favorable mass transfer.

Table 1. HPLC analysis of spruce bark polyphenolic extracts obtained by SFE, UAE and Eth E

| Peak name | Parameters | SFE 60 min, 40°C, 1200 psi | UAE 60 min, 40°C | Eth E 60 min, 40°C |
|------------------------|------------------------------|-------------------------------|---------------------|-----------------------|
| <i>Gallic acid</i> | Retention time (min) | 3.010 | 2.998 | - |
| | Area (mAU min) | 0.0635 | 0.0626 | |
| | Amount (mg L ⁻¹) | 5.4676 | 5.454 | |
| <i>Catechin</i> | Retention time (min) | 9.528 | 9.358 | - |
| | Area (mAU min) | 3.3499 | 2.165 | |
| | Amount (mg L ⁻¹) | 171.1765 | 112.084 | |
| <i>Vanillic acid</i> | Retention time (min) | 13.512 | 13.668 | 12.957 |
| | Area (mAU min) | 0.1514 | 0.532 | 0.403 |
| | Amount (mg L ⁻¹) | 7.8771 | 15.2019 | 2.321 |
| <i>Syringic acid</i> | Retention time (min) | 15.888 | 15.775 | - |
| | Area (mAU min) | 0.0758 | 0.7544 | |
| | Amount (mg L ⁻¹) | 5.1224 | 12.9180 | |
| <i>p-Coumaric acid</i> | Retention time (min) | 20.290 | 19.938 | 20.278 |
| | Area (mAU min) | 35.7026 | 13.2957 | 0.2142 |
| | Amount (mg L ⁻¹) | 260.4073 | 99.4731 | 5.5174 |
| <i>Ferulic acid</i> | Retention time (min) | 22.898 | 23.592 | 23.370 |
| | Area (mAU min) | 0.3081 | 0.5722 | 0.339 |
| | Amount (mg L ⁻¹) | 6.6290 | 9.7051 | 6.9942 |
| <i>Synapic acid</i> | Retention time (min) | 23.782 | 23.773 | - |
| | Area (mAU min) | 1.1934 | 0.3361 | |
| | Amount (mg L ⁻¹) | 35.0534 | 13.3618 | |

**a)****b)**



c)

Fig. 5. Chromatographic profile of: a) Eth E polyphenolic extract; b) UAE polyphenolic extract; c) SFE polyphenolic extract

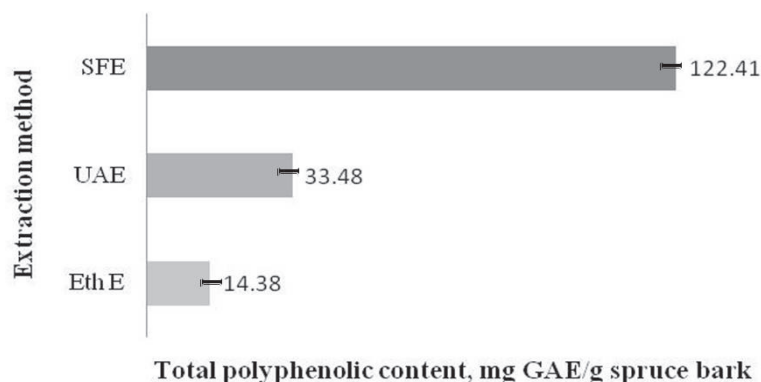


Fig. 6. Total polyphenolic content obtained by conventional and nonconventional extraction methods

Table 2. Comparative analysis between classical and non-conventional extraction techniques applied for polyphenols extraction from spruce bark.

| Method Parameters | Eth E | UAE | SFE |
|---|--------|--------|--------|
| Extraction time till maximum concentration (h) | 144 | 1 | 1 |
| Grams of spruce bark (g) | 5 | 5 | 2 |
| Volume of solvent (ethanol) ₀ (mL) | 50 | 50 | 20 |
| Total phenolic content (mg GAE g ⁻¹ spruce bark) | 14.38* | 33.48 | 122.41 |
| Total phenolic amount by HPLC (mg L ⁻¹) | 14.83 | 269.20 | 491.73 |

* Concentration of TPC after one hour of extraction

4. Conclusions

In this study different extraction techniques were used to extract polyphenolic compounds from spruce bark coming as a waste from forestry industry.

It was reported that applying supercritical CO₂ the total phenolic content extracted has a significant increasing from 14.38 mg GAE g⁻¹ spruce bark (ethanolic extraction, 60 min) to 33.48 mg GAE g⁻¹ spruce bark (UAE extraction) and to 122.41 mg GAE g⁻¹ spruce bark in case of supercritical extraction. Although SFE gives better extraction yields, allows obtaining high purity extracts and rich in terms of

polyphenolic compounds recovered, in a relatively short time extraction. This is a very important factor on operating with this technique because of the high running cost comparing with the conventional techniques and even UAE.

UAE it's also a rapid extraction technique (5-60 min), simple to operate, provides extracts with a composition similar to those obtained by SFE and have the most important advantage of a much lower operating costs.

The study recommend SFE and UAE instead of traditional ethanolic techniques, both at laboratory and pilot scale, since these provide high extraction

yields, pure extracts, with a large number of polyphenolic compounds extracted and are environmentally friendly.

References

- Adam F., Abert-Vian M., Peltier G., Chemat F., (2012), "Solvent-free" ultrasound-assisted extraction of lipids from fresh microalgae cells: a green, clean and scalable process, *Bioresource Technology*, **114**, 457-465.
- Ahluwalia S., Shivhare U.S., Basu S., (2013), Supercritical CO₂ extraction of compounds with antioxidant activity from fruits and vegetables waste -a review, *Focusing on Modern Food Industry*, **2**, 42-62.
- Azmir J., Zaidul I.S.M., Rahman M.M., Sharif K.M., Mohamed A., Sahena F., Omar K.M., (2013), Techniques for extraction of bioactive compounds from plant materials: A review, *Journal of Food Engineering*, **117**, 426-436.
- Benelli P., Riehl C., Smânia A., Smânia E.F., Ferreira, S.R.S., (2010), Bioactive extracts of orange (*Citrus sinensis* L. Osbeck) pomace obtained by SFE and low pressure techniques: Mathematical modeling and extract composition, *The Journal of Supercritical Fluids*, **55**, 132-141.
- Bodîrlău R., Spiridon I., Teacă C.A., Anghel N., Ichim M., Colceru S., Armatu A., (2009), Anti-inflammatory constituents from different plant species, *Environmental Engineering and Management Journal*, **8**, 785-792.
- Chavan Y., Singhal R.S., (2013), Ultrasound-assisted extraction (UAE) of bioactives from arecanut (*Areca catechu* L.) and optimization study using response surface methodology, *Innovative Food Science & Emerging Technologies*, **17**, 106-113.
- Cherubini F., (2010), The biorefinery concept: Using biomass instead of oil for producing energy and chemicals, *Energy Conversion and Management*, **51**, 1412-1421.
- Chupin L., Motillon C., Charrier-El Bouhtoury F., Pizzi A., Charrier B., (2013), Characterization of maritime pine (*Pinus pinaster*) bark tannins extracted under different conditions by spectroscopic methods, FTIR and HPLC, *Industrial Crops and Products*, **49**, 897-903.
- d'Alessandro L.G., Kriaa K., Nikov I., Dimitrov K., (2012), Ultrasound assisted extraction of polyphenols from black chokeberry, *Separation and Purification Technology*, **93**, 42 - 47.
- Da Porto C., Porretto E., Decorti D., (2013), Comparison of ultrasound-assisted extraction with conventional extraction methods of oil and polyphenols from grape (*Vitis vinifera* L.) seeds, *Ultrasonics Sonochemistry*, **20**, 1076-1080.
- Dey S., Rathod V.K., (2013), Ultrasound assisted extraction of β -carotene from *Spirulina platensis*, *Ultrasonics Sonochemistry*, **20**, 271-6.
- Espinosa-Pardo F., Martinez J., Martinez-Correa H., (2014), Extraction of bioactive compounds from peach palm pulp (*Bactris gasipaes*) using supercritical CO₂, *The Journal of Supercritical Fluids*, **93**, 2-6.
- Gravitis J., Abolins J., Kokorevics A., (2008), Integration of biorefinery clusters towards zero emissions, *Environmental Engineering and Management Journal*, **7**, 569-577.
- Ghiteșcu R.-E., Volf I., Carausu C., Bühlmann A.-M., Gilca I.A., Popa V.I., (2015), Optimization of ultrasound-assisted extraction of polyphenols from spruce wood bark, *Ultrasonics Sonochemistry*, **22**, 535-41.
- Hainal A., Ignat I., Volf I., Popa V.I., (2011), Transformation of polyphenols from biomass by some yeast species, *Cellulose Chemistry and Technology*, **45**, 211-219.
- Herrero M., Castro-Puyana M., Mendiola J., Ibañez E., (2013), Compressed fluids for the extraction of bioactive compounds, *Trends in Analytical Chemistry*, **43**, 67-83.
- Hidalgo D., Corona F., Martin-Marroquin J., Gomez M., Aguado A., Antolin G., (2014), Integrated and sustainable system for multi-waste valorization, *Environmental Engineering and Management Journal*, **13**, 2467-2475.
- Ignat I., Volf I., Popa V.I., (2011), A critical review of the method characterisation of polyphenolic compounds in fruits and vegetables, *Food Chemistry*, **126**, 1821-1835.
- Ignat I., Volf I., Popa V.I., (2013), *Analytical Methods of Phenolic Compounds*, In: *Natural Products, Phytochemistry, Botany and Metabolism of Alkaloids, Phenolics and Terpenes*, Ramawat K.G., Merillon J.M. (Eds.), Springer-Verlag, Berlin Heidelberg, 2061-2092.
- Kazan A., Koyu H., Turu I. C., Yesil-Celiktas O., (2014), Supercritical fluid extraction of *Prunus persica* leaves and utilization possibilities as a source of phenolic compounds, *The Journal of Supercritical Fluids*, **92**, 55-59.
- Khan M. K., Abert-Vian M., Fabiano-Tixier A.-S., Dangles O., Chemat F., (2010), Ultrasound-assisted extraction of polyphenols (flavanone glycosides) from orange (*Citrus sinensis* L.) peel, *Food Chemistry*, **119**, 851-858.
- Khoddami A., Wilkes M., Roberts T.H., (2013), Techniques for analysis of plant phenolic compounds, *Molecules (Basel, Switzerland)*, **18**, 2328-75.
- Martins S., Mussatto S.I., Martínez-Avila G., Montañez-Saenz J., Aguilar C.N., Teixeira J., (2011), Bioactive phenolic compounds: production and extraction by solid-state fermentation. A review, *Biotechnology Advances*, **29**, 365-73.
- Popa V.I., Dumitru M., Volf I., Anghel N., (2008), Lignin and polyphenols as allelochemicals, *Industrial Crops and Products*, **27**, 144-149.
- Popa V.I., (2011), *Hemicelluloses in Pharmacy and Medicine*, In: *Polysaccharides in Medicinal and Pharmaceutical Applications*, Popa V.I. (Ed.), iSmithers, U.K., 57-87.
- Popa V.I., (2013), *Lignin in Biological System*, In: *Polymeric Biomaterials, Structure and function (I)*, Dumitriu S., Popa V.I. (Eds.), CRC Press, U.S.A., 709-738.
- Roberto M., Junior M., Leite A.V., Romanelli N., Dragano V., (2010), Supercritical Fluid Extraction and Stabilization of Phenolic Compounds From Natural Sources - Review (Supercritical Extraction and Stabilization of Phenolic Compounds), *The Open Chemical Engineering Journal*, **4**, 51-60.
- Roseiro L.B., Duarte L.C., Oliveira D.L., Roque R., Bernardo-Gil M.G., Martins A.I., Rauter A.P., (2013), Supercritical, ultrasound and conventional extracts from carob (*Ceratonia siliqua* L.) biomass: Effect on the phenolic profile and antiproliferative activity, *Industrial Crops and Products*, **47**, 132-138.
- Sheldon R., (2011), Utilization of biomass for sustainable fuels and chemicals: Molecules, methods and metrics, *Catalysis Today*, **167**, 3-13.

- Stingu A., Volf I., Popa V.I., (2011), Spruce bark extract as modulator in rape plant, *Cellulose Chemistry and Technology*, **45**, 281–286.
- Sun Y., Liu Z., Wang J., (2011), Ultrasound-assisted extraction of five isoflavones from *Iris tectorum* Maxim, *Separation and Purification Technology*, **78**, 49–54.
- Tanase C., Volf I., Popa V.I., (2013), Assessment of synergic regulatory actions of spruce bark extract and deuterium depleted water on maize (*Zea mays* L.) crops, *Environmental Engineering and Management Journal*, **12**, 1287–1294.
- Tanase C., Boz I., Stingu A., Volf I., Popa V.I., (2014), Physiological and biochemical responses induced by spruce bark aqueous extract and deuterium depleted water with synergistic action in sunflower (*Helianthus annuus* L.) plants, *Industrial Crops and Products*, **60**, 160–167.
- Vilkhu K., Mawson R., Simons L., Bates D., (2008), Applications and opportunities for ultrasound assisted extraction in the food industry - A review, *Innovative Food Science & Emerging Technologies*, **9**, 161–169.
- Volf I., Stingu A., Popa V.I., (2012), New natural chelating agents with modulator effects on copper phytoextraction, *Environmental Engineering and Management Journal*, **11**, 487–491.
- Volf I., Ignat I., Neamtu M., Popa V.I., (2013), Thermal stability, antioxidant activity, and photo-oxidation of natural polyphenols, *Chemical Papers*, **68**, 121–129.
- Vongsak B., Sithisarn P., Mangmool S., Thongpraditchote S., Wongkrajang Y., Gritsanapan W., (2013), Maximizing total phenolics, total flavonoids contents and antioxidant activity of *Moringa oleifera* leaf extract by the appropriate extraction method, *Industrial Crops and Products*, **44**, 566–571.
- Wang X., Wu Y., Chen G., Yue W., Liang Q., Wu Q., (2013), Optimisation of ultrasound assisted extraction of phenolic compounds from *Sparganii rhizoma* with response surface methodology, *Ultrasonics Sonochemistry*, **20**, 846–854.



“Gheorghe Asachi” Technical University of Iasi, Romania



SELECTIVE RECOVERY OF PHENOLIC DERIVATIVES THROUGH THE TECHNIQUE OF LIQUID MEMBRANES

Ioana Diaconu^{1*}, Cristina Monica Mirea^{1,2}, Elena Ruse¹, Gheorghe Nechifor¹

¹University Politehnica Bucharest, Faculty of Applied Chemistry and Materials Science,
Department of Analytical Chemistry and Environmental Engineering, 011061 Bucharest, Romania

²Arcuda Laboratory, Water Quality Service, Joita, Giurgiu, Romania

Abstract

In the present paper we studied the competitive transport of p-nitrophenol (pNP) and 2,4-dinitrophenol (2,4-dNP) from aqueous media using the technique of liquid membranes. This technique is very efficient, economic and selective when compared to other removal techniques of phenolic derivatives. The paper presents the influence of the sodium carbonate concentration from the stripping phase, the influence of the concentration ratio $[2,4\text{-dNP}]/[p\text{NP}]$ upon the selectivity of the transport process and some kinetic aspects of the transport of 2,4-dNP in the presence of pNP through bulk liquid membranes.

Key words: 2,4-dinitrophenol, kinetics, membrane separation, p-nitrophenol

Received: November, 2014; Revised final: March, 2015; Accepted: March, 2015

1. Introduction

Phenolic compounds, especially those with – nitro groups, are toxic compounds that have harmful effects upon human beings and other terrestrial and aquatic creatures (Arsene et al., 2013; Berhanu et al., 2006; Chelba et al., 2014). For example, prolonged exposure to p-nitrophenol can cause blood disorder, methemoglobin formation, liver and kidney disease as well as eye and skin irritations (ATSDR, 1992; Zheng et al., 2009).

The carcinogenic effect of 2,4-dNP is well known, cellular growth is inhibited at a concentration of 1 ppm (Bagal et al., 2013; Cao and Shiraishi, 2010). This is why United States Environmental Protection Agency (US EPA) included these two nitrophenol compounds on the 126 proprietary pollutants list (U.S.EPA, 2009). The admitted limit for phenolic compounds is under 10 mg/L (Busca et al., 2008; Diaconu et al., 2009b), and in order the water to be drinkable the European Directive EU/440/75 has established the maximum range of

phenolic compounds at 1-10 µg/L (EC Directive, 1975).

Nitrophenols are frequently encountered in residual wastewaters from industries such as explosive manufacture, pharmaceuticals, wood preservatives, pesticides, fungicides, pigments, dyes and rubber industry where they are used as intermediary products (Chand and Shiraishi, 2013; Diaconu et al., 2011; 2010a; 2010b; Szczepański and Diaconu, 2012). These compounds can be formed as a result of the reaction of phenolic compounds in the atmosphere in aqueous or gaseous phase (Harrison et al., 2005; Lezamiz and Jönsson, 2007). Thus these compounds need to be removed from the environment.

There are several methods to remove nitrophenols such as: adsorption (Barreca et al., 2014; Jia et al., 2014), microbiological degradation (Diaconu et al., 2010a), catalytic oxidation (Das et al., 2006), electrochemical treatment (Jiang et al., 2010) and membrane separation (Diaconu et al., 2009a; 2009b). The disadvantage of certain

* Author to whom all correspondence should be addressed: e-mail: diaconuioana12@yahoo.com

techniques such as adsorption is that they have high costs and extremely selective and cheap methods must be found. An alternative is represented by the technique of liquid membrane. These technique is easy to use, low energy consumption, inexpensive and with high transport efficiency (Blaga et al., 2006; Cascaval et al., 2004; Diaconu et al., 2012; Galaction and Cascaval, 2004; Olteanu et al., 2013; Zaharia et al., 2012a, 2012b, 2013).

In the present paper a selective recovery and separation of two extremely toxic nitro-derivatives, pNP and 2,4-dNP, through the technique of liquid membranes is realized, as well as kinetic aspects of the transport of 2,4-dNP through a bulk liquid membrane.

2. Material and method

All the reagents used were analytically grade and were used without further purification. pNP was purchased from Loba Chemie Wein Fischamend and 2,4- dNP was purchased from Merck (Germany). Chloroform used as organic membrane was previously saturated with distilled water. Chloroform was purchased from Flucka. HCl and Na₂CO₃, purchased from Merck (Germany) were used to prepare the feed phase and the stripping phase, respectively. The distilled water used to prepare the aqueous phases was previously saturated with chloroform. The transport cell used was a tube in tube transport cell presented in previous papers (Diaconu et al. 2009a, 2011). The experiments were realized with an acid feed phase, pH = 2 obtained with HCl 10⁻² mol/L. The transport time was 3h and stirring speed was of 180 rot/vit.

The analytical control was realized using a LAMDA UV-VIS-NIR (Perkin Elmer Life and Analytical Sciences) spectrophotometer at pNP specific wavelength: at 317 nm-for feed phase and 404 nm-for stripping phase and at 2,4-dNP specific wavelength: at 358 nm-for feed phase and 361 nm-for stripping phase.

3. Experimental

Previous studies (Diaconu et al., 2009a; 2009b; Szczepański and Diaconu, 2012) demonstrated that pNP and 2,4-dNP can cross through an organic membrane from an aqueous acid phase (feed phase) into an aqueous alkaline phase (strip phase). In the aqueous boundary layer of the stripping phase the neutralization reaction of the two compounds takes place based on the ionization equilibriums (Eqs. 1-4), where K_{a1} and K_{a2} are acidity constants.



$$K_{a1} = \frac{[2,4\text{-dNP}^-][\text{H}_3\text{O}^+]}{[2,4\text{-dNP}]} \quad (2)$$



$$K_{a2} = \frac{[\text{pNP}^-][\text{H}_3\text{O}^+]}{[\text{pNP}]} \quad (4)$$

Keeping in mind the expression of the acidity constants the hydrogen ion concentration in the diffusion boundary layer is obtained according to Eq. (5), which will result in Eq. (6).

$$[\text{H}_3\text{O}^+] = \frac{K_{a1}[2,4\text{-dNP}]}{[2,4\text{-dNP}^-]} = \frac{K_{a2}[\text{pNP}]}{[\text{pNP}^-]} \quad (5)$$

$$\frac{K_{a1}}{K_{a2}} = \frac{[\text{pNP}]}{[\text{pNP}^-]} \cdot \frac{[2,4\text{-dNP}]}{[2,4\text{-dNP}^-]} \quad (6)$$

If $K_{a1} \gg K_{a2}$ Eq. (7) will result, with the conditions: $[\text{pNP}] \gg [2,4\text{-dNP}]$ or $[\text{pNP}] \ll [2,4\text{-dNP}]$. Therefore, the sodium carbonate reacts firstly with 2,4-dNP and than pNP.

$$\frac{[\text{pNP}]}{[\text{pNP}^-]} \gg \frac{[2,4\text{-dNP}]}{[2,4\text{-dNP}^-]} \quad (7)$$

Depending on the concentration ratio of the two compounds $[2,4\text{-dNP}]/[\text{pNP}]$, the reaction of pNP with the sodium carbonate can start the neutralization before the total neutralization of 2,4-dNP. The influence of the concentration ratio of the two compounds in the diffusion boundary layer is expressed by Eq. (8) (Liteanu and Hopârtan, 1972).

$$\frac{K_{a1}}{K_{a2}} = \frac{10^2 \alpha - 10^2 \alpha r + \alpha^2 r}{10^4 r + 2 \times 10^2 \alpha r + \alpha^2 r} \quad (8)$$

where: $r = [2,4\text{-dNP}]/[\text{pNP}]$; α = neutralization degree of harder acid (2,4-dNP).

Given these considerations in the present paper the influence of the ratio $[2,4\text{-dNP}]/[\text{pNP}]$ upon the selectivity of the transport process was studied.

3.1. Influence of the sodium carbonate concentration from the stripping phase on membrane transport

It was studied the behavior at the membrane transport of a mixture formed from the two compounds, 2,4-dNP and pNP, at different concentrations of sodium carbonate in the stripping phase. The concentration range of sodium carbonate was between 10⁻²-1 mol/L.

The experimental data obtained showed that there is no major influence of the sodium carbonate from the stripping phase in the studied concentration range upon the efficiency of the transport of 2,4-dNP, respectively pNP at the concentration ratio of $[2,4\text{-dNP}]/[\text{pNP}] = 10^{-3}/10^{-4}$ in the feed phase. This can be also observed from Fig. 1.

3.2. Influence of the concentration ration $[2,4\text{-dNP}]/[pNP]$ from the feed phase upon the selectivity of the transport process

The influence of the concentration ratio of the two compounds in the feed source at the fallowing values: $[2,4\text{-dNP}]/[pNP] = 10^{-3}/10^{-3}$; $10^{-3}/5 \cdot 10^{-4}$; $10^{-3}/10^{-4}$

We can observe from Fig. 2 that the best results are obtained at the concentration ratio in the feed source of $[2,4\text{-dNP}]/[pNP] = 10^{-3}/10^{-4}$. Thus using a concentration ratio for the feed source of $[2,4\text{-dNP}]/[pNP] = 10^{-3}/10^{-4}$ at pH=2 obtained with HCl, a chloroform membrane and a Na_2CO_3 stripping phase at a concentration of 10^{-2} mol/L the two compounds can be separated obtaining a transport efficiency for 2,4-dNP that exceed 98%.

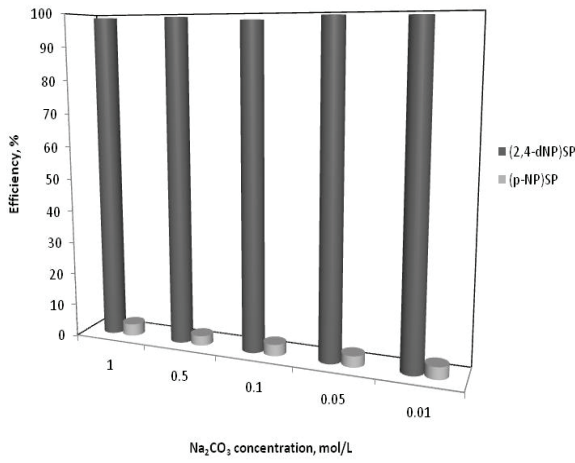


Fig. 1. Sodium carbonate concentration influence upon the transport of 2,4-dNP and pNP through bulk liquid membranes. Experimental conditions: feed phase (FP) $[2,4\text{-dNP}] = 10^{-3}$ mol/L and $[pNP] = 10^{-4}$ at pH = 2, membrane-chloroform, strip phase (SP) = 1; 0,5; 0,1; 0,05; 0,01 mol/L Na_2CO_3 , transport time = 3h

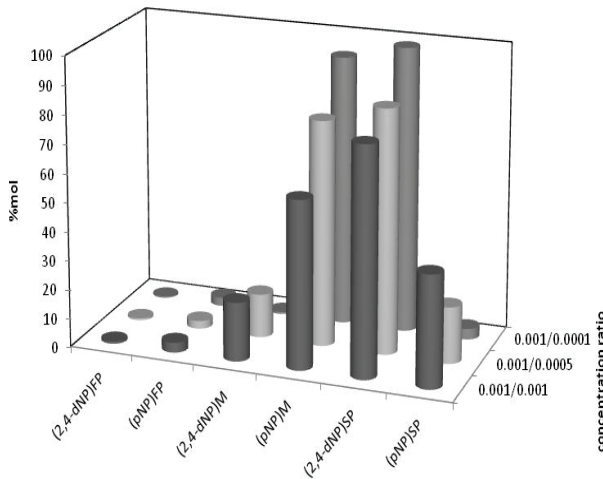
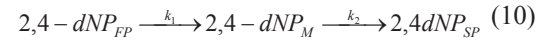


Fig. 2. The transport of 2,4-dNP and pNP at different concentration ratio for the feed phase: $[2,4\text{-dNP}]/[pNP] = 10^{-3}/10^{-3}$; $10^{-3}/5 \cdot 10^{-4}$; $10^{-3}/10^{-4}$; experimental conditions: feed phase (FP) $[2,4\text{-dNP}]/[pNP] = 10^{-3}/10^{-3}$; $10^{-3}/5 \cdot 10^{-4}$; $10^{-3}/10^{-4}$ at pH = 2, membrane (M): chloroform, stripping phase (SP): Na_2CO_3 10^{-2} mol/L, transport time = 3h

3.3. Kinetic aspects of the 2,4-dNP transport through bulk liquid membranes

The analysis of the membrane system in time allowed the assessment of some kinetic parameters of the 2,4-dNP pertraction in the presence of pNP. The experimental data confirmed a kinetic characteristic to consecutive irreversible first order chemical reaction, frequently used to describe pertraction in bulk liquid membranes (Alpaydin et al., 2011; Alpoguz et al., 2010; Gubbuk et al., 2010; León and Guzman, 2008; Minhas et al., 2010; Religa et al., 2009; Zhang et al., 2009).

The kinetic scheme which describes the pertraction of 2,4-dNP through bulk liquid membrane is given by Eqs. (10-13), where: k_1 , k_2 represent pseudo-first-order apparent membrane entrance and exit rate constants, s^{-1} ; R_{FP} , R_M and R_{SP} represent the undimensional reduced concentrations from the feed, membrane and stripping phase and are calculated with the Eqs. (14-16).



$$R_{FP} = e^{-k_1 t} \quad (11)$$

$$R_M = \frac{k_1}{k_2 - k_1} (e^{-k_1 t} - e^{-k_2 t}) \quad (12)$$

$$R_{SP} = 1 + \frac{1}{k_1 - k_2} (k_2 e^{-k_1 t} - k_1 e^{-k_2 t}) \quad (13)$$

$$R_{FP} = \frac{C_{FP} \cdot V_{FP}}{C_{FP0} \cdot V_{FP}} \quad (14)$$

$$R_M = \frac{C_M \cdot V_M}{C_{FP0} \cdot V_{FP}} \quad (15)$$

$$R_{SP} = \frac{C_{SP} \cdot V_{SP}}{C_{FP0} \cdot V_{FP}} \quad (16)$$

where: C_{FP} , C_M , C_{SP} represents the feed, membrane and stripping phase concentration, mol/L; C_{FS0} , represents the initial concentration from the feed phase, mol/L; V_M , V_{SP} represents the feed, membrane and stripping phase volume, cm^3 .

The maximum solute concentration in the membrane is calculated from the dependence $R_m = f(t)$ when $dR_m/dt = 0$ by Eqs. (17, 18):

$$R_M^{max} = \left(\frac{k_1}{k_2} \right)^{\frac{k_2}{k_1 - k_2}} \quad (17)$$

$$t_{max} = \frac{\ln \left(\frac{k_1}{k_2} \right)}{k_1 - k_2} \quad (18)$$

The pseudo-first-order apparent membrane entrance and exit rate constants can be used at the determination of the maximum flux (Eq. 19) according to the Eq. (17), where: J_{FPmax} = membrane entrance flux ; J_{SPmax} = membrane exit flux.

$$J_{max} = -k_1 \left(\frac{k_1}{k_2} \right)^{\frac{k_1}{k_1-k_2}} = k_2 \left(\frac{k_1}{k_2} \right)^{\frac{k_2}{k_1-k_2}} = -J_{FPmax} = J_{SPmax} \quad (19)$$

The experimental data confirmed a good accordance with the model. The correlation coefficient is higher than 0.99. This is illustrated in Fig. 3. Analyzing the compared results from Table 1 we have found that the pseudo-first-order apparent membrane entrance rate constant, pseudo-first-order apparent membrane exit rate constant, the time at

which the R_{max} is observed and maximum flux in the stripping phase depend on the concentration ratio $[2,4\text{-dNP}]/[pNP]$. The maximum values are obtained at the concentration ration $[2,4\text{-dNP}]/[pNP] = 10^{-3}/10^{-4}$ allowing the separation of 2,4-dNP from pNP.

4. Conclusions

In the present paper the possibility of separation of two phenolic derivatives 2,4-dNP and pNP. In order to realize this was used a membrane system formed from an acid feed phase formed from the two nitrophenols at different molar ratio, a chloroform membrane and a stripping phase formed from sodium carbonate.

The experimental data showed that the separation of the two is influenced in an essential way by the concentration ratio $[2,4\text{-dNP}]/[pNP]$.

Table 1. Kinetic aspects at the transport of 2,4-dNP in the presence of pNP. Experimental conditions: feed phase: $[2,4\text{-dNP}]/[pNP] = 10^{-3}/10^{-3}$, $10^{-3}/5 \cdot 10^{-4}$, $10^{-3}/10^{-4}$ at pH=2, membrane: chloroform, stripping phase Na_2CO_3 10^{-2} mol/L, time=3h

| Concentration ration for the substrate $[2,4\text{-dNP}]/[pNP]$ | k_1 $\times 10^3 [\text{s}^{-1}]$ | k_2 $\times 10^4 [\text{s}^{-1}]$ | R_{max} | $t_{max}, [\text{s}]$ | J_{FSmax} $\times 10^4 [\text{s}^{-1}]$ | J_{SPmax} $\times 10^4 [\text{s}^{-1}]$ |
|---|--|--|-----------|-----------------------|--|--|
| $10^{-3}/10^{-3}$ | 1.65 | 1.56 | 0.78 | 1575 | -1.22 | 1.22 |
| $10^{-3}/5 \cdot 10^{-4}$ | 1.94 | 2.24 | 0.75 | 1253 | -1.69 | 1.69 |
| $10^{-3}/10^{-4}$ | 2.02 | 3.68 | 0.68 | 1028 | -2.52 | 2.52 |

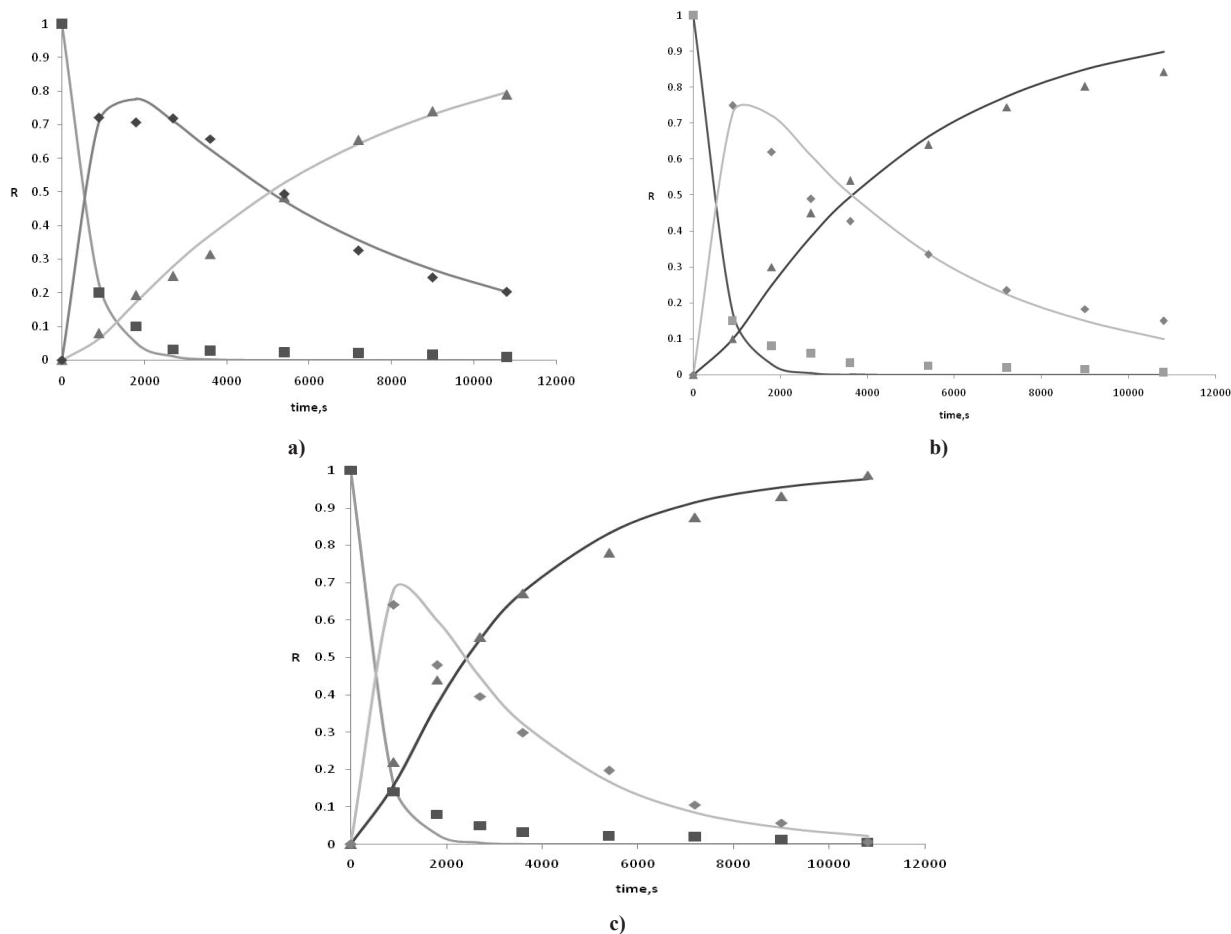


Fig. 3. Experimental results at the pertraction of 2,4-dNP through bulk liquid membranes in the presence of pNP. Feed phase (■): $[2,4\text{-dNP}]/[pNP] =$ a) $10^{-3}/10^{-3}$; b) $10^{-3}/5 \cdot 10^{-4}$; c) $10^{-3}/10^{-4}$ at pH = 2; Membrane (◆) chloroform; Stripping phase (▲): Na_2CO_3 10^{-2} mol/L, transport time = 3h; continuous line represents the values calculated using the kinetic model

Thus at the molar ratio $[2,4\text{-dNP}]/[pNP] = 10^{-3}/10^{-4}$ a separation of the two compounds can be realized. A time dependence analysis of the pertraction of 2,4-dNP in the presence of pNP allowed a kinetic assessment of the pertraction of the 2,4-dNP.

The model that describes the process is a kinetic model of two consecutive irreversible first order reactions in the system with interfaces. The results demonstrated an influence of the concentration ratio $[2,4\text{-dNP}]/[pNP]$ upon the kinetic parameters. Maximum values were obtained for the concentration ratio $[2,4\text{-dNP}]/[pNP] = 10^{-3}/10^{-4}$.

Acknowledgments

The work has been funded by the Sectoral Operational Programme Human Resources Development 2007-2013 of the Ministry of European Funds through the Financial Agreement POSDRU/159/1.5/S/132395.

Reference

- Alpaydin S., Saf A.Ö., Bozkurt S., Sirit A., (2011), Kinetic study on removal of toxic metal Cr (VI) through a bulk liquid membrane containing p-tert-butylcalix [4] arene derivative, *Desalination*, **275**, 166-171.
- Alpoguz H.K., Kaya A., Tabakci B., Yilmaz A., (2010), Facilitated transport of Cr (VI) through a bulk liquid membrane containing p-tert-butylcalix [4] arene amine derivative as a carrier, *Separation Science and Technology*, **45**, 1121-1129.
- Arsene D., Teodosiu C., Barjoveanu G., Apreutesei R.E., Apopei P., Musteret C.P., Cailean D., (2013), Combined catalytic oxidation and adsorption of priority organic pollutants for wastewater recycling, *Environmental Engineering and Management Journal*, **12**, 907-916.
- ATSDR, (1992), Agency for Toxic Substances and Disease Registry, Toxicological Profile for Nitrophenols: 2-nitrophenol and 4-nitrophenol, US Department of Health and Human Services, Public Health Service, Atlanta, USA.
- Bagal M.V., Lele B.J., Gogate P.R., (2013), Removal of 2, 4-dinitrophenol using hybrid methods based on ultrasound at an operating capacity of 7L, *Ultrasonics sonochemistry*, **20**, 1217-1225.
- Barreca S., Colmenares J.J.V., Pace A., Orecchio S., Pulgarin C., (2014), Neutral solar photo-Fenton degradation of 4-nitrophenol on iron-enriched hybrid montmorillonite-alginate beads (Fe-MABs), *Journal of Photochemistry and Photobiology A: Chemistry*, **282**, 33-40.
- Berhanu T., Liu J. F., Romero R., Megersa N., Jönsson J. Å., (2006), Determination of trace levels of dinitrophenolic compounds in environmental water samples using hollow fiber supported liquid membrane extraction and high performance liquid chromatography, *Journal of Chromatography A*, **1103**, 1-8.
- Blaga A.C., Galaction A., Cascaval D., (2006), Extraction and transport of aspartic and glutamic acids through liquid membranes, *Romanian Biotechnological Letters*, **11**, 2791-2797.
- Busca G., Berardinelli S., Resini C., Arrighi L., (2008), Technologies for the removal of phenol from fluid streams: A short review of recent developments, *Journal of Hazardous Materials*, **160**, 265-288.
- Cao X., Shiraishi F., (2010), A mechanism of photocatalytic and adsorptive treatment of 2,4-dinitrophenol on aporous thin film of TiO₂ covering granular activated carbon particles, *Chemical Engineering Journal*, **160**, 651-659.
- Cascaval D., Galaction A.I., Oniscu C., (2004), Modeling of the selective pertraction of carboxylic acids obtained by citric fermentation, *Hemijiska industrija*, **58**, 97-103.
- Chand R., Shiraishi F., (2013), Reaction mechanism of photocatalytic decomposition of 2, 4-dinitrophenol in aqueous suspension of TiO₂ fine particles, *Chemical Engineering Journal*, **233**, 369-376.
- Chelba A., Arsene D., Morosanu I., Tofan L., Teodosiu C., (2014), Secondary municipal effluent treatment by catalytic wet hydrogen peroxide oxidation, *Environmental Engineering and Management Journal*, **13**, 2401-2410.
- Das J., Aziz M.A., Yang H., (2006), A nanocatalyst-based assay for proteins: DNA-free ultrasensitive electrochemical detection using catalytic reduction of p-nitrophenol by gold-nanoparticle labels, *Journal of the American Chemical Society*, **128**, 16022-16023.
- Diaconu I., Nechifor G., Nechifor A.C., Ruse E., Totu E.E., (2009a) Membrany techniques used at the separation of some phenolic compounds from aqueous media, *UPB Scientific Bulletin, Series B: Chemistry and Materials Science*, **71**, 61-70.
- Diaconu I., Nechifor G., Nechifor A.C., Totu E.E., Ruse E., (2009b), The transport of nitrophenols through liquid membranes, *Chemistry Magazine*, **60**, 1243-1246.
- Diaconu I., Gîrdea R., Cristea C., Nechifor G., Ruse E., Totu E.E., (2010a), Removal and recovery of some phenolic pollutants using liquid membranes, *Romanian Biotechnological Letters*, **15**, 5703.
- Diaconu I., Ruse E., Totu E.E., Nechifor G., (2010b), Partition studies in biphasic systems of nitrophenols, *Chemistry Magazine*, **61**, 718-720.
- Diaconu I., Aboul-Enein H.Y., Al-Omar M.A., Nechifor G., Ruse E., Bunaciu A.A., Totu E.E., (2011), Separation of nitrophenols. Equilibriums in bi- and tri-phasic systems, *Arabian Journal of Chemistry*, **4**, 99-103.
- Diaconu I., Zaharia I., Ruse E., Radu D.A., (2012), Kinetic aspects of transport para-aminophenol through agitated bulk liquid membrane, *Chemistry Magazine*, **63**, 153-158.
- EC Directive, (1975), Council Directive 75/440/EEC of 16 June 1975 concerning the quality required of surface water intended for the abstraction of drinking water in the Member States, *Official Journal of the European Communities*, **L194**, 26-31.
- Galaction A.I., Cascaval D., (2004), New extraction techniques on bioseparations: 2. Pertraction, direct extraction, *Hemijiska industrija*, **58**, 535-547.
- Gubbuk I.H., Gungor O., Alpoguz H.K., Ersoz M., Yilmaz M., (2010), Kinetic study of mercury (II) transport through a liquid membrane containing calix [4] arene nitrile derivatives as a carrier in chloroform, *Desalination*, **261**, 157-161.
- Harrison M.A., Barra S., Borghesi D., Vione D., Arsene C., Olariu I.R., (2005), Nitrated phenols in the atmosphere: a review, *Atmospheric Environment*, **39**, 231-248.

- Jia L., Wang D., Liu L., Zhang S., Xu T., (2014), Preparation of novel poly (amide-sulfonamide)(PASA) and its application in 2, 4-dinitrophenol adsorption, *Designed Monomers and Polymers*, **17**, 425-429.
- Jiang P., Zhou J., Zhang A., Zhong Y., (2010), Electrochemical degradation of p-nitrophenol with different processes, *Journal of Environmental Sciences*, **22**, 500-506.
- León G., Guzman M.A., (2008), Facilitated transport of copper through bulk liquid membranes containing different carriers: compared kinetic study, *Desalination*, **223**, 330-336.
- Lezamiz J., Jönsson J.Å., (2007), Development of a simple hollow fibre supported liquid membrane extraction method to extract and preconcentrate dinitrophenols in environmental samples at ng L⁻¹ level by liquid chromatography, *Journal of Chromatography A*, **1152**, 226-233.
- Liteanu C., Hopârtean E., (1972), *Analytical Chemistry. Volumetric Analysis* (in Romanian), Didactic and Pedagogical Press, Bucharest, Romania.
- Minhas F.T., Memon S., Bhanger M.I., (2010), Transport of Hg (II) through bulk liquid membrane containing calix [4] arene thioalkyl derivative as a carrier, *Desalination*, **262**, 215-220.
- Olteanu C., Szczepanski P., Orbeci C., Lica C.G., Costache L., Diaconu I., (2013), Study of the transport of chromium, manganese and zinc through bulk liquid membrane using D2EHPA and Cyanex 301 as a carrier, *Revista de Chimie*, **64**, 925-929.
- Religa P., Gawroński R., Gierycz P., (2009), Kinetics of chromium (III) transport through a liquid membrane containing DNNSA as a carrier, *International Journal of Molecular Sciences*, **10**, 964-975.
- Szczepański P., Diaconu I., (2012), Transport of p-nitrophenol through an agitated bulk liquid membrane, *Separation Science and Technology*, **47**, 1725-1732.
- U.S.EPA, (2009), Water Quality Criteria, U.S.EPA, Washington DC.
- Zaharia I., Diaconu I., Nechifor G., (2012a), The pH role in the transport of active principles of drugs through agitated bulk liquid membrane, *UPB Scientific Bulletin, Series B: Chemistry and Materials Science*, **74**, 61-70.
- Zaharia I., Diaconu I., Ruse E., Nechifor G., (2012b), The transport of 3-aminophenol through bulk liquid membrane in the presence of Aliquat 336, *Digest Journal of Nanomaterials and Biostructures*, **7**, 1303-1314.
- Zaharia I., Aboul-Enein H.Y., Diaconu I., Ruse E., Bunaciu A.A., Nechifor G., (2013), Facilitated transport of 5-aminosalicylic acid through bulk liquid membrane, *Journal of the Iranian Chemical Society*, **10**, 1129-1136.
- Zhang W., Liu J., Ren Z., Wang S., Du C., Ma J., (2009), Kinetic study of chromium (VI) facilitated transport through a bulk liquid membrane using tri-n-butyl phosphate as carrier, *Chemical Engineering Journal*, **150**, 83-89.
- Zheng Y., Liu D., Xu H., Zhong Y., Yuan Y., Xiong L., Li, W., (2009), Biodegradation of p-nitrophenol by *Pseudomonas aeruginosa* HS-D38 and analysis of metabolites with HPLC-ESI/MS, *International Biodeterioration & Biodegradation*, **63**, 1125-1129.



“Gheorghe Asachi” Technical University of Iasi, Romania



SIMPLE ECO-FRIENDLY β -GALACTOSIDASE IMMOBILIZATION ON FUNCTIONALIZED MAGNETIC PARTICLES FOR LACTOSE HYDROLYSIS

Kalim Belhacene¹, Elena Florentina Grosu², Alexandra Cristina Blaga²,
Pascal Dhulster¹, Mariana Pinteala³, Renato Froidevaux^{1*}

¹Charles VIOLLETTE Institute– Equipe Laboratoire des Procédés Biologiques, Génie Enzymatique et Microbien (ProBioGEM)
– EA 1026, Université Lille 1 – Sciences et Technologies, Villeneuve d’Ascq, France

²“Gheorghe Asachi” Technical University of Iasi, Faculty of Chemical Engineering and Environmental Protection,
Department of Organic, Biochemical and Food Engineering, 73 Prof. Dr. docent Dimitrie Mangeron Str., 700050 Iasi, Romania

³“Petru Poni” Institute of Macromolecular Chemistry of Romanian Academy, Center of Advanced Research in
Bionanoconjugates and Biopolymers, 41A Aleea Grigore Ghica Voda, 700487 Iasi, Romania

Abstract

β -galactosidase from *Aspergillus oryzae* was strongly immobilized on magnetic particles functionalized with amino groups. By simple incubation without any activating agents, electrostatic interactions between amino groups and enzymes allowed obtaining a strong linkage. The immobilization efficiency was studied with the quantification of amino groups of the particles and of immobilized β -galactosidase. Kinetic parameters, especially the maximal velocity V_{max} and the affinity K_m , were determined with two substrates, o-NPG and lactose, and compared with free enzyme values in order to evaluate the influence of our immobilization methodology on the kinetic behavior of the enzyme. Therefore, magnetic capacity of the functionalized particles allows recovering and reusing the support. Results show efficient immobilization of β -galactosidase (58 μ g/mg of support), able to hydrolyze substrates during multiple cycles of use. Thus, magnetic particles functionalized with amino groups represent an attractive support for simple and efficient β -galactosidase immobilization process.

Key words: β -galactosidase, immobilization, lactose, magnetic, particles

Received: November, 2014; Revised final: March, 2015; Accepted: March, 2015

1. Introduction

β -galactosidase is an important enzyme biocatalyst used in food industry for the hydrolysis of lactose (Kim et al., 2001) necessary for lactose-intolerant people (Carpio et al., 2000). In addition, this enzyme catalyzes the formation of galacto-oligosaccharides, which are prebiotic additives for the so-called “healthy foods” (Matsumoto et al., 1989). However, since the price of β -galactosidase is quite high, the direct addition of the enzymes to the substrate is economically unacceptable (Mahoney,

1997). Immobilised β -galactosidase biocatalyst can be reused several times, which decrease the costs of the process (Genari et al., 2003). Several studies have been carried out to immobilize this enzyme to enhance the biotechnological conversion of food lactose in bioreactors (Roy and Gupta, 2003). The performance of an immobilized enzyme is mainly governed by the properties of supporting materials, the technique used to immobilize the enzyme, and the nature of reactor used (packed bed, fluidized bed or membrane reactor) (Marangoni, 2005; Roy and Gupta, 2003).

* Author to whom all correspondence should be addressed: e-mail: renato.froidevaux@univ-lille1.fr; Phone: +33(0)320417566; Fax: +33(0)328767356

A great number of methodologies (adsorption, covalent bonding, direct cross-linking, and entrapment) have been described to attach β -galactosidase to supports such as polymeric films, beads and fibrous matrices. However, most of the traditional methods require toxic reagents, surfactants, silanes or cross-linking agents such as glutaraldehyde, which may have detrimental effects on food and human health (Tanaka and Kawamoto, 1999).

Recent interest in nanotechnology has provided a wealth of diverse scaffolds (Xu et al., 2014) that could potentially support enzyme immobilization due to their potential applications in biotechnology (Sun et al., 2012), immunosensing and biomedical areas (Li et al., 2014). Immobilization of enzymes is advantageous for commercial application due to convenience in handling, ease of separation of enzymes from the reaction mixture and reuse, low product cost and a possible increase in thermal and pH stability (Husain, 2010; Lei et al., 2002; Tischer and Wedekind, 1999; Wang, 2006). An important requirement for protein immobilization is that the matrix should provide a biocompatible and inert environment (Krug, 2009), i.e. it should not interfere with the native structure of the protein, which thereby could compromise its biological activity (Mitchell et al., 2002).

Magnetic fields have been utilized in support systems to study enzyme immobilization (Bayramoglu et al., 2008; Gupta and Gupta, 2005; Kuroiwa et al., 2008; Pimentel et al., 2007; Selim et al., 2007). Several magnetic particles and magnetic supports such as microspheres of various biomaterials, encapsulating the magnetic particles and copolymers with magnetic particles have been used with good results (Dyal et al., 2003; Koneracka et al., 2002; Kouassi et al., 2005; Saiyed et al., 2003). The high surface to volume ratio provided by the magnetic particles favors high binding capacity and high catalytic specificity of the enzyme (Johnson et al., 2008; Konwarh et al., 2009). In addition, magnetic field susceptibility revealed a mechanism for efficient recovery of the enzyme complex thereby preventing the enzyme contamination of the final product.

A novel and efficient immobilization of β -galactosidase from *Aspergillus oryzae* was recently developed by using magnetic Fe_3O_4 -chitosan particles as support (Pan et al., 2009). The magnetic Fe_3O_4 -chitosan particles were prepared by electrostatic adsorption of chitosan onto the surface of Fe_3O_4 particles made through co-precipitation of Fe^{2+} and Fe^{3+} . β -galactosidase was covalently immobilized onto the composites using glutaraldehyde as activating agent. The immobilization process was optimized by examining immobilized time, crosslinking time, enzyme concentration, glutaraldehyde concentration, and initial pH values of glutaraldehyde and enzyme solution. As a result, the immobilized enzyme presented a higher storage, pH and thermal stability

than the soluble enzyme. Galactooligosaccharides were formed with lactose as substrate by using the immobilized enzyme as biocatalyst with a maximum yield of 15.5% (w/v) obtained when 50% lactose was hydrolyzed (Pan et al., 2009). In the same way, Neri et al. (2008) immobilized β -galactosidase also on polysiloxane-polyvinyl alcohol magnetic composite for lactose hydrolysis using glutaraldehyde as activating agent for immobilization (Neri et al., 2008).

All these cases of immobilization implied the preparation of support with an activating agent, like glutaraldehyde necessary for immobilization process. The utilization of this kind of agent entails risk for the user and for the environment. In this work, we used magnetic particles functionalized with amino groups to immobilize β -galactosidase only by promoting the electrostatic interactions between the amino groups and the enzyme. With this methodology, we avoided the utilization of chemicals and toxics and thus proposed a support able to retain enzyme and maintain its activity for substrate hydrolysis.

The kinetic of the hydrolysis of synthetic (o-NPG) and natural (lactose) substrate was studied, both with the β -galactosidase in solution and immobilized on functionalized magnetic particles. Firstly, some preliminary research was carried out to determine the number of amine functions on the magnetic particle surface and the immobilization capacity. Secondly, kinetic studies have been performed in a range of concentrations of substrates. With the kinetic data obtained, a comparison was performed using Lineweaver-Burk representations in order to determine the effect of immobilization on the activity of the enzyme.

2. Materials and methods

2.1. Materials

β -galactosidase (β -D-galactoside galactohydrolase, E.C. 3.2.1.23, 10.4U/mg, MW: 105kDa) from *Aspergillus oryzae* was purchased by Sigma-Aldrich Chemical Co. Synthetic β -galactosidase substrate purchased from Sigma-Aldrich Chemical Co. *ortho*-nitrophenyl- β -D-galactopyranoside (o-NPG, $\text{C}_{12}\text{H}_{15}\text{NO}_6$, MW 301.3g/mol) was prepared in 0.02M sodium acetate buffer for UV-visible measurements. In order to inactivate the enzyme in experiments where the feasibility of the process was tested, 1M Na_2CO_3 solution was prepared. All aqueous solutions were prepared in distilled water.

The immobilization support was hydrophilic magnetite particles functionalized with amine groups gifted by the Institute of Macromolecular Chemistry "Petru Poni", Iasi, Romania. These particles were constituted by a magnetic ferric core and hydrophobic shell formed by an oleic acid-oleylamine complex which modified by aminosilane monomer (Durdureanu-Angheluta et al., 2012).

2.2. Determination of the number of amine functions on the magnetic particles

In order to characterize the immobilization potential of the functionalized magnetic particles, the number of amino groups was determined by chemical tag using the 4-nitrobenzaldehyde (4-NBA). This compound reacts with the primary amine functions to form a Schiff base (Fig. 1) (Abbas, 2009). A 4-NBA 2mM solution was prepared in anhydrous methanol and incubated with a quantity of particles during 4h at 50°C. Then, the particles were washed twice 5 minutes by ethanol and methanol and dried. Finally, the particles were re-suspended in 3mL of distilled water containing 20 μ L of acetic acid during 15h at 50°C to hydrolyze the Schiff base formed. After hydrolysis, the solution was recovered and the quantity of 4-NBA was determined by spectrophotometry at 267nm and compared with a range of different concentrations of 4-NBA.

2.3. β -galactosidase immobilization on functionalized magnetic particles

One milligram of particles were weighed on microbalance (Sartorius ISO 9001 microbalance) and transferred on Eppendorf tube, washed with distilled water and sonicated fastly in order to homogenate the mix. After, the water was removed and the particles were dried and conserved at room temperature before utilization. Then, the dried particles were re-suspended in 1mL of acetate sodium buffer 0.02M pH4.5 containing 1mg of β -galactosidase. The particle and enzyme solutions were incubated together during one night at 4°C under agitation. After incubation, the mix was centrifuged and β -galactosidase solution was removed. Particles were washed several times with buffer solution to eliminate the non-fixed enzymes. The buffer used for the wash was conserved for released enzyme determination. Particles were stored dry at 4°C before enzymatic tests.

2.4. Determination of the immobilized β -galactosidase quantity

The determination of the quantity of immobilized enzyme was necessary to establish the immobilization capacity of the functionalized magnetic particles and also to determine the specific activity after carrying out of our immobilization procedure in comparison with free β -galactosidase. Then, the non-immobilized enzyme was quantified after incubation and also after particle wash, and was subtracted from the initial quantity of enzyme. For this, different quantities of particles (0.250 mg, 0.500 mg, 0.750 mg and 1mg) were incubated with 1mg of β -galactosidase on buffer, under agitation at 4°C during a night. After incubation, the mix was centrifuged at 13400 rpm, and the supernatant was removed and conserved for the enzyme quantification. Particles were washed by 1mL of

buffer solution under agitation at 4°C, centrifuged and the supernatant was removed. 6 cycles of wash were done, and the buffer was conserved for enzyme quantification. The quantity of β -galactosidase was determined by enzyme test with the synthetic substrate o-NPG. 100 μ L of buffer used for the wash were introduced in 2 mL of o-NPG 10mM. After 10 minutes, the reaction was stopped by addition of 1mL of Na₂CO₃ 1M. The absorbance of the sample was measured by spectrophotometer at 415nm. Using range of o-NP, the reaction rate of the sample was calculated and compared with a range of reaction rate determined in function of enzyme concentrations (0.01, 0.05, 0.1, 0.5 and 1mg/mL), allowing the determination of enzyme quantity (Fig. 2).

2.5. Determination of immobilized β -galactosidase activity

Two substrates were used to determine the catalytic efficiency of enzyme free and immobilized on functionalized magnetic particles: o-NPG and lactose.

2.5.1. With synthetic o-NPG substrate

The determination of β -galactosidase activity was investigated with o-NPG (o-nitrophenyl B-d-galactopyranoside) prepared in sodium acetate buffer 0.02M pH4.5. Hydrolysis gave a colored product (o-NP) easy to analyze by absorbance. Enzyme was introduced in 10mL of o-NPG, under agitation. 500 μ L were collected at different times (each minute until 10 minutes and after 15, 20, 30, 45 and 60 minutes) and mixed with 250 μ L of Na₂CO₃ 1M to stop the reaction. Collected samples were analyzed at 415nm (UV/visible spectrophotometer, Ultraspec 1100 pro, Amersham Biosciences).

For immobilized β -galactosidase on functionalized magnetic particles, substrate solution was carried out with the particles and enzymatic activity was determined with the same protocol that for free β -galactosidase. After reaction, particles were collected and washed 3 times to eliminate the potential fixation of substrate or product.

For each condition (free and immobilized β -galactosidase), in order to determine the kinetic parameters of the enzyme, different concentrations of substrate were tested (0.5, 1, 2, 5 and 10mM), the concentration of product was quantified with a range of o-NP and parameters were calculated using Michaelis-Menten and Lineweaver-Burk representations.

2.5.2. With lactose substrate

Lactose was used in order to evaluate the variation of the catalytic performance with a substrate commonly encountered in industrial process. 1mg of enzyme was introduced in 10mL of different concentration of lactose (10mM, 25mM, 50mM and 100mM prepared in acetate buffer 0.02M pH 4.5, under agitation. 300 μ L were collected at different times (each minute until 10 minutes and

after 15, 20, 30, 45 and 60 minutes) and mixed with 150 μ L of Na₂CO₃ 1M to stop the reaction. 10 μ L of the mix were added on 1mL of glucose enzymatic kit and incubated at 37°C during 10 minutes.

The glucose produced during the hydrolysis reaction reacted with the glucose oxydase to produce hydrogen peroxide which reacted with peroxydase to obtain a colored product (quinoneimine). Then, the sample was analyzed at 505nm to determine the quantity of glucose produced and compared with a range of glucose (Fig. 3). For immobilized β -galactosidase, 1mg of functionalized magnetic particles were mixed with different concentrations of lactose (80, 100, 150 and 200mM) and the reaction was studied with the same protocol that for free enzyme. Kinetic parameters were also determined with Michaelis-Menten and Lineweaver-Burk representations.

2.6. Performance of immobilized β -galactosidase on functionalized magnetic particles

In order to prove the efficiency of the immobilization procedure, the performance of the immobilized enzymes was evaluated by several activity tests with the same particles. An amount of 1mg of functionalized magnetic particles was introduced in 10mL of o-NPG 10mM. Each minute until 10 minutes then after 15, 20, 30, 45 and 60 minutes, 300 μ L were collected and mixed with 150 μ L of Na₂CO₃ 1M to stop the reaction.

Samples collected were analyzed at 415nm. The same experiment was reproduced 10 times. The reaction rate of immobilized enzyme, for each experiment, was calculated with the Michaelis-Menten equation.

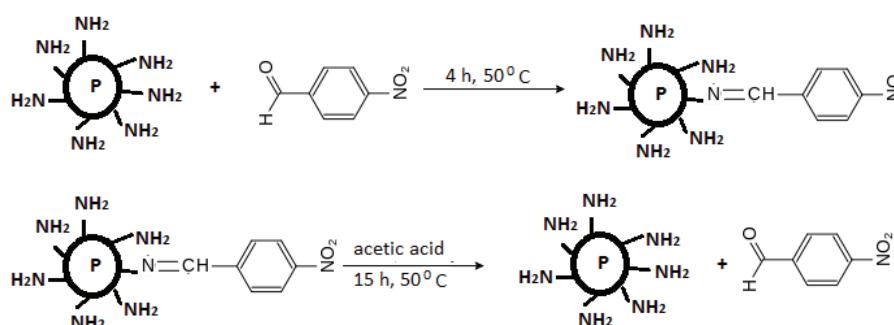


Fig. 1. Principle of reaction between amino groups and NBA; NBA is complexed with amino groups to form a Schiff base which is hydrolyzed in acidic conditions to release NBA analyzable at 267nm

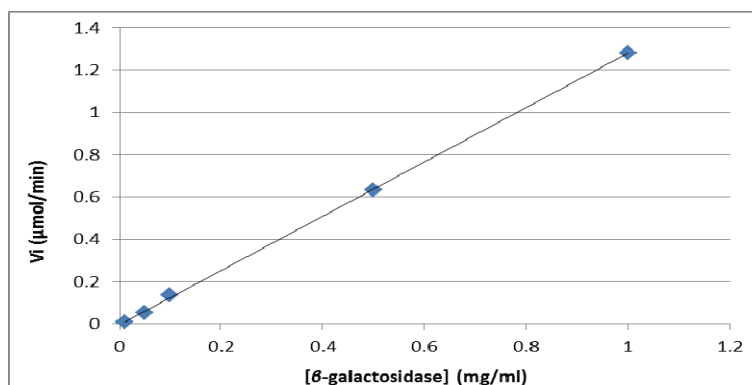


Fig. 2. Range of enzyme reaction rate in function of β -galactosidase concentration

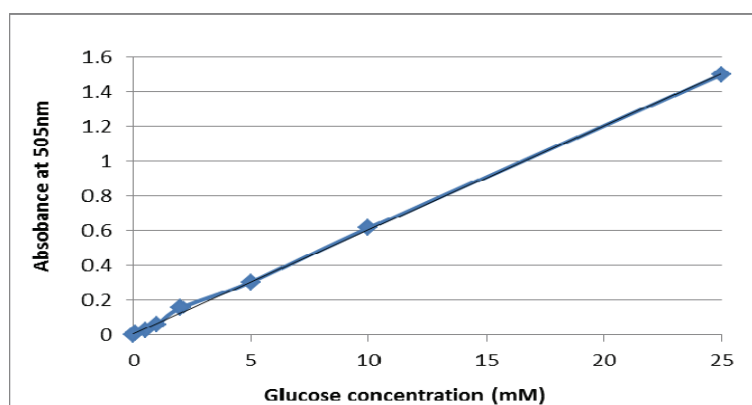


Fig. 3. Determination of glucose concentration with Glucose RTU

3. Results and discussion

3.1. Chemical characterization of magnetic particle surface

The magnetic particles used in our study were constituted by a ferric core covered by an oleic acid shell and functionalized with 3-aminopropyltriethoxysilane, leading to amino groups on the surface of the particles (Durdureanu-Angheluta et al., 2012).

In order to determine the potential of immobilization, the number of amino groups was calculated. For this, the labeling method using 4-NitroBenzAldehyde (4-NBA) as tag was used (Abbas, 2009) with four different quantities of particles (Table 1). Results allowed characterizing the chemical surface of the magnetic particles and we observed a good proportionality between the number of amine functions and the quantity of particles. Therefore, 1 mg of particles contains about $4.1 \cdot 10^{17}$ amine functions.

3.2. Immobilization capacity of functionalized magnetic particles

In order to determine the quantity of immobilized β -galactosidase, the quantity of non-adsorbed enzyme and the mass balance were calculated after each wash of functionalized magnetic particles, and compared with the initial quantity carried out. These quantities were determined with a range of reaction rate in function of the concentration of enzyme (Fig. 2). The quantity of enzyme was resumed in the Table 1. After incubation of particles with 1mg of enzyme, the solution contained between 92 and 97% of the initial quantity of enzyme (Fig. 4). Results showed a very good proportionality of the quantity of enzyme immobilized in function of particles quantity (Fig. 5). Therefore, one milligram of functionalized magnetic particles was able to immobilize 58 μ g of β -galactosidase.

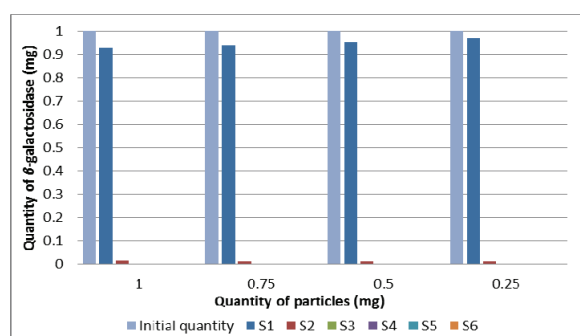


Fig. 4. Quantification of β -galactosidase after each step of particle treatment

3.3. Determination of kinetic parameters

The activity of free and immobilized β -galactosidase was determined according to the hydrolysis of synthetic substrate o-NPG.

In the study with free β -galactosidase, 100 μ g of enzyme were introduced with 10 milliliters of different concentrations of o-NPG (0.5, 1, 2, 5 and 10mM) under agitation. Each minute, 500 μ L were collected, mixed with 250 μ L of Na_2CO_3 1M and analyzed at 415nm. The kinetic parameters (K_m and V_{max}) were determined from the Lineweaver-Burk representation.

Concerning the study with immobilized β -galactosidase, one milligram of functionalized magnetic particles was introduced in 10 milliliters of o-NPG solutions (0.5, 1, 2, 5 and 10mM) under agitation. The kinetic parameters for the immobilized β -galactosidase were determined with the same procedure than with free enzyme. The values were resumed in the Table 2.

Table 1. Quantification of the number of amine functions in function of the quantity of functionalized magnetic particles

| | 0.250mg | 0.500mg | 0.750mg | 1mg |
|---------------------------|----------------------|----------------------|----------------------|----------------------|
| Concentration of NBA (mM) | 0.052 | 0.115 | 0.173 | 0.235 |
| Number of amine functions | $0.94 \cdot 10^{17}$ | $2.09 \cdot 10^{17}$ | $3.09 \cdot 10^{17}$ | $4.15 \cdot 10^{17}$ |

Table 2. Kinetic parameters of free and immobilized β -galactosidase determined with o-NPG

| | K_m (mM) | V_{max} ($\mu\text{mol}/\text{min}$) | Specific V_{max} ($\mu\text{mol}/\text{min}/\text{mg}$) | K_{cat} (s^{-1}) | K_{cat}/K_m ($\text{mM}^{-1} \cdot \text{s}^{-1}$) |
|------------------------------------|------------|--|---|-------------------------------|--|
| Free β -galactosidase | 1.899 | 1.044 | 10.44 | 17.85 | 9.39 |
| Immobilized β -galactosidase | 5.82 | 0.62 | 10.68 | 18.72 | 3.21 |

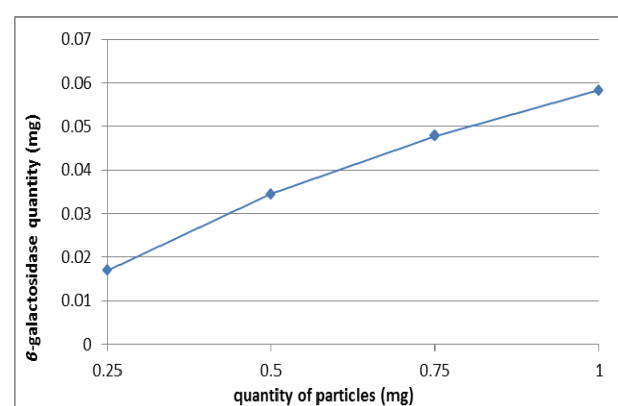


Fig. 5. Quantity of β -galactosidase immobilized in function of the quantity of functionalized magnetic particles

Results show a decrease of the maximal velocity V_{max} and an important increase of the K_m , translating a high decrease of the affinity of immobilized β -galactosidase for the substrate. Indeed, in the immobilized case, β -galactosidase adsorbed on the magnetic particles causes diffusional

limitations and consequently limited access to the active sites. Then, this phenomenon could be logically responsible of the kinetic parameter differences between free and immobilized β -galactosidase. However, when the values of V_{max} were calculated in function of the quantity of enzyme, we observed the same specific V_{max} values, indicating that our immobilization procedure did not affect the reaction rate of enzyme.

These results were confirmed with the values of the catalytic constant K_{cat} that was the same for free and immobilized β -galactosidase (~95% conserved in immobilized form compared with free form). Finally, catalytic efficiency values were different (3 times higher for free than for immobilized enzymes), translating a decrease of the global specificity of enzyme for this substrate, probably caused by the immobilization conditions of enzyme on the particles.

To conclude, the hydrolysis of o-NPG by β -galactosidase immobilized on functionalized magnetic particles showed a good conservation of the catalytic efficiency but the process slightly affected the affinity of enzyme for its substrate.

3.4. Efficiency of the immobilization procedure

The more significant advantage when enzyme immobilization is investigated is the ability to reuse the materials with adsorbed enzyme and its influence on the enzyme activity. Then, in order to evaluate the efficiency of our immobilization procedure, 11 cycles of o-NPG hydrolysis were carried out with the same functionalized magnetic particles with immobilized β -galactosidase. The residual activity was then calculated after each cycle and resumed in Fig. 6.

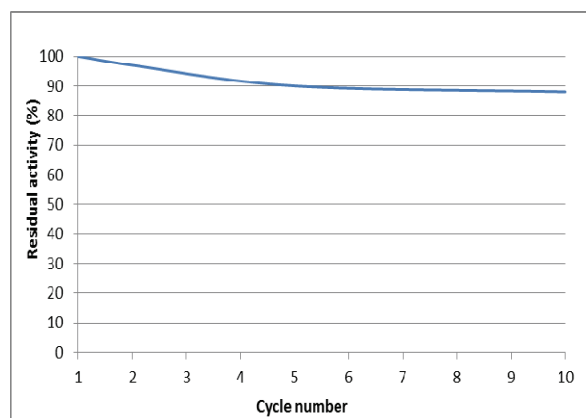


Fig. 6. Residual activity of immobilized β -galactosidase obtained after several cycles of o-NPG hydrolysis

Results show that the residual activity of immobilized β -galactosidase decreases of only 10% after 5 wash cycles. Then, the enzyme activity is always maintained after 10 cycles. This result demonstrates the efficiency of our immobilization procedure on functionalized magnetic particles and the possibility of immobilized β -galactosidase reuse while conserving its activity.

3.5. Lactose hydrolysis by β -galactosidase immobilized on functionalized magnetic particles

Hydrolysis of lactose was carried out with β -galactosidase immobilized on functionalized magnetic particles and kinetic was compared with those realized with free enzyme. Concerning the study with free β -galactosidase, one milligram of enzyme was introduced in 10mL of different concentrations of lactose (10, 25, 50 and 100mM) under agitation. Each minute, 300 μ L were collected and analyzed in order to determine the quantity of glucose produced.

Concerning the study with β -galactosidase in immobilized state, one milligram of particles was introduced in 3mL of different concentrations of lactose (80, 100, 150 and 200mM) under agitation. For each study, the kinetic of lactose hydrolysis was represented using Michaelis-Menten and Lineweaver-Burk representations (Figs. 7 and 8) and kinetic parameters were then determined in the Table 3. Results show a very important increase of K_m (45 folds) associated with a decrease of V_{max} (6 folds).

The specific enzyme activity and the catalytic constant were then affected, translating a strong impact of the immobilization process on the apparent enzyme activity. Therefore, the catalytic efficiency value was very low when the β -galactosidase was immobilized (15 folds lower than in free state), caused by the high value of K_m . By comparing the results of kinetic parameters between the two substrates (Tables 2 and 3), we observe a strong impact of our immobilization procedure on lactose hydrolysis comparing to o-NPG hydrolysis.

It seems that the diffusional effects further influence the hydrolysis kinetic, probably due to the strong quantity of enzyme molecules immobilized on the magnetic particle surface. Indeed, the surface characterization showed an important quantity of amino groups allowing the immobilization of a high amount of β -galactosidase.

However, this high quantity would strongly limit the lactose accessibility to the active sites of the enzyme, also affecting its kinetic behavior. Solution could be to decrease the quantity of β -galactosidase immobilized on the functionalized magnetic particles in order to favor its catalytic efficiency.

4. Conclusions

Utilization of magnetic particles functionalized with amino groups allowed immobilizing β -galactosidase for obtaining biofunctional support able to hydrolyze synthetic (oNPG) and natural (lactose) substrate. This support retains its activity after several assays, demonstrating the efficiency of our immobilization procedure. Without use of chemical products for immobilization process, such as glutaraldehyde commonly used, this kind of magnetic particles constitutes an interesting alternative for green process.

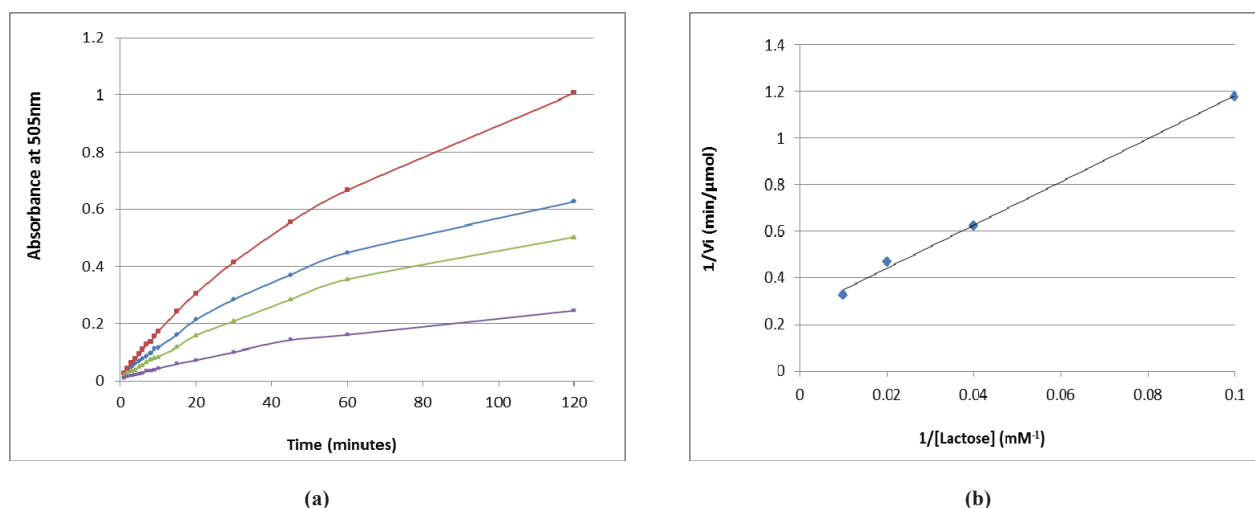


Fig. 7. Determination of kinetic parameters of free β -galactosidase for lactose hydrolysis with different concentrations of substrate (10mM, 25mM, 50mM and 100mM) with 1mg of enzyme and using Michaelis-Menten (a) and Lineweaver-Burk (b) representations

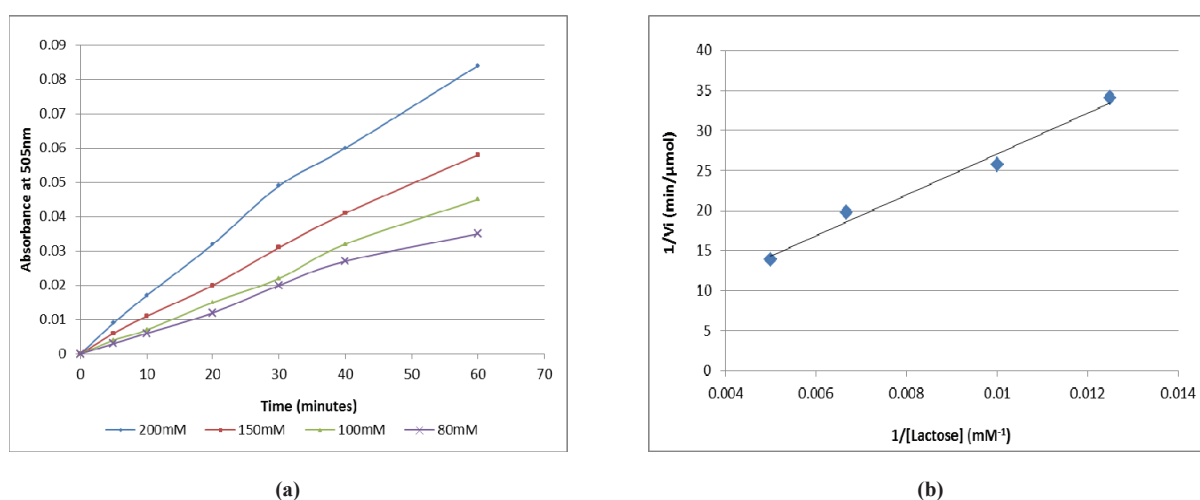


Fig. 8. Determination of kinetic parameters of β -galactosidase immobilized on one milligram of functionalized magnetic particles. Reaction carried out was lactose hydrolysis for different concentrations (80, 100, 150 and 200mM) using Michaelis-Menten (a) and Lineweaver-Burk (b) representations

Table 3. Kinetic parameters of free and immobilized β -galactosidase determined with lactose

| | K_m (mM) | V_{max} (μ mol/min) | Specific V_{max} (μ mol/min/mg) | K_{cat} (s^{-1}) | K_{cat}/K_m ($mM^{-1}.s^{-1}$) |
|------------------------------------|------------|----------------------------|--|------------------------|------------------------------------|
| Free β -galactosidase | 36 | 3.89 | 38.9 | 6.80 | 0.189 |
| Immobilized β -galactosidase | 1639 | 0.64 | 11.03 | 19.38 | 0.012 |

Moreover, the magnetic property of the particles facilitates the manipulation during the hydrolysis application and allows a fast recovery after utilization. Therefore, a continuous process for lactose hydrolysis could be envisaged.

References

- Abbas A., Vivien C., Bocquet B., Guillochon D., Supiot P., (2009), Preparation and multicharacterization of plasma polymerized allylamine films, *Plasma Processes and Polymers*, **6**, 593-604.
- Bayramoğlu G., Kiralp S., Yilmaz M., Toppare L., Arica M.Y., (2008), Covalent immobilization of chloroperoxidase onto magnetic beads: Catalytic properties and Stability, *Biochemical Engineering Journal*, **38**, 180-188.
- Carpio C., Gonzalez P., Ruales J., Batista-Viera F, (2000), Bone-bound enzymes for food industry application, *Food Chemistry*, **68**, 403-409.
- Durdureanu-Angheluta A., Dascalu A., Fifer A., Coroaba A., Pricop L., Chiriac H., Tura V., Pinteala M., Simionescu B.C., (2012), Progress in the synthesis and characterization of magnetite nanoparticles with amino

- groups on the surface, *Journal of Magnetism and Magnetic Materials*, **324**, 1679-1689.
- Dyal A., Loos K., Noto M., Chang S.W., Spagnoli C., Shafi K., Ulman A., Cowman M., Gross R.A., (2003), Activity of *Candida rugosa* lipase immobilized on γ -Fe₂O₃ magnetic nanoparticles, *Journal of American Chemical Society*, **125**, 1684-1685.
- Genari A.N., Passos F.V., Passos F.M.L., (2003), Configuration of bioreactor for milk lactose hydrolysis, *Journal of Dairy Science*, **86**, 2783-2789.
- Gupta A.K., Gupta M., (2005), Synthesis and surface engineering of iron oxide nanoparticles for biomedical applications, *Biomaterials*, **26**, 3995-4021.
- Husain Q., (2010), β Galactosidase and their potential applications, *Critical Review in Biotechnology*, **30**, 41-62.
- Johnson A.K., Zawadzka A.M., Deobald L.A., Crawford R.L., Paszczynski A.J., (2008), Novel method for immobilization of enzymes to magnetic nanoparticles, *Journal of Nanoparticle Research*, **10**, 1009-1025.
- Kim J.H., Lee D.H., Lee J.S., (2001), Production of galactooligosaccharide by galactosidase from *Kluyveromyces maxianus* var *lactis* OE-20, *Biotechnology and Bioprocess Engineering*, **6**, 337-340.
- Koneracka M., Kopčanský P., Timko M., Ramchand C.N., De Sequeira A., Trevan M., (2002), Direct binding procedure of proteins and enzymes to fine magnetic particles, *Journal of Molecular Catalysis B: Enzymatic*, **18**, 13-18.
- Konwarh R., Karak N., Rai S.K., Mukherjee A.K., (2009), Polymer-assisted iron oxide magnetic nanoparticle immobilized keratinase, *Nanotechnology*, **20**, 25-35.
- Kouassi G.K., Irudayaraj J., McCarty G., (2005), Examination of cholesterol oxidase attachment to magnetic nanoparticles, *Journal of Nanobiotechnology*, **3**, 1-9.
- Krug H.F., (2009), *Nanotechnology*, Vol. 2, *Environmental Aspects*, Wiley-VCH Verlag GmbH & Co. KGaA, Weinheim.
- Kuroiwa T., Noguchi Y., Nakajima M., Sato S., Mukataka S., Ichikawa S., (2008), Production of chitosan oligosaccharides using chitosanase immobilized on amylase coated magnetic nanoparticles, *Process Biochemistry*, **43**, 62-69.
- Lei C., Shin Y., Liu J., Ackerman E.J., (2002), Entrapping enzyme in a functionalized nanoporous support, *Journal of American Chemical Society*, **124**, 11242-11243.
- Mahoney R.R., (1997), *Lactose: Enzymatic Modification*, P. F. Fox Chapman and Hall, New York.
- Marangoni A.G., (2005), *Enzyme Kinetics: a Modern Approach*, Wiley-VCH Verlag GmbH & Co. KGaA, Weinheim.
- Matsumoto K., Kobayashi Y., Tamura N., Watanabe Y., Kan T., (1989), Production of galactooligosaccharides with β -galactosidase, *Denpun Kagaku*, **36**, 123-130.
- Mitchell D.T., Lee S.B., Trofin L., Li N., Nevanen T.K., Soderlund H., martin C.R., (2002), Smart nanotubes for bioseparations and biocatalysis, *Journal of American Chemical Society*, **124**, 11864-11865.
- Neri D.F.M., Balcao V.M., Carneiro-da-Cunha M.G., Carvalho L.G., Teixeira Jr J.R., (2008), Immobilization of β -galactosidase from *Kluyveromyces lactis* onto a polysiloxane-polyvinyl alcohol magnetic (mPOS-PVA) composite for lactose hydrolysis, *Catalysis Communications*, **9**, 2334-2339.
- Pan C., Hu B., Li W., Sun Y., Ye H., Zeng X., (2009), Novel and efficient method for immobilization and stabilization of β -D-galactosidase by covalent attachment onto magnetic Fe₃O₄-chitosan nanoparticles, *Journal of Molecular Catalysis B: Enzymatic*, **6**, 208-215.
- Pimentel M.C.B., Leao A.B.F., Melo E.H.M., Ledingham W.M., Lima-Filho J.L., Sivewright M., (2007), Immobilization of *Candida rugosa* lipase on magnetized dacron: kinetic study, *Artificial Cells Blood Substitutes and Biotechnology*, **35**, 21-35.
- Roy I., Gupta M.N., (2003), Lactose hydrolysis by LactozymTM immobilized on cellulose beads in batch and fluidized bed modes, *Process Biochemistry*, **39**, 325-332.
- Saiyed Z.M., Telang S.D., Ramchand C.N., (2003), Application of magnetic techniques in the field of drug discovery and biomedicine, *Biomagnetic Research Technology*, **1**, 2-8.
- Selim K.M.K., Ha Y.S., Kim S.J., Chang Y., Kim T.J., Lee G.H., et al., (2007), Surface modification of magnetite nanoparticles using lactobionic acid and their interaction with hepatocytes, *Biomaterials*, **28**, 710-716.
- Sun L., Yihan Li Y., Yang P., Zhu G., Dovichi N.J., (2012), High efficiency and quantitatively reproducible protein digestion by trypsin-immobilized magnetic microspheres, *Journal of Chromatography A*, **1220**, 68-74.
- Tanaka A., Kawamoto T., (1999), Cell and Enzyme Immobilization, *American Society for Microbiology*, Washington, **94**, 504-513.
- Tischer W., Wedekind F., (1999), Immobilized enzymes: methods and applications, *Topics in Current Chemistry*, **200**, 95-126.
- Wang P., (2006), Nanoscale biocatalyst systems, *Current Opinion in Biotechnology*, **17**, 574-579.
- Xu Y., Li C., Zhu X., Huang W.E., Zhang D., (2014), Application of magnetic nanoparticles in drinking water purification, *Environmental Engineering and Management Journal*, **13**, 2023-2029.



"Gheorghe Asachi" Technical University of Iasi, Romania



REMOVAL OF CARBAMAZEPINE BY ELECTROCOAGULATION: INVESTIGATION OF SOME KEY OPERATIONAL PARAMETERS

**Tania Yehya^{1,2}, Lidia Favier^{3,4*}, Yassine Kadmi^{3,4}, Fabrice Audonnet^{1,2},
Nidal Fayad^{1,2}, Maria Gavrilescu^{5,6}, Christophe Vial^{1,2}**

¹Clermont Université, Université Blaise Pascal, Institut Pascal, 24 avenue des Landais, BP 20206, 63174 Aubière cedex, France

²CNRS, UMR 6602, IP, 63171 Aubière, France

³Ecole Nationale Supérieure de Chimie de Rennes, CNRS, UMR 6226, 11 Allée de Beaulieu,
CS 50837, 35708 Rennes Cedex 7, France

⁴Université Européenne de Bretagne, France

⁵"Gheorghe Asachi" Technical University of Iasi, Faculty of Chemical Engineering and Environmental Protection,
Department of Environmental Engineering and Management, 73 Prof. dr. docent Dimitrie Mangeron Str., Iasi 700050, Romania

⁶Academy of Romanian Scientists, 54 Splaiul Independentei, RO-050094 Bucharest, Romania

Abstract

The performance of electrocoagulation (EC) process, a non-specific electrochemical technology, was investigated for the removal of carbamazepine (CBZ), an antiepileptic drug, from water. Experiments were carried out in synthetic wastewater in a batch cell. The respective influences of some key process parameters were studied, such as mixing conditions, initial pH, and current on aluminium electrodes. Experimental results showed that a CBZ removal efficiency of 62% was observed under slightly acidic initial conditions (pH 4) with a current density as high as 44 mA cm⁻² ($I=4.5$ A) using Al electrode. This clearly indicates that CBZ removal proceeds through an electrochemical mechanism, while the adsorption of CBZ onto the aluminum hydroxide flocs was shown to be negligible. Furthermore, the increase of initial pH to alkaline values was shown to decrease the drug elimination efficiency. Conversely, as expected, an increase of current intensity improved the removal of CBZ. As a result, low initial pH 4 coupled with high current elevates the electrochemical elimination of CBZ: in this case, one metabolite could also be detected.

Key words: carbamazepine, electrocoagulation, micropollutants removal, wastewater treatment

Received: November, 2014; Revised final: March, 2015; Accepted: March, 2015

1. Introduction

Water resources are contaminated when pollutants are directly or indirectly discharged into wastewater without adequate treatment to remove harmful compounds. This provides a serious threat to human health on one side, and to plants and organisms living in these bodies of water on the other side (Aziz et al., 2010; Caliman et al., 2002). Water contamination has been caused over decades by a number of natural and anthropogenic pollutions, such as the spillage of pesticides and herbicides in

agriculture, hospital discharges, industrial discharges, for example, industries involving fuels, wood preserving operations and textile production. This leads to the presence of rather different types of pollutions, such as organic products which derive for example from agro-food waste, home and personal care products, textile dyes, pharmaceuticals, but may also correspond to heavy metals cations or oxianions, or to inorganic anions, in particular sulfide, fluoride, and nitrate.

Pharmaceuticals and their bioactive metabolites are continuously introduced in the

* Author to whom all correspondence should be addressed: e-mail: lidia.favier@ensc-rennes.fr; Phone: +33223238135; Fax: +33223238120

aquatic environment, where they are detected at trace concentrations (i.e. found in the ng L^{-1} or $\mu\text{g L}^{-1}$ range, so that they are often referred to as “micropollutants”), and become pseudo-persistent (Caliman and Gavrilescu, 2009; Gavrilescu et al., 2015; Semrany et al., 2012; Sirés et al., 2012). First, most pharmaceuticals are not completely degraded after ingestion and they may be excreted directly or also produce secondary pollutants, i.e. metabolites and subsequently enter and harm the aquatic ecosystem. This results in the detection of pharmaceutically active compounds, such as lipid-regulating drugs, analgesics, antibiotics, antiseptics, antidiabetics, barbiturates, beta-agonists, psychiatrics, receptor antagonists, hormones, and chemotherapy and beta-blocking heart drugs in wastewaters, streams, and ground-water resources. Their occurrence in the environment is mainly due to:

1. the excretion of the fraction of pharmaceuticals that are not metabolized by human or animal bodies into wastewater, or their metabolites;
2. the discharge of unused or expired medications;
3. the discharge of hospital wastewater;
4. the residues from pharmaceutical manufacturing.

Carbamazepine (CBZ), commercialized as *Tegretol* (Zhang et al., 2008), is a pharmaceutical imminostilbene derivative, and a lipophilic, neutral tricyclic compound (Atkins et al., 2013; Bahlmann et al., 2014). It is mainly used as an anticonvulsant drug, and also as a specific analgesic for trigeminal neuralgia (Popa et al., 2014; Rao et al., 2010). Its efficacy and safety profiles have made it first choice for adults. It is administered chronically in high dosages of 100-2000 mg daily and, hence, its annual production is high (Kosjek et al., 2009). Approximately 72% of orally administered carbamazepine is absorbed, while 28% is unchanged and subsequently discharged through the faeces (Zhang et al., 2008). Environmental studies confirm the presence of CBZ as one of the most frequently detected pharmaceuticals in the effluents of sewage treatment plants, in river and sea water (Miao et al., 2005), in comparison to the other pharmaceutical micropollutants in Europe, America and Asia. For instance, the presence of CBZ has been reported at concentrations about $6.3 \mu\text{g L}^{-1}$ in wastewater, $1.1 \mu\text{g L}^{-1}$ in surface water, and $30 \mu\text{g L}^{-1}$ in drinking water (Mohapatra et al., 2014) in Canada. It has also been detected about 2300 ng L^{-1} in Canada in a wastewater effluent and about 258 ng L^{-1} in the USA, but below 10 ng L^{-1} in Germany (Metcalf et al., 2003). As a consequence, health-based guidance values have been established for CBZ upon fishery products consumption in both marine and freshwater, such as $2000 \mu\text{g/kg}_{\text{biota}}$ or $130 \mu\text{g L}^{-1}$.

Due to the persistence and toxic effects of this molecule, various water remediation technologies have been investigated to remove CBZ from

wastewater and drinking water, including conventional biological and physicochemical treatments, but also advanced oxidation and biological processes. Several studies showed that, the abatement yield of CBZ by the conventional activated sludge process is limited (typically below 10%) due to its high resistance to biodegradation, independent from hydraulic retention times (Hata et al., 2010).

Other studies have been investigated the removal efficiency of this molecule by white-rot fungi. A CBZ elimination yield of about 60% was obtained with fungal laccase, an enzyme from *Trametes versicolor* after 48h of treatment (Hata et al., 2010), while less than 10% CBZ elimination were achieved after treatment with membrane bioreactors using *Pseudomonas sp.* (Li et al., 2013). The efficiency of physicochemical treatments, such as coagulation and flocculation/flotation, was also investigated and these did not operate rather better than biological treatments, with typical yields of CBZ elimination from 20% to 35% (Carballa et al., 2005; Suarez et al., 2008). Conversely, many contributions from the literature showed that ozonation and advanced oxidation processes (AOPs) including Fenton, photo-Fenton and heterogeneous photocatalysis could be more efficient for the removal of this molecule from wastewater. For example, ozonation was found to remove up to 99% CBZ (Hua et al., 2006); UV/hydrogen peroxide in the presence of 25 mg L^{-1} of H_2O_2 promoted the elimination of 90% CBZ at 2.25 J cm^{-2} UV dose (Shu et al., 2013); Fenton and photo-Fenton process could possibly achieve a complete elimination of CBZ by Fenton oxidation (Mohapatra et al., 2013), and heterogeneous photocatalytic processes with more than 90% elimination (Doll and Frimmel, 2005; Martínez et al., 2011). However, AOPs are highly expensive for wastewater treatment (Betianu et al., 2008; Sirés et al., 2012). Other cheaper treatments such as electrodeposition, electrocoagulation, electroflotation, electrodisinfection, electrooxidation, and electroreduction are important alternatives for wastewater treatment, due to their high efficiency in pollution abatement, easy operation, and compact facilities (Al-Shannag et al., 2014; Behbahani et al., 2013).

The objective of this paper is to investigate the potential applicability of electrocoagulation process (EC), an electrochemical treatment, as a possible way to remove CBZ from water and wastewater. Up to now, electrochemical methods have been disregarded in the literature for the removal of CBZ. This paper will also analyze how CBZ removal is affected by mixing conditions, pH, and current intensity which is the major process parameter of EC.

2. Experimental

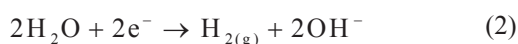
In this study, EC was applied to investigate CBZ removal from synthetic water in which the

initial concentration C_0 of CBZ is 12.5 mg L^{-1} . All solutions were prepared with carbamazepine of analytical purity (99%) supplied by *Sigma-Aldrich* (France). The composition of the synthetic water includes also KCl (6.33 g L^{-1}) as a supporting electrolyte. The initial conductivity of water is 2.8 mS cm^{-1} and pH is 8.2. Initial pH is then adjusted between 4 and 9 by the minute addition of either 0.1 M hydrochloric acid or sodium hydroxide solutions.

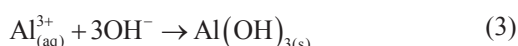
For EC process, two rectangular aluminum electrodes were used as the anode and the cathode, of surface area $S=102 \text{ cm}^2$ each, with an inter-electrode distance of 1 cm. EC consists of the controlled electrodisolution of the anodic material, as shown by Eq. (1).



At the cathode, hydrogen gas is released through the electroreduction of water (Eq. 2).



When pH is between 4 and 10, aluminium cations rapidly form insoluble oxyhydroxides and hydroxides, which readily precipitate and form flocs. This is usually summarized as given by Eq. (3).



As a result, several mechanisms can promote pollution removal, among which:

1. the coagulation of colloids or slightly soluble species;
2. the adsorption of pollutants onto the flocs;
3. the electrooxidation or electroreduction of the pollutants onto the electrodes.

To enhance these mechanisms, the EC cell consisted of a batch reactor of volume $V=4.0 \text{ L}$, mechanically stirred using a standard Rushton turbine. Tests were carried out in an intensiostatic mode by means of a *BK-Precision* (USA) generator with a current (I) ranging between 1.5A and 4.5A. The electrolysis time of each run ranged between 30 and 120 minutes. The respective effects of mixing speed (from 100 to 400 rpm), current, and initial pH (pH_i) were investigated. Experiments were done at room temperature under atmospheric pressure.

Analytical tools can be summarized as follows. The conductivity and the pH of the solution were recorded online. The concentration of soluble CBZ at time t (C_t) was obtained using a sampling procedure, followed by HPLC analysis (*Waters 2410*, UV, France) under isocratic mode using a C18 column (*Waters SAS*, Symmetry, France). The mobile phase consisted of a solution of acetonitrile (*Sigma-Aldrich*, France) and ultra-pure water at 30:70 (v/v). The flow rate was 0.5 mL.min^{-1} , leading to a retention time of 20 min for CBZ when detected at a wavelength of 230 nm. Total organic carbon in

the liquid phase was measured using a total organic carbon analyzer (*TOC-V CSN*, *Shimadzu*, Japan). At the end of EC experiment, the flocs recovered by decantation or flotation were filtered, washed, and dried at 105°C overnight before being weighted. BET surface area of the flocs was then estimated using nitrogen adsorption (*Tristar II*, *Micromeritics Instr.*, USA). To detect the presence of adsorbed species on the dried solid, the solid phase was dissolved using a 0.1 N HCl solution and, then, subjected to chemical analysis using the total organic carbon analyzer and the HPLC described above. Fig. 1 summarizes the experimental setup coupled with analytical tools.

3. Results and discussion

3.1. Influence of mixing and initial pH using Al electrodes

Preliminary results were devoted to the analysis of the influence of mixing conditions. The rotation speed of the Rushton turbine was varied between 100 and 400 rpm and its potential influence on CBZ removal was investigated. Results showed that this parameter had a limited effect in the studied range on the CBZ removal.

This means that regardless of the mechanism of depollution (oxidoreduction at the electrodes or adsorption onto the flocs), there is no apparent limitation due to mass transfer in the EC process which is in accordance with other EC studies done on wastewater containing nitrate (Yehya et al., 2014) or for the removal of trivalent chromium (Golder, 2006).

This is of utmost importance because both oxidoreduction and adsorption may be controlled by mass transfer. For this work, a rotation speed of 100 rpm has been finally retained for the Rushton turbine: this presents not only the advantage to prevent swirl, but also reduces the power input for mixing purpose.

Unlike the effect of the stirring rate which can be easily overcome, pH is always the key parameter affecting the elimination of pollutants by EC both in terms of effectiveness and operating cost (Chafi et al., 2011). In a batch cell, pH varies with time and only the initial pH, pH_i , can be controlled. Accordingly, experimental data highlighted a strong influence of pH_i on the abatement of CBZ over time during EC.

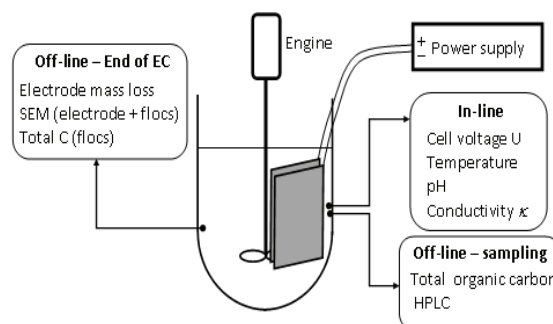


Fig. 1. Experimental setup

Concerning CBZ, it is known to have two pKa values of 13.9 and -0.49; this means that it is out of our pH range (4 to 9), and that it would be always chemically stable. However, the results obtained have shown a different behavior than expected. Fig. 2 highlighted a poor removal yield of CBZ when pH_i was 6 or 9, with values lower than 10% after 120 min of electrolysis, with a slightly higher yield when pH_i was 4. Conversely, CBZ was shown to be removed more efficiently when pH_i corresponded to acidic pH values, *i.e.* when pH_i was 4. Under these conditions the eliminated CBZ amount was up to 62%.

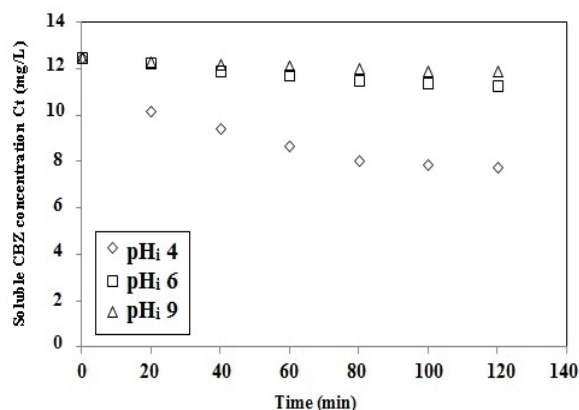


Fig. 2. Effect of initial pH during EC on the abatement of CBZ over time at $I=3\text{A}$

As pH increases during the EC process, the elimination rate of CBZ decreases, this means that CBZ removal mainly occurs when pH is between 4 and 6. This is clearly confirmed by Fig. 3: a sharp decrease of CBZ content is observed within the first five minutes, when pH varies rapidly from 4 to 6. Then, CBZ concentration passes through a plateau region when pH varies from 6 to 8.6, and then decreases again, but far slower when pH is equal or higher than 9.

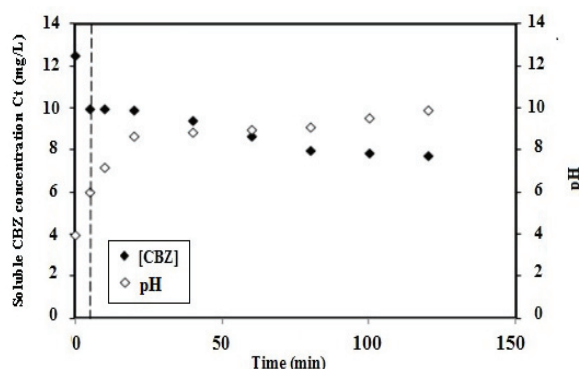


Fig. 3. Effect of the change of pH during EC on the abatement of CBZ at $I=3\text{A}$ and $\text{pH}_i 4$, as a function of time

Similar changes of pH can be observed at different current values, as shown in Fig. 4 at $I=4.5\text{A}$. This figure also shows that final pH values are close, regardless of pH_i after 120 min, which means that final pH cannot be correlated to CBZ removal yield. Moreover, it was observed that, initial pH also

affected the amount of flocs formed at the end of EC. This varied from 7.3, 9.8 and 6.1 g in the conditions of Fig. 4 when the initial pH increased from 4, 6 and 9 after 120 min of electrolysis, respectively.

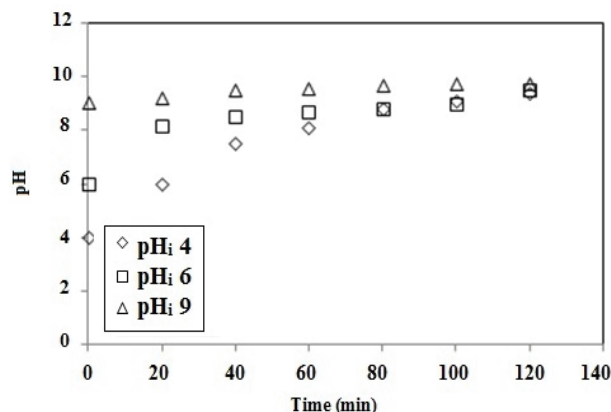


Fig. 4. Effect of initial pH on the change of pH over time during EC at $I=4.5\text{A}$

These results agree with the speciation of aluminium: soluble Al^{3+} cations dominate at low pH, soluble aluminate anions $\text{Al}(\text{OH})_4^-$ prevail at a pH higher than 10 and the insoluble $\text{Al}(\text{OH})_3$ hydroxides reign at intermediate pH. As a result, initial pH equal to 6 maximizes the mass of flocs because their formation is impaired only at the end of EC, while it is reduced at the beginning and the end when pH_i is 4 and during a large part of the electrolysis time when pH_i is 9. However, as for the final pH, no correlation could be found between the mass of flocs and CBZ removal yield.

This indicates that adsorption is unlikely to be the mechanism governing the CBZ elimination. On the contrary, HPLC highlighted the presence of a metabolite that was detected at the same wavelength as CBZ, but with a far smaller retention time (3 min). As there was no other organic compound in the synthetic water, this could only derive from CBZ. In addition, the increase in concentration of this new compound was always observed in parallel with a decrease of the CBZ concentration. As a result, its content was maximized at the end of electrolysis and was observed mainly when pH_i was 4.

A typical evolution of the metabolite production with time can be seen in Fig. 5 in which the areas of the detected peaks are compared because this compound has not been identified yet. This confirms the idea that an oxidoreduction mechanism at the electrode surface is responsible for CBZ removal.

3.2. Influence of current

The new set of experimental runs was dedicated to the study of the influence of the current intensity I on CBZ elimination using EC with Al electrodes. The results showed that an increase of current results in an acceleration of the CBZ removal at all pH_i values (Fig. 6) in particularly at $\text{pH}_i 4$ (Fig.

6a). It was shown that the elimination was rapid at early times during EC and slowed down during the EC process.

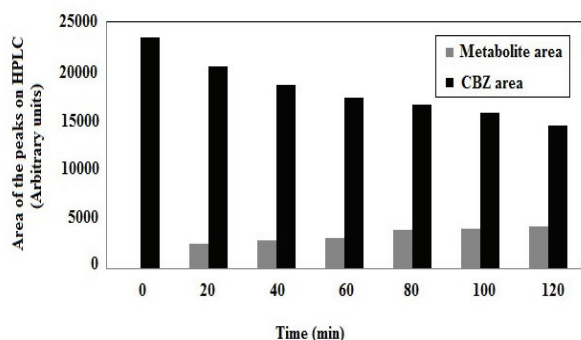


Fig. 5. Bar graph showing the peak area of a CBZ metabolite and of CBZ detected by HPLC during EC at pH_i 4 and $I=4.5A$ as a function of time

The reason is the elevation of pH and the consequent decrease in the probable oxidoreduction rate of CBZ. Current was also found to have an effect on the amount of Al^{3+} released and hence on the amount of flocs formed. Results obtained from the HPLC analysis showed the effect of the current intensity on the metabolite concentration that increased with the increase of current and with the decrease of CBZ concentration. It was also found that the pH change rate depended strongly on the current applied to the EC unit.

The highest current employed, led to the fastest rate of pH change during EC (Fig. 7) for all values of initial pH. The reason is the elevation of pH and the consequent decrease in the probable oxidoreduction rate of CBZ. Current was also found to have an effect on the amount of Al^{3+} released and hence on the amount of flocs formed.

Results obtained from the HPLC analysis showed the effect of the current intensity on the metabolite concentration that increased with the increase of current and with the decrease of CBZ concentration. It was also found that the pH change rate depended strongly on the current applied to the EC unit. The highest current employed, led to the fastest rate of pH change during EC (Fig. 7) for all values of initial pH.

3.3. Speciation of the liquid and the solid phases

The analyses of the liquid sample at $t=120$ min during EC at $I=4.5A$ and pH 4 on the HPLC found that almost 62% of CBZ has disappeared. The HPLC analysis showed that the disappearance of CBZ, was accompanied by the appearance of a new molecule that would possibly be a metabolite of CBZ having it appearing at the same wavelength of CBZ. If there was no adsorption on the solid phase or no gas release, 100% of the initial carbon should be found in the liquid samples when tested on the total organic carbon analyzer at nearly all times.

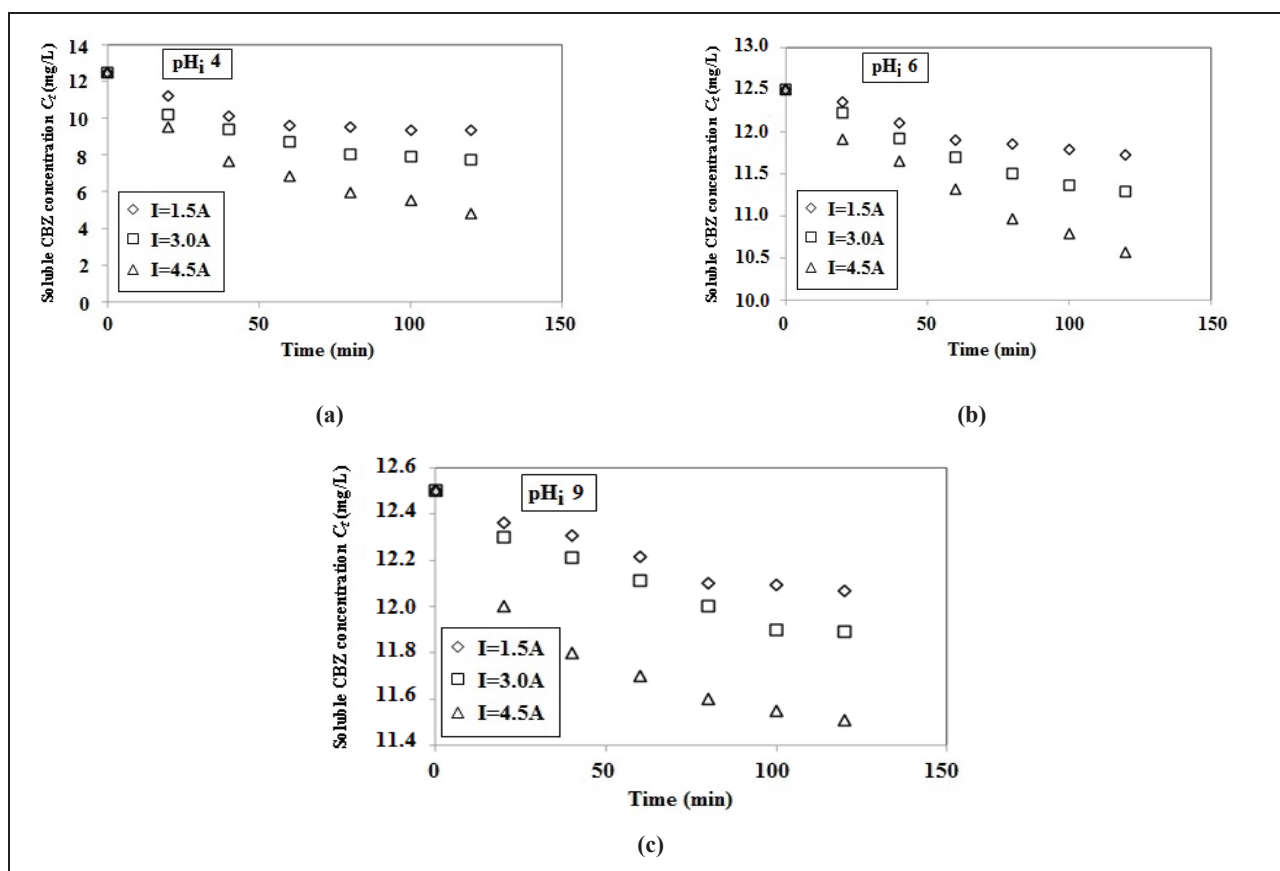


Fig. 6. Effect of current intensity on CBZ elimination: (a) at pH_i 4, (b) at pH_i 6, (c) at pH_i 9

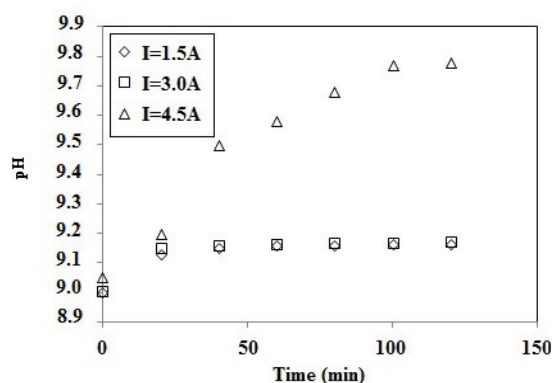


Fig. 7. Effect of current on the change of pH with pH_i 9

However, the amount of carbon found in the liquid samples when tested on the total organic carbon analyzer was about 79-82% of the initial amount of carbon found in CBZ particularly after $t=20$ min where the corresponding pH is around 7. So, this means that the rest (around 21%) was either been adsorbed on the solids throughout the experiment or released as CO_2 . Analysis of the solid phase by nitrogen adsorption isotherm showed that it exhibited a high specific surface area as the BET method provided values that varied between 200 and $320 \text{ m}^2 \text{ g}^{-1}$ floc as a function of current.

The dissolution of the flocs of EC with 0.1M HCl showed, by the analysis done on the total organic carbon analyzer, the presence of carbon entities on the solid phase that increase with the increase of current and the decrease of pH_i . The amount of these carbon entities comprises almost 20% of the total amount of carbon found as the form of CBZ at the beginning of EC.

The same samples were passed on the HPLC to test for the adsorbed species and revealed that the metabolite was found on the flocs with no minimal presence of CBZ. The inability of CBZ to adsorb on the flocs was confirmed at all the pH used in this study: the same solid phase was produced with the same composition, however, with no CBZ being added. Then, the solids were added to CBZ solutions of different concentrations. The solids were set in contact with CBZ for 24 hrs to attain equilibrium in order to test for adsorption. Analyzing the solutions on the total carbon analyzer showed no decrease of the CBZ concentration, hence no CBZ adsorption on the solid phase.

The total amount of carbon (on the solid phase and in the solution) depending on what is obtained from the total organic carbon is almost 98%, accounting for experimental error, from which we can conclude that there was no release of gaseous CO_2 , or no formation of HCO_3^- or CO_3^{2-} anions in water.

Thus, we conclude that the elimination of CBZ by EC at $I=4.5A$ and pH_i 4 is primarily an oxidoreduction mechanism comprising the change of 62% of initial CBZ concentration into a metabolite which in turn adsorbs onto the flocs at a relatively

neutral pH comprising 20% of the initial carbon amount found in CBZ.

4. Conclusions

The electrochemical treatment of a biorefractory pharmaceutical molecule, CBZ, has been tested in this work using EC process. Collected data demonstrate that the CBZ is apt to electrochemical oxidoreduction reactions. CBZ was found to be eliminated mostly at pH 4 and at the highest current density of 44 mA cm^{-2} (4.5A) on Al electrodes.

The CBZ was shown to exhibit the highest elimination at pH between 4 and 6. The solid phase was found to capture a new molecule, a probable metabolite of CBZ comprising 20% of its initial carbon content. The increase of the concentration of the soluble and the adsorbed metabolite is in harmony with the decrease of CBZ. Compared to other biological and physicochemical treatments, EC was proven to be more effective in the treatment of CBZ from water than many other conventional techniques. Moreover, by optimizing the parameters of EC, this latter can be used rather than the expensive AOP treatments.

References

- Al-Shannag M., Al-Qodah Z., Alananbeh K., Bouqellah N., Assirey E., Bani-Melhem K., (2014), COD reduction of baker's yeast wastewater using batch electrocoagulation, *Environmental Engineering and Management Journal*, **13**, 3153-3160.
- Atkins S., Jimenez-Perez R., Sevilla J.M., Blazquez M., Pineda T., Gonzalez-Rodriguez J., (2013), Electrochemical reduction of carbamazepine in ethanol and water solutions using a glassy carbon electrode, *International Journal of Electrochemical Sciences*, **8**, 2056-2068.
- Aziz H.A., Noor M.M., Omran A., (2010), Chemical oxidation of treated textile effluent by hydrogen peroxide and Fenton process, *Environmental Engineering and Management Journal*, **9**, 351-360.
- Bahlmann A., Brack W., Schneider R.J., Krauss M., (2014), Carbamazepine and its metabolites in wastewater: Analytical pitfalls and occurrence in Germany and Portugal, *Water Research*, **57**, 104-114.
- Behbahani M., Moghaddam M.R.A., Arami M., (2013), Phosphate removal by electrocoagulation process: optimization by response surface methodology method, *Environmental Engineering and Management Journal*, **12**, 2397-2405.
- Betianu C., Caliman F.A., Gavrilescu M., Cretescu I., Cojocaru C., Poullos I., (2008), Response surface optimization of Orange II photocatalytic degradation in TiO_2 aqueous suspensions, *Journal of Chemical Technology and Biotechnology*, **11**, 316-326.
- Caliman A.F., Teodosiu C., Balasanian I., (2002), Applications of heterogeneous photocatalysis for industrial wastewater treatment, *Environmental Engineering and Management Journal*, **1**, 187-196.
- Caliman A.F., Gavrilescu M., (2009), Personal care compounds, pharmaceuticals and endocrine disrupting

- agents in the environment – A review, *CLEAN – Soil, Air, Water*, **34**, 277-303.
- Carballa M., Omil F., Lema J.M., (2005), Removal of cosmetic ingredients and pharmaceuticals in sewage primary treatment, *Water Research*, **39**, 4790-4796.
- Chafi M., Gourich B., Essadki A.H., Vial C., Fabregat A., (2011), Comparison of electrocoagulation using iron and aluminium electrodes with chemical coagulation for the removal of a highly soluble acid dye, *Desalination*, **281**, 285-292.
- Doll T.E., Frimmel F.H., (2005), Photocatalytic degradation of carbamazepine, clofibric acid and iomeprol with P25 and Hombikat UV100 in the presence of natural organic matter (NOM) and other organic water constituents, *Water Research*, **39**, 403-411.
- Gavrilescu M., Demnerova K., Aamand J., Agathos S., Fava F., (2015), Emerging pollutants in the environment: present and future challenges in biomonitoring, ecological risks and bioremediation, *New Biotechnology*, **32**, 147-156.
- Golder A.K., (2006), Removal of trivalent chromium by electrocoagulation, *Separation and Purification Technology*, **53**, 33-41.
- Hata T., Shintate H., Kawai S., Okamura H., Nishida T., (2010), Elimination of carbamazepine by repeated treatment with laccase in the presence of 1-hydroxybenzotriazole, *Journal of Hazardous Materials*, **181**, 1175-1178.
- Hua W., Bennett E.R., Letcher J.R., (2006), Ozone treatment and the depletion of detectable pharmaceuticals and atrazine herbicide in drinking water sourced from the upper Detroit River, Ontario, Canada, *Water Research*, **40**, 2259-2566.
- Kosjek T., Andersen H., Kompare B., Ledin A., Heath E., (2009), Fate of carbamazepine during water treatment, *Environmental Science & Technology*, **43**, 6256-6261.
- Li A., Cai R., Cui D., Qiu T., Pang C., Yang J., Ma F., Ren N., (2013), Characterization and biodegradation kinetics of a new cold-adapted carbamazepine-degrading bacterium, *Pseudomonas* sp. CBZ-4, *Journal of Environmental Sciences*, **25**, 2281-2290.
- Metcalf C.D., Koenig B.G., Bennie D.T., Servos M., Ternes T.A., Hirsch R., (2003), Occurrence of neutral and acidic drugs in the effluents of Canadian sewage treatment plants, *Environmental Chemistry Letters*, **22**, 2872-2880.
- Martínez C., Canle M., Fernández M.I., Santaballa J.A., Fariab J., (2011), Kinetics and mechanism of aqueous degradation of carbamazepine by heterogeneous photocatalysis using nanocrystalline TiO₂, ZnO and multi-walled carbon nanotubes-anatase composites, *Applied Catalysis B: Environmental*, **102**, 563-571.
- Miao X.S., Yang J.J., Metcalfe C.D., (2005), Carbamazepine and its metabolites in wastewater and in biosolids in a municipal wastewater treatment plant, *Environmental Science and Technology*, **39**, 7469-7475.
- Mohapatra D.P., Brar S.K., Tyagi R.D., Picard P., Surampalli R.Y., (2013), A comparative study of ultrasonication, Fenton's oxidation and ferros-sonication treatment for degradation of carbamazepine from wastewater and toxicity test by Yeast Estrogen Screen (YES) assay, *Science of the Total Environment*, **447**, 280-285.
- Mohapatra D.P., Brar S.K., Tyagi R.D., Picard P., Surampalli R.Y., (2014), Analysis and advanced oxidation treatment of a persistent pharmaceutical compound in wastewater and wastewater sludge-carbamazepine, *Science of the Total Environment*, **470-471**, 58-75.
- Popa C., Favier L., Dinica R., Semrany S., Djelal H., Amrane A., Bahrim G., (2014), Potential of newly wild *Streptomyces* strains as agents for the biodegradation of a recalcitrant pharmaceutical, carbamazepine, *Environmental Technology*, **35**, 3082-3091.
- Rao S.K., Belorkar N., (2010), Development and validation of a specific stability indicating liquid chromatographic method for carbamazepine in bulk and pharmaceutical dosage forms, *Journal of Advanced Pharmaceutical Research*, **1**, 36-47.
- Sembrany S., Favier L., Djelal H., Taha S., Amrane A., (2012), Bioaugmentation: possible solution in the treatment of Bio-refractory organic compounds (Bio-ROCs), *Biochemical Engineering Journal*, **69**, 75-86.
- Sirés I., Brillas E., (2012), Remediation of water pollution caused by pharmaceutical residues based on electrochemical separation and degradation technologies: a review, *Environment International*, **40**, 212-229.
- Shu Z., Bolton J.R., Belosevic M., El Din J.M., (2013), Photodegradation of emerging micropollutants using the medium-pressure UV/H₂O₂ Advanced Oxidation Process, *Water Research*, **47**, 2881-2889.
- Suarez S., Carballa M., Omil F., (2008), How are pharmaceutical and personal care products (PPCPs) removed from urban wastewaters?, *Reviews in Environmental Science and Biotechnology*, **7**, 125-138.
- Yehya T., Chafi M., Balla W., Vial C., Essadki A., Gourich B., (2014), Experimental analysis and modeling of denitrification using electrocoagulation process, *Separation and Purification Technology*, **132**, 644-654.
- Zhang Y., Geißen S.U., Gal C., (2008), Carbamazepine and diclofenac: Removal in wastewater treatment plants and occurrence in water bodies, *Chemosphere*, **73**, 1151-1161.



“Gheorghe Asachi” Technical University of Iasi, Romania



IMPACT OF URBANIZATION ON URBAN HEAT ISLAND EFFECT BASED ON TM IMAGERY IN WUHAN, CHINA

Qijiao Xie¹, Zhixiang Zhou^{2*}

¹*School of Resources and Environmental Science, Hubei University, 430062 Wuhan, China*

²*College of Horticultural & Forestry Science/Key Laboratory of Horticultural Plant Biology (Ministry of Education),
Huazhong Agricultural University, 430070 Wuhan, China*

Abstract

As natural landscapes are increasingly replaced by impervious surface materials associated with urbanization, urban areas tend to experience higher surface temperatures when compared to rural areas, which is known as the urban heat island (UHI) effect. In this study the impact of urbanization on land surface temperature (LST) and the UHI effect were examined based on two Landsat Thematic Mapper (TM) imageries of 1987 and 2007. Results show that Wuhan experienced rapid urban expansion from 1987 to 2007, while the areal extent with higher temperatures did not always correspond to the urbanized area. The percent impervious surface area (ISA) was found to efficiently explain the LST variation in urban areas, especially in high-density ones. The normalized difference vegetation index (NDVI) was a sufficient indicator to express surface temperature variation only in natural context. These findings help urban planners and greening designers make appropriate decisions on urban planning and thermal management.

Key words: impervious surface area, land surface temperature, normalized difference vegetation index, remote sensing, urban thermal environment

Received: March, 2012; Revised final: April, 2013; Accepted: May, 2013

1. Introduction

One of the environmental consequences of urbanization and industrialization is the urban heat island (UHI) effect, a phenomenon of higher atmospheric and surface temperatures occurring in urban areas than in surrounding rural areas (Gluch et al., 2006; Voogt and Oke, 2003). Higher urban temperatures generally result in adverse economic and environmental impacts locally, regionally and globally. Persistent higher temperatures increase the demand for air conditioning, raise pollution levels, change urban thermal environments and ultimately lead to thermal discomforts and incidence of heat-related illnesses.

The UHI effect is essentially a thermal pollution caused by human activity and regarded as a

powerful force in local climate change (Du et al., 2007; Lubert and McGeehin, 2008; Zheng et al., 2014). With the rapid increase of population and buildings in urban areas, anthropogenic waste heat released from vehicles, air conditioners, power plants and industries have steadily increased (Manea et al., 2013), which heats up the urban environment directly. Urban development can tremendously alter the urban surface structures by replacing natural landscapes with a large expanse of non-evaporating impervious surfaces such as concrete and asphalt (Oke, 1982; Owen et al., 1998; Tang et al., 2014). Physical change of the urban surface (albedo, thermal capacity, heat conductivity) can affect urban surface temperatures by altering the sensible and latent heat exchange between the urban surface and boundary layers (Frey and Parlow, 2012; Mohan and Kandya,

* Author to whom all correspondence should be addressed: e-mail: whzhouzx@mail.hzau.edu.cn; Phone: +86-27-87284232; Fax: +86-27-87282010

2015). The land surface temperature (LST) will unavoidably propagate both downward into the subsurface (Baker and Baker, 2002; Taniguchi et al., 2005) and upward into atmosphere (Brazel et al., 2007; Jin et al., 2011; Jones et al., 1990). Then surface, subsurface and air urban heat islands can be detected (Roth et al., 1989; Voogt and Oke, 2003).

Urbanization typically leads to the reduction of green spaces in urban areas, which modifies urban surface water content and vegetation cover (Owen et al., 1998). Research found that, with regard to the surface energy balance, latent heat exchange was dominant in more vegetated areas, while sensible heat exchange was dominant in impervious areas (Oke, 1982). This finding is attracting mounting attention on the relationship between LST and urban vegetation. Much emphasis has been placed on the relationship between LST and the normalized difference vegetation index (NDVI) (Gallo et al., 1993; Lo et al., 1997; Nonomura et al., 2009; Owen et al., 1998; Price, 1990; Reynolds et al., 2008) or other NDVI-related parameters, such as vegetation abundance (Gillies and Carlson, 1995; Lo et al., 1997; Weng, 2001) and vegetation fraction (Gutman and Ignatov, 1998; Weng et al., 2004). Results indicate that there is a negative correlation between LST and NDVI, which is valuable for UHI and urban climate studies.

On the other hand, much attention was paid on land cover changes associated with urbanization and their impact on LST (Fabrizi et al., 2010; Hamdi, 2010; Liu and Zhang, 2011; Xiong et al., 2012). The rapid changes of land use and land cover in urban areas result in the increase of impervious surface areas (ISA) in urban area. Because the amount of ISA is closely related to population growth and urban expansion, it was used to quantify the degree of urbanization and extent of urban land use (Carlson, 2012; Civco et al., 2002; Essa et al., 2013; Lynn et al., 2009; Xian and Crane, 2006; Yang et al., 2003; Yuan and Bauer, 2007) and indicate the environmental quality (Arnold and Gibbons, 1996; Xiao et al., 2007). Increased concern has been directed to the comparative studies of NDVI and percent ISA as indicators of surface urban heat island effect based on Landsat imagery by investigating the relationships between the LST, percent ISA and the NDVI (Deng and Wu, 2013; Ma et al., 2010; Yuan and Bauer, 2007; Zhang et al., 2009). Compared to the NDVI, the percent ISA was found to be more stable and less affected by seasonal changes in urbanized environment. Therefore, it is important to analyze the relationship between the LST and percent ISA in urban areas, for it provides an effective method to study urban expansion and related UHI effect.

LST is useful to predict the energy and water exchanges between land surface and atmosphere, which plays an important role in human–environment interactions. Urban expansion and development and their adverse effect on urban thermal environment has been confirmed by analyzing the relationship

between LST, NDVI and percent ISA in past literatures. However, further investigation on the correlation between LST and NDVI at different levels of urban development is necessary. This study aims to examine the urban expansion and its impact on urban surface temperatures and the surface UHI effect and also to analyze the varied efficiency of vegetation on reducing surface temperatures in different urban developed areas. The ultimate goal is to provide a better understanding of the relationship between LST, NDVI and percent ISA, and allow urban planners and managers to control and manage the urbanization and associated thermal pollution.

2. Case studies

2.1. Study area description

The study area is Wuhan city, located at 113°41'~115°05'E, 29°58'~31°22'N. Wuhan is the capital of Hubei province, situated at the center of central China and in eastern Hubei, where the Yangtze River joins the Han River. It covers an area of over 8000 km², with a population of more than 8 million. It has a long history of more than 3500 years. It is an economic center and an important transportation pivot of China. The metropolitan area comprises three parts: Wuchang, Hankou and Hanyang, commonly called Three Towns of Wuhan. These three parts face each other across the rivers and are linked by bridges.

Wuhan is situated in the north-subtropical climatic zone with four distinctive seasons. Spring and autumn are generally mild, while winter is cool with occasional snow. Due to its oppressively hot and humid summers, Wuhan is commonly known as one of the Three Furnaces of China, along with Nanjing and Chongqing. The annual temperature is 15.8°C to 17.5°C with extreme temperatures ranging from -18.1°C to 42.0°C. The annual average precipitation is 1269 mm, concentrated during June to August. The annual frost free period lasts 211 to 272 days and annual sunlight duration is 1810 to 2100 hours.

2.2. Derivation of LST, NDVI and related indexes from Landsat TM imageries

LST data were derived from the thermal infrared (TIR) band (band6) of the radiometrically and geometrically corrected images (Voogt and Oke, 2003), which was conducted in Erdas Imagine 9.2 with several procedures: radiometric calibration, at-satellite temperature calculation, emissivity correction and LST estimation. In this study, we used two Landsat-5 Thematic Mapper (TM) images acquired on September 26, 1987 and April 10, 2007. At first, the DN value of Landsat TM band6 was converted into spectral radiance (Chander and Markham, 2003). The spectral radiance was then converted into at-satellite temperature (i.e., blackbody temperature or brightness temperature) under the assumption of uniform emissivity. The at-

satellite temperature obtained was referenced to a black body and not the real surface temperature. Therefore, emissivity corrections became necessary according to the nature of land cover when calculating LST. Built-up and bare land areas were assigned an emissivity value of 0.923 and water 0.9925 (Gong et al., 2005; Masuda et al., 1988). Emissivity of vegetated areas was modeled with the NDVI values through field measurement (Van De Griend and Owe, 1993). Then the emissivity corrected LST was computed (Artis and Carnahan, 1982).

Vegetation abundance has been identified as an important parameter to positively mitigate the UHI effect, which can be indicated through NDVI value. Together with the other two indexes: normalized difference built-up index (NDBI) and modified normalized difference water index (MNDWI), the NDVI value can be accurately calculated based on the spectral reflectances accordingly (Chander and Markham, 2003; Chander et al., 2009).

2.3. Water extraction

A great number of studies have stated that there exists a positive correlation between NDVI and LST in water bodies (Rinner and Hussain, 2011; Zakšek and Oštir, 2012). In this study, water area accounts for a large percentage, which would significantly debase the accuracy of the relationship between vegetation and LST. Thus it is important to exclude the water body from the images before quantitatively and statistically analyzing the relationships between LST and NDVI. The MNDWI was used to extract and exclude the water bodies with the appropriate threshold values.

2.4. Derivation of urban percent ISA

The urban percent of impervious surface area (ISA) was highly correlated with urban land use/land cover types and the spatial distribution patterns (Jennings et al., 2004; Xian and Crane, 2005). For rural areas, the relationship between the urban percent ISA and NDBI was used to obtain the percent ISA through thresholding the NDBI value (Zhang et al., 2009).

For built up areas, Ridd (1995) found a strong negative correlation between ISA and fractional vegetation cover. Choudhury et al. (1994) and Carlson and Ripley (1997) then quantified the relationship between the percent ISA and fractional vegetation cover based on NDVI value by the Eq. (1), where: $NDVI_{soil}$ and $NDVI_{veg}$ are the NDVI values of the pixels covered by soil or non-vegetation and full vegetation.

$$ISA = 1 - \left(\frac{NDVI - NDVI_{soil}}{NDVI_{veg} - NDVI_{soil}} \right)^2 \quad (1)$$

3. Results

3.1. Spatial pattern of the percent ISA

In this study, the percent ISA was used to indicate the extent of the urban expansion and the level of urban development. Fig. 1 illustrates the spatial distribution patterns of the percent ISA continuously ranging from 0–100%. Increasing values from natural landscape (such as green spaces and water bodies) to the built-up areas were found in both 1987 and 2007. The white color representing higher percent ISA values captured the central business districts (CBD), urban residential areas and major highways. Though the spatial patterns of percent ISA for 1987 and 2007 seemed similar, the spatial areal extent significantly varied. The area with higher percent ISA values has remarkably expanded from 1987 to 2007, with the sprawling trend of impervious surface mainly occurring around the urban core and along the major roads.

To quantify the changes in the urban development, ISA was classified into different categories by threshold values: less than 10% as non-urban (such as forest, water and park in city), 10–45% as low-density, 45–80% as medium-density and more than 80% as high-density urban areas. This classification of land-cover types involved the urban built-up areas, rural developed centers and relatively undeveloped rural areas. Detailed information on spatial extent and area change of different categories of percent ISA from 1987 to 2007 is described in Table 1. From this table, it is obvious that there has been a drastic change in urban built-up areas over this period. The areas of medium-density (45–80% ISA) and high-density (> 80% ISA) were 112.80 km² and 174.67 km² in 1987, significantly increasing to 591.45 km² and 560.69 km² respectively in 2007. The wide variation between 1987 and 2007 revealed that the city has experienced rapid urban expansion during the last two decades.

3.2. Spatial pattern of LST

Fig. 2 shows the spatial distribution of land surface temperatures derived from TM image acquired on September 26, 1987 (a) and April 10, 2007 (b) in Wuhan City. The mean summer LST of 1987 was 39.6°C (SD of 4.7°C) with the lowest one 29.7 °C occurring in water and the highest one 62.8°C appearing in built-up area (Fig. 2a), while the mean late spring LST of 2007 was 22.4°C (SD of 3.8°C) with the lowest one 12.3 °C in water and the highest one 35.7°C in farmland (Fig. 2b). From the thermal maps, not only the spatial patterns of LST but also the urban heat island effect could be detected. The higher-grade highway running through the city created interlaced ‘hot channels’. Contrastively, the Yangtze River together with other water bodies had relatively lower temperatures, which produced a ‘cool corridor’ flowing through the city.

3.3. Relationship between percent ISA and LST

Table 2 presents the mean and standard deviation (SD) of LST for different categories of percent ISA. It is obvious that for both 1987 and 2007, the high-density type (>80% ISA) exhibits the highest LST as compared to other land cover types. Difference of the mean LST values between the relatively developed areas (>10% ISA) and rural areas (<10% ISA) means the UHI effect definitely exists in the study area. The largest difference naturally occurred between high-density urban area (>80% ISA) and rural areas (<10% ISA) both for 1987 (12.27°C) and 2007 (5.66°C). The UHI intensity in different density urban areas (Table 2) in 1987 was larger than that in 2007, probably because the mean LST values were expected to be more

variable and heterogeneous over the study region in summer (1987) than in late spring (2007). The SD of LST for different categories of percent ISA (Table 2), with higher SD values in 1987 than in 2007, further supports this conclusion.

To quantify the relationship between percent ISA and the mean LST, a zonal analysis was carried out to evaluate the mean LST at each 1% increment of percent ISA from 0% to 100%. Fig. 3a and b show a relatively strong linear relationship ($R^2=0.428$) between percent ISA and the mean LST for 1987 and a weak one ($R^2=0.056$) for 2007.

However, the shapes seemed similar in both cases, indicating linear increasing trends in the rural areas (<10% ISA) and urban developed areas (>45% ISA) and a linear decreasing one in the suburbs (approximately 20-45%ISA).

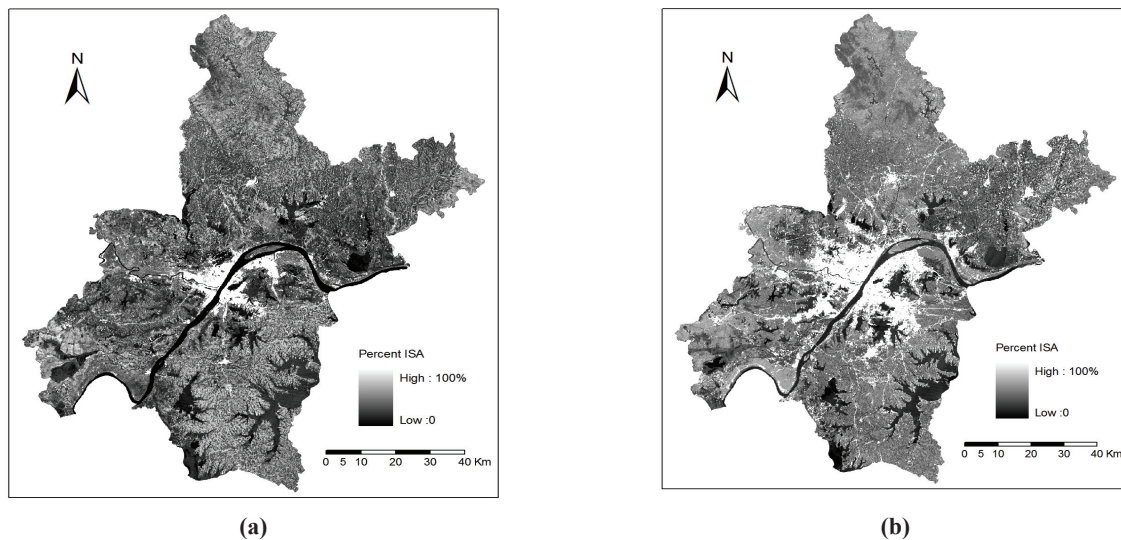


Fig. 1. Spatial distribution patterns of percent impervious surface area (ISA) from TM images acquired on September 26, 1987 (a) and April 10, 2007 (b)

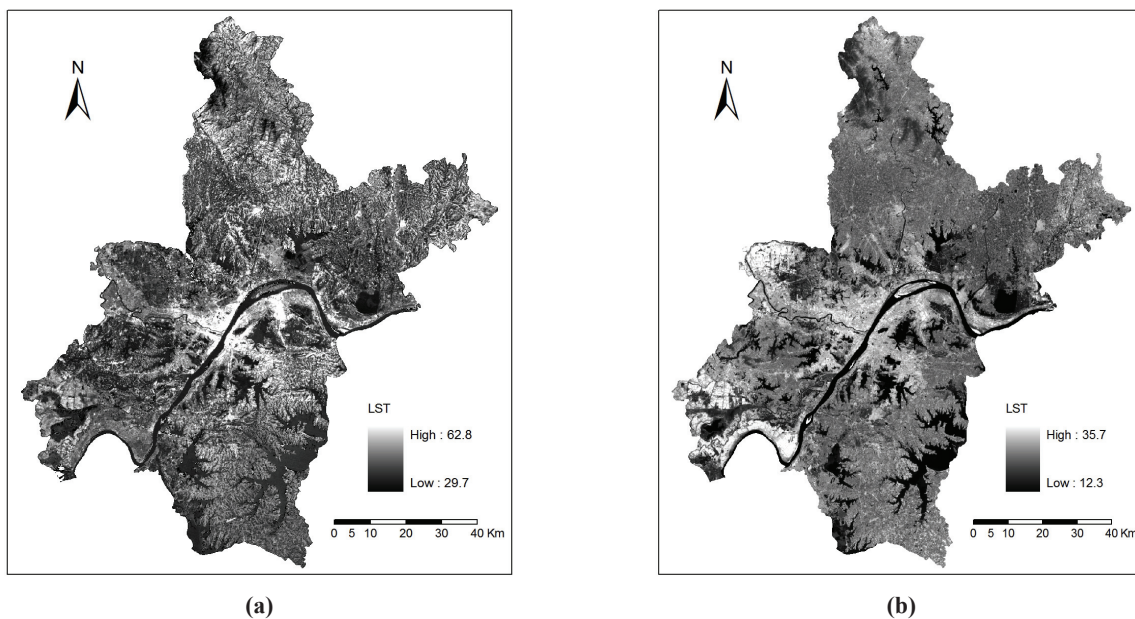


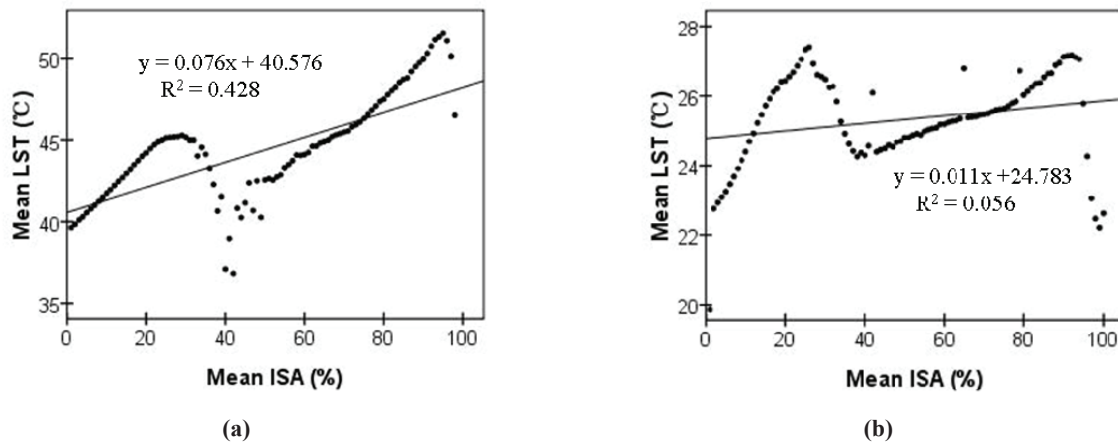
Fig. 2. Spatial distribution patterns of land surface temperature (LST) derived from TM images acquired on September 26, 1987 (a) and April 10, 2007 (b)

Table 1. Change in area from 1987 to 2007 of different categories of percent ISA

| Year/Percent ISA | <10% ISA | 10%-45% ISA | 45%-80% ISA | >80% ISA |
|-------------------------------|----------|-------------|-------------|----------|
| 1987 (km ²) | 5883.72 | 2240.81 | 112.80 | 174.67 |
| 2007 (km ²) | 5927.55 | 1418.96 | 591.45 | 560.69 |
| Difference (km ²) | 43.83 | -821.85 | 478.65 | 386.02 |
| Percent change (%) | 0.74 | -36.68 | 424.34 | 221.00 |

Table 2. Mean LST in different levels of urban development for 1987 and 2007

| Year/Percent ISA | <10% ISA | 10%-45% ISA | 45%-80% ISA | >85% ISA |
|-----------------------|----------|-------------|-------------|----------|
| Mean LST of 1987 (°C) | 36.96 | 43.20 | 45.34 | 49.23 |
| SD of 1987 (°C) | 6.42 | 4.81 | 5.69 | 4.08 |
| Mean LST of 2007 (°C) | 20.96 | 25.47 | 25.77 | 26.62 |
| SD of 2007 (°C) | 3.46 | 2.66 | 1.45 | 1.68 |

**Fig. 3.** Relationship of mean land surface temperature (LST) to percent impervious surface area (ISA): (a) 1987, (b) 2007

3.4. Relationship between LST and NDVI for different urban development density

To quantitatively investigate the relationship between the NDVI and the mean LST for each category of percent ISA, a zonal analysis was carried out to account for the mean LST at each 0.01 increment of NDVI from 0 to 1 (with water excluded). Fig. 4 shows their linear regression correlations. The highest negative correlation coefficient was found in non-urban areas (<10% ISA) for both 1987 ($R^2=0.753$) and 2007 ($R^2=0.953$). This stronger negative correlation between LST and NDVI imply that NDVI in more vegetated areas (<10% ISA) can better explain surface temperature variations than that in sparsely vegetated areas (>10% ISA).

The correlation coefficients in the other three urban areas (>10% ISA) complied with the orders: high-density (0.669) > low-density (0.397) > medium-density (0.201) for 1987 and medium-density (0.681) > low-density (0.545) > high-density (0.351) for 2007. Results show that LST values tend to negatively correlate with NDVI values in different urban development density areas in both years. The negative correlation illustrates the importance of urban vegetation in reducing urban surface temperatures. The specified effects of NDVI on cooling surface temperature significantly varied in different development density areas in both years

(shown in Fig. 4). This coefficient variation at different urban development levels between the two years indicates that the correlation of NDVI and LST can be influenced by many factors, such as land cover diversity, landscape heterogeneity and environmental complexity in urban areas.

4. Discussions

In this study, the percent ISA was selected to quantitatively represent urbanization level in Wuhan. What attracted our attention was that the degree of urbanization was defined by thresholding the values of the percent ISA. Nevertheless, the thresholds were subjectively assigned, with no unified standards. This diversity of threshold values prevented the urbanization degrees of different studied areas from being comparable.

When masking the spatial distributions of percent ISA (Fig. 1) over the corresponding LST maps (Fig. 2) for 1987 and 2007, a noticeable result appeared. The areal extent with higher temperatures did not always correspond to the urbanized area, though there was an ongoing expansion in built-up areas from 1987 to 2007.

This differs from the previous researches (Liu and Zhang, 2011; Rinner and Hussain, 2011; Xiong et al., 2012), which indicated that the UHI spatial distributions was mainly restricted to urbanized or industrialized areas.

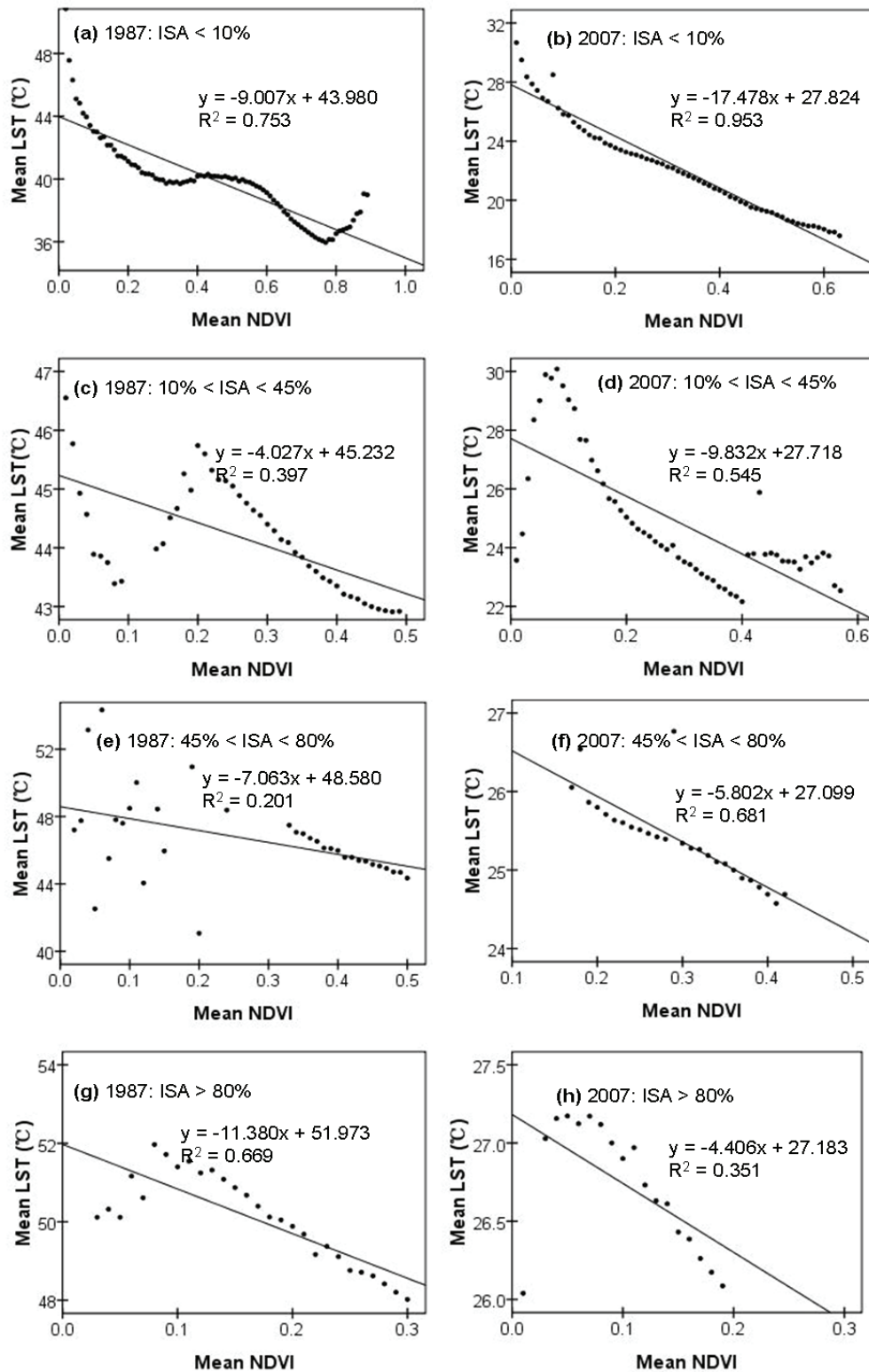


Fig. 4. Relationship of mean land surface temperature (LST) in °C to normalized difference vegetation index (NDVI) at different urban development levels (percent ISA)

Specifically, in this study, in addition to the UHI areas dominated by residential buildings, commercial areas and industrial areas in 1987 as well as in 2007 (Fig. 2a and b), another obvious heat island was found in the southwest of the city in 2007 (Fig. 2b). This is, at least in part, because the

farmlands accounted for a large percentage in the southwest and they seasonally varied in vegetation cover due to agricultural activities. They were fully covered by crops with high vegetation cover and great green biomass in summer (1987) but remained nearly fallow and bare in late spring (2007). Bare soil

was found to be similar in thermal response to impervious surface (Gluch et al., 2006; Huang et al., 2008). It is worth noting that the linear relationship between the mean LST and percent ISA in this study (Fig.3) is much weaker than those in the literatures (Yuan and Bauer, 2007; Zhang et al., 2009).

The reason is that the previous researches were conducted in relatively homogeneous urban areas, while our study in the areas with natural and impervious surface mixed. The context heterogeneity, to some extent, influenced the explanation quality of the percent ISA on LST. Remarkably, a decreasing trend was detected in the low-density urban areas due to the mixed and complex surface covers. This partly weakened the general linear relationship between percent ISA and LST.

The similar varying temperature trends to different categories of percent ISA in the two observed years are shown in Fig.3, which implied that the mean LST can be well explained by percent ISA in homogeneously covered areas. On the other hand, relatively steeper slope of linear correlation was detected in summer image than that in spring one, indicating that higher UHI magnitude appeared in summer. It is due to seasonal thermal performance associated with varied surface covers. Significant sensible heat exchange occurs mainly in areas with sparse or no vegetation cover and latent heat fluxes represent in areas characterized by vegetation cover (Lo et al., 1997). Impervious surface in urban areas expressed relatively higher warming rate in summer and higher efficiency of surface heat release in spring or winter than natural surface did (Yuan and Bauer, 2007; Yang et al., 2010).

NDVI is usually used as a parameter to indicate the biomass, percentage cover and abundance of urban vegetation (Lo et al., 1997). The NDVI value ranges generally from -1 to 1. Normally, it is positive in vegetated area, close to zero for impervious surface and negative for water bodies (Van De Griend and Owe, 1993). Typically, higher NDVI values indicate a larger amount of vegetation cover and express lower temperatures in pixels. In this study, the relationships between NDVI and LST were confirmed to be nonlinear in all categories of percent ISA except for in non-urban areas (<10% ISA).

That is to say, sparsely vegetated areas experience a wider variation in LST than densely vegetated ones (Owen et al., 1998; Price, 1990). This suggests that NDVI can be a sufficient indication to express surface temperature variation only in natural context.

5. Conclusions

Anthropogenic activities associated with urbanization and industrialization were the most important driving force in land cover changes and UHI formation, as expected. Agricultural activity was another artificial factor contributing to the

seasonal variation of land covers and land surface temperatures.

The percent ISA was suitable for LST studies in urbanized areas and NDVI was sufficient to express surface temperature variation in vegetated areas. What has yet to be examined is how to select appropriate threshold values of the percent ISA to define urbanization degree. Future studies need to focus on better understanding the seasonal influence on the relationship between NDVI, percent ISA and LST variation.

Acknowledgments

This research was sponsored by the National Science and Technology Supporting Program (No. 2013BAJ02B01), the National Natural Science Foundation of China (Grant No. 41401186), the Natural Science Foundation of Hubei Province of China (2014CFB346), the Fund No. 200951999569 and the Program No. 2013PY133. The authors would like to thank Elizabeth Lord from the University of Toronto, Canada for reviewing and correcting the paper. We are also grateful to the Editor and the anonymous referees for their helpful comments and suggestions.

References

- Arnold C.L., Gibbons C.J., (1996), Impervious surface coverage: The emergence of a key environmental indicator, *Journal of the American Planning Association*, **62**, 243-258.
- Artis D.A., Carnahan W.H., (1982), Survey of emissivity variability in thermography of urban areas, *Remote Sensing of Environment*, **12**, 313-329.
- Baker J.M., Baker D.G., (2002), Long-term ground heat flux and heat storage at a mid-latitude site, *Climate Change*, **54**, 295-303.
- Brazel A., Gober P., Lee S.J., Grossman-Clarke S., Zehnder J., Hedquist B., (2007), Determinants of changes in the regional urban heat island in metropolitan Phoenix (Arizona, USA) between 1990 and 2004, *Climate Research*, **33**, 171-82.
- Carlson T.N., Ripley D.A., (1997), On the relation between NDVI, fractional vegetation cover, and leaf area index, *Remote Sensing of Environment*, **62**, 241-252.
- Carlson T.N., (2012), Land use and impervious surface area by county in Pennsylvania (1985-2000) as interpreted quantitatively by means of satellite imagery, *The Open Geography Journal*, **5**, 59-67.
- Chander G., Markham B., (2003), Revised Landsat-5 TM radiometric calibration procedures and postcalibration dynamic ranges, *IEEE Transactions on Geoscience and Remote Sensing*, **41**, 2674-2677.
- Chander G., Markham B.L., Helder D.L., (2009), Summary of current radiometric calibration coefficients for Landsat MSS, TM, ETM+ and EO-1 ALI sensors, *Remote Sensing of Environment*, **113**, 893-903.
- Choudhury B.J., Ahmed N.U., Idso S.B., Reginato R.J., Daughtry C.S.T., (1994), Relations between evaporation coefficients and vegetation indices studied by model simulations, *Remote Sensing of Environment*, **50**, 1-17.
- Civco D.L., Hurd J.D., Wilson E.H., Arnold C.L., Prisloe Jr. M.P., (2002), Quantifying and describing urbanizing landscapes in the northeast United States, *Photogrammetric Engineering and Remote Sensing*, **68**, 1083-1090.

- Deng C.B., Wu C.S., (2013), Examining the impacts of urban biophysical compositions on surface urban heat island: A spectral unmixing and thermal mixing approach, *Remote Sensing of Environment*, **131**, 262-274.
- Du Y., Xie Z.Q., Zeng Y., Shi Y.F., Wu J.G., (2007), Impact of urban expansion on regional temperature change in the Yangtze River Delta, *Journal of Geographical Sciences*, **17**, 387-398.
- Essa W., van der Kwast J., Verbeiren B., Batelaan O., (2013), Downscaling of thermal images over urban areas using the land surface temperature–impervious percentage relationship, *International Journal of Applied Earth Observation and Geoinformation*, **23**, 95-108.
- Fabrizi R., Bonafoni S., Biondi R., (2010), Satellite and Ground-Based Sensors for the Urban Heat Island Analysis in the City of Rome, *Remote Sensing*, **2**, 1400-1415.
- Frey C.M., Parlow E., (2012), Flux measurements in Cairo. Part 2: On the determination of the spatial radiation and energy balance using ASTER satellite data, *Remote Sensing*, **4**, 2635-2660.
- Gallo K.P., McNab A.L., Karl T.R., Brown J.F., Hood J.J., Tarpley J.D., (1993), The use of NOAA AVHRR data for assessment of the urban heat island effect, *Journal of Applied Meteorology*, **32**, 899-908.
- Gillies R.R., Carlson T.N., (1995), Thermal remote sensing of surface soil water content with partial vegetation cover for incorporation into climate models, *Journal of Applied Meteorology*, **34**, 745-756.
- Gluch R., Quattrochi D.A., Luvall J.C., (2006), A multi-scale approach to urban thermal analysis, *Remote Sensing of Environment*, **104**, 123-132.
- Gong A.D., Jiang Z.Y., Li J., Chen Y.H., Hu H.L., (2005), Urban land surface temperature retrieval based on landsat TM remote sensing images in Beijing, *Remote Sensing Information*, **3**, 18-20.
- Gutman G., Ignatov A., (1998), The derivation of the green vegetation fraction from NOAA/AVHRR data for use in numerical weather prediction models, *International Journal of Remote Sensing*, **19**, 1533-1543.
- Hamdi R., (2010), Estimating urban heat island effects on the temperature series of uccle (Brussels, Belgium) using remote sensing data and a land surface scheme, *Remote Sensing*, **2**, 2773-2784.
- Huang L.M., Li J.L., Zhao D.H., Zhu J.Y., (2008), A fieldwork study on the diurnal changes of urban microclimate in four types of ground cover and urban heat island of Nanjing, China, *Building and Environment*, **43**, 7-17.
- Jennings D.B., Jarnagin S.T., Ebert D.W., (2004), A modeling approach for estimating watershed impervious surface area from national land cover data 92, *Photogrammetric Engineering and Remote Sensing*, **70**, 1295-1307.
- Jin M.S., Kessomkiat W., Pereira G., (2011), Satellite-observed urbanization characters in Shanghai, China: aerosols, urban heat island effect, and land-atmosphere interactions, *Remote Sensing*, **3**, 83-99.
- Jones P.D., Groisman P.Y., Coughlan M., Plummer N., Wang W.C., Karl T.R., (1990), Assessment of urbanization effects in time-series of surface air-temperature over land, *Nature*, **347**, 169-72.
- Liu L., Zhang Y.Z., (2011), Urban heat island analysis using the landsat TM data and ASTER data: A case study in Hong Kong, *Remote Sensing*, **3**, 1535-1552.
- Lo C.P., Quattrochi D.A., Luvall J.C., (1997), Application of high-resolution thermal infrared remote sensing and GIS to assess the urban heat island effect, *International Journal of Remote Sensing*, **18**, 287-304.
- Luber G., McGeehin M., (2008), Climate change and extreme heat events, *American Journal of Preventive Medicine*, **35**, 429-435.
- Lynn B.H., Carlson T.N., Rosenzweig C., Goldberg R., Druyan L., Cox J., Gaffin S., Parshall L., Civerolo K., (2009), A modification of the NOAA LSM to simulate heat mitigation strategies in the New York City metropolitan area, *Journal of Applied Meteorology and Climatology*, **48**, 199-216.
- Ma Y., Kuang Y.Q., Huang N.S., (2010), Coupling urbanization analyses for studying urban thermal environment and its interplay with biophysical parameters based on TM/ETM+ imagery, *International Journal of Applied Earth Observation and Geoinformation*, **12**, 110-118.
- Manea D.L., Manea E.E., Robescu D.N., (2013), Study on greenhousegas emissions from wastewater treatment plants, *Environmental Engineering and Management Journal*, **12**, 59-63.
- Masuda K., Takashima T., Takayama Y., (1988), Emissivity of pure and sea waters for the model sea surface in the infrared window region, *Remote Sensing of Environment*, **24**, 313-332.
- Mohan M., Kandya A., (2015), Impact of urbanization and land-use/land-cover change on diurnal temperature range: A case study of tropical urban airshed of India using remote sensing data, *Science of the Total Environment*, **506–507**, 453-465.
- Nonomura A., Kitahara M., Masuda T., (2009), Impact of land use and land cover changes on the ambient temperature in a middle scale city, Takamatsu, in Southwest Japan, *Journal of Environmental Management*, **90**, 3297-3304.
- Oke T.R., (1982), The energetic basis of the urban heat island, *Quarterly Journal of the Royal Meteorological Society*, **108**, 1-24.
- Owen T.W., Carlson T.N., Gillies R.R., (1998), An assessment of satellite remotely-sensed land cover parameters in quantitatively describing the climatic effect of urbanization, *International Journal of Remote Sensing*, **19**, 1663-1681.
- Price J.C., (1990), Using spatial context in satellite data to infer regional scale evapotranspiration, *IEEE Transactions on Geoscience and Remote Sensing*, **28**, 940-948.
- Raynolds M.K., Comiso J.C., Walker D.A., Verbyla D., (2008), Relationship between satellite-derived land surface temperatures, arctic vegetation types, and NDVI, *Remote Sensing of Environment*, **112**, 1884-1894.
- Ridd M.K., (1995), Exploring a V-I-S (vegetation-impervious-surface-soil) model for urban ecosystem analysis through remote sensing: comparative anatomy for cities, *International Journal of Remote Sensing*, **16**, 2165-2185.
- Rinner, C.; Hussain, M., (2011), Toronto's Urban Heat Island—Exploring the Relationship between Land Use and Surface Temperature, *Remote Sensing*, **3**, 1251–1265.
- Roth M., Oke T.R., Emery W.J., (1989), Satellite-derived urban heat islands from three coastal cities and utilization of such data in urban climatology, *International Journal of Remote Sensing*, **10**, 1699-1720.

- Tang Z., Shi C.B., Bi K.X., (2014), Impacts of land cover change and socioeconomic development on ecosystem service values, *Environmental Engineering and Management Journal*, **13**, 2697-2705.
- Taniguchi M., Uemura T., Sakura Y., (2005), Effects of urbanization and groundwater flow on subsurface temperature in three megacities in Japan, *Journal of Geophysics and Engineering*, **2**, 320-5.
- Van De Griend A.A., Owe M., (1993), On the relationship between thermal emissivity and the normalized difference vegetation index for nature surfaces, *International Journal of Remote Sensing*, **14**, 1119-1131.
- Voogt J.A., Oke T.R., (2003), Thermal remote sensing of urban areas, *Remote Sensing of Environment*, **86**, 370-384.
- Weng Q., (2001), A remote sensing-GIS evaluation of urban expansion and its impact on surface temperature in the Zhujiang Delta, China, *International Journal of Remote Sensing*, **22**, 1999-2014.
- Weng Q.H., Lu D.S., Schubring J., (2004), Estimation of land surface temperature-vegetation abundance relationship for urban heat island studies, *Remote Sensing of Environment*, **89**, 467-483.
- Xian G., Crane M., (2005), Assessments of urban growth in the Tampa Bay watershed using remote sensing data, *Remote Sensing of Environment*, **97**, 203-215.
- Xian G., Crane M., (2006), An analysis of urban thermal characteristics and associated land cover in Tampa Bay and Las Vegas using Landsat satellite data, *Remote Sensing of Environment*, **104**, 147-156.
- Xiao R.B., OuYang Z.Y., Zheng H., Li W.F., Schienke E.W., Wang X.K., (2007), Spatial pattern of impervious surfaces and their impacts on land surface temperature in Beijing, China, *Journal of Environmental Sciences*, **19**, 250-256.
- Xiong Y.Z., Huang S.P., Chen F., Ye H., Wang H., Zhu C.B., (2012), The impacts of rapid urbanization on the thermal environment: a remote sensing study of Guangzhou, South China, *Remote Sensing*, **4**, 2033-2056.
- Yang L., Huang C., Homer C.G., Wylie B.K., Coan M.J., (2003), An approach for mapping large-area impervious surfaces: Synergistic use of Landsat 7 ETM+ and high spatial resolution imagery, *Canadian Journal of Remote Sensing*, **29**, 230-240.
- Yang S. B., Zhao X. Y., Shen S. H., Hai Y. L., Fang Y.X., (2010), Characteristics of urban heat island seasonal pattern in beijing based on landsat TM / ETM+ Imagery (in Chinese), *Transactions of Atmospheric Sciences*, **33**, 427-435.
- Yuan F., Bauer M.E., (2007), Comparison of impervious surface area and normalized difference vegetation index as indicators of surface urban heat island effects in Landsat imagery, *Remote Sensing of Environment*, **106**, 375-386.
- Zakšek K., Oštir K., (2012), Downscaling land surface temperature for urban heat island diurnal cycle analysis, *Remote Sensing of Environment*, **117**, 114-124.
- Zhang Y.S., Odeh Inakwu O.A., Han C.F., (2009), Bi-temporal characterization of land surface temperature in relation to impervious surface area, NDVI and NDBI, using a sub-pixel image analysis, *International Journal of Applied Earth Observation and Geoinformation*, **11**, 256-264.
- Zheng B.J., Myint S.W., Fan C., (2014), Spatial configuration of anthropogenic land cover impacts on urban warming, *Landscape and Urban Planning*, **130**, 104-111.



“Gheorghe Asachi” Technical University of Iasi, Romania



RESEARCH ON THE PRODUCTION OF FORAGE FOR THE AGRO -TOURISTIC FARMS IN ROMANIA BY CULTIVATING PERENNIAL LEGUMINOUS PLANTS

Aurel Călina*, Jenica Călina

University of Craiova, Faculty of Agriculture, 19 Libertății Str., 200421 Craiova, Romania

Abstract

The paper is the result of research conducted for approximately 20 years in the agro tourism field and also rural tourism, as well as in natural and cultivated pastures, at the Faculty of Agriculture and Horticulture, University of Craiova. Based on these studies it was concluded that the research in this field has been less realistic so far, because it was strictly oriented towards obtaining high forage production, but of questionable quality due to high content of residual chemicals. Currently, in tourism activities and other specific areas of food production, the demand for natural products (bio or eco) has greatly increased to ensure a quality taste and high security and traceability. To assist the forage manufacturers and workers in tourism activity we considered appropriate and necessary to study this particularly valuable forage, to which by applying minimal chemical treatments, high yields with a very low degree of chemical residues will be obtained, with a high nutritional quality and traceability, while a cuisine with higher value taste and food safety can be obtained.

Key words: agri-tourism, food safety, protein feed, traceability

Received: April, 2013; Revised final: June, 2014; Accepted: June, 2014

1. Introduction

The agro tourism activity in Romania must develop constantly, as from the research and studies conducted it was concluded that this is a complex activity, with considerable advantages on the economic and socio-cultural landscape, which was almost entirely forgotten during the communist period (Călina, 2007; Călina et al., 2011a).

The impact of this activity is visible, quick and significant, manifesting itself in the Romanian rural area by: acquisition of new professional skills, stopping the exodus of people from rural to urban areas (Moinet, 2006; Călina, 2008), increasing the number of jobs and substantially reducing rural unemployment (Gartner, 2004; Grolleau, 1987), increasing the income of farms and households engaged in such work (Călina et al., 2009, 2010a), increasing the number and volume of investments in

the area, direct source of capitalization and modernization of agricultural holdings, improving housing (Stoian, 2006), increasing the level of education, culture and civilization of villagers, harnessing typical products from agriculture and traditional cuisine of the region (Călina et al., 2010a, 2011b), assuring sustainable development of rural communities through wise use of all resources, the decrease of the removal process of agricultural and forest lands from the agricultural and forestry circuit (Hernández-Mogollón et al., 2013; Jeangros, 2006; Louwagie et al., 2009).

Due to these advantages and favorable quality/price ratio of the agro tourism activity recorded by Plog (2003), the research team sought to support small farms and agro tourism farms in our country by conducting research regarding the production of protein forage with high nutritional

* Author to whom all correspondence should be addressed: e-mail: aurelcalina@yahoo.com

value and a lower percentage of chemicals, to be used in animal feed, grown on the farm.

Obtaining such feed with high nutritional and ecological value is particularly important because the activity of farms and agro pensions should be attached to the function of recreation and leisure and also that of protection and conservation of natural ecosystems and anthropic resources (Barke, 2004).

2. Materials and methods

To assess the agro touristic phenomenon, specific methods frequently encountered in specialized literature were used, which permitted the accomplishment of a clear, pertinent and realist analysis and diagnosis of the phenomena, from a quantitative as well as a qualitative point of view.

The experiences regarding the protein forage production were conducted at the Experimental Center for the Meadows Culture, Preajba, of the Faculty of Agriculture, University of Craiova, Romania, on an albic luvisol, characterized by physico - chemical properties which produce low fertility, to truly make use of this soil aeration processes are needed as well as applying organic and mineral fertilizers in high doses and amendments to correct the acid reaction (Peț et al., 2005, 2006).

Since the research was conducted in an area with strongly acidic soils where some perennial legumes such as alfalfa or sainfoin cannot be sustained for long periods of usage, and because the trefoil gives lower production quantities with high expendability, red clover (*Trifolium pratense*) was chosen in both pure culture and mixed with perennial forage grasses, under the form of temporary meadows. Ionescu (1998, 2001) confirms that the red clover cultivated on acid soils provides high yields of superior quality feed.

2.1. Objectives of research

The research undertaken during 2009 - 2010 had two main objectives:

1. the production of feed with high protein and ecological value;
2. determining the chemical composition of forage and its influence on the quality and traceability of food products (Dragomir, 2001);

In order to achieve these complex objectives, the investigations have taken into account the following major aspects:

- the behavior of the *Trifolium pratense* species in pure culture, used for forage;
- the influence of amendment under the form of calcium carbonate (CaCO_3) on dry matter production of the red clover (*Trifolium pratense*) in pure culture;
- the effect on the quantity and quality of dry matter production of the red clover (*Trifolium pratense*) produced by applying organic fertilizer (manure) in pure culture (Iepema et al., 2006; Muntean, 2002);

- the influence of lime amendments and organic fertilizer on annual growth in production; the influence of lime amendments and organic fertilizer on the quality of red clover forage.

2.2. Working method

During the experiments, the Merviot soil was sown with red clover in 2009, on April 5th, being considering the method of subdivided parcels with 3 factors (Vântu, 2004). It was generated a schema of 2 x 3 x 2 type in 4 repetitions as follows:

A: Factor - soil amendment with 2 graduations:

a1 – unchanged

a2 –amended with 5.5 t/ha of calcium carbonate (CaCO_3)

B: Factor - organic fertilizer with 3 graduations:

b1 – unfertilized

b2 - 20 t / ha manure

b3 - 40 t / ha manure

The surface of a large lot was of 15 m x 5.6 m = 84 m², of a small lot of 5.6 m x 2.5 m = 14 m², from which harvest, 10 m².

Harvesting was performed at the beginning of flowering transition, at a height of 4 to 5 cm with a mower. Concurrently with every mowing, samples were gathered in order to determine the dry substance and chemical composition.

3. Results and discussion

The studies and researches performed have lead to the conclusion that providing animal food in sufficiently high quantity and quality, along with other products, determines an increase in the living standards of the population. Achieving this goal involves increasing the number of animals and their production, which is possible only by ensuring an adequate forage base in terms of quantity and quality (Abberton, 2007; Muntean, 2002). In Romania, the predominant source of forage is represented by the permanent grassland with a high share and also temporary meadows that even though currently occupy small areas, provide significant productions. Among fodder plants, the perennial legumes are of particularly importance, whether used in pure culture or mixed with perennial grasses, the productions made by these are always of a high level (Vantu, 2004).

The perennial leguminous crops coupled with other measures (amendments, fertilizers etc.) could play an important role in increasing soil fertility through the ameliorative qualities they possess and furthermore contribute to obtaining, within farms and agro tourism households, a constant and ecological animal productions of a high quantity and quality (Croitoru and Miluț, 2008; Dragomir, 2001).

Within this context, the research conducted at the Experimental Center for Meadows Culture Preajba - Gorj have looked at determining factors of the culture technology that can be considered as

viable solutions for spreading these valuable forage plants, grown single or in mixture with perennial grasses, as temporary grasslands in farms and agro tourism households, across the Subcarpathian area of Oltenia and the entire country.

Considering that the produced forage is designed primarily for agro touristic farms and households, the research was focused primarily on two directions, obtaining forage high in protein, of a high a quality and environmentally friendly and the development of food products with a high nutritional value and low in residual chemicals accumulated from the treatment applied to plants (Charles, 1988).

The achievement of such natural products that ensure a high degree of traceability and food safety to tourists visiting farms and agro pensions in Romania and other regions should represent a primary concern for all researchers in our country and all over the world (Stoll, 2007). The research team arrived to this conclusion considering that so far all investigations conducted nationally and internationally have mainly focused on obtaining high productions of low ecological quality, with large side effects on human health.

This research aimed to demonstrate that culinary dishes prepared from animal products produced by feeding with forage of nutritional and environmental quality are highly recommended, as they provide a high quality taste and the highest level of security and traceability. Furthermore the research based on the experiences carried out on poorer acid soils, specific to sub mountain and hill areas, must prove that these areas can obtain high productions with a high nutritional and ecological quality, through a technology that involves applying reduced chemical treatments to forages (Ionescu, 2003).

In order to meet the objectives, the influence of amendments and organic fertilizers on the production and on the quality of forage produced on pastures grown with red clover (*Trifolium pratense*) in pure culture, in the form of temporary grassland was taken into account.

3.1. Effects of amendments on red clover (*Trifolium pratense*) crop production

The first phase was aimed at analyzing the effect of amendments on crop production of red clover. The results have shown that 7.32 t/ha dry matter (s.u.) resulted without amendment, and 8.45 t/ha s.u. (1.13 t/ha more, meaning about 16%), when 5.5 t/ha calcium carbonate were applied to correct the soil acidity (Fig. 1). Statistical analysis of the data showed that the difference between amended and not amended crop production was around 1 t/ha s.u., which was found as insignificant.

The values obtained cannot confirm with adequate certainty that the application of lime amendments to clover is inefficient, whereas calcium carbonate has positive effects not only on mass production plant and plant chemical composition, but

also on the characteristics of the soil, by correcting its acidity (Dunea, 2008).

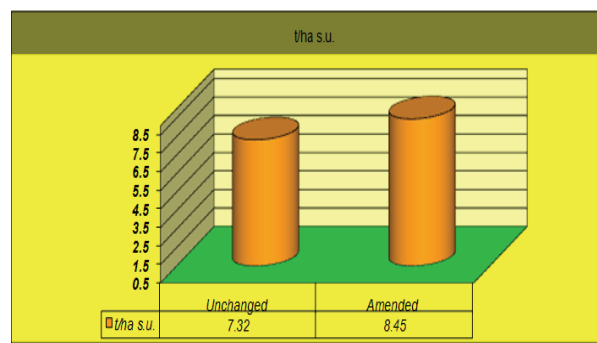


Fig. 1. Culture production of red clover (*Trifolium pratense*) under the influence of calcareous amendments (t / ha s.u., average 2009 - 2010)

3.2. Effect of organic fertilizer on red clover (*Trifolium pratense*) crop production

Very significant results were obtained by applying organic fertilizers on the culture of *Trifolium pratense* (Table 1). The sizes of these improvements depend on the fertilizer dose. Considering the alternative with 40 t/ha manure added during two years, an average production of 9.28 t/ha s.u. resulted, with more than 3.37 t (almost 37%) than in the alternative without manure. The dose of manure of 20 t/ha resulted in a production of 8.75 t s.u. (more than the witness with 2.84 t, almost 20%), high enough to be considered for use in practice (Table 1). The high value of the production obtained after fertilization with manure and substantial gains in comparison with the unfertilized soil recommend organic fertilizers to be used with priority for the clover crops.

The results confirm that, by applying organic fertilizers even on acid soils with lower natural fertility, large productions with high nutritional and ecological value can be obtained.

3.3. Effect of amendments combined with organic fertilizer on red clover (*Trifolium pratense*) crop production

At this stage, the way in which the manure application had undergone both on amended background and also on unchanged background was observed (Table 2). It can be noticed that the manure used in doses of 20 and 40 t/ha improved crop production comparative with the variants without manure as described above, the data being comparable to those obtained by other researchers (Hatch et al., 2014; Ionescu, 2001). In all working variants, the increases in crop production given by lower doses of organic fertilizer were significantly distinct, and those given by the double dose were very significant.

The experiments conducted at the Center for the Meadows Culture, under the hill region of

Oltenia, display that the area offers good conditions for this culture, which spread over larger areas, can help in improving soil characteristics and provide animals with large quantities of forage of excellent quality.

3.4. Dynamics of red clover (*Trifolium pratense*) crop production

Careful monitoring of red clover production showed that the crop can be exploited in economic conditions for only two years, meaning 2009 and 2010, while in the following years the plants disappeared massively. This resulted in changing the culture and plowing the land in order to cultivate it with other plant species (this phenomenon was also noted by Mosimann, 2008).

In the first year, the clover production was enhanced with 29-36%, but we were not able to find some correlations between the experienced factors and the production share in the total amount collected in the two years of operation (Fig. 2). In the second year (2010) much higher yields were harvested that reported to the amount of dry matter produced in the two years, represented 64-72% of the total production. Thus it can be asserted, with some approximation, that the clover expresses about 1/3 of the production potential in the first year and the remaining 2/3 in the second year of vegetation.

3.5. Chemical composition of red clover crop

Analyzing the red clover forage in terms of chemical composition it was found the applied amendments and organic fertilizers had a strong influence. The data in Table 3 underline that, under the influence of different treatments, the gross protein content of the forage was at a higher level, ranging between 17.99% and 22.58%. The cellulose content ranged from 21.19% to 26.33%.

Slightly lower values were recorded in the levels of phosphorus, potassium and calcium. Phosphorus was determined at a rate of 0.31-0.45%, being therefore present in optimal amounts in the plants. The potassium content of plants was found of 1.22 - 1.92%, as deficient in all variants, while calcium in the plants ranged from 0.33 - 0.55%.

Similar results were obtained in other areas with acidic soils. It was also found that the presence of large quantities of mobile aluminum favored strong leaching of the potassium and decreased the plants absorption capacity for this element (Ionescu, 1998, 2001).

The correct exemplification of the effect of the separate impact of amendments and organic fertilizers on the chemical composition of the red clover forage is shown in Table 4. The percentage of gross protein as it is displayed has increased, reaching the value of 20.58% on amended soil, in comparison with the content of the forage on unchanged soil of 19.66%, which can demonstrate the qualitative role of calcium used as amendment, but the results have not statistical significance.

Comparing the two doses of organic fertilizer used, it was identified that the highest amount of protein was obtained at a dose of 20 t/ha (20.85%). The dose of 40 t/ha manure resulted in a protein content of 19.48%, lower even for the variant without manure (20.03%), which demonstrates that there is no direct correlation between the amount of proteins in the forage and the quantity of organic fertilizer applied.

The dynamics of the chemical composition of forage can be explained as follows: a larger amount of manure is found due to increased nitrogen input into the soil, which help plants to develop stronger tissues. This resulted in a high content of cellulose (24.87%) in the working variant when the soil was amended with 40 t/ha manure, compared to 20 t organic fertilizer variants or without manure (cellulose, 22.55% respectively 22.94%).

Table 1. The influence of organic fertilizers on the production of cultivated *Trifolium pratense* (average from 2009 to 2010, t / ha s.u.)

| No. | Version | Absolute production (t/ha s.u.) | % | Difference | Significance |
|-----|----------------|---------------------------------|-----|------------|--------------|
| 1 | Unfertilized | 5.91 | 100 | - | Witness |
| 2 | 20 t/ha manure | 8.75 | 148 | 2.84 | *** |
| 3 | 40 t/ha manure | 9.28 | 157 | 3.37 | *** |

DL 5 % = 1.05 t/ha s.u.; DL 1 % = 1.43 t/ha s.u.; DL 0.1 % = 2.12 t/ha s.u.

Table 2. The combined influence of organic fertilizers with the amendment on the production of cultivated *Trifolium pratense* (average from 2009 to 2010, t / ha s.u.)

| No. | Amendment | Organic fertilizers | Absolute production (t/ha s.u.) | % | Difference | Significance |
|-----|------------------------------------|---------------------|---------------------------------|-----|------------|--------------|
| 1 | Unchanged | 0 | 5.91 | 100 | - | Witness |
| 2 | | 20 t/ha manure | 8.75 | 148 | 2.84 | ** |
| 3 | | 40 t/ha manure | 9.28 | 157 | 3.37 | *** |
| 4 | Amended 5,5 t/ha CaCO ₃ | 0 | 6.75 | 100 | - | Witness |
| 5 | | 20 t/ha manure | 8.96 | 133 | 2.21 | ** |
| 6 | | 40 t/ha manure | 9.77 | 145 | 3.02 | *** |

DL 5 % = 1.39 t/ha s.u.; DL 1 % = 1.99 t/ha s.u.; DL 0.1 % = 3.01 t/ha s.u.

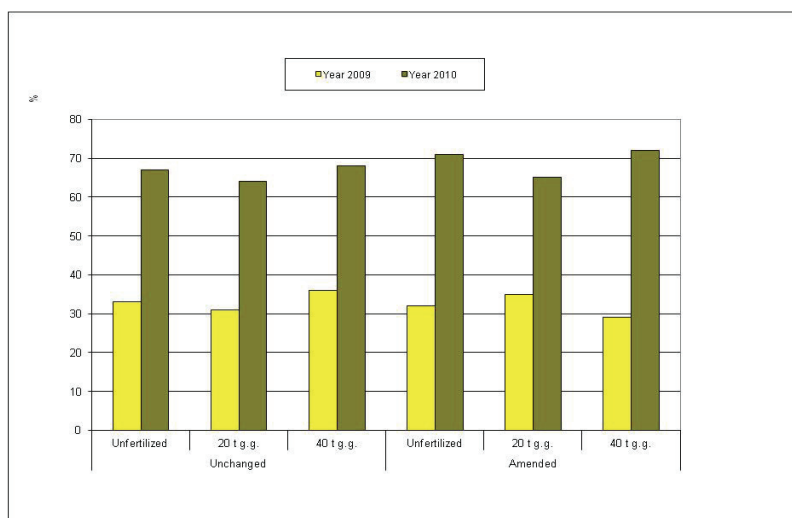


Fig. 2. The yearly dynamic of the red clover crop production (*Trifolium pratense*), (%)

Table 3. The chemical composition of the *Trifolium pratense* cultivated forage (%)

| No. | Amendment | Organic fertilizers | Gross proteins% | Gross cellulose % | P% | K% | Ca% |
|-----|-------------------------------------|---------------------|-----------------|-------------------|------|------|------|
| 1 | Unchanged | 0 | 21.95 | 21.95 | 0.37 | 1.63 | 0.33 |
| 2 | | | 18.88 | 23.57 | 0.41 | 1.92 | 0.39 |
| 3 | | 20 t/ha manure | 22.33 | 21.19 | 0.31 | 1.28 | 0.46 |
| 4 | | | 18.96 | 25.15 | 0.35 | 1.47 | 0.41 |
| 5 | | 40 t/ha manure | 21.32 | 26.03 | 0.41 | 1.39 | 0.55 |
| 6 | | | 17.99 | 26.33 | 0.43 | 1.42 | 0.47 |
| 7 | Amended, 5.5 t/ha CaCO ₃ | 0 | 21.55 | 22.46 | 0.37 | 1.53 | 0.36 |
| 8 | | | 20.60 | 24.44 | 0.38 | 1.87 | 0.39 |
| 9 | | 20 t/ha manure | 22.58 | 21.52 | 0.35 | 1.29 | 0.53 |
| 10 | | | 20.14 | 23.10 | 0.33 | 1.58 | 0.41 |
| 11 | | 40 t/ha manure | 21.51 | 23.37 | 0.42 | 1.22 | 0.54 |
| 12 | | | 19.36 | 24.85 | 0.45 | 1.51 | 0.47 |

Table 4. The separate influence of amendments, organic fertilizers on nutritional parameters of *Trifolium pratense* cultivated forage (%)

| Nutritional parameter Version | Gross proteins (%) | Gross cellulose (%) | P (%) | K (%) | Ca (%) |
|----------------------------------|--------------------|---------------------|-------|-------|--------|
| Unchanged | 19.66 | 23.99 | 0.38 | 1.51 | 0.46 |
| Amended 6 t/ha CaCO ₃ | 20.58 | 23.32 | 0.37 | 1.49 | 0.50 |
| 0 | 20.03 | 22.94 | 0.39 | 1.75 | 0.40 |
| 20 t/ha manure | 20.85 | 22.55 | 0.36 | 1.44 | 0.42 |
| 40 t/ha manure | 19.48 | 24.87 | 0.43 | 1.39 | 0.48 |

Analyzing the evolution of cellulose content in red clover crop, it can be noted that this is inversely proportional with the protein percentage: the lowest cellulose content was determined when the protein registered the highest values (amended, 20 t/ha manure) and vice versa. The phosphorus was within the optimal range, not being influenced by amendments, and the effect of organic fertilizers is not significant, because they have low phosphorus content.

The potassium content was in all cases below the limit of 2%. The amount of this macro-element decreased from 1.51% (unchanged) to 1.49% (amended) and 1.75% (without manure) to 1.39%

(manure 40 t / ha). The decrease is explained by the antagonism that exists between calcium and potassium: in the presence of calcium (from amendment or manure) the potassium is blocked in insoluble forms. The percentage of calcium in plants was positively influenced by the amendments, increasing from 0.46% (unchanged) to 0.50%. Its percentage increased under the influence of organic fertilizers from 0.40% (without manure) to 0.48%.

4. Conclusions

The red clover grown on amendment conditions of over 5.5 t/ha CaCO₃ has averaged

insignificant increases, while manure, applied when preparing the ground work had a very large influence on the production of dry matter. The best results were obtained with the dose of 40 t/ha, but higher production costs and lower profitability were obtained. The dose of 20 t/ha led to a higher production, similar to that of the maximum dose of organic fertilizer, with important economic efficiency.

The analysis of the chemical composition of red clover forage showed that the application of chemical products, such as lime amendments and a dose of 20 t/ha manure led to a substantial increase in the proportion of protein and lower percentage of cellulose; the phosphorus is present in optimum values, the potassium is below 2%, while calcium is stimulated to some extent by the dose of amendment and organic fertilizer.

By analyzing and interpreting the percentage values of the main chemicals contained in the red clover forage it was demonstrated that addressing this research topic is necessary for agro tourism farms and households, as high yields were obtained with a lower residual chemicals content in the case of amended cultures.

It was determined that the red clover (*Trifolium pratense*) is a profitable crop, recommended for high capitalization of acidic soils. The organic fertilizers in dose of 20 t/ha are profitable due to relevant increases in production, since the amendments applied do not raise the cost of production, bringing substantial benefits and high food security for the animal food specialties, obtained from this forage.

Therefore, relevant and documented interpretation and analysis of our research demonstrated that protein forage with a high nutritional and ecologic value was obtained, revealed by chemical analyses. They can be designated for agro tourism farms and households, through which food products of animal origins can be manufactured, which would offer a high degree of food security and traceability to the local traditional culinary specialties offered to tourists since the soil can support the rotation of cultures due to its improvements. The results confirm that this crop is a viable solution for obtaining large productions with a high nutritional and ecological value, due to its capacity to diminish the effects of land degradation in a changing climate and its integration into sustainable food production systems.

References

- Abberton M.T., (2007), Interspecific hybridization in the genus *Trifolium*, *Plant Breeding*, **126**, 337–342.
- Barke M., (2004), Rural tourism in Spain, *The International Journal of Tourism Research*, **6**, 137–149.
- Călina A., (2007), *Agri-Tourism and C.G.A.T.*, Sitech Publishing House, Craiova, Romania.
- Călina J., (2008), *Agri-Tourism*, Sitech Publishing, Craiova, Romania.
- Călina A., Calina J., Romulus I., Croitoru A., (2009), *Researches on the Potential and Impact of Agrotourism upon the Economic and Social-Cultural Development of Rural Areas in the South-West of Romania*, Proc. of the 44rd Croatian & 4rd International Symposia on Agriculture, University of Zagreb, Faculty of Agriculture, Croatia, 139-143.
- Călina A., Calina J., Iagaru R., Milut M., Iagaru P., (2010a), *Researches Concerning the Evolution and Influence of Agrotourism in Durable Development of Gorj County – Romania*, Proc. 45rd Croatian & 5rd Int. Symp. on Agriculture, University of Zagreb, Faculty of Agriculture, Croatia, 214-218.
- Călina J., Calina A., Croitoru A., (2010b), *Stimulation of border and intercounty cooperation by capitalization of agrotouristical resources from Dolj County – Romania*, Proc. -45 rd Croatian & 5 rd Int. Symp. on Agriculture, University of Zagreb, Faculty of Agriculture, Croatia, 219-223.
- Călina A., Călina J., (2011a), Study regarding the determination of the agro tourism resources in Cozia national park and the impact of this activity development on the contiguous rural space, *Bulletin UASVM Agriculture*, **68**, 103-109.
- Călina J., Călina A., (2011b), Technical – material basis of agro tourism support of touristic potential in Romania, *Bulletin UASVM Agriculture*, **68**, 234-240.
- Călina J., Călina A., Stoian M., (2011), Evolution of main indicators of the offer and tourist movement from Brasov County, *Annals of University of Craiova, Series Agriculture - Montanologie – Cadastre*, **XLI**, 234-239.
- Charles I., (1988), Essays on the variety of violet clover (*Trifolium pratense*, 1985 – 1987), *Swiss Magazine of Agriculture*, 25-36.
- Croitoru A., Miluț M., (2008), Researches concerning red clover (*Trifolium pratense*) technology, cultivated in the hill area of Oltenia, *Annals of University of Craiova, Series Agriculture - Montanologie – Cadastre*, **XXXVIII**, 405-411.
- Dragomir N., (2001), *The Reaction of Some Genotypes of Fodder Leguminous Plants when Treated of Artificial Bacteria*, Colloquium Romanian - French Current trends in research on permanent grassland, Delhi – Brasov, 19-24.
- Dunea D., (2008), Persistence assessment of red clover (*Trifolium Pratense* L.) in Târgoviste plain, *Animal Science and Biotechnologies Scientific papers*, **41**, 245-253.
- Gartner W.C., (2004) Rural tourism development in the USA, *The International Journal of Tourism Research*, **6**, 151-164.
- Grolleau H., (1987), *Rural Tourism in the 12 States of CEE*, General Direction of Transport TER, 23-28.
- Hatch D., Joynes A., Roderick S., Shepherd M., Goodlass G., (2014), Effects of cutting, mulching and applications of farmyard manure on the supply of nitrogen from a red clover/grass sward, *Organic Agriculture*, **4**, 15-24.
- Hernández-Mogollón JM., Campón-Cerro AM., Alves A., (2013), Authenticity in environmental high-quality destinations: a relevant factor for green tourism demand, *Environmental Engineering and Management Journal*, **12**, 1961-1970.
- Ionescu I., (1998), The influence of perennial leguminous plants on temporary grassland production and on nitrogen fertilizer capitalization, *Annals of University of Craiova*, **XXIX**, 252-257.

- Ionescu I., (2001), *Meadows Culture*, Sitech Publishing, Craiova, Romania.
- Ionescu I., (2003), *Temporary Meadows in the Sub-Carpathian area of Oltenia*, Sitech Publishing, Craiova, Romania.
- Iepema G., Van Eekeren N., Van Dongen M., (2006), Production and persistency of red clover (*Trifolium pratense*) varieties when grown in mixtures, *Grassland Science in Europe*, **11**, 388-392.
- Jeangros B., (2006), Perennial leguminous plants of the sustainable grassland production, *Swiss Magazine of Agriculture*, 4-9.
- Louwagie G., Gay S.H., Burre A., (2009), *SoCo: Sustainable Agriculture and Soil Conservation, 2007-2009*, European Communities, On line at: <http://eusoils.jrc.ec.europa.eu/projects/SOCO/>.
- Moinet F., (2006), *Rural Tourism*, Editions France Agricole, Paris.
- Mosimann E., (2008), Standard mixture of the production grasslands 2009-2012, *Swiss Magazine of Agriculture*, 6-10.
- Muntean L., (2002), *Study of genetic resources of red clover (Trifolium pratense) for improvement*, PhD Thesis, USAMV Cluj – Napoca, Romania.
- Peț E., Dragomir N., Selegean M., Dragomir C., (2005), *Studies looking upon the effect of some biostimulants on the quantity and quality production of birdsfoot trefoil*, Quality Production and Quality of the Environment in the Mountain Pastures of Enlarged Europe, Udine, Italy, 15-21.
- Peț E., Dragomir N., Peț I., Dragomir C., (2006), *The economic efficiency obtained after the application of biostimulants on red clover culture*, Animal husbandry, veterinary and agroecology in transitional processes, Faculty of Agriculture, University of Novi Sad, 303-310.
- Plog S.C., (2003), *Travelling for Pleasure - Marketing Manual*, Pearson Prentice Hall Publishing House, Upper Saddle River, New Jersey.
- Stoian M., (2006), *Management of the Pension, Manual and Legislative Supplement*, ANTREC Publication, Alba-Iulia, Romania.
- Stoll W., (2007), Grass, the base for nutrition of ruminants, *Swiss Magazine of Agriculture*, 12-17.
- Vântu V., (2004), *Grassland and Forage Crop*, Ion Ionescu de la Brad Publishing House, Iasi, Romania.



“Gheorghe Asachi” Technical University of Iasi, Romania



EFFECT OF HYDROGEN ADDITION ON EXHAUST EMISSIONS AND PERFORMANCE OF A SPARK IGNITION ENGINE

Yasin Karagöz*, Emre Orak, Levent Yüksek, Tarkan Sandalcı

*Yıldız Technical University, Mechanical Engineering Faculty, Laboratory of Internal Combustion Engines,
Automotive Division, 34349 Istanbul, Turkey*

Abstract

The use of hydrogen in spark ignition engines as a supplementary fuel can enhance combustion and reduce toxic emissions. Difficulties in hydrogen storage and production limit its use in internal combustion engines. This paper investigates the performance of a spark ignition engine with the addition of a mixture of hydrogen (H_2) and oxygen (O_2) into the intake manifold. Hydrogen is produced by an alkaline electrolyser and consumed simultaneously to eliminate the need for a storage device. Flow rates of 0 and 10 L/min H_2 - O_2 mixture were introduced into the manifold. No flow, or 0 L/min, refers to the case without hydrogen, and 10 L/min represents the case with hydrogen. Brake torque, fuel consumption, nitrogen oxides, carbon monoxide, and total unburned hydrocarbons were measured. The results show that brake power, brake torque, and nitrogen oxide emissions increased with the addition of H_2 - O_2 , while total unburned hydrocarbons, carbon monoxide emissions, and brake-specific energy consumption decreased.

Key words: electrolysis, hydrogen fuel, spark ignition engine

Received: August, 2013; Revised final: June, 2014; Accepted: July, 2014

1. Introduction

Increasing energy demand and environmental concern have stimulated researchers' interest in non-polluting alternatives to petroleum-derived fuels. Today, a significant part of the energy demand is met by fossil fuels. In spite of the measures taken by the *Kyoto Protocol to the United Nations Framework Convention on Climate Change* during the period of 1990-2004, CO_2 emissions increased by 27% and the energy consumption of the transportation sector increased by 37%, which was not forecast (Sopena et al., 2010). Petroleum-based fuels can be replaced in part by an alternative energy source such as hydrogen (Al-Baghdadi, 2004; Lako et al., 2008; Sastri, 1987). Automotive manufacturers have developed different technologies, such as fuel cell, hydrogen fuelled internal combustion engine (ICE), hybrid, and electric vehicle configurations (Offer et al., 2010; Pasculete et al., 2007). Some manufacturers have

been making progress on polymer electrolyte membrane fuel cells (PEMFC), but investment costs are high and a PEMFC requires high purity hydrogen. Thus, investment and operation costs of fuel cell systems are even more expensive than other hydrogen fuelled engines (Sopena et al., 2010). One way to increase performance of a spark ignition (SI) engine is to use supplementary fuels, which improve thermal efficiency and reduce emissions (Bari and Esmaeil, 2010).

Hydrogen has unique combustion properties, and using hydrogen as a supplementary fuel in internal combustion engines improves thermal efficiency and tail-pipe emissions. The diffusion coefficient of hydrogen is higher than gasoline, which improves the homogeneity of the combustible mixture (Ji and Wang, 2009a). The flame speed of hydrogen is five times higher than that of gasoline, which improves thermal efficiency because the combustion of hydrogen is much closer to ideal

* Author to whom all correspondence should be addressed: e-mail: ykaragoz@yildiz.edu.tr; Phone: +902123832901; Fax: +90 212 2616659

constant volume combustion in ICEs (Ji and Wang, 2009b; Ma et al., 2008).

Alternative fuels can be used as bulk or supplements; the most common instance for this type of application is biodiesel (Dai et al., 2014; Lapuerta et al., 2008; Nita and Mandopol, 2009; Opera et al., 2009). Using supplementary fuels is a promising method to reduce the cost of fossil fuels. Hydrogen is the most promising additive that can significantly reduce fuel consumption and harmful emissions in ICEs (Bari and Esmaeil, 2010; Pasculete et al., 2007). Bari and Esmaeil (2010) used an H_2 - O_2 mixture as an additional fuel in a diesel engine at 1500 rpm under different loads. The authors reported that the brake thermal efficiency and nitrogen oxide (NO_x) emissions increased, while total hydrocarbons (THC), carbon dioxide (CO_2), and carbon monoxide (CO) emissions decreased with H_2 - O_2 addition. Ji and Wang (2009a) investigated hydrogen as a supplementary fuel in 3% and 6% volume fractions of total fuel intake at a constant engine speed of 1400 rpm. An increase in brake thermal efficiency of the engine was reported with hydrogen addition. Furthermore, the authors indicated that THC and CO emissions were reduced with hydrogen addition. Kumar et al. (2003) investigated hydrogen addition in an SI engine. The authors reported an increase in brake thermal efficiency and a reduction in tail-pipe emissions. Tomita et al. (2001) published similar results. In the study of Saravanan et al. (2008) hydrogen was introduced into cylinders as a supplementary fuel at rates of 10 L/min and 20 L/min, and performance parameters with and without exhaust gas recirculation (EGR) were investigated (Saravanan et al., 2008). The authors obtained an increase in brake thermal efficiency. Stebar and Parks (1974) carried out a study on a single-cylinder SI engine fuelled with a hydrogen-gasoline mixture. According to the authors, the lean burn limit of the engine was extended by hydrogen enrichment, and NO_x emissions decreased. However, THC emissions increased with the increase in excess air in the air-fuel mixture. Apostolescu and Chiriac (1996) studied the effect of hydrogen addition to a single cylinder SI engine. Shortened combustion durations, reduced cycle-to-cycle variations, and extended lean limits of operation were reported by the authors. Ma and Wang (2008) investigated the performance of hydrogen-enriched methane. According to their results, thermal efficiency was improved with hydrogen addition and toxic emissions were decreased. Additionally, cyclic variations were improved and the lean burn limit of the natural gas engine was extended with hydrogen addition. Ji and Wang (2009b) investigated the effect of hydrogen addition on SI engine performance at idle and stoichiometric conditions. The authors found that the engine thermal efficiency and emissions were improved after hydrogen enrichment. Ceviz et al. (2012) investigated hydrogen addition of 0%, 2.14%, 5.28%, and 7.74% by volume to a spark ignition engine at 2000 rpm constant engine speed.

According to their results, brake-specific fuel consumption, THC, and CO emissions decreased, whereas NO_x emissions increased with hydrogen addition. Wang et al. (2012) experimentally investigated the effect of hydrogen-oxygen blends as supplementary fuel on engine performance and emissions of a gasoline engine. The blends were called hydroxygen in this study (Wang et al., 2012). A hybrid electronic control unit (ECU) was developed to control spark timing and the overall volume fraction of hydroxygen. The hydroxygen was varied from 0% to 100% by varying the injection duration of the injectors. According to their results, flame development and propagation duration periods were shortened and emissions were reduced. Ji et al. (2012) carried out a study of a hybrid hydrogen-gasoline engine with a hydrogen injection system and a hybrid ECU that they developed. The engine was operated with hydrogen at cold start and was operated with hydrogen-gasoline blends at idle and part loads. According to their results, thermal efficiency was improved and emissions were reduced with hydrogen addition. Ji et al. (2013) studied the emissions of a passenger car powered by a hydrogen-gasoline engine under the New European Driving Cycle. The hydrogen was produced by a water electrolyser, and they found that CO and THC emissions were reduced by 62.1% and 64.1%, respectively. Several studies offer similar results for hydrogen enrichment (D'Andrea et al., 2004; Li et al., 1998; Varde, 1981; Wang et al., 2011).

Most of the studies that investigated hydrogen implementation indicated a fuel storage problem. Hydrogen has a very low density. It can be stored in pressurized tanks or it can be combined chemically with a metal alloy (Bari and Esmaeil, 2010). However, a tank is required to store hydrogen on-board a vehicle, which increases overall system weight (Fontana et al., 2002). Alternatively, when hydrogen is stored as a liquid, on-board cryogenic container costs are high and a significant amount of energy is needed to convert gaseous hydrogen into liquid phase (White et al., 2006). To solve the storage difficulties, the hydrogen can be produced on-board through the electrolysis of water. On-board production eliminates the need for a high pressure tank and provides for safer operation. A simultaneous producing-consuming operation makes the application safer.

In this study, the effect of hydrogen addition on SI engine performance and emissions was investigated. Hydrogen fuel was produced by electrolysis of water in an alkaline solution. The flow rate of supplementary fuel was set to a constant 10 L/min.

2. Experimental setup

2.1. Test engine and modifications

Tests were carried out on a multi-cylinder spark ignition engine with an electronically

controlled port fuel injection system. The main engine specifications are listed in Table 1. The test bench was modified for hydrogen injection. The H₂-O₂ mixture and gasoline were separately introduced into the intake manifold for each cylinder.

A schematic diagram of the hydrogen line is shown in Fig. 1. The H₂-O₂ mixture was delivered into the engine with an additional fuel supplement system. A pressure regulator was used to reduce the pressure of the H₂-O₂ gas mixture produced by the electrolyser. The H₂-O₂ gas mixture passed through a bubbler before being fed to the engine to prevent backfires. A relief valve was used to prevent overpressure, and a second pressure regulator was

installed to regulate line pressure. A thermal mass-flow meter was used to measure flow rate. A rotameter was also used to check the hydrogen fuel flow rate against the thermal mass-flow meter. A buffer tank was installed between the flow meters and engine to reduce H₂-O₂ mixture flow fluctuations. A check valve and a flame arrestor were used before the engine intake manifold to prevent backfiring. The gas pressure regulator and hydrogen line were made of 316 stainless steel to fulfil ECE R110, EIHP Draft, and ECE R67 standards (ECE R67, 2013; ECE R110, 2013; EIHP regulations, 2000).

Table 1. Specifications of the engine

| Definition | Value/Specification |
|--|----------------------------|
| Manufacturer & Type | Peugeot-1B53318F |
| Displacement volume (cm ³) | 1124 |
| Number of cylinders | 4 |
| Bore/stroke (mm) | 72/69 |
| Compression ratio | 10.2:1 |
| Number of valves per cylinder | 4 |
| Rated power | 44 kW@5500 rpm |
| Aspiration | Naturally aspirated |
| Ignition system | Electronic |
| Fuel system | Multi-point fuel injection |
| Cylinder arrangement | In-line |

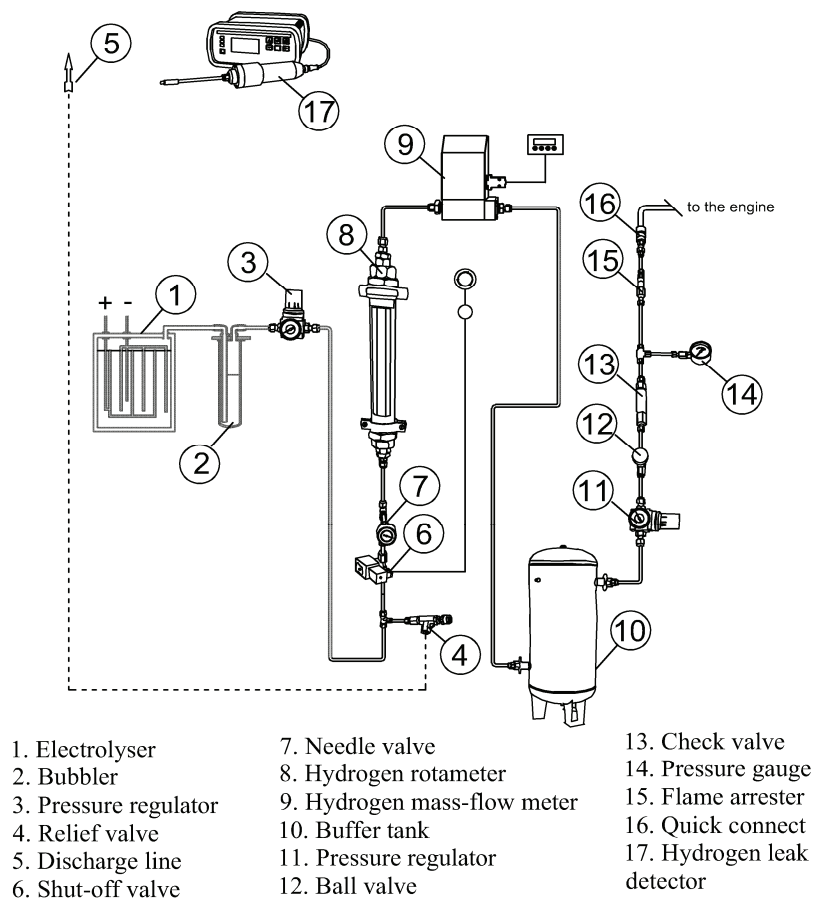


Fig. 1. Schematic diagram of hydrogen fuel system

No modification was made to the original ECU of the test engine. A self-developed ECU was used to trigger the hydrogen injectors. The flow rates of injectors were determined according to the signal length with a series of preliminary tests. A power supply with constant current capability was used to control the current and the voltage of the electrolyser. The safety system of the test cell was upgraded to prevent possible hazards. An air venting system was used to prevent hydrogen accumulation, and a hydrogen leak detector was installed to detect hydrogen leaks.

2.2. Test bench

The test bench scheme is shown in Fig. 2. A hydrokinetic dynamometer was used to load the test

engine, where the load was varied by controlling the servo motor position. A turbine-type flow meter was used to measure the gasoline flow rate. The exhaust emissions were measured with an AVL Dicom 4000 exhaust gas analyser.

During experiments, the brake torque, brake power, brake-specific energy consumption (BSEC), NO_x , THC, and CO measurements were acquired with a data acquisition system (DAS) at a sampling rate of 1 Hz. The accuracies of the measurements and the uncertainties in the calculated results are listed in Table 2. All of the tests were performed at steady-state and part-load conditions with constant throttle position. Additionally, tests were conducted with a stoichiometric air-fuel ratio (AFR) value, which is typical for a catalyst-equipped SI engine.

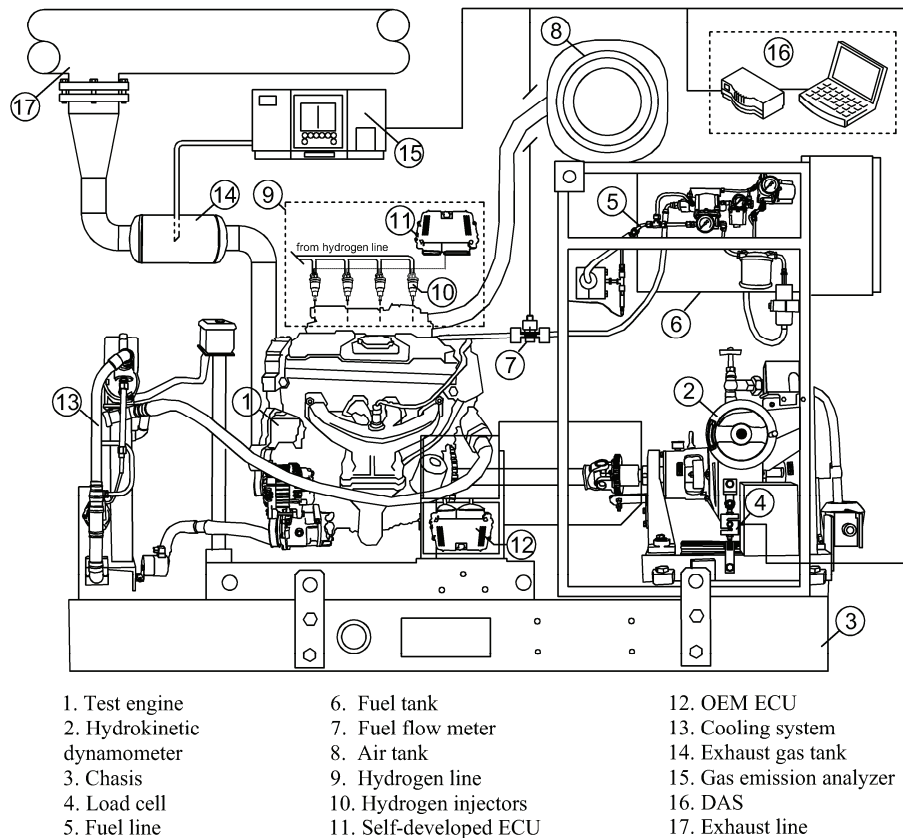


Fig. 2. Schematic diagram of test bench

Table 2. Accuracies of the measurements and uncertainties of calculated results

| Measured parameter | Measurement device | Accuracy |
|---------------------------|---------------------|---|
| Engine torque | Load cell | ± 0.05 Nm |
| Engine speed | Incremental encoder | ± 5 rpm |
| Fuel flow rate | Sika VZ 0.2 | $\pm 1\%$ |
| Hydrogen mass-flow rate | New-flow TLF | $\pm 1\%$ |
| CO | AVL Dicom 4000 | ± 0.01 vol.% |
| THC | AVL Dicom 4000 | ± 1 ppm |
| NO_x | AVL Dicom 4000 | ± 1 ppm |
| Calculated results | | Uncertainty (entire speed range) |
| Brake power | | $\pm 0.09 \div 0.12\%$ |
| BSEC | | $\pm 0.43 \div 0.56\%$ |

The flow rates of 0 L/min and 10 L/min H_2 - O_2 mixture were introduced into the intake manifold as additional fuel at 1500, 2000, 2500, 3000, and 3500 rpm engine speeds. The H_2 - O_2 flow rate was set at 10 L/min constantly to demonstrate that using a small amount of hydrogen can enhance gasoline combustion.

Using higher levels of hydrogen requires high levels of electrical energy, making it very difficult to implement this system on the electrical architecture of current vehicles. During the study, the introduced hydrogen to oxygen molar ratio was 2:1. The energy content of additional H_2 - O_2 at 1500, 2000, 2500, 3000, and 3500 rpm was equal to 3.3%, 2.7%, 2.2%, 1.9% and 1.7% of the total energy of the charge, respectively.

3. Results and discussion

Brake power and brake torque variation are shown in Fig. 3. According to the results, engine performance improved with hydrogen addition for the entire engine speed range measured. The maximum brake power of the engine increased by 1% at 3500 rpm engine speed with 10 L/min H_2 - O_2 enrichment.

BSEC is defined as the amount of energy consumed per kilowatt of power produced by the engine. For comparing the fuel economy of test fuels, BSEC is better than brake-specific fuel consumption because the heating value and density of the fuels exhibit different trends. The variation of BSEC is shown in Fig. 4. The figure reveals that adding a small amount of H_2 - O_2 decreases BSEC regardless of the engine speed. The higher flame speed of the mixture has a positive effect on improving BSEC because the flame speed of hydrogen is five times as large as that of gasoline (Ji and Wang, 2009b; Ji and Wang, 2010a). Additionally, hydrogen has a wider flammability range than gasoline (Ji and Wang, 2009a). Consequently, the shorter burning duration and wider flammability range of the hydrogen gasoline mixture lead to higher combustion efficiency (Ma et al., 2008). For this reason, it can be concluded that a higher degree of constant volume combustion is completed, which means that an SI engine operates much closer to its theoretical cycle (Ji and Wang, 2009b). According to the test results, BSEC reduction reached its maximum value of 8.64% at 1500 rpm, while the minimum of 1.17% was obtained at 2500 rpm.

The results clearly indicate that the thermodynamic improvement of the test engine minimizes BSEC in the high efficiency region and vice-versa. Improvement in BSEC mainly originated in lower amount of gasoline injection which was a result of engine control unit algorithm. Neither an interruption nor a signal modification was implemented on the ECU. However, as shown in Fig. 5, the gasoline injection quantity decreased significantly. The main reason for this situation is the

decrease in the inducted air due to the gas phase injection of the H_2 - O_2 mixture. Hydrogen possesses many unique combustion properties that improve the more complete combustion in ICEs (Ji and Wang, 2009a). THC, CO, and NO_x are the main toxic pollutants that are emitted from ICEs, and these toxic pollutants can be reduced by inducing hydrogen into gasoline (Ji and Wang, 2009b). The variation of THC is depicted in Fig. 6.

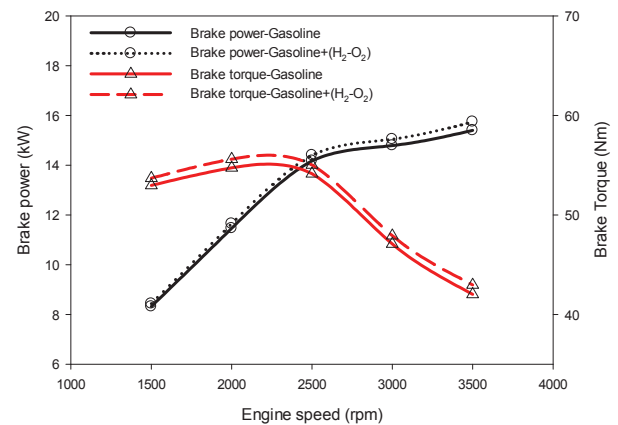


Fig. 3. Variations in brake power and brake torque at part-load operation versus engine speed

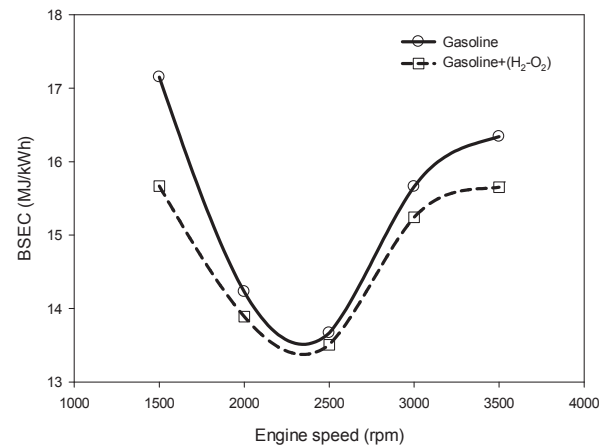


Fig. 4. Variation of BSEC versus engine speed

According to the Fig. 6, THC emissions were decreased regardless of the engine speed by inducing H_2 - O_2 mixture. Similar results are explained in the literature as the formation of OH radicals accelerated by hydrogen addition (Ji and Wang, 2009b). Due to the accelerated formation of OH and the improved chain reaction, a gasoline-hydrogen mixture can be more completely burnt and will emit less THC (Ji and Wang, 2009a). Additionally, the decrease in THC emissions can be related to H_2 - O_2 induction because of the absence of carbon in hydrogen fuel (Bari and Esmaeil, 2010).

Lastly, the shorter quenching distance of hydrogen causes a reduction in THC emissions (Ji and Wang, 2010b). The quenching distance of

hydrogen is one-third that of gasoline (Ji and Wang, 2010b). Therefore, the flame of a gasoline hydrogen mixture can be propagated much closer to cylinder walls and crevices than can gasoline fuel (Ji and Wang, 2009a). A maximum reduction in THC of 13.3% was obtained at 2000 rpm.

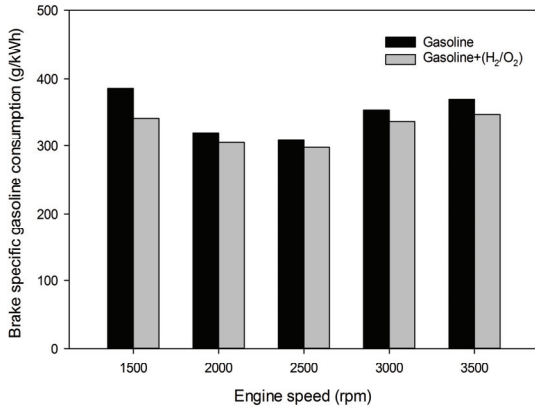


Fig. 5. Brake-specific gasoline consumption of the test engine

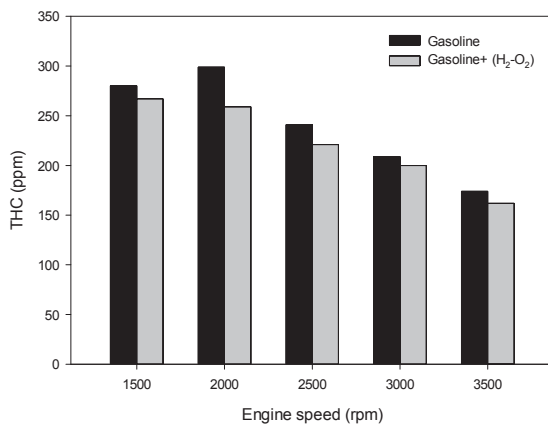


Fig. 6. Variation of THC emissions versus engine speed

The variation of NO_x emissions at part-load conditions with 10 L/min H₂-O₂ addition is shown in Fig. 7. According to test results, NO_x emissions were increased with hydrogen addition regardless of the engine speed. A maximum increase of 17.6% was obtained at 3000 rpm, while the minimum gain measured was 3.7% at 2000 rpm. When the increase of NO_x emissions and improvement of engine performance are considered together, it is concluded that peak cylinder pressure and bulk cylinder temperature were increased with hydrogen addition (Bari and Esmail, 2010).

Both high temperature and more available oxygen in the charge may cause NO_x emissions to rise (Heywood, 1988). It is expected that the maximum NO_x emission will occur at maximum torque range in ICEs, but higher NO_x measurements in test results can be attributed to additional oxygen introduced into the cylinder. Almost equal NO_x at low engine speeds indicates the improvement of combustion. Due to a constant flow rate of the H₂-O₂

mixture, the inducted oxygen amount per cycle decreased at higher engine speeds. Significant reduction of NO_x emissions at higher engine speeds indicates the importance of the oxygen ratio. Additionally, the higher flame temperature and speed of hydrogen combustion cause higher local in-cylinder temperatures and a larger amount of NO_x emissions (Ji et al., 2012).

As shown in Fig. 8, CO emissions were lower than those from pure gasoline. The minimum CO reduction was observed at 2500 rpm, while the positive effect of H₂-O₂ addition on CO emission reached up to 10.7% at 3000 rpm. Considering the increase in CO emissions of gasoline fuel at higher engine speeds, one can easily conclude the reduction of combustion efficiency. Additionally, Fig. 7 clearly indicates the importance of H₂-O₂ mixture addition in the high rpm region. With respect to tail-pipe emissions, H₂-O₂ mixture addition improved combustion efficiency while NO_x emissions increased.

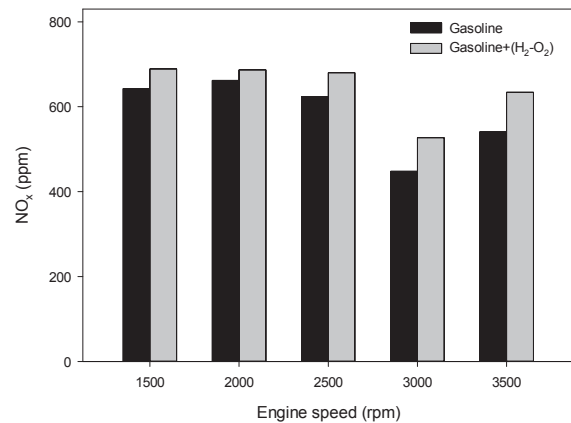


Fig. 7. Variation of NO_x versus engine speed

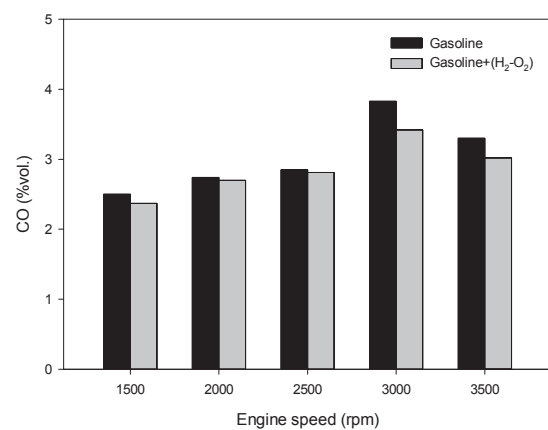


Fig. 8. Variation of CO versus engine speed

4. Conclusions

An experimental study was conducted to investigate the effects of hydrogen addition on emissions and performance of a gasoline engine. During the experiments, an SI engine was operated at part-load, and the throttle was kept at a constant

position; 0 L/min and 10 L/min of an H₂-O₂ mixture as supplementary fuel was introduced into the intake manifold, where 0 L/min is referring to the case without hydrogen and 10 L/min refers to the case with hydrogen.

The required amount of H₂-O₂ mixture was produced by an alkaline water electrolyser and simultaneously consumed by the engine. The high diffusion coefficient of hydrogen improves the homogeneity of the combustible mixture. The flame speed of hydrogen is higher than gasoline, so using a small amount of H₂-O₂ mixture as additional fuel improves combustion efficiency. Additionally, engine performance and emissions were evaluated. It was proved that by using a small amount of hydrogen, stringent emission regulations will be met, and the hydrogen will have a positive effect on the environment. The effect is positive because emissions of greenhouse gases from combustion of fossil fuels cause global warming and are responsible for adverse environmental effects such as photochemical smog, acid rain, and the death of forests.

The emissions of THC and CO are reduced by hydrogen addition, but NO_x emissions are increased due to higher in-cylinder temperatures.

Further studies are required to reveal the effect of different amounts of the H₂-O₂ mixture on engine parameters. In particular, higher engine-out NO_x emissions will have to be considered, so a possible optimisation and/or trade-off solution may be required. Lowering nitrogen oxides without a penalty from the findings mentioned above can be maintained by varying the engine control parameters such as the ignition timing and EGR ratio. Finally, hydrogen has the potential to reduce tail-pipe emissions, and the instantaneous production and consumption method is a safe means of integration into gasoline engine-powered vehicles.

Nomenclature

| | |
|-----------------|---|
| BSEC | Brake-specific energy consumption, MJ/kWh |
| CO | Carbon monoxide |
| CO ₂ | Carbon dioxide |
| DAS | Data acquisition system |
| ECE | Economic Commission for Europe |
| ECU | Electronic control unit |
| EIHP | European Integrated Hydrogen Project |
| EGR | Exhaust gas recirculation |
| H ₂ | Hydrogen |
| ICE | Internal combustion engine |
| NO _x | Nitrogen oxide |
| OH | Hydroxyl radical |
| O ₂ | Oxygen |
| PEMFC | Polymer electrolyte membrane fuel cell |
| rpm | Revolutions per minute (engine speed) |
| SI | Spark ignition |
| THC | Total hydrocarbons |

References

- Al-Baghdadi M.A.R.S., (2004), Effect of compression ratio, equivalence ratio and engine speed on the performance and emission characteristics of a spark ignition engine using hydrogen as a fuel, *Renewable Energy*, **29**, 2245-2260.
- Apostolescu N., Chiriac R., (1996), A study of combustion of hydrogen-enriched gasoline in a spark ignition engine, SAE International, 960603, On line at: <http://papers.sae.org/960603/>.
- Bari S., Esmail M.M., (2010), Effect of H₂/O₂ addition in increasing the thermal efficiency of adiesel engine, *Fuel*, **89**, 378-283.
- Ceviz M.A., Sen A.K., Küleri A.K., Öner İ.V., (2012), Engine performance, exhaust emissions, and cyclic variations in a lean-burn SI engine fueled by gasoline-hydrogen blends, *Applied Thermal Engineering*, **36**, 314-324.
- Dai H., Peng J., Qiu T., Li X., Lei Y., (2014), Investigation on impact of biodiesel on injection process of unit pump fuel system, *Environmental Engineering and Management Journal*, **13**, 1843 - 3707.
- D'Andrea T., Henshaw P., Ting D.S.K., (2004), The addition of hydrogen to a gasoline-fuelled SI engine. *International Journal of Hydrogen Energy*, **29**, 1541-1542.
- ECE R110, (2013), Proposal for Supplement 1 to the 01 series of amendments to Regulation No. 110 (CNG vehicles), Economic Commission for Europe-Inland Transport Committee (World Forum for Harmonization of Vehicle Regulations), Geneva, On line at: <http://www.unece.org/fileadmin/DAM/trans/doc/2013/wp29/ECE-TRANS-WP29-2013-101e.pdf>.
- ECE R67, (2013), Proposal for Supplement 1 to the 01 series of amendments to Regulation No. 110 (CNG vehicles), Economic Commission for Europe-Inland Transport Committee (World Forum for Harmonization of Vehicle Regulations), Geneva, On line at: <http://www.unece.org/fileadmin/DAM/trans/doc/2013/wp29/ECE-TRANS-WP29-2013-097e.pdf>.
- EIHP regulations, (2000), European Integrated Hydrogen Project, Geneva, On line at: <http://www.eihp.org/>.
- Fontana G., Galloni E., Jannelli E., Minutillo M., (2002), *Performance and Fuel Consumption Estimation of a Hydrogen Enriched Gasoline Engine at Part-Load Operation*, SAE International 2002-01-2196, On line at: <http://papers.sae.org/2002-01-2196/>.
- Heywood J.B., (1988), *Internal Combustion Engine Fundamentals*, McGraw-Hill, New York.
- Ji C.W., Wang S.F., (2009a), Effect of hydrogen addition on combustion and emissions performance of a spark ignition gasoline engine at lean conditions, *International Journal of Hydrogen Energy*, **34**, 7823-7834.
- Ji C.W., Wang S.F., (2009b), Effect of hydrogen addition on the idle performance of a spark ignited gasoline engine at stoichiometric condition, *International Journal of Hydrogen Energy*, **34**, 3546-3556.
- Ji C.W., Wang S.F., (2010a), Combustion and emissions performance of a hybrid hydrogen-gasoline engine at idle and lean conditions, *International Journal of Hydrogen Energy*, **35**, 346-55.
- Ji C.W., Wang S.F., (2010b), Experimental study on combustion and emissions performance of a hybrid hydrogen-gasoline engine at lean burn limits, *International Journal of Hydrogen Energy*, **35**, 1453-1462.
- Ji C., Wang S., Zhang B., (2012), Performance of a hybrid hydrogen-gasoline engine under various operating conditions, *Applied Energy*, **97**, 584-589.

- Ji C., Wang S., Zhang B., Liu X., (2013), Emissions performance of a hybrid hydrogen-gasoline engine-powered passenger car under the New European Driving Cycle, *Fuel*, **106**, 873-875.
- Kumar M.S., Ramesh A., Nagalingam B., (2003), Use of hydrogen to enhance the performance of a vegetable oil fuelled compression ignition engine, *International Journal of Hydrogen Energy*, **28**, 1143-1154.
- Lakó J., Hancsók J., Yuzhakova T., Marton G., Utasi A., Rédey Á., (2008), Biomass – a source of chemicals and energy for sustainable development, *Environmental Engineering and Management Journal*, **7**, 499-509.
- Lapuerta M., Armas O., Rodriguez-Fernandez J., (2008), Effect of biodiesel fuels on diesel engine emissions, *Progress in Energy and Combustion*, **34**, 198-223.
- Li J.D., Guo L.S., Du T.S., (1998), Formation and restraint of toxic emissions in hydrogen-gasoline mixture fueled engines, *International Journal of Hydrogen Energy*, **23**, 971-975.
- Ma F.H., Wang Y., (2008), Study on the extension of lean operation limit through hydrogen enrichment in a natural gas spark-ignition engine, *International Journal of Hydrogen Energy*, **33**, 1416-1424.
- Ma F.H., Wang Y., Liu H.Q., Li Y., Wang J.J., Ding S.F., (2008), Effects of hydrogen addition on cycle-by-cycle variations in a lean burn natural gas spark-ignition engine, *International Journal of Hydrogen Energy*, **33**, 823-831.
- Nita I., Mandalopol D., (2009), Study of the viscosity of some biodiesel – diesel oil blends, *Environmental Engineering and Management Journal*, **8**, 639-643.
- Offer G.J., Howey D., Contestabile M., Clague R., Brandon N.P., (2010), Comparative analysis of battery electric, hydrogen fuel cell and hybrid vehicles in a future sustainable road transport system, *Energ Policy*, **38**, 24-29.
- Oprea I., Pişă I., Mihăescu L., Prisecaru T., Lăzăroiu G., Negreanu G., (2009), Research on the combustion of crude vegetable oils for energetic purposes, *Environmental Engineering and Management Journal*, **8**, 475-482.
- Păsculete E., Condrea F., Rădulescu C., (2007), Hydrogen and sustainable energy. Research for hydrogen production, *Environmental Engineering and Management Journal*, **6**, 45-49.
- Saravanan N., Nagarajan G., Kalaiselvan K.M., Dhanasekaran C., (2008), An experimental investigation on hydrogen as a dual fuel for diesel engine system with exhaust gas recirculation technique, *Renewable Energy*, **33**, 422-427.
- Sastri M.V.C., (1987), Hydrogen Energy Research-and-Development in India - an Overview, *International Journal of Hydrogen Energy*, **12**, 137-145.
- Sopena C., Dieguez P.M., Sainz D., Urroz J.C., Guelbenzu E., Gandia L.M., (2010), Conversion of a commercial spark ignition engine to run on hydrogen: Performance comparison using hydrogen and gasoline, *International Journal of Hydrogen Energy*, **35**, 1420-1429.
- Stebar R.F., Parks F.B., (1974), *Emission Control with Lean Operation Using Hydrogen-Supplemented Fuel*, SAE International, 740187.
- Tomita E., Kawahara N., Piao Z., Fujita S., Hamamoto Y., (2001), *Hydrogen Combustion and Exhaust Emissions Ignited with Diesel Oil in a Dual Fuel Engine*, SAE International, 2001-01-3503, On line at: <http://papers.sae.org/2001-01-3503/>.
- Varde K.S., (1981), *Combustion Characteristics of Small Spark Ignition Engines Using Hydrogen Supplemented Fuel Mixtures*, SAE International, 810921, On line at: <http://papers.sae.org/810921/>.
- Wang S., Ji C., Zhang B., (2011), Starting a spark-ignited engine with the gasoline-hydrogen mixture, *International Journal of Hydrogen Energy*, **36**, 4461-4468.
- Wang S., Ji C., Zhang B., Liu X., (2012), Performance of a hydroxygen-blended gasoline engine at different hydrogen volume fractions in the hydroxygen, *International Journal of Hydrogen Energy*, **37**, 3209-3218.
- White C.M., Steeper R.R., Lutz A.E., (2006), The hydrogen-fuelled internal combustion engine: a technical review, *International Journal of Hydrogen Energy*, **31**, 1292-1305.



"Gheorghe Asachi" Technical University of Iasi, Romania



GRIDDED POPULATION DISTRIBUTION MAP FOR THE HEBEI PROVINCE OF CHINA

Yu Zhang^{1,2*}, Chun Dong², Jiping Liu², Shouzhi Xu³, Tinghua Ai¹, Fengguang Kang²

¹*School of Resource and Environmental Science, Wuhan University, 129 Luoyu Road, Wuhan, 430079 Hubei, China*

²*Chinese Academy of Surveying and Mapping, 28 Lianhuachi West Road, Haidian District, 100830 Beijing, China*

³*School of Geodesy and Geomatics, Wuhan University, 129 Luoyu Road, Wuhan, 430079 Hubei, China*

Abstract

Mapping the distribution of populations has become an important issue in geographical and relative researchers. Combining population and spatial data allows for socio-graphic information to be visualized, in order to evaluate the total numbers of people at risk of environmental health hazards, who have died in natural disasters etc. Therefore, spatial distribution of population data is an effective way to integrate statistical and spatial data. This paper presents a multi-factor data fusion modeling method for population estimation, which is based on spatial relationships that determine the factors affecting population distribution. The factors that have a strong correlation with population distribution in the Hebei Province were extracted using Geographic Information Systems (GIS). Their standardized weight coefficients were factored as weight coefficients of population distribution in a given spatial unit. The unit (1 km × 1 km) population database was established, allowing for the computation of the relevant population data error. The accuracy of the map was then assessed by comparing predicted population data with that collected from the local government. The results show that the population correlated with geographical factors. The population of the Hebei Province was distributed heterogeneously, increasing from the northwest to southeast. There was relatively low population density in the Taihang Mountains in the west and in the Yanshan Mountains in the northeast, with less than 100 people per square kilometer. The population density in the central Hebei Province was higher, with about 2,000 people per square kilometer, which was higher and denser than that in Handan, Shijiazhuang, Langfang, and Tangshan. These findings may be important for data mining (DM), Decision-making Support Systems (DSS), and regional sustainable development.

Key words: data fusion, grid population, Hebei Province, multi-factor fusion, partial correlation coefficient

Received: September, 2013; Revised final: January, 2015; Accepted: January, 2015

1. Introduction

Extrapolating information from large amounts of data from different sources, such as geographical, statistical, text, and image data is important for policy-making. However, more than eighty percent of all information is related to geographic location in our productive life (Wu, 2009). This information may also be related to different geographical factors in a given spatial unit. Thus, fusing statistical and spatial data provides a scientific basis for administrative planning, land improvement, urban and rural construction, and environmental planning and protection (Balk et al., 2006). Resources, energy,

food, environmental issues, and population concerns are among the most pressing global issues today. Resource shortages, environmental degradation, and other problems negatively affect sustainable, social, and economic development (Liu et al., 2006; Small and Cohen, 2004). Apart from playing an increasingly important role in monitoring these changes, Geographic information systems (GIS) also contribute towards regional social development decisions.

Estimations of the total population in irregular areas must be performed quickly and accurately when the need arises, such as in areas affected by nuclear contamination, epidemics, floods, or other

* Author to whom all correspondence should be addressed: e-mail: zhangyu6242@163.com; Phone: +86 10 6388 0559; Fax: +86 10 6388 0540

disasters (Hay et al., 2005; Linard et al., 2010). Several methods have utilized geographical elements and indicators of economic and social development to spatially integrate statistical and quantitative data to address this issue (Liu et al., 2003; Linard et al., 2012). However, these methods are far from ideal. Social statistics primarily focus on the spatial distribution of population-based data (Martin, 2006; Yan and Bian, 2007), while thematic layout charts visualize population and spatial data but are unable to describe population distributions within distinct geographical units or regions.

Current population databases also often fail to take environmental conditions into account. The first (V1) and second (V2) versions of the global population database only use population and administrative boundary data (Zhao et al., 2010), while UNEP/GRID is based only on population density and accessibility (Dobson et al., 2000; Yang et al., 2009). These methods lack precision and are inappropriate for analyzing structured data and environmental conditions, such as topographical features. In northwest China, for instance, the Gobi Desert dominates much of the environment; thus, people tend to settle near oases and the wetlands. Methods using social statistics, however, would fail to identify the significance of the geography in this case. Most existing solutions to this problem focus on selection and quantification of influencing factors in order to take into account the correlation among selected factors. The least squares method has been used to simulate population density in Zhengzhou using population statistics (Lu et al., 2003), while a database of urban layout parameters has also been combined with unit population information for data mining and decision making (He, 2011). These methods include remote-sensing inversion (Jensen et al., 1990), regression-based analysis (Briggs et al., 1997), multi-factor analyses of statistical models (Lloyd, 2010; Niu et al., 1998), Distance Weighted (DW) interpolation, Genetic Programming (GP) and Genetic Algorithms (GA) (Liao et al., 2010), and methods based on night-time imagery and land use data (Zeng et al., 2011). However, few data fusion models can handle the complexity that arises when multiple factors are included (Dong et al., 2000, 2003; Liao, 2005).

The multi-factor data fusion model is the most common approach for analyzing the spatial distribution of social data. In this type of analysis, a multi-factor fusion model is presented based on the weighted coefficients measured between geographical factors and population count to redistribute county unit populations to grid cells in the Hebei Province.

2. Material and methods

2.1. Study area

The area selected for this study was the Hebei Province (longitude: 113°30'-119°54'E, latitude:

36°6'-42°36'N; Fig. 1). The Hebei Province (marked in blue in Fig. 1), an administrative province of China, is located in the Northern China, and embraces capital Beijing and Tianjin municipality. The Hebei Province has an area of 187,693 km² and a population of 72.8 million, with 170 administrative counties. The geomorphology is mountainous and hilly with watersheds. The relative elevation difference ranges from about 52 to 2836 meters, with a mean elevation of about 450 meters.



Fig. 1. Location of the study area in China

2.2. Data sources

The data collected from various sources includes population count, a digital elevation model (DEM) and topographical, land cover, and landform data. The population count data for 2010 in the Hebei province were sourced from the 2011 Statistical Yearbook (National Bureau of Statistics of China, 2011). The data was at the county level.

Digital elevation model (DEM) data, topographical features, landform, and land cover datasets were used to reallocate county-based spatial population count data. DEM data were obtained from topographic mapping at the 1:250 000 scale, provided by the Hebei Bureau of Geoinformation, which were capable of reflecting micro-factors in the complex terrain of cities. Topographical features and land cover datasets were obtained from a topographic database at a scale of 1:100 000, provided by National Administration of Surveying, Mapping and Geoinformation (NASMG). Land cover factors included farmland, forests, meadows, water, residential areas, and unused land. Landform data at a scale of 1:250 000 were used by scanning and digitizing the National Physical Atlas of China from SinoMaps Press. Landform factors included plain, hill, platform, mountain, and plateau. The boundaries of administrative divisions, including provincial and county boundaries for Hebei Province at the 1:250

000 scales were obtained from National Basic Geographic Information Center of China.

2.3. Multi-factor data fusion model

2.3.1. Extracting geographical factors

The geographical factors database was established including topographical features, landform, altitude, slope, land cover, and land area by overlaying and analyzing with grid cells. We first created the grid with a $1 \text{ km} \times 1 \text{ km}$ cell size and geocoded each cell. Secondly, we extracted the layers, such as inhabitant sites, railways, highways, and waterways from the topographical database, and then overlaid this with the grid created above. Thirdly, the DEM database was used as a data source. According to the relative altitude and slope difference in the Hebei province, classification with the quantile method was taken as a basis to reflect regional differences, and then altitude was reclassified and resampled into nine categories from DEM with the surface analysis function, using ArcGIS10.0 software. Same software was used for obtaining slope.

The spatial analyst function of the software was adopted for resampling and reclassifying slope values into seven categories based on 4° intervals. In the fifth step, the landform layer was overlaid with a grid, and summary statistics for the area of each factor were calculated. Finally, a summary statistics area for each class of land cover was calculated.

2.3.2. Calculating and normalizing geographical factor weighted coefficients

A partial correlation coefficient between the geographical factors and the population was taken as the single-factor weight. The weight coefficient was then normalized for each factor in every county of the Hebei Province in China.

Taking a highway's length factor for example, if there are n grids in a county, the normalized length in the i^{th} grid is equal to the total length in the number of n grid divided by the highway length in the i^{th} grid. Moreover, the standardized weighted coefficient for highway length in the i^{th} grid is equal to the normalized weight coefficient multiplied by the highway weight coefficient.

The factors such as land cover factors included 6 categories: farmland, forest, meadow, water, residential, and unused land. For these factors, the land cover weight in the i^{th} grid is equal to the sum of the weight coefficient of each category multiplied by the area of each category. Additionally, the standardized weighted coefficient for land cover in the i^{th} grid is equal to the sum of the weight coefficient of land cover in the number of n grid divided by the land cover weight in the i^{th} grid. The calculation for the landform factor is the same as that for the land cover factor. The standardized multi-factor weight in the i^{th} grid was obtained from the sum of all factor weights divided by the multi-factor weight in the i^{th} grid, and finally the population in the

i^{th} grid is equal to the population count multiplied by the standardized multi-factor weight in the i^{th} grid.

2.3.3. Establishing a data fusion model for population data and geographic factors

Six factors from the geographical databases were selected: topographical factors, altitude, slope, landform, land cover, and land area. These factors were considered important because of their geographical particularity and diversity. Landform factors were omitted to avoid correlations with similar factors, represented as polygons in the databases. The landform factors included in these analyses were those represented in the databases as lines and points (e.g., the entries to habitat sites and the lengths of railways, highways, and waterways).

Geographical factors from the databases were extracted using ArcGIS10.0, in order to generate the data fusion model. The grid module was used to translate factors into a $1 \text{ km} \times 1 \text{ km}$ grid. Next, Mask was used to set the Nodata grid to zero for all geographic factors to ensure that results for the geographical factors were equal to actual values. Zonegrid was used to determine regional boundaries, and Valuegrid determined the grids for each geographic factor. Zonal statistics were used to generate an index of geographical factors for each city and county by dividing the final results by 106. This index was used with the Intersect module and overlay function. The average population was calculated by dividing the total population by its total region area. The framework for grid transformation for population data of the Hebei Province is presented in Fig. 2.

2.3.4. Multi-factor data fusion

A multi-factor fusion model was used to examine the relationships between geographical factors and population data. A significant correlation between two variables did not necessarily signify a causal relationship. Two variables can be highly correlated if both are affected by a third shared variable. Consequently, partial correlation coefficients (Fisher, 1924) were used to more accurately portray the relationships between the factors. Partial correlation coefficients (Rao and Sievers, 1995) were used as the weighted coefficients and then normalized (the sum of all weighted coefficients divided by the weighted coefficient). Correlation coefficients generally varied from -1 to 1, and a larger coefficient absolute value reflected a stronger association (Fisher, 1924). Three types of correlation coefficients were used. Pearson correlation coefficients (Dong et al., 2005) were used to analyze continuous variables, such as distance, while Spearman rank and Kendall correlation coefficients were used to analyze ranks.

The population database is divided into $1 \text{ km} \times 1 \text{ km}$ grid units for all of the Hebei Province. The weighted coefficient of each grid unit in relation to population distribution W_{mn} is calculated as given by Eq. (1), where: F_{ij} is the area of topographical

features for all individual classes, when $i=1$, it refers to topographical features, and $j=1, \dots, 4$ means habitat sites, railways, highways, and waterways; F_{ij} is the altitude area of 9 categories, $i=2$ means altitude, and $j=1, 2, \dots, 9$ means altitude of less than 10m, 10-30 m, 30-50 m, 50-70 m, 70-230 m, 230-350 m, 350-660 m, 660-1100 m, >1100 m; F_{ij} is the area for each all individual slope classes, $i=3$ means slope, and $j=1, 2, \dots, 7$ means slope is in the range $0^\circ-4^\circ$, $4^\circ-8^\circ$, $8^\circ-12^\circ$, $12^\circ-16^\circ$, $16^\circ-20^\circ$, $20^\circ-24^\circ$, $24^\circ-26^\circ$; F_{ij} is the landform area of each individual second class, $i=4$ means landform, and $j=1, 2, \dots, 5$ means plain, hill, platform, mountain, plateau; F_{ij} is the land cover area of 6 individual second classes, $i=5$ means land cover, and $j=1, 2, \dots, 6$ means farmland, forest, meadow, water, residential area, unused land; F_{ij} is the land area, $i=6$ means land cover, and $j=1$ means land area; b_{ij} is expressed as the standardized weighted coefficient between geographic factors and population, and the range of i and j is equal to F and that of each geographical (sort) factor; a_i is the partial correlation coefficient of the multi-geographical factors with population, and $i=1, 2, \dots, 6$; $a_i b_{ij}$ is the final weighted coefficient between geographic factors and population; m is the sequence number for each county in the Hebei province; n is the sequence number for each grid in a county.

$$W_{mn} = \frac{a_i b_{ij} F_{ij}}{\sum_{i=1}^6 \sum_{j=1}^x a_i b_{ij} F_{ij}} \quad (1)$$

2.5. Accuracy test

Accuracy tests were conducted by aggregating the gridded population counts to the county level. We then used those counts to produce gridded population distributions and compared the observed population totals at the administrative level with the summed estimates from the output gridded datasets. Root mean square error (RMSE), expressed as a percentage of the mean population size of the administrative level and the mean absolute error (MAE) were used to verify accuracy. This is a better way to compare the estimated population value to the statistical population value and obtain useful information about the quality of our mode (Goovaerts, 2001, 2005; Wang et al., 2005), in order to ensure that the quintiles and probability depend on the interpolation standard errors as much as the predictions. The average standard errors are close to the roots mean squared prediction errors, and the roots mean squared standardized errors should be close to 1. The root mean square error was then calculated with Eq. (2):

$$RMSE = \sqrt{\frac{1}{n} \sum_{i=1}^n (P_{si} - P_{ei})^2} \quad (2)$$

where n is the county number in the Hebei province, P_{si} and P_{ei} represent the statistical population value to the estimated population value in i county in the Hebei province.

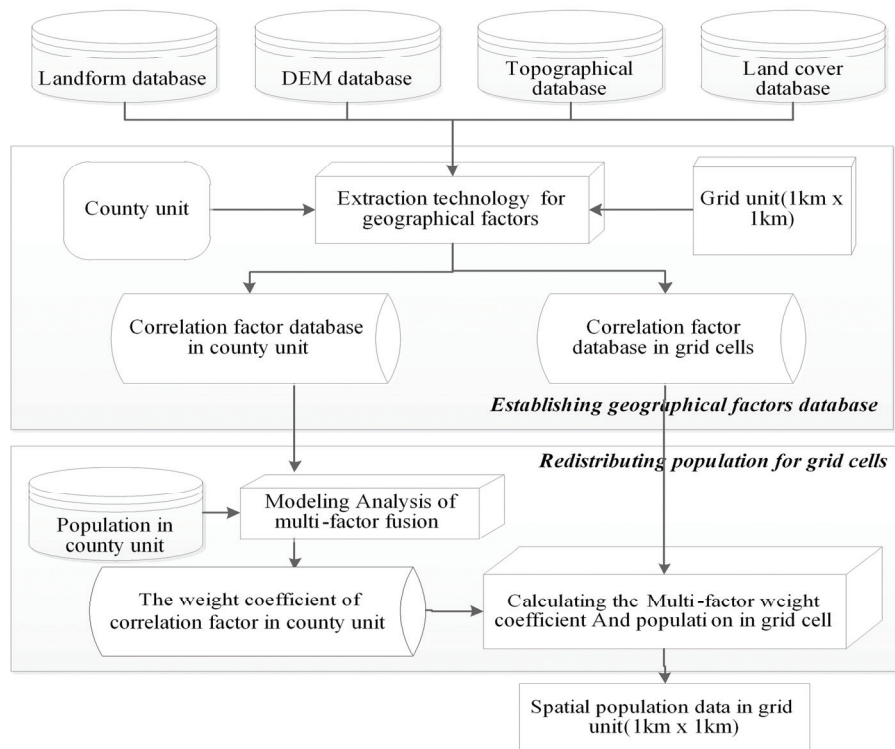


Fig. 2. Framework for establishing a data fusion model for gridded population distribution

3. Results

3.1. Single-factor weight analysis

(1) Topographical features

Inhabited sites, railways, highways, and waterways are the main topographical factors, but are also closely related to the population distribution factor. The quantitative value of a geographical unit is defined as its total length (arc), point size (point), or area (polygon). Polygonal factors, such as residential parcels and rivers, were omitted, and only the parameters represented as lines and points were included in the analysis. Table 1 shows the weighted and standardized weighted coefficients of landforms as they relate to total population data.

weighted coefficients (Table 6) were calculated. It is evident that the topographical factors, land cover, and altitude, have the strongest relationship with population in the Hebei Province.

Table 1. The impact of topographical features on population distribution

| <i>Topographical feature</i> | <i>Weighted coefficients</i> | <i>Standardized weighted coefficients</i> |
|------------------------------|------------------------------|---|
| habitat sites (entries) | 0.842 | 0.401 |
| railways (length) | 0.674 | 0.321 |
| highways (length) | 0.253 | 0.120 |
| waterways (length) | 0.331 | 0.158 |

Table 2. The impact of elevation on population distribution

| <i>Altitude (meters)</i> | <i>Weighted coefficients</i> | <i>Standardized weighted coefficients</i> |
|--------------------------|------------------------------|---|
| <10 | 0.87 | 0.207 |
| 10-30 | 0.533 | 0.127 |
| 30-50 | 0.635 | 0.151 |
| 50-70 | 0.652 | 0.155 |
| 70-230 | 0.615 | 0.146 |
| 230-350 | 0.37 | 0.088 |
| 350-660 | 0.273 | 0.065 |
| 660-1100 | 0.143 | 0.034 |
| >1100 | 0.119 | 0.028 |

Table 3. The impact of slope on population distribution

| <i>Slope (°)</i> | <i>Weighted coefficients</i> | <i>Standardized weighted coefficients</i> |
|------------------|------------------------------|---|
| 0-4 | 0.786 | 0.254 |
| 4-8 | 0.496 | 0.160 |
| 8-12 | 0.347 | 0.112 |
| 12-16 | 0.341 | 0.110 |
| 16-20 | 0.415 | 0.134 |
| 20-24 | 0.381 | 0.123 |
| 24-26 | 0.334 | 0.108 |

Table 4. The impact of landform on population distribution

| <i>Landform (area)</i> | <i>Weighted coefficients</i> | <i>Standardized weighted coefficients</i> |
|------------------------|------------------------------|---|
| plain | 0.729 | 0.420 |
| hills | 0.199 | 0.115 |
| platform | 0.038 | 0.022 |
| mountain | 0.577 | 0.333 |
| plateau | 0.192 | 0.111 |

(2) Altitude

As altitude increases, population density rapidly declines. In the Hebei Province, population density was higher at lower altitudes (Table 2), and the weighted coefficient was highest for altitudes less than 10 meters. This is consistent with the generalization that population distribution follows a vertical gradient.

(3) Slope

The two rainy areas of the Hebei Province are formed by the slopes of the Yanshan and Taihang Mountains in the north and west, respectively. The population was primarily distributed below a slope of 4° (Table 3). As slope increased, the corresponding weighted coefficient decreased, which is consistent with the principle of upright population distribution.

(4) Landform

The northwest region of the Hebei Province is characterized by mountains, hills, and plateaus, while the southeast and center of the Province are characterized by basins, valleys, and a vast central plain. The population was mainly distributed among the mountains and plains (Table 4).

(5) Land cover

Land cover was highly correlated with the agricultural population of the Hebei Province (Table 5). The population was primarily distributed among farmlands and forests.

(6) Land area

Land area was positively correlated with total population and had a partial correlation coefficient of 0.769.

3.2. Multi-factor weight analysis

In this study, the relative factors were classed with the population distribution of the Hebei Province into six categories: main topographical factors, altitude, slope, landform, land cover, and land area; the weighted coefficients and standardized

3.3. Population distribution derived from local governmental offices and calculated using our model

The weighted coefficients between geographical factors and population in the Hebei Province were obtained, and the fundamental geographical factor database covering county administrative boundaries in a 1km x 1km grid were set up. The population database based on a county level was also compiled. Considering the differences in geographical conditions and particularity the distribution of population in different regions of the

Hebei Province, both geographical factor and population databases were helpful for quantitative analysis.

Table 5. The impacts of land cover on population distribution

| <i>Land cover (area)</i> | <i>Weighted coefficients</i> | <i>Standardized weighted coefficients</i> |
|--------------------------|------------------------------|---|
| farmland | 0.984 | 0.243 |
| forest | 0.974 | 0.240 |
| meadow | 0.925 | 0.228 |
| water | 0.244 | 0.060 |
| residential area | 0.312 | 0.077 |
| unused land | 0.617 | 0.152 |

Table 6. Partial correlation coefficients of the geographical factors

| <i>Geographical factors</i> | <i>Weighted coefficients</i> | <i>Standardized weighted coefficients</i> |
|-----------------------------|------------------------------|---|
| topographical feature | 0.685 | 0.158 |
| Altitude | 0.638 | 0.178 |
| Slope | 0.753 | 0.174 |
| Landform | 0.771 | 0.176 |
| Land cover | 0.786 | 0.182 |
| Land area | 0.691 | 0.160 |

The population data was calculated for both administrative and geographical units using the multi-factor fusion model, which incorporated both spatial and statistical data. The model determined the total population data of distinct regions (Fig. 2a) and compared the results with the population distribution calculated using 1 km grids (Fig. 2b). A darker color

indicates a larger population and vice versa. The average population distribution within each region did not accurately characterize that of the same region when population distribution was calculated by grid units. The population clustered near administrative centers, such as in Zhangjiakou, Chengde, Langfang, Qinhuangdao, and Hengshui, which show a higher population concentration of about 2000 persons per square kilometer. These regional trends were not reflected by the regional population distribution, however. The population distribution gradually increased from the northwest to southeast, most likely due to a higher slope in the northwest. The northwest also has mountains, hills, and plateaus, while the central and southeast regions are comprised of basins, valleys, and plains. Population density was relatively low in the Taihang Mountains and was less than 100 persons per square kilometers for the Yanshan Mountains.

The population density in the central Hebei Province was higher, with about 2,000 people per square kilometer. Overall, the population distribution in Hebei is higher and denser than that seen in Handan, Shijiazhuang, Langfang, and Tangshan. In addition, the spatial population distribution was uneven.

3.4. Accuracy assessment

Mapping accuracies are consistently higher when incorporating geographical factor information. Since spatially detailed county data for the Hebei Province were available, we aggregated the small administrative units into a coarser administrative unit level by summing the small units.

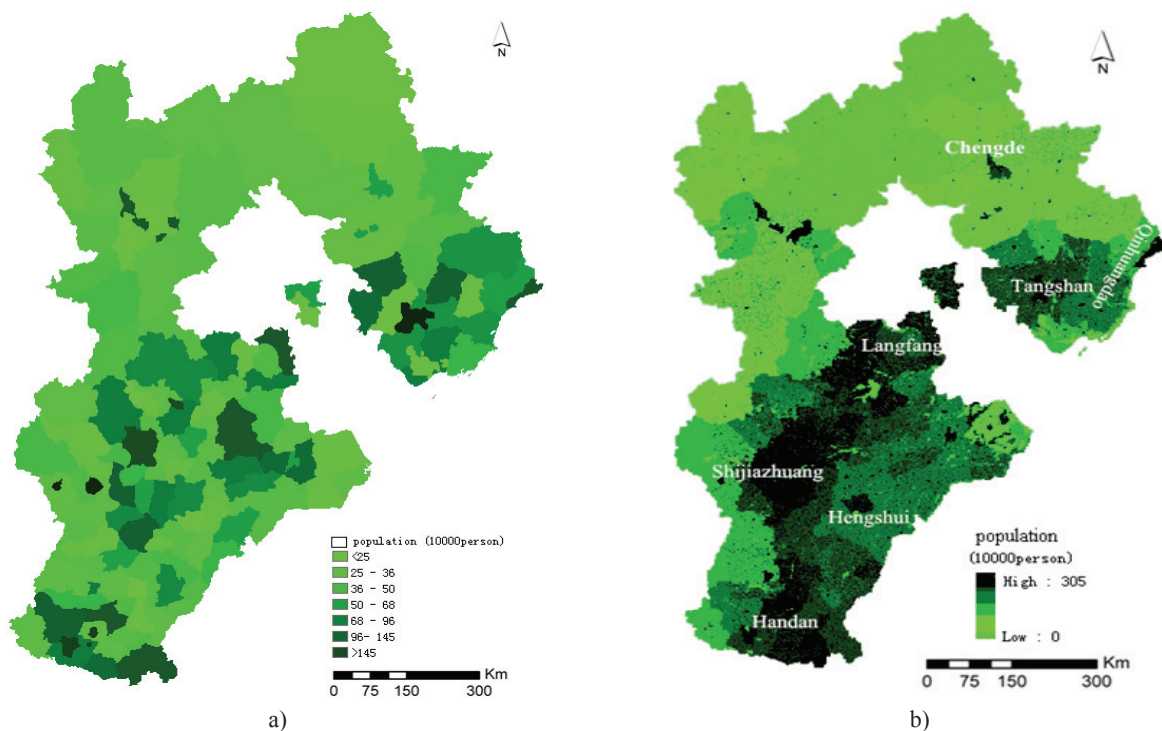


Fig. 2. Spatial population distribution maps in the Hebei Province, China (a) Population derived by municipality; b) Population calculated with our model

Then, these coarse units and population sums were used to generate gridded population maps and the sums of those gridded estimates were compared with the numbers from the original unit population (Fig. 3). The population statistical error is in the range of 6.84 percent. The average standard errors are close to the root mean squared prediction errors, and the root mean squared standardized error was 0.94, which is quite close to 1. Compared with calculating the average population in all counties, the population accuracy with spatial population distribution in grid cells improved to a certain extent; the overall average error was less than the simulation based on land use (Tang et al., 2012; Tian et al., 2004).

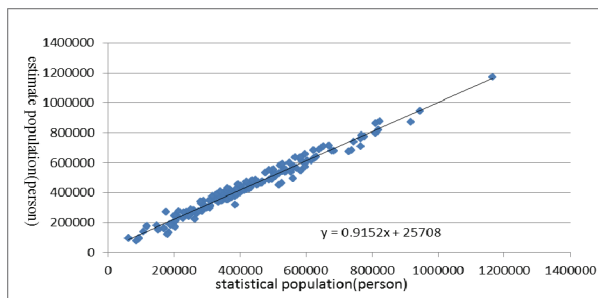


Fig. 3. Scatter diagram of estimated population value and statistical population value

4. Conclusions

In order to analyze the relationship between geographical factors and population data in a spatial unit, in this study, the geographical factors database was established with GIS software, including topographical features, landform, altitude, slope, land cover, and land area. Based on the analysis of geographical factors and population by partial correlation coefficient, there was a significant correlation between population and geographical factors. However, we must be noted that the effect of each factor on population is not the same as that in other regions due to China's topographical features.

The gridded dataset presented here more accurately characterizes population distribution in the defined regions than other existing global datasets (e.g., Gridded Population of the World) with small-scale data. The gridded population dataset takes advantage of the growing collection of geographical features and land cover data to more accurately map human population distributions at a finer spatial scale. Additionally, weighting the distribution of a population by different land cover types, especially through incorporating detailed datasets on roads and developed areas, provides a more accurate representation of population density.

The results prove that it is much more effective than other methods in counting the population in an arbitrary region in China. Measuring population distribution is very complicated, since it relies on the distribution of other statistical factors,

some of which are hard to quantitate. There are multiple other factors affecting population distribution, as well.

Analyzing statistical data in an irregular and random geographical region is important for policy making. Thus, spatializing population data can help develop new ideas and models for space-time data integration and the fusion of multi-source and multi-scale data. In addition, social-pixel and pixel-society concepts can be cemented, promoting a social and public service-oriented e-government. These problems affect the accuracy of the calculated population distribution and should be improved in our future studies.

Acknowledgements

This research was funded by the National Key Technology R&D Program under grant No.2012BAH28B03, and by National High Technology Research and Development Program of China (863 Program) under grant No. 2012AA12A402. We wish to thank the invited reviewers for their time and comments, which improved the manuscript.

References

- Balk D.L., Deichmann U., Yetman G., Pozzi F., Hay S.I., Nelson A., (2006), Determining global population distribution: methods, applications and data, *Advances in Parasitology*, **62**, 119-156.
- Briggs D.J., Collins S., Elliott P., Fischer P., Kingham S., Lebet E., Pryl K., Reeuwijk H.V., Smallbone K., Veen A.V.D., (1997), Mapping urban air pollution using GIS a regression-based approach, *International Journal of Geographical Information Science*, **11**, 699-718.
- Dong C., Zhang Q.P., Zhang J.Q., Liu J.P., Wang L., (2000), The application research of establishing geographical parameter (in Chinese), *Remote Sensing Information*, **1**, 12-17.
- Dong C., Zhao R., Liu J.P., (2003), An application of geographical parameters database in establishment of unit population database, *Chinese Geographical Science*, **13**, 34-38.
- Dong C., Luo Y.B., Liu J.P., Wu X.Z., Wang G.X., (2005), Study on correlation between residential points and geographical factors based on poisson logarithm linearity model (in Chinese), *China Population, Resources and Environment*, **15**, 79-84.
- Fisher R.A., (1924), The Distribution of the Partial Correlation Coefficient, *Metron*, **3**, 329-332.
- Goovaerts P., (2001), Geostatistical assessment and validation of uncertainty for three-dimensional dioxin data from sediments in an estuarine river, *Environmental Science and Technology*, **35**, 3294-3301.
- Goovaerts P., (2005), Geostatistical modeling of the spatial variability of arsenic in groundwater of southeast Michigan, *Water Resources Research*, **41**, 1-19.
- Hay S.I., Noor A.M., Nelson A., Tatem A.J., (2005), The accuracy of human population maps for public health application, *Tropical Medicine and International Health*, **10**, 1073-1086.
- He L.N., (2011), A discussion of population spatial distribution based on urban layout parameter (in

- Chinese), *Science of Surveying and Mapping*, **36**, 38-41.
- Dobson J.E., Bright E.A., Coleman P.R., Durfee R.C., Worley B.A., (2000), LandScan: a global population database for estimating populations at risk, *Photogrammetric Engineering & Remote Sensing*, **66**, 849-857.
- Jensen J.R., Ramsey III E.W., Holmes J.M., Michel J.E., Savitsky B., Davis B.A., (1990), Environmental sensitivity index (ESI) mapping for oil spills using remote sensing and geographic information system technology, *International Journal of Geographical Information Systems*, **4**, 181-201.
- Liao Y.L., (2005), *The study for-scaling with socio-economic data*, (in Chinese), MSc Thesis, Nanjing Normal University, Nanjing, China.
- Liao Y.L., Wang J.F., Meng B., Li X.H., (2010), Integration of GP and GA for mapping population distribution, *International Journal of Geographical Information Science*, **24**, 47-67.
- Linard C., Alegana V.A., Noor A.M., Snow R.W., Tatem A.J., (2010), A high resolution spatial population database of Somalia for disease risk mapping, *International Journal of Health Geographics*, **9**, 1-13.
- Linard C., Gilbert M., Snow R.W., Noor A.M., Tatem A.J., (2012), Population distribution, settlement patterns and accessibility across Africa in 2010, *PLoS ONE*, **7**, 1-8.
- Liu J.P., Liu Z., Wang L., (2006), Research on the spatial information service for e-government based on function collaboration (in Chinese), *Acta Geodaetica et Cartographica*, **35**, 299-302.
- Liu J.Y., Yue T.X., Wang Y.A., Qiu D.S., Liu X.Z., Deng M.L., Yang X.H., Huang Y.J., (2003), Digital simulation of population density in China, (in Chinese), *Acta Geographica Sinica*, **58**, 17-24.
- Lloyd C.D., (2010), Exploring population spatial concentrations in Northern Ireland by community background and other characteristics: an application of geographically weighted spatial statistics, *International Journal of Geographical Information Science*, **24**, 1193-1221.
- Lu A.M., Li C.M., Lin Z.J., Shi W.Z., (2003), Spatial continuous surface model of population density, (in Chinese), *Acta Geodaetica et Cartographica*, **32**, 344-348.
- Martin D., (2006), *Grid models of population: temporal comparison by fixing the geography*, ESRC Research Methods Festival, University of Southampton, On line at: <http://slideplayer.com/slide/786548/>.
- National Bureau of Statistics of China, (2011), *Statistical Yearbook of Hebei* (in Chinese), China Statistics Press, Beijing, China.
- Niu H.E., Meng Q.M., Hu Q.C., Chen Y.C., (1998), Economic interaction analysis between regions of Gansu Province and their surrounding areas (in Chinese), *Economic Geography*, **18**, 51-56.
- Small C., Cohen J.E., (2004), Continental physiography, climate, and the global distribution of human population, *Current Anthropology*, **45**, 269-289.
- Rao S.H., Sievers G.L., (1995), A robust partial correlation measure, *Journal of Nonparametric Statistics*, **41**, 1-20.
- Tang Q., Xu X.Y., Yu S., Xin D., (2012), Population spatial distribution and its application based on GIS: Case of northern China, *Journal of Beijing Normal University (Natural Science)*, **48**, 654-659.
- Wang C.J., Tang X.H., (2004), GIS-based Specialization of population census data in Fujian Province (in Chinese), *Geography and Geo-Information Science*, **20**, 71-74.
- Wang H., Liu G., Gong P., (2005), Use of co-kriging to improve estimates of soil salt solute spatial distribution in the yellow river delta, *Acta Geographica Sinica*, **60**, 511-518.
- Wu X.C., (2009), *Principal and Method of Geographical Information Systems* (Second Edition), Publishing House of Electronics Industry, Beijing, China.
- Yan Q.W., Bian Z.F., (2007), Method of pixelizing social statistical data based on the GIS, (in Chinese), *Yunnan Geographic Environment Research*, **19**, 92-97.
- Yang X., Huang Y., Dong P., Jiang D., Liu H., (2009), An updating system for the gridded population database of china based on remote sensing, GIS and Spatial Database Technologies, *Sensors*, **9**, 1128-1140.
- Zeng C.Q., Zhou Y., Wang S.X., Yan F.L., Zhao Q., (2011), Population spatialization in China based on night-time imagery and land use data, *International Journal of Remote Sensing*, **32**, 9599-9620.
- Zhao J., Yang D. H., Pan J.H., (2010), A study on spatial pattern of GDP in Lanzhou city based on spatialization and land utilization, (in Chinese), *Journal of Northwest Normal University (Natural Science)*, **46**, 92-97.



"Gheorghe Asachi" Technical University of Iasi, Romania



OPTIMIZATION OF ISE_s FOR SIMULTANEOUS NH₄⁺, NO₃⁻ AND NO₂⁻ MONITORING IN SYNTHETIC WASTEWATER USING *SOLVER*

Natalija Velić¹, Olivera Galović², Milan Sak-Bosnar^{2*}, Tonči Rezić³,
Božidar Šantek³, Ana Stanić²

¹Faculty of Food Technology, J.J. Strossmayer University of Osijek, F. Kuhača 18, HR-31000 Osijek, Croatia

²Department of Chemistry, J. J. Strossmayer University of Osijek, Cara Hadrijana 8A, HR-31000 Osijek, Croatia

³Faculty of Food Technology and Biotechnology, University of Zagreb, Pierottijeva 6, HR-10000 Zagreb, Croatia

Abstract

The adaptation of commercially available ion-selective electrodes (ISEs) for use in wastewater matrices was demonstrated using multivariate analysis and optimization with the Microsoft Excel *Solver* tool. The electrodes were characterized in pure analyte solutions, and their parameters were estimated using multivariate analysis and *Solver* optimization. The ammonium, nitrate, and nitrite ions were measured in model systems that were designed to simulate wastewater. The accuracy of the measurements (95.3% - 101.0%) was satisfactory for the determination of ammonium, nitrate, and nitrite in complex matrices. The adapted ISEs were then successfully used for bioprocess (synthetic wastewater treatment) dynamics and efficiency studies in a horizontal rotating tubular bioreactor (HRTB) by monitoring the concentrations of the substrates and intermediates in the samples collected from the bioreactor. The simultaneous determination of ammonium, nitrate, and nitrite in the samples through the use of adapted ISEs considerably shortened the time required for ion determination.

Key words: ammonium, ion-selective electrodes, nitrate, nitrite, wastewater

Received: September, 2013; Revised final: March, 2014; Accepted: March, 2014

1. Introduction

Wastewater may contain several different forms of nitrogen, including organic nitrogen, ammonia nitrogen, nitrate nitrogen, and nitrite nitrogen. Nitrogen compounds are some of the most common pollutants in aquatic environments and pose a threat to both aquatic organisms and humans (Sumino et al., 2006). Therefore, it is important that these compounds are monitored and removed from wastewater to an appropriate concentration prior to its discharge into the environment (Seifi and Fazaelpoor, 2012).

Biological nitrogen removal is an effective method for reducing the concentrations of nitrogen compounds in wastewaters, which is typically accomplished in two sequential steps: nitrification

and denitrification. During nitrification by autotrophic nitrifying bacteria, the oxidation of ammonium into nitrite is followed by the oxidation of nitrite into nitrate. Under anoxic conditions, the nitrate is then reduced to N₂ (or denitrification intermediates) by denitrifying bacteria. In simultaneous nitrification and denitrification (SND), the nitrification and denitrification occur simultaneously in the same reactor under aerobic conditions (Guo et al., 2013; Holman and Wareham, 2005; Pochana and Keller, 1999; Walters et al., 2009). The pure microorganism cultures capable of performing SND are *Paracoccus denitrificans* and *Nitrosomonas europaea* (Ahn, 2006; Helmer and Kunst, 1998). Different types of bioreactors can be used for wastewater treatment, especially those containing microbial biofilms, e.g., trickling filters,

* Author to whom all correspondence should be addressed: e-mail: msbosnar@kemija.unios.hr; Phone:+385(0)31399950; Fax:+385(0)31399969

biodisc bioreactors, packed bed bioreactors, fluidized bed bioreactors (Nicolella et al., 2000) or moving bed biofilm reactors (Quan et al., 2013).

The horizontal rotating tubular bioreactor (HRTB), which was developed by Šantek et al. (1996a, 1996b), combines the characteristics of thin layer and biodisc reactors. HRTBs have been used to conduct both aerobic (Slavica et al., 2004) and anaerobic (Ivančić et al., 2004) bioprocesses. In further studies, the HRTB was used for the heterotrophic cultivation of *P. denitrificans* bacteria, i.e., the SND of synthetic wastewater (Rezić et al., 2007), and for the monitoring and removal of heavy metals from textile wastewaters (Zeiner et al., 2012; Zeiner et al., 2010).

The on-line monitoring of the primary bioprocess variables, such as the concentrations of the substrates, the metabolites and the suspended cells, is often difficult or expensive; thus, off-line measurements must be employed. This is even more evident in the case of the HRTB, where on-line monitoring is further enabled by the design and construction of the bioreactor. Therefore, the development of simple, accurate, and fast methods of measuring these variables off-line and preferably on-site is of vital importance. The most commonly used methods for the determination of ammonium, nitrate, and nitrite are colorimetric (spectrophotometric) techniques that require tedious sample pre-treatment steps (Michalski and Kurzyca, 2006). Several other methods for the simultaneous determination of ammonium, nitrate and nitrite include ion chromatography (IC), high-performance liquid chromatography (HPLC), sequential injection analysis (SIA), flow injection analysis (FIA), capillary electrophoresis (CE), fluorimetry, chemiluminescence, and direct potentiometry by ion-selective electrodes (ISEs) (Bouvier et al., 2008). ISEs are a promising approach because of their small size, rapid response, simplicity of use, low cost, portability, and ability to directly measure the analyte across a wide range of concentrations (Kim et al., 2007). Recently, research efforts have been dedicated to the development of multisensory systems, such as voltammetric electronic tongues, for monitoring the above-mentioned ions in waters (Campos et al. 2012; Nuñez et al., 2013).

Incorporated into Microsoft Excel for Windows, *Solver* is a tool used for mathematical simulation, optimization, and modeling and has the capability to solve an extensive range of linear, nonlinear, and integer problems. It is an affordable substitute to expensive commercial software packages because it can yield the same results when applied to the same sets of data (Sak-Bosnar et al., 2011). In this investigation, *Solver* was used for fitting of the data with nonlinear functions via an iterative algorithm.

The aim of this investigation was to adapt commercially available ISEs using multivariate analysis and *Solver* for the detection of ammonium, nitrate, and nitrite in wastewater matrices.

Furthermore, the overall aim was to shorten the time required to monitor the bioprocess in the HRTB by developing a method for the simultaneous determination of these ions using ISEs.

2. Materials and methods

2.1. Simultaneous determination of ammonium, nitrate, and nitrite by ISEs

2.1.1. Standard solutions and calibrations

Stock solutions ($c=1 \text{ mol L}^{-1}$) of NaNO_2 , NaNO_3 , and NH_4Cl were used in the calibration procedure. A conditioning solution (CS), which consists of $\text{CH}_3\text{COONa} \times 3\text{H}_2\text{O}$ ($c=7.351 \times 10^{-2} \text{ mol L}^{-1}$), KH_2PO_4 ($c=2.204 \times 10^{-3} \text{ mol L}^{-1}$), K_2HPO_4 ($c=4.650 \times 10^{-3} \text{ mol L}^{-1}$), and $\text{MgSO}_4 \times 7\text{H}_2\text{O}$ ($c=1.623 \times 10^{-3} \text{ mol L}^{-1}$), was prepared to adjust the ionic strength.

The chemicals were reagent grade quality and were supplied by Kemika (Croatia), except for $\text{CH}_3\text{COONa} \times 3\text{H}_2\text{O}$, which was supplied by Mallinckrodt Baker (Holland).

Deionized water was used in the preparation of all solutions. The synthetic wastewater (SW), and trace elements solution (TES) were prepared as described below in section 2.2. A synthetic wastewater blank (SWB) was also prepared, which contained all of the chemicals listed below except for the ions to be determined.

2.1.2. Electrode

Ammonium (ELIT 8051), Nitrite (ELIT 8071), and Nitrate (ELIT 8021) solid ISEs were used in the measurements. A silver/silver(I) chloride maintenance-free Single Junction Reference Electrode (ELIT 001, with gel 4 mol L^{-1} solution of KCl saturated with AgCl) was used as a reference. All of the electrodes were supplied by NICO2000 Ltd. (UK). Between measurements, the electrodes were stored in the preconditioning/standard solutions that were recommended by the manufacturer.

2.1.3. Apparatus

The potentiometric measurements were performed on an EA 168 Quad pH/mV Amp 4 channel amplifier connected to an e-corder 821, which is an 8 channel, high-resolution, high-speed, computer-based data recording system that uses Chart software for data acquisition and analysis (supplied by eDAQ Pty Ltd., Australia). The solutions were magnetically stirred during the measurements (801 Stirrer; Metrohm, Switzerland).

2.1.4. Procedure

The electrodes were calibrated in solutions containing four different concentrations of the analytes, ranging from $c=10^{-5}$ - $10^{-2} \text{ mol L}^{-1}$. Each solution was diluted in 25 mL of the CS. The electrodes were recalibrated every 30 measurements. The sample aliquots were diluted in 25 mL of the CS, and the electrode potentials were recorded at room

temperature under constant stirring. Stable values of the potential (± 0.1 mV) were achieved within 5 minutes, although the exact time varied for each sensor depending on the concentration of the species being determined.

2.1.5. Optimization strategy using Solver

Microsoft Excel (2007) for Windows contains a spreadsheet optimization modeling system called *Solver*. The activation of *Solver* is simple and can be selected by choosing *Add ins* in the *Tools* menu. *Solver* was used to predict the results of the model for an initial set of parameters over a range of values of the dependent variables and to compare these results with the experimental data. The sum of the squared residuals between the two arrays was calculated, and the error between the two data sets was minimized by varying the values of the parameters according to an iterative search algorithm.

2.2. Simultaneous nitrification and denitrification experiment in the HRTB

2.2.1. Microorganism, SW and growth conditions

The working microorganism was a pure culture of *P. denitrificans* DSM 413 (obtained from the Deutsche Sammlung von Mikroorganismen und Zellkulturen GmbH) cultivated at room temperature (20 ± 1 °C) in the SW, which was composed of $\text{CH}_3\text{COONa} \times 3\text{H}_2\text{O}$ ($c = 7.351 \times 10^{-2}$ mol L⁻¹), KH_2PO_4 ($c = 2.204 \times 10^{-3}$ mol L⁻¹), K_2HPO_4 ($c = 4.650 \times 10^{-3}$ mol L⁻¹), NH_4Cl ($c = 5.613 \times 10^{-2}$ mol L⁻¹), NaNO_3 ($c = 3.235 \times 10^{-2}$ mol L⁻¹), $\text{MgSO}_4 \times 7\text{H}_2\text{O}$ ($c = 1.623 \times 10^{-3}$ mol L⁻¹), and 3 mL L⁻¹ of TES. TES was prepared according to Robertson and Kuenen (1992) and was composed of the following trace elements: ZnSO_4 ($c = 1.362 \times 10^{-2}$ mol L⁻¹), $\text{CoCl}_2 \times 6\text{H}_2\text{O}$ ($c = 6.767 \times 10^{-3}$ mol L⁻¹), $\text{CuSO}_4 \times 5\text{H}_2\text{O}$ ($c = 6.288 \times 10^{-3}$ mol L⁻¹), $\text{C}_{10}\text{H}_{16}\text{N}_2\text{O}_8$ (EDTA) ($c = 0.171$ mol L⁻¹), $(\text{NH}_4)_6\text{Mo}_7\text{O}_{24} \times 4\text{H}_2\text{O}$ ($c = 8.899 \times 10^{-4}$ mol L⁻¹), $\text{FeSO}_4 \times 7\text{H}_2\text{O}$ ($c = 1.798 \times 10^{-2}$ mol L⁻¹), $\text{MnCl}_2 \times 4\text{H}_2\text{O}$ ($c = 2.557 \times 10^{-2}$ mol L⁻¹), and CaCl_2 ($c = 4.956 \times 10^{-2}$ mol L⁻¹). The medium was sterilized at 121 °C for 20 minutes. The chemicals were reagent grade quality and supplied by Kemika (Croatia), except for $\text{CH}_3\text{COONa} \times 3\text{H}_2\text{O}$, which was supplied by Mallinckrodt Baker (Holland).

2.2.2. HRTB and experimental set-up

The HRTB design and construction used herein, has been described elsewhere (Rezić et al., 2007). The microbial culture was first cultivated on a rotary shaker (72 h, 20 ± 1 °C, 150 min⁻¹, eccentricity 50 mm) and further propagated by batch cultivation (inoculum, 7.5% v/v) in a stirred tank bioreactor. The bacterial biomass obtained by batch cultivation (7.5 L) in the stirred tank bioreactor was used for the inoculation of the HRTB (liquid volume, 15 L; total volume, 98 L). A constant airflow rate of 152 L h⁻¹ was used throughout the experiment, except for the periods when the aeration was turned off to enhance the denitrification process. The bioprocess dynamics

were studied at different combinations of the process parameters: the medium inflow rate was varied from 0.5 to 2 L h⁻¹ and the HRTB rotation speed was varied from 5 to 20 min⁻¹. Samples were collected in duplicate at five positions along the length of the HRTB. After establishing a new set of process parameters, five residence times (37.5-150 h, depending on the medium inflow rate) were allowed to pass before the samples were collected.

2.2.3. Determination of biomass, acetate, ammonium, nitrate, and nitrite concentrations

To determine the concentration of the biomass in the SW/biomass suspension, a 35-mL sample was centrifuged for 20 minutes at 4500 min⁻¹, washed twice with demineralized water, dried at 105 °C for 48 h, cooled and weighed. The supernatant was stored at -20 °C. The liquid samples were thawed and homogenized before the acetate, ammonium, nitrate, and nitrite concentrations were determined. The acetate concentration was determined spectrophotometrically (UV/Vis spectrophotometer model 1700, Shimadzu, Japan) using Boehringer Mannheim/R-Biopharm enzymatic test kits (Cat. No. 10 148 261 035).

The concentrations of ammonium, nitrate, and nitrite were simultaneously determined using ISEs, as described above. All values were expressed as the average of 4 measurements.

2.2.4. Bioprocess efficiency parameters

The removal efficiencies of acetate, ammonium, and nitrate (substrate, S) were calculated using Eq. (1), where γ_0 is the concentration of the substrate in the inflow to the HRTB, and γ_{out} is the concentration of the substrate in the outflow from the HRTB.

$$RE_S = [(\gamma_0 - \gamma_{\text{out}}) / \gamma_0] \times 100 \quad (1)$$

The volumetric consumptions of acetate, ammonium, and nitrate were estimated using Eq. (2), where τ is the hydraulic residence time of the liquid in the HRTB.

$$Q_S = (\gamma_0 - \gamma_{\text{out}}) / \tau \quad (2)$$

3. Results and discussion

3.1. Characterization and estimation of the electrode parameters

Before determining the ammonium, nitrate, and nitrite content in the synthetic wastewater samples that were withdrawn from the HRTB, it was necessary to adapt commercially available ISEs for use in complex wastewater matrices. Additionally, before estimating the electrode parameters with multivariate analysis and *Solver* optimization, the response of each ISE in pure analyte solutions was characterized. The electrodes responded to the ammonium, nitrate, and nitrite ions according to the

Nernst equations (Eqs. 3 - 5), where E is the potential difference between the sensing and reference electrodes, E^0 is a constant potential, S is the electrode slope and $a_{\text{NH}_4^+}$, $a_{\text{NO}_3^-}$ and $a_{\text{NO}_2^-}$ are the activities of the ions.

$$E = E^0 + S \times \log a_{\text{NH}_4^+} \quad (3)$$

$$E = E^0 - S \times \log a_{\text{NO}_3^-} \quad (4)$$

$$E = E^0 - S \times \log a_{\text{NO}_2^-} \quad (5)$$

The response characteristics and the corresponding statistics of the electrodes in the pure ion solutions are summarized in Table 1. The electromotive force of the cell consisting of each particular electrode and the reference cell was measured in the series of corresponding ion solutions, covering the concentration range of 1×10^{-6} - 1×10^{-1} mol/L. The correlation between the measured E values and logarithm of the concentrations, defined by Eqs. (3) - (5), was confirmed by using the linear regression analysis. Therefore, the slope value (S) and constant potential term (E^0) were determined. The high correlation coefficient (R^2) values indicated the strong linear relation between the variables.

The confidence intervals for S and E^0 were calculated from the corresponding standard deviation values. In real systems, which are typically more complex, ISEs can be affected by numerous analytical interferents, which can either increase or decrease the detected analyte concentration. The response of the ISE to the primary ion and the interferents is described by the Nikolsky-Eisenman equation (Eq. 6). Here, a_i is the activity of the

primary (measured) ion (I), K_{ij} is the selectivity coefficient of the electrode against the interfering ion, a_j is the activity of the interfering ion (j), and z_i and z_j are the charges of the primary and the interfering ions, respectively. The activity coefficients were calculated according to the Davies equation.

$$E = E^0 + S \times \log(a_i + \sum K_{ij} a_j^{z_i/z_j}) \quad (6)$$

Potassium ions can seriously interfere with the determination of ammonium using ISEs (Jin et al., 2004) and they are present at a high concentration in the SW formulation that was used in this investigation. The mixed solution method was used for the determination of the potentiometric selectivity coefficients.

A multivariate calibration of this electrode set (ammonium, nitrate, and nitrite) was performed by varying the concentrations of the important interferents, including potassium. This procedure allowed for the calculation of the selectivity coefficient, electrode slope, and constant potential term of each electrode. The Nikolsky-Eisenman parameters for each electrode were modeled using a matrix of the potentials that were measured by the electrodes in the calibration solutions. A set of potentials was predicted based on the model and calibration solution parameters, and the validity of the model was estimated by examining the residuals between the predicted and observed potentials.

Table 2 shows a portion of the spreadsheet that displays the potentiometric calibration data and the model parameters for the ammonium electrode after optimization using *Solver*.

Table 1. The response characteristics and the corresponding statistics of the ammonium, nitrate, and nitrite electrodes in the pure analyte solutions

| ISE | $\frac{S}{\text{mV/decade}}$ | E^0 / mV | R^2 | Linearity range $c / \text{mol L}^{-1}$ | Detection limit* $c / \text{mol L}^{-1}$ |
|----------|------------------------------|-------------------|--------|--|---|
| Ammonium | 53.2 ± 0.8 | 420.4 ± 4.8 | 0.9997 | $5 \times 10^{-5} - 5 \times 10^{-1}$ | 2×10^{-5} |
| Nitrate | 55.8 ± 1.9 | 205.0 ± 3.4 | 0.9977 | $5 \times 10^{-6} - 1 \times 10^{-1}$ | 2×10^{-6} |
| Nitrite | 55.5 ± 2.3 | 12.5 ± 4.2 | 0.9973 | $1 \times 10^{-5} - 1 \times 10^{-2}$ | 4×10^{-6} |

*DL (detection limit) = 3 SD (standard deviation) number of measurements, $n = 5$

Table 2. Potentiometric calibration data and model parameters for the ammonium electrode after optimization using *Solver* (with an initial analyte volume of 25.0 mL and an initial ammonium concentration of 1.0 mol L^{-1})

| Model parameter | | | | | | | |
|-----------------|---|---------------------------|---|--------------------------------------|-----------------------|-----------------------------|----------------|
| E^0 | 425.433 | | | | | | |
| S | 57.197 | | | | | | |
| K_{ij} | 1.14×10^{-1} | | | | | | |
| $\log K_{ij}$ | -0.9427 | | | | | | |
| E/mV | $c_{\text{NH}_4^+} / \text{mol L}^{-1}$ | $a^* / \text{mol L}^{-1}$ | $a_{\text{NH}_4^+} / \text{mol L}^{-1}$ | $C_{\text{K}^+} / \text{mol L}^{-1}$ | $^b E_{\text{model}}$ | $^c \text{res.}$ | $^d \text{SR}$ |
| 288.86 | 3.98×10^{-3} | 9.98×10^{-2} | 3.07×10^{-3} | 1.15×10^{-2} | 288.79 | 0.0710 | 0.0050 |
| 314.32 | 1.38×10^{-2} | 1.09×10^{-1} | 1.06×10^{-2} | 1.14×10^{-2} | 314.66 | -0.3310 | 0.1095 |
| 338.64 | 3.85×10^{-2} | 1.31×10^{-1} | 2.90×10^{-2} | 1.11×10^{-2} | 338.29 | 0.3510 | 0.1232 |
| 385.45 | 2.86×10^{-1} | 3.54×10^{-1} | 2.00×10^{-1} | 8.22×10^{-3} | 385.54 | -0.0911 | 0.0083 |
| | | | | | | $^e s_{\text{sr}} = 0.2461$ | |

$^a I^*$ = ionic strength, $^b E_{\text{model}}$ = calculated value obtained by the Nikolsky-Eisenman equation after optimization, $^c \text{res.}$ = difference between measured E and E_{model} values, $^d \text{SR}$ = square of residuals (res.), $^e s_{\text{sr}}$ = sum of squares of residuals

The experimental data have been compared to an appropriate theoretical model in which the unknown parameters (E^0 , S , K_{ij}) were optimized. By using *Solver*, the values for those variables that would minimize the sum of the squares of the differences between the theoretical and the experimental data were determined. In other words, the least-squares criterion was used to fit a theoretical model to the experimental data using the entire data set.

3.2. Determination of the ammonium, nitrate, and nitrite concentrations in the model systems

An SWB solution was prepared that contained all of the ingredients except the analytes (ammonium, nitrate, and nitrite), thus simulating a real system. Known amounts of the analytes were added to this solution to verify the impact of the SWB ingredients on the quantitation of the analytes. The measured electrode parameters and the corresponding statistics are given in Table 3. The generated potentiometric experimental data were compared to the appropriate theoretical model in which the sensor response parameters were optimized.

Solver was used to determine the values for those variables that would minimize the sum of the squares of the differences between the theoretical model and experimental data, using the same methodology as previously described. The SWB solutions contained the three analytes at two concentrations over two orders of magnitude that covered the expected concentration range of the bioprocess.

The calculated K_{ij} value is in good accordance with the literature data. No other interfering ions were present in the system investigated herein. The results of these investigations are given in Table 4. The accuracy of the measurements (95.3% - 101.0%) is satisfactory for the determination of ammonium, nitrate, and nitrite in complex matrices. A good fit of the theoretical models to the experimental values was obtained for all the electrodes and calibration parameters that were tested. Using these methodologies, the values of the selectivity coefficient, K_{ij} ; the slope, S ; the constant potential term, E^0 , (Table 3) and the sample concentration, expressed as the recovery (Table 4) were calculated.

The estimates of the standard errors of the parameters, the standard error of the output variable, and the correlation coefficients proved the validity of the model.

3.3. Bioprocess dynamics and efficiency studies

The investigation in the HRTB was a continuation of a previous study by Rezić et al. (2007), which confirmed that acetate and ammonium removal in the HRTB by *P. denitrificans* in a one-step process can be achieved. The commercial ISEs adapted to wastewater matrices were used for

bioprocess dynamics and efficiency studies by monitoring the concentrations of the substrates and the intermediates/products in samples that were collected from the HRTB.

Table 3. The parameters and corresponding statistics of the electrodes in the model SWB solutions containing known concentrations of ammonium, nitrate, and nitrite

| Parameter | Electrode investigated | | |
|-------------------------|------------------------|------------------|------------------|
| | Ammonium | Nitrate | Nitrite |
| $^a S/\text{mV/decade}$ | 53.9 ± 1.4 | 52.6 ± 0.1 | 51.4 ± 0.1 |
| $^a E^0/\text{mV}$ | 376.2 ± 2.3 | 210.0 ± 0.3 | -11.7 ± 0.2 |
| $\log K_{ij}^*$ | -0.80 ± 0.04 | -3.90 ± 0.02 | -3.60 ± 0.01 |
| R^2 | 0.9999 | 1.000 | 1.000 |
| $^b SE(y)$ | 0.494 | 0.126 | 0.041 |

^avalue \pm standard deviation; ^b $SE(y)$ = standard error of measurement

Table 4. The results of the direct potentiometric measurements of ammonium, nitrate, and nitrite in the model SW solutions

| Analyte used | $c_{\text{added}}/\text{mol L}^{-1}$ | $^a c_{\text{found}}/\text{mol L}^{-1}$ | $a_{\text{recovery}}/\%$ | RSD / % |
|--------------|--------------------------------------|---|--------------------------|---------|
| Ammonium | 5.61×10^{-2} | 5.43×10^{-2} | 96.8 | 1.22 |
| | 5.61×10^{-4} | 5.35×10^{-4} | 95.3 | 1.67 |
| Nitrate | 3.24×10^{-2} | 3.27×10^{-2} | 101.0 | 0.49 |
| | 3.24×10^{-4} | 3.21×10^{-4} | 99.2 | 0.78 |
| Nitrite | 4.00×10^{-3} | 3.89×10^{-3} | 97.2 | 1.32 |
| | 4.00×10^{-5} | 3.82×10^{-5} | 95.5 | 1.63 |

^a Average of 5 measurements

Ammonium, nitrate, and nitrite, the latter of which is an intermediate of the bioprocess, were simultaneously determined in the samples, thus shortening the ion determination time. This is of vital importance when employing off-line/on-site analysis of bioprocess variables. The obtained data were then compared to data obtained by Rezić et al. (2007), in which the spectrophotometric determination of ammonium and nitrite was applied.

In the investigation by Rezić et al. (2007), the SW contained ammonium as a source of N and acetate as a source of C; however, in the current study, nitrate was included in the SW as an additional source of N. Furthermore, the aeration regime was changed during the cultivation to enhance the denitrification process within the microbial biofilm. The concentrations of the substrates in the inlet feed were 4.3 g L^{-1} acetate, 1.0 g L^{-1} ammonium and 2.0 g L^{-1} nitrate. After a stable microbial biofilm had formed, the effect of the bioreactor process parameters on the bioprocess dynamics in the HRTB was studied. The process parameters that were investigated included the medium inflow rate ($F=0.5 - 2 \text{ L h}^{-1}$) and the HRTB rotation speed ($n = 5 - 20 \text{ min}^{-1}$), as well as changes in the aeration regime (Fig. 1). The concentration profiles of acetate, ammonium, and suspended biomass concentration as well as pH along the length of the HRTB were similar to those obtained by Slavica et al. (2004) and Rezić et al. (2007) and are presented in Fig. 2.

A bacterial culture of *P. denitrificans* grew in a suspension of single cells and cell aggregates and attached to the inner surface of the bioreactor as a biofilm. The preliminary results of biofilm thickness measurements (data not shown) as well as the characteristics of the formed biofilm were similar to the previous study conducted by Rezić et al. (2007). The concentration profile of the suspended biomass, shown in Fig. 2, exhibits a gradual increase along the length of the HRTB, which agrees with the results of the investigation conducted by Rezić et al. (2007). A similar pattern was observed for all other combinations of the process parameters (data not shown).

An increase in the pH was observed along the length of the HRTB (Fig. 2) for all combinations of process parameters because of acetate degradation. Tubular bioreactors are characterized by a liquid plug flow that leads to the formation of concentration and/or temperature gradients along the length of the

bioreactor (Moser, 1985). The concentration gradients were also observed for ammonium, nitrate, and nitrite ions. The ammonium ion concentration profile and range were in agreement with those obtained by Rezić et al. (2007), as previously mentioned. As a result of dilution, the concentrations of all the substrates were lower at the place of medium inflow to the HRTB (0% l_{HRTB}) than their initial concentrations in the inlet feed. The nitrite ion in the output flow of the HRTB, however, was significantly higher (100 to 1000 times) than that measured by Rezić et al. (2007). This disparity is expected considering that the cultivation medium in this investigation contained nitrate at a concentration of 2.0 g L^{-1} , which is subsequently reduced to nitrite by *P. denitrificans*.

The removal efficiency and volumetric consumption of acetate, ammonium, and nitrate for different combinations of bioprocess parameters are presented in Table 5.

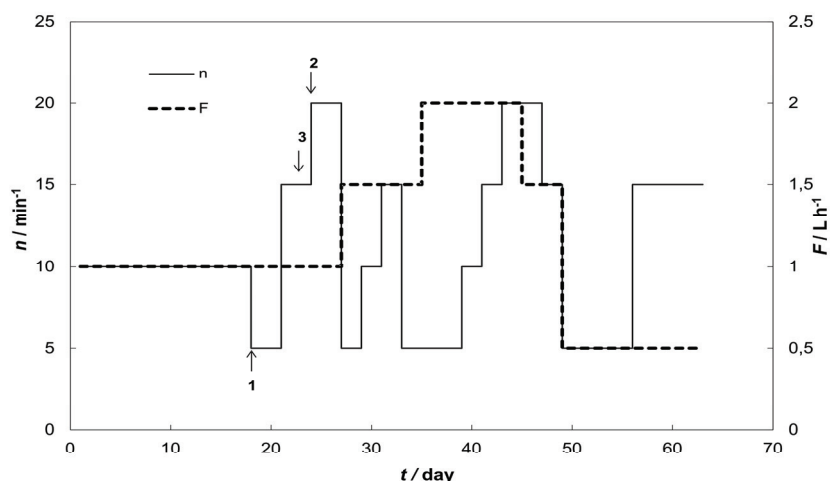


Fig. 1. The changes in the medium inflow rate (F , ---) and the bioreactor rotation speed (n , —) of the HRTB during the investigation. Arrows 1, 2 and 3 indicate the changes in the aeration regime

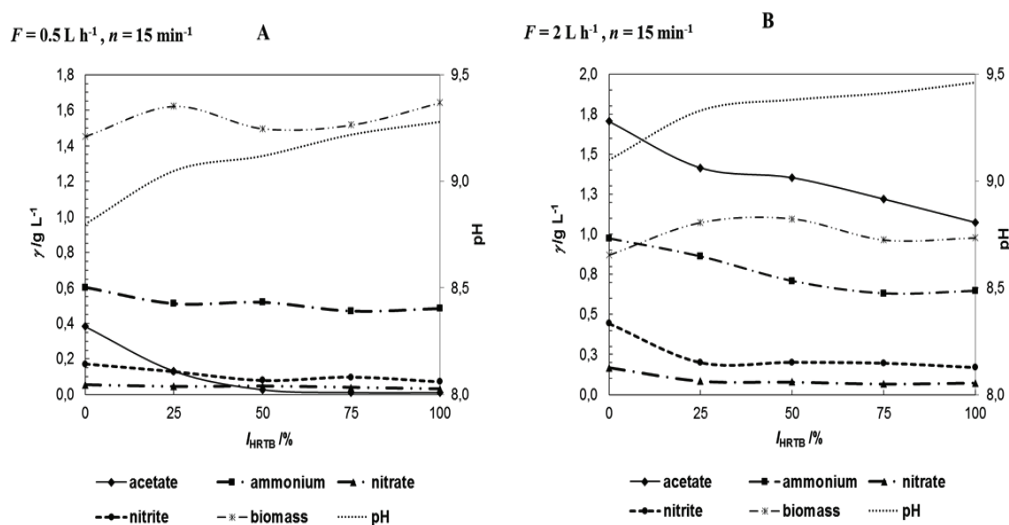


Fig. 2. The biomass, acetate, ammonium, nitrate, and nitrite concentrations as well as the pH along the length of the HRTB (l) at medium inflow rates of $F = 0.5 \text{ L h}^{-1}$ (A) and 2 L h^{-1} (B) and at rotation speed of $n = 15 \text{ min}^{-1}$

Table 5. The removal efficiency (RE_S) and volumetric consumption (Q_S) of acetate, ammonium, and nitrate at different combinations of the process parameters

| $F/L\ h^{-1}$ | τ/h | n/min^{-1} | Aeration regime | $\frac{U_{Ac}}{\%}$ | $\frac{U_{NH_4^+}}{\%}$ | $\frac{U_{NO_3^-}}{\%}$ | $\frac{Q_{Ac}}{g\ L^{-1}\ h^{-1}}$ | $\frac{Q_{NH_4^+}}{g\ L^{-1}\ h^{-1}}$ | $\frac{Q_{NO_3^-}}{g\ L^{-1}\ h^{-1}}$ |
|---------------|----------|---------------------|--------------------|---------------------|-------------------------|-------------------------|------------------------------------|--|--|
| 0.5 | 30 | 5 | aerobic | 99.78 | 62.00 | 96.91 | 0.143 | 0.021 | 0.065 |
| | | 15 | aerobic | 99.75 | 51.48 | 98.41 | 0.143 | 0.017 | 0.066 |
| 1 | 15 | 5 | anaerobic | 62.04 | 16.80 | 99.31 | 0.178 | 0.011 | 0.132 |
| | | 10 | aerobic | 98.31 | 25.70 | 0.00 | 0.282 | 0.017 | 0.000 |
| | | 15 | aerobic/anaerobic* | 97.72 | 25.34 | 80.31 | 0.280 | 0.017 | 0.107 |
| | | 20 | anaerobic | 69.30 | 19.00 | 97.62 | 0.199 | 0.013 | 0.130 |
| 1.5 | 10 | 5 | aerobic | 93.74 | 52.70 | 98.99 | 0.403 | 0.053 | 0.198 |
| | | 10 | aerobic | 92.45 | 44.40 | 99.05 | 0.398 | 0.044 | 0.198 |
| | | 15 | aerobic | 95.75 | 61.56 | 97.94 | 0.412 | 0.062 | 0.196 |
| | | 20 | aerobic | 96.15 | 35.40 | 99.12 | 0.413 | 0.035 | 0.198 |
| 2 | 7.5 | 5 | aerobic | 81.73 | 41.80 | 0.00 | 0.469 | 0.056 | 0.000 |
| | | 10 | aerobic | 81.36 | 58.40 | 94.12 | 0.466 | 0.078 | 0.251 |
| | | 15 | aerobic | 75.02 | 35.40 | 96.35 | 0.430 | 0.047 | 0.257 |
| | | 20 | aerobic | 84.91 | 39.60 | 96.01 | 0.487 | 0.053 | 0.256 |

* 4 residence times aerobic, and 1 residence time anaerobic

A complete consumption of acetate was achieved at an inflow rate of $0.5\ \text{L}\ \text{h}^{-1}$. At an inflow rate of $1.0\ \text{L}\ \text{h}^{-1}$, the aeration regime was changed more than once (Fig. 1), and the acetate consumption decreased. The volumetric consumption of acetate ranged from 0.143 to $0.282\ \text{g}\ \text{L}^{-1}\ \text{h}^{-1}$ at medium inflow rates between 0.5 and $1.0\ \text{L}\ \text{h}^{-1}$. When the medium inflow rate was increased to $1.5 - 2.0\ \text{L}\ \text{h}^{-1}$, the volumetric acetate consumption increased by a factor of two ($0.398 - 0.487\ \text{g}\ \text{L}^{-1}\ \text{h}^{-1}$). This increase can be attributed to a higher volumetric acetate overload. The calculated efficiencies and volumetric consumption rates for ammonium and nitrate were based on data obtained by using adapted ISEs and were calculated for all combinations of selected bioprocess parameters.

In comparison to the results based on the spectrophotometric determination of ammonium ion obtained by Rezić et al. (2007), the removal efficiency and volumetric consumption of ammonium obtained in this study using adapted ISEs were similar. The ammonium consumption efficiency ranged from 35.4 to 62.0% for medium inflow rates of $F=0.5$, 1.5 and $2.0\ \text{L}\ \text{h}^{-1}$ at all bioreactor rotation speeds. The volumetric consumption of ammonium (for the same process parameters) ranged from 0.017 to $0.078\ \text{g}\ \text{L}^{-1}\ \text{h}^{-1}$. The minimum ammonium consumption efficiency ($0.011 - 0.017\ \text{g}\ \text{L}^{-1}\ \text{h}^{-1}$) and the minimum volumetric consumption of ammonium ($0.011 - 0.017\ \text{g}\ \text{L}^{-1}\ \text{h}^{-1}$) were observed at an inflow rate of $1\ \text{L}\ \text{h}^{-1}$ for all bioreactor rotation speeds. The low efficiency and consumption of ammonium are results of the multiple changes in the aeration regime that were observed for these combinations of the process parameters (Fig. 1).

The nitrate consumption efficiency was high ($> 94\%$) for almost every combination of the process parameters. A decrease in the nitrate concentration was observed along the length of the HRTB, which indicates that denitrification occurred. For $F=1.0\ \text{L}\ \text{h}^{-1}$ and $n=10\ \text{min}^{-1}$ as well as for $F=2.0\ \text{L}\ \text{h}^{-1}$ and $n=5\ \text{min}^{-1}$, the efficiency was 0% and the nitrate

concentrations along the bioreactor were higher than the input concentrations. Sudden environmental changes occurred in both cases: for $F=1.0\ \text{L}\ \text{h}^{-1}$ and $n=10\ \text{min}^{-1}$ there was an anaerobic-aerobic transition, and for $F=2.0\ \text{L}\ \text{h}^{-1}$ and $n=5\ \text{min}^{-1}$ there was a biofilm regeneration preceded by a sudden drop in the pH and a peeling of the biofilm. Therefore, the 0% efficiency is a result of an insufficiently rapid metabolic adjustment to the changes in the conditions.

Nitrite was detected at concentrations ranging from 17.54 to $443.74\ \text{mg}\ \text{L}^{-1}$ along the length of the HRTB. The lowest nitrite concentrations in the bioreactor occurred at a flow rate of $F=1.0\ \text{L}\ \text{h}^{-1}$ and rotation speeds of $n=5$ and $20\ \text{min}^{-1}$ during the anaerobic regime and a rotation speed of $n=15\ \text{min}^{-1}$ during the final working bioreactor volume when the aeration was turned off. The lowest input and output concentrations were determined under these same conditions.

These conditions favor the denitrification process; therefore, nitrite was reduced to its gaseous intermediates and no nitrite accumulated in the medium. The consumption of acetate, ammonium, and nitrate and the presence of nitrite confirmed that SND processes occurred in the HRTB.

4. Conclusions

Multivariate analysis and *Solver* optimization were used to adapt and optimize commercially available ISEs for the detection of ammonium, nitrate, and nitrite in wastewater matrices.

Apart from being cheaper and simpler compared with ion chromatography and spectrophotometry, this technique reduced the time required for the off-line analysis of these ions in synthetic wastewater samples during and after treatment in the HRTB.

The simultaneous determination of the consumption of ammonium and nitrate and the presence of nitrite by adapted commercial ISEs

confirmed that SND processes occurred in the HRTB. Thus, it can be concluded that the adaptation and optimization of commercial ISEs by using *Solver* was performed successfully.

Acknowledgements

The authors gratefully acknowledge the financial support of the Croatian Ministry of Science, Education and Sports that was given to project No. 291-0580000-0169 and project No. 058-0581990-2004.

References

- Ahn Y.-H., (2006), Sustainable nitrogen elimination biotechnologies: A review, *Process Biochemistry*, **41**, 1709-1721.
- Bouvier J.-C., Bekri M., Mazouni D., Schoefs O., Harmand J., Ribeiro T., Pham H.N., Pauss A., (2008), On-line Monitoring of Nitrate and Nitrite by UV Spectrophotometry in a SBR Process Used for the Treatment of Industrial Wastewaters, *International Journal of Chemical Reactor Engineering*, **6**, 1542-6580.
- Campos I., Alcañiz M., Aguado D., Barat R., Ferrer J., Gil L., Marrakchi M., Martínez-Mañez R., Soto J., Vivancos J.-L., (2012). A voltammetric electronic tongue as tool for water quality monitoring in wastewater treatment plants, *Water Research*, **46**, 2605-2614.
- Guo J., Thang J., Chen W., Ma F., Liu H., Tian Y., (2013), The regulation and control strategies of a sequencing batch reactor for simultaneous nitrification and denitrification at different temperatures, *Bioresource Technology*, **133**, 59-67.
- Helmer C., Kunst S., (1998), Simultaneous nitrification/denitrification in an aerobic biofilm system, *Water Science and Technology*, **37**, 183-187.
- Holman J.B., Wareham D.G., (2005), COD, ammonia and dissolved oxygen time profiles in the simultaneous nitrification/denitrification process, *Biochemical Engineering Journal*, **22**, 125-133.
- Ivančić M., Šantek B., Novak S., Marić V., (2004), Fermentative bioconversion in a horizontal rotating tubular bioreactor, *Process Biochemistry*, **39**, 995-1000.
- Jin H.Y., Kim T.H., Kim J., Lee S.S., Kim J.S., (2004), Tetrahydrofuran-containing Crown ethers as ionophores for NH_4^+ - Selective Electrodes, *Bulletin of the Korean Chemical Society*, **25**, 59-62.
- Kim H.-J., Hummel J.W., Sudduth K.A., Motavalli P.P., (2007), Simultaneous analysis of soil macronutrients using ion-selective electrodes, *Soil Science Society of America Journal*, **71**, 1867-1877.
- Michalski R., Kurzyca I., (2006), Determination of nitrogen species (nitrate, nitrite and ammonia ions) in environmental samples by ion chromatography, *Polish Journal of Environmental Studies*, **15**, 5-18.
- Moser A., (1985), *Imperfectly Mixed Bioreactor Systems*, In: *Comprehensive Biotechnology*, Moo-Young M. (Ed.), Vol. 2, Pergamon Press, Oxford, 77-98.
- Nicolella C., van Loosdrecht M. C. M., Heijnen J.J., (2000), Wastewater treatment with particulate biofilm reactors, *Journal of Biotechnology*, **80**, 1-33.
- Núñez L., Cetó X., Pividori M.I., Zannoni M.V.B., del Valle M., (2013), Development and application of an electronic tongue for detection and monitoring of nitrate, nitrite and ammonium levels in waters, *Microchemical Journal*, **110**, 273-279.
- Pochana K., Keller J., (1999), Study of factors affecting simultaneous nitrification and denitrification (SND), *Water Science Technology*, **39**, 61-68.
- Quan X., Gu L., Qian Y., Pei Y., Yang Z., (2013), Characterization of nitrification performance and microbial community in a MBBR and integrated GBBR-MBBR treating heavily polluted river water, *Environmental Engineering and Management Journal*, **12**, 1335 -1344.
- Rezić T., Šantek B., Novak S., Marić V., (2007), Heterotrophic cultivation of *Paracoccus denitrificans* in a horizontal rotating tubular bioreactor, *World Journal of Microbiology and Biotechnology*, **23**, 987-996.
- Robertson L.A., Kuenen J.G., (1992), *Nitrogen Removal from Water and Wastewater*, In: *Microbial Control of Pollution*, Fry J. C., Gadd G. M., Herbert R. A., Jones C. W., Watson-Craik I.A. (Eds.), University Press, Cambridge, 227-267.
- Sak-Bosnar M., Madunić-Čačić D., Sakač N., Samardžić M., Kurtanek Ž., (2011), Estimation and optimization of potentiometric sensor response parameters from surfactant titration data using microsoft excel solver and mathematica, *Sensor Letters*, **9**, 1-8.
- Seifi M., Fazelipour M.H., (2012), Modeling simultaneous nitrification and denitrification (SND) in a fluidized bed biofilm reactor, *Applied Mathematical Modelling*, **36**, 5603-5613.
- Slavica A., Šantek B., Novak S., Marić V., (2004), Microbial acetate oxidation in horizontal rotating tubular bioreactor, *Journal of Biosciences*, **29**, 169-177.
- Sumino T., Isaka K., Ikuta H., Saiki Y., Yokota T., (2006), Nitrogen removal from wastewater using simultaneous nitrate reduction and anaerobic ammonium oxidation in single reactor, *Journal of Bioscience and Bioengineering*, **102**, 346-351.
- Šantek B., Horvat P., Novak S., Mayr B., Moser A., Marić V., (1996a), Mathematical modeling of mixing in a horizontal rotating tubular bioreactor: "Simple flow" model, *Bioprocess Engineering*, **14**, 195 – 204.
- Šantek B., Horvat P., Novak S., Mayr B., Moser A., Marić V., (1996b), Mathematical modeling of mixing in a horizontal rotating tubular bioreactor: "Spiral flow" model, *Bioprocess Engineering*, **14**, 223 – 229.
- Zeiner M., Rezić T., Šantek B., (2010), Monitoring of Cu, Fe, Ni, and Zn in wastewater during treatment in a horizontal rotating tubular bioreactor, *Water Environment Research*, **82**, 183-186.
- Zeiner M., Rezić T., Šantek B., Rezić I., Hann S., Stinger G., (2012), Removal of Cr, Mn, and Co from textile wastewater by horizontal rotating tubular bioreactor, *Environmental Science and Technology*, **46**, 10690-10696.
- Walters E., Hille A., He M., Ochmann C., Horn H., (2009), Simultaneous nitrification/denitrification in a biofilm airlift suspension (BAS) reactor with biodegradable carrier material, *Water Research*, **43**, 4461-4468.



"Gheorghe Asachi" Technical University of Iasi, Romania



CHALLENGES AND OPORTUNITIES IN GREEN PLASTICS: AN ASSESSMENT USING THE ELECTRE DECISION-AID METHOD

Elena-Diana Comaniță^{1,2*}, Cristina Ghinea^{1,3}, Raluca Maria Hlihor¹,
Isabela Maria Simion¹, Camelia Smaranda¹, Lidia Favier⁴,
Mihaela Roșca¹, Irina Gostin², Maria Gavrilescu^{1,5*}

¹"Gheorghe Asachi" Technical University of Iasi, Faculty of Chemical Engineering and Environmental Protection,
Department of Environmental Engineering and Management, 73 Prof.dr.docent D. Mangeron Str., 700050 Iasi, Romania

²"Alexandru Ioan Cuza" University of Iasi, 11 Carol I Blvd., 700506 Iasi, Romania

³"Stefan cel Mare" University of Suceava, Faculty of Food Engineering, 13 Universitatii Str., 720229 Suceava, Romania

⁴Superior National School of Chemistry in Rennes, UMR CNRS 6226, Institute of Chemical Sciences Rennes,
Department of Chemistry and Process Engineering, 11 Beaulieu Str., CS 50837, 35708 Rennes Cedex 7, France

⁵Academy of Romanian Scientists, 54 Splaiul Independentei, RO-050094 Bucharest, Romania

Abstract

Bioplastics are biobased materials, usually easy biodegradable, derived from renewable resources. Evolution of bioplastics production is related to: bio starch and starch mixtures (74.5%); bioplastic products from fermentation (13%), bioplastic from petrochemicals materials (12.5%). They are seen as a viable solution to avoid some environmental impacts caused by the use of fossil-based conventional plastics. In this context, the general objectives of this study entail the analysis and selection of the optimal alternative of bioplastics able to be used for packaging production, considering social, economic and environmental criteria. In order to accomplish these objectives, we applied the ELECTRE method (*ELimination Et Choix TRaduisant la Realité*), a multi-criteria analysis method. Application of this method enables the use of qualitative and quantitative discrete criteria, making also possible alternatives ranking. The application of ELECTRE method in our study consisted in selecting different types of bioplastics which were compared considering some consistent criteria so as to assess their economic and environmental performances. Based on the application of multiple criteria evaluation we concluded that bioplastics, in particular polyhydroxyalkanoates (PHAs) are suitable from economic and environmental points of views for manufacturing and utilization of packaging.

Key words: bioplastic, indicators, ELECTRE method, multi-criteria analysis, polyhydroxyalkanoates

Received: November, 2014; Revised final: March, 2015; Accepted: March, 2015

1. Introduction

Human society continuously aspires to achieve economic development and well-being in order to secure higher living standards and to protect and improve the environment, both for present and future generations (Fortuna et al., 2012; Gavrilescu, 2004; Ghinea et al., 2014a; Koroneos et al., 2012). It is considered that these two aspirations are in the

core of sustainable development concept based on ecosystem - eco-efficiency dualism (Simion et al., 2013; Teng and Wu, 2014). Movements towards sustainability address, among others, various categories of materials which incorporate nonrenewable resources, such as fossil fuels, and energy. All these generate economic, social and environmental negative impacts and high carbon footprints during the whole life cycle. This is why

* Author to whom all correspondence should be addressed: e-mail: comanita_elena_diana@yahoo.com; mgav@tuiasi.ro

today, biobased production largely seen as a central element of bioeconomy is gaining against the conventional oil and petrochemicals industries (Gavrilescu and Chisti, 2005; OECD, 2014). Biofuels, bio-based chemicals and bio-based plastics represent a vast network in the public policy which try to reconsider the balance among sustainability of materials, energy, fuel (Gavrilescu, 2014a, b; OECD, 2014).

In particular, the challenges for the future of bio-based plastics are particularly important, both in terms of sufficient material resources supplying, and waste management (Iwata, 2015; Peelman et al., 2013; Yu et al., 1998). Currently, there are a number of obstacles that should be overcome to ensure a sustainable life cycle for bioplastics (emergence of renewable biomass sources of carbon, price in comparison to oil-based plastics). Therefore, it is necessary to intensify the analyses of strengths and weaknesses, threats and opportunities regarding sustainability biodegradable plastics in terms of considering the economic, social and environmental challenges, along the whole life cycle (Iles and Martin, 2013).

Apart from resource conservation goal, the current policy on bioplastics is focused on bio-waste management considering prevention, reuse and recycling in order to reduce and valorize the amount of waste produced (Briassoulis, 2001; Dace et al., 2014; Fortuna et al., 2011; Ghinea et al., 2014b; Şchiopu and Ghinea, 2013). Waste composition makes the process of degradation and natural elimination by the action of microorganisms more difficult, leading to increased remanence period, especially when waste contains conventional plastics (De Feo et al., 2013; Gavrilescu, 2008; Heaney et al., 2011; Hermann et al., 2011; Hlihor et al., 2014a). Environmental and landscape degradation, emissions and odors create a negative impact (pollution by organic substances, nitrites, nitrates, heavy metals and other elements) on life quality for the surrounding communities.

All these can lead to soil, water and air pollution (Gavrilescu et al., 2015; Hlihor et al., 2014b; Pogăcean et al., 2014; Simion et al., 2013b). Some efficient solutions addressing packaging end-of-life can play an important role in the development of sustainable waste management, because resource waste and environmental impact can be reduced, while providing economic and social benefits (Gavrilescu and Chisti, 2005; Rossi et al., 2015).

In this framework, the main objective of this work was to find from several alternatives the most sustainable bioplastics for packaging production, which use material resources and energy without compromising the possibilities of meeting the needs of future generations. We applied the ELECTRE method for a set of bioplastics in order to choose the most suitable for packaging considering the economic, social and environmental criteria.

2. Plastics – characteristics and impacts on environment and human health

2.1. Some characteristics of plastic products and waste

The global plastic production was 230 million tons in 2009, and more than 99% was due to polymeric materials obtained from fossil resources (Rose and Palkovits, 2011).

According to ISO 472 (2013) plastic “contains as an essential ingredient, a polymer with a high average molecular weight and at some point in the processing, can be poured through the flow into final products”.

Plastic materials are used for a large variety of products, in particular for packaging (bags, cups, glasses, cutlery, casseroles, plastic bottles, recipients for shampoos and toys). At the end of their life they become waste generating additional pollution, which can induce negative impacts on the environment and human health, because of their composition (Gregory, 2009; PlasticsEurope, 2011; Peelman et al., 2013) (Table 1).

Table 1. Impacts of plastic waste in aquatic environment

| <i>Impact</i> | <i>Effect</i> | <i>References</i> |
|---|--|---|
| Landscape degradation | Economic repercussions for the tourism industry | Barnes et al. (2009); Sivan (2011) |
| Hindering activities in marine industry | Repercussions to maritime transport, fisheries, energy production, aquaculture | Barnes et al. (2009) |
| Destruction of the aquatic environment | Damage (fall of feathers from birds) and death marine birds, mammals, fish and reptiles | Gregory (2009) |
| | "Suffocation" and the destruction of plankton and phytoplankton due to the accumulation of "plastic mountains" | Weiss et al. (2012) |
| | Disequilibrium of marine habitat due to "plastic mountains" expansion (disappearance of marine species) | Hall et al. (2010); Weiss et al. (2012) |
| | Issue of toxins from the plastic on fish communities (death of fish species) | Rochman et al. (2013) |

Plastics can be classified in many ways, depending on polymeric molecules contained and procedure of polymerization and processing (Sahoo and Ali, 2008; Tachwali et al., 2007). The most known polymers are (Fig. 1): polyethylene terephthalate (PET or PETE); high density polyethylene (HDPE); polyvinyl chloride (PVC); low density polyethylene (LDPE); polypropylene (PP); polystyrene (PS); other plastics (polycarbonate and polylactide).

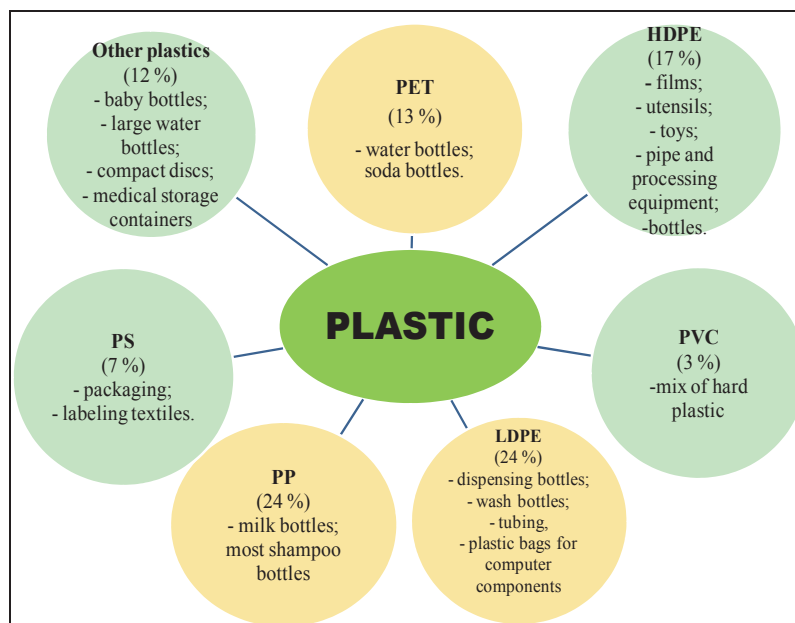


Fig. 1. Areas of utilization for various plastics

Petroleum deriving plastics are widely used not only due to their outstanding mechanical properties, low cost, light weight and high energy efficiency, but also for their stability, durability and chemical and biological inertness. Half of plastic wastes generated in Europe are landfilled. This situation should be prevented, because plastic can contain dangerous elements and undesirable emissions can be generated by landfilling (Groot et al., 2014; Song et al., 2009). The plastic wastes disposed in landfills frequently experience photo oxidation and degradation, resulting in small fragments and particles, which can absorb toxins and toxic chemicals, entering into the food chain, where they can exert toxic effects (Roy et al., 2011).

2.2. Challenges and opportunities in green plastics

Information on biodegradation of petroleum-deriving polymers and plastics is generally limited to biodegradable synthetic polymers, such as poly(vinyl alcohol), aliphatic polyesters, polycaprolactone, and polyamides, oligomeric ethylene, styrene, isoprene, butadiene, acrylonitrile, and acrylate (Shah et al. 2008). In this context, another category of plastics, based on biopolymers (polymeric biomolecules) starts to become increasingly more a sustainable alternative to fossil-based polymers (Gavrilescu and Chisti, 2005).

According to IUPAC, “*biobased polymer derived from the biomass or issued from monomers derived from the biomass and which, at some stage in its processing into finished products, can be shaped by flow*” (Vert et al., 2012).

The advantage of biopolymers against conventional petrobased polymers is represented by the fact that they can be produced by living organisms, from renewable bio-based resources.

Some biopolymers can be used as plastics, replacing the conventional, and petrobased plastics.

In terms of biodegradability, all plastics will be degraded in time, but the conventional plastics face with a long duration of degradation, for hundreds of years (Groot et al., 2014). On the other hand, bioplastics are biodegradable products that can degrade quickly in raw materials (under defined conditions of degradation process) and can improve the soil quality and support plant growth. Bioplastics obtained from renewable bio-based resources or organic wastes are considered environmentally friendly, having the potential to alleviate pollution issues caused by plastics.

A significant increase in the production of bioplastics at a level comparable to that of conventional plastics could have a positive impact on the environment, by reducing greenhouse gas emissions, space for waste storage, and the risk of for marine pollution and on human health (Sheldon, 2014). Although research in the field of bioplastics began a few decades ago, the products made of these materials have appeared on the market in the past decades (Freemantle, 2005). Since the 80s, researches were undertaken throughout the world for biopolymers assimilation, but the most funds for these types of researches were allocated in the United States and Japan (Ritter, 2002). The development perspective of material production from biodegradable bioplastic is primarily optimistic, the experts estimating a production of over 5 million tons by the end of 2020 (Shen et al., 2009).

The assimilation of bioplastics could be an optimal solution both for reducing plastic waste and food waste prevention and valorization, given the loss of about 1.3 billion tonnes of food in each year at global level, according to program of the United Nations Environment Programme (UNEP)

(Melikoglu et al., 2013). Vegetable fats and oils, corn starch, pea starch or microbiota are considered as raw materials for bioplastics. According to production method, bioplastics can be classified as (Cooper, 2013):

- made from vegetable resources (BMS): corn, potato, wheat, rice, beets, cellulose, starch etc.;
- synthesized from renewable sources: polylactic acid (PLA), poly glycolic acid (PGA), polycaprolactone (PCL);
- produced by microorganisms or genetically modified: polyhydroxyalkanoates (PHAs), PolyHydroxyButyrate (PHB), PolyHydroxyButyrate-co-valerate (PHBV);
- mixtures with biodegradable polymers: Poly vinyl alcohol (PVOH), Polycaprolactone (PCL).

The new bioplastics are characterized by a specific combination of rigidity and elasticity compared with both existing bioplastics and with traditional plastics. For example, a plastic obtained from spinach is more elastic, while plastic produced from rice husk is more firmly (Zhao et al., 2002).

Bioplastics are used extensively in modern society for packaging, agriculture, transport, household utilities (Fig. 2).

3. Methodology

3.1. Multicriteria decision analysis (MCDM)

Multicriteria analysis was developed in 1960 as an instrument for decision making, and has become increasingly used in the projects management (Phillips, 1984). The main steps of multi-criteria analysis are (San Cristobal, 2012; Tsioporkova and Boeva, 2006):

1. establishment of the decisional context, such as goals of project which is evaluated and its feasibility;
2. definition of options, which meant to identify alternatives that will be considered;

3. definition of criteria, identification and definition of all the criteria relevant to the problem decision;

4. achievement of the performance matrix, which describes the intended performance of each option according to the criteria;

5. standardization of scores for each criterion to a common scale interval (usually with values ranging from 0-1 or -100);

6. weighting of criteria for relative quantification of each criterion in the decision process;

7. hierarchy of options: in this stage the decision maker has to select the most appropriate method for ranking alternatives;

8. examination of results: in this step the expert analyzes the results and presents them in a comprehensive manner;

9. sensitivity analysis: to validate alternative assessment, and ranking the alternatives resulted from decision process.

Multicriteria analysis methodology includes complex methods such as (Choi et al., 2015; Milutinović et al., 2014; Soltani et al., 2015): Analytical Hierarchy Process (AHP); ELECTRE I; ELECTRE II; ELECTRE III; Organization, Rangement et Synthese De Donnes Relationnelles (ORESTE); - Preference Ranking Organization Method for Enrichment Evaluation (PROMETHEE); Simple Multi-Attribute Ranking Technique (SMART).

The models of multicriteria analysis can be used in different areas such as: waste management (Generowicz et al., 2011; Ghinea and Gavrilescu, 2010; Ghinea et al., 2014a; Soltani et al., 2015), hydrology and water management (Hyde et al., 2005; Pedrero et al., 2011; Scholten et al., 2015; Sudhakaran et al., 2013), energy management (Kowalski et al., 2009; Troldborg et al., 2014; Wang et al., 2009), and others.

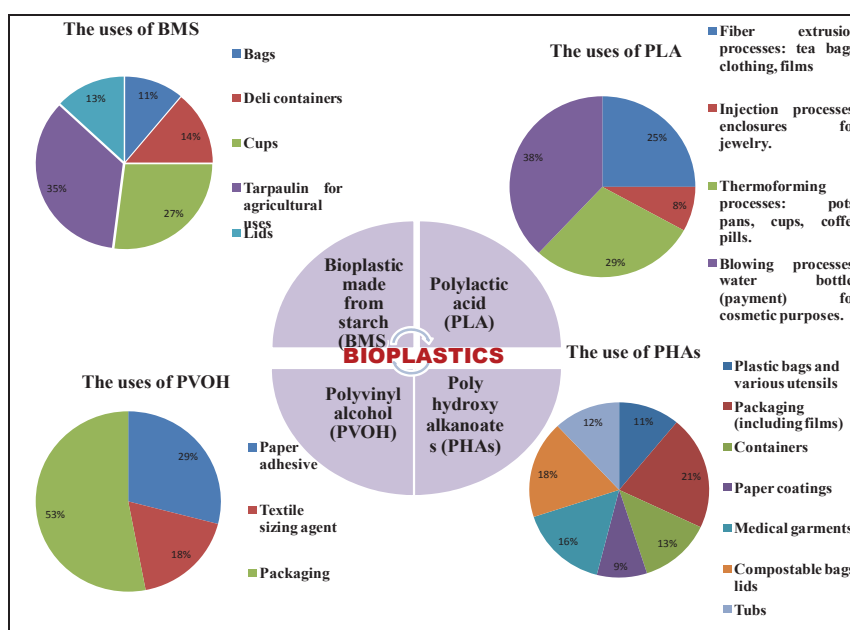


Fig. 2. Applications of bioplastics

3.2. ELECTRE method

In order to achieve the objectives of this paper, ELECTRE - a multicriteria evaluation method was applied. This method was developed in France, and applied particularly in European countries (Roy, 1993; Roy and Vanderpooten, 1996). It is based on the concept of *Upgrademay* to eliminate alternatives that are in a certain sense “dominated”. The notion of “dominance” within the framework provided by *Upgrademay* is a generalization of the classical dominance and uses weightings to rank the criteria (some of them have more influence than others on the decision).

Roy (1993) described *Upgrademay* concept as follows: alternative A_i , outperforms the alternative A_k , if, given the preferences of the decision maker, the quality evaluation of alternatives and problem context, there exist enough arguments to decide that A_i is at least as good as A_k and there is no obvious reason to contradict the affirmation. Based on this idea, a series of procedures for concretizing *Upgrademay* concept as a way of multicriteria decision support have been developed (Iazzolino et al., 2012). In general, two steps are necessary for applying ELECTRE method (Hatami-Marbini and Tavana, 2011):

- specifying a precise way of determining the *Upgrademay* existence between two alternatives;
- combining *Upgrademay* evaluations for ranking of the alternatives.

Application of multi-criteria analysis methods, such as ELECTRE, in environmental management is based on (Kaya and Kahraman, 2011):

- existence of multiple criteria evaluation;
- participation of decision makers;
- complexity and subjectivity of the evaluation process.

ELECTRE Methodology has been developed through a series of different versions (I-IV); ELECTRE I is designed for a problematic choice of alternatives considered, ELECTRE II, III and IV are designed for extreme situations arising from the proposed variants and ELECTRE TRI has been designed for a problematic sorting from considered variants. Another type of variant from ELECTRE is TOPSIS method (Wang and Triantaphyllou, 2008). ELECTRE method is based on the evaluation of two indices, the concordance and discordance indexes, defined for each pair of alternatives (Bojković et al., 2010). Like other methods of multi-criteria analysis, ELECTRE has the same steps (Vahdani et al., 2010):

- specifying alternatives and criteria;
- performance evaluation according to criteria;
- establishing the weights associated criteria that determine their relative importance.

The essence of ELECTRE method is to identify the relationships of dominance, and its purpose is that a subset noted “ E ” should have as few elements that will represent the alternative candidate

for final decision (Vahdani et al., 2010). The main advantages offered by ELECTRE method in the environmental decision-making can be synthesized as follows (Aiello et al., 2013; Kaya and Kahraman, 2011):

- possibility to analyse complex environmental issues;
- active participation of environmental factors in the decision making process;
- application of scientific methods in decision making.

ELECTRE method was used in several areas: Kaya and Kahramanv (2011) combined AHP and ELECTRE methods for environmental impact assessment; Hatami-Marbini et al. (2013) used a fuzzy group ELECTRE method for safety and health assessment in hazardous waste recycling facilities; Choi et al. (2015) applied this method for rehabilitation of water distribution system.

In our study, the bioplastic evaluation was performed by applying ELECTRE method and by using selected criteria that address both objectives associated with current trends in waste management as well as global environmental indicators (e.g. quantity of emissions generated). The alternatives were established in order to minimize the amount of waste landfilled, increase the quantity of produced energy, obtain raw materials for bioplastic and reduce greenhouse gases emissions.

The ELECTRE method was applied in order to find the most suitable solution for obtaining bioplastics used for packaging production, by respecting the criteria of sustainable development, from the economical, social and environmental points of view, thus contributing to the development of the market for raw materials and to promote the use of products derived from biopolymers. We also used concordance and discordance indicators and threshold values for calculation purposes. Each type of bioplastic was evaluated from social, economical and environmental point of view. The steps followed in this study are illustrated in Fig. 3.

4. Case study

Starting from the premise of Environmental Action Programme 7: “Turning Waste into Resources”, which proposes to increase the sustainability towards “zero waste”, and transform waste into valuable materials and energy resources, in this study we evaluated the economical, social and environmental performance of various bioplastics used for packaging production.

Most used bioplastics, to obtain packaging are: polylactic acid (PLA); polyhydroxyalkanoates (PHAs); bioplastic made from starch (BMS); cellulose and its derivatives; polyvinyl alcohol (PVOH); biodegradable aliphatic and aromatic copolyesters (European Bioplastics, 2013). To achieve our objectives we focused on the use of polylactic acid (PLA), Polyhydroxyalkanoates (PHAs), bioplastics obtained from starch (BMS) and polyvinyl alcohol (PVOH).

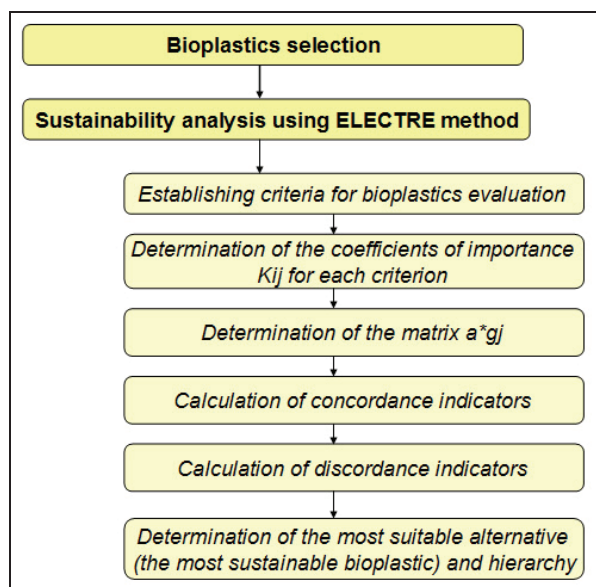


Fig. 3. Stages developed in the study of plastics sustainability applying ELECTRE method

(i) *Polylactic Acid (PLA)*

Polylactic acid is thermoplastic aliphatic polyester produced from renewable resources. It is biodegradable under certain conditions, such as in the presence of oxygen, and is difficult to recycle. PLA possesses high values of tensile strength and modulus, is a polymer that has many properties comparable to other plastics (Auras et al., 2004).

(ii) *PolyHydroxyAlcanoate (PHA) and PolyHydroxyButyrate (PHB)*

PHA and PHB are bioplastics in the form of granules. PHA is more rigid, being used in a more limited area for bottles and agricultural land cover, when is necessary, while PHB is used for plastic bags and various utensils (Cavalheiro et al., 2009; Chen et al., 2007). The process for producing these bioplastics consists of incubating in bioreactors large amounts of bacteria, until their number increase greatly, reaching to point of "stress" as an alarm caused by environmental change. When bacteria transform nutrients through fermentation, until get to 80% by weight, bacteria are "purified" and the bioplastics are extracted (Adamus, 2012).

Shen et al. (2014) obtained PHB from organic waste through a process consisting of two stages and which is focused on volatile fatty acids intermediaries. Cavalheiro et al. (2009) obtained PHB using *Cupriavidus necator* and waste based on glycerol. PHA was obtained from waste pulp by Queirós et al. (2014). Polyhydroxybutyrate-co-valerate (PHBV), a member of the family of PHB has gained a lot of attention as a green material. It is a brittle and crystalline material with short pendent side-groups on its backbone (Singh et al., 2008).

(iii) *Bioplastic made from starch (BMS)*

Current bioplastics are generally made from starch derived from corn, rice, sugar cane or potato. Starch from plant sources is very attractive due to

low costs, its existence in large quantities in renewable materials, and processing due to the possibility of the extruder and thermoforming used in the processing of biopolymers (Freire et al., 2009; Singh and Nath, 2013).

Bioplastics made from starch can be processed using common methods of processing synthetic polymers (Chaudhary et al., 2008). Making biodegradable protective packaging will help in building top of starch and starch reactivation of domestic factories, and bring substantial benefits to the environment and society, by preserving and protecting ecosystems (Araujo et al., 2004).

(iv) *Polyvinyl alcohol (PVOH)*

Polyvinyl alcohol is a biodegradable vinyl polymer, used for coatings, adhesives, and as additive in paper and board production.

The advantages of bioplastics types used in our study are presented in Fig. 4 (Accinelli et al., 2012; Akaraonye et al., 2010).

5. Results and discussion

5.1. Sustainability evaluation of bioplastics using ELECTRE method

Multi-criteria analysis was applied to rank and select the best type of bioplastic used for packaging production considering the social, technical and functional performances and the influence of economic and financial factors, according to specific legislation on public procurement.

Also, the aim of this work was to investigate the biodegradation potential benefits, achieved by applying the proposed solutions, harmonization with the priorities of EU legislation, cost of project implementation, and amount of waste possible to recover, energy recovered from bioplastics waste such as BMS, PLA, PHAs and PVOH.

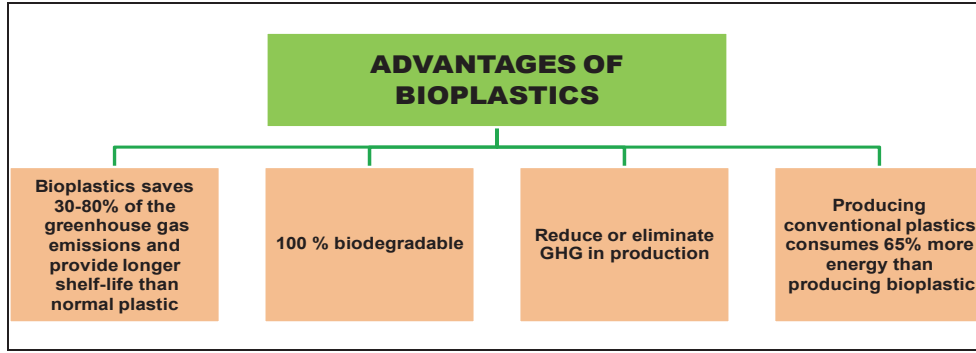


Fig. 4. Advantages of bioplastics

We applied the ELECTRE method to compare the alternatives (bioplastic categories) noted V_1 – V_4 in terms of the criteria C_1 – C_6 , which are described below.

To achieve the objectives of this study, we have applied the ELECTRE method considering the steps described in the section 2, as follows:

a. Establishing criteria for bioplastics evaluation

We proposed the following type of bioplastics denoted as V_1 – V_4 , which are considered project alternatives, (Table 2):

- V_1 – Bioplastic Made from Starch (BMS);
- V_2 – Polylactic Acid (PLA);
- V_3 – Polyhydroxyalkanoates (PHAs);
- V_4 – Polyvinyl Alcohol (PVOH);

Criteria for assessment of variants are denoted as C_1 – C_6 :

- C_1 – benefit achieved by applying the solution (reporting in thousands EUR);
- C_2 – harmonization with the priorities of EU legislation (will give marks);
- C_3 – the degree of degradation for bioplastics (will give marks);
- C_4 – cost of project implementation (reporting in thousands EUR);
- C_5 – amount of waste recovery (reporting in %);
- C_6 – energy recovered from waste (reporting in %).

These criteria focused on sustainable development indicators (social, economical and environmental) (Fig. 5).

b. Determination of the coefficients of importance K_{ij} for each criterion

After we established alternatives of bioplastics and evaluation criteria, we have selected the evaluation team, which is represented by a biologist, an analyst, a process engineer, and an engineer specialized in waste management.

Also, we gave scores from 6 to 10 (6 represents low participation for each criterion and 10 means active participation) to each team member according to the six criteria established. The importance coefficient K_{ij} was calculated with Eq. (1), where: $\sum n_{ij}$ is the sum of the importance coefficients according to some criteria where the notes for variant i are greater or equal compared to

the notes for variant j ; $\sum \sum n_{ij}$ is the sum of the importance coefficients.

$$K_{ij} = \frac{\sum n_{ij}}{\sum \sum n_{ij}} \quad (1)$$

The results obtained after the calculation of K_{ij} are presented in Table 3. Determination mark from notes of appreciation a^*_{ij} helped us to bring in the same unit mass concentrations, which are expressed in different units.

Application of ELECTRE method is based on two groups of indicators, namely: concordance (C_c) and discordance (C_d) indicators.

c. Calculation of concordance indicators

Determination of concordance indicators that indicate in which way a^*_{gj} version is surpassed to the variant a^*_{hj} was performed using Eq. (2) (Herghiligi and Lupu, 2012; Herghiligi et al., 2013; Lupu et al., 2006, 2012), where: C_{vgvh} is the concordance indicator; K_j is importance coefficient from the j criterion; a^*_{gj}, a^*_{hj} represent the appreciation notes.

$$C_{vgvh} = \frac{1}{\sum_{k=1}^n} \sum_j k_j; a^*_{gj} \geq a^*_{hj} \quad (2)$$

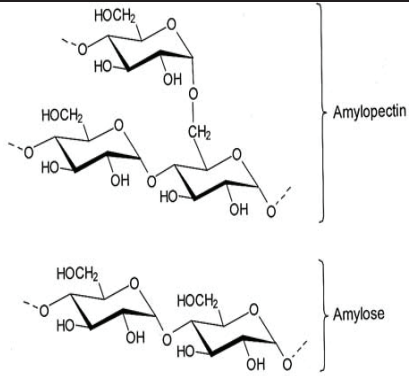
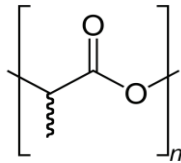
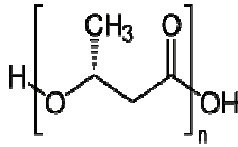
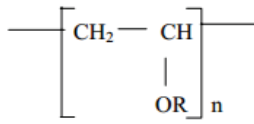
After finalizing calculations, we obtained the following indicators of concordance: 0.7, 0.5, 0.5 for BMS 0.49, 0.69, 0.5 for PLA, 0.48, 0.48, 0.48 for PHAs and 0.5, 0.5, 0.68 for PVOH. The structure of the concordance matrix is presented in Table 4.

d. Calculation of discordance indicators

Eq. (3) was used for the calculation of discordance indicators (Herghiligi and Lupu, 2012; Herghiligi et al., 2013; Lupu et al., 2006, 2012), where: $d=ecart$ represents the maximum distance a^*_{gj} between the appreciation notes awarded = 1.

$$D_{vgvh} = \begin{cases} a^*_{gj} > a^*_{hj} \\ \frac{1}{d} \max |a^*_{gj} - a^*_{hj}|; a^*_{gj} \leq a^*_{hj} \end{cases} \quad (3)$$

Table 2. Characteristics of bioplastic types used in this study

| Type of bioplastic | Characteristics | Chemical formula |
|--|---|--|
| Bioplastic made from starch (BMS) | <p>Bioplastics obtained from starch (extracted from corn, potato, etc.) are currently the most widely used, accounting for about 50% of the bioplastics market. Due to their thermal characteristics, these bioplastics can help bring additives (Butterworth et al., 2013). Starch-based bioplastics can be mixed with the polyester to produce mixtures such as polycaprolactone. These mixtures are used in industrial applications are also compostable (Mahasukhonthachat et al., 2010).</p> <p>Bioplastic made from starch can be used for (Hasjim and Jane, 2009): bags; Deli containers; cups; Tarpaulin for agricultural uses; lids.</p> |  <p>Amylopectin</p> <p>Amylose</p> |
| Polylactic acid (PLA) | <p>Polylactic acid is made from dextrose (sugar) extracted from renewable materials. This is the most popular bioplastic material or biopolymer and only product currently in a world-class factory (Undri et al., 2014).</p> <p>This biopolymer is suitable for fiber extrusion, and can easily be replaced by polypropylene (PP). PLA can be easily degraded (respecting certain conditions of temperature and humidity). The products of the PLA can be composted in industrial installations where the temperature (700 °C) and humidity (70% RH) can be controlled (Garlotta, 2001).</p> <p>PLA can be used for (Bordes et al., 2009; Petersson et al., 2007): fiber extrusion processes: tea bags, clothing, films; injection processes: enclosures for jewelry; thermoforming processes: pots, pans, cups, coffee pills; blowing processes: water bottles (payment) for cosmetic purposes.</p> |  |
| Polyhydroxyalkanoates (PHAs) | <p>PHAs are biological polyesters are produced by microorganisms, and may also be biodegradable by a large number of different microorganisms. The polymers are produced through a fermentation process, which involves feeding sugar and microorganisms (Cyras et al., 2007).</p> <p>PHAs can be used for (Reddy et al., 2003): plastic bags and various utensils; packaging (including films); containers; paper coatings; medical garments; compostable bags, lids; tubs.</p> |  |
| Polyvinyl alcohol (PVOH) | <p>Polyvinyl alcohol is produced by conversion of biobased ethylene (from biobased ethanol) to biobased vinyl acetate, polymerization polyvinyl acetate and to biobased, biobased hydrolysis to PVOH. As the main raw material used in the manufacture of polyvinyl alcohol is vinyl acetate monomer type (Guohua et al., 2006).</p> <p>PVOH is a bioplastic; in the form of a granular powder with white or cream color. Depending on the obtaining method, PVOH can be of two types, partially hydrolyzed or fully hydrolyzed. PVOH partially hydrolyzed, is used in the food industry (for obtaining packages). This type of bioplastic is used to obtain packaging with protective role of moisture absorption (Pavol et al., 2002).</p> <p>Areas of use the Polyvinyl alcohol (PVOH) (Guohua et al., 2006; Pavol et al., 2002): paper adhesive; textile sizing agent; packaging.</p> |  <p>where R = H or COCH₃</p> |

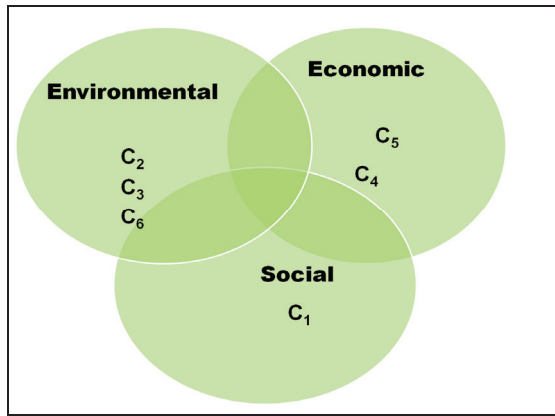


Fig. 5. Criteria taken into account for obtaining sustainable bioplastics

After the calculation of discordance indicators the following values were obtained: 0.6, 0.8, 1 for BMS indicators, 0.5, 0.5, 1 for PLA; 0.6, 0.9, 0.4 for PHAs and 0.8, 1, 0.5 for PVOH. In Table 5 is presented the discordance matrix structure.

e. Determination of the most suitable alternative

Establishing of the suitable alternative was performed by using the difference method and the concordance and discordance matrices.

The difference between the two matrices represents the best option. We have evaluated all variants, the final selection, favoring the variant V_3 (PHAs) followed by V_1 (BMA), V_4 (PVOH) and V_2 (PLA)(Fig. 6).

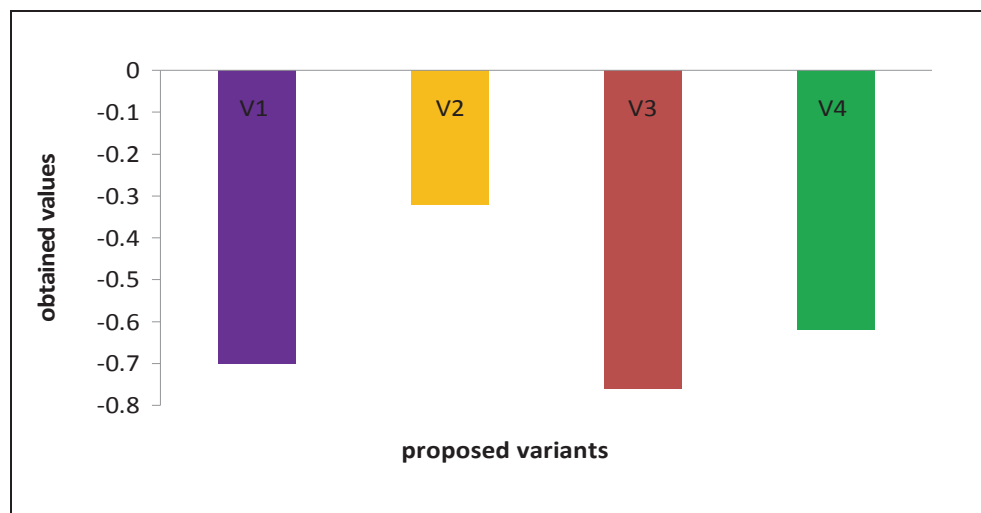


Fig. 6. Results obtained after applying the difference method

Table 3. Determination of appreciation notes matrix, function, utility

| | C_1 | C_2 | C_3 | C_4 | C_5 | C_6 |
|----------|-------|-------|-------|-------|-------|-------|
| V_1 | 0 | 0 | 1 | 1 | 0.8 | 1 |
| V_2 | 0.3 | 0.5 | 0 | 0.5 | 0.8 | 1 |
| V_3 | 1 | 0.5 | 0.5 | 0.1 | 0.5 | 0.3 |
| V_4 | 0.5 | 0.8 | 0.5 | 0.50 | 0 | 0.2 |
| K_{ij} | 0.15 | 0.16 | 0.16 | 0.17 | 0.18 | 0.18 |

5.2. Analysis of solution from the point of view of ELECTRE method

ELECTRE method is specially adapted to environmental and sustainability problems, because this it searches the best compromise between all decision criteria and not the solution (if only some criteria are optimized).

The type of decision problem approach resulted by applying ELECTRE method leads to results oriented for decision making. Following the development of this problem, with entering values instead of the criteria, the results of this case are more precise and easier to interpret.

The final classification of multi-criteria analysis process by applying ELECTRE method was conducted based on selected criteria which addressed both objectives: current trends of waste recovery (recovery material and energy resources) and environmental global indicators (amount of emissions generated).

The results depend on the input data, criteria such as the: benefit achieved through applying the solution, harmonization variant, with the priorities of legislation, possibility of bioplastics degradation, the quantity of emissions for greenhouse gases responsible for global warming emitted by stations / installations in the environment, cost of project implementation, quantity of waste recovery and the quantity of material resources and energy recovered. Four criteria were represented as beneficial attributes and two criteria were represented as cost attributes.

Table 4. Concordance matrix

| $V \backslash V$ | V_1 | V_2 | V_3 | V_4 |
|------------------|-------|-------|-------|-------|
| V_1 | | 0.7 | 0.5 | 0.5 |
| V_2 | 0.49 | | 0.69 | 0.5 |
| V_3 | 0.48 | 0.48 | | 0.48 |
| V_4 | 0.5 | 0.5 | 0.68 | |

Table 5. Discordance matrix

| $V \backslash V$ | V_1 | V_2 | V_3 | V_4 |
|------------------|-------|-------|-------|-------|
| V_1 | | 0.6 | 0.8 | 1 |
| V_2 | 0.5 | | 0.5 | 1 |
| V_3 | 0.6 | 0.9 | | 0.4 |
| V_4 | 0.8 | 1 | 0.5 | |

Fig. 6 illustrates the results obtained by applying ELECTRE method. The results are favorable for the alternative addressing the polyhydroxyalkanoate, followed by alternative that involves obtaining bioplastic made from starch. The lowest results are for bioplastics as polylactic acid and polyvinyl alcohol.

Results are mainly confirmed by high rates of material resources or energy recovery and reduction of the amount of emissions generated by PHAs. The conclusion is supported by the fact that polyhydroxyalkanoate are biological polyesters which are produced by microorganisms, and may also be biodegradable by a great number of different microorganisms.

6. Conclusions

In this study a multicriteria evaluation method was applied for the determination of the bioplastics optimal alternative which can be used in packaging production. The analysis was performed using the ELECTRE method, which quantifies the relative importance of the criteria considered. The choice of thresholds is determined by the specificity of each criterion in order to reflect the decision maker preference.

The alternatives proposed (BMS, PLA, PHAs, PVOH) are evaluated based on six criteria considering three sustainable development indicators: social, economical and environmental. The *environmental criteria* aspects focused on harmonization with the priorities of EU legislation, the degree of bioplastics degradation and energy recovered from waste. *Economic criteria*, focused on benefits achieved by applying the solution and cost of project implementation, while social criteria includes benefits of project implementation.

The alternatives can be ranked after the evaluation from the most favorable option to the less favorable as following: PHAs>BMS>PVOH>PLA. PHAs are the most suitable alternative in terms of production from both environmental and economical criteria. Our analysis nevertheless shows that PHAs may have some advantages, compared to the BMS, PVOH and PLA. This result is an important step for

sustainable development in terms of the use of biomass, the possibility of plastic recycling, and waste energy recovery. The interest and usefulness of this variant should be analyzed further.

It can be concluded that ELECTRE is an efficient method which can respond directly to the concerns of policy makers by ranking of criteria and will remain a valuable instrument for decision making.

Acknowledgments

This work was supported by a strategic grant POSDRU/159/1.5/S/133652, co-financed by the European Social Fund within the Sectorial Operational Program Human Resources Development 2007 – 2013 and by a grant of the Romanian National Authority for Scientific Research, CNCS – UEFISCDI, project number PN-II-ID-PCE-2011-3-0559, Contract 265/2011.

References

- Accinelli C., Saccà M.L., Mencarelli M., Vicari A., (2012), Deterioration of bioplastic carrier bags in the environment and assessment of a new recycling alternative, *Chemosphere*, **89**, 136–143.
- Adamus G., Sikorska W., Janeczek H., Kwiecień M., Sobota M., Kowalczyk M., (2012), Novel block copolymers of atactic PHB with natural PHA for cardiovascular engineering: Synthesis and characterization, *European Polymer Journal*, **48**, 621–631.
- Aiello G., La Scalia G., Enea M., (2013), A non dominated ranking Multi Objective Genetic Algorithm and electre method for unequal area facility layout problems, *Expert Systems with Applications*, **40**, 4812–4819.
- Akaraonye E., Keshavarz T., Roy I., (2010), Production of polyhydroxyalkanoates: the future green materials of choice, *Journal of Chemical Technology and Biotechnology*, **85**, 732–743.
- Andrady A.L., (2011), Microplastics in the marine environment, *Marine Pollution Bulletin*, **62**, 1596–1605.
- Araujo M.A., Cunha A.M., Mota M., (2004), Changes in morphology of starch-based prosthetic thermoplastic material during enzymatic degradation, *Journal of Biomaterials Science Polymer Edition*, **15**, 1263–1280.
- Auras R., Harte B., Selke S., (2004), An overview of polylactides as packaging materials, *Macromolecular Bioscience*, **4**, 835–864.

- Barnes D.K.A., Galgani F., Thompson R.C., Barlaz M., (2009), Accumulation and fragmentation of plastic debris in global environments, *Philosophical Transactions of the Royal Society B: Biological Sciences*, **364**, 1985–1998.
- Bojković N., Anić I., Pejčić-Tarle S., (2010), One solution for cross-country transport-sustainability evaluation using a modified ELECTRE method, *Ecological Economics*, **69**, 1176–1186.
- Bordes P., Pollet E., Avérous L., (2009), Nano-biocomposites: biodegradable polyester/nanoclay systems, *Progress in Polymer Science*, **34**, 125–55.
- Briassoulis H., (2001), Sustainable development and its indicators: through a (planner's) glass darkly, *Journal of Environmental Planning and Management*, **44**, 409–427.
- Butterworth P.J., Warren F.J., Grassby T., Patel H., Ellis P.R., (2012), Analysis of starch amyolysis using plots for first-order kinetics, *Carbohydrate Polymers*, **87**, 2189–2197.
- Caliman F.A., Gavrilescu M., (2009), Pharmaceuticals, personal care products and endocrine disrupting agents in the environment – a review, *CLEAN - Soil, Air, Water*, **37**, 277–303.
- Cavalheiro J.M.B.T., de Almeida M.C.M.D., Grandfils C., da Fonseca M.M.R., (2009), Poly (3-hydroxybutyrate) production by *Cupriavidus necator* using waste glycerol, *Process Biochemistry*, **44**, 509–515.
- Chaudhary A.L., Miller M., Torley P.J., Sopade P.A., Halley P.J., (2008), Amylose content and chemical modification effects on the extrusion of thermoplastic starch from maize, *Carbohydrate Polymers*, **74**, 907–913.
- Chen J., Zhang L., Chen J., Chen G., (2007), Biosynthesis and characterization of Polyhydroxyalkanoate copolymers in *Ralstonia eutropha* PHB-4 harboring a low-substrate-specificity PHA Synthase PhaC2Ps from *Pseudomonas stutzeri* 1317, *Chinese Journal of Chemical Engineering*, **15**, 391–396.
- Choi T., Han J., Koo J., (2015), Decision method for rehabilitation priority of water distribution system using ELECTRE method, *Desalination and Water Treatment*, **53**, 2369–2377.
- Cooper T.A., (2013), *Developments in bioplastic materials for packaging food, beverages and other fast-moving consumer goods*, In: *Woodhead publishing series in food science, technology and nutrition*, Farmer N. (Eds.), Woodhead Publishing, New York, 108–152.
- Cyras V.P., Commisso M.S., Mauri A.N., Vázquez A., (2007), Biodegradable double-layer films based on biological resources: polyhydroxybutyrate and cellulose, *Journal of Applied Polymer Science*, **160**, 749–756.
- Dace E., Bazbauers G., Berzina A., Davidsen P.I., (2014), System dynamics model for analyzing effects of eco-design policy on packaging waste management system, *Resources, Conservation and Recycling*, **87**, 175–190.
- De Feo G., De Gisi S., Williams I.D., (2013), Public perception of odour and environmental pollution attributed to MSW treatment and disposal facilities: a case study, *Waste Management*, **33**, 974–987.
- European Bioplastics, (2013), Institute for Bioplastics and Biocomposites, On line at: www.bio-based.eu/markets.
- Fortuna M.E., Simion I.M., Gavrilescu M., (2011), Sustainability in environmental remediation, *Environmental Engineering and Management Journal*, **10**, 1987–1996.
- Fortuna M.E., Simion I.M., Ghinea C., Petraru M., Cozma P., Apostol L.C., Hlihor R.M., Tudorache Fertu D., Gavrilescu M., (2012), Analysis and management of specific processes from environmental engineering and protection based on sustainability indicators, *Environmental Engineering and Management Journal February*, **11**, 333–350.
- Freemantle M., (2005), Green polymer field blossoming, *Chemical & Engineering News*, **83**, 36–39.
- Freire C.A., Fertig C.C., Podczek F., Veiga F., Sousa J., (2009), Starch-based coatings for colon-specific drug delivery. Part I: The influence of heat treatment on the physico-chemical properties of high amylose maize starches, *European Journal of Pharmaceutics and Biopharmaceutics*, **72**, 574–586.
- Garlotta D., (2001), A literature review of poly (lactic acid), *Journal of Polymers and the Environment*, **9**, 63–84.
- Gavrilescu M., (2004), Cleaner production as a tool for sustainable development, *Environmental Engineering and Management Journal*, **3**, 45–70.
- Gavrilescu M., Chisti Y., (2005), Biotechnology – a sustainable alternative for chemical industry, *Biotechnology Advances*, **23**, 471–499.
- Gavrilescu M., (2008), Biomass power for energy and sustainable development, *Environmental Engineering and Management Journal*, **7**, 617–670.
- Gavrilescu M., (2014a), *Biorefinery System: An Overview*, In: *Bioenergy Research: Advances and Applications*, Gupta V.K., Tuohy M., Kubicek C.P., Saddler J., Xu F. (Eds.), Elsevier, 219–242.
- Gavrilescu M., (2014b), *Biomass Potential for Sustainable Environment, Biorefinery Products and Energy*, In: *Sustainable Energy in the Built Environment - Steps Towards nZEB*, Visa I. (Ed.), Springer International Publishing Switzerland, 169–194.
- Gavrilescu M., Demnerová K., Aamand J., Agathos S., Fava F., (2015), Emerging pollutants in the environment: present and future challenges in biomonitoring, ecological risks and bioremediation, *New Biotechnology*, **32**, 147–156.
- Generowicz A., Kulczycka J., Kowalski Z., Banach M., (2011), Assessment of waste management technology using BATNEEC options, technology quality method and multi-criteria analysis, *Journal of Environmental Management*, **92**, 1314–1320.
- Ghinea C., Gavrilescu M., (2010), Decision support models for solid waste management – An overview, *Environmental Engineering and Management Journal*, **9**, 869–880.
- Ghinea C., Petraru M., Bressers H., Gavrilescu M., (2012), Environmental Evaluation of Waste management Scenarios – Significance of the Boundaries, *Journal of Environmental Engineering and Landscape Management*, **20**, 76–85.
- Ghinea C., Bressers H.Th.A., Gavrilescu M., (2014a), Multicriteria evaluation of municipal solid waste management scenarios: Case study Iasi, Romania, *Journal of Faculty of Food Engineering, Ștefan cel Mare University of Suceava, Romania*, **XIII**, 38 – 47.
- Ghinea C., Petraru M., Simion I.M., Sobariu D., Bressers H., Gavrilescu M., (2014b), Life cycle assessment of waste management and recycled paper systems, *Environmental Engineering and Management Journal*, **13**, 2073–2085.
- Gregory M.R., (2009), Environmental implications of plastic debris in marine settings-entanglement, ingestion, smothering, hangers-on, hitch-hiking and

- alien invasions, *Philosophical Transactions of the Royal Society B: Biological Sciences*, **364**, 2013–2025.
- Groot J., Bing X., Bos-Brouwers H., Bloemhof-Ruwaard J., (2014), A comprehensive waste collection cost model applied to post-consumer plastic packaging waste, *Resources, Conservation and Recycling*, **85**, 79–87.
- Guohua Z., Ya L., Cuilan F., Min Z., Caiqiong Z., Zongdao C., (2006), Water resistance, mechanical properties and biodegradability of methylated-cornstarch/poly(vinyl alcohol) blend film, polymer degradation and stability, *Polymer Degradation and Stability*, **91**, 703–711.
- Hall C.R., Campbell B.L., Behe B.K., Yue C., Lopez R.G., Dennis J.H., (2010), The appeal of biodegradable packaging to floral consumers, *HortScience*, **45**, 583–591.
- Hasjim J., Jane J.L., (2009), Production of resistant starch by extrusion cooking of acid-modified normal-maize starch, *Journal of Food Science*, **74**, C556–C562.
- Hatami-Marbini A., Tavana M., (2011), An extension of the ELECTRE I method for group decision-making under a fuzzy environment, *Omega*, **39**, 373–386.
- Hatami-Marbini A., Tavana M., Moradi M., Kangi F., (2013), A fuzzy group Electre method for safety and health assessment in hazardous waste recycling facilities, *Safety Science*, **51**, 414–426.
- Heaney C.D., Wing S., Campbell R.L., Caldwell D., Hopkins B., Richardson D., (2011), Relation between malodor, ambient hydrogen sulfide, and health in a community bordering a landfill, *Environmental Research*, **111**, 847–852.
- Herghilighiu I.V., Lupu M.L., (2012), Stakeholder role in environmental decision, *Quality-Access to Success*, **13**, 179–182.
- Herghilighiu I.V., Lupu M.L., Robledo C., Kobi A., (2013), A new conceptual framework for environmental decision based on fractal philosophy, *Environmental Engineering and Management Journal*, **12**, 1095–1102.
- Hermann B.G., Debeer L., De Wilde B., Blok K., Patel M.K., (2011), To compost or not to compost: Carbon and energy footprints of biodegradable materials' waste treatment, *Polymer Degradation and Stability*, **96**, 1159–1171.
- Hlihor R.M., Diaconu M., Leon F., Curteanu S., Tavares T., Gavrilescu M., (2014a), Experimental analysis and mathematical prediction of Cd(II) removal by biosorption using support vector machines and genetic algorithms, *New Biotechnology*, <http://dx.doi.org/10.1016/j.nbt.2014.08.003>.
- Hlihor R.M., Bulgariu L., Sobariu D.L., M. Diaconu, Tavares T., Gavrilescu M., (2014b), Recent advances in biosorption of heavy metals: Support tools for biosorption equilibrium, kinetics and mechanism, *Revue Roumaine de Chimie*, **59**, 527–538.
- Hyde K.M., Maier H.R., Colby C.B., (2005), A distance-based uncertainty analysis approach to multi-criteria decision analysis for water resource decision making, *Journal of Environmental Management*, **77**, 278–290.
- Iazzolino G., Laise D., Marraro L., (2012), Business multicriteria performance analysis: a tutorial, *Benchmarking: An International Journal*, **19**, 395–411.
- Iles A., Martin A.N., (2013), Expanding bioplastics production: sustainable business innovation in the chemical industry, *Journal of Cleaner Production*, **45**, 38–49.
- ISO 472, (2013), International Organization for Standardization, Plastics, Subcommittee SC 1, Terminology, On line at: <https://www.iso.org/obp/ui/#iso:std:iso:472:ed-4:v1:en>.
- Iwata T., (2015), Biodegradable and bio-based polymers: future prospects of eco-friendly plastics, *Angewandte Chemie International Edition*, **54**, 3210–3215.
- Kaya T., Kahraman C., (2011), An integrated fuzzy AHP–ELECTRE methodology for environmental impact assessment, *Expert Systems with Applications*, **38**, 8553–8562.
- Koroneos C.J., Nanaki E.A., (2012), Integrated solid waste management and energy production - a life cycle assessment approach: the case study of the city of Thessaloniki, *Journal of Cleaner Production*, **27**, 141–150.
- Kowalski K., Stagl S., Madlener R., Omann I., (2009), Sustainable energy futures: Methodological challenges in combining scenarios, *European Journal of Operational Research*, **197**, 1063–1074.
- Lithner D., Larsson Å., Dave G., (2011), Environmental and health hazard ranking and assessment of plastic polymers based on chemical composition, *Science of the Total Environment*, **409**, 3309–3324.
- Lupu M.L., Oniciuc N., Rusu B., Rusu C., (2006), *The Environmental Performance Indicators System*, (in Romanian), Performantica Publishing House, Iași, Romania.
- Lupu M.L., Trofin O., Trofin N., (2012), Environmental performance – part of management performance, *Environmental Engineering and Management Journal*, **11**, 393–405.
- Mahasukhonthachai K., Sopade P.A., Gidley M.J., (2010), Kinetics of starch digestion in sorghum as affected by particle size, *Journal of Food Engineering*, **96**, 18–28.
- Melikoglu M., Lin C.S.K., Webb C., (2013), Analyzing global food waste problem: pinpointing the facts and estimating the energy content, *Central European Journal of Engineering*, **3**, 157–164.
- Milutinović B., Stefanović G., Dassisti M., Marković D., Vučković G., (2014), Multi-criteria analysis as a tool for sustainability assessment of a waste management model, *Energy*, **74**, 190–201.
- OECD, (2014), Biobased Chemicals and Bioplastics. Finding the Right Policy Balance, OECD Science, Technology and Industry Policy Papers, No. 17, OECD Publishing, <http://dx.doi.org/10.1787/5jxwwfjx0djf-en>.
- O'Brine T., Thompson R.C., (2010), Degradation of plastic carrier bags in the marine environment, *Marine Pollution Bulletin*, **60**, 2279–2283.
- Pavol A., Darina K., Miroslav K., Dusan B. Barbora S., (2002), Poly (vinyl alcohol) stabilisation in thermoplastic processing, *Polymer Degradation and Stability*, **78**, 413–421.
- Pedrero F., Albuquerque A., Marecos do Monte H., Cavaleiro V., Alarcón J.J., (2011), Application of GIS-based multi-criteria analysis for site selection of aquifer recharge with reclaimed water, *Resources, Conservation and Recycling*, **56**, 105–116.
- Peelman N., Ragaert P., De Meulenaer B., Adons D., Peeters R., Cardond L., Van Impe F., Devlieghere F., (2013), Application of bioplastics for food packaging, *Trends in Food Science & Technology*, **32**, 128–141.
- Petersson L., Kvien I., Oksman K., (2007), Structure and thermal properties of poly(lactic acid)/cellulose whiskers nanocomposite materials, *Composites Science and Technology*, **67**, 2535–44.

- Phillips L.D., (1984), A theory of requisite decision models, *Acta Psychologica*, **56**, 29–48.
- PlasticsEurope, (2011), Eco-profiles and Environmental Declarations Plastics Europe, Version 2.0, On line at: http://www.plasticseurope.org/documents/document/20110421141821-plasticseurope_eco-profile_methodology_version2-0_2011-04.pdf.
- Pogăcean M.O., Hlihor R.M., Gavrilescu M., (2014), Monitoring pesticides degradation in apple fruits and potential effects of residues on human health, *Journal of Environmental Engineering and Landscape Management*, **22**, 171–182.
- Queirós D., Rossetti S., Serafim L.S., (2014), PHA production by mixed cultures: A way to valorize wastes from pulp industry, *Bioresource Technology*, **157**, 197–205.
- Reddy C.S.K., Ghai R., Kalia V.C., (2003), Polyhydroxyalkanoates: an overview, *Bioresource Technology*, **87**, 137–146.
- Ritter S., (2002), Green challenge, *Chemical & Engineering News*, **80**, 26–30.
- Rochman C.M., Hoh E., Hentschel B.T., Kaye S., (2013), Long-term field measurement of sorption of organic contaminants to five types of plastic Pellets: implications for plastic marine debris, *Environmental Science & Technology*, **47**, 1646 – 1654.
- Rose M., Palkovits R., (2009), Cellulose-based sustainable polymers: state of the art and future trends, *Macromolecular Rapid Communications*, **32**, 29–311.
- Rossi V., Cleeve-Edwards N., Lundquist L., Schenker U., Dubois C., Humbert S., Jolliet O., (2015), Life cycle assessment of end-of-life options for two biodegradable packaging materials: sound application of the European waste hierarchy, *Journal of Cleaner Production*, **86**, 132–145.
- Roy B., Bouyssou D., (1993), *Multicriteria Decision: Methods and Case*, (in French), Economica, LAMSADE, Paris.
- Roy B., Vanderpooten D., (1996), An overview on “The European school of MCDA: Emergence, basic features and current works”, *European Journal of Operational Research*, **99**, 26–27.
- Roy P.K., Hakkarainen M., Varma I.K., Albertsson A.-C., (2011), Degradable polyethylene: fantasy or reality, *Environmental Science and Technology*, **45**, 4217–4227.
- Sahoo P., Ali S.M., (2008), Elastic–plastic adhesive contact of non-Gaussian rough surfaces, *Sadhana*, **33**, 367–384.
- San Cristobal J.R., (2012), *Multi Criteria Analysis in the Renewable Energy Industry*, Springer, Amsterdam.
- Scholten L., Schuwirth N., Reichert P., Lienert J., (2015), Tackling uncertainty in multi-criteria decision analysis – An application to water supply infrastructure planning, *European Journal of Operational Research*, **242**, 243–260.
- Shah A.A., Hasan F., Hameed A., Ahmed S., (2008), Biological degradation of plastics: A comprehensive review, *Biotechnology Advances*, **26**, 246–265.
- Sheldon R.A., (2014), Green and sustainable manufacture of chemicals from biomass: state of the art, *Green Chemistry*, **16**, 950–963.
- Shen L., Haufe J., Patel M.K., (2009), Product Overview and Market Projection of Emerging Bio-based Plastics, PRO-BIP 2009, Final Report, Report Commissioned by European Polysaccharide Network of Excellence (EPNOE) and European Bioplastics, Group Science, Technology and Society, Universiteit Utrecht, The Netherlands.
- Shen L., Hu H., Ji H., Cai J., He N., Li Q., Wang Y., (2014), Production of poly(hydroxybutyrate–hydroxyvalerate) from waste organics by the two-stage process: Focus on the intermediate volatile fatty acids, *Bioresource Technology*, **166**, 194–200.
- Simion I.M., Ghinea C., Maxineasa S.G., Taranu N., Bonoli A., Gavrilescu M., (2013a), Ecological footprint applied in the assessment of construction and demolition waste integrated management, *Environmental Engineering and Management Journal*, **4**, 779–788.
- Simion I.M., Fortuna M.E., Bonoli A., Gavrilescu M., (2013b), Comparing environmental impacts of natural inert and recycled construction and demolition waste processing using LCA, *Journal of Environmental Engineering and Landscape Management*, **21**, 273–287.
- Singh A.V., Nath L.K., (2013), Evaluation of chemically modified hydrophobic starch as a carrier for controlled drug delivery, *Saudi Pharmaceutical Journal*, **21**, 193–200.
- Singh S., Mohanty Amar K., Sugie T. Takai Y., Hamada H., (2008), Renewable resource based biocomposites from natural fiber and polyhydroxybutyrate-co-valerate (PHBV) bioplastic, *Composites Part A: Applied Science and Manufacturing*, **39**, 875–886.
- Sivan A., (2011), New perspectives in plastic biodegradation, *Current Opinion in Biotechnology*, **22**, 422–426.
- Soltani A., Hewage K., Reza B., Sadiq R., (2015), Multiple stakeholders in multi-criteria decision-making in the context of Municipal Solid Waste Management: A review, *Waste Management*, **35**, 318–328.
- Song J.H., Murphy R.J., Narayan R., Davies G.B.H., (2009), Biodegradable and compostable alternatives to conventional plastics, *Philosophical Transactions of the Royal Society B: Biological Sciences*, **364**, 2127–2139.
- Sudhakaran S., Lattemann S., Amy G.L., (2013), Appropriate drinking water treatment processes for organic micropollutants removal based on experimental and model studies — A multi-criteria analysis study, *Science of the Total Environment*, **442**, 478–488.
- Șchiopu A.-M., Ghinea C., (2013), Municipal solid waste management and treatment of effluents resulting from their landfilling, *Environmental Engineering and Management Journal*, **12**, 1843 – 3707.
- Tachwali Y., Al-Assaf Y., Al-Ali A.R., (2007), Automatic multistage classification system for plastic bottles recycling, *Resources, Conservation and Recycling*, **52**, 266–285.
- Teng J., Wu X., (2014), Eco-footprint-based life-cycle eco-efficiency assessment of building projects, *Ecological Indicators*, **39**, 160–168.
- Troldborg M., Heslop S., Hough R.L., (2014), Assessing the sustainability of renewable energy technologies using multi-criteria analysis: Suitability of approach for national-scale assessments and associated uncertainties, *Renewable and Sustainable Energy Reviews*, **39**, 1173–1184.
- Tsiporkova E., Boeva V., (2006), Multi-step ranking of alternatives in a multi-criteria and multi-expert decision making environment, *Information Sciences*, **176**, 2673–2697.
- Undri A., Rosi L., Frediani M., Frediani P., (2014), Microwave assisted pyrolysis of corn derived plastic bags, *Journal of Analytical and Applied Pyrolysis*, **108**, 86–97.

- Vahdani B., Jabbari A.H.K., Roshanaei V., Zandieh M., (2010), Extension of the ELECTRE method for decision-making problems with interval weights and data, *International Journal of Advanced Manufacturing Technology*, **50**, 793–800.
- Vert M., Doi Y., Hellwich K.-H., Hess M., Hodge P., Kubisa P., Rinaudo M., Schué F., (2012), Terminology for biorelated polymers and applications (IUPAC Recommendations 2012), *Pure and Applied Chemistry*, **84**, 377-410.
- Wang J.-J., Jing Y.-Y., Zhang C.-F., Zhao J.-H., (2009), Review on multi-criteria decision analysis aid in sustainable energy decision-making, *Renewable and Sustainable Energy Reviews*, **13**, 2263–2278.
- Wang X., Triantaphyllou E., (2008), Ranking irregularities when evaluating alternatives by using some ELECTRE methods, *Omega*, **36**, 45–63.
- Weiss M., Haufe J., Carus M., Brandão M., Bringezu S., Hermann B., (2012), A review of the environmental impacts of biobased materials, *Journal of Industrial Ecology*, **16**, S169–S181.
- Yu P.H., Huang A.L., Lo W., Chua H., Chen G.Q., (1998), *Conversion of Food Industrial Wastes into Bioplastics*, In: *Biotechnology for Fuels and Chemicals*, Finkelstein M., Davison B.H., Humana Press, 603-614.
- Zhao K., Yang X., Chen G.Q., Chen J.C., (2002), Effect of lipase treatment on the biocompatibility of microbial polyhydroxyalkanoates, *Journal of Materials Science: Materials in Medicine*, **13**, 849–854.



“Gheorghe Asachi” Technical University of Iasi, Romania



FACILE SYNTHESIS OF BISMUTH OXIDE NANOPARTICLES BY A HYDROLYSIS SOLVOTHERMAL ROUTE AND THEIR VISIBLE LIGHT PHOTOCATALYTIC ACTIVITY

Xiaowen Luan, Jian Jiang, Qingya Yang, Minmin Chen, Maolin Zhang, Longfeng Li*

Huaibei Normal University, School of Chemistry and Materials Science, Huaibei 235000, China

Abstract

The bismuth oxide (Bi_2O_3) nanoparticles are easily synthesized from a solution of bismuth nitrate pentahydrate ($\text{Bi}(\text{NO}_3)_3 \cdot 5\text{H}_2\text{O}$) in ethylene glycol by a hydrolysis solvothermal route at temperatures of 120-150°C. X-ray diffraction, scanning electron microscopy and UV-visible diffuse reflectance spectroscopy are used to characterize the products. The results show that the reaction temperature, the reaction duration and the initial solution concentration play important roles in the formation of the Bi_2O_3 nanoparticles, and all the as-synthesized Bi_2O_3 samples have the cubic phase structure. In addition, studies of the photocatalytic properties by exposure to visible light irradiation demonstrate that the as-obtained Bi_2O_3 nanoparticles show potential photocatalytic application.

Key words: bismuth oxide, nanocrystalline materials, photocatalyst, semiconductors

Received: March, 2014; Revised final: July, 2014; Accepted: July, 2014

1. Introduction

Bi_2O_3 is an advanced functional material with potential applications such as functional electronic material, burning rate catalyst, photocatalytic decomposition material, optical material, medical composite material and anti-radiative material. Among various applications, Bi_2O_3 arouses increasing attentions as a photocatalyst over the last few years, and bismuth oxide in different forms such as nanoparticles, nanostructures and thin films have been developed for studying their photocatalytic properties (Chen et al., 2011; Duan et al., 2010; Hao et al., 2014; He et al., 2007a; Iyyapushpam et al., 2012; Sood et al., 2015; Wu et al., 2007; Xiao et al., 2013; Zhang et al., 2010). At present, various methods are introduced for the synthesis of the nanoscale Bi_2O_3 particles including sol-gel method (Anilkumar et al., 2005; He et al., 2007a, 2007b; Pan et al., 2008; Wu et al., 2007), magnetron sputtering

deposition (Sirota et al., 2012), precipitation process (Iyyapushpam et al., 2012; Jha et al., 2005; Li, 2006; Wu et al., 2013; Yang et al., 2014), gel to crystal conversion route (Patil et al., 2005), chemical-bath method (Hajra et al., 2014), low-temperature oxidation method (Xia et al., 2012), oxidative metal vapor transport deposition technique (Qiu et al., 2006), flame spray pyrolysis (Mädler and Pratsinis, 2002), polyol method (Jungk and Feldmann, 2001), hydrolysis route (Schlesinger et al., 2013a, 2013b), microwave-assisted method (Huang et al., 2011), solvothermal method (Qin et al., 2012) etc.

Although the previous methods have been proven to be successful in the synthesis of Bi_2O_3 , they normally requires high temperature heating, long synthesis period, post treatment and so on. At the same time, the common chemical synthesis method based on the polyol medium has been well developed for the synthesis of bismuth oxide. However, the previous polyol method required the

* Author to whom all correspondence should be addressed: e-mail: lilongfeng@chnu.edu.cn

alkali as precipitation reagent during the synthesis process. Hence, it is expected that a more simple synthesis method, which is precipitant-free, additive-free and low costing, is proposed for the synthesis of Bi_2O_3 nanoparticles.

In the present work, we have developed a facile hydrolysis solvothermal method to synthesize Bi_2O_3 nanoparticles, including a rapid self-hydrolysis of bismuth nitrate pentahydrate in ethylene glycol and subsequent solvothermal dehydration and crystallization processes, and no catalysts and additives are added to the reaction system during the synthesis process. In addition, the obtained sample is tested for its performance as a photocatalyst.

2. Experimental section

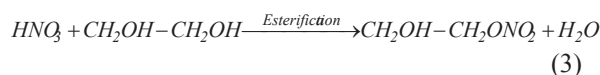
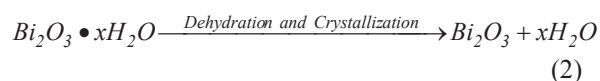
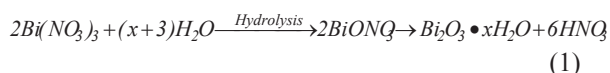
2.1. Materials and apparatus

All chemicals (bismuth nitrate pentahydrate, ethylene glycol etc.) used in the study were of analytical grade quality. A powder diffractometer (Bruker D8 Advance, Germany) with Cu K α radiation ($\lambda = 0.15418$ nm), the accelerating voltage of 40 kV and the emission current of 40 mA was used to determine the crystal phase composition and the crystallite size of the synthesized samples. A scanning electron microscope (LEO1530VP, Germany) was employed to observe the shape and size of the synthesized samples.

The UV-Vis diffuse reflectance spectroscopy was obtained using a UV-visible spectrophotometer (TU-1901, Beijing Purkinje General Instrumental Co., China).

2.2. Synthesis procedure

All chemicals used in the study were commercial available without further treatment. In a typical synthesis, a given amount of $\text{Bi}(\text{NO}_3)_3 \cdot 5\text{H}_2\text{O}$ was firstly dissolved in 80ml ethylene glycol under vigorously stirring, and the resulting solution was then transferred into a Teflon-lined stainless steel autoclave with a capacity of 100 mL. Subsequently, the sealed autoclave was heated at a given temperature for a certain time, and naturally cooled to room temperature. Finally, the as-synthesized products were separated from the solid-liquid mixture by the high-speed centrifugation, washed with ethanol for several times, dried in vacuum at 80°C for 2h, and the Bi_2O_3 nanoparticles were obtained. In the synthesis process, uniform hydrolysis of $\text{Bi}(\text{NO}_3)_3 \cdot 5\text{H}_2\text{O}$ was accomplished to form an amorphous or nano-grain sized hydrated oxide precursor via its own crystallization water in ethylene glycol acting as solvent and esterification agent, followed by solvothermal dehydration and crystallization processes. The chemical reactions for synthesis of Bi_2O_3 can be formulated as Eqs. (1-3):



2.3. Photocatalytic activity measurement

The photocatalytic degradation experiments were carried out in a photochemical reactor using a 500 W Xe lamp with a 420-nm UV cutoff filter, and the photocatalytic performance of the prepared Bi_2O_3 was evaluated by the photodegradation of methyl orange (MO). The reaction temperature was kept at room temperature by cooling water to prevent any thermal catalytic effect. The reaction suspension was prepared by adding 0.25 g of the Bi_2O_3 powder into 100 ml MO aqueous solutions with the concentration of 20 mg/L. Prior to irradiation, the suspension was stirred in a dark to establish adsorption-desorption equilibrium between photocatalyst and MO.

Once the concentration of methyl orange got stabilized, the reaction mixture was irradiated, signaling the start of photocatalysis. At given time intervals, the sample was collected, centrifuged, and filtered through a 0.2 μm millipore filter. Then the filtrate was analyzed on a spectrophotometer at 464 nm, which is the maximum absorption wavelength of MO, to determine the concentration of MO.

3. Results and discussion

3.1. Influence of reaction temperature on phase composition and crystallite size

To determine the crystal phase composition and crystallite size of the synthesized samples, the powder X-ray diffraction (XRD) measurements are carried out at room temperature in the diffraction angle (2θ) range from 20° to 80°. Fig. 1 shows the XRD patterns of samples synthesized with the bismuth nitrate initial concentration of 0.1 mol/L at 120, 130, 140, 150 °C for 2 h, respectively.

In Fig. 1, the spectra are indexed to the crystal planes of the cubic phase bismuth oxide (JCPDS Card No. 27-0052), when the solvothermal temperature is below 140°C, and there are a continuous sharpening and intensifying of the diffraction peaks for Bi_2O_3 with increasing solvothermal temperature, indicating that the crystallite size of Bi_2O_3 increases with the reaction temperature going up. The crystallite size of Bi_2O_3 synthesized at different reaction temperatures can be calculated according to the Scherrer equation.

The results show that the mean sizes of Bi_2O_3 are 8.3, 13.7 and 26.1 nm at 120, 130 and 140°C, respectively. In addition, the characteristic diffraction peaks of Bi (JCPDS Card No. 44-1246) are observed from Fig. 1 at 150°C. While below 140°C, only the diffraction peaks of Bi_2O_3 appear in patterns. It indicates that Bi_2O_3 will be partly reduced to form

the metal bismuth when the solvothermal temperature is 150 °C and above.

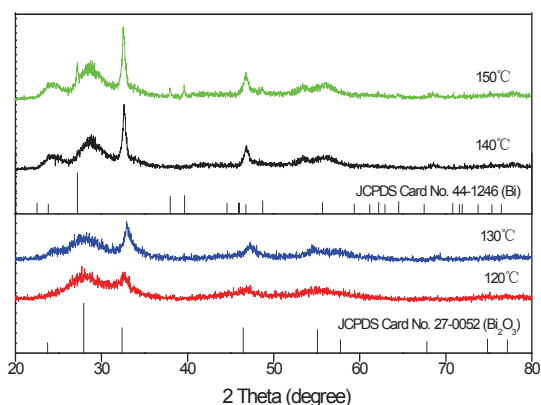


Fig. 1. XRD patterns of samples synthesized at different solvothermal temperatures

3.2. Influence of bismuth nitrate initial concentration on crystallite size

Fig. 2 shows the XRD patterns of the products synthesized at 140 °C for 2 h with the different initial bismuth nitrate concentrations. The average crystallite sizes of the as-prepared products are calculated by the Scherrer equation and are ca. 30.7, 26.1, 17.2 and 13.4 nm corresponding to the initial concentrations of 0.05, 0.1, 0.2 and 0.3 mol/L, respectively. The results indicate that the initial bismuth nitrate concentration has significant influence on the crystallite sizes of products, and the crystallite sizes of the Bi_2O_3 decrease gradually with the increasing of the initial bismuth nitrate concentrations.

It can be explained that the nucleation rate of the predecessor $\text{Bi}(\text{OH})_3$ is greater than the its growth rate under the condition of the higher initial bismuth nitrate concentrations, and the small predecessor results in the formation of small Bi_2O_3 .

3.3. Morphology and size distribution of the sample

In order to study the morphology and size distribution of the synthesized samples, scanning electron microscopy (SEM) is used.

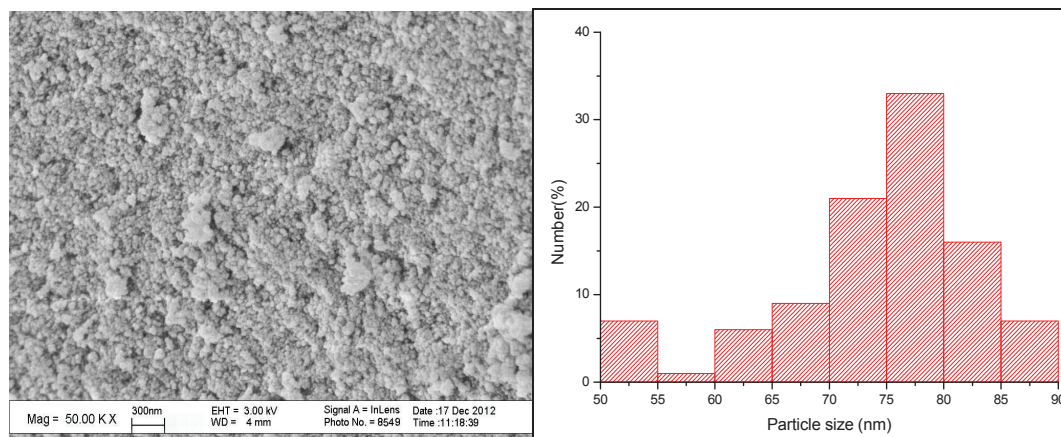


Fig. 3. SEM image and particle size distribution of the synthesized sample

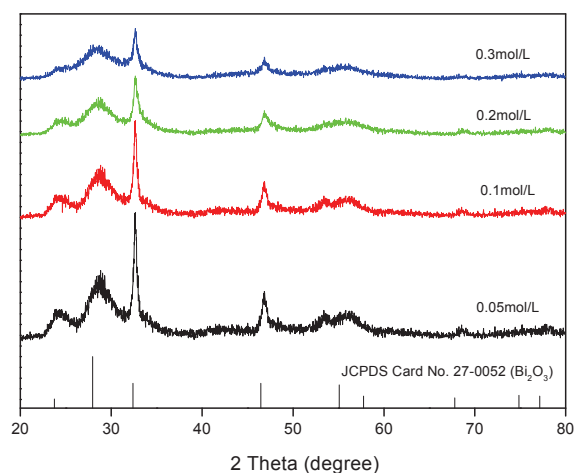


Fig. 2. XRD patterns of samples synthesized under the condition of the different initial bismuth nitrate concentrations

Fig. 3 shows the SEM image of the Bi_2O_3 sample synthesized at the solvothermal temperature of 140 °C for 2 h with the initial bismuth nitrate concentration of 0.1 mol/L. SEM micrograph reveals that the obtained sample is the approximate spherical particles with a little agglomeration, and the particle sizes of them are in the range of 50–90 nm, which are larger compared with the results obtained from XRD analysis. The result declares that the synthesized product is a polycrystalline state.

3.4. UV-Vis diffuse reflectance spectra

The absorption spectra of commercial Degussa P25 TiO_2 and Bi_2O_3 synthesized at the solvothermal temperature of 140 °C for 2 h with the initial bismuth nitrate concentration of 0.1 mol/L are shown in Fig. 4. It can be seen that both the samples have a strong absorption at the wavelength range from 230 to 400 nm.

In addition, it can be observed from Fig. 4 that the absorption band of the Bi_2O_3 sample is red-shifted compare with that of TiO_2 , which is a well known largely studied material for photo-degradation, and the Bi_2O_3 sample has obvious absorption in the visible region (>400 nm).

The absorption band of the Bi_2O_3 is extended to a visible region due to its low-energy band-gap of ca. 2.8 eV, responding to visible irradiation.

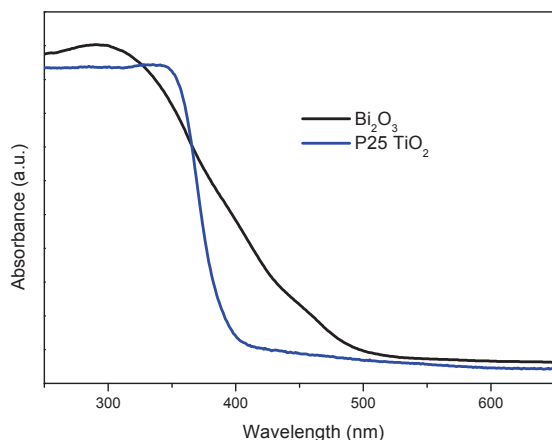


Fig. 4. UV-Vis diffuse reflection spectra

3.5. Photocatalytic activity

The photocatalytic activity of the Bi_2O_3 synthesized at the solvothermal temperature of 140 °C for 2 h with the initial bismuth nitrate concentration of 0.1 mol/L is evaluated through the photodegradation of MO under the visible light irradiation. The experimental results are illustrated in Fig. 5.

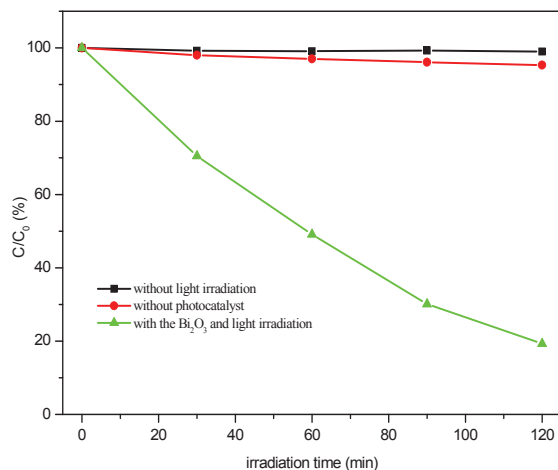


Fig. 5. Photocatalytic activity of the synthesized Bi_2O_3

It shows that the synthesized Bi_2O_3 sample exhibits a high photocatalytic activity for decomposition of MO under the visible light irradiation, and the photocatalytic degradation ratio of MO reaches to 81.3% after irradiation for 2 h. For the purpose of comparison, both blank experiments are also carried out.

The result shows that the MO is not decomposed in the absence of irradiation and has only less than 5% of degradation for 2 h irradiation without the Bi_2O_3 . It suggests that the as-synthesized Bi_2O_3 is an effective photocatalyst for the degradation of MO under irradiation of visible light.

4. Conclusions

The Bi_2O_3 has been successfully synthesized by a simple and cost-effective hydrothermal method. The hydrothermal reaction temperature and the initial bismuth nitrate concentrations obviously influence the phase composition and crystallite size of synthesized powders, and the crystallite sizes of Bi_2O_3 nanoparticles are controlled in the range of 13.4 – 30.7 nm with the initial bismuth nitrate concentrations of 0.05 – 0.3 mol/L at 140 °C for 2 h.

The synthesized Bi_2O_3 shows red shift compared with TiO_2 , and exhibits a higher photocatalytic activity in degradation of MO under visible light irradiation.

Acknowledgments

This work is financially supported by Anhui Provincial Natural Science Foundation (No. 1208085MB30), Natural Science Foundation of Anhui Provincial Department of Education (Nos. KJ2013A231, KJ2014A230, and KJ2010A302).

References

- Anilkumar M., Pasricha R., Ravi V., (2005), Synthesis of bismuth oxide nanoparticles by citrate gel method, *Ceramics International*, **31**, 889-891.
- Chen R., Shen Z.R., Wang H., Zhou H.J., Liu Y.P., Ding D.T., Chen T.H., (2011), Fabrication of mesh-like bismuth oxide single crystalline nanoflakes and their visible light photocatalytic activity, *Journal of Alloys and Compounds*, **509**, 2588-2596.
- Duan F., Zheng Y., Liu L., Chen M.Q., Xie Y., (2010), Synthesis and photocatalytic behaviour of 3D flowerlike bismuth oxide formate architectures, *Materials Letters*, **64**, 1566-1569.
- Jungk H.-O., Feldmann C., (2001), Polyol mediated synthesis of sub-micrometer Bi_2O_3 particles, *Journal of Materials Science*, **36**, 297-299.
- Hajra P., Shyamal S., Mandal H., Fageria P., Pande S., Bhattacharya C., (2014), Photocatalytic activity of Bi_2O_3 nanocrystalline semiconductor developed via chemical-bath synthesis, *Electrochimica Acta*, **123**, 494-500.
- Hao W.C., Gao Y., Jing X., Zou W., Chen Y., Wang T.M., (2014), Visible light photocatalytic properties of metastable $\gamma\text{-Bi}_2\text{O}_3$ with Different Morphologies, *Journal of Materials Science & Technology*, **30**, 192-196.
- He W.D., Qin W., Wu X.H., Ding X.B., Chen L., Jiang Z.H., (2007a), The photocatalytic properties of bismuth oxide films prepared through the sol-gel method, *Thin Solid Films*, **515**, 5362-5365.
- He W.D., Qin W., Wu X.H., Ning H.L., (2007b), Thin bismuth oxide films prepared through the sol-gel method, *Materials Letters*, **61**, 4100-4102.
- Huang Q.Q., Zhang S.N., Cai C.X., Zhou B., (2011), β - and $\alpha\text{-Bi}_2\text{O}_3$ nanoparticles synthesized via microwave-assisted method and their photocatalytic activity towards the degradation of rhodamine B, *Materials Letters*, **65**, 988-990.
- Iyyapushpam S., Nishanthi S.T., Pathinettam Padiyan D., (2012), Synthesis of room temperature bismuth oxide and its photocatalytic activity, *Materials Letters*, **86**, 25-27.

- Jha R.K., Pasricha R., Ravi V., (2005), Synthesis of bismuth oxide nanoparticles using bismuth nitrate and urea, *Ceramics International*, **31**, 495-497.
- Li W., (2006), Facile synthesis of monodisperse Bi₂O₃ nanoparticles, *Materials Chemistry and Physics*, **99**, 174-180.
- Mädler L., Pratsinis S.E., (2002), Bismuth oxide nanoparticles by flame spray pyrolysis, *Journal of the American Ceramic Society*, **85**, 1713-1718.
- Pan C.Y., Li X.H., Wang F.R., Wang L.F., (2008), Synthesis of bismuth oxide nanoparticles by the polyacrylamide gel route, *Ceramics International*, **34**, 439-441.
- Patil M.M., Deshpande V.V., Dhage S.R., Ravi V., (2005), Synthesis of bismuth oxide nanoparticles at 100 °C, *Materials Letters*, **59**, 2523-2525.
- Qin F., Li G.F., Wang R.M., Wu J.L., Sun H.Z., Chen R., (2012), Template-free fabrication of Bi₂O₃ and (BiO)₂CO₃ nanotubes and their application in water treatment, *Chemistry- A European Journal*, **18**, 16491-16497.
- Qiu Y., Liu D., Yang J., Yang S., (2006), Controlled synthesis of bismuth oxide nanowires by an oxidative metal vapor transport deposition technique, *Advanced Materials*, **18**, 2604-2608.
- Schlesinger M., Weber M., Schulze S., Hietschold M., Mehring M., (2013a), Metastable β-Bi₂O₃ nanoparticles with potential for photocatalytic water purification using visible light irradiation, *ChemistryOpen*, **2**, 146-55.
- Schlesinger M., Schulze S., Hietschold M., Mehring M., (2013b), Metastable β-Bi₂O₃ nanoparticles with high photocatalytic activity from polynuclear bismuth oxido clusters, *Dalton Transactions*, **42**, 1047-1056.
- Sirota B., Reyes-Cuellar J., Kohli P., Wang L., McCarroll M.E., Aouadi S.M., (2012), Bismuth oxide photocatalytic nanostructures produced by magnetron sputtering deposition, *Thin Solid Films*, **520**, 6118-6123.
- Sood S., Umar A., Mehta S.K., Kansal S.K., (2015), α-Bi₂O₃ nanorods: An efficient sunlight active photocatalyst for degradation of Rhodamine B and 2,4,6-trichlorophenol, *Ceramics International*, **41**, 3355-3364.
- Wu X.H., Qin W., He W.D., (2007), Thin bismuth oxide films prepared through the sol-gel method as photocatalyst, *Journal of Molecular Catalysis A - Chemical*, **261**, 167-171.
- Wu Y.-C., Chaing Y.-C., Huang C.-Y., Wang S.-F., Yang H.-Y., (2013), Morphology-controllable Bi₂O₃ crystals through an aqueous precipitation method and their photocatalytic performance, *Dyes and Pigments*, **98**, 25-30.
- Xia J.Y., Tang M.T., Chen C., Jin S.M., Chen Y.M., (2012), Preparation of α- Bi₂O₃ from bismuth powders through low-temperature oxidation, *Transactions of Nonferrous Metals Society of China*, **22**, 2289-2294.
- Xiao X., Hu R.P., Liu C., Xing C.L., Qian C., Zuo X.X., Nan J.M., Wang L.S., (2013), Facile large-scale synthesis of β-Bi₂O₃ nanospheres as a highly efficient photocatalyst for the degradation of acetaminophen under visible light irradiation, *Applied Catalysis B: Environmental*, **140-141**, 433-443.
- Yang L.-L., Han Q.-F., Zhao J., Zhu J.-W., Wang X., Ma W.-H., (2014), Synthesis of Bi₂O₃ architectures in DMF-H₂O solution by precipitation method and their photocatalytic activity, *Journal of Alloys and Compounds*, **614**, 353-359.
- Zhang H., Wu P., Li Y., Liao L.F., Fang Z., Zhong X.H., (2010), Preparation of bismuth oxide quantum dots and their photocatalytic activity in a homogeneous system, *ChemCatChem*, **2**, 1115-1121.



"Gheorghe Asachi" Technical University of Iasi, Romania



DEGRADATION AND ADSORPTION BEHAVIOR OF DIBUTYL PHTHALATE IN METHANOGENIC PHASE REFUSE

Chengran Fang^{1,2*}, Yuyang Long², Dongsheng Shen²

¹*Research Institute of Eco-environmental Science, School of Civil Engineering and Architecture,
Zhejiang University of Science and Technology, Hangzhou 310023, China*

²*Zhejiang Provincial Key Laboratory of Solid Waste Treatment and Recycling, School of Environmental Science and Engineering,
Zhejiang Gongshang University, Hangzhou 310018, China*

Abstract

The degradation and adsorption behavior of dibutyl phthalate (DBP) in methanogenic phase refuse was investigated through laboratory microcosm experiments. The results showed that the half-life of DBP in the sterilized refuse was 5.9 times higher than in unsterilized samples, but that it decreased by 35.8% when dominant bacterial strains were added. Different concentrations of DBP did not have obvious effects on its degradation. The half-lives of DBP were decreased by 53.0%, 37.2% and 20.8% when the refuse moisture increased from 20%, 40% and 60% to 80%, respectively. The pH of refuse was an important factor influencing DBP biodegradation, with the optimal pH being around 7.0. The optimal temperature for DBP degradation in refuse was around 30°C. In addition, the Freundlich model fits the adsorption and desorption isotherm of DBP for refuse with n values that suggest nonlinear adsorption characteristics. The free energy change ΔG value ($-23.5 \text{ kJ mol}^{-1}$) indicates that the adsorption of DBP on refuse was a physical reaction. Desorption hysteresis was observed in the DBP desorption experiments. Overall, the results indicate that DBP may accumulate in refuse, and that its transformation and bio-availability may be limited under landfill conditions.

Key words: adsorption, degradation, dibutyl phthalate, refuse

Received: November, 2013; Revised final: February, 2015; Accepted: February, 2015

1. Introduction

Dibutyl phthalate (DBP) belongs to the family of phthalic acid esters (PAEs), which are widely used as plasticizers (Blount et al., 2000). DBP is suspected to cause cancer and interfere with the reproductive systems and development of humans and animals (Mo et al., 2008; Wu et al., 2011). The United States Environmental Protection Agency, European Union, and China National Environmental Monitoring Center have classified DBP as a top priority pollutant (Lu et al., 2009; Wu et al., 2011). DBP can be released from plastic products and leach into the environment during their use or after disposal (Amir et al., 2005). As a result, DBP has been detected in surface water, sediments, municipal wastewater,

sludge and soil (Cai et al., 2007; Chang et al., 2007; Liu et al., 2010; Wang et al., 2008; Xu et al., 2008).

Biodegradation plays an important role in the decomposition of DBP because of its low rate of hydrolysis and photolysis (Xu et al., 2005); therefore, many research regarding the biodegradation of DBP has been conducted (Chi and Cai, 2012; Wang et al., 2004; Xu et al., 2007; Yuan et al., 2010). In addition, several DBP-degrading bacterial strains have been isolated from different environments, including activated sludge, mangrove sediments and wastewater (Li et al., 2005; Lu et al., 2009; Roslev et al., 2007; Wang et al., 2012; Xu et al., 2005, 2007; Yuan et al., 2010).

Most materials containing DBP are disposed of in landfills with other municipal solid waste

* Author to whom all correspondence should be addressed: e-mail: fangchengr@163.com; Phone: +86-571-85070518; Fax: +86-571-85070518

(MSW); accordingly, these facilities are an important DBP pollution source and a sink in the natural environment. Degradation of DBP in landfills is difficult owing to the complex anaerobic environment. Ejlertsson et al. (2003) and Mersiowsky et al. (2001) confirmed that biodegradation plays an important role in the fate of DBP under landfill conditions. Additionally, Jonsson et al. (2003) investigated the degradation of DBP to monobutyl phthalate and phthalic acid under methanogenic conditions in a landfill. In our previous research, the behavior of DBP in simulated landfill bioreactors was evaluated and its concentration was found to decrease greatly during decomposition of waste in bioreactors, with major loss of DBP from landfills with active methanogenic environments being observed (Fang et al., 2009a, 2009b). Furthermore, some bacterial strains capable of using DBP as their sole source of carbon and energy were isolated from MSW (Fang et al., 2010). However, the mechanism of dynamic degradation of DBP in the refuse has yet to be identified.

It is well known that there are methanogens in refuse when a landfill enters the methanogenic phase; however, these organisms cannot degrade complicated organic materials such as DBP. Nevertheless, previous studies confirmed that the loss of DBP from landfills was much higher in active methanogenic environments than acidic environments (Ejlertsson et al., 2003; Fang et al., 2009b; Jonsson et al., 2003; Mersiowsky et al., 2001). Despite this, no studies have investigated the reason for this phenomenon, and the factors influencing DBP degradation in refuse are still unclear. In addition, adsorption is a fundamental process controlling the transformation and biological activity of hydrophobic organic contaminants in the environment (Chefetz and Xing, 2009; Wen et al., 2007). However, few studies have been conducted to investigate the adsorption behavior of DBP and its effects on DBP transformation and fate in landfills.

This study was conducted to measure the dynamic degradation and adsorption behavior of DBP in methanogenic phase refuse through laboratory microcosm experiments. To accomplish this, the influences of microorganisms, DBP initial concentration, moisture, pH of refuse and temperature on DBP degradation in the refuse were investigated. Moreover, the adsorption characteristics of DBP in methanogenic refuse were analyzed with consideration of the adsorption isotherm and desorption hysteresis. The overall goal of this study

was to further reveal the mechanism of DBP biodegradation in the refuse and provide a basis for accelerated removal of DBP under landfill conditions.

2. Materials and methods

2.1. Chemicals and instruments

HPLC-grade hexane and isopropanol, as well as reagent grade dibutyl phthalate ($\geq 99\%$) and all other reagents were obtained from Tianjin Siyou Co. (Tianjin, China). Purified water from a Milli-Q system was used in all experiments.

The following equipment was used in this study: a liquid chromatograph (Agilent 1100, USA), rotatory evaporator (BUCHI R200), biochemical incubator (LRH-250), oven oscillator (HZ-9211K) and ultrapure water equipment (Millipore Milli-Q, USA), etc.

2.2. Tested refuse

The refuse for the test was collected from a leachate recirculation landfill bioreactor located in our lab on day 120 after the refuse was loaded. The landfill bioreactor was constructed of brick and concrete and had an effective size of 0.55 m \times 0.55 m \times 2.0 m (L \times W \times H). The system was comprised of a methanogenic reactor that received leachate from the landfill. The leachate was subjected to methanogenesis in the methanogenic reactor, after which it was recycled into the landfill. Leachate was continuously circulated between the landfill and the methanogenic reactor for 8 h daily using pumps with adjusted flow rates that varied with leachate volume during waste decomposition.

The recycling ratio of leachate was 100%. To avoid the effects of DBP in the refuse itself, the components of the plastics and rubber were removed from the MSW. The initial physical composition of the refuse (by weight) was as follows: kitchen waste 70.0 \pm 1.2%; paper 11.7 \pm 0.5%; sand and soil 8.1 \pm 0.1%; cellulose textile 1.5 \pm 0.2%; glass 7.3 \pm 0.5%; metal 0.7 \pm 0.1%; and wood 0.7 \pm 0.1%. Analysis of the refuse indicated that the simulated landfill had completed the acidic phase and entered the methanogenic phase, and refuse samples collected on day 120 are defined as samples from the methanogenic phase. The physicochemical and biochemical properties of the refuse are shown in Table 1.

Table 1. Physicochemical and biochemical properties of refuse used in this study

| Diameter (cm) | Moisture (%) | pH | VSS (%) | BDM (%) | CEC (cmol Kg ⁻¹) | Specific surface area (m ² g ⁻¹) | Population of microorganisms | | | Redox enzyme activities | | |
|---------------|-------------------|--------------------|-------------------|-------------------|------------------------------|---|------------------------------|--------------------|--------------------|-------------------------|-------------------|------------------|
| | | | | | | | M1 | M2 | M3 | E1 | E2 | E3 |
| ≤ 2 | 62.3 ± 0.3 | 7.03 ± 0.02 | 14.7 ± 0.3 | 13.4 ± 0.6 | 79.4 ± 1.7 | 4.58 ± 0.78 | 7.59 ± 0.07 | 6.72 ± 0.10 | 5.50 ± 0.09 | 434.5 ± 48.6 | 14.2 ± 1.6 | 4.9 ± 1.2 |

VSS: volatile suspended solids; BDM: biodegradable materials; CEC: cation exchange capacity; M1: bacteria (lg CFU g⁻¹); M2: fungi (lg CFU g⁻¹); M3: actinomycetes (lg CFU g⁻¹); CFU: colony forming units; E1: dehydrogenase (mg TF g⁻¹ dw, 12 h); E2: hydrogen peroxidase (mL KMnO₄ g⁻¹ dw, 1 h); E3: polyphenol oxidase (mg purple gall pigment g⁻¹ dw, 2 h)

2.3. Tested bacterial strain

The bacteria strain *Enterobacter* sp. T5 used in this study was previously isolated from MSW obtained from a simulated landfill bioreactor and found to have the ability to use DBP as its sole source of carbon and energy.

The optimal pH and temperature for its biodegradation activities were 7.0 and 35°C, and the degradation half-life was about 20.9 h when the concentration of DBP was < 1000 mg L⁻¹ in inorganic salt culture (Fang et al., 2010). When the cultures reached the logarithmic growth phase, samples were centrifuged at 150 rpm and 30°C. The bacteria were then washed three times with buffer solution Na₂HPO₄-NaH₂PO₄ (pH 7.0, 0.02 mol L⁻¹), after which a bacterial suspension with a weight ratio of 1g bacteria: 3 g buffer solution was prepared (Fang et al., 2010).

2.4. Effects of microorganisms on DBP degradation in refuse

Three types of refuse were prepared, sterilized refuse (a), unsterilized refuse (b) and inoculated refuse (c). For sample (a), the refuse was intermittently sterilized for 30 minutes at 121°C and 1.1 kg·cm⁻². For sample (c), the refuse was inoculated with 10⁸ CFU g⁻¹ (*Enterobacter* sp. T5). Each refuse sample was prepared in triplicate. DBP was dissolved in acetone and added to the tested refuse samples to give a concentration of 20 µg g⁻¹ (0.05% acetone addition), after which the samples were mixed thoroughly and the acetone was allowed to evaporate. Aliquots of refuse (40 g) were then transferred into serum bottles, tightly sealed and incubated under stationary conditions at 25°C in the dark to avoid photolysation.

To avoid experimental errors caused by non-uniform sampling, all refuse of each sample was withdrawn from the serum bottle on day 0, 1, 3, 7, 14, 21, 28, 35 and 50 and analyzed for residual DBP. Removal of DBP was assessed by measuring disappearance of the parent chemical by HPLC.

2.5. Effects of different concentrations of DBP on its degradation

DBP was added to the tested refuse samples to give concentrations of 5, 10, 20 and 30 µg g⁻¹. Aliquots of refuse were transferred into serum bottles and incubated under stationary conditions at 25°C in the dark. Each refuse sample was prepared in triplicate and sampled for DBP as described in 2.4.

2.6. Effects of refuse moisture on DBP degradation

The refuse was air dried first, after which the moisture contents of the refuse were adjusted to 20%, 40%, 60% and 80% with sterile water. DBP was added to the tested refuse samples to give a

concentration of 20 µg g⁻¹. Aliquots of refuse were transferred into serum bottles and incubated under stationary conditions at 25°C in the dark. Each refuse sample was prepared in triplicate and sampled for DBP as described in 2.4.

2.7. Effects of refuse pH on DBP degradation

DBP was added to the tested refuse samples to give a concentration of 20 µg g⁻¹, after which the pH was adjusted to 5.0, 6.0, 7.0, and 8.0, respectively. Aliquots of refuse were then transferred into serum bottles and incubated under stationary conditions at 25°C in the dark. Each refuse sample was prepared in triplicate and sampled for DBP as described in 2.4.

2.8. Effects of the temperature on DBP degradation

DBP was added to the tested refuse samples to give a concentration of 20 µg g⁻¹, after which aliquots of refuse were transferred into serum bottles and incubated under stationary conditions at 15°C, 25°C, 35°C, 45°C and 55°C in the dark. Each refuse sample was prepared in triplicate and sampled for DBP as described in 2.4.

2.9. Adsorption experiment

Adsorption experiments were performed using the batch equilibrium approach. Briefly, DBP solutions of 40.0–400.0 µg L⁻¹ (150 mL amended with 0.02% sodium azide to inhibit bacterial growth with pH 7.0) and 0.5 g refuse were placed into a series of 250 mL conical flasks. After initial mixing, flasks were shaken at 200 rpm and 25°C for 24 h (based on the results of a preliminary experiment), then centrifuged at 10,000 rpm for 10 min. Once equilibrium had been reached, the supernatant was used for DBP analysis.

The difference in initial DBP and equilibrium concentration in the liquid phase was the adsorption capacity of the refuse. For the desorption experiments, the supernatant from the adsorption experiments was removed and 150 mL of background solution (0.02% sodium azide in sterilized distilled water) was added to the solid phase, after which the samples were shaken for 24 h, at which time the DBP concentrations in the liquor phase were measured. This test was performed in triplicate. In addition, background samples containing refuse and no DBP and controls containing sample but no refuse were run under the same conditions and the results were considered in the final calculations.

2.10. Analytical methods

Extraction of DBP from the refuse and liquid phase and the subsequent HPLC analysis were conducted as described by Fang et al. (2009b), with minor modification. Briefly, the pH value of sample

of refuse or liquid phase was adjusted to 7–8 with 1N NaOH or 1N HCl if necessary, after which the samples were extracted three times with hexane (2:1, v/v). The hexane extracts were then passed through a small glass hopper containing Na₂SO₄ to eliminate contaminating water. Next, the extracts were concentrated to 1.0 mL prior to analysis by HPLC. This procedure was performed in triplicate for each sample. The samples were then injected onto an AE LICHROM column (CN-5 μ m) using a mixture of hexane and isopropanol (99:1, v/v) applied at a flow rate of 1.5 mL min⁻¹ as the mobile phase, and DBP was detected using a UV detector at a wavelength of 272 nm. The recovery rates of DBP from refuse and the liquid phase were 82.5%–99.1% and 84.2–98.7%, respectively. The detection limits were 0.1 μ g g⁻¹ and 0.1 μ g l⁻¹ for DBP in the refuse and liquid phase, respectively.

3. Results and discussion

3.1. Effects of microorganisms on DBP degradation in refuse

Fig. 1 shows the degradation characteristics of DBP in the sterilized, unsterilized and inoculated refuse from the methanogenic phase. The degradation rate of DBP was significantly higher in the unsterilized refuse than the sterilized refuse ($p < 0.05$). The degradation rate of DBP in the refuse from the methanogenic phase increased after addition of the dominant bacterial strain, *Enterobacter* sp. T5. The degradation rate of DBP was significantly higher in the inoculated refuse than the unsterilized refuse ($p < 0.05$). On day 50, the removal rate of DBP was 12.3%, 54.7% and 70.1% in the sterilized, unsterilized and inoculated refuse, respectively. DBP biodegradation in the refuse was fit to the first-order kinetic equation (1), where: C is the DBP concentration; K is the first-order kinetic constant; t is the time; A is the constant.

$$\ln C = -Kt + A \quad (1)$$

The kinetic equations are shown in Table 2. The half-life of DBP in the sterilized refuse was 5.9 times higher than that of unsterilized samples. In addition, the half-life of DBP was decreased by 35.8% when the dominant bacterial strains were added. These findings suggest that the effects of hydrolyzation and other chemical degradation on DBP were much lower than biodegradation, again demonstrating that biodegradation plays an important

role in DBP decomposition in landfill refuse (Ejlertsson et al., 2003; Mersiowsky et al., 2001). The residual DBP in the refuse was determined based on the metabolic activities of the microbes in the refuse. In previous studies, more loss of DBP from a landfill was observed in active methanogenic environments than in acidic environments (Ejlertsson et al., 2003; Fang et al., 2009b; Jonsson et al., 2003; Mersiowsky et al., 2001), indicating that a methanogenic environment is beneficial to the growth of DBP dominant bacteria.

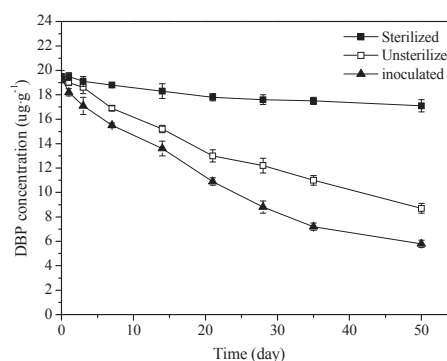


Fig. 1. Effects of microorganisms on degradation of DBP in refuse

3.2. Effects of concentrations of DBP, moisture, pH of refuse and temperature

Variations in the concentration of DBP in the refuse with different initial concentrations, moistures, pH and temperatures are shown in Fig. 2. Plots of the decline of DBP in the refuse all followed the first-order kinetic model (Table 3). The removal rate of DBP was 58.0%, 57.9%, 54.7% and 55.8% in the refuse when the DBP initial concentrations were 5, 10, 20 and 30 μ g g⁻¹, respectively. In addition, the half-life periods of DBP in the refuse did not differ significantly among groups, with values of 42.3 d, 42.5 d, 43.3 d and 44.1 d being observed, respectively. The acute toxicity of DBP was not serious (Piersma et al., 2000), and the DBP concentration was relatively low; therefore, the inhibitory effects of DBP on microorganisms in the refuse were weak. Overall, these findings clearly demonstrate that different concentrations of DBP had no effects on its degradation ($p < 0.05$).

The removal rate of DBP was influenced by the refuse moisture. The removal rate of DBP was highest in refuse with 80% moisture, while it was lowest in refuse with 20% moisture (Fig. 2b).

Table 2. Degradation kinetic parameters of DBP in sterilized, unsterilized and inoculated refuse

| Refuse | Kinetic equations | K (d ⁻¹) | R^2 | $t_{1/2}$ (d) |
|--------------|---------------------------|------------------------|--------|---------------|
| Sterilized | $\ln C = -0.0027t + 2.96$ | 0.0027a* | 0.9218 | 256.7 |
| Unsterilized | $\ln C = -0.0160t + 2.95$ | 0.0160b | 0.9946 | 43.3 |
| Inoculated | $\ln C = -0.0249t + 2.92$ | 0.0249c | 0.9878 | 27.8 |

*Parameters followed by different letters (a, b, c) in the same column differ significantly at $p < 0.05$.

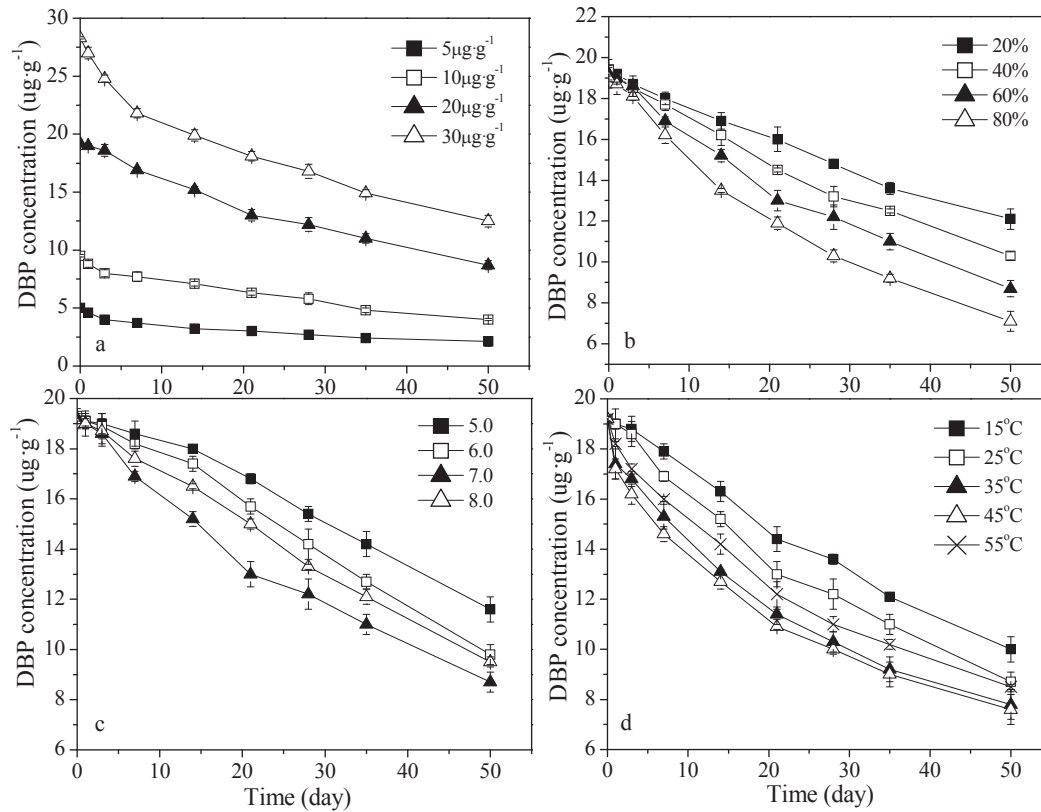


Fig. 2. Effects of DBP concentration, moisture, pH and temperature on degradation of DBP in refuse (a) DBP concentration; (b) Moisture; (c) pH; (d) Temperature

Table 3. Degradation kinetic parameters of DBP in refuse at different DBP concentrations, moistures, pH and temperatures

| DBP concentration ($\mu\text{g/g}$) | Kinetic equations | K (d^{-1}) | R^2 | $t_{1/2}$ (d) |
|---------------------------------------|---------------------------|------------------|--------|---------------|
| 5 | $\ln C = -0.0164t + 1.48$ | 0.0164a | 0.9372 | 42.3 |
| 10 | $\ln C = -0.0163t + 2.18$ | 0.0163a | 0.9820 | 42.5 |
| 20 | $\ln C = -0.0160t + 2.95$ | 0.0160a | 0.9946 | 43.3 |
| 30 | $\ln C = -0.0157t + 3.26$ | 0.0157a | 0.9666 | 44.1 |
| Refuse moisture (%) | Kinetic equations | K (d^{-1}) | R^2 | $t_{1/2}$ (d) |
| 20 | $\ln C = -0.0095t + 2.96$ | 0.0095a | 0.9974 | 73.0 |
| 40 | $\ln C = -0.0127t + 2.96$ | 0.0127b | 0.9971 | 54.6 |
| 60 | $\ln C = -0.0160t + 2.95$ | 0.0160c | 0.9946 | 43.3 |
| 80 | $\ln C = -0.0202t + 2.93$ | 0.0202d | 0.9931 | 34.3 |
| Refuse pH | Kinetic equations | K (d^{-1}) | R^2 | $t_{1/2}$ (d) |
| 5.0 | $\ln C = -0.0098t + 2.99$ | 0.0098a | 0.9666 | 70.7 |
| 6.0 | $\ln C = -0.0132t + 2.99$ | 0.0132b | 0.9776 | 52.5 |
| 7.0 | $\ln C = -0.0160t + 2.95$ | 0.0160c | 0.9946 | 43.3 |
| 8.0 | $\ln C = -0.0138t + 2.97$ | 0.0138b | 0.9931 | 50.2 |
| Temperature ($^{\circ}\text{C}$) | Kinetic equations | K (d^{-1}) | R^2 | $t_{1/2}$ (d) |
| 15 | $\ln C = -0.0133t + 2.96$ | 0.0133a | 0.9971 | 52.1 |
| 25 | $\ln C = -0.0160t + 2.95$ | 0.0160b | 0.9946 | 43.3 |
| 35 | $\ln C = -0.0178t + 2.87$ | 0.0178c | 0.9724 | 38.9 |
| 45 | $\ln C = -0.0179t + 2.84$ | 0.0179c | 0.9610 | 38.7 |
| 55 | $\ln C = -0.0163t + 2.90$ | 0.0163b | 0.9812 | 42.5 |

*Parameters followed by different letters (a, b, c, d) in the same condition differ significantly at $p < 0.05$

The half-lives of DBP were decreased by 53.0%, 37.2% and 20.8% when the refuse moisture increased from 20%, 40% and 60% to 80%, respectively. These results indicate that appropriate refuse moisture was beneficial to the growth and reproduction of microorganisms. In addition, moisture can change the porosity, oxidation-reduction potential of refuse and adsorption effect between the DBP and the refuse (Ingerslev et al.,

2001), which will ultimately influence DBP degradation.

Leachate recirculation landfill bioreactors are superior to conventional landfills and provide an advantage for the transformation of organic materials (Calli et al., 2006; He et al., 2007) owing to their effects on microbial populations, as well as the increased refuse moisture in response to circulation of the leachate.

The removal rate of DBP was 39.6%, 49.2%, 54.7% and 50.1% when the refuse pH was 5.0, 6.0, 7.0 and 8.0, respectively. The shortest degradation half-life of DBP was achieved (43.3d) at pH 7.0 (Table 3). The removal rate of DBP decreased significantly when the pH was <7.0 ($p < 0.05$). Specifically, the half-life of DBP was increased by 63.3% when the refuse pH decreased from 7.0 to 5.0. This may have been because of the low pH of refuse, which influenced bacterial growth (Fan et al., 2004; Fang et al., 2010). Therefore, the pH of refuse may be an important factor influencing DBP biodegradation. Within the specific limits of the present study, a neutral pH was beneficial for DBP degradation, confirming that the loss of DBP from the landfill would be much higher in an active methanogenic environment than an acidic environment (Ejlertsson et al., 2003; Fang et al., 2009b; Jonsson et al., 2003; Mersiowsky et al., 2001).

The degradation rate constants for DBP loss from the refuse at 15°C, 25°C and 35°C were 0.0133, 0.0160 and 0.0178 d^{-1} , respectively. Accordingly, the half-lives of DBP were 52.1 d, 43.3 d and 38.9 d, respectively (Table 3). Although there was no significant difference in the degradation rates of DBP when the temperature increased from 35°C to 45°C ($p < 0.05$), the rate decreased significantly when the temperature increased to 55°C ($p < 0.05$). The removal rate of DBP was 59.4%, 60.4% and 55.7% in refuse at 35°C, 45°C and 55°C, respectively. Temperatures between 25°C and 35°C are most suitable for microbial growth (Kurola et al., 2007), and the degradation rate of DBP increased obviously when the temperature increased from 15°C to 35°C ($p < 0.05$). Overall, these findings suggested that the optimal temperature for DBP degradation in refuse was around 30°C considering degradation and the energy cost.

3.3. Adsorption behavior of DBP by refuse

DBP is a hydrophobic organic compound with an octanol-water partition coefficient $\lg K_{ow}$ of 4.45 (Cui et al., 2010). Many studies have shown that nonlinear adsorption exists in hydrophobic organic matter (Liu et al., 2011; Pan et al., 2006; Xing and Pingnatello, 1997); therefore, the Freundlich model was used to describe quantitative DBP adsorption and desorption in refuse according to Eq. (2), where: Q_e is the equilibrium adsorption capacity of DBP on refuse ($\mu\text{g kg}^{-1}$); c_e is the equilibrium concentration of DBP in the liquid phase ($\mu\text{g L}^{-1}$); K_f is the Freundlich adsorption coefficient ($[\mu\text{g kg}^{-1}]/[\mu\text{g L}^{-1}]^n$) in the desorption formula, instead of $K_{f,des}$; n is the nonlinear exponent, expressed as n_{ads} and n_{des} in the adsorption and desorption models, respectively.

$$Q_e = K_f c_e^n \quad (2)$$

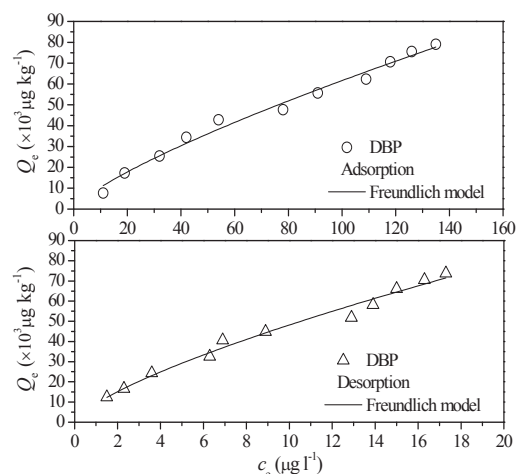


Fig. 3. Results of Freundlich model fits to adsorption and desorption isotherms of DBP on refuse

Table 4. Parameters of Freundlich model of adsorption, free energy change, and desorption isotherms of DBP

| Adsorption | r^2 | n_{ads} | K_f | |
|--------------------|--------------------|--------------------|-------------------------|-------|
| | 0.9861 | 0.772 | 1.76×10^3 | |
| Free energy change | K_f | K_{oc} | ΔG | |
| | 1.76×10^3 | 1.31×10^4 | -23.5 (kJ mol $^{-1}$) | |
| Desorption | r^2 | n_{des} | $K_{f,des}$ | H^* |
| | 0.9811 | 0.720 | 9.17×10^3 | 0.933 |

*H: hysteresis exponent

As shown in Fig. 3, the Freundlich model fits the adsorption isotherm of DBP on refuse. The fitting parameters of the Freundlich model to the adsorption isotherm of DBP are listed in Table 4. The n_{ads} of DBP adsorption on refuse in the Freundlich model was significantly less than 1, indicating that the adsorption isotherm of DBP has nonlinear characteristics. As refuse contains different organic components with various structures and properties and the adsorption point of organics is not uniform, several mechanisms may exist during adsorption. The nonlinear characteristic adsorption isotherm of DBP was attributed to the organic matter heterogeneity, which has been confirmed as the most important factor in nonlinear adsorption (Jiang et al., 2012).

The maximum removal efficiency of DBP by refuse was a little lower than that reported in most previous studies (Table 5). This difference may have occurred due to differences in the adsorbent type and condition of the experimental operation in each study.

To investigate the adsorption mechanism of DBP by the refuse, the free energy change ΔG for adsorption was calculated using Eqs. (3-4) (Ozgul, 2015):

$$\Delta G = -RT \ln K_{oc} \quad (3)$$

$$K_{oc} = K_f / f_{oc} \times 100 \quad (4)$$

Table 5. Comparison of adsorption behavior of DBP in literature

| Constituents | | | | | | | | References |
|-----------------|--------------------------|-------------------------------|-------------|-----------------------|---------------|--------------|----------------------------|------------------------|
| Wastewater type | Adsorbent (dosage) | Initial DBP concentration | Reaction pH | Operating temperature | Sample volume | Contact time | Maximum removal efficiency | |
| Seawater | Montmorillonite (687 mg) | 3930 $\mu\text{g L}^{-1}$ | 8.1 | 30°C | 10 mL | 12 h | 11% | Sullivan et al. (1982) |
| Seawater | Sediment (0.05 g) | 3~12 mg L^{-1} | 7.5 | 25°C | 100 mL | 4 h | 71% | Xu et al. (2008) |
| Purified water | Sediment (1.0 g) | 150~500 mg L^{-1} | 7.0 | 30°C | 20 mL | 24 h | 98% | Guo et al. (2009) |
| Purified water | Soil (2 g) | 400~6000 $\mu\text{g L}^{-1}$ | 7.0 | 20°C | 50 mL | 10 h | 77% | Li et al. (2006) |
| Purified water | Refuse (0.5 g) | 40~400 $\mu\text{g L}^{-1}$ | 7.0 | 25°C | 150 mL | 24 h | 66% | This study |

where: T is the solution temperature (K); R is the gas constant ($8.314 \times 10^{-3} \text{ kJ mol}^{-1} \text{ K}^{-1}$); K_{oc} is the carbon normalized partition coefficient; K_f is the Freundlich adsorption coefficient ($[\mu\text{g kg}^{-1}]/[\mu\text{g L}^{-1}]^n$); f_{oc} is the organic carbon fraction of the refuse (%).

As shown in Table 4, the negative value of ΔG indicates that the adsorption of DBP on refuse is spontaneous. In addition, the ΔG value was less than 40 kJ mol^{-1} , indicating that the adsorption of DBP on refuse was a physical reaction (McCall et al., 1980).

3.4. Desorption hysteresis

The adsorption of organic matter often exhibits hysteresis because of its irreversible adsorption on the adsorbent. Several indicators are used for the characterization of adsorption hysteresis (Jiang et al., 2012). The hysteresis exponent (H), which was used in this study, was determined using Eq. (5), where: n_{ads} and n_{des} are the fitting parameters of the Freundlich model for the adsorption and desorption isotherms, respectively.

$$H = n_{des} / n_{ads} \quad (5)$$

The fitting parameters of the Freundlich model to the desorption isotherm of DBP and the hysteresis exponent are listed in Table 4. The Freundlich model can be used to fit the desorption isotherm of DBP on refuse. The $K_{f,des}$ value of DBP from the desorption isotherm was higher than the K_f from the adsorption isotherm, while the nonlinear exponent n_{des} from the desorption process was lower than the n_{ads} from the adsorption process. The hysteresis exponent H of DBP was less than 1, indicating that desorption hysteresis exists in the desorption process.

The desorption hysteresis of the DBP may be attributed to the properties of the refuse. Organic matter content, specific surface area, adsorption points for DBP and bonding strength are key factors contributing to desorption hysteresis in refuse. Pore deformation is also believed to contribute to irreversible desorption (Li et al., 2013). In the desorption process, pore deformation of the refuse

formed part of a confined space to fix DBP into deeper pores. This irreversible process prevents the adsorbate from being desorbed completely, causing desorption hysteresis. As a result, large amounts of DBP can be adsorbed for long periods of time by the refuse because of the desorption hysteresis. Therefore, the transformation and bio-availability of this hydrophobic organic compound may be limited in landfill conditions, resulting in accumulation of DBP.

4. Conclusions

Biodegradation plays an important role in DBP decomposition in refuse. The removal of DBP was greatly enhanced in response to the addition of bacterial strains; however, its degradation did not appear to be influenced by its initial concentrations. The half-lives of DBP decreased when the refuse moisture increased.

The optimal pH and temperature for DBP degradation in the refuse were 7.0 and 30°C. The Freundlich model fits the adsorption and desorption isotherm of DBP, and desorption hysteresis occurred in the DBP desorption experiments. Taken together, the results of this study indicate that DBP may be a potential environmental risk in landfills.

Acknowledgements

This work was financially supported by the National Natural Science Foundation of China (51108419), the Zhejiang Province Natural Science Foundation of China (Y5090073).

References

- Amir S., Hafidi M., Merlina G., Hamdi H., Jouraiphy A., Gharous M., (2005), Fate of phthalic acid esters during composting of both lagooning and activated sludges, *Process Biochemistry*, **40**, 2183-2190.
- Blount B.C., Milgram K.E., Silva M.J., (2000), Quantitative detection of eight phthalate metabolites in human urine using HPLC-APCI-MS, *Analytical Chemistry*, **72**, 4127-4134.
- Cai Q.Y., Mo C.H., Wu Q.T., Zeng Q.Y., Katsoyiannis A., (2007), Occurrence of organic contaminants in sewage

- sludges from eleven wastewater treatment plants, China, *Chemosphere*, **68**, 1751-1762.
- Calli B., Mertoglu B., Roest K., Inanc B., (2006), Comparison of long term performances and final microbial compositions of anaerobic reactors treating landfill leachate, *Bioresource Technology*, **97**, 641-647.
- Chang B.V., Wang T.H., Yuan S.Y., (2007), Biodegradation of four phthalate esters in sludge, *Chemosphere*, **69**, 1116-1123.
- Chefetz B., Xing B.S., (2009), Relative role of aliphatic and aromatic moieties as sorption domains for organic compounds: A review, *Environmental Science & Technology*, **43**, 1680-1688.
- Chi J., Cai X.D., (2012), Effects of nitrogen on the removal of dibutyl phthalate from surface water in the presence of *Potamogeton crispus* L., *Ecological Engineering*, **41**, 70-73.
- Cui X.H., Li B.H., Chen H.H., Wan P.Q., (2010), A review of phthalic acid esters contamination and sorption in soil and sediment, China (in Chinese), *Ecology and Environmental Sciences*, **19**, 472-479.
- Ejlertsson J., Karlsson A., Lagerkvist A., Hjertberg T., Svensson B.H., (2003), Effects of co-disposal of wastes containing organic pollutants with municipal solid waste - a landfill simulation reactor study, *Advances in Environmental Research*, **7**, 949-960.
- Fang C.R., Long Y.Y., Shen D.S., (2009a), Comparison on the removal of phthalic acid diesters in a bioreactor landfill and a conventional landfill, *Bioresource Technology*, **100**, 5664-5670.
- Fang C.R., Long Y.Y., Wang W., Feng H.J., Shen D.S., (2009b), Behavior of dibutyl phthalate in a simulated landfill bioreactor, *Journal of Hazardous Materials*, **167**, 186-192.
- Fang C.R., Yao J., Zhen Y.G., Jiang C.J., Hu L.F., Wu Y.Y., Shen D.S., (2010), Dibutyl phthalate degradation by *Enterobacter* sp. T5 isolated from municipal solid waste in landfill bioreactor, *International Biodeterioration & Biodegradation*, **63**, 732-738.
- Fan Y., Wang Y., Qian P.Y., Gu J.D., (2004), Optimization of phthalic acid batch biodegradation and the use of modified Richards model for modeling degradation, *International Biodeterioration and Biodegradation*, **53**, 57-63.
- Guo H., Zhou M., Tong D., Chen H., (2009), Adsorption of phthalate esters on sediments of Yellow River (in Chinese), *Environmental Science & Technology*, **32**, 6-9.
- He R., Liu X.W., Zhang Z.J., Shen D.S., (2007), Characteristics of the bioreactor landfill system using an anaerobic-aerobic process for nitrogen removal, *Bioresource Technology*, **98**, 2526-2532.
- Ingerslev F., Torang L., Loke M.L., (2001), Primary biodegradation of veterinary antibiotics in aerobic and anaerobic surface water simulation systems, *Chemosphere*, **44**, 865-872.
- Jiang L., Wang J.H., Li J.Z., Xin J., Li M., Liu X., (2012), Sorption and desorption of 17 α -ethinyl estradiol and 4-n-nonylphenol in soil (in Chinese), *Environmental Science*, **33**, 3885-3892.
- Jonsson S., Ejlertsson J., Ledin A., Mersowsky I., Svensson B.H., (2003), Mono- and diesters from o-phthalic acid in leachates from different European landfills, *Water Research*, **37**, 609-617.
- Kurola J., Salkinoja-Salonen M., (2007), Potential for biodegradation of anthropogenic organic compounds at low temperature in boreal soils, *Soil Biology and Biochemistry*, **39**, 1206-1212.
- Li J., Shu W.Q., Chen J.A., Qiu Z.Q., (2005), Studies on isolation, identification and degradation characteristics of DBP-degradation strain CQ0302 (in Chinese), *China Environmental Science*, **25**, 47-51.
- Li J.Z., Fu J., Xiang X., Wu M.M., Liu X., (2013), Kinetics, equilibrium, and mechanisms of sorption and desorption of 17 α -ethinyl estradiol in two natural soils and their organic fractions, *Science of the Total Environment*, **452-453**, 404-410.
- Li L., Liu Z., Sun J., (2006), Adsorption of phthalic esters by loam clay (in Chinese), *Journal of South-Central University for Nationalities*, **25**, 15-17.
- Liu H., Liang H.C., Liang Y., Zhang D., Wang C., Cai H.S., Shvartsev S.L., (2010), Distribution of phthalate esters in alluvial sediment: a case study at Jiang Han Plain, Central China, *Chemosphere*, **78**, 382-388.
- Liu W.X., Ling X., Chen J.L., Li W.B., Dou H., Tao S., (2011), Sorption behaviors of BDE-28 on natural soils, (in Chinese), *Environmental Science*, **32**, 749-757.
- Li L., Liu Z., Sun J., (2006), Adsorption of phthalic esters by loam clay, (in Chinese), *Journal of South-Central University for Nationalities*, **25**, 15-17.
- Lu Y., Tang F., Wang Y., Zhao J.H., Zeng X., Luo Q.F., Wang L., (2009), Biodegradation of dimethyl phthalate, diethyl phthalate and di-n-butyl phthalate by *Rhodococcus* sp. L4 isolated from activated sludge, *Journal of Hazardous Materials*, **168**, 938-943.
- McCall P.J., (1980), *Test protocol for environmental fate and movement of toxicants*, Proceedings of AOAC, Washington D.C., Association of Official Analytical Chemists, 89-109.
- Mersowsky I., Weller M., Ejlertsson J., (2001), Fate of plasticized PVC products under landfill conditions: A laboratory-scale landfill simulation reactor study, *Water Research*, **35**, 3063-3070.
- Mo C.H., Cai Q.Y., Li Y.H., Zeng Q.Y., (2008), Occurrence of priority organic pollutants in the fertilizers, China, *Journal of Hazardous Materials*, **152**, 1208-1213.
- Ozgul G., (2015), Adsorption properties of activated carbon from wild plant prepared by chemical activation, *Environmental Engineering and Management Journal*, **14**, 129-137.
- Pan B., Xing B., Liu W., (2006), Two-compartment sorption of phenanthrene on eight soils with various organic carbon contents, *Journal of Environmental Science and Health, Part B*, **41**, 1333-1347.
- Piersma A.H., Verhoefa A., Biesebeeka J., Pietersa M.N., Sloba W., (2000), Developmental toxicity of butyl benzyl phthalate in the rat using a multiple dose study design, *Reproductive Toxicology*, **14**, 417-425.
- Roslev P., Vorkamp K., Aarup J., Frederiksen K., Nielsen P., (2007), Degradation of phthalate esters in an activated sludge wastewater treatment plant, *Water Research*, **41**, 969-976.
- Sullivan F.K., Atlas E.L., Glam C.S., (1982), Adsorption of phthalic acid esters from seawater, *Environmental Science & Technology*, **16**, 428-432.
- Wang F., Xia X.H., Sha Y.J., (2008), Distribution of phthalic acid esters in Wuhan section of the Yangtze River, China, *Journal of Hazardous Materials*, **154**, 317-324.
- Wang J.L., Zhao X., Wu W.Z., (2004), Biodegradation of phthalic acid esters (PAEs) in soil bioaugmented with acclimated activated sludge, *Process Biochemistry*, **39**, 1837-1841.

- Wang Y.Y., Miao B., Hou D.M., Wu X.L., Peng B., (2012), Biodegradation of di-n-butyl phthalate and expression of the 3,4-phthalate dioxygenase gene in *Arthrobacter* sp. ZH2 strain, *Process Biochemistry*, **47**, 936-940.
- Wen B., Zhang J.J., Zhang S.Z., (2007), Phenanthrene sorption to soil humic acid and different humin fraction, *Environmental Science & Technology*, **41**, 3165-3171.
- Wu X.L., Wang Y.Y., Liang R.X., Dai Q.Y., Jin D.C., Chao W.L., (2011), Biodegradation of an endocrine-disrupting chemical di-n-butyl phthalate by newly isolated *Agrobacterium* sp. and the biochemical pathway, *Process Biochemistry*, **46**, 1090-1094.
- Xing B.S., Pingnatello J.J., (1997), Dual-mode sorption of low-polarity compounds in glassy poly (vinyl chloride) and soil organic matter, *Environmental Science & Technology*, **31**, 792-799.
- Xu G., Li F.H., Wang Q.H., (2008), Occurrence and degradation characteristics of dibutyl phthalate (DBP) and di-(2-ethylhexyl) phthalate (DEHP) in typical agricultural soils of China, *Science of Total Environment*, **393**, 333-340.
- Xu X.R., Li H.B., Gu J.D., (2005), Biodegradation of an endocrine-disrupting chemical di-n-butyl phthalate ester by *Pseudomonas fluorescens* B-1, *International Biodeterioration and Biodegradation*, **55**, 9-15.
- Xu X.R., Li H.B., Gu J.D., Li X.Y., (2007), Degradation of n-butyl benzyl phthalate by a pure bacterial culture from mangrove sediment, *Journal of Hazardous Materials*, **140**, 194-199.
- Xu X.R., Li X.Y., (2008), Adsorption behaviour of dibutyl phthalate on marine sediments, *Marine Pollution Bulletin*, **57**, 403-408.
- Yuan S., Huang I., Chang B., (2010), Biodegradation of dibutyl phthalate and di-(2-ethylhexyl) phthalate and microbial community changes in mangrove sediment, *Journal of Hazardous Materials*, **184**, 826-831.



INSTRUCTIONS FOR AUTHORS

1. Introduction

Environmental Engineering and Management Journal (EEMJ) is an international medium for publication of Original Papers, Reviews, Case Studies, Book Reviews on the fundamentals, applications in environmental engineering and technologies, applied environmental sciences, environmental health, management, sustainable development, education for sustainability. Advertising is also accepted with contractual payment forms.

Submission of a manuscript implies that the work described has not been published before (except in the form of an abstract or as part of a published lecture, or thesis); that it is not under consideration for publication elsewhere; that its publication has been approved by all coauthors, if any, as well.

Papers, books for review, offers to review, suggestions and commercials (advertising) should be submitted to the *Editor-in-Chief*. All papers will be published in English. Non-English speaking authors should seek the advice of a professional language expert or an English speaker to help translate the paper.

2. Legal requirements

The author(s) guarantee(s) that the manuscript is/will not be published elsewhere in any language without the consent of the copyright holders, that the rights of third parties will not be violated, and that the publisher will not be held legally responsible should there be any claims for compensation. Authors wishing to include figures or text passages that have already been published elsewhere are required to obtain permission from the copyright holder(s) and to include evidence that such permission has been granted when submitting their papers. Any material received without such evidence will be assumed to originate from the authors. The author(s) are encouraged to transfer the copyright of the article to the publisher upon acceptance of an article by the journal, using the Authors' Warranty and Assignment of Copyright agreement. This transfer enables the Editor to protect the copyrighted material for the authors, but does not relinquish the author's proprietary rights. The publication of an article is conditioned by the signature of the author to whom correspondence should be addressed on this Authors'

Warranty and Assignment of Copyright that is provided by the Editor.

Ethics in Publishing

For information on ethics in publishing for journal publication see
<http://omicron.ch.tuiasi.ro/EEMJ/plagiarism.htm>

Conflict of interest

All authors are requested to disclose any actual or potential conflict of interest such as any financial, personal or other relationships with other people or organizations concerning the submitted work that could inappropriately influence, or be perceived to influence, their work.

3. Editorial procedure

For original papers, an upper limit of 7000 words is recommended (including Abstract, Keywords, References, Figures and Tables), processed with MS editing facilities.

For review papers (critical evaluation of existing data, defined topics or emerging fields of investigation, critical issues of public concern), an upper limit of 15000 words is recommended (including Abstract, Keywords, References, Figures and Tables).

Manuscripts should be written in English (American or British usage is accepted, but not a mixture of these) and submitted **electronically**, in .doc format (please do not use .docx) to the *Editor-in-Chief*, at **one (and only one)** of the following e-mail addresses: **eemjournal at yahoo dot com; eem_journal at yahoo dot com; eemjeditor at yahoo dot com; eemj_editor at yahoo dot com; eemjournal at gmail dot com; eemjeditor at gmail dot com; eemjoffice at gmail dot com.**

Please be sure to include your full affiliation and e-mail address (see Sample manuscript).

When submitting the manuscript, it is mandatory to include a cover letter to the editor. The cover letter must state:

- that all authors mutually agree that the manuscript can be submitted to EEMJ;
- that the manuscript contains the original work of the authors;

- the novelty in results/findings, or significance of results;
- that the manuscript has not already been published, or is not under consideration for publication elsewhere.

Manuscripts are evaluated first in the Editorial Office (as a preliminary condition for acceptance) in terms of meeting the requirements of the journal, including attempts of plagiarism. The authors are responsible for the accuracy of the whole paper and references. Authors will be notified about the registration of their contribution. Only those contributions, which conform to the following instructions, can be considered for the peer-review process. Otherwise, the manuscripts are returned to the authors, with observations, comments and annotations.

The peer review process is decisive for paper acceptance. It could be done in several stages, depending on the revision quality of the manuscript in accordance with the requirements of paper evaluators. Please do not transmit electronic data or requirements to the publisher until your manuscript has been reviewed and accepted for publication. Please follow the instructions below.

A minimum of four suitable *potential reviewers* should be provided by the authors. Please provide their name, email addresses, and institutional affiliation. When compiling this list of potential reviewers please consider the following important criteria: they must be knowledgeable about the manuscript subject area of the manuscript; they must not be from the authors' own institution or country; they should not have recent (less than five years) joint publications with any of the authors. However, the final choice of reviewers is at the editors' discretion.

4. Manuscript preparation

General:

Authors must follow the Instructions for authors strictly, failing which the manuscripts would be rejected without review. Editors reserve the right to adjust the formatting style to conform to the standards of the journal.

Manuscripts should be concise, in 1.5 line spacing, and should have 2 cm all over margins. The font should be Times New Roman of size 12 points. The numbering of chapters should be in decimal form. Ensure that each new paragraph is clearly indicated, using TAB at 1.25 pts.

The text layout should be in single-column format.

Keep the layout of the text as simple as possible. Most formatting codes will be removed and replaced on processing the manuscript. However, do use bold face, italics, subscripts, superscripts etc. Add line numbering and page numbers. To avoid unnecessary errors it is strongly advised to use the 'spell-check' and 'grammar-check' functions of your word processor.

Title page will contain:

- A concise and informative title (Times New Roman bold, all caps of size 14 points); the maximum length

of the title should be maximum 100 letters and spaces; The full name(s) of the author(s) (first name, then last name, with Times New Roman bold 12 points) should be written below the title. The affiliation(s) and complete postal address(es) of the author(s) will be provided immediately after the full name of the authors and will be written with Times New Roman 12 points. When the paper has more than one author, their name will be followed by a mark (Arabic numeral) as superscript; for the corresponding author, an asterisk will be added using *Word Insert Reference Footnote Symbol* sequence. Also, the full and e-mail addresses, telephone and fax numbers of the corresponding author will be provided in the footer of the first page, as: Author to whom all correspondence should be addressed: email....., Phone....., Fax.....

- **Abstract:** each paper must be preceded by an abstract presenting the most important results and conclusions in no more than 250 words. Do not include citations in the Abstract.
- **Keywords:** three to five keywords should be supplied after the Abstract for indexing purposes, separated by comma, **ordered alphabetically**, using American spelling and avoiding general and plural terms and multiple concepts (avoid, for example, "and", "of"). Be sparing with abbreviations: only abbreviations firmly established in the field may be eligible.
- The text of the paper should be divided into **Introduction, Materials and methods (or Experimental), Results and discussion, Conclusions, References** (for papers dealing with environmental management, policy, education etc., the Experimental part can be replaced by case-studies presentation).

1. Introduction

State the objectives of the work and provide an adequate background, avoiding a detailed literature survey or a summary of the results.

2. Material and methods (or 2. Experimental)

Provide sufficient detail to allow the work to be reproduced. Methods already published should be indicated by a reference: only relevant modifications should be described.

3. Results and discussion

Results should be clear and concise. Discussion should explore the significance of the results of the work, not repeat them. Avoid extensive citations and discussion of published literature.

4. Conclusions

The main conclusions drawn from results should be presented in a short Conclusions section. Do not include citations in this section.

Formulae, symbols and abbreviations:

Formulae will be typeset in Italics (preferable with the Equation Editor of Microsoft Office 2003) and should be written or marked as such in the manuscript, unless they require a different styling. The formulae should be numbered on the right side, between brackets:

$$a^3 = 3M / 4N \quad (1)$$

Always refer in the text to Equations as (Eq. 1), Eqs. (1-4) etc.

The more complex Chemical Formulae should be presented as Figures.

Abbreviations should be defined when first mentioned in the abstract and again in the main body of the text and used consistently thereafter.

SI units must be used throughout.

Footnotes should be avoided.

References:

The list of References should only include works that are cited in the text and that have been published. References should be cited in the text in brackets (**Harvard style**) as in the following examples:

(Chisti, 1989), (Gavrilescu and Roman, 1996), (Moo-Young et al., 1999).

References should be alphabetically listed at the end of paper, with complete details, as follows:

Books: Names and initials of authors, year (between brackets), chapter title, title of the book (italic), editors, edition, volume number, publisher, place, page number:

Mauch K., Vaseghi S., Reuss M., (2000), *Quantitative Analysis of Metabolic and Signaling Pathways in Saccharomyces cerevisiae*, In: *Bioreaction Engineering*, Schügerl K., Bellgardt K.H. (Eds.), Springer, Berlin Heidelberg New York, 435-477.

Faber K., (2000), *Biotransformations in Organic Chemistry – A Textbook*, vol. VIII, 4th Edition, Springer, Berlin-Heidelberg-New York.

Handbook, (1951), *Handbook of Chemical Engineer*, vol. II, (in Romanian), Technical Press, Bucharest, Romania.

Symposia volumes: Names and initials of authors, year (between brackets), paper title, symposium name, volume number, place, date, page numbers:

Clark T.A., Steward D., (1991), *Wood and Environment*, Proc. 6th Int. Symp. on Wood and Pulping Chemistry, Melbourne, vol. 1, 493-498.

Journal papers: Names and initials of authors, year (between brackets), full title of the paper, full name of the journal (italic), volume number (bold), first and last page numbers:

Tanabe S., Iwata H., Tatsukawa R., (1994), Global contamination by persistent organochlorines and their ecotoxicological impact on marine mammals, *Science of the Total Environment*, **154**, 163-177.

Patents: Names and initials of authors, year (between brackets), patent title, country, patent number (italic):

Grant P., (1989), *Device for Elementary Analyses*. USA Patent, No. 123456.

Dissertations: Names and initials of authors, year (between brackets), title, specification (PhD Thesis, MSc Thesis), institution, place:

Aelenei N., (1982), *Thermodynamic study of polymer solutions*, PhD Thesis, Institute of Macromolecular Chemistry Petru Poni, Iasi, Romania.

Star K., (2008), *Environmental risk assessment generated by natural hazards*, MSc Thesis, Institute of Hazard Research, Town, Country.

Legal regulations and laws, organizations:

Abbreviated name, year (between brackets), full name of the referred text, document type, author, URL address:

ESC, (2007), Improving access to modern energy services for all fundamental challenge, Economic and Social Council, ENV/DEV/927, On line at: <http://www.un.org/News/Press/docs/2007/envdev927.doc.htm>.

EPA, (2007), Biomass Conversion: Emerging Technologies, Feedstocks, and Products, Sustainability Program, Office of Research and Development, EPA/600/R-07/144, U.S. Environmental Protection Agency, Washington, D.C., On line at: <http://www.epa.gov/Sustainability/pdfs/Biomass%20Conversion.pdf>.

EC Directive, (2000), Directive 2000/76/EC of the European Parliament and of the Council of 4 December 2000, on the incineration of waste, Annex V, *Official Journal of the European Communities*, L 332/91, 28.12.2000, Brussels.

GD, (2004), Governmental Decision No. 1076/2004 surnamed SEA Governmental Decision, regarding the procedure for strategic environmental impact assessment for plans or programs, *Romanian Official Monitor*, Part I, No. 707 from 5th of August, 2004.

Web references

The full URL should be given in text as a citation, if no other data are known. If the authors, year, title of the documents are known and the reference is taken from a website, the URL address has to be mentioned after these data:

Burja C., Burja V., (2008), Adapting the Romanian rural economy to the European agricultural policy from the perspective of sustainable development, MPRA, Munich Personal RePEc Archive, On line at: http://mpra.ub.uni-muenchen.de/7989/1/MPRA_paper_7989.pdf

Web references must not be listed separately, after the reference list.

All references must be provided in English with a specification of original language in round brackets.

Citation in text

Please ensure that every reference cited in the text is also present in the reference list (and vice versa). Do not cite references in the abstract and conclusions.

Unpublished results, personal communications as well as URL addresses are not recommended in the references list.

Citation of a reference as "in press" implies that the item has been accepted for publication.

Papers which have been accepted for publication should be included in the list of references with the name of the journal and the specification "in press".

References style

Text: All citations in the text may be made directly (or parenthetically) and should refer to:

- *single author:* the author's name (without initials, unless there is ambiguity) and the year of publication: "as previously demonstrated (Smith, 2007)"; "as Smith (2007) demonstrated"
- *two authors:* both authors' names and the year of publication: (Arnold and Sebastian, 2008; Smith and Hansel, 2006; Stern and Lars, 2009)
- *three or more authors:* first author's name followed by "et al." and the year of publication: "As has recently been shown (Werner et al., 2005)...", "Kramer et al. (2000) have recently shown"

Citations of groups of references should be listed first alphabetically, then chronologically.

Examples: ".....as demonstrated (Aden, 1996a, 1996b, 1999; Allan and Jones, 1995; Han et al., 2007; Weiss and Schmidt, 1988)".

Abbreviations

Define all abbreviations at their first mention in the text. Ensure consistency of abbreviations throughout the article.

Acknowledgements

Include acknowledgements in a separate section at the end of the article before the references and do not, therefore, include them on the title page, as a footnote to the title or otherwise. List here those individuals who provided help during the research (e.g., providing language help, writing assistance or proof reading the article, funding supports etc.).

Footnotes

Footnotes must be avoided. Do not include footnotes in the Reference list.

Table footnotes

Indicate each footnote in a table with a superscript lowercase letter.

Tables

Draw the Tables in grid format using a basic, solid line style without shadows.

Ensure that the data presented in Tables do not duplicate results described in Figures or elsewhere in the paper.

Figures

Number Figures consecutively in accordance with their appearance in the text. All illustrations should be provided in camera-ready form, suitable for reproduction, which may include reduction without retouching.

Photographs, charts and diagrams are all to be referred to as Figure(s) and should be numbered consecutively, in the order to which they are referred.

Figures may be inserted preferably as black line drawings. They should be pasted on, rather than taped, since the latter results in unclear edges upon reproduction.

Ensure that each illustration has a caption, placed below the Figure. Supply also captions separately, not attached to the figure. A maximum limit of 8 Figures are allowed per manuscript.

A caption should comprise a brief title (**not** on the Figure itself) and a description of the illustration. Keep text in the illustrations themselves to a minimum but explain all symbols and abbreviations used. Multiple Figures can be expressed as one Figure (for e.g. 1a, 1b, 1c etc...), while retaining the maximum limit of 6.

ALL Figures must be submitted in either .jpg or .tiff format with a very good resolution (but do not submit graphics that are disproportionately large for the content).

Figures and Tables must be embedded in the text.

Proofs

Proofs will be sent to the corresponding author (by e-mail) and should be returned within 72 hours of receipt. Corrections should be restricted to typesetting errors; any other changes may be charged to the authors.

Paper in Electronic Format:

Authors are asked to submit their final and accepted manuscript as an attachment to one of the above-mentioned e-mail addresses. Use the .doc format (not .docx !).

5. Page charge

There is no charge per printed page for regular papers.

6. Reprints

The corresponding author will be provided with a .pdf file of the paper via e-mail, free of charge. A hard copy of the issue containing the paper can be provided on request, for a fee. This request will be formulated when the final form of the manuscript (the electronic one) is provided.

7. Additional procedures for the editorial management of *Environmental Engineering and Management Journal*

Starting with volume 13/2014, the members of the Scientific Advisory Board and the Corresponding authors will receive each issue of the journal in electronic .pdf format. Printed copies can be delivered on request.

An author cannot appear on more than two papers per regular issue. An author cannot appear on more than three papers in a Guest Editor/ Conference issue.

The evaluation/peer-review process of manuscripts submitted for Guest Editor / Conference issues published according to journal *Editorial Procedure and Policy* will be handled and evaluated as with regular manuscripts, so that only consistent papers will be published. The manuscripts must be sent at least six months before the presumed date of publication. Those manuscripts which do not fulfill the journal requirements will be rejected. This is to discourage superficiality in the development of the manuscript, from formal and scientific points of view. No amount of money will be refunded following the rejection of manuscripts.

No more than 160 pages and no more than 20 papers are acceptable for regular issues. No more than 180 pages and no more than 25 papers are opportune for special issues. The number of pages is based on the published version of an article, not on the submitted version (for instance, when page breaks are changed and when images are enlarged for easier viewing).

An issue can include, as an exception, a number of 25-30 papers as a maximum. This situation could appear when the authors of an already accepted paper need and ask for early publication, from the position in the list of accepted papers. In this circumstance, a yearly submission to our journal (500 Euro) will be asked for each already accepted paper, for its publication in advance.

A newly-received manuscript can be evaluated by priority, when a deposit of 200 Euro shall be paid by authors in advance. If the manuscript is deemed

unsuitable for publication, the authors will not be eligible for a refund.

Failure to pay mandatory charges may result in the paper being withheld from early publication.

In all cases, the corresponding author will sign an agreement with the *Editor-in-Chief*, and the *Director* of the *EcoZone* Publishing House according to journal *Editorial Procedure and Policy*.

Automated software is used for checking against plagiarism. In order to avoid false results, the generated reports are cautiously checked and confirmed by journal staff. We do not send plagiarism reports to authors. Any manuscripts which do not prove to be at least 90% original will be rejected. The rejection for plagiarism may arise at any phase of the editorial / review process, even if the manuscript was accepted for publication. The authors are solely responsible for the originality of their submission. Therefore, any manuscript should be carefully checked for such inconsistencies before submitting to EEMJ.

The authors are required to follow academic publishing rules, to adhere to the principles of scientific ethics and to sign the Authors' warranty and Copyright transfer.

Detailed information concerning these issues may be found of the EEMJ website, under *Editorial Procedure and Policy*.

Environmental Engineering and Management Journal is edited by the
Publishing House **ECOZONE** of the
Academic Organization for Environmental Engineering and Sustainable Development (OAIMDD)
within the **Department of Environmental Engineering and Management – Faculty of Chemical Engineering and
Environmental Protection under the aegis of "Gheorghe Asachi" Technical University of Iasi**
73 Prof.Dr.docent Dimitrie Mangeron Street, 700050-Iasi, Romania



"Gheorghe Asachi" Technical University of Iasi